BIOBASED SYNTHESIS OF SILVER AND TITANIUM DIOXIDE NANOPARTICLES AND THEIR APPLICATIONS
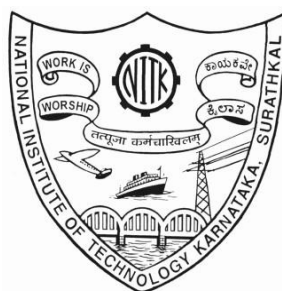
Thesis

Submitted in partial fulfilment of the requirement for the degree of

DOCTOR OF PHILOSOPHY

By

AISHWARYA DEVADIGA

DEPARTMENT OF CHEMICAL ENGINEERING
NATIONAL INSTITUTE OF TECHNOLOGY KARNATAKA,
SURATHKAL, MANGALORE-575 025
NOVEMBER, 2016.

DECLARATION

I hereby *declare* that the Research thesis entitled **"Biobased synthesis of silver and titanium dioxide nanoparticles and their applications"** which is being submitted to the National Institute of Technology Karnataka, Surathkal in partial fulfilment of the requirements for the award of the Degree of **Doctor of Philosophy** in the Department of Chemical Engineering**,** is a *bonafide report of the research work carried out by me*. The material contained in this Research Thesis has not been submitted to any University or Institution for the award of any degree.

Place: NITK, Surathkal   Name   : AISHWARYA DEVADIGA

Date: Register Number: 100527CH10F01

                                         Department of Chemical Engineering

CERTIFICATE

This is to *certify* that the that the Research Thesis entitled **"Biobased synthesis of silver and titanium dioxide nanoparticles and their applications"** submitted by **Ms. Aishwarya Devadiga (Register Number: 100527CH10F01)** as the record of the research work carried out by her, *is accepted as the Research Thesis submission* in partial fulfilment of the requirements for the award of Degree of **Doctor of Philosophy.**

Research Guides

Dr.Vidya Shetty.K,
Associate Professor,
Department of Chemical
Engineering.

Dr. M.B Saidutta,
Professor,
Department of Chemical
Engineering

Chairman – DRPC

ACKNOWLEDGEMENT

Saving the most important for the last, I would like to thank my husband, **Mr. Ambadas Nambivalap,** for his unconditional love, patience and encouragement especially when the tasks seemed arduous and insurmountable. For his continual support of my academic endeavours over the past years that enabled me to complete this research work.

The last word of love and thanks goes for *Reyansh Ambadas*, my baby boy, who has been the new light of happiness in my life and has given me the extra strength and motivation to achieve this goal of my life.

Above all, I owe it all to Almighty God for granting me the wisdom, health and strength to accomplish this research work.

-Aishwarya Devadiga

DEDICATED TO MY FAMILY

ABSTRACT

Silver nanoparticles (AgNPs) and titanium dioxide nanoparticles (TiO$_2$-NPs) have found wide range of applicability in engineering, healthcare, consumer goods, pollution abatement and electronics. Biobased routes for their synthesis is gaining prominence, as they are safer and environmental friendly routes with low chemical footprint compared to physical and chemical routes. In the present research work, the plant sources such as leaves of *Terminalia catappa* and *Tectona grandis* Linn F leaves were selected based on their ability to synthesize AgNPs. The bacterial sources were isolated from the silver rich environment based on their ability to reduce the silver ions extracellularly and were identified as *Brevundimonas vancanneytii, Leucobacter aridicollis, Enterobacter cloacae* and *Alcaligenes aquatilis.* AgNPs could be synthesized effectively using aqueous extracts of the leaves and the cell free culture supernatants of these bacterial strains. Extracellular TiO$_2$-NPs were also synthesized using the bacterial cell free culture supernatants. The synthesis parameters influencing the conversion of precursor ions and the morphological characteristics such as size, shape, isotropy and monodispersity of the nanoparticles being synthesized were studied and optimized. In plant based synthesis, plant bioactive components acted as reducing and capping agents, while the bacterial based synthesis was brought about by the extracellular enzymes. AgNPs and TiO$_2$-NPs synthesized in the present research work were found to be capped with biobased moieties which imparted stability to the particles. The AgNPs exhibited antibacterial efficacy and colorimetric mercury sensing property, while the TiO$_2$-NPs exhibited photocatalytic activity. Crystalline AgNPs synthesized with a conversion of 98.98% using the bacterial strain *Alcaligenes aquatilis* were of average particle size of 23±0.9 nm, isotropic, quasispherical shaped along with narrow size range and exhibited the best antibacterial property and colorimetric mercury sensing ability as compared to other AgNPs synthesized. TiO$_2$-NPs synthesized using the cell free culture supernatant of the same bacterial strain were isotropic, monodispersed, quasi spherical shaped, and with an average size of 4.0±0.5 nm containing brookite phase of titania. They exhibited higher photocatalytic activity as compared to Degussa P-25 in terms of degradation of Acid blue and Remazol brilliant blue R dyes, with complete degradation of 50 mg/L of dyes in 120 min. Thus the process developed in the current study could harness the biobased components from the selected plant and bacterial sources for the synthesis of AgNPs and TiO$_2$-NPs under ambient conditions with promising large scale applicability.

Keywords: Nanoparticles; Photocatalyst, Colorimetric sensors; Antibacterial property

TABLE OF CONTENTS

LIST OF FIGURES

LIST OF TABLES

CHAPTER 1

INTRODUCTION

1.1 Background of research work and motivation

Nanotechnology is a highly multidisciplinary field, covering a broad range of topics, including biology, physics, chemistry, and engineering. With the technological advancements in the field of nanotechnology, it has gained prominence as the third industrial revolution and is emerging as one of the promising and lucrative fields of current research areas due to the growing demand of commercial products produced using this technology. Nanostructured materials, nanoparticles/nanocomposites, nanocapsules, nanoporous materials, nanofibres, fullerenes, nanowires, single-walled & multi-walled (Carbon) nanotubes, dendrimers, molecular electronics, quantum dots and thin films are some of the products of nanotechnology. Due to their myriad and exuberant properties at the nanoscale level, nanoproducts have found their major applicability in predominant sectors such as energy and power, healthcare and medical, engineering, consumer goods, environmental applications and electronics (Jain et al. 2011; Willems, 2005). They are used in cosmetics, food and feed, mechanics, optics, biomedical sciences, chemical industries, space industries, drug-gene delivery, optoelectronics, catalysis, single electron transistors, light emitters, nonlinear optical devices, and photo-electrochemical application (Mansur et al. 1995; Colvin et al. 1994, Wang and Herron, 1991, Schmid, 1992, Hoffman et al. 1992, Hamilton and Baetzold, 1979).

Nano-products are generally synthesized using two methods-the top down approach and the bottom up approach. In bottom up method, materials and devices are built from molecular components (Lu and Lieber, 2007; Balzani et al. 2002). In the "top-down" approach, nano-objects are constructed from larger materials (LaBean and Li, 2007; Spatz et al. 2002). Ordinary materials, when reduced to the nanoscale, often exhibit novel and unpredictable traits such as extraordinary strength, chemical reactivity, electrical conductivity, or other characteristics like the specific surface area they offer, optical (Evanoff and Chumanov, 2005), magnetic (Garcia et al. 2007), thermal (El-Sayed et al. 2001), mechanical and electrical (Shi et al. 2006) properties. Nanoparticles are defined as the particles having one or more dimensions of the order of 100 nm or less and have attracted great attention due to their unusual and fascinating properties, and applications advantageous over their bulk counterparts

(Daniel and Astruc, 2004). Nanoparticles can be made out of a wide range of materials, the most common being organic, ceramics, metal oxides, metals, silicates and non oxide ceramics.

Noble metal nanoparticles exhibit enhanced properties based on their nanoscale size and structure enabling their use in various applications (Sun and Xia, 2002; Daniel and Astruc, 2004). These enhanced properties exhibited by nanoparticles are due to large surface to volume ratio, large surface energy, and reduced imperfections (El-Nour et al. 2010; Dong and Zhu, 2003; Yoffe, 2001). Among all the noble metal nanoparticles, silver nanoparticles (AgNPs) have gained boundless interest because of their unique properties (Ahmed et al. 2016) such as chemical stability, good conductivity, catalytic (Santos et al. 2012; Jiang et al. 2005), optical (Evanoff and Chumanov, 2005), electrical properties (Chen et al, 2009), electromagnetic (Zhao et al. 2008), thermodynamic (Luo et al. 2008), antimicrobial (Rai et al, 2009), antiangiogenic property (Gurunathan et al. 2009b), antiplatelet (Shrivastava et al. 2009), in addition to anti-inflammatory activities. AgNPs can be incorporated into composite fibers, cryogenic superconducting materials, cosmetic products, food industry and electronic components (Klaus-Joeger et al. 2001).

A broad spectrum of antibacterial and antifungal activities exhibited by AgNPs make them extremely popular in a diverse range of consumer products, including plastics, soaps, pastes, cosmetics (Kokura et al. 2010), food and textiles (Perelshtein et al. 2008; Dubas et al. 2006), healthcare sector (Worchester and This, 2011), water purification (Jain and Pradeep, 2005) and are already integrated into applications such as wound treatment, sterilization, food sanitation, antibacterial textiles and more recently drug delivery, thus increasing their market value (Rauwel et al. 2015). AgNPs are used as plasmonic light traps in solar cells. These properties make them valuable in applications such as inks, microelectronics, medical imaging, and waste management (Rauwel et al. 2015). They are also used for sensing and imaging applications (Kumar and Anthony, 2014).

Another widely used nanoparticle with broad range of applicability is titanium dioxide (TiO$_2$-NPs). TiO$_2$ belongs to the family of transition metal oxides. There are four commonly known polymorphs of TiO$_2$: anatase (tetragonal), brookite (orthorhombic), rutile (tetragonal), and TiO$_2$ (B) (monoclinic) (Carp et al. 2004). TiO$_2$

4

is a large band semiconductor, with band gaps of 3.2 and 3.02 eV for the anatase and rutile phases respectively (Di Paola et al. 2013). The brookite phase has been reported to have the band gap values ranging from 3.26 to 3.4eV (Di Paola et al. 2013; Shibata et al. 2004). TiO_2 exhibits good photo catalytic property, hence is used in degradation of organic contaminants (Fujishima and Zhang, 2006; Turchi and Ollis, 1990) and germs (Cheng et al. 2009; Kühn et al. 2003), antiseptic and antibacterial compositions (Kangwansupamonkon et al. 2009; Machida et al. 2005), as a UV-resistant material (Katangur et al. 2006; Yang et al. 2004), manufacture of printing ink (Comiskey et al. 1998), self-cleaning ceramics, glass and coatings (Benedix et al. 2000, Nakajima et al. 2000), making of cosmetic products such as sunscreen creams, whitening creams, morning and night creams, skin milks, etc (Contado and Pagnoni, 2008; Popov et al. 2005), used in the paper industry for improving the opacity of paper (Park et al. 2007a; Gregory and Vinson,1990). TiO_2 has been used widely as a photocatalyst due to its low cost, non-toxicity, long-term stability, and environmental application potential (Zhang et al. 1998; Linsebigler et al. 1995). Owing to the wide and diverse applicability of AgNPs and TiO_2-NPs, the present study focuses on the synthesis of these nanoparticles.

Production or synthesis of nanoparticles can be achieved through various methods which can be categorized into physical (Kabashin et al. 2003; Zhu et al. 2000), chemical (Guzmán et al. 2009; Maaz et al. 2007; Lyon et al. 2004) and biological (Parashar et al. 2009; Shankar et al. 2004) routes. The physical and chemical methods involve attrition or milling (Tsuzuki and McCormick, 2004), spray pyrolysis (Widiyastuti et al. 2011), inert gas condensation or chemical vapour deposition (Iskandar, 2009; Wegner et al. 2002), pulsed laser ablation (Marine et al. 2000), spark discharge generation (Tien et al. 2008) and ion sputtering (Urban et al. 2002), chemical vapour synthesis or chemical vapour condensation (Jones and Chalker, 2003), Laser pyrolysis/photothermal synthesis (Rice, 1987),thermal plasma synthesis (Tanaka et al. 2011), flame synthesis (Kammler et al. 2001), solvothermal or hydrothermal reaction (Jeon and Braun, 2003; Rajamathi and Seshadri, 2002), sol-gel method (Valencia et al. 2010), micellar structured media (Capek, 2004).

Most of the contemporary, traditional chemical and physical routes used for synthesis of nanoparticles employ hazardous, toxic and expensive solvents and other

chemical reagents in large quantities, involvement, monitoring and control of elevated physical process parameters like temperature and pressure (Saxena et al. 2010). Thus, these processes lead to difficulties involved with handling of large volumes of reagents, stable control of physical process parameters throughout the synthesis, achievement of monodispersed nanoparticles, the capital involved in the process and disposal of the remnant. Most of these processes are energy and chemical intensive making them uneconomical and causing pollution risks.

Recently, there is a growing need to develop environmentally and economically friendlier processes generally referred as greener processes which do not use toxic chemicals in the synthesis. Selection of solvent medium and selection of eco-friendly, nontoxic reducing and stabilizing agents are the most important issues which must be considered in green synthesis of nanoparticles (Iravani et al. 2014). This has conducted researchers to look at the organisms which are the biological resources for the green synthesis. The potential of organisms in nanoparticle synthesis ranges from simple prokaryotic bacterial cells to eukaryotic fungi and plants (Mohanpuria et al. 2008). The key aspect of bio-based synthesis process involves the production of nanoparticles by employing biological resources like plants and microbes like bacteria, fungi, yeast and viruses. The extract of plant parts or the microorganisms helps in the formation of nanoparticles of varying physico-chemical properties, size, shape and controlled dispersity.

The biobased synthesis of nanoparticles has been proven to be cost effective, ecofriendly and involves the usage of biological resources under ambient conditions of synthesis (Bhainsa and D'Souza, 2006) while providing a lower chemical foot print on the environment and considered as greener and cleaner process. More over the bio-based processes are the best platforms for synthesis of nanoparticles; being free from toxic chemicals as well as providing natural capping agents for their stabilization (Ahmed et al. 2016). The bio-based routes for the synthesis of nanoparticles are majorly classified as plant based and microbial based synthesis.

The biological sources like plants are found competent in this regard. Plants have evolved as pioneers in survival on earth throughout evolution due to their ability to adapt and survive even in harsh climatic conditions, the advent of industrialization and the subsequent pollution in the atmosphere though adaptive measures (Berry and

Bjorkman, 1980; Walley et al. 1974). Plant biomass is abundantly available and possesses huge paraphernalia of the bioactive components that demonstrate myriad chemical properties hence can be harnessed for these properties and utilized for the synthesis of nanoparticles.

Plant parts like fruits, seeds, leaves, bark, latex, roots and flower find their way into many high value commercial products. The use of plant or plant part extracts as the production assembly of nanoparticles has drawn attention, because of rapid, eco-friendly and economical nature of the synthesis process and for providing a single step technique for the synthesis (Ahmed et al. 2016). Certain plant parts have been established to contain variety of bioactive components such as alkaloids, tannins, phenolics, saponins, terpinoids etc, which are environmentally benign, yet chemically complex structures and they bring about the formation of nanoparticles (Kulkarni and Muddapur, 2014).

Majority of the research on plant based synthesis of nanoparticles deals with the use of plant products which already possess/carry a good commercial or food value. AgNPs have been reported to be synthesized using the extracts of various plant parts such as *Citrus limon* fruit (Prarthna et al. 2011), *Terminalia chebula* fruit (Edison and Sethuraman, 2012), *Aloe vera* (Chandran et al. 2006), *Coriandrum sativum* leaf (Sathyavathi et al. 2010), coffee and tea (Nadagouda and Varma, 2008), *Cinnamomum camphora* (Huang et al. 2010), *Emblica officinalis* (Ankamwar et al. 2005). TiO$_2$-NPs are also synthesized using certain plant parts such as extract of *Nyctanthes arbor-tristis* leaves (Sundrarajan et al.2011), *Jatropha curcas* L. latex (Hudlikar et al. 2012), *Eclipta prostrate* leaves (Rajakumar et al. 2012a), *Annona squamosa* peel (Roopan et al. 2012), *Catharanthus roseus* leaves (Velayutham et al. 2012), *Calotropis gigantean* flower (Marimuthu et al. 2013) and *Solanum trilobatum* leaves (Rajakumar et al. 2014).

Many plant parts bearing commercial and agricultural value have been diverted towards the synthesis of nanoparticles. A better alternative in the avenue of plant based synthesis of nanoparticles would arise from harnessing the bioactive components from plant material that generally form a refuse of agro or food based industries. These discarded resources include the foliage of certain trees that go untapped while the wood of the trees bearing commercial value are lumbered, the

unused peels and rinds of fruits that are majorly used in the preparation of fruit pulp juices, jams and marmalades generated in huge proportions from the food processing industries. These refuses are seen as a major promising contender in comparison to other valuable plant based sources for biosynthesizing nanoparticles. The resources are readily available in surplus quantities as a refuse and prove to be a cost effective source for the bioactive components required for the synthesis of nanoparticles. A dual edged benefit arises in the efficacious utilization of the unharnessed bioactive components that go untapped for the synthesis of nanoparticles.

Microorganisms such as bacteria, fungi and yeast have also been used for the synthesis of nanoparticles. The microbial based synthesis of nanoparticles has been based on randomly chosen strains. Considerable number–of research reports are available on the synthesis of nanoparticles by different microbial strains belonging to the genera of fungi such as *Fusarium oxysporum* (Duran et al. 2005; Ahmad et al. 2002)*, Fusarium accuminatum* (Ingle et al. 2008), Aspergillus *niger* (Gade et al. 2008), *Aspergillus fumigatus* (Bhainsa and D'Souza, 2006), yeast such as *S.cerevisiae* (Geriecke and Pinches, 2006) and bacteria such as *Lactobacillus* sp. (Jha et al., 2009a; Nair and Pradeep. 2002)*, Bacillus subtilis* (Dhandapani et al. 2012; Kirthi et al. 2011)*, Pseudomonas stutzeri* (Geriecke and Pinches, 2006), *E.coli* (Sondi and Sondi, 2004) and *Staphylococcus aureus* (Nanda and Saravanan, 2009) for the synthesis of metal and metal oxide nanoparticles. Microbes such as *Morganella* sp. (Parikh et al. 2008), *Klebsiella pneumoniae* (Mokhtari et al. 2009), *Phaenerochaete chrysosporium* (Vigneshwaran et al. 2006), *Fusarium accuminatum* (Ingle et al. 2008), *Verticillium* (Mukherjee et al. 2001a) have been used in the synthesis of AgNPs, while strains such as *Bacillus subtilis* (Kirthi et al. 2011), *Bacillus subtilis* (Dhandapani et al. 2012), *Planomicrobium* sp. (Malarkodi et al. 2013), *Propionibacterium jensenii* (Babitha et al. 2013), *Aeromonas hydrophila* (Jayaseelan et al. 2013) are used in the synthesis of TiO$_2$-NPs.

Microbial based synthesis of nanoparticles can be classified based on its location of synthesis. The particles may be synthesized extracellularly (Parikh et al. 2008; Ingle et al. 2008; Bhainsa and D'Souza, 2006; Vigneshwaran et al. 2006) or intracellularly (Klaus et al. 2009; Mukherjee et al. 2001a). Thus, the synthesized particles can be located inside the cell (Ahmad et al. 2003), periplasmically confined

(Pugazhenthiran et al. 2009) or extracellular (Basavaraja et al. 2008). However, the challenges faced in terms of recovery of nanoparticles from the synthesis mixture containing microbial cells and the separation of microbial biomass associated with the intracellular or periplasmically confined nanoparticles need to be countered. These challenges can be overcome by adopting a cell free, extracellular enzymatic/metabolite based synthesis process. However, for a cell free synthesis process, isolation of strains from the specific environment with the ability to synthesize extracellular nanoparticles is a promising approach.

1.2 Scope of the study

Both plant and microbial based synthesis approach are very promising as they are greener, cost effective, less energy intensive and eco friendly processes. Both the methods are advantageous by providing natural capping agents for the stabilization of the nanoparticles, thus needing no further addition of surfactants and organic chemicals during the synthesis to enhance stability as in chemical processes. Microbial based synthesis, involves the maintenance of microbial cultures under aseptic conditions. The use of plant extracts is potentially advantageous over microorganisms due to the ease of improvement, the less biohazard and elimination of elaborate process of maintaining cell cultures (Kalishwaralal et al. 2010). However, the morphological characteristics, size, dispersity and surface capping agents may be different based on the synthesis route adopted and the varied characteristics offer varied application potential for the nanoparticles. Based on the literature reports, synthesis of nanoparticles using yeast and fungi is slower compared to that of bacterial based synthesis of nanoparticles (Ingle et al. 2008).

As the plant parts and microbial resources such as bacteria, have proven themselves as successful candidates for the biobased synthesis of nanoparticles, the presently reported study was focused on harnessing the potential microbial isolates and plant based wastes for the efficient synthesis of AgNPs and TiO_2-NPs. As discussed earlier, most of the research on plant based synthesis of nanoparticles deals with the use of plant resources that already carry good food, agronomical and commercial value, thereby leading to injudicious utilization of these limited high value resources. Plant resources with high nutritional value are being diverted to cater

to nanotechnological applications and may amount to their depletion as food source. Though, there are reports on plant based synthesis using the waste plant or plant part material such as Banana peels (Bankar et al. 2010), water melon rind (Lakshmipathy et al. 2015), Orange peels (Kahrilas et al. 2013), Pomegranate peels (Edison and Sethuraman, 2013; Ahmad and Sharma, 2012) and Mango peel (Yang and Li, 2013) for AgNPs and sources such as *Annona squamosa* (Custard apple) peels (Roopan et al. 2012) for TiO_2-NPs, there is a need to explore other alternate resources which are readily available as by product or wastes of food, agricultural or forestry sector so that the society is benefitted through the potency of these waste material. In the present study, various plants resource material such as fruit peels and plant foliage that possess less commercial or agro economic value and which are readily available in surplus quantities have been screened for their potential to synthesize AgNPs. The waste material from food, agricultural or forestry sector were selected for screening based on the literature reports suggesting the presence of bioactive components in them, which can contribute as reducing and stabilizing agents in the synthesis of nanoparticles.

Studies on bacterial based synthesis of AgNPs and TiO_2-NPs are reported in literature. However, search for the bacterial isolates with the ability to synthesize nanoparticles extracellularly may prove beneficial as extracellular synthesis eliminates the challenges involved in recovery of nanoparticles from the cellular material. It was hypothesized that, if the microbial strains were isolated from silver rich environment, they would possess the metabolic machinery required for the reduction of Ag^+ ions to zerovalent silver thus being able to synthesize AgNPs.

In the presently reported study, the plant resources and isolated strains were screened based on their potential to synthesize AgNPs. These resources were also tested for their efficacy to synthesize TiO_2-NPs. The yield of nanoparticles which is based on the conversion of precursor salt to the nanoparticles and the morphological characteristics of the nanoparticles depend on the synthesis parameters. In plant based synthesis, the parameters which control morphological characteristics of the nanoparticles and the conversion are the concentration of the precursor salt solution and the plant extract, volume ratio of the plant extract to the precursor salt solution, pH and temperature of the synthesis mixture (Sathishkumar et al. 2014; Moghaddam

and Dabanlou, 2014; Veerasamy et al. 2011; Thakkar et al. 2010; Dubey et al. 2010). The process used for the preparation of plant extract may also determine the conversion and the nanoparticle characteristics as it controls the concentration of bioactive components in the synthesis mixture. In microbial based synthesis the important synthesis parameters which control the morphological characteristics of the nanoparticles and the conversion are the concentration of the precursor salt solution and pH of the synthesis mixture (Hebbalalu et al. 2013; Vahabi et al. 2011; Gurunathan et al. 2009; Kowshik et al. 2009).

The development of any synthesis process for the nanoparticles using any new resource demands for optimization of the above said process parameters which govern the synthesis, so as to maximize the synthesis of nanoparticles with the desired morphological characteristics. There is a also need for testing the synthesized nanoparticles for their application potential, as the efficacy of nanoparticles for the given application depends on their morphological characteristics such as size, shape, dispersity, stability, presence of capping agents etc.

As reported in the literature review presented in Chapter 2, there are limited reports available on the synthesis of AgNPs and TiO$_2$-NPs with the isolated bacterial strains and with the food, agricultural or forestry sector waste. Reports on optimization of parameters influencing the microbial and plant based synthesis process are limited.

Thus, based on the extensive review of literature and as demanded for the development of a synthesis process with the new resources the following key research questions were raised

(i) Whether the various plants resource material such as fruit peels and plant foliage that possess less commercial or agro economic value and which are readily available in surplus quantities as waste material from food, agricultural or forestry sector selected in the present study possess the potential to synthesize AgNPs?

(ii) Whether the bacterial strains isolated from the silver rich environment possess the potential to synthesize extracellular AgNPs?

(iii) If so, what are the optimum conditions for the synthesis to maximize the conversion and to obtain narrow size ranged, small sized, isotropic, monodispersed AgNPs?

(iv) Are the resources selected for the synthesis of AgNPs can be used for the synthesis of TiO_2-NPs and if so, what are the optimum conditions for the synthesis to maximize the conversion and to obtain narrow size ranged, small sized, isotropic, monodispersed TiO_2-NPs?

(v) What are the characteristics of synthesized AgNPs and TiO_2-NPs?

(vi) What are the application potential of synthesized AgNPs and TiO_2-NPs?

(vii) Are these nanoparticles (AgNPs and TiO_2-NPs) of comparable efficacy in their application potential to the chemically synthesized counterparts?

(viii) What is the mechanism of plant and bacterial based sources synthesis of these nanoparticles?

Based on literature review, the research questions raised and the scope of the work, following objectives have been formulated for the research work:

1.3 Objectives of the Research Work

The main objective of the research work is to synthesize AgNPs and TiO$_2$-NPs by microbial and plant based routes and to compare their efficacy in terms of their application potential with those synthesized by chemical methods.

Specific objectives are:

- Screening of potential leaf and fruit peel sources for synthesis of AgNPs

- Isolation of bacteria from metal rich soil; screening and identification of the bacteria capable of synthesizing extracellular AgNPs.

- Optimization of the various physico-chemical parameters for microbial and plant based synthesis of AgNPs.

- To test the ability of chosen plant resources and isolated bacteria for the synthesis of TiO$_2$-NPs and to optimize the synthesis parameters

- Characterization of the synthesized nanoparticles for their size, shape, surface capping, dispersity, stability etc.

- Identification of bioactive components present in the extract of the plant resources which are responsible for the synthesis of nanoparticles

- Identification of the metabolic machinery responsible for the bacterial based synthesis of nanoparticles

- To study the application potential of AgNPs as antibacterial agents and sensors in comparison with the chemically synthesized AgNPs

- To study the application potential of the synthesized TiO$_2$-NPs as photocatalysts and compare with the chemically synthesized (commercial) TiO$_2$-NPs

1.4 Organization of the Thesis

This thesis is divided into following five chapters:

Chapter 1 presents the **Introduction**.

This chapter discusses the background of research, need for the study and problem statement. The objectives based on the extensive literature review and the key research questions raised through it were specified for the currently reported research work and are presented at the end of this chapter.

Chapter 2 presents the detailed **Literature Review**.

This chapter summarizes the relevant literature review carried out during the current study, highlighting the research gaps in the existing literature reports. It also presents the review of literature on the methodologies adopted and salient finding in the existing literature.

Chapter 3 presents the **Materials and Methods**.

This chapter lists the materials used, followed by description of the experimental methods and the analytical procedures adopted to achieve the stated objectives.

Chapter 4 presents the **Results and Discussions** on the studies performed according to the methodologies presented in Chapter 3. The results obtained are presented as tables and figures as suitable for the better representation and interpretation of results. The detailed discussion, validation and rationalization of the results and findings of the present study with the related research work from the literature are presented in this chapter.

This chapter is divided into two parts; Part A and Part B.

Part A: This part of Chapter 4 presents the results of experiments on **Plant and bacterial based synthesis of metallic AgNPs,** the screening and selection of suitable plant material and the isolation, screening and selection of bacterial strains for the synthesis of AgNPs, influence of various synthesis parameters on the conversion and morphological characteristics of the AgNPs, characterization of the AgNPs synthesized and their application as potential antibacterial agent and mercury sensors.

Part B: This part of Chapter 4 presents the results of the experiments on **the bacterial based synthesis of TiO$_2$-NPs**, factors influencing the synthesis of TiO$_2$-NPs, characterization of the TiO$_2$-NPs synthesized, their application as photocatalysts in the degradation of dyes, factors influencing the photocatalytic degradation of the dyes and study of kinetics.

Chapter 5 presents the **Summary and Conclusions** of the present research work along with the future scope for research.

CHAPTER 2

REVIEW OF LITERATURE

This chapter presents the salient details of the reported literature relevant to the present research work. It summarizes the literature on synthesis methods, resources used for biobased synthesis, mechanism of synthesis, properties and the applications of AgNPs and TiO_2-NPs.

2.1 Concept of nanotechnology

Nanotechnology has become one of the most important and exciting frontier research fields encompassing basic areas of science like Physics, Chemistry, Engineering and Biology (Bhushan, 2010; Dai, 2006; Roco, 2002). The concept of nanotechnology is based on the recognition that particles less than the size of 100 nanometres (a nanometre is a billionth of a meter), exhibit new properties and behaviour (Chol, 1995). This happens because particles that are smaller than the characteristic lengths associated with particular phenomena often display new physiochemical aspects, leading to new behaviour, which depends on the size. The dependence of the behaviour on the particle sizes can allow one to engineer their properties. The nanoscale technology is often described as the "enabling technology" and has been proclaimed to impact the human lifestyle widely (Higashisaka, 2015; Bradley et al. 2011). The specific area of applicability for nanotechnology is quite multidisciplinary in nature as the unique properties offered by the products of this technology fascinate researchers.

The earliest concept of nanotechnology was introduced to mankind by Michael Faraday through his lecture to the Royal Society of London in 1857 regarding his genius observation of interaction between light with the gold metal colloid (Edwards and Thomas, 2007; Faraday, 1991). The major findings of the research were based on the facets of particle formation, shape and properties of ruby gold (Thompson, 2007). The aspect of nanoscale size was later elaborated by Nobel Laureate Richard Feynman in his visionary lecture at Caltech in 1959 and the term nanotechnology was used by Noria Taniguchi, (1974). With the understanding of the basic concepts and the refinement in the available technology to support the nanotechnology frontier, researchers are currently changing the aspect of Nanotechnology with nanomaterials at the leading edge of the rapidly developing field. Nanomaterials have found their usage for instance, in the microelectronics (Wong et al. 2010; Bruce et al. 2008), cosmetics (Kogure, 2015; Mu and Sprando,

2010), pharmaceutical (Dobrovolskaia and McNeil, 2007; Kumar, 2006) and food industries (Weiss et al. 2006; Sanguansri and Augustin, 2006). It has been forecasted that the global nanotechnology industry will grow to reach US$ 75.8 Billion by 2020 (RNCOS, 2015).

2.2 Properties of nanoparticles

Nanoparticles are one of the most important products of nanotechnology as they exhibit exceptionally remarkable characteristics at their size range (Jain et al. 2008; Tjong, 2007; Park et al. 2007). At size less than 100 nm, quantum effects rule the behaviour and properties of particles. Properties of materials are size-dependent in this scale range. Thus, when particle size is of nanoscale, properties such as melting point, fluorescence, electrical conductivity, magnetic permeability, and chemical reactivity change as a function of the size of the particle. This display of properties is due to the increase in the surface area to volume ratio in a progression which is relative to the gradual decrease in size from the bulky nature of the material towards nanoscale level (Weiss et al. 2006). The increase of the surface area leads to the dominance in the behaviour of atoms present at the surface of the particle than those on the interior. Observance of this behaviour, affects the properties of the nanoparticles in an isolated condition and its interaction with other materials.

Nanoparticles have varied applications based on their specific surface area, magnetic (López-Ortega et al. 2015; Kačenka et al. 2014; Garcia et al. 2007), optical (Nasrollahzadeh et al. 2014; Elghanian et al. 1997), electrical (Chen et al. 2009; Vollath, 2008; Park et al. 2002), thermal (Philip et al. 2008; El-Sayed et al. 2001), chemical (Lévy et al. 2010; Daniel and Astruc, 2004) and mechanical (Shi et al. 2006) properties compared to large particles of bulk materials hence offer great potential to influence various sectors in the areas of energy, environment, agriculture, healthcare and consumer goods (Jain et al. 2011; Sastry et al. 2003).

Nanoparticles have emerged as the highly endowed nanoproducts as they impact the daily life style of living beings. Properties exhibited by the nanoparticles make them suitable candidates as antimicrobial agents in toys, sports gear (Zhao and Shen, 2012), clothes (Benn and Westerhoff, 2008; Tarimala et al. 2006), water purifiers and health care products (Tolaymat et al. 2010).

The current and projected applications of nanoparticles include catalysts (Chimentao, 2004; Sun and Xia, 2002; Zhong and Maye, 2001), lubricants and fuel additives (Sajith et al. 2010; Hu et al. 2002), paints, pigments and coatings (Kaiser et al. 2013; Kumar et al. 2008), cosmetics and personal care products (Weir et al. 2012), medical, dental, drug delivery and bionanotechnology (Kayser et al. 2005), functional coatings (Roguska et al. 2014; Kainz and Reiser, 2014), hydrogen storage and fuel cells (Arico et al. 2005), nanoelectronics and sensor devices (Shipway et al. 2000), optics and optical devices (Barnes et al. 2003), security and authentication applications (Creran et al. 2012); structural (composite) materials (Shipway and Willner, 2001), conductive inks and printing (Li et al. 2005a), UV-absorbers and free-radical scavengers (Berneth et al. 2007; Ammala et al. 2002), construction materials (Sobolev et al. 2009), detergents (Shengrong et al. 2005), food processing and packaging (Duncan, 2011), agrochemicals (Wanyika et al. 2012), plant protection products (Khot et al. 2012), plastics (Roe et al. 2008), weapons and explosives (Senesac and Thundat, 2008). AgNPs and TiO$_2$-NPs are some of the most sought after candidates for several applications owing to their optical, electrical, thermal properties, electrical conductivity, stability, catalytic and antibacterial properties.

2.3 Silver nanoparticles

AgNPs at nanoscale exhibit unique optical properties which vary due to the shape and size of the nanoparticles. Fine tuning of the synthesis methods allows the researchers to control the shape and size and to synthesize AgNPs with desired morphological characteristics based on their suitability for a particular application as there exists a strong correlation between these parameters and optical, electrical and catalytic properties (Noguez, 2007). AgNPs also exhibit remarkable colours in colloidal forms varying from light yellow to deep brown based on the optical properties of AgNPs (Wilcoxon et al. 1993) and photoluminescence property which is again dependent on the size, and the spectra shift to higher energies with decreasing particle size (Zhao et al. 2006). Surface plasmon resonance (SPR) are collective excitations of the electrons at the interface between a conductor and an insulator and are described by evanescent electromagnetic waves that are not necessarily located at the interface (Noguez, 2007) and can be studied by UV- Vis spectrophotometer. Mie

(1908) studied the interaction between the electromagnetic radiation and the nanoparticle sphere as a function of its radius. In case of nanoparticles with larger radius the SPR band is the sum of absorption and scattering modes with higher order modes (Multipole, quadrapole) becoming dominant in case of increasing particle size causing the plasmon to redshift with an increase in the bandwidth. With the AgNPs size decreasing or being smaller than the incident wavelength dipole resonances are dominant with the plasmon being blueshifted and the plasmon width being narrow.

Several studies show that the surface plasmon resonance of AgNPs depends on its geometric shape, size, composition and energetic structures and crystalline nature (Yao et al. 2005; Barnard et al. 2005; Sosa et al. 2003). These characteristic optical signals (SPR) of AgNPs are also used as a characterization tool. SPR of AgNPs along with the high surface to volume ratio and transition from the bulk band structure to individual localized energy levels at nanoscale level allows their application into surface-enhanced Raman scattering (Haes et al. 2005), catalytic processes (Haruta et al. 1989) and plasmonic devices (Li et al. 2005b), biosensing (Ravi et al. 2013; Farhadi et al. 2012), in optical data storage devices (Ditlbacher, et al. 2000), conversion of solar energy to chemical energy (Linic et al. 2011), in photovoltaic devices (Atwater and Polman, 2010) and in electronics (Chen et al. 2009).

Due to the high applicability credentials offered by AgNPs, various routes have been adopted for the synthesis of AgNPs which are classified as three predominant routes; chemical, physical and biobased/biological synthesis routes. Chemical and physical routes comprise of chemical reduction methods for the preparation of colloidal dispersions of AgNPs in water or organic solvents by using reductants such as borohydride (Hyning and Zukoski, 1998), citrate (Lee and Meisel, 1982), ascorbate and elemental hydrogen (Wiley et al. 2005; Lee and Meisel, 1982), electrochemical reduction methods (Zhu et al. 2001), sonodecomposition synthesis (Salkar et al. 1999), Mechanical grinding and milling (Magana et al. 2008), Microwave synthesis (Jiang et al. 2006), synthesis by thermal decomposition in organic solvents (Esumi et al. 1990), chemical and photoreduction synthesis in reverse micelles (Sun et al. 2001; Pileni, 2000), spark discharge synthesis (Tien et al. 2008) and cryochemical synthesis (Sergeev et al. 1999).

Chemical and physical routes are high yielding and are employed at a large scale. Chemical synthesis routes are generally employed in the preparation of colloidal solutions of AgNPs. Generally, the chemical methods are low-cost for high volume; however, their drawbacks include contamination from precursor chemicals, use of toxic solvents and harsh chemicals, maintenance of high temperature and pressure, generation of hazardous by-products, difficulties in handling of toxic and corrosive chemicals, disposal of the toxic remnant after synthesis (Thakkar et al. 2010). The remnant from these processes may cause environmental pollution. Thus, the spent chemicals are to be treated to convert or degrade them into less toxic forms. There arises a need to employ expensive techniques and equipments for the treatment. The scaled up processes for physical or chemical synthesis face difficulties in handling large quantities of corrosive chemicals, monitoring and control of the process due to the requirement for extreme conditions of synthesis and energy demand is higher (Saxena et al. 2010).

In many of the chemical and physical methods, the particles do not at once undergo the process, resulting in agglomeration in them as well as poor dispersity (Dubey et al. 2010). The AgNPs synthesized through chemical and physical methods are mostly non uniform in size and tend to reaggregate together to form clusters.

However, chemical methods for the synthesis of AgNPs have proved to be better than physical routes. Various capping agents, solvents and templates are employed to control the size, shape and stability of the nanoparticles in the chemical approach. Capping agents such as simple ions, polymers and biomolecules are routinely used for the capping and stabilization of nanoparticles (Warner et al 2000; Naka et al. 1999). Chemically synthesized nanoparticles need to be pre-treated with surfactants as they are covered up with capping agents, it reduces the activity and renders them bio-incompatible (Iravani et al. 2014). The surfactants as well as the capping agents are predominantly chemical in nature and act as pollutants in the environment. In order to overcome these short comings, and in an attempt to develop safer and energy efficient synthesis processes with reduced wastage and derivatives, green methods are being employed.

Biobased synthesis of AgNPs usually employs two different classes of sources; Plants and Microorganisms. Both the sources are found to be equally

competent to chemical and physical routes of AgNPs synthesis. Biobased synthesis of AgNPs has received a large amount of credential as it engages mild experimental conditions like temperature, pH and pressure (Fayaz et al. 2009). These green methods employed to synthesize AgNPs have an edge over their counter parts as they provide slow kinetics and better stabilized products. Moreover these methods conveniently help to design nanomaterials with new properties, increasing their dimension of applications (Narayanan and Sakthivel, 2010). Biological routes utilize nature's most efficient machines i.e. living cells for the synthesis of nanoparticles and also involve the use of biomolecules as templates or scaffolds for synthesis and assembly of nanoparticles.

Biological sources such as microorganisms and plant materials can catalyze specific reactions and act as subtle alternatives for physical and chemical methods of AgNP synthesis (Narayanan and Sakthivel, 2010). Biological sources chiefly bacteria (Wen et al. 2009; Kalishwaralal et al. 2008; He et al. 2007; Duran et al. 2005), fungi (Gade et al. 2008; Ingle et al. 2008; Mukherjee et al. 2001a), yeast (Kowshik et al. 2002) and several plant parts (Ashokkumar et al. 2014; Bar et al. 2009) have been exploited by researchers for the synthesis of AgNPs.

2.3.1 Plant based synthesis of AgNPs

Plants possess different parts, each with its functionality and huge paraphernalia of the bioactive components that assist it in its role. These bioactive compounds demonstrate myriad chemical properties hence can be harnessed for these properties and utilized for the synthesis of AgNPs. Biological sources like plants are found competent in this regard, as these are abundant in nature and have the ability to adapt to and withstand extreme climatic conditions. Plant based synthesis seems to be promising as it can overcome the shortcomings of physical and chemical synthesis methods such as requirement of elevated process conditions, handling large quantities of hazardous chemicals and the disposal of the toxic remnants into the environment.

Plant parts such as leaves, bark, roots, leaves, fruit and floral parts of various sources mentioned in Table 2.1 have been harnessed to synthesize AgNPs. Plant extracts contain various bioactive compounds such as polyphenols, carotenoids and anthocyanins, phenolic acids, flavonoids such as flavanols and isoflavones (Ajila et al.

2007) that aid in the synthesis of nanoparticles. The types of bioactive components and their content in plants also vary depending upon their growth conditions (Canter et al. 2005; Anttonen and Karjalainen, 2005). The content of bioactive compounds varies in different parts of the plant (Biswas et al. 2002) which are subsequently harnessed by various extraction procedures to be used in the synthesis of nanoparticles (Annamalai et al. 2011). These bioactive compounds are known to act as reducing and capping agents in the AgNPs synthesis process.

Plants can scavenge metal ions from large volume of soil and bioconcentrate into their biomass. The presence of various secondary metabolites, enzymes, proteins and/or other reducing agents with electron-shuttling compounds is usually involved in the synthesis of nanoparticles by plant components. In bioaccumulation, the localization of nanoparticles is based on the presence of particular enzymes or proteins involved in it. The recovery of intracellular nanoparticles from plant tissues is tedious and expensive and needs enzymes to degrade the cellulosic materials that surround it increasing the number of downstream purification steps. Thus, the synthesis of various metal nanoparticles using plant extracts is easy in downstream processing and in scaling up of the synthesis process (Narayanan and Sakthivel, 2008).

Various extraction techniques have been adopted by researchers to prepare plant extracts. Majority of the extract used for the synthesis of AgNPs was prepared using open solvent heating in water at a temperature of 60-95ºC (Gopinath et al. 2012; Dubey et al. 2010; Krishnaraj et al. 2010) using a steam bath (Ahmad et al. 2010), soxhlet extraction (Ramamurthy et al. 2013) and Reflux extraction (Kumar et al. 2015; Maria et al. 2015; Murugan et al. 2014). Water has been widely used for the synthesis of AgNPs (Gopinath et al. 2012; Dubey et al. 2010; Krishnaraj et al. 2010; Song and Kim, 2009) followed by other solvents such as methanol (Zargar et al. 2014; Priyadarshini et al. 2012; Santhoshkumar et al. 2011), ethanol (Suganya et al. 2013); benzene, hexane and chloroform (Muthukumaran et al. 2015). However use of water as a solvent has been favoured as it increases the overall efficiency of the synthesis process in offering a benign, non toxic and non corrosive and ecofriendly solvent (Jagtap and Bapat, 2013; Rajakumar and Rahuman, 2011; Thakkar et al. 2010).

Table 2.1 Plant based biological resources used in the synthesis of AgNPs

Plant Resources	Plant part used to prepare extract	Reference
Azadirachta indica	Leaf	Shankar et al. 2004
		Tripathy et al. 2010
Emblica officinalis	Fruit	Ankamwar et al. 2005a
Aloe vera	Plant	Chandran et al. 2006
		Dinesh et al. 2015
Cinnamomum camphora	Leaf	Huang et al. 2007
Coriandrum sativum	Leaf	Narayanan and Sakthivel, 2008;
		Sathyavarthi et al. 2010
Camelia sinensis	Leaf	Vilchis-Nestor et al. 2008
		Loo et al. 2012
Mentha piperita	Leaf	Parashar et al. 2009a
		MubarakAli et al. 2011
Eclipta prostrata	Leaf	Jha et al. 2009
		Rajakumar and Abdul Rahuman, 2011
Medicago sativa	Seed	Gardea-Torresdey et al. 2009
	Sprouts	Lukman et al. 2011
Eucalyptus hybrid	Leaf	Dubey et al. 2009
Carica papaya	Fruit	Jain et al. 2009
	Callus	Mude et al. 2009
Jatropha curcas	Latex and seed	Bar et al. 2009

Table 2.1 Continued…

Plant Resources	Plant part used to prepare extract	Reference
Cinnamomum zeylanicum	Bark	Sathishkumar et al. 2009
Carica papaya	Fruit	Mude et al. 2009
		Jain et al. 2009
Datura metel	Leaf	Kesharwani et al. 2009
Hibiscus rosa sinensis	Flower	Philip, 2010
Musa paradisiaca	Fruit peel	Bankar et al. 2010
Acalypha indica	Leaf	Krishnaraj et al. 2010
Stevia rebaudiana	Leaf	Varshney et al. 2010
		Yilmaz et al.2011
Euphorbia hirta	Leaf	Elumalai et al. 2010
		Priya et al. 2011
		Priyadarshini et al. 2012
Curcuma longa	Tuber powder	Sathishkumar et al. 2010
		Shameli et al. 2012a
Psidium Guajava	Leaf	Raghunandan et al. 2011
		Gupta et al. 2014
Eclipta prostrata	Leaf	Rajakumar and Rahuman, 2011
Zingiber officinale	Root	Singh et al. 2011
Citrullus colocynanthis	Leaf	Satyavani et al. 2011
Nelumbo nucifera	Leaf	Santhoshkumar et al. 2011
Citrus sinensis	Peel	Kaviya et al. 2011
		Konwarh et al. 2011

Table 2.1 Continued...

Plant Resources	Plant part used to prepare extract	Reference
Desmodium triflorum	Plant	Ahamed et al. 2011
Coleus amboinicus Lour	Leaf	Subramanian and Suja, 2012
Piper betle	Leaf	Mallikarjuna et al. 2012
Myrica esculanta	Leaf	Phanjom et al. 2012
Coleus aromaticus	Leaf	Vanaja and Annadurai, 2013
Prunus armeniaca	Fruit	Dauthal and Mukhopadhyay, 2013
Vitex nigundo	Leaf	Prabhu et al. 2013
		Zargar et al. 2014
Manilkara zapota	Seed	Otari et al. 2014
Myrmecodia pendan	Plant	Zuas et al. 2014
Crataegus douglasii	Fruit	Moghaddam and Dabanlou, 2014
Ficus carica	Leaf	Ulug et al. 2015
Pistacia atlantica	Seed	Sadehegi et al. 2015
Nyctanthes arbor-tristis	Seed	Basu et al. 2016
Clerodendrum phlomidis	Leaf	Sriranjani et al. 2016

The research on AgNPs synthesis needs to be channelled towards utilization of alternate plant resources which are available in huge quantities and that form as industrial wastes or as biowaste from either agricultural or forestry sectors and which carry less food, agronomical and commercial value to prevent injudicious utilization of limited high value resources and depletion as food source. This route of employing the bioactive components from the agro, forestry or industrial wastes does not employ harsh and elevated process conditions, toxic reagents or solvents if aqueous extraction is adopted and is ecofriendly, hence is termed as 'green route' of synthesis. In addition, it has been analyzed that bioactive compounds such as tannins, phenols,

enzymes, antioxidants and flavonoids play an important role in reducing the precursor salt into nanoparticles (Parashar et al. 2009; Vilchis-Nestor et al. 2008).

The use of various plant parts possessing the necessary bioactive components for the synthesis of the nanoparticles allows for the production of particles without physical confinement of the particle within unwanted matrices, as in plant or microbial based extracellular synthesis. The location of nanoparticles in case of intracellular synthesis in either plant or microbial based synthesis routes, plays a crucial role as the location of the particle makes it difficult to provide better control over size distribution, shape and crystallinity and increases the downstream processing steps involved in the recovery of the nanoparticles (Mohanpuria et al. 2008). The drawbacks of microbial based synthesis such as, maintenance of sterile conditions, subsequent culturing of microbes and regular replenishment of the exhausted nutrients are absent in plant based synthesis route (Kalishwarlal et al. 2010).

2.3.2 Parameters affecting plant based synthesis of AgNPs

The production of monodispersed nanoparticles with faster rate of synthesis can be achieved by controlling the synthesis parameters governing the plant based synthesis of nanoparticles. Understanding the influence of various factors governing the rate of the synthesis reaction can aid in controlling the shape, size, characteristics and the properties of nanoparticles as desired.

Researchers have demonstrated that physical parameters like concentration of the extract as well as the precursor salt used for the synthesis of the nanoparticles, the initial pH of the synthesis mixture, temperature of synthesis, the mixing ratios of the reactants (Extract and precursor salt) in the synthesis medium play a fundamental role in determining the rate of synthesis, controlling the monodispersity of the nanoparticle, size and shape of the nanoparticle being synthesized (Kirthi et al. 2011; Kathiresan et al. 2009). Synthesis time duration is also crucial in determining the size and shape.

2.3.2.1 Concentration of the extract, precursor salt and their mixing ratios in the synthesis mixture

The plant resources contain a large number of bioactive components such as proteins, amino acids, enzymes, polysaccharides, alkaloids, tannins, phenolics, saponins, terpinoids and vitamins that bring about the reduction of the precursor salt to the desired nanoparticle as well as cap the particles being synthesized (Arunachalam et al. 2015; Kulkarni and Muddapur, 2014; Huang et al. 2011; Zhou et al. 2010).

In a detailed study carried out by researchers Moghadamm and Dabanlou, (2014) pertaining to the synthesis of AgNPs using various concentrations of *C. douglasii* extract, it is reported that the concentration of the extract used for the synthesis of the nanoparticles controls their morphological aspects in terms of the size. While the variation in size of the nanoparticles being synthesized depends on reducing agents that reduce the precursor salt to nanoparticles and the capping agents available for imparting the stability to them. Bar et al. (2009) reported that using lower concentration of *Jatropha curcus* latex for the synthesis of AgNPs did not result in the formation of AgNPs. Ibrahim (2014) found an increase in the intensity of the SPR peak of the AgNPs being synthesized using increased concentrations of banana peel extract and reported that increased concentration of the extract led to the formation of a large number of AgNPs in the synthesis mixture. Bindhu and Umadevi (2014) reported that increase in the concentration of the extract of *S. lycopersicums* in the synthesis mixture led to the formation of small sized and more monodispersed AgNPs. Similarly, Christensen et al. (2011) also reported that increased concentration of *M. Koengii* Leaf extract concentration to the precursor salt concentration in the synthesis mixture plays a pivotal role in conferring the morphological aspects of AgNPs being synthesized, as increased concentration of the Leaf extract led to the formation of large number of small sized spherical shaped AgNPs with monodispersity. Similar have been reported by Ganaie et al. (2015); Umadevi et al. (2012); Dubey et al. (2010). Hence, it is crucial to study and optimize the concentration of the extract being used to aid in the controlled synthesis of monodispersed, smaller sized and isotropic nanoparticles.

Various researchers have studied and determined that the concentration of the precursor salt used for the synthesis of nanoparticles is a decisive controlling synthesis parameter (Mittal et al. 2014; El- Sherbiny et al. 2013; Bar et al. 2009). Mittal et al. (2014) in their study pertaining to the synthesis of AgNPs using *S. cumini* extract and various concentrations of $AgNO_3$ salt solutions concentrations concluded that increase in the concentration of the precursor salt used for the synthesis led to the increased formation of the nanoparticles. While Satishkumar et al. (2014) and Bar et al. (2009) concluded that increase in the concentration of the precursor salt beyond the optimal concentration led to the formation of large anisotropic nanoparticles while lower concentrations of the precursor salt solution formed small and isotropic shaped nanoparticles. Rastogi and Arunachalam (2011) also reported that there was a remarkable increase in the number of nanoparticles being synthesized with an increase in the concentration of precursor salt solution without any change in the size of the nanoparticles being synthesized. Increasing concentrations of $AgNO_3$ in the synthesis mixture led to an increase in the intensity of the SPR peak indicating the formation of large number of AgNPs as reported by Kora et al. (2012) and has been attributed to the increased availability of Ag^+ ions for reduction into (Zerovalent silver) Ag^0 by the bioactive components present in the extract. On the contrary, El-Sherbiny et al. (2013) reported the formation of smaller sized nanoparticles with increase in the concentration of the precursor salt solution in the synthesis mixture along with an increase in the intensity of the SPR peak indicating the formation of large number of particles. Thus, it can be well understood that the precursor salt solution plays a pivotal role in governing the morphological characteristics of the nanoparticles being synthesized and determines the yield. However, the concentration of the precursor salt solution along with the constituents of the extract being used for the synthesis of nanoparticles play a synergistic role.

As discussed earlier, plant extracts are known to possess various bioactive components that aid in the reduction of the precursor salt to nanoparticles and cap them. The concentration of the precursor salt affects the number as well as the shape of the nanoparticles being synthesized in the synthesis mixture. But the quantity of reducing agents as well as the capping agents present in the extract determines the formation of the nuclei and their subsequent growth as nanoparticles with definite

shape and size. Hence, it is highly essential that there must be an adequate balance between the precursor salt and the bioactive components in the synthesis mixture to yield a large number of monodispersed, small sized and isotropic shaped nanoparticles. Researchers have carried out detailed studies to evaluate the balance between the two by varying the mixing ratios between the extract and the precursor salt for the synthesis of AgNPs. The concentration of the precursor salt and extract was kept constant while the volume mixing ratios of their solution in the synthesis mixtures were varied typically by Rajan et al. (2015); Ashokkumar et al. (2014); Khalil et al. (2014) and Philip et al. (2011). With the variation in the mixing ratios of the extract and the precursor salt solution, the morphological characteristics of the nanoparticles in terms of size, shape and monodispersity varied depending on the concentration of the extract and precursor salt solution being used. Rajan et al. (2015) have reported that by increasing the volume ratio of the extract to the precursor salt beyond an equilibrium, increases the number as well as the size of the nanoparticles being synthesized in the synthesis mixture and this has been attributed to the growth of the nuclei leading to larger sized nanoparticles rather than the formation of small sized nuclei. However, Ashokkumar et al. (2014); Philip et al. (2011); Guidelli et al. (2011); Dubey et al. (2010) have reported a decrease in the size of the nanoparticles with an increase in the volume ratio of the extract to the precursor salt, favouring the formation of nuclei over growth of the nanoparticles. They also observed large anisotropic shaped AgNPs were synthesized resulting in wider SPR bands with low volume ratios of the extract to the precursor salt. In an elaborate study to determine effect of mixing ratios of the extract to the precursor salt solution in the AgNPs synthesis mixture using the aqueous Leaf extract of *A. absinthium* conducted by Ali et al. (2016), it was concluded that lower volume ratio of the extract to the precursor salt solution favoured the synthesis of AgNPs while higher extract to precursor salt solution ratio did not favour the synthesis of AgNPs.

Thus, literature suggests that the concentration of the reducing and capping agents present in the extract must be balanced or present in sufficient quantities to reduce the number of Ag^+ ions to Ag^0 nuclei, followed by their growth to form nanoparticles and subsequently cap them to bring about the formation of large number of monodispersed and isotropic shaped nanoparticles. The study of different mixing

volume ratios of the extract and precursor salt solution indicates that the shapes and sizes of the AgNPs being synthesized can be manoeuvred, controlled and synthesized by using suitable mixing volume ratios and with the choice of appropriate plant parts irrespective of the natural variation present in the chemical composition of the bioactive components present in the source (Ganaie et al. 2015).

2.3.2.2 pH of the synthesis medium

pH of the synthesis medium influences the morphological characteristics of the AgNPs being synthesized and also play a crucial role in the synthesis mechanism. Various researchers have reported that a variation of pH influences the formation of the nanoparticles in relation to the morphology and its size.

Tripathi and co-workers, (2013) conducted a well defined study to analyze the effect of pH of the synthesis medium upon synthesis of AgNPs by the aqueous extract of *Ficus panda* leaves. They observed that alkaline pH of the reaction medium at units 8 and 9 led to the formation of well dispersed, smaller and monodispersed AgNPs that was characterized from the wide, less intense and red shifted SPR peak observed, while acidic pH conditions of 5 and 6 led to the formation of polydispersed, larger and agglomerated AgNPs. Variation of pH influences the shape and size of AgNPs being synthesized as observed by Satishkumar et al. (2009) in their studies on synthesis using *Cinnamon zeylanicum* bark extract as well as powder over a pH range of 1 to 11. It was observed that larger sized particles were formed at lower pH while smaller sized particles at a slightly alkaline pH. Lower pH value promoted the nucleation of the AgNPs while higher pH caused electrostatic repulsion among them thereby leading to formation of smaller nanoparticles. Stability of the nanoparticles in the reaction medium depends upon the pH as the hydroxide ions present in the medium can change the surface charge on the nanoparticles (Moghaddam and Dabanlou, 2014, Maria et al. 2015).

Generally neutral to basic pH of the synthesis medium have been reported to favour the rapid formation of well dispersed, stable and isotropic shaped AgNPs (Mittal et al. 2014; Saware and Venkatraman, 2014; Dauthal and Mukhopadhyay, 2013; Edison and Sethuram, 2012). Acidic pH offers slow rate of AgNPs synthesis due to electrostatic repulsion of anions present in the synthesis solution (Ramesh et al.

2015; Chowdhary et al. 2015; Maria et al. 2015; Tripathy et al. 2010, Thakkar et al. 2010, Dubey et al. 2010) by binding to the reducing agents thereby rendering them unavailable for the reduction of the Ag^+ ions in the synthesis mixture. Aggregation of the AgNPs is favoured over nucleation of the AgNPs at acidic pH due to the ionization of the phenolic groups that act as reducers of Ag^+ ions to AgNPs. Ibrahim (2015) and Roopan et al. (2013) have reported that extreme acidic pH of 2 did not result in the synthesis of AgNPs rather a white precipitate was observed to form.

At neutral to alkaline pH conditions of the synthesis medium nucleation of the Ag^+ ions to Ag^0 is favoured as the large number of functional groups available for Ag^+ binding facilitated the formation of higher number of AgNPs with smaller diameters (Moghaddam and Dabanlou, 2014). According to Lee et al. (2004) increase in the alkalinity of the synthesis medium by addition of NaOH increases the reducing potential of the reducing agents. Also, alkalinity of the synthesis mixture increases the surface reactivity of the Ag^+ ions making it more readily available for reduction by the reducing agents present in the plant Leaf extract, favouring the formation of a large number of nuclei with smaller sizes and increased stability of the AgNPs being synthesized in the medium (Sathishkumar et al. 2014; Tripathi et al. 2010). Tran et al. (2013) in their study pertaining to the synthesis of AgNPs using *T. diversifolia* found that neutral pH of 7 favoured the synthesis of AgNPs while higher alkaline pH of the medium led to the formation of AgOH with large sizes. Similar findings were reported by Moghaddam and Dabanlou, (2014), Khalil et al. (2014), Vivek et al. (2012). Maria et al. (2015) also studied the effect of pH on the synthesis of AgNPs and determined that alkaline pH 11 favoured the formation of smaller sized spherical shaped AgNPs compared to lower pH conditions of the AgNPs synthesis medium.

Thus, pH of the synthesis medium influences the stability as well as the morphological characteristics of the AgNPs being synthesized in a controlled manner and enables the researcher to manoeuvre the shape and size of the nanoparticles as desired for certain applications. The morphological characteristics of the AgNPs can be controlled by fine-tuning the initial pH of the synthesis mixture. pH of the synthesis medium confers control of the morphological characteristics by exhibiting the ability to change the electrical charges of the bioactive components of the extract

involved in the reduction and capping of the Ag$^+$ ions that might affect their capping and stabilizing abilities and subsequently the growth of AgNPs.

2.3.2.3 Temperature of AgNPs synthesis

Generally most of the green synthesis of AgNPs is carried out at ambient conditions of synthesis (Maria et al. 2015; Tran et al. 2013; Njagi et al. 2010; Philip, 2011; Sathishkumar et al. 2009; Kasthuri et al. 2009; Jha et al. 2009; Medina-Ramirez et al. 2009; Li et al. 2007a). Synthesis of AgNPs under room temperature leads to less energy intensive process. An increase in the temperature of the synthesis medium can also lead to the disruption of the native structures of the reducing and capping agents present in the plant extract leading to electrostatic interactions occurring at the surface of the AgNPs thereby causing particle growth and decreased stability of the nanoparticles (Kumar et al. 2014). In the large-scale synthesis of nanoparticles, controlling a high temperature during synthesis may be challenging. High temperature synthesis makes the overall process energy and capital intensive, thereby reducing the overall efficiency of the green synthesis method.

In case of plant based synthesis of AgNPs, an extensive study by Mittal and co-workers (2014) using the extract of *Syzygium cumini* fruit was carried out at various synthesis temperatures ranging from 25 ^{0}C to 65 ^{0}C. They reported the increase in the sharpness of the SPR peak of the reaction mixture with an increase in the temperature of the reaction mixture, thereby indicating the formation of a large number of AgNPs. The increase in SPR peak intensity with increase in temperature was attributed to increase in the rate of the conversion of the metal ion to nanoparticles at higher temperature (Dwivedi and Gopal et al. 2010) resulting in large number of Ag$^+$ ions being reduced to Ag^0 due to elevated temperature of synthesis; favouring nucleation, thereby leading to faster formation of small sized AgNPs. Higher temperature of 95 ℃ was also found to be favourable for the synthesis of large number of small sized AgNPs as reported by Sukirtha et al. (2012) in the synthesis of AgNPs using the aqueous extract of *Melia azedarach* Linn. Leaves.

In consideration of industrial applicability of the synthesis process, it is always beneficial if the synthesis of nanoparticles occurs under ambient conditions. Employment of higher temperature may lead to denaturation of bioactive components

responsible for synthesis of nanoparticles. Moreover, synthesis under ambient conditions is advantageous as it may prove to be cost effective and less energy intensive with ease of operation.

2.3.2.4 Synthesis time duration

Shah et al. (2015) in their study pertaining to the synthesis of AgNPs using the aqueous Leaf extract of *Ferocactus echidne* reported that AgNPs require a "optimum" time for the synthesis as this time duration highly influenced the morphological characteristics of the AgNPS being synthesized. They studied the morphological characteristics of AgNPs using SPR analysis at different synthesis time intervals of AgNPs, varying from 2-24 h and found that synthesis time duration of 8h for AgNPs was optimum. The AgNPs were large in number, smaller in size and spherical at 8 H of synthesis time duration beyond which the formation of large sized, polydispersed and aggregated AgNPs was observed. Sathishkumar et al. (2012) studied the effect of incubation time on the synthesis of AgNPs using *M. citrifolia* Leaf extract and reported that increased synthesis time duration favoured the synthesis of AgNPs. However Gao et al. (2014) in their studies on the synthesis of AgNPs using kiwi fruit extract reported that prolonged synthesis period led to the aggregation of the AgNPs as well as the formation of large sized particles when the synthesis time duration of 0.5 h to 3 h was employed. Similar reports of synthesis time duration influencing the morphological characteristics of the AgNPs being synthesized were studied and reported by Ganaie et al. (2015), Mittal et al. (2014), Veerasamy et al. (2011) and Dubey et al. (2010). Thus, synthesis time duration influences the number as well as the morphological characteristics of AgNPs being synthesized and is a crucial parameter in the optimization of plant based synthesis of AgNPs.

2.3.3 Microbial based synthesis of AgNPs

Microbes have been a predominant life sustaining entity on our planet since time immemorial and their distribution throughout is directly based on their adaptive capability to live and reproduce in extreme conditions (Roszak and Colwell, 1987). They generally are an integral part of many processes that occur in nature and are known to carry out most of the vital process like degradation of pollutants, bioremediation as well as playing a crucial role in certain nutrient cycles (Thakkar et

al. 2010). Among the milieu of natural resources, prokaryotic bacteria have been most extensively researched on for synthesis of AgNPs. One of the reasons for "bacterial preference" for nanoparticles synthesis is their relative ease of manipulation. In one of the earliest studies in this technology, Slawson et al. (1992) found that a silver-resistant bacteria strain isolated from silver mines, *Pseudomonas stutzeri* AG259, accumulated AgNPs within the periplasmic space. Although the usage of microbes for the synthesis of nanoparticles is a recent approach (1990s), these metal–microbe interactions have important role in several biotechnological applications including the fields of bioremediation, biomineralization, bioleaching and microbial corrosion. However, it is only recently that microorganisms have been explored as potential biofactory for synthesis of AgNPs (Gericke and Pinches, 2006).

Synthesis of AgNPs depends upon the microorganism's capacity to reduce a particular metal salt and either deposits it as a nanoparticle within itself as intracellular nanoparticles or attached onto its surface as extracellular nanoparticles. This eco-friendly process, referred to as green technology, can be used to obtain better AgNPs from microbial cells (Mandal et al. 2006).

Although fungi (Bhimba et al. 2011; Bansal et al. 2005; Bansal et al. 2004; Ahmad et al. 2003a), yeast (Kowshik et al. 2002) and viruses have been proven to successfully synthesize AgNPs, the synthesis time duration of nanoparticles from these sources is too long (Ahmad et al. 2003a) making bacterial resources quite lucrative. Table 2.2 shows the different microbial strains that have been employed successfully for the synthesis of AgNPs.

Microbial-based technology for the synthesis of AgNPs presents an economic alternative for synthesis of AgNPs at a time when high grade mineral resources are being depleted, energy costs are increasing, and adverse environmental effects are becoming more apparent. Reports pertaining to the isolation of microbial strains from environment containing the metal to be reduced to form AgNPs are very less. Microbes already persistent in "metal rich" environment may offer a better reduction capability and tolerance towards high concentration of the metal leading to the increased yield and better morphological characteristics of AgNPs being synthesized. Selection of such strains with the ability to survive and reduce metal precursor salts to nanoparticles as well as their screening with this regard can enhance efficiency of the

process of synthesis of nanoparticles. Among the different microbes employed for the synthesis of nanoparticles, bacteria are preferred due to their ability to withstand high concentrations of heavy metal ions, ease of culturing, manipulation of genetic make-up and downstream processing in terms of procurement of nanoparticles (Thakkar et al. 2010; Parikh et al. 2008).

Based on the location of synthesis by the microbe, the nanoparticles are known to be intracellular (Nair and Pradeep, 2002; Lengke et al. 2007; Klaus et al. 1999), extracellular (Müller et al. 2016; Deljou and Rhamjou, 2016; Parikh et al. 2008; Bhainsa and D' Souza, 2006) or periplasmically confined (Klaus et al. 2009; Konishi et al. 2007; Klaus-Joeger et al. 2001). Separation of intracellular and periplasmically confined nanoparticles from the unwanted bacterial biomass involves several downstream processing steps wherein the cell needs to be lysed as well as the unwanted bacterial associated material needs to be eliminated from the AgNPs. This process is energy, labour and capital intensive while extracellular synthesis of nanoparticles overcomes these shortcomings. Microbial sources with the ability to synthesize extracellular AgNPs are highly preferred as the nanoparticles as they are not embedded or confined within any matrix, hence can be easily obtained without the involvement of additional downstream processing steps that reduce the overall efficacy of the synthesis process. Synthesis of extracellular nanoparticles in a cell free synthesis medium addresses the shortcomings of intracellular or cell associated synthesis of nanoparticles, by reducing the number of synthesis steps required in intracellular synthesis of nanoparticles.

Table 2.2 Microbial based biological sources used for the synthesis of AgNPs

Microbial Resources	References
Fungi:	
Verticillium sp.	Mukherjee et al. 2001
Phoma sp. 3.2883	Chen et al. 2003
F. oxysporum	Duran et al. 2005
Aspergillus fumigatus	Bhainsa and D'Souza, 2006
Phanerochaete chrysosporium	Vigneshwaran et al. 2006
Aspergillus flavus	Vigneshwaran et al. 2007
Plectonema boryanum	Lengke et al. 2007
Fusarium semitectum	Basavaraja et al. 2008
Trichoderma viridae	Fayaz et al. 2009
Fusarium solani	Ingle et al. 2009
Coriolus versicolor	Sanghi and Verma, 2009b
Aspergillus clavatus	Verma et al. 2010
Hypocrea lixii	Bhimba et al. 2011.
Candida glabrata &F.oxysporum	Namasivayam et al. 2011.
Bacteria:	
P. stutzeri AG259	Klaus et al. 1999
Bacillus megaterium	Fu et al. 1999
Lactobacillus sp.	Nair and Pradeep. 2002
Acetobacter xylinum	Mouxing et al. 2007
Morganella sp.	Parikh et al. 2008
Aeromonas sp. SH10	Mouxing et al. 2008
B. licheniformis	Kalimuthu et al. 2008
Enterobacter cloacae	Minaeian et al.2008
Lactobacillus fermentum	Sintubin et al. 2009
Klebsiella pneumonia	Mokhtari et al. 2009
Proteus mirabilis	Samadi et al. 2009
Bacillus sp.	Pugazenthiran et al. 2009
Bacillus subtilis	Saifuddin et al. 2009

Table 2.2 Continued...

Microbial Resources	References
Escherichia coli	Gurunathan et al. 2009a
	El. Shanshoury et al. 2011;
Brevibacterium casei	Kalishwaralal et al. 2010
Streptomyces sp.	Shirley et al. 2010.
Corynebacterium glutamicum	Sneha et al. 2010
K.pneumoniae, E. coli & P. jessinii	Müller et al. 2016
Bacillus Sp. AZ1	Deljou and Rhamjou, 2016
Sporosarcina koreensis DC4	Singh et al. 2016
Yeast:	
MKY3	Kowshik et al. 2002

Shaverdi et al. (2007) were the first to report the extracellular synthesis of AgNPs using the culture supernatants of bacterial strains *Enterobacteriaceae* (*K. pneumonia*, *E. coli* and *E. cloacae*). Saifuddin (2009) also reported the synthesis of AgNPs using the cell free culture supernatants of *B. subtilis* as a facile route for synthesis. In addition, various researchers have exploited microbes with the potency to synthesize extracellular AgNPs such as Priyadarshini et al. (2013); Prakash et al. (2011); Parikh et al. (2010); Fayaz et al. (2010) and Kowshik et al. (2002).

Selection, screening and employment of strains that can synthesize extracellular nanoparticles can make the synthesis process more efficient by being an ecofriendly approach with a low chemical footprint, energy and cost effective process.

2.3.3.1 Selection of microbial strains specific to synthesis of nanoparticles

As previously cited, the selection of an environmentally benign agent is required for the synthesis of the nanoparticles. The microorganism must have the ability to withstand the high metal stress in its vicinity and facilitate the reduction of the metal salt provided to it as the substrate for reduction (Vaidyanathan et al. 2010; Raveendran et al. 2003). The first report of isolating strains with specificity towards the metal precursor salt of the nanoparticles is by Slawson and Co-workers (1992) from silver mine. *Pseudomonas stutzeri* AG259 was used as the specific strain to synthesize AgNPs confined in the periplasmic space by them. The isolated strains

were further used in synthesizing AgNPs. It can be beneficial if the microbe to be isolated thrives in an area which is enriched with the element that is required to be reduced into the nanoparticles. Mukherjee et al. (2001a) isolated a strain of acidophilic fungus, *Verticillium* sp. from the *Taxus* plant and maintained it on potato dextrose agar medium that was further used to synthesize AgNPs. Isolation of a *Bacillus sp.* of bacteria to synthesize AgNPs nanoparticles was carried out from air, through agar plating method by Pugazenthiran et al. (2009). Geriecke and Pinches (2006) isolated various microorganisms like fungi, bacteria and yeast from metal waste dump area for the synthesis of AgNPs. However, in all these studies the microorganisms were not isolated and screened based on their metal reducing capacity, but only based on the metal tolerance. Singh et al. (2013) also isolated 18 strains of *Acenitobacter* based on their tolerance of silver metal. Attempts to isolate organisms based on their ability to withstand the metal stress and their metal reduction capacity is scarce, except the research work by Rammohan and Balakrishnan, (2011), who selected the microorganisms that were capable of reduction of metal salts from the soil samples collected from metal enriched area by agar plating method. In their studies, reduction of the metal was characterised by the change in colour of the microbial colony. These isolated strains were capable of intracellular synthesis of nanoparticles. Separation of these intracellular nanoparticles may turn out to be an expensive process. Isolation of specific strains with the ability to synthesize nanoparticles extracellularly in the medium seems promising with regard to eliminating the disadvantages of cell associated nanoparticle synthesis, thereby reducing the synthesis cost.

2.3.3.2 Mechanism of extracellular synthesis of AgNPs by bacterial sources

Usually only those bacteria that exhibit resistance to silver possess the ability to reduce silver precursor salt in the synthesis medium. These bacteria are capable of reducing the Ag^+ ions upto a certain concentration limit, to AgNPs using the enzymes secreted by them into the medium. Each bacterium has its own reduction mechanism as well as ability to reduce the precursor salt to AgNPs. The bacteria that secrete the reducing agents also secrete certain small biomolecules such as peptides, aminoacids and polysaccharides that may further cap the AgNPs synthesized. However it is

widely accepted that extracellular AgNPs synthesis using microorganisms occurs through the action of an extracellular enzyme secreted by the microbe-Nicotinamide Adenine Dihydrophosphate dependant Nitrate reductase (NADH dependant nitrate reductase) (Kalimuthu et al. 2008; Gade et al. 2008; Ingle et al. 2008; Kumar et al. 2007a; Duran et al. 2005).

The silver detoxification mechanism is used for the synthesis of AgNPs by employing the NADH dependant nitrate reductase enzyme (Ahmad et al. 2003a). Duran et al. (2005) have identified nitrate reductase enzyme secreted by the fungi *Fusarium oxysporum* to synthesize AgNPs; that forms an integral part of the nitrogen cycle, bringing about the reduction of nitrate to nitrite. This mechanism of AgNPs synthesis involving NADH dependant nitrate reductase enzyme was further validated by Kumar et al. (2007a) wherein the enzyme-NADH dependant nitrate reductase was purified by dialysis, DEAE-Sephadex negative adsorption and Gel filtration on Sephacryl S-300, from *F. oxysporum* and was allowed to react with $AgNO_3$ and NADPH in a test tube. Formation of AgNPs *in vitro* using the purified NADH dependant nitrate reductase enzyme was confirmed by the appearance of characteristic brown colour in the test tube indicating the synthesis of AgNPs. The molecular weight of the enzyme NADH dependant nitrate reductase was determined to be 44 kDa using (Sodium Dodecyl Sulphate–Poly Acrylamide Gel Electrophoresis) SDS PAGE analysis. Vaidyanathan et al. (2010) have employed the NADH dependent nitrate reductase enzyme secreted by *B.subtilis* for the synthesis of AgNPs.

SDS-PAGE has been ideally used by researchers to determine the molecular weight of the protein and can be identified in comparison with a molecular weight marker (Fayaz et al. 2009; Kathiresan et al. 2009).

A NADH dependent reductase is secreted by several species of fungi which assist in the synthesis of nanoparticles (Gajbhiye et al. 2009; Ahmad et al. 2003a). Kathiresan et al. (2009) have proved the reduction of the $AgNO_3$ in the medium by fungus *P. fellutanum* takes place by a NADH dependant reductase. In their studies, AgNPs were synthesized extracellularly using the fungal cell filtrate challenged with $AgNO_3$ as the precursor salt. The protein responsible for the reduction was partially purified using ammonium sulphate precipitation method and dialysed, the dialysed samples were used for SDS PAGE.

2.3.4 Parameters influencing microbial based synthesis of AgNPs

Microbial based synthesis of nanoparticles is regarded as safe, cost-effective, sustainable and environment friendly processes, however to enhance the rate of nanoparticles synthesis and to control the morphological characteristics of the nanoparticles being synthesized, the synthesis parameters involved must be manoeuvred.

Parameters such as pH, concentration of $AgNO_3$ and temperature of synthesis control the size of the nanoparticles being synthesized. Hence careful manoeuvring of these parameters allows the precise control of the morphological characteristics in terms of isotropy, monodispersity, shape and size of the nanoparticle being synthesized. Fine control of suitable conditions of synthesis is important to achieve higher yield as well as to ensure that the activity of microbial reducing agents are retained. Several reports suggest that the optimization of process parameters increases the overall efficacy of the synthesis process.

2.3.4.1 Concentration of the precursor salt used for the synthesis of nanoparticles

Monodispersity of the nanoparticles has always been a concern for researchers during the synthesis of nanoparticles as it controls the functionality of the particles in specific application.

Ag^+ ions as such are known to be toxic to the cells; however, for the synthesis of AgNPs the bacteria selected for the synthesis possess the necessary mechanism of reducing the high levels of Ag^+ ions to AgNPs. The reducing efficacy of each strain varies in terms of the concentration of silver salt being used as precursor that it can reduce leading to the formation of various shapes and sizes of nanoparticles. The precursor salt such as $AgNO_3$ is first reduced to Ag^0 nuclei and subsequent growth of the nuclei along with the capping of the nanoparticles occurs (Sharma et al. 2009). Several low molecular weight peptides, enzymes such as NADH-dependent reductases (Otari et al. 2012; Vaidyanathan,et al. 2010), nitroreductases (Gurunathan et al. 2009a) and cysteine desulfhydrases (Srivastava et al. 2013; Prabhawathi et al. 2012) have been established to bring about the synthesis of AgNPs.

Several reports suggest that the concentration of the precursor salt in the synthesis medium is known to control the monodispersity and morphological

characteristics of the nanoparticles being synthesized (Priyadarshini et al. 2013; Millstone et al. 2009; Saifuddin et al. 2009).

Ahluwalia et al. (2014) studied the effect of AgNO$_3$ on the synthesis of AgNPs using the cell free supernatant of *Trichoderma harzianum* and concluded that increasing the concentration of AgNO$_3$ from 1 mM to 9 mM led to an increased yield of the AgNPs. This was monitored by the observation of the intensity of the brown colour formation that was found to increase with an increase in the AgNO$_3$ concentration along with increase in the intensity of the SPR peak indicating the synthesis of large number of AgNPs. Oza et al. (2012) and Mukherjee et al. (2010) through their studies pertaining to the synthesis of AgNPs proved that increasing the concentration of AgNO$_3$ in the synthesis medium led to the formation of increased number of AgNPs.

Katherisan et al. (2009) conducted a study of synthesizing AgNPs using a marine fungus *Penicillium fellutanum* involving concentration of AgNO$_3$ in the range of 0.5, 1, 1.5, 2.0, 2.5 mM and reported 1mM as the optimum concentration for the synthesis of AgNPs, as it gave rise to the SPR peak with the highest intensity indicating the formation of a large number of AgNPs. Kuber and Bhainsa (2006) also conducted their studies with 1mM silver nitrate as their precursor salt concentration. A salt concentration of 3.5 mM was used by Zaki et al. (2011) in their study. Otari et al. (2012) used a final concentration of 3 mM silver nitrate in their study of AgNPs synthesis using *Rhodococcus* sp. Singh et al. (2013) screened 18 strains of *Acenitobacter* sp. to synthesize AgNPs, and studied the effect of AgNO$_3$ concentration on the synthesis of AgNPs. They concluded that the bacterial supernatant could efficiently reduce the concentration of AgNO$_3$ of 0.7 mM however at concentrations higher than this value led to the formation of wide and redshifted SPR peaks signifying the synthesis of polydispersed and large sized nanoparticles. The formation of polydispersed and large sized AgNPs and lower reduction of the precursor salt was attributed enzyme-substrate kinetics; with the active site in the enzyme being saturated with the silver ions, and no site is available for excess ions to get reduced, hence causing reduction in the synthesis of AgNPs.

Thus it can be deduced that each organism has its own limit in reducing the precursor salt solution for the synthesis of AgNPs wherein increase in precursor salt

concentration beyond a particular concentration would lead to the reduction efficiency of the enzyme either by disrupting it native form or by inactivation of the active sites.

2.3.4.2 pH of the synthesis mixture

pH of the synthesis mixture containing the bacterial reducing agents and the precursor salt solution plays a pivotal role in determining the kinetics, shape and size of the nanoparticles being synthesized. Each microbe is capable of secreting several enzymes or metabolites that result the highest yield of AgNPs at a particular pH. This can be attributed to the stabilization of the surface charges on the reducing agent by the pH of the synthesis medium. In a study conducted by Gurunathan et al. (2009), the effect of pH on the synthesis of AgNPs using the culture supernatant of *Escherichia coli* (*E.coli*) in the range of pH 5 to 12, they reported that maximum reduction of the precursor salt solution occurred at pH 10, while increment in the pH beyond this to 12 led to the decrease in the yield and aggregation of the AgNPs. Also, determined that the addition of alkaline ion is necessary to carry out the reduction of metal ions to AgNPs and in the absence of alkaline ion the reduction was slower. They also reported that increasing alkalinity of the medium increased the efficiency of the reducing enzymes that brought about the synthesis of AgNPs thus concluding that increasing or decreasing the pH of the synthesis mixture led to the aggregation of the particles.

Singh et al. (2013) found alkalinity of the synthesis medium to increase the reduction rates of Ag^+ ions to Ag^0 as most of the Ag^+ ions get reduced to form the nuclei thus limiting the secondary reduction process on the surface of the preformed nuclei, leading to the formation of smaller sized AgNPs. Sowani et al. (2016) reported alkaline pH to favour the synthesis of AgNPs compared to acidic and neutral pH conditions of the synthesis medium using actinomycete *Gordonia amicalis* HS-11.

2.3.4.3 Synthesis temperature

Several researchers have studied the synthesis of nanoparticles at different temperatures reported increased rate of nanoparticles synthesis with increase in temperature (Juibari et al. 2011; Fayaz et al. 2009; Babu and Gunasekaran, 2009; Nair and Pradeep, 2002). Fayaz et al. (2009) studied the effect of synthesis temperature of 10 ºC, 27 ºC and 40 ºC on the synthesis of AgNPs and their sizes. It was observed in

their study that at increased reaction temperature, the size of the nanoparticles synthesized was smaller in comparison to the ones synthesized at lower temperature. Gurunathan et al. (2009) reported 60ºC as the optimum temperature for the synthesis of AgNPs using *E.coli* and explained it on the basis of thermal kinetics, i.e., as temperature is increased more nucleation is favoured and smaller sized AgNPs are formed. However, after a certain temperature, deposition of Ag^0 was favoured for the growth leading to improper capping of the nanoparticles and aggregation may also result. Singh et al. (2013) reported 70 ºC as the optimum temperature for the synthesis of AgNPs using *A. calcoaceticus* LRVP54.

Considering the fragile nature of proteinaceous moieties in the synthesis medium, increased synthesis temperature of nanoparticles is known to disrupt the native–active forms of their structure causing decreased yields of the nanoparticles (Gurunathan et al. 2009). In addition, maintenance of elevated temperature for the large scale synthesis of nanoparticles increases the energy requirement and affects the economics of the process required for the process rendering it less efficient. Thus if synthesis occurs readily at ambient conditions of synthesis with high yield and desired morphological characteristics then it is highly advantageous.

2.4 Applications of AgNPs

Silver in its bulk form has been renowned for its antibacterial properties and has been used for making water potable since ages (Castellano et al. 2007). The first record of usage of silver was from the Greek period where it was used in utensils to preserve water and the first medicinal usage dates back to the 8th century. In fact, silver was used in the treatment of wounds and infection in World War I before the advent of antibiotics (Vaidhyanathan et al. 2009). Silver salts have been used for various antibacterial and disinfection purposes (Klasen, 2000; Fox and Modak, 1974). AgNPs however exhibit a large surface to volume ratio, thereby being highly reactive compared to bulk silver and thus exhibiting higher antibacterial properties.

Due to their antibacterial properties AgNPs are well sought after by researchers and have been extensively used in commercial products, consumer and medical products (Rai et al. 2009). Apart from antimicrobial properties larvicidal action of AgNPs against filariasis and malaria vectors have been reported by

Rajakumar and Rahuman, (2011) and Santhoshkumar et al. (2011). AgNPs are also known to effectively kill plasmodial pathogens (Ponarulselvam et al. 2012) and cancer cells (Sukirtha et al. 2012; Fortina et al. 2007).

The antimicrobial activity of AgNPs by researchers has been generally evaluated on solid media in terms of zone of inhibition (ZOI) by Agar well/ disc diffusion technique (Priyadarshini et al. 2013; Gopinath et al. 2012; Dipankar and Murugan, 2012; MubarakAli et al. 2011) and in colloidal form in terms of Minimum inhibitory concentration (MIC) (Dipankar and Murugan, 2012). ZOI technique for the determination of antibacterial efficacy is semi-quantitative while MIC provides better quantification of antibacterial activity of the AgNPs.

The mechanism which AgNPs employ to cause antimicrobial effect is not clearly known and is a debated topic. AgNPs have the ability to anchor to the bacterial cell wall and subsequently penetrate it, thereby causing structural changes in the cell membrane like the permeability of the cell membrane and death of the cell. The formation of free radicals by the AgNPs may be considered to be another mechanism by which the cells die. There might also occur oxidation of the AgNPs, which may lead to the formation of Ag^+ ions and these ions can interact with the thiol groups of many vital enzymes and inactivating them. Also the bacterial cells in contact with AgNPs may ingest the Ag^+ ions, which inhibit several functions in the cell and damage the cells. Possibility of generation of reactive oxygen species can also take place through the inhibition of a respiratory enzyme by silver ions and attack the cell itself (Prabhu and Paulose, 2012). Silver is a soft acid, and there is a natural tendency of an acid to react with a base, in this case, a soft acid to react with a soft base (Morones et al. 2005). The cells are majorly made up of sulfur and phosphorus that are soft bases. The action of these nanoparticles on the cell can cause the reaction to take place and subsequently lead to cell death. Another fact is that the DNA (Deoxy ribose nucleic acid) has sulfur and phosphorus as its major components; the AgNPs can act on these soft bases and destroy the DNA, which would definitely lead to cell death (Prabhu and Paulose, 2012). The interaction of the AgNPs with the sulfur and phosphorus of the DNA can lead to problems in the DNA replication of the bacteria and thus terminate the microbes. It has also been found that the nanoparticles can modulate the signal transduction in bacteria. It is a well-established fact that

phosphorylation of protein substrates in bacteria influences bacterial signal transduction. Dephosphorylation is noted only in the tyrosine residues of gram-negative bacteria. The phosphotyrosine profile of bacterial peptides is altered by the nanoparticles. It was found that the AgNPs dephosphorylate the peptide substrates on tyrosine residues, which leads to signal transduction inhibition and thus the stops the growth (Prabhu and Paulose, 2012).

Many researchers have proposed several hypotheses on the mechanism of antibacterial activity of AgNPs based on their research findings. Kim et al. (2007) have reported that AgNPs synthesized by them demonstrated lower efficacy against *Staphylococcus aureus* (*S.aureus*) strain in comparison to that of *E.coli* and have attributed this activity to the thickness in the peptidoglycan layer of Gram-positive and Gram-negative bacteria. Sondi and Salopek-Sondi (2004) reported that the antimicrobial activity of AgNPs on Gram-negative bacteria was dependent on the concentration of AgNPs, and was closely associated with the formation of pits in the cell wall of bacteria. The AgNPs are known to get accumulated in the bacterial membrane causing the permeability, resulting in cell death. Uncontrolled generation of free radicals on the surface of the AgNPs that can attack the microbial cell membrane lipids leading to a breakdown of membrane function as a result of the formation of irregularly shaped pits in the outer membrane as well as change in membrane permeability, which is caused by progressive release of lipopolysaccharide molecules and membrane proteins. This in turn causes the leakage of the intracellular material eventually leading to cell death. AgNPs are also known to enter the cell and bind to the intracellular structures leading to inhibition of vital cell metabolism such as transcription and translation (Jung et al. 2008; Bury et al. 1999). Although most studies have utilized spherical particles, truncated triangular shaped particles are reported to have greater bactericidal effect compared to that of spherical and rodshaped particles (Pal et al. 2007). It is also reported that bactericidal efficiency is affected by the type of microorganism.

Baker et al. (2005) attributed the antibacterial effect to the increased surface area of the AgNPs and reported that smaller sized AgNPs exhibited more pronounced antibacterial effect on *E. coli* as the test pathogen compared to large sized AgNPs. The concentration based studies on the antibacterial effect of AgNPs was examined

by Morones et al. (2005). They studied the inhibitory effect of AgNPs (0 μg/mL to 100 μg/mL) on the test pathogens by using agar well dilution method, wherein the concentration of the AgNPs was varied and the inhibitory effect of the AgNPs was observed beyond a concentration of 75 μg/mL. Panáček et al. (2005) reported the antibacterial effect of AgNPs to be size as well as concentration dependent against several Gram-positive and Gram-negative strains including multidrug resistant strains. The combinatorial antibiotic effect of AgNPs along with antibiotics was studied by Shahverdi et al. (2007). They proposed that AgNPs along with antibiotics exhibited higher antibacterial effect compared to individual agents. The shape dependent antibacterial effect of AgNPs was reported by Pal et al. (2007) wherein the spherical shaped AgNPs exhibited higher antibacterial efficacy over triangular truncated AgNPs on solid media, while in colloidal solutions the converse was reported. The antiparasitic activity of AgNPs was reported by Rai et al. (2014). Dankovich and Gray, (2011) impregnated blotting paper with AgNPs for the point of use treatment of water. This was evaluated by passing water samples containing *E. coli* through the increasing concentration of AgNPs impregnated paper and the viability of the bacterial pathogen was tested later by growing it in culture medium. They observed that the microorganism after passing through the filter paper with highest concentration was completely deactivated. Thus, their study showed that percolation of bacteria contaminated water through paper embedded with AgNPs could be an effective emergency water treatment. Similarly the AgNPs also used as an antibacterial textile finish for cotton fabric. The antibacterial coating of AgNPs synthesized using *F. oxysporum* was incorporated onto textiles and its antibacterial effect was studied by Duran et al. (2005). AgNPs synthesized by Maneerung et al. (2008) were impregnated onto bacterial cellulose and used as antibacterial wound dressing thus proving the applicability of the antibacterial nature of the AgNPs. In the study conducted by Zhang et al. (2009), cotton fabric was coated with AgNPs by immersing it in a silver colloid. The whiteness, silver content, antibacterial activity and washing durability of the AgNPs treated fabrics were determined. The results indicated that AgNPs treated cotton fabric showed 99.01 % bacterial reduction of *Staphylococcus aureus* and 99.26 % bacterial reduction of *Escherichia coli* while silver content on cotton was about 88 mg/kg. The antimicrobial activity of the AgNPs

treated cotton fabric was maintained at over 98.77 % reduction level even after being exposed to 20 consecutive home laundering conditions.

Researchers have been fascinated by the exuberant array of colours displayed by metal dispersions and the understanding of nanoscale properties such as the type of metal, size, shape and dielectric local environment along with the ability to analyse these features have opened new avenues for nanoparticles in sensor applications. It is the optical property of the nanoparticles that can reveal highly significant data and have been exploited for sensing various molecules of organic and inorganic forms. The variations produced by the optical properties of nanoparticles can provide vital information of molecules being analyzed in a predictable manner and have been used in applications such as materials for optical filters (Kahl et al. 1998; Freeman et al. 1995), plasmonic devices (Maier et al. 2003 and 2001) and sensors (McFarland and Van Duyne, 2003).

AgNPs exhibits better extinction coefficients, sharper extinction bands, higher ratio of scattering to extinction, and extremely high field enhancements compared to gold nanoparticles but have been gaining momentum in the sensory application arena. Unlike dyes AgNPs are quite photostable and can be easily detected by naked eye due to its colour, allowing the rapid detection with the use of minimal chemical wastage. Also the dispersion properties of AgNPs in the dielectric medium can be exploited and employed making it an ideal candidate for biosensing. Nanosilver biosensors can effectively biosense a large number of proteins that normal biosensors find hard to detect (Caro et al. 2016). As discussed earlier, AgNPs are known to exhibit electric fields on the surface of the particle due to SPR of surface electrons which is based on the size, shape and dielectric properties of the medium. These electric fields are known to interact when the particles come into close proximity of each other i.e aggregate and cause plasmon coupling leading to a shift in the SPR (Kreibig and Vollmer, 1995). AgNPs are generally stable in the dispersions due to the capping present on the surface, however minute changes in the pH or the ionic concentration of the medium are known to cause aggregation of the particles due to destabilization of the particles (Badawy et al. 2010). On the basis of this property, small molecules, DNA, proteins, toxic metal ions and pollutants can be assayed in a simple, highly sensitive and low cost colorimetric method with accuracy (Ravi et al. 2013).

Researchers have been constantly employing AgNPs in various sensing application. Ling et al. (2008) developed a colorimetric analytical method for the detection of an anti-inflammatory drug, berberine hydrochloride using citrate stabilized AgNPs. It was reported that the citrate stabilized AgNPs exhibited yellow stable dispersions in water due to negatively charged surface causing electrostatic repulsion between nanoparticles. When positively charged berberine hydrochloride was added to the AgNPs colloidal solution, the nanoparticles aggregate and suspension colour changes from yellow to green or blue, depending on the aggregation degree. A good correlation between the absorbance change at the plasmon wavelength of the nanoparticle and berberine concentration was achieved by adjusting pH and ionic strength values of the medium.

AgNPs have also been conjugated to oligonucleotides and have emerged as a powerful and highly accurate tool for the detection of target DNA sequences and have been used in the design of colorimetric assays based on aggregation induced by sequence-specific hybridization. Several combinations of conjugates of nanoparticle-oligonucleotide have been used for the colorimetric sensing abilities (Lee et al., 2007; Liu et al., 2007). Zhang et al. (2007) have used AgNPs for the development of an assay wherein proteins can be detected. While Wei et al. (2008) have used AgNPs to detect enzymatic reactions wherein Adenosine Triphosphate has been consumed during the reaction. Several highly sensitive and selective colorimetric assays have thus been accomplished for the detection of histidine (Li et al. 2009), pesticides (Xiong and Li, 2008) and Yb^{3+} ions (Han et al. 2009). Farhadi et al. (2012) and Ravi et al. (2013) have reported the use of AgNPs synthesized using biological route in the development of a colorimetric assay to detect mercury ions in contaminated water. The assay did not involve the conjugation of the nanoparticle with any other molecule allowing the direct use of as synthesized AgNPs for mercury sensing properties. This analysis method involving the as synthesized AgNPs as colorimetric sensors for detection of mercury is rapid, simple and promising in terms of its applicability. AgNPs can be synthesized using different biological sources and explored for their potential use as sensors for the detection of mercury levels in various samples.

AgNPs also exhibit catalytic properties. Ganaie et al. (2014) studied the catalytic property of AgNPs synthesized using aqueous extract of *Ipomea carnea* Leaf

extract in the degradation of Alizarin Red S and Remazol Brilliant Blue dye, wherein the degradation of the dye was monitored by studying the change in the spectral characteristics of the AgNPs. While Edison and Sethuraman, (2013) reported the catalytic activity of AgNPs synthesized using the aqueous extract of *Terminalia chebula* in the degradation of methylene blue dye wherein the degradation of the dye was monitored by decrease in the intensity of the SPR peak characteristic of AgNPs using UV-Vis spectrophotometer. These studies signify that the spectral characteristics of AgNPs play a crucial role in determining the applicability of these particles for various applications. Suvith and Philip (2014) also studied the applicability of AgNPs synthesized using Guggulutiktham Kashayam as catalysts in the degradation of methylene blue dye.

2.5 Titanium dioxide nanoparticles

TiO_2 as a semiconductor photocatalyst has encompassed various fields of applicability as it is highly sought after for its photocatalytic efficiency. However as the size of the bulk TiO_2 decreases to nanoscale, the properties change (O'regan and Grfitzeli, 1991). The physicochemical properties include shape, size, surface characteristics and inner structure lead to the wide spread application of TiO_2-NPs as paints, coatings, plastics, papers, inks, medicines, pharmaceuticals, food products, cosmetics, and toothpaste (Kaida et al. 2003; Wolf et al. 2003), as a pigment to whiten skim milk and sunscreens (Trouiller et al. 2009), as a component for articulating prosthetic implants, especially for the hip and knee (Sul, 2010; Jacobs et al. 1991), as a photocatalyst in reactions pertaining to the treatment of water contaminated with hazardous industrial by-products (Ni et al. 2007), Water splitting for hydrogen production (Fujishima et al. 1975) as a photoactive material in solar cells (Mor et al. 2006), as self-cleaning and anti-fogging agents for tiles, windows, textiles, car mirrors (Parkin and Palgrave, 2005), as useful tools in advanced imaging and nanotherapeutics (Montazer et al. 2011), photosensitizers for use in photodynamic therapy (Wiesenthal et al. 2011).

TiO_2-NPs are generally synthesized using chemical vapour deposition (CVD) method (Jones and Chalker, 2003), oxidation of titanium tetrachloride (Jang et al. 2001), thermal decomposition and sol-gel technique via hydrolysis of titanium

alkoxides (Valencia et al. 2010; Su et al.2004), sputtering (Song et al. 2009b), spray deposition (Uzunova-Bujnova et al. 2010), thermal plasma (Tanaka et al. 2011), flame combustion method (Nagaveni et al. 2004) and microwave assisted hydrothermal synthesis (Truong et al. 2011). However due to the shortcomings of chemical and physical methods involved in the synthesis as discussed in section (2.3), biobased sources are being sought after for the synthesis of TiO_2-NPs. The biobased routes involve mild process conditions and have a negligible chemical footprint on the environment as they do not use toxic solvents or other chemicals.

2.6 Biobased synthesis of TiO_2-NPs

Apart from conventional chemical and physical methods of TiO_2-NPs synthesis, biological sources such as various plant parts and microbes are being used for the synthesis of TiO_2-NPs. Table 2.3 enlists the biological sources used for the synthesis of TiO_2-NPs.

Synthesis of TiO_2-NPs using various precursor salts such as titanium hydroxide (Kirthi et al. 2011), dipotassium hexafluorotitanate (Bansal et al. 2005), and titanium isopropoxide (Sundrarajan and Gowri, 2011) has been reported, while bulk TiO_2 was also reduced to nanoscale TiO_2 using biological reductants (Velayutham et al. 2012; Sundrarajan and Gowri, 2011). However, there is no report based on the optimization of any synthesis parameter on biobased synthesis of TiO_2-NPs and its influence on the morphological characteristics of the TiO_2-NPs being synthesized. Thus, this initiates the necessity to study the various parameters influencing the overall synthesis.

Table 2.3 Biological sources used for the synthesis of TiO$_2$-NPs.

Sources	Reference
Plant leaf extracts:	
Nyctanthes arbor-tristis	Sundrarajan and Gowri, 2011
Annona squamosa	Roopan et al. 2012
Catharanthus roseus	Velayutham et al. 2012
Jathropha Curcas and Citrus aurantium	Nwanya et al. 2012
Eclipta prostrate	Rajakumar et al. 2012a
Aloe vera	Nithya et al. 2013
Calotropis gigantean	Marimuthu et al. 2013
Psidium guajava	Santhoshkumar et al. 2014
Solanum trilobatum	Rajakumar et al. 2014
P. dulce and Lagenaria siceraria	Kalyanasundharam and Prakash, 2015
Azadirachta indica	Sankar et al. 2015
Microbial :	
Fungi:	
Fusarium oxysporium	Bansal et al. 2005
Aspergillus flavus TFR 7.	Raliya et al. 2015
Bacteria:	
Lactobacillus sp.	Azhar et al. 2014
Bacillus subtilis	Jha et al. 2009a Dhandapani et al. 2012; Kirthi et al. 2011
Bacillus mycoides	Órdenes-Aenishanslins et al. 2014
Bacillus lichenciformis	Suriyaraj and Selvakumar, 2014
Aeromonas hydrophilia	Thamima and Karuppuchamy, 2014
Lactobacillus crispatus	Ibrahem et al. 2014
Bacillus cereus	Sunkar et al. 2014
Lactobacillus subtilis	Krajarathinam et al. 2014
Yeast:	
Sacharromyces cerevisiae	He et al. 2011

2.6.1 Factors affecting the synthesis of TiO$_2$-NPs

Though substantial quantum of research has been carried out in identifying the biobased sources that possess the efficacy to synthesize TiO$_2$-NPs, reports pertaining to the study of various synthesis parameters such as concentration of the precursor salt and the reducing agent, the pH and temperature of the synthesis mixture are scarce. Predetermined concentrations of precursor salt has been used for the synthesis of TiO$_2$-NPs (Dhandapani et al. 2012; Kirthi et al. 2011; Jha et al. 2007) and acidic pH was found to promote the synthesis of TiO$_2$-NPs using *Lactobacillus* sp. (Jha et al. 2009). Report of TiO$_2$-NPs synthesis from *Bacillus* sp., by Kirthi et al. (2011) suggested that the higher temperatures could also be employed in order to enhance the reaction process as the synthesis mixture containing the culture solution along with the precursor salt was heated on a steam bath at 60^{0}C yielded TiO$_2$-NPs at a faster rate. However, synthesis of TiO$_2$-NPs was also observed to occur at room temperature leading to less energy intensive process (Zhang et al. 2011; Pugazenthiran et al. 2009; Nair and Pradeep, 2002).

A detailed and in depth study of the synthesis parameters affecting the biobased synthesis of TiO$_2$-NPs would facilitate researchers with the ease of manoeuvring the morphological characteristics as well as the yield of the nanoparticles being synthesized to cater to the desired applications.

2.7 Mechanism of bio-based synthesis of TiO$_2$-NPs by microbial sources

Ahmad and co-workers (2005) employed plant pathogenic fungi, *F. oxysporum* for synthesizing TiO$_2$-NPs from K$_2$TiF$_6$ as the precursor salt. The protein machinery was proposed to be a hydrolytic enzyme present in the fungus. Also TiO$_2$-NPs were synthesized using *Lactobacillus sps.* and it was proposed that oxido reductases must be the responsible enzymes for the reduction of the precursor salt into the TiO$_2$-NPs (Jha et al. 2009). While Dhandapani et al. (2012) and Kirthi et al. (2011) have attributed oxido-reductases enzymes present in the organism *A.flavus* for the synthesis of TiO$_2$-NPs.

In case of plant based synthesis of TiO$_2$-NPs, the bioactive components such as phenols and amines (Kalyanasundharam and Prakash, 2015), terpenoids, flavonoids and proteinsin (Sankar et al. 2015) and flavones (Rajakumar et al. 2012a) present in

the plant source extract have been attributed to serve as reducing agents thereby facilitating the synthesis of TiO_2-NPs (Sankar et al. 2015; Santhoshkumar et al. 2014; Sundrarajan and Gowri, 2011).

2.8 Application of TiO_2-NPs as photocatalysts

TiO_2 is considered as an ideal photocatalyst with a favourable chemical structure and ability to absorb light radiation, having both a high oxidation potential and can oxidise almost all toxic organic compounds to CO_2 (Ohko et al. 1998) and a band gap that allows for absorption of sunlight (Fujishima et al. 2000). The use of TiO_2 as a semiconductor is particularly useful as strong oxidising agent, antibacterial agent, self-cleaning when in contact with surfaces, depolluting agent, stable and superhydrophilic entity. With these aforementioned properties TiO_2 becomes the most sought after nanomaterial for various applications such as photocatalysis, separations, sensor devices, paints, and dye-sensitized solar cells (Chen and Mao, 2007; Hoffmann et al. 1995; Linsebigler et al. 1995) and have been used profoundly in research pertaining to photocatalysis (Diebold, 2003).

TiO_2 is considered the best choice for general photocatalytic needs despite low solar radiation absorption as it is cheap, nontoxic, photolytically and chemically stable, and reusable with a high turnover rate. Also the chemical and physical characteristics of TiO_2, including absorption range and particle size, which can be considered the most important means of modification of its oxidation capabilities can be modified by adopting simple procedures.

The photocatalytic reaction is initiated by absorption of UV light, an electron-hole pair is then formed on the titanium dioxide, each of which are then able to react with nearby molecules (Nakata and Fujishima, 2012). There are a number of reactions that can then lead to the production of hydroxyl radicals or reactive oxygen species. The hydroxyl radical or any of the reactive oxygen species are capable of oxidising pollutants on or near the TiO_2. TiO_2 was first used as a photocatalyst for the splitting of water for the production of hydrogen by Fujishima (1972). TiO_2 as photocatalysts offer remedies for the reduction of environmental and biological pollution by degradation of environmental pollutants in air (Zhang et al. 2010; Noguchi et al. 1998) or water (Shet and Shetty, 2015; Matthews, 1991) and for the elimination of

pathogenic microbes such as fungi, viruses and bacteria (Nakata and Fujishima, 2012; Sunada et al. 1998).

TiO$_2$-NPs have been largely employed as photoinduced hydrophilic coatings and self-cleaning devices owing to their photocatalytic properties. Self-cleaning surfaces are highly sought after as the deposition of dirt, soot, vehicular exhaust and other particulates results in the tainting of these surfaces. Also mechanical weakening and eventual destruction of buildings can be prevented by a coat of TiO$_2$ as it prevents the growth of organisms, such as bacteria, algae and fungi that disfigure the facades of buildings (Mills et al. 2005).

The dirt coated on the surfaces is eliminated from the surfaces by photocatalysis that takes place in the presence of light with the energy corresponding to the band gap energy of the photocatalyst and causes the coating to chemically breakdown the organic particles adsorbed on the surface of the photocatalyst. Along with the breakdown of organic particles to simpler molecules, the contact angle of water is increased, which allows the dirt to be washed away easily (Parkin and Palgrave, 2005). Sprayed TiO$_2$ coatings, as studied by Toma et al. (2008) were successfully used for the degradation of gaseous nitrogen oxide pollutants like NO and NO$_x$ (around 52% for NO and 34% for NOx). TiO$_2$ was also used as an antibacterial coating on silicone catheters that were further used in the photocatalytic abatement of microbial strains such as *E. coli*, *S. aureus*, *P. aeruginosa* and *S. marcescens* in the liquid inside the catheter when exposed to UV light irradiation as reported by Sekiguchi et al. (2007). Thus, TiO$_2$-NPs have been proved to be efficient in self-cleaning and self sterilizing applications.

Photocatalysis has been widely studied as a possible system to produce hydrogen from water ever since the Honda-Fujishima effect was first reported in 1972 (Fujishima and Honda, 1972), thus establishing the potential of hydrogen fuel production by photocatalysis. Hydrogen fuel production by photocatalysis has also been studied and reported by Seger and Kamath, (2009), Yoshida et al. (2008) and Fujishima et al. (1975). However, the large scale application of photocatalytic applicability is in the wastewater treatment especially in the photocatalytic degradation of dyes which constitute as a major pollutant from various industries. Dyes, especially textile dyes and other industrial dyestuffs are the largest group of

organic pollutants constituting of around 1-20% (Houas et al. 2001; Zollinger, 1991) of the wastewater and impose serious implications on the environment leading to non aesthetic pollution and eutrophication, thereby leading to the generation of dangerous byproducts through oxidation, hydrolysis, or other chemical reactions taking place in the wastewater phase.

TiO$_2$-NPs have also been successfully used in the photocatalytic degradation of pesticides, thereby playing a pivotal role in environmental remediation as reported by several researchers (Ali and Hassan, 2008; Dai et al. 2008; Konstantinou et al. 2001).

Though TiO$_2$- NPs as semiconductor nanoparticles are highly sought after for their photocatalytic activity, TiO$_2$- NPs have also exhibited their antimicrobial activity against several pathogenic strains such as *E.coli* (Sunada et al. 2003; Sunada et al. 1998), *S.aureus, Shigella flexneri and Acinetobacter baumannii* (Cheng et al. 2009). The antimicrobial activity of TiO$_2$- NPs has been accredited to the reactive oxygen species, $-OH^\bullet$ radical generation which interacts with the bacterial cell and causes cell death (Jeng et al. 2006). The Reactive oxygen species, generated interact with the cell wall and bring about its decomposition while $-OH^\bullet$ radicals bring about the phospholipid peroxidation leading to cell death (Nadtochencko et al. 2006; Jeng et al. 2006; Maness et al. 1999).

2.8.1 Mechanism of TiO$_2$ photocatalysis

Photocatalytic degradation of organic (molecules) on the surface of the TiO$_2$ involves absorption of incident light which has higher energy than the band gap of TiO$_2$ (Konstantinou and Albanis, 2004).This leads to the excitation of the electrons from the valence band to the conduction band of TiO$_2$, as a result conduction band electrons (e^-) and valence band holes (+) are generated (Fig 2.1).

The photogenerated electron-hole pairs serve as powerful oxidizing and reducing agents. The photogenerated electrons in the conduction band can either reduce the adsorbed organic molecule or react with the oxygen adsorbed on its surface thereby reducing it to superoxide radical anion. The photogenerated holes in valence band either oxidize the dye or react with hydroxyl ions or water molecules to oxidize them into hydroxyl radicals. TiO$_2$ is known to bring about the heterogeneous

photocatalytic degradation of organic molecules by the production of oxidizing species such as Hydroxyl or peroxide radicals (Hashimoto et al. 2005; Linsebigler et al. 1995).
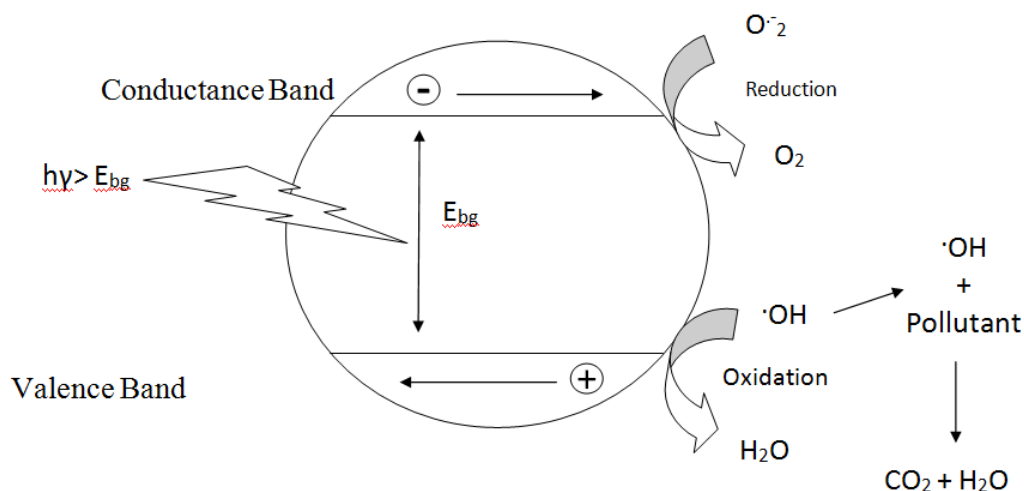
Figure 2.1: General mechanism of TiO$_2$ photocatalysis (Modified from Robert and Malato 2002; Dijkstra et al. 2001).

The chemical mechanism of heterogeneous photocatalysis of TiO$_2$ is shown in the following equations:

$$TiO_2 + h\upsilon \quad \rightarrow \quad TiO_2\ (e^- + h^+) \qquad\qquad ...(i)$$
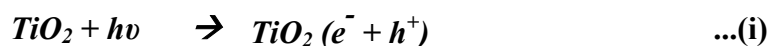
Eq.(i) shows the initial reaction of TiO$_2$ with light, producing a hole (h^+) and an electron (e^-) that act as the active excited species, which then react with water and oxygen. In aqueous conditions, Ti-OH groups are abundant and are the major source of hydroxyl radicals (OH^-) on the TiO$_2$ surface. The downstream products of reactions with molecular oxygen being superoxide ($^\bullet O_2{}^-$) and often hydroxyl radical ($^\bullet OH$) that react with a nearby organic molecule.

2.8.2 Factors effecting photocatalytic degradation of organic molecules using TiO$_2$-NPs

Though semiconductors such as ZnO, ZrO$_2$, CdS, MoS$_2$, Fe$_2$O$_3$ and WO$_3$ have been examined and used as photocatalysts (Carp et al. 2004), TiO$_2$-NPs exhibit better characteristics as a photocatalyst compared to others such as; photo-stability, inert

nature, availability and low cost, ability to adsorb reactants under efficient photonic activation (Konstantinou et al. 2002).

TiO$_2$ exists in many polymorphs; anatase, rutile, brookite and an unknown monoclinic phase (Carp et al. 2004). Rutile is the stable form, whereas anatase and brookite are metastable and are readily transformed to rutile when heated. While Anatase and Rutile phases are highly researched after forms with anatase phase being reported to exhibit the highest photocatalytic activity compared to rutile (Perkowski et al. 2003). Synthesis of brookite phase and its photocatalytic activity is least reported. Synthesis of pure brookite without rutile or anatase is rather difficult to be prepared hence the photocatalytic properties of this phase have been not much studied (DiPaola et al. 2013). The knowledge of the electronic band structure of the TiO$_2$ polymorphs (Anatase, rutile and brookite) is useful to understand the photocatalytic behaviour of the pure phases and of their mixtures. The separation between the energy of the lowest conduction band and that of the highest valence band is called the band-gap, energy gap or forbidden energy gap (E$_g$), which determines the photoactivity of the semiconductor. Rutile has an E$_g$ value of 3.02 eV, anatase of 3.23 eV while the E$_g$ value of brookite is uncertain between 3.1 to 3.4 eV (DiPaola et al. 2013).

Several factors are known to affect the photocatalytic degradation of the organic molecules by TiO$_2$-NPs. The photocatalytic degradation is known to increase with the increase in the light intensity (Qamar et al. 2006). Increase in the concentration of the organic compound in the reaction mixture leads to decrease in the photocatalytic degradation of the compound by TiO$_2$-NPs as the surface gets saturated with the organic compound leading to catalyst deactivation (Arana et al. 2004, Sakthivel et al. 2003). The decrease in the photocatalytic efficacy due to increase in the substrate concentration can also be attributed to the light screening effect caused by the high concentration of the substrate (So et al. 2002; Epling and Lin, 2002; Tang, 1995). Similarly factors such as light screening, agglomeration and settling of the catalyst caused by an increased concentration of the catalyst loading beyond definite value causes diminished photocatalytic degradation rates (So et al. 2002; Tang, 1995).

The pH of the reaction medium also is known to influence the photocatalytic efficiency of the catalyst as pH changes can influence the adsorption of dye molecules onto the TiO$_2$ surfaces (Bahnemann et al. 1994). Drastic change in the pH of the

reaction medium can lead to low photocatalytic activity (Naskar et al. 1998; Neppolian et al. 1998) and aggregation of the catalyst (Fox and Dulay, 1993). Addition of oxidants to the photocatalytic reaction mixture is also known to either increase or decrease the overall efficacy of the photocatalysis (Augugliaro et al. 2002; Malato et al. 1998) and is dependent on the type of the oxidant added as well as the pH of the synthesis mixture. Addition or presence of humic substances, naturally occurring ions and solvents may reduce the photocatalytic efficiency of the catalyst by the combination effects of light attenuation, competition for active sites and surface deactivation (Daneshvar et al. 2003; Epling and Lin, 2002). A precise control of these conditions during the photocatalytic degradation of the organic molecules can enhance the overall efficiency and yield higher degradation rates.

2.9 Characterization of nanoparticles

Characterization of the nanoparticles is the most crucial aspect in the synthesis of nanoparticles as it is helpful in the determination of the morphology, structure and properties of the nanoparticle, thus important in determining its suitability for a specific application. It is through characterization of the nanoparticles synthesized that vital information about the effect of various parameters upon the physio-morphological characteristics can be understood. Appropriate tools with the ability to adequately characterize the structural and surface details at atomic levels are available and thus make it easier for characterizing.

AgNPs and TiO_2-NPs have been characterized using various techniques; the spectral analysis of the AgNP in colloidal form can be determined using spectrophotometer (Nanda and Saravanan, 2009; Fayaz et al. 2010), while the morphological characteristics of AgNPs and TiO_2-NPs such as size, shape and particle size can be determined by Scanning electron microscopy (SEM) analysis (Sun and Xia, 2002; Burnside et al. 1998), Transmission electron microscopy (TEM) analysis (Pottier et al. 2001; Ahmad et al. 2010), Dynamic light scattering (DLS) analysis for particle size analysis (Fayaz et al. 2010; Burnside et al. 1998). The crystalline structure of nanoparticles can be determined using X- Ray diffraction (XRD) analysis (Parikh et al. 2008; Tan and Wu, 2006). The stability of the nanoparticles in terms of their surface charge is generally determined using zeta potential analyzer (Fayaz et al.

2010; Zhang et al. 2007). The surface functional groups indicating the presence of various capping agents on the surface of the nanoparticles can be determined using Fourier transform Infrared (FTIR) spectroscopy (Dubey et al. 2008; Su et al. 2008). Energy Dispersive X-ray analysis (EDX) analysis provides the compositional analysis of the nanoparticle sample (Dubey et al. 2010; Burda et al. 2003). Band Gap energy of TiO_2-NPs was determined by spectral analysis of the nanoparticles using spectrophotometer (Ghobadi et al. 2013).

It can be inferred from the literature review that biobased methods of synthesis of nanoparticles are advantageous. Selection of new plant resources that are produced as wastes from different sectors and isolation and screening of bacteria from metal rich environment for extracellular synthesis of nanoparticles may prove economical and beneficial. When a nanoparticle synthesis process is developed with the new resources the synthesis conditions need to be optimized to obtain required characteristics and high yield. The research questions along with the detailed scope and objectives of the research work devised based on the review of literature are presented in Chapter 1.

CHAPTER 3

MATERIALS AND METHODS

This chapter furnishes details of materials used for the execution of experiments, analytical techniques and methodologies adopted to attain the objectives set forth in this research work.

3.1 Materials

Chemicals used for the experiments in the present research work were of analytical (AR) grade. Silver nitrate ($AgNO_3$) was purchased from Merck India Pvt Ltd, Mumbai, Dipotassium hexafluorotitanate (K_2TiF_6), Acid Blue 129 dye (AB 129), Remazol Brilliant Blue R dye (RBB), quercitin, gallic acid, Folin-Ciocalteau reagent were purchased from Sigma-Aldrich Chemicals Pvt. Ltd., Bangalore, India. SDS-PAGE kit was purchased from Genei, Bangalore. Chemicals such as acetic acid (CH_3COOH), hydrochloric acid (HCl), nitric acid (HNO_3), Ethylenediaminetetraacetic acid (EDTA) were purchased from Merck India Pvt. Ltd, Mumbai. Ferrous sulphate ($FeSO_4$), Aluminium chloride (Al_2Cl_3), Sodium bicarbonate (Na_2CO_3) were purchased from Nice chemicals, Chennai, India. Nutrient broth, Nutrient Agar, Mueller Hilton broth, Mueller Hilton agar was purchased from Himedia Ind. Pvt. Ltd, Bangalore, India. Degussa P-25 was obtained as a gift pack from Evonik Degussa India Pvt. Ltd. It consists of 75% anatase and 25% rutile TiO_2 with Brunauer–Emmett–Teller (BET)-specific surface area of 50 m^2/g and primary particle size of 20 nm.

3.2 Plant based synthesis of AgNPs

All the experiments in the present study were performed in triplicates and the average values have been reported.

3.2.1 Selection of plant resources

The plant resources to carry out the synthesis of nanoparticles were chosen on the basis of the following criterion:

- Their availability in surplus as refuse generated from fruit processing units or as waste from agricultural or forestry sectors.
- Low economic value of plant resource material
- Presence of bioactive components such as antioxidants, phenolics and flavonoids in the plant resources which are known to act as reducing agents

Plant resources fulfilling the above mentioned criteria were identified and selected for the synthesis of nanoparticles. The leaves of various trees were collected from the campus neighbourhood of National Institute of Technology, Karnataka, Surathkal, India, Geographically located at 12°58'60 N latitude and 74° 46' 60 E longitude. The fruit peels were collected from a local fresh fruit juice centre located in Surathkal, India

The following plant resources were selected and processed suitably to synthesize AgNPs.

- Leaves of cashew nut tree (*Anacardium occidentale*),
- Leaves of Indian Gooseberry tree (*Phyllanthus embilica*),
- Plantain leaves (*Musa paradisiaca*),
- Teak leaves (*Tectona grandis* Linn. f),
- Leaves of the Indian almond tree (*Terminalia catappa*),
- Leaves of Pongamia tree (*Milletia pinnata*),
- Leaves of Mango tree (*Mangifera indica*),
- Exocarps of Pineapple fruit (*Ananas comosus*),
- Orange Exocarps (*Citrus sinensis*),
- Exocarp of Watermelons (*Citrullus lanatus*).

3.2.2 Processing of the plant resource material

Undamaged and healthy plant material, either leaves or fruit exocarp peels without any signs of micro or macro-infestation were collected. The plant material was sorted, cut into small pieces measuring approximately 1cm x1cm in size and washed several times under running tap water to eliminate dust and other physical impurities. Excess of water from the plant material was drained and final three rinses were performed using deionized water.

The plant materials were then shade dried for 10 days in a dust free area. Dried plant material was then powdered using a motor operated blade mixer (Ultra, India) and the powder obtained from each of the plant material used was stored for subsequent usage in preparation of the extract and was used for the synthesis of AgNPs.

3.2.3 Preparation of the plant extract for synthesis of AgNPs

The aqueous extract of the plant resource material was prepared by adding required quantity of the processed plant material powder to 100 mL of boiling deionized water in a beaker and the suspension was further boiled for 2 min under slow heating with continuous stirring. The suspension was then cooled to a room temperature of 28 ± 2 ºC and filtered through Whatman No. 1 filter paper to eliminate any plant material, thus obtained extract was stored in amber colored air tight bottles at 4 ºC for further usage. To prepare the extract with 1% (w/v) plant material powder suspension, 1 g of the powder was used with 100 mL water.

3.2.4 Preparation of silver nitrate solution

8.4935 g of $AgNO_3$ was made upto 100 mL in a standard flask using deionized water to obtain a stock solution of 500 mM. 0.2 mL, 1 mL, 2 mL, 4 mL, 10 mL and 20 mL of the stock solutions were made upto 100 mL in a standard flask using deionized water to prepare 1 mM, 5 mM, 10 mM, 20 mM, 50 mM and 100 mM $AgNO_3$ solutions respectively and were used for the synthesis of AgNPs.

3.2.5 Synthesis of AgNPs using the plant material extract

Aqueous $AgNO_3$ solution was used as the precursor salt solution for the synthesis of AgNPs. The precursor salt solution of the known concentration and the plant material extract (prepared from the suspension of the processed plant material powder at the concentration, as required for the experiment) were made to react in the required volume ratio with total volume of 10 mL at 28 ± 2 ºC with constant stirring for 24 h. The synthesis mixture containing the extract and $AgNO_3$ solution was observed for the visible change in colour of the synthesis mixture to brown, characteristic of AgNPs. 0.3 mL aliquot sample of the synthesis mixture was collected after 24 h (unless otherwise specified) and diluted to 3 mL using deionized water for spectral analysis. The spectral analysis of the sample was performed using a dual wavelength UV- Vis spectrophotometer (Labomed, USA) to further confirm the formation of AgNPs from the SPR peak around 420 nm, characteristic of AgNPs. The samples were analyzed at a resolution of 1nm in a scan range of 200- 800nm against deionized water as a blank.

3.2.6 Screening of the plant resource material for synthesis of AgNPs

The synthesis mixture was prepared with 1 mM AgNO$_3$ solution and the plant material extract prepared with 1% w/v of the plant material powder suspension. The synthesis of AgNPs was carried out with 1:1 volume ratio of the precursor salt solution and the extract as described in Section 3.2.5 with each of the plant material listed in section 3.2.1. The plant materials were chosen based on the characteristics of the SPR peak for AgNPs obtained from the synthesis mixture.

3.2.7 Effect of process parameters on the synthesis of AgNPs using aqueous extracts of *T.catappa* leaves (ALE) and *Tectona grandis* Linn f. leaves (TLE)

3.2.7.1 Effect of reaction time

Aqueous extracts of *T.catappa* leaves (Almond leaf extract 'ÁLE') and *Tectona grandis* Linn f. leaves extract (Teak leaves extract 'TLE') were prepared by the method described in section 3.2.3 with 1% w/v of the leaf powder suspension. These extracts were hereinafter referred as 1% ALE and 1 % TLE respectively. The synthesis of AgNPs was carried out for a total reaction time of 24 h using 1% ALE or TLE and 1 mM of AgNO$_3$ solution in volume ratio of 1:1 as described in Section 3.2.5. The samples from the synthesis mixtures were withdrawn at time intervals of 1 min, 5 min, 10 min, 30 min, 1 h, 6 h, 12 h and 24 h and spectrally analyzed for SPR peak of AgNPs using UV- Vis spectrophotometer as described in section 3.2.5 over a wavelength range of 350 to 700 nm to determine the influence of the reaction time on the synthesis of AgNPs.

3.2.7.2 Effect of concentration of leaf powder suspension used for the preparation of aqueous extracts of the plant leaves on synthesis of AgNPs

1%, 5% and 10% ALE or TLE were prepared by open solvent heating method described in Section 3.2.3 using the leaf powder suspensions consisting of 1g, 5g and 10 g of the leaf powder respectively in 100 mL water.

To evaluate the effect of the concentration of leaf powder suspension used in preparation of the extract, synthesis of AgNPs was carried out with 1%, 5% and 10% ALE or TLE and 1 mM AgNO$_3$ solution in 1:1 volume ratio as described in Section 3.2.5. The synthesis mixture remaining after the synthesis of AgNPs was analyzed for

residual Ag^+ ions concentration using Atomic absorption spectrophotometer (AAS GBC-932plus) and the conversion of Ag^+ ions was calculated using Eq.A1 as described in Appendix I. The optimum leaf powder suspension concentration was selected based on the spectral characteristics and the conversion.

3.2.7.3 Effect of precursor salt (AgNO$_3$) concentration on the synthesis of AgNPs

To determine the effect of precursor salt solution on the synthesis of AgNPs, synthesis was carried out with 5% ALE or 10% TLE (optimum leaf powder suspension concentration) and with different concentrations of precursor salt solutions in 1:1 volume ratio. The concentration of AgNO$_3$ solution was varied while keeping the total volume and the ratio of the extract to precursor salt solution in the synthesis mixture constant. The synthesis was carried out as described in Section 3.2.5 with 1 mM, 5 mM, 10 mM, 20 mM and 100 mM AgNO$_3$ solutions. The sample of synthesis mixture after 24 h of synthesis time was analyzed for spectral characteristics using UV–Vis spectrophotometer, morphological characteristics using SEM analysis (Section 3.6.3) and residual concentration of Ag^+ ions in the synthesis mixture after the synthesis of AgNPs was analyzed using Atomic absorption spectrophotometer (Appendix I). The conversion of Ag^+ ions was calculated using Eq.A1 according to the procedure described in Appendix I. The optimum concentration of AgNO$_3$ solution was determined based on the spectral characteristics, morphological characteristics and the conversion.

3.2.7.4 Effect of ratio of aqueous leaf extract to precursor salt solution (v/v) in synthesis mixture on the synthesis of AgNPs

To evaluate the effect of the volume ratio of plant leaf extracts and AgNO$_3$ solution in the synthesis mixture on the synthesis of AgNPs, synthesis was carried out as described in Section 3.2.5 using 20 mM AgNO$_3$ solution (optimum concentration obtained by the studies described in Section 3.2.7.3) and 5% ALE or 10% TLE. The volume ratio of the extract to the AgNO$_3$ solution was varied in the range of 1:1, 1:4, 1:7, 1:10, 1:20, 1:50 and 1:100, while keeping the total volume of the synthesis mixture constant.

After 24 h of the reaction time, the samples of synthesis mixture were subjected to spectral analysis as described in Section 3.2.5, and morphological

characteristics were studied using SEM analysis (Section 3.6.3). The residual concentration of Ag^+ ions in the synthesis mixture after the synthesis of AgNPs was analyzed using Atomic absorption spectrophotometer (Appendix I). The percentage conversion of Ag^+ ions was determined according to the procedure described in Appendix I using Eq.A1. The optimum ratio was chosen based on the spectral, morphological characteristics of AgNPs and the conversion.

3.2.7.5 Effect of initial pH of the synthesis mixture on plant based synthesis of AgNPs

To study the effect of pH, the synthesis was carried out for 24 h as described in Section 3.2.5 with different initial pH conditions of (i) unadjusted pH: 4.87 ± 0.01 for ALE and 5.3 ± 0.01 for TLE, (ii) acidic pH 4, (iii) neutral pH 7 and (iv) alkaline pH of 11. 0.1 N NaOH and 0.1 N HNO_3 were used to adjust the pH. The synthesis mixture was prepared with 5% ALE or 10% TLE with 20 mM $AgNO_3$ solution in the volume ratio of 1:4 (optimum ratio obtained by the studies described in Section 3.2.7.4). The synthesis mixture remaining after the synthesis of AgNPs was analyzed for residual Ag^+ ions concentration using Atomic absorption spectrophotometer and the conversion of Ag^+ ions was calculated using Eq.A1 as described in Appendix I. The spectral and morphological characteristics of the particles were analyzed using UV–Vis spectrophotometer and SEM (Section 3.6.3) respectively. The optimum pH was chosen based on the spectral, morphological characteristics of the particles and the conversion.

3.2.7.6 Effect of the processes adopted for extraction of bioactive components from the leaves of *T.catappa* and *T.grandis* Linn f on synthesis of AgNPs

The following three extraction processes were adopted for preparation of ALE and TLE:

- Open Solvent heating (OS): ALE and TLE were prepared with 5% and 10% leaf powder suspensions respectively by the open solvent heating method described in section 3.2.3.
- Reflux heating (REF): Reflux extraction was performed in a in a 250 mL round bottomed flask equipped with a reflux condenser at the temperature of 100ºC for 1 h with 5 g almond leaf powder in 100 mL of deionized water to

obtain 5 % ALE. Similarly, for obtaining 10% TLE, the reflux extraction was performed using 10 g of teak leaf powder suspended in 100 mL of deionized water. The obtained extracts were cooled to 28±2 ºC and filtered through Whatman No.1 filter paper and stored in amber colored air tight bottles at 4ºC for further use in the synthesis of AgNPs.

- Sonication (SON): 5 g of processed *T.catappa* leaf powder or 10 g of processed *T.grandis* Linn F. leaf powder were suspended in 100 mL deioninzed water. The mixture was sonicated in a probe type sonicator (Vibracell, USA) at an amplitude of 90%, pulse of 50 seconds for 5 minutes. The extracts obtained were filtered through Whatman No.1 filter paper and stored in sterile amber colored air tight bottles at 4ºC for further use in the synthesis of AgNPs. 5 % ALE or 10% TLE were thus prepared by sonication.

The extracts obtained by the above mentioned extraction techniques were used to synthesize AgNPs according to the methodology described in Section 3.2.5 under the optimized conditions of 5 % ALE or 10 % TLE and 20 mM of AgNO$_3$ solution in the volume ratio of 1:4 with initial alkaline pH 11 (optimum pH determined through the studies described in Section 3.2.7.5) of the synthesis mixture.

Spectral analysis of the samples of synthesis mixtures after 24 h of reaction time was carried out according to the methodology described in section 3.2.5. The conversion of Ag$^+$ ions was determined by the analysis of residual silver content in the synthesis mixture using AAS as described in Appendix I.

3.2.7.7 Determining the role of bioactive components present in the plant leaf extracts in the synthesis of AgNPs

The synthesis of AgNPs was carried out with initial pH 11 using 5% ALE or 10% TLE prepared by different extraction methods described in Section 3.2.6.7. The volume ratio of the extract and 20 mM of AgNO$_3$ solution used for the synthesis was 1:4 (total volume 10 mL). The concentration of bioactive components such as phenolics, flavonoids and antioxidants present in the synthesis mixture before and after the synthesis of AgNPs was determined using the procedures described in Section 3.2.7.8, 3.2.7.9 and 3.7.2.10 respectively. After 24 h of reaction time, the synthesis mixture containing AgNPs was centrifuged and the supernatant was used for

the determination of bioactive components. To determine the initial concentration of bioactive components in the synthesis mixture, 2 mL of the extract was diluted to 10 mL using deioninzed water and the sample was analyzed for the bioactive components.

3.2.7.8 Determination of Total Phenolic Content

The total phenolic content (TPC) was measured using Folin-Ciocalteu method (Singleton et al. 1999). 1.5 mL Folin-Ciocalteu's phenol reagent (10% v/v) and 1.2 mL 7.5% (w/v) Na_2CO_3 solution were added to 0.3 mL of the sample. The reaction mixture was thoroughly mixed and was kept in the dark for 30 minutes before the absorbance was measured at 765 nm using UV-Vis spectrophotometer (Labomed, USA). Total phenolic content in the samples was determined in terms of µg of gallic acid equivalents (GAE) /mL using the precalibrated data with gallic acid standards. The detailed procedure for the reagent preparation and calibration along with the calibration plot is provided in Appendix II.

3.2.7.9 Determination of Total Flavonoid Content

The flavonoids content was determined spectrophotometrically using the method described by Ordon-Ez et al. (2006), which based on the formation of a complex flavonoid-aluminium. 0.5 mL of 2% $AlCl_3$ solution in ethanol was added to 0.5 mL of the sample. After 1 h, the absorbance was measured at 420 nm using UV-Vis spectrophotometer (Labomed, USA). Formation of yellow color indicated the presence of flavonoids. Flavonoid concentration as Quercitin equivalent (QE) was determined using precalibrated data. The amount of flavonoids was expressed as µg of Quercitin equivalent (QE)/mL. The detailed procedure for the reagent preparation and calibration along with the calibration plot is provided in Appendix III.

3.2.7.10 Determination of Total Antioxidant Activity

Total antioxidant activity was determined by Ferric Reducing Antioxidant power (FRAP) (Benzie and Strain, 1996) assay. 0.2mL of the sample was allowed to react with 3 mL of the FRAP solution at $37^{o}C$ for 30 min in the dark condition. Absorbance of the colored product (ferrous tripyridyltriazine complex) was taken at 593 nm using UV-Vis Spectrophotometer and the total antioxidant concentration

expressed in µM/mL of the Ferrous Equivalent (FE) was determined using the precalibrated data. The detailed procedure for the reagent preparation and calibration along with the calibration plot is provided in Appendix IV.

3.3 Bacterial based synthesis of AgNPs

3.3.1 Collection of soil sample for isolation of bacteria

Silver rich dust laden soil from the silversmith's work bench in a silver jewellery workshop located in Mangalore, India was collected aseptically in a presterilized sampling bottle, as the source for isolation of bacterial strains.

3.3.2 Preparation of Nutrient agar medium with AgNO$_3$ salt

250 mL Nutrient agar (HiMedia, India) medium was prepared in distilled water as per the manufacturer's instructions. The medium was sterilized by autoclaving at 121˚C, 115kPa for 20 minutes. Silver Nitrate (AgNO$_3$) (Merck, India) 100 mM stock solution in required volume was added to the molten media to prepare nutrient agar medium with required concentration of AgNO$_3$ was as added to the molten media, when the temperature was about 40-45˚C and stirred well to ensure uniform distribution of the precursor salt avoiding the formation of air bubbles. The molten agar was then carefully poured into pre-sterilized Petri dishes (Autoclaved at 121˚C, 115kPa for 20 minutes) and allowed to solidify in the laminar air flow chamber for further inoculation.

3.3.3 Isolation and screening of bacterial strains with the efficiency to synthesize extracellular AgNPs

The collected soil sample was processed using serial dilution method. 100 mL soil slurry containing 1 gram of the soil sample was prepared using sterilized distilled water. The soil slurry was serially diluted with sterile saline solution of 0.7 % (w/v) to obtain dilutions varying from 10^{-1} to 10^{-10}.

100 µL of aliquots were drawn from each of the dilution tubes and inoculated onto the nutrient agar plates enriched with 100 mg/L of AgNO$_3$ salt using spread plate technique. The inoculated plates were incubated at 35$^{\text{o}}$C for 24 to 48 h and were observed for bacterial growth. Un-inoculated control plate was also maintained. Single isolated colonies exhibiting brown colour along with a clear zone around them

with a brown band, within 24 h of the incubation period were and selected for further studies. These colony characteristics indicated that the bacterial isolates could extracellulary reduce the Ag^+ ions to Ag^0 within 24 h of time duration.

The bacterial colonies exhibiting the above mentioned characteristics were selected and further subcultured onto nutrient agar plates enriched with $AgNO_3$ in the concentration of 0.2 g /L, 0.4 g/L, 0.6 g/L, 0.8 g/L and 1 g/L to screen them based on their efficacy to reduce the higher concentrations of Ag^+ ions to Ag^0. The inoculated petriplates were further incubated at 28 ± 2^oC for 24 h and observed for the characteristics exhibited by the bacterial strains for the extracellular reduction of Ag^+ ions to Ag^0.

Further, the isolates which were able to tolerate and produce a clear zone around the colonies with brown band even in higher concentrations of $AgNO_3$ in 24 h of incubation were selected for further studies. The reducing ability of the bacterial strains were indicated by the formation of clear zones around them, these colonies turned brown in colour along with the presence of silver metallic sheen at the bottom of the colony and Petridish. These isolated, screened and selected strains were further separately subcultured onto nutrient agar plates by quadrant streaking method and incubated for 24 h at 28 ± 2^oC.

The selected strains were further individually inoculated into 100 mL of presterilized nutrient broth medium (Himedia, India) under aseptic conditions and incubated in a rotary shaker at 28 ± 2^oC for 24 h at 120 rpm. These cultures served as inocula for the synthesis of AgNPs.

3.3.4 Identification of the bacterial isolates by partial sequencing of 16S ribosomal RNA

The selected pure strains of the bacterial isolates 4S1, 4S2, 4S3, 6S1 and 8S1 were subcultured on the nutrient agar plates as described in Section 3.3.3. The fresh subcultured colonies of the isolates were characterized by Agharkar Research Institute, Pune, Maharashtra, India for 16S ribosomal RNA partial sequencing of bacterial chromosome. The protocol adopted for the sequencing technique is described in Appendix V.

The partial gene sequence of 16S ribosomal RNA of the bacterial strains provided by Agharkar Research Institute was subjected to BLAST-n algorithm to obtain the closest phylogenetic match with the GenBank database by using BLASTn algorithm (http://blast.ncbi.nlm.nih.gov/Blast.cgi) on National Centre for Biotechnology Information (NCBI) site.

3.3.5 Synthesis of AgNPs using the cell free culture supernatant of the isolated bacterial strains.

For obtaining the cell free culture supernatants of the bacterial strains, 1 mL of the inoculum from the 24 h culture of each of the selected bacterial isolates namely, 4S1, 4S2, 4S3, 6S1 and 8S1 was inoculated separately into Erlenmeyer flasks containing 100 mL of presterilized (Autoclaved at 121°C, 115 kPa for 20 minutes) nutrient broth medium (HiMedia, India) under aseptic conditions and further incubated at 28±2 ºC for 24 h at 120 rpm on a rotary shaker for the growth. Individual culture broth of isolates were then centrifuged at 10000 rpm for 10 minutes at 4ºC to eliminate the bacterial cells and the supernatant was used for the synthesis of AgNPs and hereinafter referred as 24 h grown cell free culture supernatant.

For the synthesis of AgNPs, $AgNO_3$ solution of known concentration was added to 100 mL of the 24 h grown cell free culture supernatant of the bacterial isolates in equal volume. The synthesis mixture containing the cell free culture supernatant of the bacterial strain and the precursor salt was kept in a rotary shaker at room temperature of 28±2ºC for 24 h at 120 rpm. The synthesis mixture was observed for the formation of brown colour characteristic of AgNP synthesis. 0.3 mL aliquot of the sample was drawn at 24 h of synthesis time duration and analyzed using a dual wavelength UV- Vis spectrophotometer (Labomed, USA) at a resolution of 1nm in a scan range of 350-700 nm against deionized water as a blank, for spectral characteristics to further confirm the formation of AgNPs. The percentage conversion of the Ag^+ ions was calculated by determination of the residual Ag^+ content present in the synthesis mixture as described in Appendix I.

The synthesis mixture containing the AgNPs was centrifuged at 15000 rpm for 20 min at 4ºC to separate the AgNPs and the supernatant was discarded. The AgNPs thus obtained was washed twice with deionized water to remove any contaminants.

The AgNPs were dried at 130ºC for 24 h and stored in moisture free conditions for characterization. The AgNPs synthesized using the 24 h grown cell free culture supernatant of the isolated bacterial strains 4S1, 4S2, 4S3, 6S1 and 8S1 were analyzed for their morphological characteristics using SEM as described in section 3.6.3.

3.3.6 Studies on the effect of synthesis process parameters on the bacterial based synthesis of AgNPs

3.3.6.1 Effect of precursor salt solution concentration

Effect of precursor salt solution concentration on the synthesis of AgNPs by the bacterial isolates 4S1, 4S2, 4S3, 6S1 and 8S1.

Synthesis of AgNPs was carried out according to the method described in Section 3.3.3 by varying the concentration of $AgNO_3$ solution used for the synthesis in the range of 1 mM, 5 mM, 10 mM, 20 mM, 75 mM, 100 mM and 500 mM.

Spectral and morphological analysis of the AgNPs synthesized after 24 h of reaction time were carried out as described in Section 3.3.5 and Section 3.6.3 respectively. The conversion of Ag^+ ions was determined as described in Appendix I by the analysis of residual Ag^+ concentration in the synthesis mixture. The optimum precursor salt solution concentration was chosen based on the spectral, morphological characteristics of the particles and the conversion.

3.3.6.2 Effect of initial pH of the synthesis mixture

To determine the influence of initial pH of the synthesis mixture on the synthesis of AgNPs using the bacterial isolates 4S1, 4S2, 4S3, 6S1 and 8S1, the synthesis was carried out according to the methodology described in Section 3.3.5 with each of the bacterial isolates and by varying the initial pH. The synthesis mixture was prepared by mixing the cell free culture supernatants of the bacterial isolate and the $AgNO_3$ solution of optimum concentrations (75 mM for 4S1, 4S2, 4S3 and 100 mM for 6S1, 8S1) in equal volumes. The initial pH of the synthesis mixture was adjusted to acidic pH 4, neutral unadjusted pH 7.0±0.2 and alkaline pH 11 using 1 N HCl or 1 N NaOH wherever necessary. Spectral and morphological analysis of the AgNPs synthesized after 24h of reaction time were carried out as described in Section 3.3.5 and Section 3.6.3 respectively. The conversion of Ag^+ was determined as described in Appendix I by analysis of residual Ag^+ concentration. The optimum

initial pH was chosen based on the spectral, morphological characteristics of the particles and the conversion.

3.4 Biobased synthesis of TiO$_2$-NPs

3.4.1 Synthesis of TiO$_2$-NPs using the leaf extracts of *T.catappa* and *T.grandis* Linn F.

For the synthesis of TiO$_2$-NPs, 100 mL of 5% ALE prepared using the procedure described in section 3.2.7.2 and 3.2.3 was taken and 1 g of K$_2$TiF$_6$ salt was added to it as the precursor salt. The synthesis mixture was kept in a rotary shaker operated at 120 rpm at ambient temperature of 28±2ºC and observed for the reaction time of 24 h for the appearance of any turbidity indicating the synthesis of TiO$_2$-NPs.

Similar procedure was followed for the synthesis of TiO$_2$-NPs using 10 % TLE. However, no turbidity in the synthesis mixture was observed indicating that the plant leaf extracts of *T.catappa* and *T.grandis* Linn F. were unable to synthesize TiO$_2$-NPs.

3.4.2 Synthesis of TiO$_2$-NPs using the cell free culture supernatant of the isolated bacterial strains

The isolated bacterial strains, 4S1, 4S2, 4S3, 6S1 and 8S1 were used to synthesize extracellular TiO$_2$-NPs. The 24 h grown cell free culture supernatant of the bacterial strains was obtained by following the procedure presented in section 3.3.5.

To 100 mL of the 24 h grown cell free culture supernatant of the bacterial isolate, desired quantity of K$_2$TiF$_6$ salt was added as the precursor salt to form the synthesis mixture. The synthesis mixture was kept for 24 h in a rotary shaker maintained at 120 rpm at ambient temperature of 28±2ºC. Control flasks containing only 100 mL of the 24 h cell free culture supernatant of the bacterial isolate was also maintained under the same conditions of synthesis. The synthesis mixture was observed for change in colour of the medium indicating turbidity and any white colored deposition confirming the synthesis of TiO$_2$-NPs.

The percentage conversion of the Ti^{+4} ions was calculated by determination of the residual Ti^{+4} content present in the synthesis mixture as described in Appendix II.

The synthesis mixture containing the TiO$_2$-NPs was centrifuged at 15000 rpm for 20 min at 4ºC to separate the nanoparticles and the supernatant was discarded. The

TiO$_2$-NPs thus obtained was washed twice with deionized water to remove any contaminants, dried at 100ºC for 24 h and stored in moisture free conditions for characterization. The TiO$_2$-NPs synthesized using the 24 h grown cell free culture supernatant of the isolated bacterial strains were analyzed for their morphological characteristics using SEM as described in section 3.6.3.

3.4.3 Effect of synthesis process parameters on bacterial based synthesis of TiO$_2$-NPs

3.4.3.1 Effect of precursor salt concentration in the synthesis mixture

In order to determine the effect of precursor salt concentration on bacterial based synthesis of TiO$_2$-NPs, synthesis was carried out with the 24 h grown cell free culture supernatants of bacterial isolates 4S1, 4S2, 4S3, 6S1 and 8S1 prepared by the methodology described in section 3.4.2.

Concentration of K$_2$TiF$_6$ as the precursor salt in 100 mL of the synthesis mixture was varied as 5 g/L, 10 g/L and 15 g/L. The synthesis of TiO$_2$-NPs was carried out for a time duration of 24 h as described in section 3.4.2. The conversion of Ti^{+4} ions was determined as described in Appendix II by the measurement of residual concentration of Ti^{+4}. The morphological characteristics of the TiO$_2$-NPs were determined using SEM analysis (Section 3.6.3).

The optimum precursor salt concentration was determined based on the conversion and the morphological characteristics.

3.4.3.2 Effect of initial pH of the synthesis mixture

In order to determine the influence of initial pH of the synthesis mixture on the synthesis of TiO$_2$-NPs, synthesis was carried out under different initial pH conditions of pH 4, unadjusted pH 7.0±0.2 and pH of 11, by adjusting the pH using 1 N HCl or 1 N NaOH wherever necessary. The synthesis of TiO$_2$–NPs was carried out as described in Section 3.4.2, with the synthesis mixture containing the cell free culture supernatant of the bacteria with optimum K$_2$TiF$_6$ salt concentration (determined according to the methodology described in section 3.4.3.1).

The conversion of Ti^{+4} ions was determined as described in Appendix II by the measurement of residual concentration of Ti^{+4}. The morphological characteristics of the TiO$_2$-NPs were determined using SEM analysis (Section 3.6.3).The optimum

initial pH was determined based on the conversion and the morphological characteristics.

3.5 Determination of the bacterial metabolic machinery responsible for the synthesis of AgNPs and TiO$_2$-NPs

The 24 h grown cell free culture supernatants of the bacterial isolate obtained through the methodology described in section 3.3.5 were subjected to partial purification of the proteins to determine the proteins present in the culture supernatant that brought about the synthesis of AgNPs or TiO$_2$-NPs. The proteins present in the bacterial cell free culture supernatants of isolates 4S1, 4S2, 4S3, 6S1 and 8S1 were partially purified using traditional and classical protein purification methods like ammonium sulphate precipitation and membrane dialysis, followed by the concentration of the protein by reverse osmosis. SDS PAGE was used to identify the molecular weight of the proteins responsible for the bacterial based synthesis of AgNPs and TiO$_2$-NPs.

3.5.1 Ammonium sulphate protein precipitation method

Ammonium sulphate precipitation is a classical method adapting the principle of salting out of proteins. The proteins from the bacterial cell free culture supernatants of the isolates 4S1, 4S2, 4S3, 6S1 and 8S1 obtained as described in section 3.3.5 were precipitated using ammonium sulphate salt at 25ºC using the following methodology.

100 mL of the cell free culture supernatant of each of the isolate was salted out using dry and preweighed ammonium sulphate. The approximate amount of ammonium sulphate required for 100% saturation was calculated using ammonium sulphate calculator ([www.encorbio.com/protocols/AM-SO$_4$.htmL](http://www.encorbio.com/protocols/AM-SO4.htmL)) for 100 mL of the supernatant to be precipitated at 25ºC. The salting out procedure of the bacterial proteins was carried out under continuous stirring of the crude culture supernatants using a magnetic stirrer. Ammonium sulphate salt was added pinch by pinch to ensure proper salting out of the protein. Saturation was determined by the salting out of the proteins in the medium; as the medium turned turbid indicating the precipitation of the proteins, addition of ammonium sulphate salt was then ceased. The percentage saturation was calculated using the unused amount of ammonium sulphate salt. To

further ensure proper salting out of the proteins the solutions were maintained at 4 °C overnight.

Centrifugation of the salt saturated solutions containing the precipitated proteins was carried at 4°C at 15000 rpm for a time duration of 10 minutes. The proteinaceous deposit obtained after centrifugation was resuspended in 20 mM phosphate buffer of pH 7.4 to avoid denaturation of the native structures of the proteins and maintained at 4 °C for further purification.

3.5.2 Membrane Dialysis of the precipitated proteins

Membrane dialysis is a separation technique based on the principle of diffusion that facilitates the removal of small, unwanted compounds from macromolecules in solution by selective and passive diffusion through a semi-permeable membrane. The smaller molecules of salt that caused the precipitation of the proteins can permeate out of the membrane into the dialysate of lower concentration thereby increasing the purity of the protein to acceptable levels.

The dialysis membrane was activated as follows: Desired lengths of the Dialysis membrane-150 (Himedia, India) was cut and boiled in 1 mM of Ethylenediaminetetraacetic acid (EDTA) solution for a time duration of 8 minutes to ensure unclogging of the membrane pores and its activation. The membrane tubing was rinsed several times with deionized water and carefully handled after activation to avoid clogging of pores which could possibly hinder the dialysis process.

Dialysis of the bacterial proteins obtained from the precipitation of the crude supernatants was carried out in a large beaker containing 0.2 mM of 2 L phosphate buffer as the dialysate. The dialysate was changed 5 times at regular intervals to ensure attainment of equilibria. The proteinaceous samples obtained as mentioned in section 3.4.2 were packed in the activated dialysis membrane in a leak proof manner and the packed membranes were immersed in the dialysate for the removal of excess salt. The dialyzed samples were further subjected to reverse osmosis for the concentration of proteins.

3.5.3 Reverse Osmosis

The dialyzed sample contains excess of water molecules that enter the membrane during the dialysis. To concentrate the dialyzed samples, the dialysis

membrane containing the sample was placed in high molecular weight PEG (poly ethylene glycol) hygroscopic compound instead of ordinary dialysate for the removal of excess of water in the sample during the osmotic swell of the sample by dialysis.

3.5.4 Determination of molecular weight of the bacterial proteins by SDS-PAGE

SDS PAGE is the most popular biochemical method of determining the molecular weight of the proteins (Lamelli, 1970). To identify the proteins responsible for the biosynthesis of AgNPs and TiO_2-NPs, the processed protein samples (obtained after reverse osmosis) from culture supernatant of each isolate and the broad range marker (Genei, India) were subjected to SDS PAGE with a stacking gel composition of 6% and a resolving gel composition of 15%. The molecular weight of the proteins present in each of the bacterial cell free culture supernatant were determined by using Alphaimager MINI (Protein Simple, Japan) Gel documentation Instrument. The composition of the gels and buffer used for SDS PAGE is mentioned in Appendix VI.

3.6 Characterization of AgNPs and TiO_2–NPs synthesized using plant and bacterial based sources

3.6.1 Preparation of nanoparticles sample for characterization

The synthesis mixtures containing the nanoparticles were centrifuged at 15000 rpm for 20 min at 4 ºC (Kubota-6930, Japan). The AgNPs synthesized by using plant leaf extracts were washed twice with 70% ethanol, dried in a hot air oven overnight at 130^oC.

For AgNPs and TiO_2-NPs synthesized using the bacterial isolates, the pellet obtained after centrifugation was washed twice with deionized water to remove any contaminants and then dried. The dried powder of nanoparticles was used for characterization by XRD, SEM, TEM, EDS, DLS, Zeta potential analyzer and FTIR.

3.6.2 XRD Analysis

In order to determine the crystallographic nature and the crystallite size of the nanoparticles synthesized in the study, X-Ray diffractograms of the nanoparticles were obtained using the X-Ray Diffractometer (JEOL, Japan), operated at Cu kα 1.5418 Aº, at 30 kV voltage and current at 20mA and at a scan speed of 2 nm with a step size of 2° over the range of 2θ values from 20° to 80°. Crystallographic details

corresponding to the XRD peaks were determined using respective Joint Committee on Powder Diffraction Standards (JCPDS) data cards.

The average crystallite size of the nanoparticles was calculated using Full width at half maximum data through Scherrer's Formula given in Eq. (3.1):

$$D = \frac{K\lambda}{\beta_{\frac{1}{2}} cos\theta} \qquad \text{........ (3.1)}$$

The equation uses the reference peak width at angle θ, where λ is the X-ray wavelength (1.5418 A°), $\beta_{1/2}$ is the width of the XRD peak at half height and K is a shape factor (0.9).

3.6.3 SEM and EDS Analysis

The dried AgNPs powder was drop coated onto carbon tapes and gold sputtered (JFC- 1600 Auto fine coater, JEOL, Japan) twice before carrying out the analysis.

Scanning electron microscopy and EDS analysis of the nanoparticles was performed (JEOL-6807, Japan) and the SEM images were obtained at suitable magnifications at the operating voltage of 20 kV, to determine their morphological characteristics such as size and shape using Image J analyzer software. Elemental composition of the nanoparticles was obtained by EDS analysis.

3.6.4 FTIR spectroscopy analysis

In order to identify the functional groups present on the synthesized nanoparticles and to determine the involvement of various reducing and capping agents in the synthesis, FTIR analysis of the nanoparticle samples was performed and the spectra was recorded using Avatar 360 IR spectrophotometer in the range of 4000-400cm^{-1}.

3.6.5 Particle size analysis by DLS technique and zeta potential analysis

The DLS technique represents the particle size as a hydrodynamic diameter while particle size distribution is based on scattering intensities of the incident laser light. The scattered light undergoes either constructive or destructive interference by the surrounding particles (Merkus, 2009).

The colloidal solutions of the synthesized nanoparticles of concentration 0.1 mg/mL were prepared in HPLC grade water in dust free conditions. The sample was analyzed for particle size distribution using Zetasizer NZ-100 instrument (Horiba, Japan) in the scattering light intensity mode at an angle of 173º at 25 ºC holding temperature. Zeta potential values of the colloidal samples were also measured under the same conditions with an electrode voltage of 3.3 V.

3.6.6 Transmission electron microscopic (TEM) analysis

TEM is a standard and conventional tool for the analysis of nanomaterials. The nanoparticles were suspended in 10 mL of suitable solvent (methanol for nanoparticles synthesized using plant resources and ethanol for those synthesized using bacterial sources) and sonicated to ensure uniform dispersion, drop coated onto carbon coated copper grids (200 square mesh size), dried under dust free conditions and analyzed using TEM (JEOL JEM 2100 F TEM, Japan) at an accelerating voltage of 200 kV to obtain a better insight into the morphological characteristics using Image J analyzer software.

3.6.7 Studies on the stability of AgNPs synthesized using the plant leaf extracts and cell free culture supernatants of the isolated bacteria

The colloidal solution of AgNPs synthesized in the present study was prepared in deionized water with concentration of 0.1 g/ mL. Spectral analysis of the prepared colloidal solution of AgNPs was performed over the time duration of 6 months using a dual beam UV-Vis Spectrophotometer (Labomed, USA) at resolution of 1 nm from 350 to 700 nm and the spectral characteristics were observed for any possible changes indicating the stability of AgNPs.

3.6.8 Determination of Band Gap energy of TiO$_2$-NPs synthesized using the cell free culture supernatant of the isolated bacterial strains

In the present study the band gap of the TiO$_2$-NPs was determined using two different methods.

For both the methods; a colloidal solution of 0.1 g/mL of TiO$_2$-NPs in deionized water was prepared. 3 mL of this colloidal solution was taken in a clean quartz cuvette with deionized water as a blank and the absorbance of the colloidal

solution was measured at a scan range of 200 nm to 800 nm with a scan speed of 1 nm using UV-Vis Spectrophotometer (Labomed, USA). The spectral data in terms of absorbance was plotted and further used for the determination of the band gap energy values.

Method A (Dharma and Pisal, Perkin Elmer, 2012)

In this method, on the absorbance spectrum, the point of strong cut-off was identified by drawing tangents to the two distinct regions of the curve. The value of the wavelength corresponding to the cut off (λg) was further substituted in Eq.3.2 to obtain the band gap energy.

$$\text{Band Gap Energy (E}_g) = \frac{hC}{\lambda g} \qquad \dots\dots\dots \text{(Eq.3.2)}$$

Where h = Planks constant = 6.626 x 10^{-34} Js, C = Speed of light = 3.0 x 10^{8} ms^{-1}, λg = Cut off wavelength (nm)

Method B (Ghobadi et al. 2013)

In this method, using the spectral data of the nanoparticles, a plot of $\left(\frac{Abs(\lambda)}{\lambda}\right)^{1/m}$ against $\frac{1}{\lambda}$ was plotted, where m is the index which can have different values of 1/2, 3/2, 2, and 3. The value of m for which the plot exhibited the best linear fit was chosen and the linear portion of the curve was extrapolated to the X-axis to obtain the value of λ_g corresponding to $\left(\frac{Abs}{\lambda}\right)^{1/m}$ =0. The value of band gap energy in electron volt was calculated by using the Eq. 3.2.

3.7 Application of AgNPs

The antibacterial and sensor application potential of AgNPs and the photocatalytic application potential of TiO_2-NPs synthesized in the present study by biobased methods were evaluated and compared with those of chemically synthesized nanoparticles. AgNPs, chemically synthesized by citrate reduction and capping method and Degussa P-25, commercially available TiO_2-NPs were used for comparison of the nanoparticles synthesized in the present study in terms of their application potential. The citrate reduction method for the synthesis of AgNPs is provided in Appendix VII in detail.

3.7.1 Antibacterial and sensor application studies of the AgNPs synthesized using plant and bacterial sources

3.7.1.1 Evaluation of antibacterial activity of AgNPs by Agar well diffusion method

Antibacterial activity of the AgNPs synthesized using of the plant leaf extracts of *T. catappa* and *T. grandis* Linn F and the bacterial cell free culture supernatants of strains 4S1, 4S2, 4S3, 6S1 and 8S1 were tested using agar well diffusion technique (David et al., 2010). Sterile Mueller Hinton (MH) agar plates were swabbed with 10^8 CFU/mL (0.5 Mac Farland) culture solutions of water borne pathogens, *S. aureus* (NCIM No. 5021;ATCC- 25923) and *E.coli* (NCIM No. 2350; ATCC No. 8134) strains. A well was punched into the Mueller Hinton agar plates. The antimicrobial activity of the AgNPs synthesized in the present study and those of chemically synthesized AgNPs were evaluated as follows.

50µL colloidal solution of the AgNPs with a concentration of 1g/L was prepared. The AgNPs were uniformly dispersed in the solution by sonication (5 min at 28±2ºC) and the solution was further dispensed carefully into the wells punched in the agar plates with the test pathogens. These plates were incubated at 35ºC for 24 h to observe the ZOI and measured.

3.7.1.2 Evaluation of antibacterial activity of AgNPs by determination of MIC

In order to determine the antibacterial activity of AgNPs quantitatively in terms of their MIC on *E. coli* or *S. aureus* strains, broth macrodilution method (Wanger et al. 1995) was used. Culture strains of *E. coli* and *S. aureus* (Mc Farland-0.5 standard) in MH broth were prepared. The stock colloidal solution of AgNPs of 102.4 1 µg/mL concentration in sterilized MH broth was suitably diluted with the liquid media containing the test pathogen to prepare the suspensions with AgNP concentrations ranging from 51.2 µg/mL, 25.6 µg/mL, 12.8 µg/mL, 6.4 µg/mL, 3.2 µg/mL, 1.5 µg/mL, 0.8 µg/mL, 0.4 µg/mL to 0.2 µg/mL. These suspensions were incubated at 120 rpm in a rotary shaker at 30 ºC for 24 h. The minimum concentration of AgNPs at which no visual growth was observed was indicative of MIC of the AgNPs. Thus, the minimum concentration of AgNPs at which the bacterial growth was completely inhibited was noted as the MIC value. The MIC of the AgNPs

synthesized in the present study and those of chemically synthesized AgNPs were evaluated

3.7.1.3 Antibacterial activity of AgNPs coated on cotton fabric

To evaluate the efficacy of AgNPs as an antibacterial coating upon cotton fabric, cotton swatches were coated with the AgNPs The method reported by Sathishkumar et al. (2010) was adopted for coating of cotton fabric with AgNPs.

White cotton fabric material was purchased from a local textile shop in Surathkal, Karnataka, India and washed in distilled water, dried in dust free conditions to eliminate any dust or contaminant. The dried fabric material was then cut into several swatches measuring 1cm x 1cm. The swatches were then sterilized by autoclaving them at 15 psi for 20min at 121° C.

The pre-sterilized cotton fabric swatches were separately coated with 50 μL of AgNP colloidal solution of 0.1 mg/mL concentration under aseptic conditions by drop coating. The individual drop coated swatches were further placed onto Mueller Hinton agar plates that were previously swabbed with 10^8 CFU/mL (0.5 Mac Farland) culture solutions of water borne pathogens, S. *aureus* and *E.coli.* A cotton fabric swatch without any AgNPs was used as a control.

These plates were incubated at 35^oC for 24-48h and observed for the appearance of the zone of inhibition formed around the cotton swatches coated with AgNPs. The antibacterial effect of AgNPs synthesized by plant based and bacterial based synthesis routes were compared with those of chemically synthesized AgNPs in terms of ZOI when coated on cotton fabric.

3.7.1.4 AgNPs as colorimetric sensors for mercury

The mercury sensing property of AgNPs synthesized in the present study was evaluated and compared with that of chemically synthesized AgNPs. A colloidal solution of the AgNPs was made with deionized water (0.1 mg/mL). Mercuric chloride solution was prepared at a concentration of 1 mg/mL. 10 μl of the $HgCl_2$ solution was consecutively added to 3 mL of the AgNP colloidal solution and spectra were obtained after each addition of $HgCl_2$ solution, using UV-Vis spectrophotometer by scanning in the wavelength range of 200-800nm a scan speed of 1 nm/s. The

addition of HgCl$_2$ was stopped when the colour of the AgNPs colloidal solution turned colourless.

The absorbance at the wavelength of absorbance maxima vs. Hg^{2+} content in the colloidal suspension of AgNPs were plotted and linearity of the plot was tested. The maximum detectable level of Hg^{2+} by AgNPs was determined by addition of Hg^{2+} ions to the colloidal solution till the solution turned colourless and no SPR peak was observed, followed by the calculation of the total amount of Hg^{2+} added.

The minimum detectable level was determined by preparing a working solution of 0.1 mg/mL of HgCl$_2$ and 10 µL of the solution was consecutively added to 3 mL of colloidal solution of AgNPs (0.1 mg/mL) and the SPR peak obtained after each addition of HgCl$_2$ solution was analyzed to detect for any change in the spectral peak of the AgNPs being evaluated. Maximum amount of Hg^{2+} ions addition that brought about reduction in the intensity of the SPR peak along with blue shift indicated the minimum detectable level of Hg^{2+} by AgNPs.

3.8 Application of TiO$_2$-NPs

3.8.1 Photocatalytic activity of the TiO$_2$-NPs synthesized using the cell free culture supernatant of the isolated bacterial strains

The photocatalytic efficacy of TiO$_2$-NPs synthesized using the cell free culture supernatants of the isolated bacterial strains was tested in terms of degradation of two model organic dye compounds; Acid Blue 129 (AB 129) and Remazol Brilliant Blue R (RBB) dye.

3.8.1.1 Preparation of aqueous dye solutions and analysis of the dyes
Preparation of aqueous dye solutions

100 mg/L of stock dye solution of AB 129 was prepared by dissolving 0.04 g of AB 129 dye (Purity- 25%) in distilled water to make upto 100 mL . 100 mg/L of stock solution of RBB dye was prepared by dissolving 0.022 g of RBB dye (Purity- ~50%) in distilled water to make upto 100 mL. Required concentrations of the dye solutions were prepared by suitably diluting the stock solutions with distilled water.

Analysis of dyes

The dye concentrations in the aqueous samples were analyzed by measurement of the absorbance of the solutions at the corresponding wavelengths (at

629 nm for AB129 and at 592 nm for RBB) using dual beam UV-Vis spectrophotometer (Hitachi, UV-160A) and then by obtaining the corresponding concentration from the calibration plot.

3.8.2 Photocatalysis experiments

Batch photocatalysis experiments using the extracellular TiO_2-NPs synthesized using the cell free culture supernatant of the isolated bacterial strains for the degradation of AB 129 and RBB dyes were conducted to study their efficacy as potential photocatalysts. The photocatalysis experiments were performed under UV as well as visible light irradiation. The photocatalytic efficacy of the TiO_2-NPs synthesized using the biobased routes was compared with those of commercially available, chemically synthesized TiO_2 (Degussa P-25) nanoparticles in terms of degradation of the dyes.

3.8.2.1. Photocatalytic degradation of dyes in batch stirred reactor

The experimental setup for carrying out photocatalysis of the dyes is shown in Fig 3.1. A borosilicate glass reactor was used for the batch photocatalysis experiments. The reactor contents were stirred continuously during the photocatalysis using a magnetic stirrer which could facilitate the homogenous mixing of the reaction mixture. Air was continuously bubbled through the reactor contents, at a flow rate of 2 LPM. The reactor was placed equidistant from the two lamps, each mounted vertically on the side walls of an aluminium chamber used as an enclosure for the reactor. The lamps were held in a holder at a distance of 22 cm apart. The aluminium chamber was of dimensions 40 cm×70 cm×70 cm. To maintain a constant temperature in the reactor, an exhaust fan was fitted on top of the chamber to drive out the heated air. For experiments under UV irradiation, two numbers of 18 W UV lamps (wavelength, $\lambda = 365$ nm, Philips) were used. The lamps are specified to radiate 80 % UV-A and 20 % UV-B light. The same experimental setup was used for visible light photocatalysis studies wherein the UV lamps were replaced with two 18 W visible light lamps (Percolate Gold, Mysore lamp) of similar dimensions.

UV light intensity on the reactor walls was measured using a UV light intensity meter (model: UV-340A, Lutron). An average UV light intensity of 5.85 mW/cm^2 was found at the reactor walls. The visible light intensity was measured

using LUX meter (KM-LUX-100K) and the average intensity was found to be 84.7×10^3 Lux.
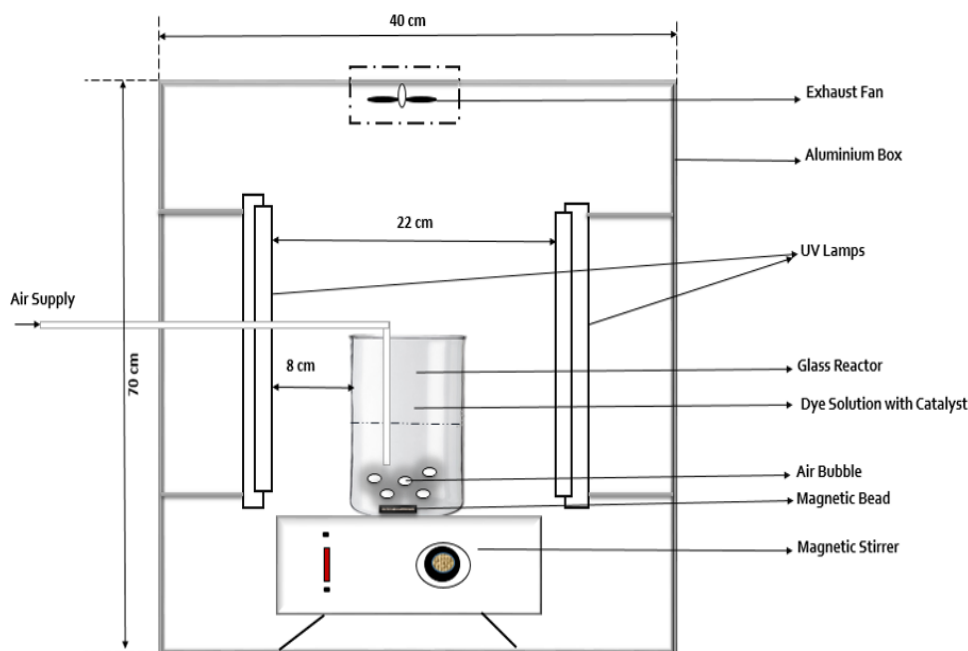
Figure 3.1 Schematic diagram of the stirred batch reactor.

Experimental procedure

Batch photocatalytic degradation experiments were performed in a batch stirred reactor for photocatalytic degradation of the dyes with TiO_2-NPs synthesized in the present study under UV or visible light irradiation. In all the experiments 100 mL aqueous dye solution with the required concentration of the dye, containing appropriate quantity of the photocatalyst was used. Initial pH of the solution was adjusted to a required value by adding 0.01 N NaOH or 0.01 N HNO_3 and by measuring the pH with a pH meter (Equip-Tronics model no.EQ-610). Aqueous dye solutions were magnetically stirred and air supply was provided. Each batch experiments were performed for a period of 80 minutes. At regular intervals 1.5 mL of the samples were withdrawn and made upto 3 mL and centrifuged at 15000 rpm for 10 min at 25ºC to separate the nanoparticles and the supernatant was used for the analysis of dye concentration according to the methodology described in section 3.8.1.1. Percentage degradation of the dye was calculated using the following Eq. 3.3

$$Perccentage\ dye\ degrdation = \frac{Co - Cf}{Co} \times 100 \qquad ...\ Eq.\ 3.3$$

Where Co = Initial concentration of the dye in the reaction mixture and Cf = Final concentration of the dye in the reaction mixture after time 't'. The procedures for calibration of the spectrophotometer, calibration data and calibration plot with the corresponding equation for both the dyes are presented in Appendix VII.

The studies carried out in batch stirred reactor, the experimental conditions such as initial dye concentration, initial pH and the catalyst loading used in the study are presented in Chapter 4 along with the results and discussions.

3.8.2.2 Photocatalytic degradation of dyes in immersion well quartz reactor under UV light irradiation

Batch photocatalysis experiments were also carried out for the degradation of dyes using TiO_2-NPs in an immersion well photochemical reactor (Scientific Aids and Instruments Corporation, Chennai, India). The experimental reactor is shown in Fig 3.2. It consists of a double walled immersion well made of quartz (IWQ1), which houses the 80 W UV lamp (80 W medium pressure mercury vapour that radiate predominantly 365-366 nm radiation with smaller amounts in the wavelength of 265, 297, 303, 313 nm, as well as small amounts in the visible region). The Inlet and outlet tubes were provided in the annular space between the double walls of the immersion well for circulation of water for cooling of the reaction mixture to avoid rise in the reaction temperature.

The immersion well is placed inside a borosilicate cylindrical reaction flask of 150 mL volume (Model A/150), with a round bottom and the entire setup was placed on a magnetic stirrer to facilitate the homogenous mixing of the reaction mixture during the photocatalysis. The reaction flask consisted of two angle sockets and a vertical socket made of glass. Cooling water was circulated through the annular space in immersion well. Tubing for air supply was inserted into the reaction flask through one of the sockets on the wall of the reaction flask and air was supplied at 2 LPM. Samples from reaction mixture were withdrawn through a tube inserted into another socket on the reaction flask wall. The reactor content was irradiated with the 80 W UV lamp. The UV light intensity on the reactor walls was measured using UV intensity meter (model: UV-340A, Lutron) and average intensity was found to be 5.85

mW/cm^2. The entire immersion well photoreactor was housed in an aluminium chamber so as to protect the personnel from UV radiations and to avoid radiation loss.
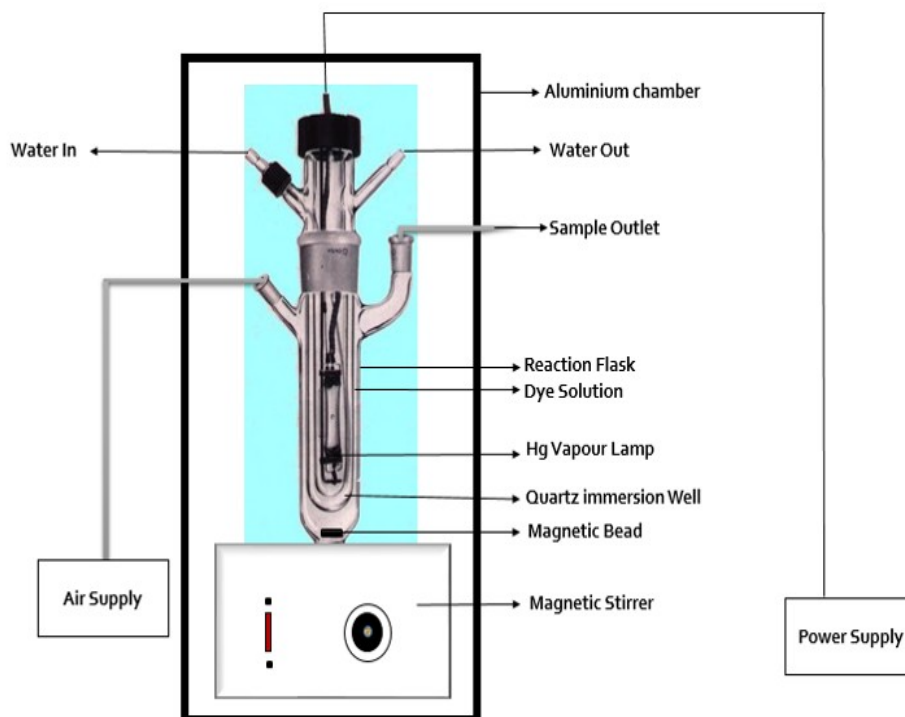
Figure 3.2 Schematic diagram of the immersion well UV light quartz photoreactor.

Experimental procedure

Batch photocatalytic degradation experiments were performed in an immersion well quartz photoreactor for photocatalytic degradation of the dyes with the 8S1-TiO$_2$-NPs under UV light irradiation. In all the experiments 100 mL aqueous dye solution with the required concentration of the dye, containing appropriate quantity of the photocatalyst was used. Initial pH of the solution was adjusted to a required value by adding 0.01 N NaOH or 0.01 N HNO$_3$ and by measuring the pH with a pH meter (Equip-Tronics model no.EQ-610). Aqueous dye solutions were magnetically stirred and air supply was provided. Control experiment with the above mentioned experimental conditions was performed in dark conditions. To determine the occurrence of any photodegradation of the dyes under UV light irradiation an experiment with the above mentioned experimental conditions was performed in the absence of photocatalyst. Each batch experiments were performed for a period of 2 hours.

At regular intervals, 1.5 mL of the sample was withdrawn from the reactor, made upto 3 mL and centrifuged at 15000 rpm for 10 min at 25ºC to separate the nanoparticles and the supernatant was analyzed for dye concentration according to the methodology described in section 3.8.1.1. Percentage degradation was calculated using Eq. 3.3.

The studies carried out in quartz reactor, the experimental conditions such as initial dye concentration, initial pH and the catalyst loading used in the study are presented in Chapter 4 along with the results and discussions.

3.8.2.3 Studies on photocatalysis

The studies on photocatalytic activity of TiO_2-NPs in the present research work involved the comparison of UV and visible light activity of TiO_2-NPs synthesized in the current study with that of Degussa P25 and choice of the bacterial based photocatalyst with the highest activity.

Studies on photocatalytic degradation of dyes in Quartz immersion well photoreactor with medium pressure mercury vapour lamp to test for the improvement in photocatalytic activity of the chosen photocatalyst (8S1-TiO_2-NPs) under high power irradiation.

Studies on photocatalytic degradation of dyes Quartz immersion well photoreactor to study the effect of various parameters such as–initial dye concentration, catalyst loading and initial pH of the reaction mixture affecting the photocatalysis with the chosen photocatalyst (8S1-TiO_2-NPs)

The experimental conditions such as initial dye concentration, initial pH and the catalyst loading used in these studies are presented in Chapter 4 along with the results and discussions

CHAPTER 4

RESULTS AND DISCUSSIONS

PART A

Plant based synthesis of AgNPs

4.1 Screening of plant material for the synthesis of AgNPs

In the present work, several plant resources were screened for the synthesis of AgNPs. Further, the effect of various parameters affecting the synthesis were studied and optimized. The plant resources that were screened in terms of their potency for the synthesis of AgNPs are mostly fruit peels and plant foliage that possess less commercial or agro economic value and which are readily available in surplus quantities.

As discussed in section 3.2.1 of Chapter 3 the following plant resources such as Leaves of cashew nut tree (*Anacardium occidentale*), Leaves of Amla (Gooseberry) fruit tree (*Phyllanthus embilica*), Plantain leaves (*Musa paradisiaca*), Teak leaves (*Tectona grandis* Linn.), Leaves of the Indian almond tree (*Terminalia catappa*), Leaves of Pongamia tree (*Milletia pinnata*), Leaves from Mango tree (*Mangifera indica*), exocarps of Pineapple fruit (*Ananas comosus*), Orange (*Citrus sinensis*) and Watermelon (*Citrullus lanatus*) were subjected to the screening studies for nanoparticle synthesis. These resources are abundantly available as the plants that provide these resources are abundantly grown in the tropical belt of South East Asia (Opeke, 1992) owing to the high demand for their commercial and high value nutritional products. The sources and the major classes of bioactive phytocomponents of these plant resources are presented in Table 4.1. The bioactive phytocomponents belonging to the class of Phenols, Antioxidants and Flavonoids present in these plant resources are known to possess the capability to reduce the precursor salt into AgNPs and simultaneously serve as capping agents (Khalil et al. 2014; Prarthna et al. 2011; Dubey, 2010; Satishkumar et al. 2009). The refuse generated after the commercial utilization of the plant resources for commercial products is in large proportions and these abundantly available wastes were harnessed for the synthesis of AgNPs.

AgNPs were synthesized by the reduction of $AgNO_3$, the precursor salt using the aqueous extracts of the plant resources as described in section 3.2.5 of Chapter 3. The aqueous extracts of the plant resources were prepared using open solvent heating method as described in section 3.2.3 of Chapter 3. AgNPs synthesis was carried out with synthesis mixture containing 1% extract (prepared using 1% w/v plant material powder suspension) and 1 mM $AgNO_3$ solution in 1:1 volume ratio. The potency of these plant resource extracts to synthesize AgNPs was tested through the appearance

of characteristic surface plasmon resonance (SPR) peak generated by metallic AgNPs in the colloidal synthesis solution as shown in Figure 4.1.

Table 4.1 Native plant, source and major classes of bioactive phytocomponents of various plant resources used in the study for synthesis of AgNPs

Native plant resource	Source	Major classes of bioactive phytocomponents
Anacardium occidentale (Cashew tree) leaves	Agrowaste	Phenols, Antioxidants, Flavonoids (Kuiters and Denneman, 1987. Konan and Bacchi, 2007 Kögel and Zech, 1985)
Ananas comosus exocarp peels (Pineapple) fruit	Food processing industry waste	Phenols and antioxidants, cellulose, hemicellulose and other carbohydrates(Rani and Nand, 2004)
Citrullus lanatus (Watermelon) Exocarp peels	Food industry waste	Antioxidants, Phenols and Citrulline (Tarazona-Díaz el al. 2011)
Citrus sinensis (Orange)exocarps	Food industry waste	Antioxidants, Phenols and Aromatic oils (Bocco et al.1998; Boelens and Jimenez, 1989)
Phyllanthus embilica/ Emblica officinalis (Amla) leaves	Agrowaste	Tannin, amlaic acid, astragalin, ellagic acid, gallo-tannin, kaempferol, kaempferol-3-o-glucoside, phyllantidine, phyllantine and rutin (Bajpai et al. 2005; Nain et al. 2012)
Mangifera indica (Mango) Leaves	Agrowaste	Steroids, flavonoid, reducing sugar anthraquinone, tannin and saponin, steroids (Aiyelaagbe and Osamudiamen, 2009)

Table 4.1 Continued…

Native plant resource	Source	Major classes of bioactive phytocomponents
Milletia pinnata (Honge) leaves	Agrowaste from Biodiesel industry	Antioxidants, flavonoids, Sterols, fatty acids (Chopade et al. 2008 and Raut et al. 2010)
Musa Paradisiaca (Plantain) leaves	Agrowaste	Lignins, proteins and pentosans, saponins, Antioxidant and phenols (Karuppiah and Mustaffa, 2013
Tectona grandis Linn f.(Teak) leaves	Timber industry waste	Quinones, Antioxidants, Flavonoids and Phenols (Kore et al.2011)
Terminalia catappa (Indian Almond) leaves	Agrowaste	Flavonoids- kaempferol, tannins, polyphenols and phenols (Owolabi et al. 2013; Chyau et al. 2002; Ko et al. 2002; Mau et al. 2003)

The UV-Vis spectroscopic analysis of the synthesis mixtures containing the aqueous leaf extracts of *Tectona grandis* Linn. F and *Terminalia catappa* showed the presence of characteristic peak of AgNPs centered at 420 nm as shown in Figure 4.1, indicating that these plant resources possessed necessary bioactive compounds in considerable quantities that contributed in the reduction of the precursor salt into metallic AgNPs. Hence, *Tectona grandis* Linn f. leaves and *Terminalia catappa* leaves were chosen for the synthesis of AgNPs.

The synthesis mixture containing the aqueous leaf extract of Pongamia tree (*Milletia pinnata*) did not reduce the $AgNO_3$ salt to AgNPs as a blue shifted peak centering at 244 nm was observed in Figure 4.1 indicating the presence of a plant bioactive phytocomponent rather than that of AgNPs, as the characteristic peak for AgNPs is generally centered at 420 nm.
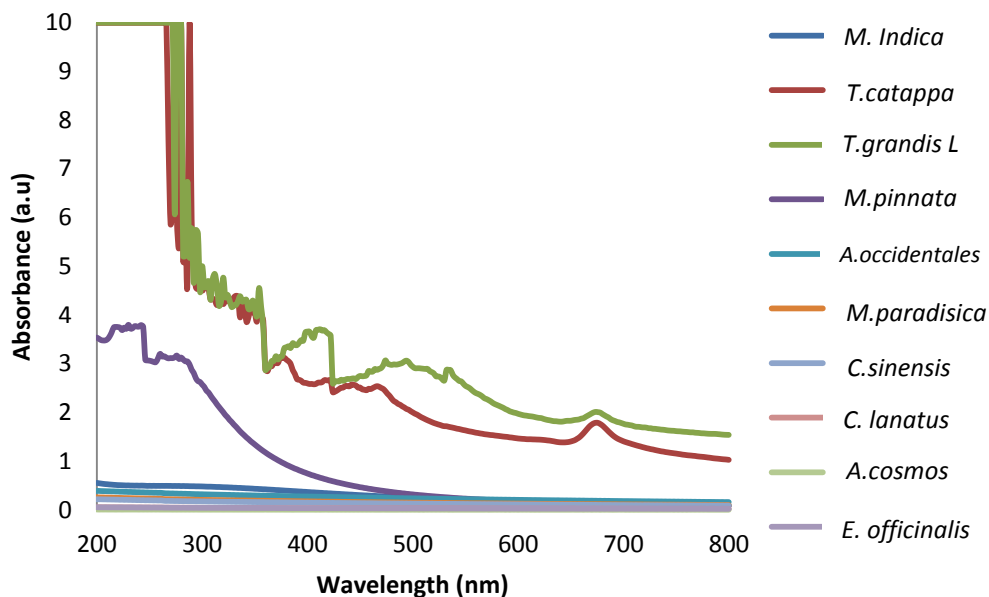
Figure 4.1 SPR spectra of synthesis mixture for AgNPs at 24 h obtained from different plant resources.

The synthesis mixtures containing the aqueous extracts of *Phyllanthus embilica* leaves, *Musa paradisiaca* leaves, *Mangifera indica l*eaves, exocarp of *Ananas comosus*, exocarp of *Citrus sinensis*, and Exocarp of *Citrullus lanatus* did not emit the characteristic SPR peak of AgNPs indicating that these plant resources did not contain plant bioactive phytocomponents in significant quantities to reduce AgNO$_3$ salt to AgNPs.These studies indicated that not all the plant resources used in the present study possess the required bioactive compounds with high reduction potential as that of *T.grandis* Linn f. and *T.catappa* leaves to reduce the precursor salt into AgNPs.

Tectona grandis. Linn (Teak) is a large deciduous tree, native of tropical Asia and the growing demand of it as the World`s premium hardwood has initiated several countries lying in the tropical belt to grow them in huge plantations. It is reputed as Sagwan (Hindi), Saka (Sanskrit) and teak tree (English).Teak tree being indigenous to Asia, accounts for almost 90% of the global teakwood supply. Consequently the proportion of foliage that forms the refuse of the timber industry is large.

Teak leaf extracts are found to contain Quinones such as tectoquinone, lapachol, deoxylapachol and its isomer, tectoleafoquinone, anthraquinone-napthaquinone pigment, steroidal compounds such as squalene, poly isoprene-a-tolyl

methyl ether betulinic acid, tectograndone, monoterpene, apocarotenoids such as tectoinols-A, tectoionols-B, glycosides such as anthraquinone glycosides, phenolic acids such as tannic acid, gallic acid, ferulic acid, caffeic acid and ellagic acid, flavonoids such as rutin and quercitin, saponins, proteins, calcium, phosphorous and dye (Kore et al.2011). Extracts obtained from teak leaves have demonstrated antioxidant activities, free radical scavenging properties (Rao et al.2011), diuretic and antibacterial property (Nidvani and Mahalakshmi, 2014). It can hence be affirmed that teak leaves are known to contain a repertoire of bioactive compounds that possess the strong ability to reduce the $AgNO_3$ salt to AgNPs.

Teak leaves are known for their high antioxidant value (Peteros and Uy, 2010) and the decoction of the leaves is used in Chinese therapeutic medicine; it also forms an ingredient in certain staple food delicacies of South East Asia (Kaosa-ard, 1981). These "reservoirs" of bioactive phytocomponents go untapped as the timber obtained from these trees is used for lumbering while the leaves end up as agrowaste. In the present study, the extract of *T.grandis* Linn F. leaves exhibited an ability to synthesize AgNPs. Owing to the abundant availability of teak leaves as an agrowaste, they form a suitable plant bioresource for the synthesis of AgNPs.

Terminalia catappa, a large tropical tree belonging to the *Combretaceae* family is a native of Asia, northern Australia and tropical America. Huge plantations of the tree have been cultivated for harvesting seeds (Almonds). *Terminalia catappa* is popularly known as Indian almond tree (English). The leaves are known to contain several bioactive components like flavonoids- kaempferol, tannins, polyphenols and phenols (Owolabi et al. 2013; Chyau et al. 2002; Ko et al. 2002; Mau et al. 2003) Therefore it can be deduced that these bioactive compounds may be responsible for the reduction of the precursor salt into AgNPs. The leaves of the Indian almond tree have been reported as a folk remedy (Chen et al. 2000) for various skin diseases in medicine (Fan et al. 2004; Gao et al. 2004) and also widely reported in the breeding of Betta fish which require tannin rich and acidic water.

Commercial exploitation of the tree for the sake of its high nutritional value seeds has led to wide spread cultivation of these trees. Leaves of the tree remain as an unharnessed reservoir of various bioactive compounds; the seeds are harvested for their high commercial value as a dry fruit and as oil source. These "bioreservoirs" of

active components go untapped as the leaves are shed off from the tree naturally, during the fall season. As the aqueous extract of *T.catappa* leaves exhibited an ability to synthesize AgNPs (Figure 4.1) the potency of these leaves can be steered towards the route of biobased synthesis of AgNPs.

The plants *T. grandis* Linn f. and *T. catappa* were classified by The Principal Scientist of Dr. Shivram Karantha Pilikula Nisarga Dhama, Mangalore, India; based on the identification of vegetative and fruiting bodies. The herbarium for both the plant materials were prepared and preserved. The herbarium certifications are furnished in Appendix X.

4.2. Parameters influencing plant based synthesis of AgNPs

Potential use of AgNPs for various applications depends on their morphological and physiochemical characteristics, presence of capping agents on the nanoparticle surface, yield of the nanoparticles and their dispersion. Thus these are the determining factors during the synthesis. Therefore, an exquisite control of size, composition, morphology, stability and environmental friendly synthesis are the features that are desirous of a 'given method' of synthesis (Basavaraja et al. 2008). The influence of various physical parameters such as the time required for the synthesis of AgNPs, concentration of the leaf powder suspension used for preparation of aqueous extracts of plant leaves for the synthesis of AgNPs, concentration of precursor salt solution, volume ratios of the aqueous leaf extract to the precursor salt solution, pH of the synthesis mixture and the method of extraction of plant bioactive phytocomponents from the plant resource influences the morphological and physiochemical characteristics of the nanoparticles being synthesized (Jagtap and Bapat; 2013; Vanaja et al. 2013; Christensen et al. 2011; Guidelli et al. 2011; Badawy et al. 2010; Dwivedi and Gopal, 2010; Song and Kim, 2008; Noguez et al. 2007).

Thus in the present study the effect of these parameters on the conversion of Ag^+ ions and characteristics of AgNPs synthesized using the aqueous leaf extracts of *T.catappa* leaves and *Tectona grandis*. Linn f. were studied.

4.2.1 Influence of reaction time on the synthesis of AgNPs using aqueous extracts of *T.catappa* leaves and *T. grandis.* Linn f. leaves

The synthesis of AgNPs proceeds with the reduction of the precursor salt ($AgNO_3$) by the bioactive phytocomponents of the extract which are present in the synthesis mixture. The number and characteristics of AgNPs synthesized depends on the reaction time provided. The AgNPs were synthesized using aqueous extracts of the plant leaves according to the methodology described in section 3.2.5 of Chapter 3 using 1% ALE or TLE and 1 mM $AgNO_3$ solution in 1:1 volume ratio. The detailed method is presented in section 3.2.7.1 of Chapter 3.

A) Synthesis of AgNPs using ALE

The effect of reaction time on the synthesis of AgNPs was studied by analysing the SPR spectra of the synthesis mixture at various time periods during the synthesis of AgNPs using the aqueous extracts of *T.catappa* leaves (ALE). The characteristic brown colour of the AgNPs appeared after 1 h of reaction time. The colour intensity increased over a period of around 24 h. However no visibly noticeable change in colour intensity occurred after 24 h. Figure 4.2 (a) and Figure 4.2 (b) presents the photograph of the synthesis mixture at the start of the synthesis and after 24 h of synthesis time duration due to formation of AgNPs respectively indicating the change in colour from yellow to dark brown.

(a)   (b)
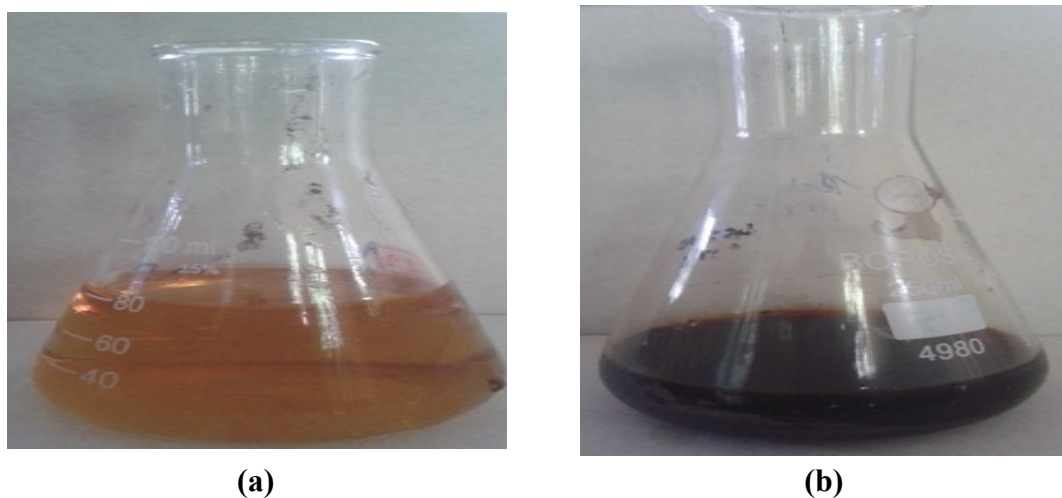
Figure 4.2 (a) Synthesis mixture with ALE at the start of the synthesis, (b) Synthesis mixture with ALE characteristic of AgNPs at 24 h
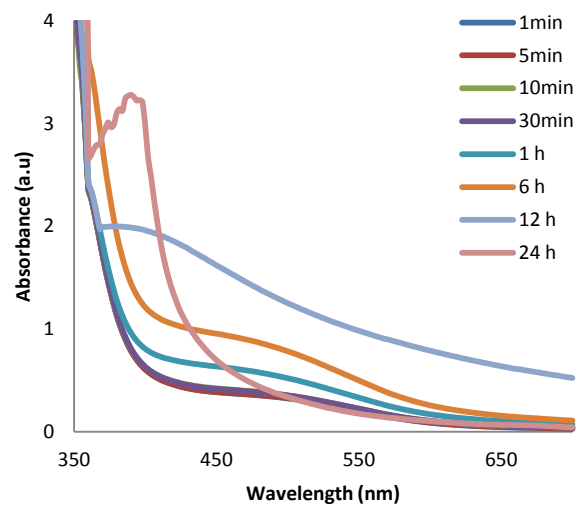
Figure 4.3 SPR spectra of synthesis mixture for AgNPs as a function of time. Synthesis mixture containing 1% ALE and 1mM AgNO$_3$ in 1:1 volume ratio.

Figure 4.3 depicts the SPR spectra of the synthesis mixture at various time periods of reaction during the synthesis of AgNPs carried out with 1 % ALE and 1 mM AgNO$_3$ solution in 1:1 volume ratio. As observed in Figure. 4.3, the SPR peak characteristic of AgNPs did not appear upto 1 h of synthesis time. SPR peak characteristic of AgNPs appeared at around 450 nm wavelength range after 1 h of synthesis time. The intensity of the peak was found to increase with time indicating that the number of Ag$^+$ ions being reduced to Ag^0 by the bioactive phytocomponents present in the leaf extract and subsequent formation of AgNPs increase with the passage of reaction time period (Rodríguez-León et al. 2013; Darroudi et al. 2012; Guidelli et al. 2011). The highest intensity of the SPR peak occurred at 24 h of the synthesis time indicating that, 24 h of reaction time is required for the conversion of the Ag$^+$ ions present in the synthesis mixture to Ag^0 or all the bioactive components in 1% ALE required for the reduction of Ag$^+$ ions exhausted in the synthesis mixture over a time period of 24 h. Through this study it can be concluded that the time required for the maximum conversion of Ag$^+$ ions into Ag^0 in the synthesis mixture containing 1% ALE and 1 mM AgNO$_3$ solution in 1:1 volume ratios is 24 h.

B) Synthesis of AgNPs using TLE

The reaction time duration required to achieve maximum conversion of Ag^+ ions into Ag^0 in the synthesis mixture for the formation of AgNPs by the aqueous extract of *T.grandis* Linn f leaves (TLE) was also determined through SPR analysis of the synthesis mixture at various reaction time periods. The colour of the medium changed from light brown to dark brown due to the formation of AgNPs in the synthesis mixture containing 1% TLE and 1 mM $AgNO_3$ solution in 1:1 volume ratio at the end of 24 h of synthesis time as shown in Fig 4.4 (a) and 4.4 (b). The colour intensity increased over a period of around 24 h. No change in colour intensity was visible after 24 h.
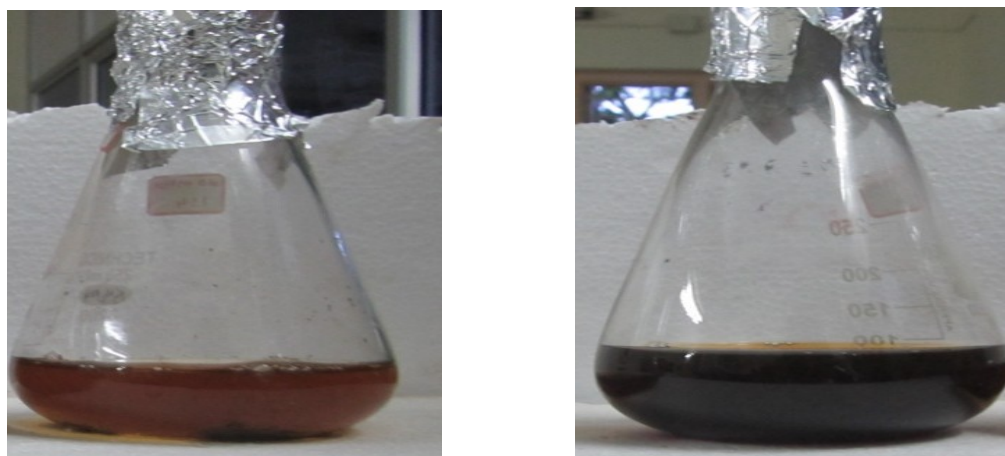
Figure 4.4 (a) Synthesis mixture with TLE at the start of the synthesis, (b)Synthesis mixture characteristic of AgNPs at 24 h
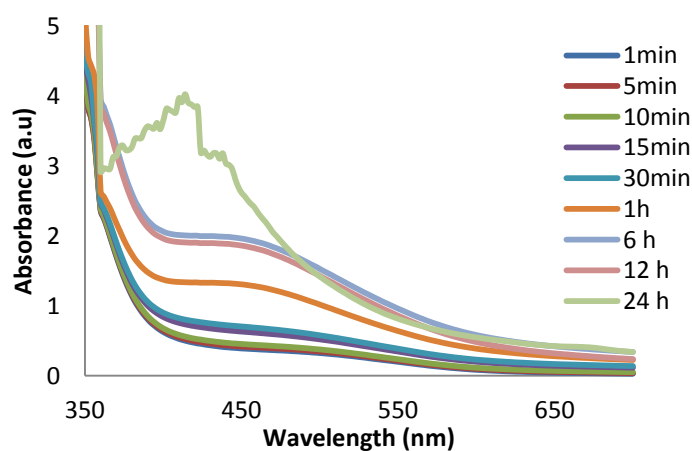
Figure 4.5 SPR spectra of synthesis mixture for AgNPs as a function of time. Synthesis mixture containing 1% TLE and 1mM $AgNO_3$ in 1:1 volume ratio

Figure 4.5 shows the SPR spectra of the synthesis mixture at various time periods of reaction during the synthesis of AgNPs. The results were found to be in similar lines with those obtained with ALE. The analysis of the spectra showed that the maximum conversion of Ag^+ ions into Ag^0 leading to the formation of AgNPs in the synthesis mixture containing 1% TLE and 1 mM $AgNO_3$ solution in equal volume ratios require a reaction time duration of 24 h as indicated by a peak of highest intensity at 414 nm. Thus for further studies on the optimization of synthesis parameters, the synthesis of AgNPs with ALE and TLE were carried out for a reaction time period of 24 h.

4.2.2 Effect of concentration of leaf powder suspension used for the preparation of aqueous extracts of the plant leaves on the synthesis of AgNPs

The concentration of bioactive components which possess the ability to reduce Ag^+ ions in the synthesis mixture is an important parameter that determines the reduction of Ag^+ ions to Ag^0 and thus the yield of nanoparticles. The concentration of bioactive components present in the synthesis mixture in turn depends on the amount of leaf powder used to prepare the extract, if other factors such as extraction conditions, concentration of $AgNO_3$ solution, and volume ratio of the extract to the leaf extract used in the synthesis mixture and initial pH are maintained constant.

To evaluate the influence of concentration of leaf powder suspension used for preparation of aqueous extracts of the plant leaves on the synthesis of AgNPs, ALE and TLE were prepared by open solvent heating extraction method using 1%, 5% and 10% concentrations of leaf powder suspension. The extraction was carried out using water as a solvent as described in Section 3.2.3 of Chapter 3. The synthesis of nanoparticles was carried out as described in Section 3.2.5 of Chapter 3, using these extracts in synthesis mixture containing equal volumes of the extract and 1 mM $AgNO_3$ solution. The detailed method is presented in section 3.2.7.2.

A) Synthesis of AgNPs using ALE

The synthesis of AgNPs was monitored by the spectral analysis of the synthesis mixture. The UV-Vis spectra showing the SPR peak generated by the colloidal AgNPs synthesized using the synthesis mixture containing the extracts prepared with different concentrations of leaf powder suspensions and 1 mM of

precursor salt solution at the synthesis time period of 24 h is shown in Figure 4.6. Table 4.2 presents the conversion of Ag^+ ions to AgNPs obtained after 24 h of synthesis time period with different concentrations of leaf powder suspensions. The aqueous leaf extract prepared using 1%, 5% and 10% concentration of *T.catappa* leaf powder suspension is hereafter referred as 1%, 5% and 10% ALE respectively.
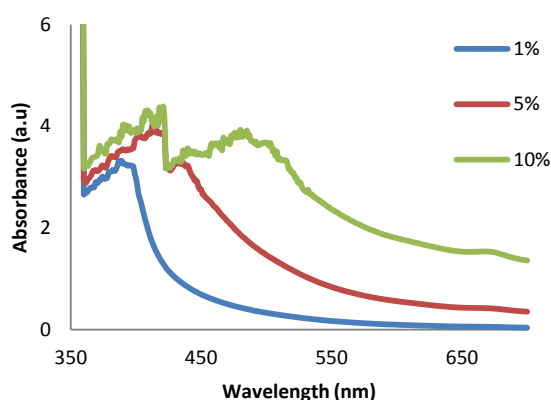
Figure 4.6 SPR spectra of synthesis mixture of AgNPs at 24 h. Synthesis mixture containing 1%, 5% and 10% ALE and 1 mM AgNO₃ solution in volume ratio of 1:1.

As observed in Figure 4.6 the SPR peak generated by AgNPs from the synthesis mixture containing 1% ALE and 1 mM of precursor salt solution in equal volume ratio is blue shifted towards 380 nm indicating the reduction of the precursor salt into silver nuclei with a conversion of 79.81% (Table 4.2). The blue shift of the SPR peak from the characteristic wavelength of 420 nm indicates the formation of smaller sized AgNPs (Rodríguez-León et al. 2013; Guidelli et al. 2011; Noguez et al. 2007; Abe et al. 1982). The SPR peak of AgNPs being synthesized is highly influenced by their shape, size and the dielectric constant of the medium (Stamplecoskie and Scaiano, 2010; Stepanov, 1997). The SPR peak of the synthesis mixture prepared with 1% ALE (Figure 4.6) is sharp but with lower intensity than that with 5% ALE indicating that lesser number of smaller sized AgNPs were formed with ALE from the lowest concentration of leaf powder suspension. The amount of bioactive phytocomponents such as polyphenols, flavonoids and antioxidants present in the synthesis mixture containing ALE prepared from 1% leaf powder suspension, which serve as reducing agents is inadequate to bring about complete reduction of Ag^+ ions to Ag^0, thus resulting in lesser number of AgNPs synthesis as indicated by

the least   SPR peak intensity. These results are also supported by the lowest conversion of 79.81 % of Ag^+ ions (Table 4.2) obtained with 1% ALE.

The SPR peak at 420 nm emanated by the AgNPs synthesized using 5% ALE is also sharp, narrow and with higher intensity as compared to that with 1% ALE. The red shifted higher intensity peak with similar sharpness as that with 1% ALE signifies the formation of large number of monodispersed AgNPs with larger particle size (Bindhu and Umadevi, 2013; Oluwafemi et al. 2013; Zheng et al. 2007). The conversion of Ag^+ ions to Ag^0 obtained using 5% ALE is 89% and higher than that obtained with 1% ALE, which is in agreement with the results obtained from the SPR studies. The SPR peak intensities increased with the increase in concentration of leaf powder suspensions used for the synthesis of AgNPs and such an increase in SPR peak intensities is due to increase in the number of nanoparticles formed. (Prarthna et al. 2011a; Šileikaitė et al, 2009). The synthesis mixture containing 10% ALE along with 1 mM of precursor salt solution in equal volume ratio yields a broad, intense and red shifted SPR peak as compared to the SPR peaks of AgNPs synthesized using 1% ALE and 5% ALE. The SPR peak is broader and a split is observed in case of 10% ALE. The red shift of the SPR peak observed with 10% ALE indicates the formation of larger sized nanoparticles wherein the surface electrons of the particles upon excitation by the incident electromagnetic field radiate energy in all directions and lose their energy due to secondary scattering, this results in the damping effect and yields a redshifted, and wider SPR band (Zhang and Noguez, 2008). As the formation of a large number of AgNPs occurs in the synthesis mixture, the particles aggregate and the conduction electrons near each particle surface becomes delocalized and shared amongst the neighbouring particles resulting in the plasmon coupling. The decreasing interparticle distance and the increasing size of the aggregates determines the extent to which the SPR redshifts. The redshift of the SPR at higher wavelength occurs due to the dipolar resonances being red-shifted by the presence of the electric field generated by higher multipolar resonances which result from the formation of anisotropic particles (nanoComposix, 2003; Jain et al. 2007). The split occurring in the SPR peak of AgNPs with 10% ALE is due to the difference in the energy levels of the dipole and multipole resonances resulting from the anisotropy of the particles. The split indicates the extent of longitudinal and transverse polarization of the particles

(Wang et al. 2010). The SPR band of AgNPs synthesized using 10% ALE also contains several small peaks indicating the highly anisotropic nature of the AgNPs being synthesized in the synthesis mixture (Tian et al. 2005). Thus, the appearance of the redshift, broadening and splitting of the SPR peak emanating from AgNPs synthesized with 10% ALE indicates the formation of large sized, anisotropic AgNPs with a wider size distribution.

Polydispersity of AgNPs is also found to increase as the leaf powder suspension concentration increased from 5% to 10%, as indicated by the broadening of the SPR peak shown in Figure 4.6. Polydispersity may be the result of aggregation of nanoparticles caused by faster conversion of Ag^+ ions into Ag^0 nuclei and increase in their subsequent collisions in the colloidal suspension (Hotze et al. 2010). The high conversion of around 93% (Table 4.2) obtained from 10% ALE may be due to the formation of many silver nuclei and its subsequent growth and aggregation into larger sized nanoparticle (Akaighe et al. 2011; Philip, 2010).

The studies on the effect of leaf powder suspension concentration on the conversion of Ag^+ ions to Ag^0 and SPR characteristics of the AgNPs revealed the dependency of these parameters on the ratio of Ag^+ ions to the bioactive components present in the synthesis medium. As the concentration of leaf powder suspension used for extraction increases under a fixed set of extraction conditions, the concentration of bioactive components serving as capping, reducing or/and stabilizing agents present in the extract and thus in the synthesis mixture increase leading to higher ratio of bioactive components to Ag^+ ions which result in higher conversion of Ag^+ ions. However, size, shape and monodispersity of the nanoparticles are also governed by the concentration of bioactive components in the media, which changes the refractive index and the dielectric characteristics of the medium surrounding the nanoparticles (Khlebstov et al. 2005). Moghaddam and Dabanlou, (2014) through their studies on the synthesis of AgNPs using different concentrations of *C. douglasii* extracts have also reported that, the size of AgNPs depends on the ratio of Ag^+ ions to the bioactive phytocomponents which serve as capping, reducing or/and stabilizing agents present in the synthesis mixture.

From this study it can be inferred that monodispersed AgNPs with higher conversion and better morphological characteristics could be synthesized with 5%

ALE and thus the synthesis approach using 5% ALE is superior in comparison to 1% ALE and 10% ALE. Thus 5% leaf powder suspension of *T.catappa* (ALE) was considered as the optimum for the synthesis of AgNPs and further studies were continued with AgNPs synthesized using 5% ALE.

Table 4.2 Percentage Conversion of Ag$^+$ ions in the synthesis mixture by various concentrations of *T.catappa* leaf powder suspension

Percentage of leaf powder suspension used for the synthesis of AgNPs (% ALE)	Percentage Conversion of Ag$^+$ ions
1%	79.41
5%	88.87
10%	93.70

B) Synthesis of AgNPs using TLE

Effect of concentration of leaf powder suspension of *T.grandis* Linn f. used for the preparation of the extract on the synthesis of AgNPs was also studied using SPR analysis and percentage conversion of Ag$^+$ ions obtained from the synthesis mixtures containing 1%, 5% or 10% TLE and 1 mM of precursor salt. 1%, 5% and 10% TLE is referred to the extracts prepared using 1%, 5% and 10% (w/v) *T.grandis* Linn f leaf powder suspension by open solvent heating method described in section 3.2.3 of Chapter 3. The SPR peaks of AgNPs obtained from the synthesis mixtures containing TLE prepared with different concentrations of the leaf powder suspensions are shown in Figure 4.7 and were analyzed to study the effect of concentration of leaf powder suspension on the synthesis of AgNPs.
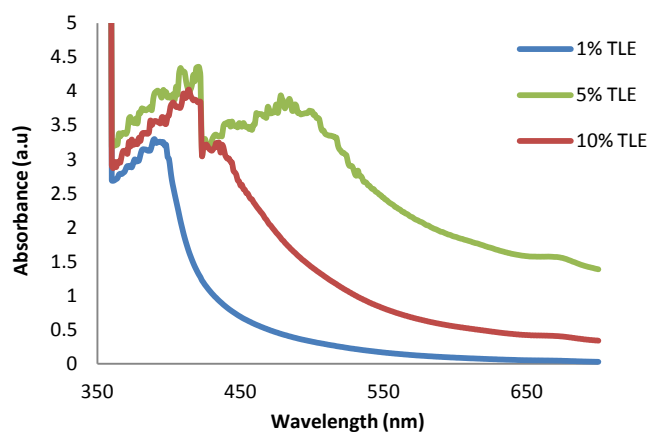
Figure 4.7 SPR spectra of synthesis mixture for AgNPs synthesized using of 1%, 5% and 10% TLE at synthesis time period of 24 h.

Table 4.3 Percentage Conversion of Ag⁺ ions in the synthesis of AgNPs by various concentrations of *T.grandis* Linn f leaf powder suspension

Percentage of leaf powder suspension used for the synthesis of AgNPs (% TLE)	Percentage Conversion of Ag^+ ions
1%	41.60
5%	95.92
10%	97.78

The synthesis mixtures containing 1%, 5% and 10% TLE exhibited the characteristic SPR peak of AgNPs. The SPR peak of AgNPs synthesized using 1% TLE is blue shifted to 380 nm from the characteristic position of 420 nm of AgNPs indicating the formation of smaller sized AgNPs. The low conversion of 41.6% of AgNPs obtained using 1% TLE as shown in Table 4.3 is indicative of the inadequate amount of reducing agents in 1% TLE required for the reduction of Ag^+ ions present in the synthesis mixture. As the concentration of leaf powder suspension increased to 5% TLE and 10% TLE, the conversion of Ag^+ ions to Ag^0 increased to around 96% and 98 % respectively as presented in Table 4.3. Thus, maximum conversion of nanoparticles was obtained with 10% TLE. This proves the existence of adequate quantities of bioactive phytocompounds in the synthesis mixture with 10% TLE to provide an adequate balance between Ag^+ ions and the bioactive phytocomponents to bring about maximum conversion Ag^+ ions to Ag^0.

The SPR band of the AgNPs synthesized from the synthesis mixture containing 5% and 10% TLE showed a split in the peak at 422 nm (Figure 4.7). Two peaks appeared for 5% and 10% TLE. The peaks for 5% and 10% TLE are redshifted in comparison to that with 1% TLE. Smaller sized nanoparticles with diameters less than that of the incident wavelength produce only dipole type resonance which becomes evident as a single SPR peak but as the particle size increases the charge distribution over the particles become non-uniform resulting in the phase retardation that broadens the dipole resonance and excites higher multipole resonances like quadruple, octupole resonances leading to the formation of several peaks in the spectra. The difference in the energy level of the resonances is manifested as a split in the SPR peak and the distance between the peaks (Evanoff and Chumanov, 2005).

The two peaks in the spectra for 5% and 10% TLE show the quadrapole and dipole maximum. It is apparent from Figure 4.7 that the dipole maximum rapidly shifted to longer wavelengths as the leaf powder suspension concentration decreased from 10% to 5% with dipole maximum at 440 nm and 485 nm for 10% and 5% TLE. According to Evanoff and Chumanov, (2005), the shift in dipole maximum is attributed to larger size of the particles. The observed spectral shift results from the "spreading" of the particle's surface charge over a larger surface area so that the surrounding medium better compensates the restoring force thus slowing the electron oscillations (Evanoff and Chumanov, 2005). However, the quadrapole peak remained centred at around 422 nm.

Plasmon peak splits into several anisotropic SPR modes depending on specific morphology of the particles (Tian et al. 2005). Two peaks were observed by Wang et al. (2010) for ellipsoidal nanoparticles, due to splitting of SPR peak into different modes caused by longitudinal and transverse polarization of the surface plasmon. Tian et al. (2005) have observed peak splits for tabular nanoparticles. Thus peak split due to two different polarization may also occur due to anisotropic nanoparticles (Zhang and Noguez, 2008). The SPR peak with 5% TLE is broader and the distance between the two resonances is very large of about 80 nm indicating the formation of highly polydispersed and anisotropic AgNPs. The dipolar peak is more red shifted than that with 10% TLE, indicating larger sized nanoparticles with 5% TLE. The formation of a large number of polydispersed anisotropic AgNPs may be due to inadequate quantity of bioactive phytocomponents in 5% TLE leading to limited growth of the nanoparticles in spite of adequate nucleation.

The nanoparticles with 10% ALE seem to be with narrow size distribution, isotropic as represented by narrower SPR band and smaller particle size as represented by the peak at lower wavelength as compared to that with 5% TLE. Noguez, (2007) studied the influence of the particle shape upon the SPR and stated that as the truncation of the particle increases the dipolar resonance is always blue-shifted and the SPRs occurring at smaller wavelength are closer to the dominant mode and the width of the SPR also increases. This indicates that 10% TLE possessed the optimal quantity of bioactive compounds that were responsible in bringing about the

efficient synthesis of AgNPs with better characteristics than those with lower concentrations of TLE.

Highest conversion of Ag^+ ions was obtained with 10% TLE as compared to 1% and 5% TLE. Thus, owing to high conversion and smaller size AgNPs with narrow size distribution being synthesized with 10% TLE as compared to that with 1% and 5% TLE, the extract prepared with 10% TLE was considered the optimum for the synthesis of AgNPs and was used for further studies. Dubey et al. (2010) have also reported the decrease in the size of the AgNPs as the extract concentration was increased in the synthesis mixture containing the precursor salt and Tansy fruit extract. Decrease in the size of the AgNPs with increase in the extract concentration was also reported by Ashokkumar et al. (2014) in the synthesis of AgNPs using the aqueous extract of *Tribulus terrestris* leaf.

4.2.3 Effect of precursor salt concentration on plant based synthesis of AgNPs

The concentration of the $AgNO_3$ (precursor salt) solution in the synthesis mixture, plays an important role during the synthesis of AgNPs as the shape, size and conversion of Ag^+ ions depends on it (Tripathi et al. 2013; Prarthna et al. 2011a; Zhang et al. 2013; Philip et al. 2011). The amount of precursor salt used in the synthesis mixture should be in adequate ratio with the reductants and stabilizers present in the extract to obtain maximum conversion of Ag^+ ions with the desirable characteristics. The pivotal role of concentration of Ag^+ ions in the path of AgNP synthesis can be understood by varying the number of Ag^+ ions available for conversion into Ag^0 by the bioactive components. Thus, to evaluate the optimum concentration of precursor salt solution to be added into the synthesis mixture with 1:1 v/v extract to $AgNO_3$ solution, the methodology mentioned in section 3.2.7.3 of Chapter 3 was followed. The optimum concentration of the leaf powder suspension to prepare ALE and TLE was determined through studies presented in section 4.2.2 as 5 % and 10% respectively for 1 mM of $AgNO_3$ solution. Thus the synthesis mixture was prepared with leaf extract (5% ALE or 10% TLE) and $AgNO_3$ solution of concentrations 1 mM, 5 mM, 10 mM, 20 mM and 100 mM in 1:1 ratio to determine the optimal $AgNO_3$ solution concentration for the synthesis of AgNPs. The total volume of the synthesis mixture was kept constant and the volume ratio of the leaf

extract to the AgNO$_3$ solution was also kept constant, while the concentration of AgNO$_3$ solution added to synthesis mixture was varied from 1 mM to 100 mM. Therefore, as the concentration of AgNO$_3$ solution added to the synthesis mixture varied from 1 mM to 100 mM, the concentration of AgNO$_3$ in the synthesis mixture varied from 0.8 mM to 80 mM. UV-Vis spectral analysis of the AgNPs being synthesized was performed to determine the characteristics of the SPR peak.

A) Synthesis of AgNPs using ALE

To evaluate the effect of precursor salt solution concentration in the synthesis of AgNPs using ALE, the leaf powder suspension concentration of 5% was used in the preparation of the extract. The SPR spectra of the synthesis mixture prepared with different concentrations of precursor salt solution at 24 h of synthesis time duration are presented in Figure 4.8. The SEM images of the AgNPs synthesized with different concentrations of precursor salt solution are presented as Figure 4.9 (a)-(e) and 4.10 (a)-(e) with 10000X and 50000X magnifications respectively. The average size of AgNPs synthesized was determined from the SEM image by using Image J software. The effect of precursor salt solution concentration on the conversion of Ag$^+$ ions and the average size of AgNPs synthesized is presented in Table 4.4.
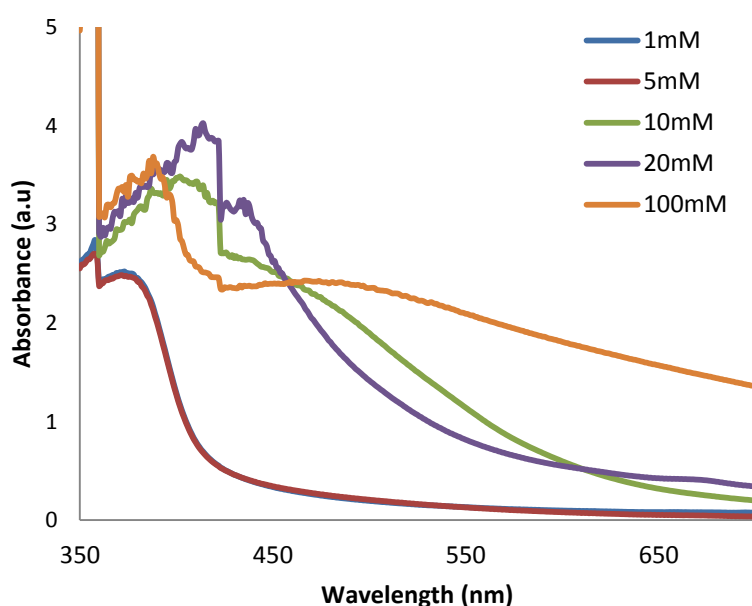
Figure 4.8 SPR spectra of synthesis mixture of AgNPs synthesized using 5% ALE and different concentrations of precursor salt solution.

Table 4.4 Percentage conversion of Ag$^+$ ions and approximate size range of AgNPs synthesized using 5% ALE with varying precursor salt concentrations

Precursor salt concentration	Percentage conversion of Ag$^+$ ions	Particle size range	Average particle size
1mM	88.87	38-171nm	104.1nm
5mM	95.03	41-180nm	110 nm
10mM	94.94	28-83nm	55.5 nm
20mM	97.31	33-48nm	40.5
100mM	99.91	Polydispersed and aggregated	ND

As observed in Figure 4.8, the intensity of SPR peak emanated by AgNPs increased with an increase in AgNO$_3$ concentration from 1 mM to 20 mM, expressive of the result that increased concentration of Ag$^+$ ions are being converted to Ag^0 by the bioactive components present in the synthesis mixture which act as reducing agents, yielding a large quantity of AgNPs. The same is supported by increase in conversion of Ag$^+$ ions with increased AgNO$_3$ concentration as presented in Table 4.4. The conversion of Ag$^+$ ions increased from 88.7% to 99.9%, with increase in the concentration of AgNO$_3$ solution from 1 mM to 100 mM. As the Ag$^+$ concentration in the AgNO$_3$ solution increases, the Ag$^+$ ions available in the synthesis mixture increases. Higher concentration of Ag$^+$ ions in the mixture increases the rate of reduction of Ag$^+$ ions to Ag^0, thus the nucleation and subsequent growth of nanoparticles occur at a higher rate. The increased rate of growth at the Ag nuclei may be owing to higher rate of mass transfer of Ag$^+$ ions to the surface of Ag nuclei due to higher concentration gradient and subsequent reduction to Ag^0 on the surface resulting in faster growth of the nanoparticles. Mittal et al. (2014) have reported the increase in the yield of AgNPs with the increasing concentration of AgNO$_3$ in the synthesis mixture.

As presented in Table 4.4, almost complete conversion of Ag$^+$ ions occurred in 24 h with 100 mM AgNO$_3$ solution, which indicates that the reducing agents present in aqueous extract of *T. catappa* leaves are adequate for reducing all the Ag$^+$ present in the solutions with concentrations lesser than or equal to 100 mM. However, with concentrations lesser than 100 mM, complete conversion could not take place in 24 h, due to lower rate of reduction to Ag^0.

As observed in Figure 4.8, at lower concentration of $AgNO_3$ of 1 mM and 5 mM, the SPR peaks are less intense than that with 10 mM and 20 mM $AgNO_3$ salt solutions. Formation of less intense peaks at lower concentrations of 1 mM and 5 mM are indicative of the formation of lesser number AgNPs (Dubey et al. 2010) in 24 h owing to lower rate of AgNPs formation at lower concentration of $AgNO_3$. However, the peak intensities increased with increase in $AgNO_3$ concentrations upto 20 mM, showing that larger numbers of nanoparticles were formed when the concentration of Ag^+ ions was increased owing to higher rate of nucleation and growth. Prathna et al. (2011a) had also reported that higher intensity of the SPR peaks obtained from higher concentrations of $AgNO_3$ signifies large number AgNPs being synthesized owing to the larger rate of formation of AgNPs. However in spite of highest rate of formation of AgNPs in the case with 100 mM $AgNO_3$ solution as indicated by highest conversion at 24 h, the peak intensity is lower than that with 20 mM. Though almost all the Ag^+ ions present in 100 mM solution were converted to Ag^0, due to the presence of very large number of particles in the solution, the particles collide with each other at a higher rate resulting in agglomeration of the nanoparticles forming smaller number of large sized aggregates. Presence of smaller number of larger size particles as compared to that with 20 mM $AgNO_3$ solution, resulted in peak of lower intensity with 100 mM solution.

The formation of distinct AgNPs with 1 mM to 20 mM $AgNO_3$ solution are clearly visible in the SEM images shown in Figure 4.9 (a)- (d) [10000X] and in Figure 4.10 (a)-(d) [50000X]. The SEM images of AgNPs synthesized using 100 mM of $AgNO_3$ solution are shown as Figure 4.9 (e) and Figure 4.10 (e) clearly indicating the formation of aggregates.

The SPR peak (Figure 4.8) belonging to the AgNPs synthesized using 100mM of $AgNO_3$ solution has a shoulder centring at 390 nm which may be attributed to the multiple transitions of surface plasmon as reported by Bar et al. (2009). The dipole peak is redshifted to 490 nm indicating the formation of large sized (Evanoff and Chumanov, 2005) and polydispersed AgNPs (Sosa et al. 2003; Brause et al. 2002) and also resulted in the multipole transitions of surface plasmon, which is undesirable. SEM images shown in Figure 4.9 (e) and 4.10 (e) indicating the aggregation of the

AgNPs provided no scope for identification of definite shape and size to support the analysis and interpretation of SPR characteristics analysis.

The SPR peak formed by the AgNPs synthesized using 20 mM AgNO$_3$ solution is sharp, intense and is centered at 420 nm indicating the formation of monodispersed AgNPs (Singha et al. 2014; Bindhu and Umadevi, 2013). The split in the SPR peak is obtained due to longitudinal and transverse polarization of the surface Plasmon (Wang et al. 2010).

The size ranges of the AgNPs obtained with different concentration of AgNO$_3$ solution are presented in Table 4.4. The size ranges of AgNPs obtained with 1 mM and 5 mM AgNO$_3$ solutions are very wide indicating highly polydispersed nature. The AgNPs synthesized with 1 mM and 5mM solutions lie in almost similar size range supporting the overlapping of the SPR bands shown in Figure 4.8. The SEM images of AgNPs synthesized with 1 mM and 5 mM AgNO$_3$ solutions presented as Figure 4.9 (a), Figure.4.10 (a) and Figure 4.9 (b), Figure.4.10 (b) respectively, show varied structural morphology with particles which are spherical, cubes and other polyhedral shapes of varying number of faces. As the concentration of AgNO$_3$solution increased, the size range of synthesized AgNPs narrowed down considerably, the narrowest size range being that with 20 mM AgNO$_3$ solution as presented in Table 4.4. Similar observation of narrowing down of the size range of AgNPs being synthesized with increase in the precursor salt concentration was made by Bar et al. (2009) in the synthesis of AgNPs using the seed extract of *Jatropha curcus.*

The average size of AgNPs synthesized with 20 mM AgNO$_3$ solution was found to be 40.5 nm and the size range was 33-48 nm as determined using Image J software. The SEM images of the nanoparticles synthesized with 10 mM and 20 mM AgNO$_3$ solution are presented as Figure 4.9 (c) and (d) respectively and Figure 4.10 (c) and (d) respectively also show that the particles are more uniform as compared with those obtained with lower concentrations of AgNO$_3$ solution and are spherical. As discussed earlier the particle aggregation occurred with 100 mM AgNO$_3$ solution, though the conversion was the maximum.

(a)

(b)

(c)

(d)

(e)
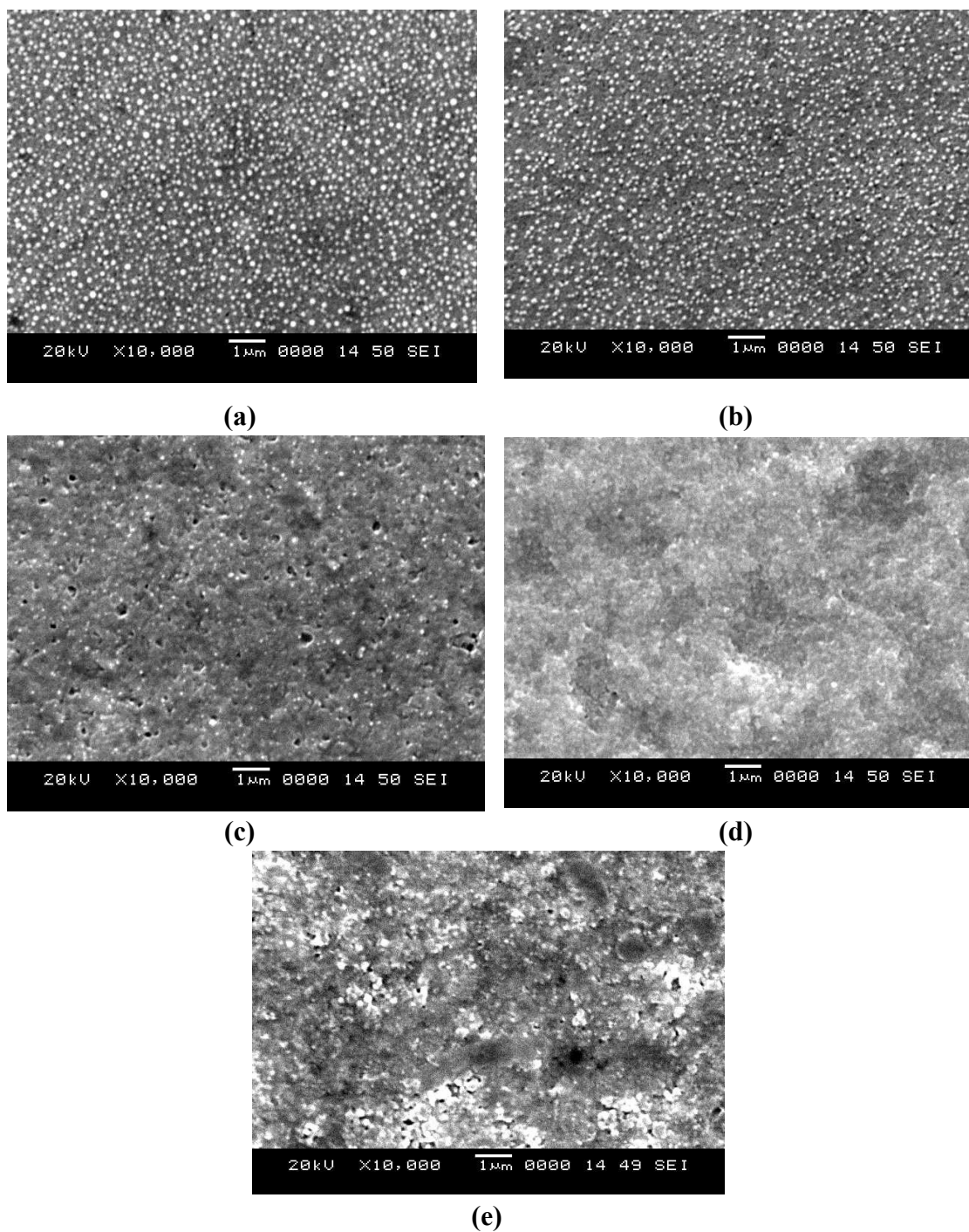
Figure. 4.9 SEM images of AgNPs synthesized from the synthesis mixture containing 5%ALE and a precursor salt concentration of (a) 1mM (b) 5mM (c) 10mM (d) 20mM and (e) 100mM.

(a)

(b)

(c)

(d)

(e)
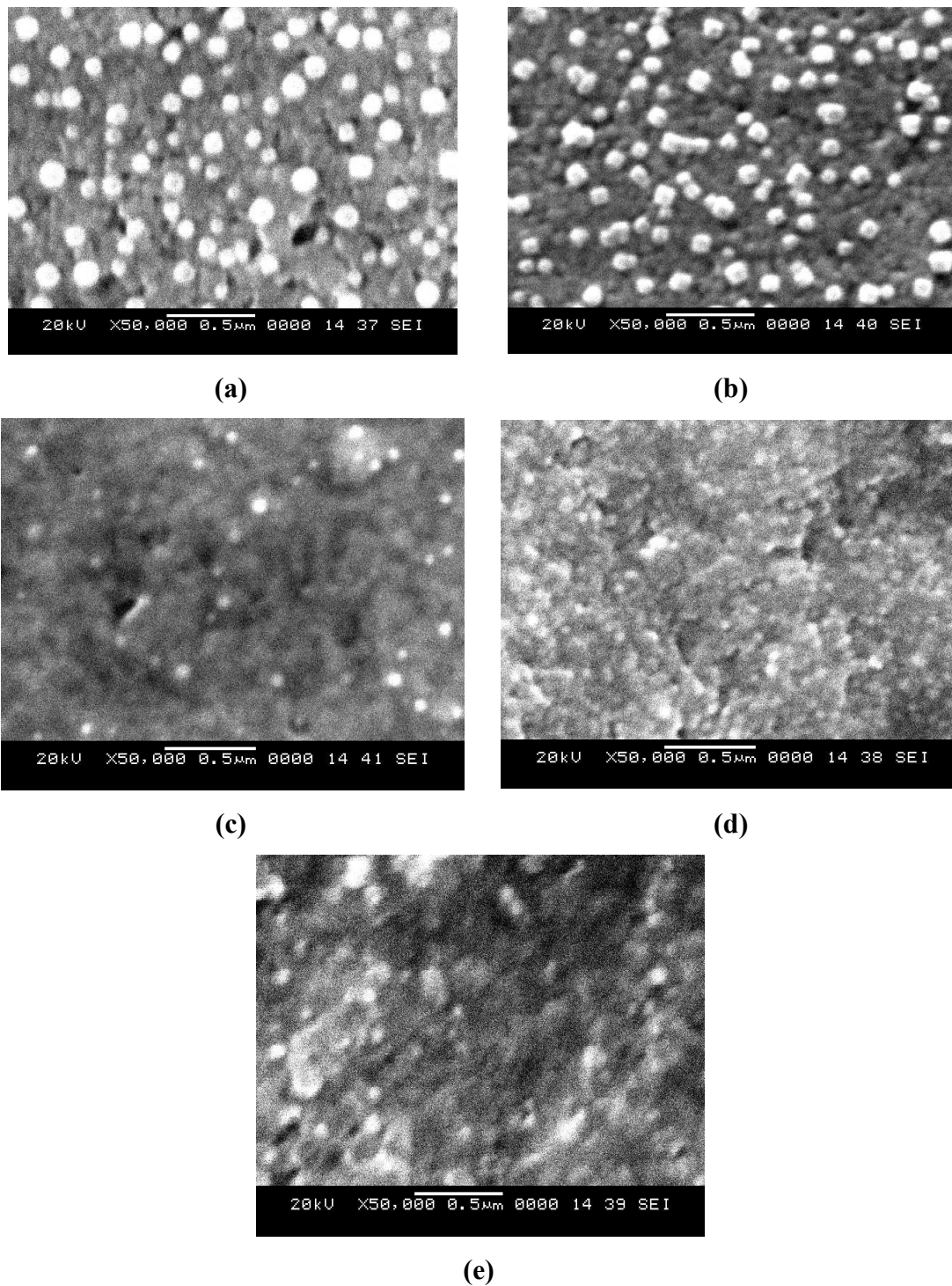
Figure 4.10 SEM images of AgNPs synthesized from synthesis mixtures comprising of 5% ALE using (a) 1mM (b) 5mM (c) 10mM (d) 20mM and (e) 100mM concentration of precursor salt

Thus, the morphological insight of AgNPs provided by SEM analysis (Figure 4.9 and 4.10) is supportive of the SPR data (Figure 4.8) acquired by spectral analysis of the AgNPs synthesized by using different $AgNO_3$ solution concentrations. The results obtained by both spectral data and morphological characterization indicate that increase in precursor salt concentration leads to the formation of smaller and monodispersed AgNPs but there exists a delicate balance between the concentration of the precursor salt and that of the bioactive components in the aqueous extract of the leaves. A further increase in the concentration of the precursor salt leads to the faster reduction of the Ag^+ ions in the synthesis mixture into AgNPs by the bioactive components of the plant extract leading to agglomeration and aggregation of the AgNPs resulting in the formation of larger AgNPs.

Owing to the formation of spherical, monodispersed AgNPs of narrow size range and lowest average size with significant conversion of around 97% of Ag^+ ions to AgNPs, 20 mM $AgNO_3$ solution was found to be the optimum for AgNP synthesis using ALE prepared from 5% leaf powder suspension in equal volume ratio with the $AgNO_3$ salt solution.

B) Synthesis of AgNPs using TLE

The similar studies for determining the optimum precursor salt concentration for the synthesis of AgNPs with TLE were conducted. The *T.grandis* Linn f leaf powder suspension concentration of 10 % was used in the preparation of TLE.

The SPR spectra obtained by UV-Vis spectrophotometric analysis of AgNPs synthesized using 10% TLE and varying concentrations of $AgNO_3$ solutions are shown in Figure 4.11. The percentage conversion of Ag^+ ions is presented in Table 4.5.

AgNPs synthesized using lower concentrations of 1 mM and 5 mM of $AgNO_3$ yielded no prominent SPR peaks indicating that AgNPs being synthesized by TLE are negligible at these concentrations, in spite of very large conversion (greater than 97%) of Ag^+ ions to Ag^0 as presented in Table 4.5. It indicates that the formation of AgNPs did not occur in noticeable quantities with 1 mM and 5mM $AgNO_3$ solution. A characteristic SPR peak of low absorption intensity was observed in the case of synthesis mixture prepared with 10 mM $AgNO_3$ solutions.
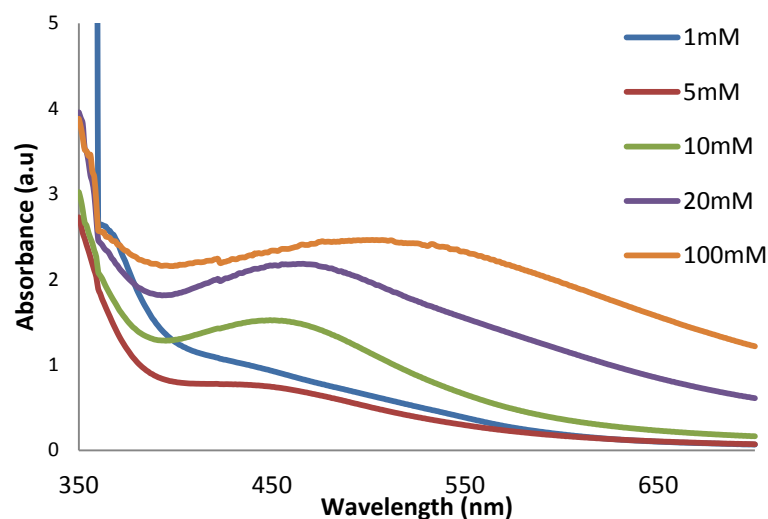
Figure 4.11 SPR spectra of synthesis mixture of AgNPs synthesized using 10% TLE and different concentrations of precursor salt solution at 24 h.

When AgNPs were synthesized using lower concentrations of 1 mM, 5 mM and 10 mM of $AgNO_3$ solutions, the SPR peaks were either absent or with low absorption intensities indicating negligibly small or lesser number of AgNPs being synthesized by TLE, in spite of very large conversion (greater than 97%) of Ag^+ ions to Ag^0 as presented in Table 4.5.

Table 4.5 Conversion of Ag^+ ions and approximate size range of AgNPs synthesized using 10%TLE with varying precursor salt concentrations

Precursor salt concentration	Percentage conversion of Ag^+ ions	Particle size range	Average Particle size
1mM	97.78	48-102nm	75 nm
5mM	97.8	32-97nm	49.5 nm
10mM	97.91	39-92nm	65.5 nm
20mM	98.88	34-47nm	37.5 nm
100mM	99.92	Polydispersed and Aggregated	ND

The rate of reduction of Ag^+ ion to Ag^0 is faster with TLE as indicated by very high conversions (Table 4.5) even at lower concentrations of $AgNO_3$. However, at lower concentrations of $AgNO_3$, large number of Ag^0 nuclei may form but the rate of growth of nuclei into AgNPs may be lesser owing to slower mass transfer rate caused

by lower concentration gradient. Negligibly small number of AgNPs would have formed at 1 mM and 5 mM as indicated by the absence of prominent peak. Due to lesser number of AgNPs formed in the synthesis mixture at 10 mM, peak intensity was less.

However, at higher concentrations of 20 mM the number of Ag^+ ions available per unit volume of the synthesis mixture for reduction into Ag^0 are larger and thus, the rate of formation of AgNPs is high, leading to the formation of large number of AgNPs, hence the peak is sharper, narrower and intense (Rodriguez-León et al. 2013; Guidelli et al. 2011) in comparison to that with 10 mM as observed in Figure 4.11. Even though for AgNPs synthesized with 100 mM $AgNO_3$ solution the peak intensity of SPR is higher than that at 20 mM, the SPR band is broader indicating the formation of large sized, polydispersed AgNPs due to aggregation. As observed in Table 4.5 the conversion of Ag^+ ions to Ag^0 increased from around 97% to approximately 100% as the $AgNO_3$ solution concentration increased from 1 mM to 100 mM. The rate of reduction of Ag^+ to Ag^0 seems to be very high even with 1 mM $AgNO_3$ solution and further increase in concentration has resulted in only marginal increase in the conversion. 100 mM of $AgNO_3$ solution resulted in conversion of 99.9 % of Ag^+ and the SPR band emanating from the AgNPs is broader, and red shifted indicating polydispersity of the AgNPs (Chen et al. 2003). This may have occurred through the rapid reduction of the Ag^+ ions to Ag^0 and their consecutive collisions at a faster rate owing to the presence of large number of nanoparticles in the suspension that led to aggregation of AgNPs forming larger sized particles. In spite of 100 mM $AgNO_3$ solution yielding almost complete conversion, the aggregation of AgNPs resulted as indicated by broad SPR band and the SEM image presented in Figure 4.12 (e) and 4.13 (e). Thus, 100 mM concentration is not suitable for the synthesis of AgNPs.

Table 4.5 shows that the AgNPs formed with 1 mM $AgNO_3$ solution are larger and the particle size distribution range is broader. SEM image presented as Figure 4.12 (a) and 4.13 (a) also shows smaller number of larger size nanoparticles with 1 mM $AgNO_3$ solution. With increase in $AgNO_3$ solution concentration, from 1 mM to 20 mM, the size distribution range narrowed down and the average particle size was found to reduce. These results are supported by the SEM images shown in Figure 4.12 (a) to (d) and 4.13 (a) to (d). AgNPs prepared with 5 mM and 10 mM $AgNO_3$ solution

appeared to be smaller and larger in number as compared to those synthesized with 1 mM. However Figure 4.12 (b), (c) and 4.13 (b), (c) indicates that the particle size distributions are wide.

(a)

(b)

(c)

(d)

(e)
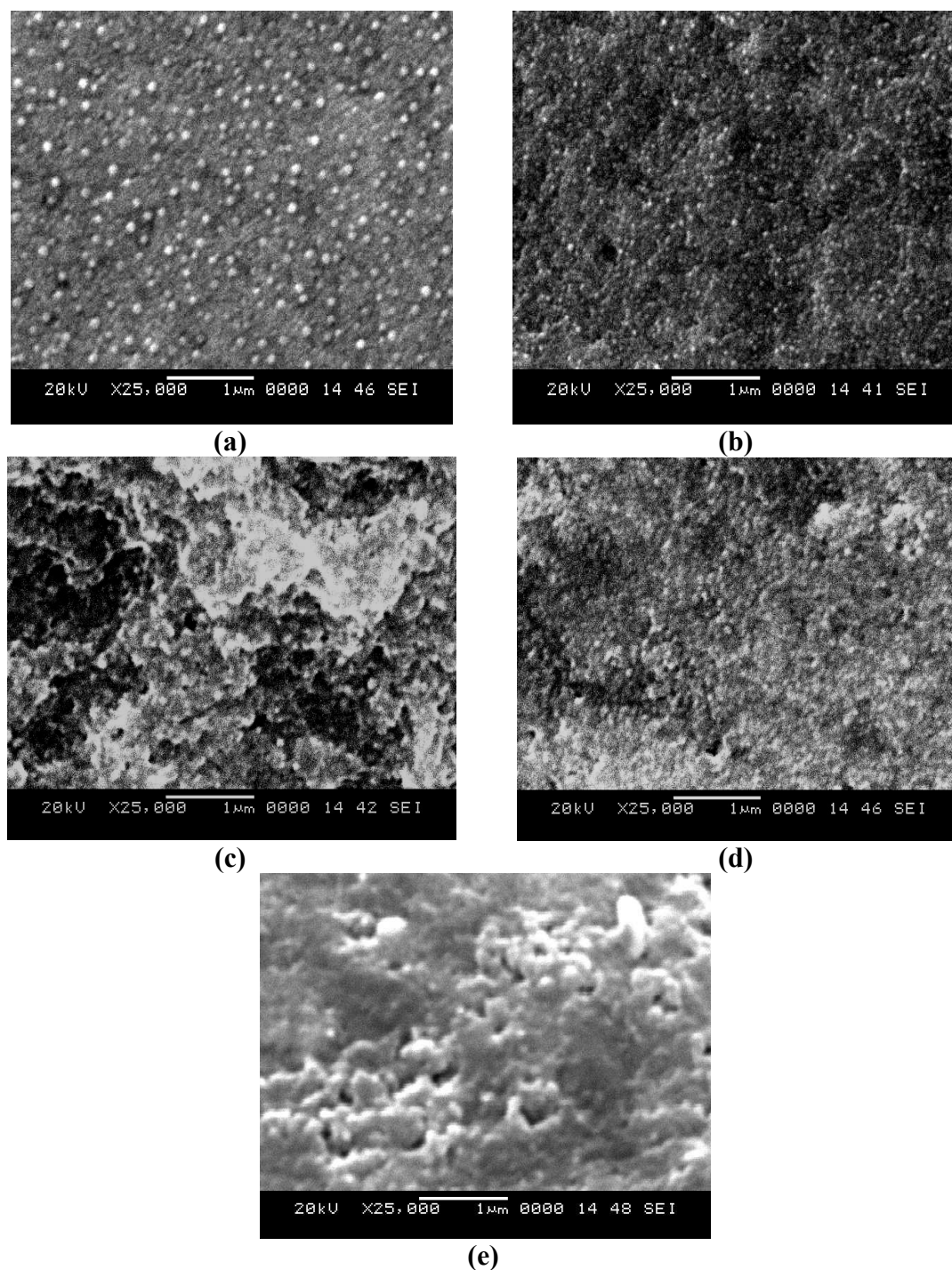
Figure. 4.12 SEM images of AgNPs (25000 X)synthesized using 10 % TLE with precursor salt concentration of (a) 1 mM (b) 5 mM (c) 10 mM (d) 20 mM and (e) 100 mM
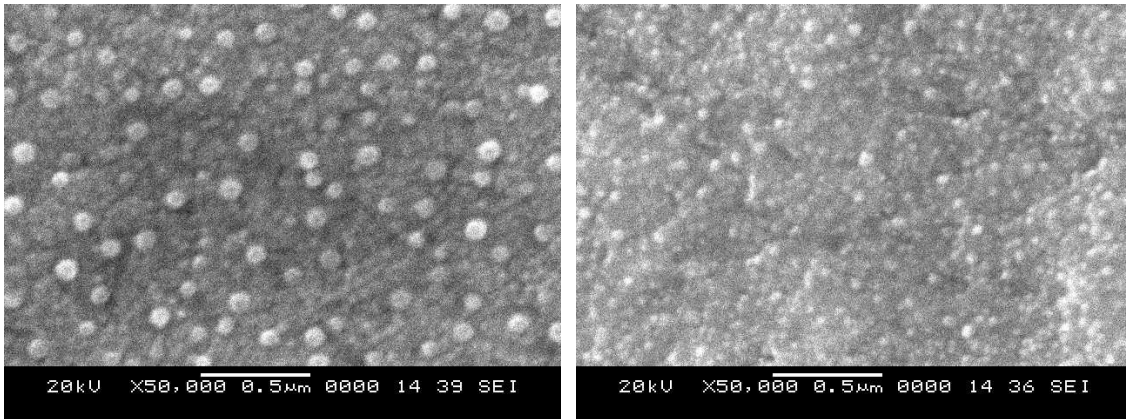
(a)

(b)
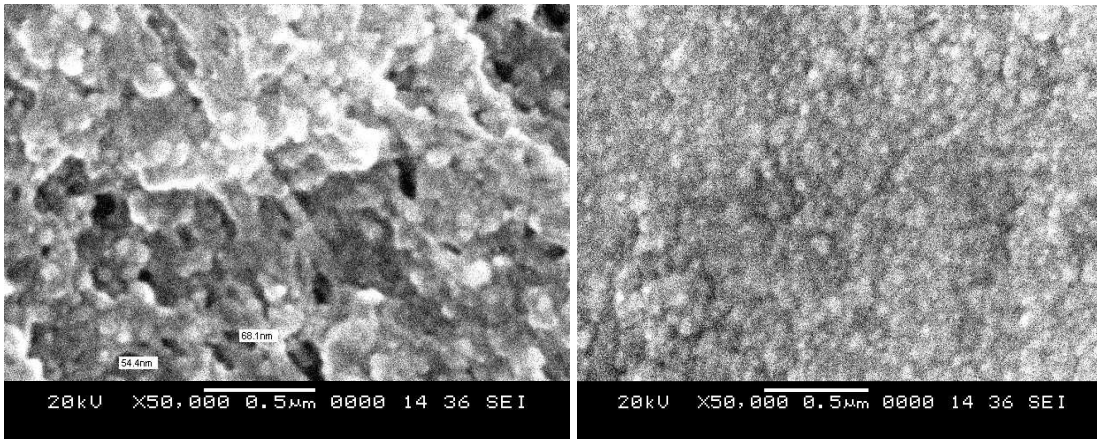
(c)

(d)
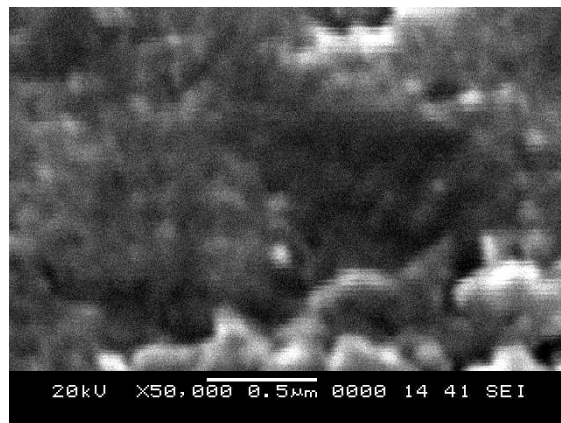
(e)

Figure 4.13 SEM images of AgNPs (50000 X) synthesized from the synthesis mixture containing 10 % TLE and precursor salt concentration of (a) 1 mM (b) 5 mM and (c) 10 mM (d) 20 mM (e) 100 mM

124

Table 4.5 shows that the AgNPs formed with 20 mM AgNO$_3$ solution are smaller in size (37.5 nm) with a very narrow size distribution of 34-47 nm. The SEM images of these AgNPs shown in Figure 4.12 (d) and 4.13 (d) also show that large numbers of smaller sized spherical nanoparticles are formed with 20 mM AgNO$_3$ solution.

The AgNPs synthesized with 20 mM of AgNO$_3$ solution exhibited a SPR peak centering at 420 nm, that is narrow and sharp indicating the formation of monodispersed AgNPs and the conversion is 98.88% (Table 4.5). The results obtained from the spectral analysis (Figure 4.11) and morphological analyses by SEM (Figure 4.12 (d) and 4.13 (d)) are found to be concurrent. Owing to conversion of around 99% of Ag$^+$ ions and the formation of monodispersed, smaller sized quasi spherical nanoparticles with narrow size distribution range, 20 mM AgNO$_3$ solution may be considered as the optimum for synthesis of AgNPs using TLE.

For the synthesis of AgNPs using the plant leaf extracts of *T.catappa* and *T.grandis* Linn f., 20 mM of AgNO$_3$ solution concentration was determined to be optimum when 5% ALE and 10% TLE were used for the synthesis based on the spectral analysis, size, monodispersity of the AgNPs and also from the conversion of Ag$^+$ ions obtained in Table 4.4 and Table 4.5.

These studies confirm that the precursor salt solution concentration plays a major role in determining the size and morphological characteristics of the AgNPs being synthesised using ALE or TLE. The plant leaf extracts of *T.catappa* and *T.grandis* Linn f. used in the synthesis of AgNPs possess necessary bioactive phytocomponents with Ag$^+$ reducing efficiency and capping potential. It may also be inferred that the stoichiometric balance between the bioactive phytocomponents and the Ag$^+$ ions cannot be taken as the sole decisive parameter in optimizing the precursor salt concentration that provides an optimum ratio between the bioactive phytocomponents and the Ag$^+$ ions. The conversion of Ag$^+$ ions to Ag^0 at a fixed time depicting the rate of formation of AgNPs along with their size and morphological characteristics contribute as the collective decision parameters in optimization.

The optimum AgNO$_3$ solution concentration for the synthesis of AgNPs using 5 % ALE (leaf extract of *T.catappa*) and 10 % TLE (leaf extract of *T.grandis* Linn f)

was determined to be 20 mM and further studies were carried out with synthesis of AgNPs using 20 mM AgNO$_3$, solution.

4.2.4 Effect of ratio of aqueous leaf extract to precursor salt solution (v/v) in synthesis mixture on the synthesis of AgNPs

The volume ratios of the plant extract to the precursor salt solution in the synthesis mixture is known to have a pronounced effect on the morphological characteristics of the AgNPs being synthesized and has been studied and reported widely by researchers (Ganaie et al. 2015; Rao and Paria, 2013; Dauthal and Mukhopadhyay, 2013; Ahmad et al .2013; Prathna et al. 2011a; Tripathy et al. 2010; Singh et al. 2010). For a fixed concentration of leaf powder suspension and precursor salt solution, on varying the volume ratio between the extract and the precursor salt solution, the availability of bioactive components for reduction of Ag$^+$ ions in the synthesis mixture varies. Such a variation, not only alters the rate of formation of the AgNPs but also their characteristics.

To obtain a better insight into the balance between the bioactive components in the leaf extract and the precursor salt solution, the reacting solutions (extract and precursor salt solution) were used in different volume ratios in the synthesis mixture. The studies were carried out as described in section 3.2.7.4 of Chapter 3. The AgNPs synthesized from the synthesis mixtures were spectrally analyzed using UV-Vis spectrophotometer for SPR characteristics. The conversion of Ag$^+$ ions was also determined. In these studies 20 mM of AgNO$_3$ solution was used in the synthesis mixture.

A) Synthesis of AgNPs using ALE

The volumes of 5% ALE and 20 mM of AgNO$_3$ solution were varied in the ratios 1:1, 1:4, 1:7, 1:10, 1:20, 1:50 and 1:100 while keeping the total volume of the synthesis mixture constant. The SPR spectra obtained from the AgNPs synthesized using different volume ratios of the reactants are presented in Figure 4.14. The percentage conversion of Ag$^+$ ions obtained by varying the volume ratios of ALE and the precursor salt solution are presented in Table 4.6.
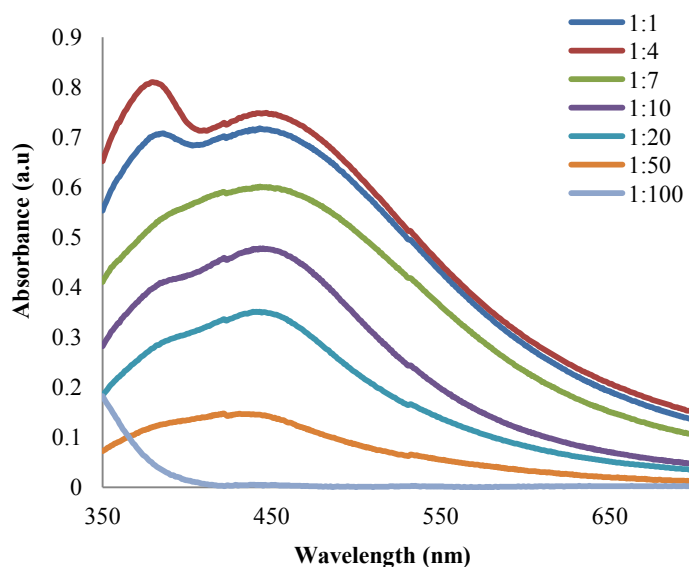
Figure 4.14 SPR spectra of the synthesis mixture of AgNPs synthesized using different volume ratios of 5% ALE and 20mM AgNO$_3$ solution at synthesis time period of 24 h

Table 4.6 Percentage conversion of Ag$^+$ ions in the synthesis mixture containing different volume ratios of 5% ALE extract to 20mM precursor salt solution

Ratios of leaf extract and precursor salt solution (v/v)	Percentage conversion of Ag$^+$ ions
1:1	97.31
1:4	99.91
1:7	99.92
1:10	99.89
1:20	99.92
1:50	99.9
1:100	99.96

It can be noted from Figure 4.14 that the absorption maxima of the SPR peaks obtained from of the synthesis mixtures containing varying volume ratios of ALE and precursor salt solution, varied in terms of the intensity. The intensity of the SPR peak obtained from the synthesis mixture containing ALE and 20 mM of precursor salt solution in the volume ratio of 1:4 was the highest (Figure 4.14) as compared to those obtained from synthesis mixtures with other volume ratios. The SPR peak intensity increased as the ratio was varied from 1:1 to 1:4. Higher intensity of the SPR peak of AgNPs synthesized with ALE to precursor salt solution volume ratio of 1:4 reveals

the formation of large number of particles with 99.9% conversion of Ag^+ ions (Table 4.6). A split in the SPR peak is observed revealing two separate peaks in a single spectra in case of AgNPs synthesized using 1:1 and 1:4 (Extract: Precursor salt solution) volume ratios. As discussed in Section 4.2.1 the split results from the polarization of the AgNPs in two different modes of dipole and quadrapole mode (Zhang et al. 2011; Evanoff and Chumanov, 2005; Mie, 1908). The two plasmonic peaks are observed due to the polarization of longitudinal and transversal vibrations of the electrons on the surface of the AgNPs (Zhang et al. 2011; Evanoff and Chumanov 2005) which may be caused by non-spherical or anisotropic nanoparticles (Tian et al,2005; Sun and Xia, 2002).

According to Mie's theory small spherical or quasi-spherical nanocrystals exhibit a single SPR band; whereas anisotropic particles show two or three bands, depending on their shape. The symmetry of nanostructures determines the polarization ways which leads to the number of plasmonics being emitted (Ashkarran and Bayat, 2013; Xia et al. 2009). Presence of two SPR peaks in single spectra with the AgNPs synthesized using volume ratios of 1:1 and 1:4 between ALE and precursor salt solution (Figure 4.14) indicate the formation of non spherical, anisotropic AgNPs. The intensity of SPR peak reduced as the volume ratio of ALE to precursor salt solution was varied from 1:4 to 1:50. With volume ratio of ALE to precursor salt solution of 1:100, no SPR peak was observed, indicating that the particles in the mixture settled completely after aggregation.

The intensity of the SPR peak resulting from the mixtures with higher volume percent of precursor salt solution i.e volume ratio of ALE to precursor salt solution of 1:7 and beyond led to diminished SPR peaks as seen in Figure 4.14. It may be due to the availability of a larger concentration of the Ag^+ ions leading to faster reduction by the bioactive compounds present in the leaf extract into Ag^0 (Dwivedi and Gopal, 2010). The rate of mass transfer of Ag^+ ions to the surface of nuclei also occurs at a faster rate owing to large concentration gradient, thus resulting in faster growth of nanoparticles. Owing to longer time of 24 h given for the synthesis process and presence of insufficient number of molecules of capping agents present in the mixture to cap all the synthesized AgNPs, the nanoparticles may aggregate forming less number of large sized particles. Aggregation of AgNPs may also result due to their

presence in large number leading to collisions between them which causes aggregation resulting in the diminished intensity of SPR peak (Dwivedi and Gopal, 2010).

The reports pertaining to optimization of the volume ratios of the extract and the precursor salt solution has been widely studied by researchers (Moghaddam and Dabanlou, 2014; Sathishkumar et al. 2014; Veerasamy et al.2011).

As observed in Table 4.6, the conversion remained unchanged when the volume ratios of the extract and precursor salt solution was varied from 1:4 till 1:100, with around 99.9% conversion occurring at all the ratios from 1:4 to 1:100. It shows that the available bioactive components present in the mixture are sufficient to provide stoichiometric ratio between the reducing agents and the Ag^+ ions in the synthesis mixture with the volume ratio of 1:4 (extract to precursor salt solution) to 1:100. Thus, the bioactive phytocomponents present in the extract were capable of reducing almost all the Ag^+ ions to Ag^0 with the extract to precursor salt solution volume ratio of 1:4 to 1:100, even though the Ag^+ ions concentration in the synthesis mixture increased. But, the rate of nucleation and growth may be governed by the rate of mass transfer which depends on the concentration gradient. However, the growth and size distribution of the AgNPs might be governed by a number of factors such as mass transfer rate, availability of capping agents (Cruz et al. 2010), dielectric constant of the medium (Kvítek et al. 2013; Mubayi et al. 2012; Sadhasivam et al. 2010) that changes as the conversion increases and the interparticle collisions (Imam et al. 2013) occurring in the colloidal suspension.

The results on conversion of Ag^+ ions shown in Table 4.6 is in concurrence with the SPR spectral data shown in Figure 4.14 with the SPR peak of highest intensity and highest conversion of approximately 100% being observed at the volume ratio 1:4 (Extract: $AgNO_3$). The SEM image of AgNPs synthesized using 5% ALE and 20 mM of $AgNO_3$ solution in the volume ratio of 1:4 is shown in Figure 4.15 which reveals the formation of a large number of AgNPs with quasi spherical shaped particles. The size distribution range for the AgNPs synthesized with volume ratio of 1:4 between the extract to $AgNO_3$ solution was found to be in the size range of 33.8 nm to 45.27 nm with average size of 38.46 nm. The size range of AgNPs synthesized using 1:1 volume ratio between the extract and precursor salt in as shown

in Table 4.4 of section 4.2.3 was determined using Image J software and was found to be between 33-48 nm with the average size of the particles was found to decrease from 40.5 nm to 38.46 nm.. The average size of the AgNPs synthesized was found to decrease and the conversion was found to increase as the volume ratio of the extract and the precursor salt solution was varied from 1:1 to 1:4. Owing to the higher conversion and similar morphological characteristics of quasi spherical shaped AgNPs obtained with the volume ratio of 1:4 between ALE and 20 mM of precursor salt solution as compared to that with 1:1 and the formation of more dispersed nanoparticles without aggregation as compared to that with volume ratios of 1:7 to 1:100, 1:4 volume ratio was considered as the optimum and was used in further studies for the synthesis of AgNPs with ALE.
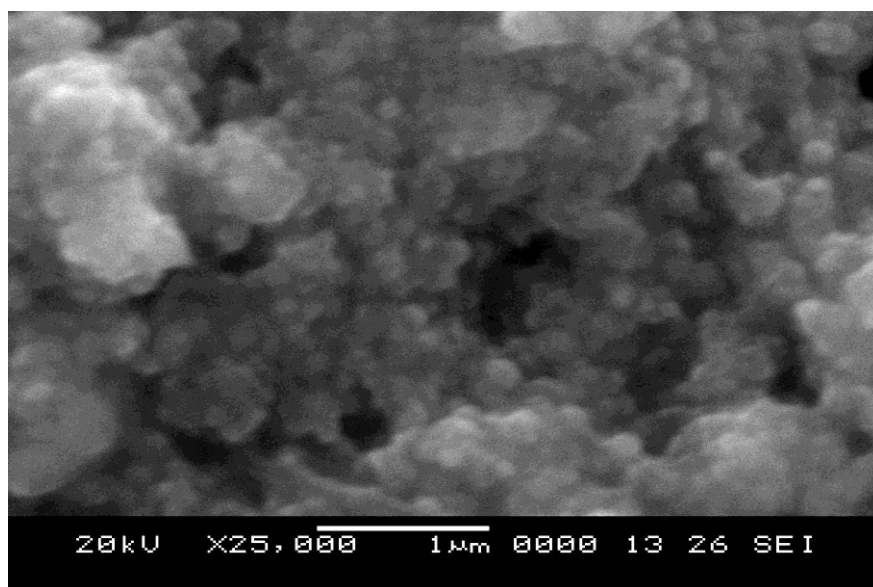
Figure 4.15 SEM image of AgNPs synthesized using synthesis mixture containing 5%ALE and 20mM AgNO$_3$ solution in volume ratio of 1:4

B) Synthesis of AgNPs using TLE

The volumes of 10 % TLE and 20 mM of precursor salt in the synthesis mixture were varied in the ratios 1:1, 1:4, 1:7, 1:10, 1:20, 1:50 and 1:100 while keeping the total volume of the synthesis mixture constant. AgNPs were synthesized as described in Section 3.2.7.4 of Chapter 3. The SPR spectra obtained by the AgNPs synthesized using different volume ratios of the reactants in the synthesis solution is presented in Figure 4.16. The conversion of Ag$^+$ ions obtained by varying the volume ratios of extract to the precursor salt solution is presented in Table 4.7.
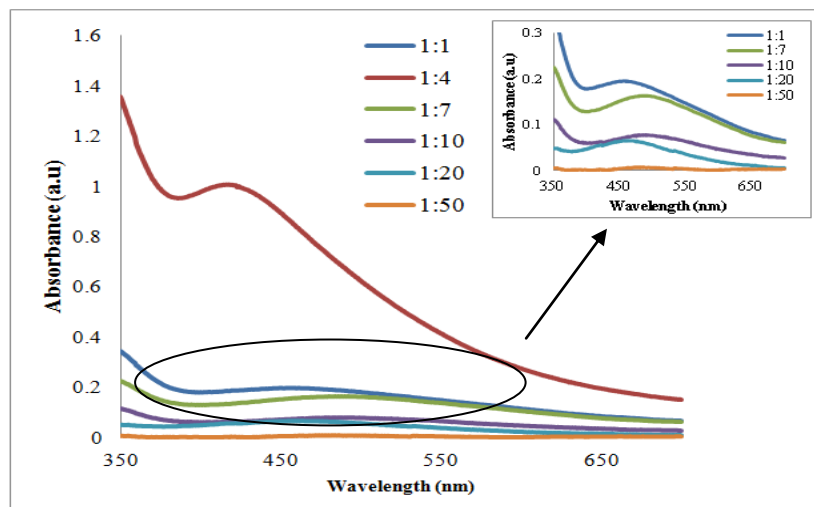
Figure 4.16 SPR spectra of synthesis mixtures for AgNPs synthesized using different volume ratios of 10% TLE and 20 mM precursor salt solution at 24 h

Table 4.7 Percentage conversion of Ag$^+$ ions by different mixing ratios of TLE and precursor salt solution.

Ratios of leaf extract and precursor salt (v/v)	Percentage conversion of Ag$^+$ ions
1:1	98.88
1:4	99.99
1:7	99.86
1:10	99.94
1:20	99.91
1:50	99.93

As observed in Figure 4.16, the SPR peak emanated at a wavelength of 418 nm from the synthesis mixture containing TLE to AgNO$_3$ solution in volume ratio of 1:4 at 24 h indicating the reduction of the precursor salt to AgNPs. The SPR peak has the highest intensity showing the presence of considerable number AgNPs. A sharp peak centred at 418nm indicates the presence of small monodispersed nanoparticles. The conversion of Ag$^+$ ions to Ag^0 in the synthesis mixture with the volume ratio of 1:4 of TLE and precursor salt solution was determined to be 99.99% (Table 4.7), indicating that the amount of bioactive phytocomponents present in TLE provides adequate balance with the Ag$^+$ ions in the synthesis mixture and thus were sufficient

for almost complete reduction of Ag^+ ions. The SPR spectra obtained from the synthesis mixture with 1:1 volume ratio (TLE:AgNO$_3$ solution) is of considerably lower intensity as compared to that with 1:4, indicating the presence of lesser number of AgNPs owing to lower quantity of Ag^+ ions present in the mixture initially. The conversion is lower than that with 1:4, as indicated in Table 4.7. Lower conversion may be due to lower rate of reduction of Ag^+ ions owing to their lesser concentration in the mixture and thus 24 h of reaction time would not have been sufficient for the reaction to go to completion.

But as the volume ratio of TLE to AgNO$_3$ solution was varied from 1:4 to 1:7,1:10,1:20 and 1:50, the peak intensities reduced and the peaks were red shifted. Red shift indicates larger size particles and reduced peak intensity indicates less number of nanoparticles. As the volume percent of AgNO$_3$ in the synthesis mixture was increased, the nucleation and growth occurred at a faster rate and the number of molecules of capping agents present in the synthesis mixture may be insufficient to cap all the AgNPs thus causing the aggregation and agglomeration of AgNPs resulting in broader, less intense and redshifted peaks. Frequent interparticle collisions may also lead to their aggregation and subsequent settling causing the emanation of an SPR band with diminished intensity as observed in Figure 4.16.

The SEM image of AgNPs synthesized using 20 mM of precursor salt solution and 10 % TLE in the volume ratio of 1:4 (Figure 4.17) shows the formation of many quasi spherical shaped, monodispersed AgNPs. The size of AgNPs synthesized under these conditions were determined using Image J software and were found to be of the approximate size distribution range of 31 nm to 48 nm and the average size was 38.6 nm. The size range of AgNPs synthesized with 1:1 volume ratio of the extract and precursor salt solution was found to be within 34-47 nm with an average size range of 37.5 nm (Table 4.6 of section 4.2.3). A marginal increase in the average size of the AgNPs synthesized with 1:4 compared to 1:1 volume ratio from 37.5 to 38.6 was observed along with an increase in the conversion of Ag^+ ions as seen in Table 4.7. Thus the morphological characteristics of AgNPs synthesized using 1:1 and 1:4 volume ratios of reactants were found to be almost similar and quasi spherical and monodispersed. However, the conversion with 1:4 volume ratio was higher compared to that obtained using 1:1 volume ratio.

Thus, owing to higher conversion of around 99.9% and formation of quasi spherical shaped, monodispersed AgNPs obtained with synthesis mixture containing 1:4 volume ratio and absence of aggregation as with other volume ratios, the optimum volume ratio of 10% TLE and 20mM of precursor salt solution for AgNP synthesis was found to be 1:4.
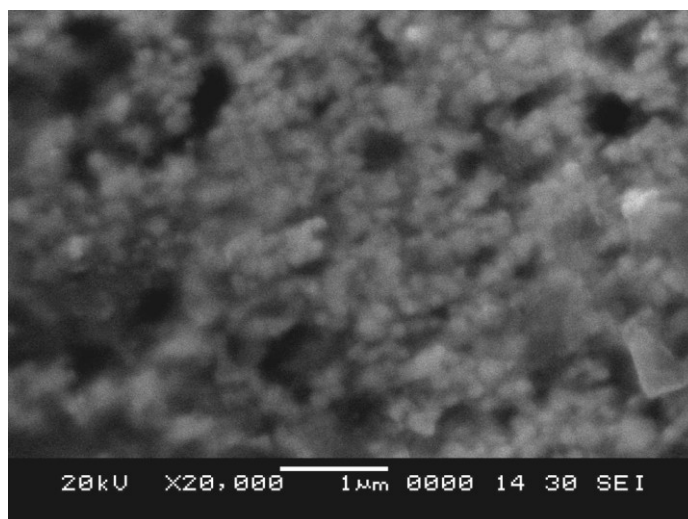
Figure 4.17 SEM image of AgNPs synthesized using synthesis mixture containing 10 % TLE and 20mM AgNO$_3$ in volume mixing ratio of 1:4 (v/v)

4.2.5 Effect of initial pH of the synthesis mixture on plant based synthesis of AgNPs

As discussed in Section 2.3.2.2 of Chapter 2, pH of the synthesis mixture plays an important role in determining the morphology and characteristics of AgNPs. To determine the influence of initial pH of the synthesis mixture on the synthesis of AgNPs using the plant leaf extracts, the initial pH of the synthesis mixtures was varied from acidic to alkaline as described in section 3.2.7.5 and its effect on the synthesis of AgNPs was studied through the spectral analysis of the SPR band obtained from them.

A) Synthesis of AgNPs using ALE

5% ALE and 20 mM of the precursor salt solution in 1:4 (v/v) ratio was mixed to prepare the synthesis mixtures and the initial pH of this medium was set at the desired value as mentioned earlier. AgNPs were also synthesized under normal (unadjusted) initial pH condition of 4.87±0.1. The synthesis of AgNPs was carried out

for time duration of 24 h and the spectra of the synthesis mixtures are presented in Figure 4.18. The percentage conversion of Ag^+ ions was determined by measurement of residual Ag^+ ions in the mixture and the conversions at different pH are presented in Table 4.8.
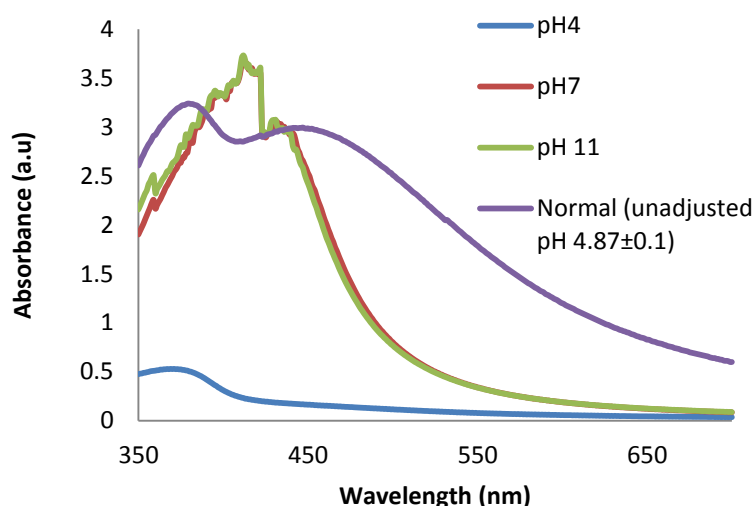
Figure 4.18 SPR spectra of the synthesis mixtures containing 5% ALE and 20mM AgNO₃ solution (1:4 v/v) at 24 h under different pH

Table 4.8 Percentage conversion of Ag^+ ions obtained by varying the Initial pH of the synthesis mixture

Initial pH of the synthesis mixture	Percentage conversion of Ag^+ ions
pH 4	68.63
pH 7	88.45
pH 11	99.85
pH 4.87±0.1(unadjusted)	99.9

From Figure 4.18, it can be seen that there is no noticeable characteristic SPR peak showing the presence of AgNPs at acidic pH 4 it indicates that the acidic pH did not favour the nucleation of Ag^0 and also led to the aggregation of AgNPs, which may be due to the electrostatic repulsion of the anions in the acidic synthesis mixture favoured by the dominance of hydrogen bonding on the –COOH groups in the capping agents (Sun et al. 2008). The SPR peaks obtained from the AgNPs synthesized in the synthesis mixture with neutral pH and at alkaline pH of 11 are sharp, intense and narrow, centred at 420nm in comparison to the SPR band obtained from the AgNPs synthesized under normal pH conditions. The split in the SPR peak

under neutral and alkaline pH conditions of synthesis occurs due to the excitation of the surface electrons in longitudinal and transversal modes leading to the formation of dipole and multipole transitions (Evanoff and Chumanov, 2005). Though the split in the peaks occur at neutral and alkaline pH, the two peaks are closer to each other indicating that the difference in energy levels of excitation in longitudinal and transversal modes is lesser in the SPR spectra. It shows that AgNPs synthesized at neutral and alkaline pH are nearly spherical (Evanoff and Chumanov, 2005). The higher intensity of the SPR peak with neutral and alkaline pH in comparison to the normal conditions indicate larger number of AgNPs being synthesized at higher pH conditions of neutral and alkaline.

The SPR peaks obtained from the synthesis mixtures with neutral and alkaline pH are higher in intensities and narrower, compared to that of the normal pH of synthesis. The conversion is found to be similar with alkaline pH and normal pH conditions at∼ 99.9 %. The intensity of the AgNPs synthesized under alkaline pH condition was found to be higher than that synthesized with normal pH indicating the formation of large number of AgNPs with smaller size range at pH 11 while those synthesized with normal pH condition were larger in size and fewer in number as indicated by the low intensity and broadness of the peak. Two peaks were observed in the SPR band obtained from AgNPs synthesized at normal (unadjusted) pH. Presence of two peaks that are farther and broader indicated that at normal pH the AgNPs are anisotropic and large sized as compared to AgNPs synthesized under neutral and alkaline pH conditions of the synthesis mixture. The conversion of Ag^+ ions is shown in Table 4.8 is in agreement with the results of the SPR spectral analysis. The conversion of the Ag^+ ions is found to increase from 68.4% under acidic synthesis condition to around 99.9% under alkaline synthesis conditions. The morphological analysis by SEM in Figure 4.19 of AgNPs synthesized from the synthesis mixture containing 5%ALE and 20 mM of $AgNO_3$ in the volume ratio 1:4 with an initial pH of 11 reveals the formation of large number of monodispersed, quasi spherical shaped AgNPs with an average size of 20.8 nm and size range of 18 nm to 38 nm which are smaller in comparison to the AgNPs synthesized with normal (unadjusted) pH of size range of 33.8 nm to 45.27 nm with average size of 38.46 nm.

Addition of NaOH to the synthesis mixture may increase the surface reactivity of the Ag^+ ions making it more readily available for reduction by the reducing agents present in the plant leaf extract. At acidic pH, the aggregation of AgNPs to form larger nanoparticles is favoured over the nucleation but at alkaline pH, many Ag^0 nuclei tend to bind and subsequently form a large number of nanoparticles with smaller size. Alkaline pH condition also increases the reactivity of the reducing agents and while subsequently increasing the stability of the AgNPs by the capping agents. Thereby it is concluded that alkaline pH promotes the synthesis of monodispersed nearly isotropic, quasi spherical shaped AgNPs and plays a crucial role in keeping the AgNPs stable. Seo and Co-workers (2008) through their studies on fine-tuning the synthesis parameters by varying pH as one of the physical parameter concluded that when $AgNO_3$ was reduced under acidic conditions, non uniform sized AgNPs were formed whereas monodispersed nanoparticles were formed under alkaline conditions.

In the study conducted by Tripathi et al. (2010), the stability of AgNPs in the presence of additives has been found to be a function of sol pH since OH^- ions can change the surface charge on the nanoparticles. The stability of the cluster distribution was enhanced at alkaline pH range owing to complete charging of the clusters thus maximizing the repulsive electrostatic/electrosteric interactions. Saware and Venkataraman, (2014) have also studied the effect of initial pH of the synthesis mixture on AgNPs synthesis using *Ficus religiosa* leaf extract and have reported that acidic pH brought about slow rate of formation and aggregation of AgNPs while increase in the pH from acidic to alkaline led to the blueshift and increase in the absorbance of the SPR peaks suggesting that the rate of formation of AgNPs is higher in neutral and basic pH than in acidic pH. They also reported that acidic condition suppresses the formation of AgNPs but the basic condition enhances the formation of AgNPs. The results obtained in the present study are also in agreement with the literature reports.
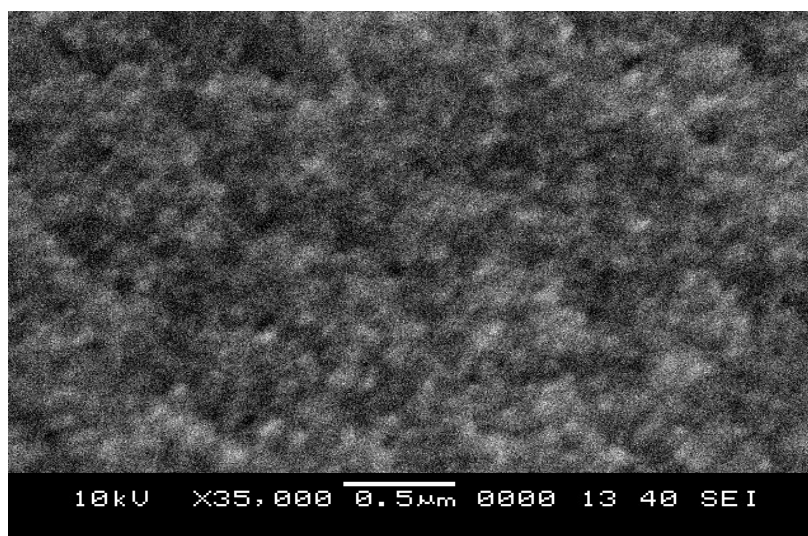
Figure 4.19 SEM image of AgNPs synthesized from the synthesis mixture prepared with 5 % ALE and 20 mM AgNO$_3$ (1:4 v/v) under initial alkaline pH condition of 11.

B) Synthesis of AgNPs using TLE

The influence of initial pH of the synthesis mixture on the synthesis of AgNPs using 10% TLE and 20 mM precursor salt in the volume ratio of 1:4 was studied. The influence of initial pH of the synthesis mixture on AgNPs synthesized using TLE is similar to the ALE based synthesis. Figure 4.20 shows the SPR spectra emanating from the synthesis mixtures of AgNPs obtained by varying the initial pH of the synthesis mixture. Table 4.9 presents the percentage conversion of Ag^0 ions under the influence of varying initial pH of the synthesis mixture.

Table 4.9 Percentage conversion of Ag$^+$ ions obtained with 10% ALE by varying the initial pH of the synthesis mixture

Initial pH of the synthesis medium	Percentage conversion of Ag$^+$ ions
pH 4	51.0
pH 7	85.35
pH 11	99.07
unadjusted pH 5.3±0.1	99.9

137
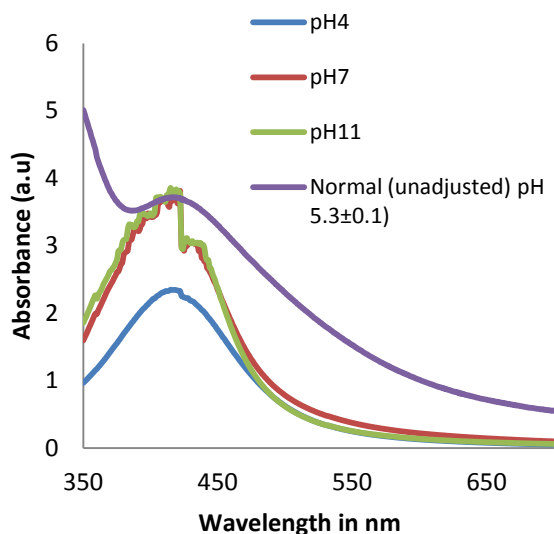
Figure 4.20 SPR spectra of the synthesis mixture for AgNPs synthesized using 10 % TLE and 20 mM AgNO₃ (1:4 v/v) under different pH conditions at 24 h.

The SPR peaks belonging to AgNPs synthesized with alkaline and neutral initial pH conditions of AgNPs synthesis from TLE were found to be narrower in comparison to that obtained with normal (unadjusted) pH of 5.3±0.1 indicating the formation of AgNPs with smaller size distribution at alkaline and neutral pH. From Figure 4.20, the intensity of the SPR peaks formed from the synthesis mixtures with normal (unadjusted) initial pH, neutral and alkaline are similar implying the formation of a similar number of AgNPs, but the peak is broad in the case of AgNPs synthesized at normal (unadjusted) initial pH conditions while the SPR peaks obtained from AgNPs synthesized at neutral and alkaline pH conditions were narrower indicating the formation of monodispersed AgNPs. A sharp and intense SPR peak is observed under alkaline pH of 11 and neutral pH of 7 indicating the formation of large number of small sized AgNPs being synthesized. Around 99% conversion of Ag⁺ ions was obtained for alkaline pH condition of 11. TLE is able to bring about significant rate of AgNPs synthesis even at acidic pH range of 4 with a conversion of 51%. Percentage conversion of Ag⁺ ions obtained through (Table 4.9) reveals that acidic pH does not favour the synthesis of AgNPs and the synthesis of AgNPs at alkaline condition is more and leads to the formation of monodispersed nanoparticles (owing to the narrow SPR peak).
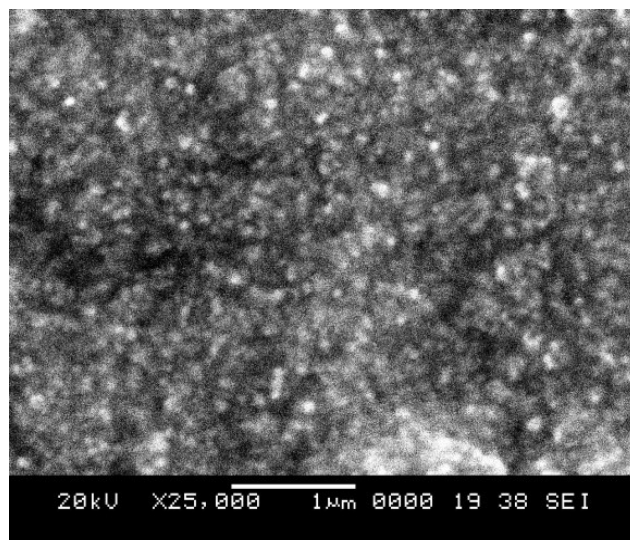
Figure 4.21 SEM image of AgNPs synthesized from the synthesis mixture comprising 10% TLE and 20 mM AgNO$_3$ (1:4 v/v) under initial alkaline pH condition of 11 at 24 h.

SEM image of AgNPs synthesized from the synthesis mixture comprising 10% TLE and 20 mM AgNO$_3$ (1:4 v/v) under initial alkaline pH condition of 11 is shown in Figure 4.21. The size range of AgNPs was determined using Image J software from the SEM image. The average size range of AgNPs obtained with alkaline pH condition of synthesis was found to be 21.6 nm with an approximate size range of 18.6 nm to 38 nm as shown in Figure 4.21 in comparison to the size range of 31 nm to 48 nm and the average size of 38.46 nm of AgNPs obtained from normal (unadjusted) pH conditions of synthesis as presented as Figure 4.17 of section 4.3.4 (B). Thus in spite of conversion of Ag$^+$ ions being above 99 % with both alkaline and normal (unadjusted) pH conditions, the size of the AgNPs synthesized are smaller and with narrower size distribution range with alkaline pH as compared to the AgNPs synthesized using normal (unadjusted) pH.

Thus on the basis of formation of monodispersed, smaller sized AgNPs with high conversion, initial alkaline pH 11 was found to be the optimum for the synthesis of monodispersed and stable AgNPs in case of TLE based AgNPs synthesis.

Sathishkumar et al. (2014) have also studied the effect of pH on the synthesis of AgNPs using *Cinnamon zeylanicum* bark extract as well as powder. They varied the pH of the synthesis medium from acidic and alkaline and reported that lower pH value promoted the nucleation of the nanoparticles without their growth, while higher

alkaline pH of the synthesis medium caused electrostatic repulsion between the AgNPs, thereby leading to formation of smaller nanoparticles. Acidic pH has been reported to be unfavourable for the synthesis of the AgNPs by several other researchers (Chowdhury et al. 2015; Ramesh et al. 2015; Thakkar et al. 2010; Dubey et al. 2010; Edison and Sethuram, 2012).

The studies reported in the current work show that initial alkaline pH is favourable for the synthesis of AgNPs using ALE and TLE.

4.2.6 Effect of the processes adopted for extraction of bioactive components from the leaves of *T.catappa* and *T.grandis* Linn f on synthesis of AgNPs

The process for extraction of bioactive components from the leaves determines the composition of the extract used for the synthesis of AgNPs, which in turn governs the rate of formation of AgNPs and their morphology. Thus, different extraction processes such as open solvent heating, extraction with reflux heating and sonication were adopted for preparation of ALE and TLE. The ALE and TLE were prepared by three different extraction processes (a) Open solvent heating (b) Reflux heating and (c) Sonication as described in Section 3.2.7.6 of Chapter 3. The extracts thus prepared were then used for the synthesis of AgNPs. AgNPs were synthesized using optimum conditions of initial pH 11 at room temperature with (a) 5% ALE and 20 mM $AgNO_3$ solution in 1:4 (v/v) ratio (b) 10% TLE and 20 mM $AgNO_3$ solution in 1:4 (v/v) ratio. The conversion of Ag^+ ions and the SPR characteristics were compared to study the effect of extraction process adopted in preparation of ALE and TLE on AgNPs synthesis. The major classes of bioactive components such as phenolics, antioxidants and flavonoids present in the extracts, which are considered to be responsible for reduction of Ag^+ ions to Ag^0 and capping of AgNPs were determined by analytical procedures described in Section 3.2.7.7 of Chapter 3 and are presented in Table 4.10.

Table 4.10 Content of bioactive components in ALE and TLE obtained through various extraction processes

Source	Process	Bioactive Components		
		Total Phenolic Content (µg GAE/mL)	Total Flavonoid Content (µg QE/mL)	Total Antioxidant Content (µM FE/ mL)
ALE	Open Solvent Heating	4583.9	5864.6	6808.3
	Reflux heating	5048.7	8062.5	6400
	Sonication	2282.2	3656.25	6183.3
TLE	Open Solvent Heating	2464.7	2604.2	6554.2
	Reflux heating	2851.6	2270.8	6025.0
	Sonication	1995.1	2989.6	5308.3

As observed in Table 4.10, the amount of antioxidants present in ALE and TLE were higher in the extracts prepared by open solvent heating method as compared to those prepared by extraction with reflux and sonication. However, the total phenolic content is higher in the extracts prepared by reflux heating in case of both ALE and TLE. However, the flavonoid content in TLE prepared by sonication is the highest as compared to that prepared by other methods, while that for ALE was the highest with reflux heating. Table 4.11 shows the conversion of Ag^+ ions in the synthesis using the ALE and TLE prepared by different extraction procedures and the SPR spectra for the synthesis mixtures with ALE and TLE are shown as Figure 4.22 (a) and (b) respectively.

Table 4.11 Influence of different extraction procedures on the synthesis of based AgNPs using ALE and TLE

Method of extraction	Percentage Conversion of Ag^+ ions	
	ALE	TLE
Open solvent heating	99.86	97.01
Reflux heating	99.55	88.65
Sonication	89.6	89.45
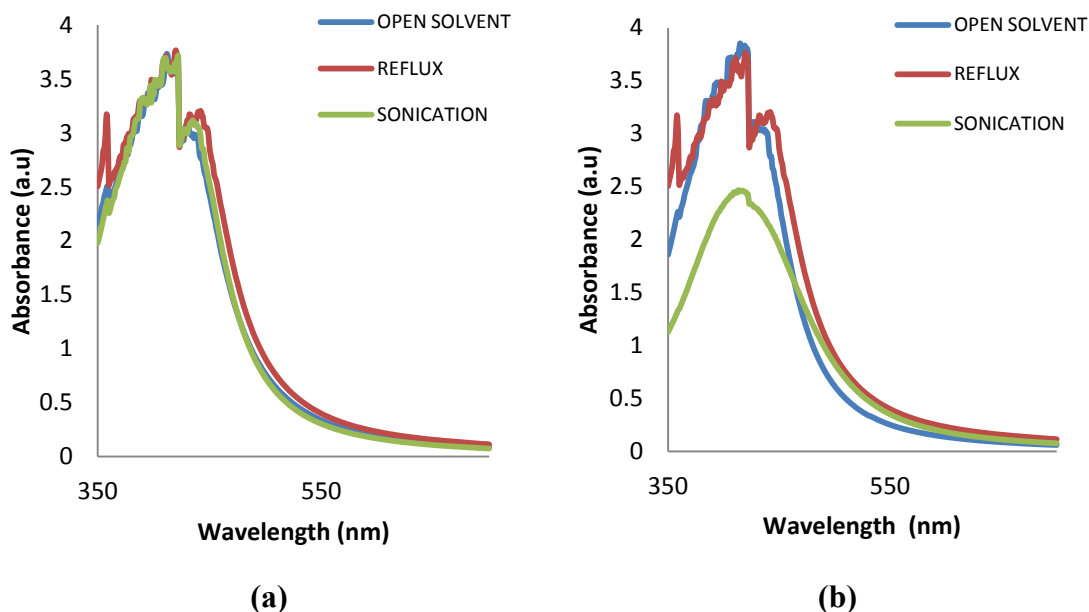
Figure 4.22 SPR spectra of synthesis mixtures of AgNPs synthesized using different extraction techniques for (a) ALE (b) TLE at 24 h

As observed in Table 4.11, the conversion is higher in the extracts prepared by open solvent heating method as compared to that prepared by extraction with reflux heating or sonication. The antioxidant contents are in the order of open solvent > reflux > sonication and the conversion followed the same order. However, total phenolic content and flavonoids were not the highest in extract prepared by open solvent method, in spite of conversion being the maximum in this case. It indicates that antioxidants are majorly responsible for reduction of Ag^+ to Ag^0. Thus, the major part of phenols and flavonoids may act as capping agents for AgNPs, rather than aid in reduction (Mittal et al. 2014; Bunghez et al. 2012; Vijayaraghavan et al. 2012; Gade et al. 2010).

The SPR peaks of AgNPs obtained (Figure 4.22 (a) and (b)) from the extracts prepared by the above mentioned extraction methods were analyzed. It is observed in Figure 4.22 (a) that the SPR characteristics for AgNPs prepared with ALE are similar for cases with open solvent extraction, extraction with reflux and sonication, indicating that the morphological characteristics of nanoparticles remain unchanged. It is observed in Figure 4.22 (b) that the SPR characteristics for AgNPs prepared with TLE are similar for cases with open solvent extraction and extraction with reflux, whereas AgNPs prepared using TLE from sonication showed SPR peak with lower

intensity indicating lesser number of particles. These results suggest that ALE and TLE prepared by open solvent extraction or extraction with reflux yield nanoparticles with similar characteristics. The spectra in cases of ALE and TLE, prepared by reflux extraction showed an additional peak at around 360nm in addition to the characteristic peak for AgNPs. The additional peak at 360nm corresponds to the flavonoids present in the extract (Fang et al. 2007) which remained in the synthesis mixture after AgNPs synthesis.

The SPR peaks for the AgNPs synthesized using open solvent extraction method were found to be sharp and narrower in comparison to the SPR peaks of AgNPs obtained by using reflux and sonication method of extraction procedures. Narrower SPR peak is indicative of monodispersed AgNPs which is highly desirable in a synthesis process. However, the conversion as seen in Table 4.11 is marginally higher (ALE) or higher (TLE) in case of extracts prepared by open solvent method. Owing to the presence of large quantity of antioxidants in the extract prepared, higher conversion of Ag^+ ions to Ag^0 and similar spectral characteristics depicting the morphology of AgNPs as those prepared by other extraction processes, as well as due to less time and energy consumption involved in open solvent extraction process, open solvent process was recommended for preparation of ALE and TLE.

4.3 Utilization of various bioactive components present in the aqueous leaf extracts in synthesis of AgNPs

As discussed in section 2.3.1 of Chapter 2, various bioactive components such as antioxidants, polyphenols and flavonoids present in the leaf act like reducing agents and as capping/stabilizing agents in AgNPs synthesis. The presence of these bioactive components in ALE and TLE are demonstrated in Section 4.2.6. As observed during optimization in Section 4.2.3, adequate balance between these bioactive components and Ag^+ ions must exist in the synthesis mixture, though it is not the sole decisive parameter. Song and Kim (2009) have also reported that a delicate balance exists between the bioactive compounds of a plant material and, the precursor salt concentration.

In order to gain a better perspective of biobased synthesis of AgNPs by ALE and TLE, the major classes of bioactive components in the plant leaf extracts of

T.catappa and *T.grandis* Linn f prepared by open solvent extraction process were assessed and the reduction in the content of these components in the synthesis mixture after AgNP synthesis was determined. The AgNPs were synthesized using (a) 5% ALE and 20 mM $AgNO_3$ in the volume ratio of 1:4 (v/v) of the synthesis mixture (b) 10% ALE and 20 mM $AgNO_3$ in the volume ratio of 1:4 (v/v) of the synthesis mixture, both with initial alkaline pH condition of 11 and the utilization of the bioactive components in the synthesis of AgNPs is shown in Figure 4.23 and Figure 4.24 respectively.
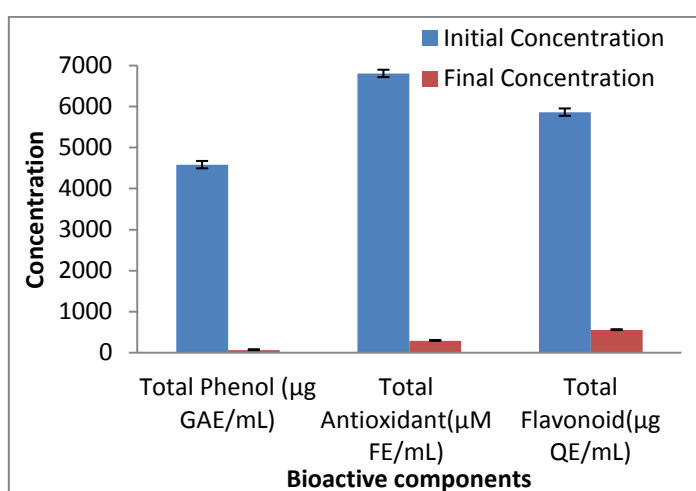
Figure 4.23 TPC, TFC and TAC content in the synthesis mixture before and after the synthesis of AgNPs using 5% ALE
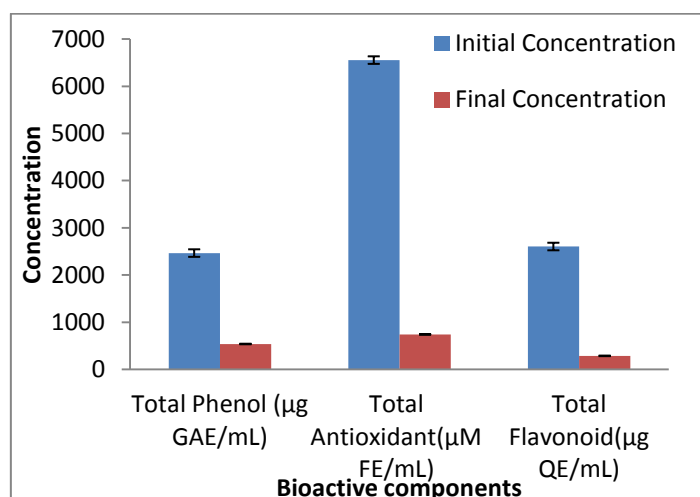
Figure 4.24 TPC, TFC and TAC content in the synthesis mixture before and after synthesis of AgNPs using 10% TLE

144

The total phenolics content (TPC), total antioxidant content (TAC) and Total flavonoid content (TFC) were analyzed using the methodologies described in section 3.2.7.8, 3.2.7.9, 3.2.7.10 of Chapter 3. A percentage reduction of 98.67% in the total phenolic content, 89% reduction in the total antioxidant content and 90.65% reduction in the total flavonoid content of ALE (Figure 4.23) after synthesis of AgNPs was observed indicating that these bioactive components present in ALE played a role in the synthesis of AgNPs.

As shown in Figure 4.24, total phenolic content in TLE reduced by 78%; total antioxidant content by 96.56% and total flavonoid content reduced by 89% after the synthesis of AgNPs using TLE. The evident utilization of these three major classes of bioactive components, depict the role of these components in the synthesis of AgNPs.

The decrease in content of these components in the synthesis mixture was observed in the case of ALE and TLE (Figure 4.23 and Figure 4.24) which is suggestive of the fact that the bioactive components present in the leaf extracts play an intrinsic role in the synthesis of AgNPs as they are responsible for the reduction of the Ag^+ ions into Ag^0 nuclei and subsequent capping and stabilization of the formed AgNPs. The major classes of plant bioactive compounds that play a role in the reduction of the precursor salt in the synthesis mixture are antioxidants (Niraimathi et al. 2013; Ahmad et al. 2010b; Park et al. 2011) while phenols and flavonoids majorly contribute as capping agents (Mittal et al. 2014; Bunghez et al. 2012; Vijayaraghavan et al. 2012; Gade et al. 2010). High conversion of Ag^+ ions (Table 4.11) and decrease in the levels of bioactive components in the synthesis mixture shows that both ALE and TLE possess natural antioxidants, phenolics and flavonoids which reduce the $AgNO_3$ to AgNPs with subsequent capping and stabilization (Mittal et al. 2014; Huang et al. 2011; Philip, 2011; Zhou et al. 2010).

Under optimum set of conditions of leaf powder suspension concentration, precursor salt solution concentration and the volume ratio between the two, a perfect balance between the reducing/capping agents and the number of Ag^+ ions in the synthesis mixture exist, to form monodispersed AgNPs with small size range and with high conversion level .

4.4 Synthesis time duration for the synthesis of AgNPs using ALE and TLE under optimal conditions of synthesis

The synthesis of AgNPs using ALE and TLE was performed to determine if the synthesis time could be reduced under optimal conditions of synthesis. The extracts were prepared by open solvent heating method and the synthesis was carried out under optimum conditions of initial pH 11 at room temperature with (a) 5% ALE and 20 mM $AgNO_3$ solution in 1:4 (v/v) ratio (b) 10% TLE and 20 mM $AgNO_3$ solution in 1:4 (v/v) ratio respectively. The UV-Vis spectroscopy of the synthesis mixture containing the AgNPs was performed at a regular time interval period of 1.5 min. The SPR spectra of the synthesis mixture containing ALE and TLE at different synthesis time duration indicating the formation of AgNPs is presented in Figure 4.25 (a) and Figure 4.25 (b) respectively.

(a)   (b)
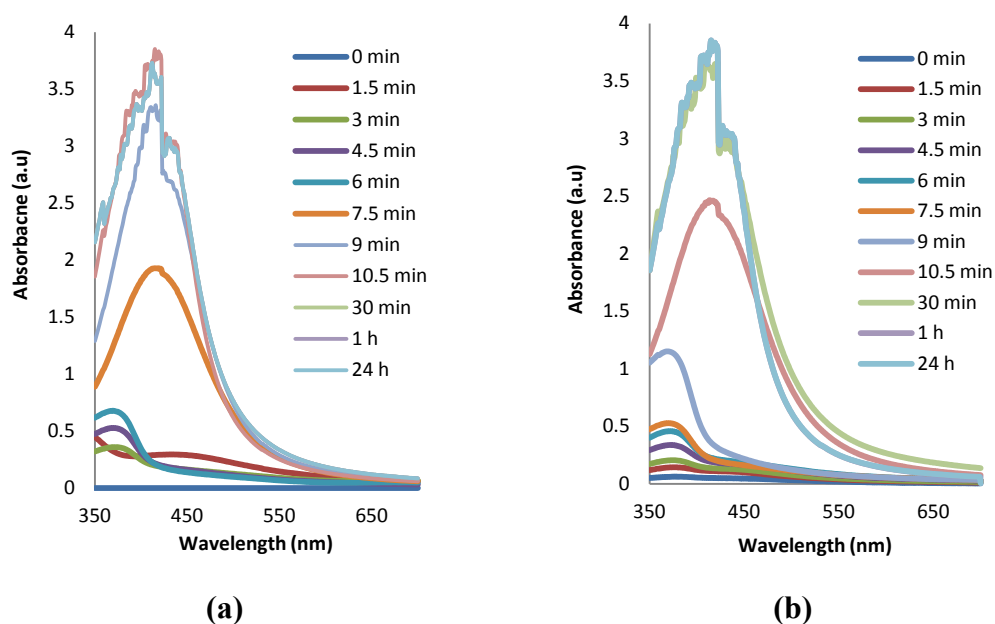
Figure 4.25 SPR spectra of synthesis mixtures showing the synthesis of AgNPs as a function of time under optimized conditions using (a) ALE and (b) TLE

As seen in Figure 4.25 (a) the SPR peak characteristic of AgNPs synthesized using ALE originated after 3 min of the start of the reaction, this indicates the beginning of the reduction process of Ag^+ ions to Ag^0 and the beginning of nucleation. The peak was of low intensity indicating the formation of a small number of Ag^0 nuclei but as the synthesis proceeded with time, the intensity of SPR peak

centered at 380 nm increased till 6 min of the synthesis time duration. The increase in the peak intensity indicated the increase in the nucleation by reduction of the available Ag^+ ions in the synthesis mixture by the bioactive components of ALE. However at 7.5 min of synthesis time the SPR peak increased in intensity and the characteristic peak of AgNPs centred at 420 nm with highest intensity appeared. The increase in intensity of the SPR peak indicated the growth process of the AgNPs and the layering of Ag^0 nuclei to form AgNPs with small diameters.

The SPR peak of AgNPs in Figure 4.25 (a) exhibited the maximum intensity at time interval of 10 min with no shift or change in the characteristics of the SPR peak of the AgNPs synthesized using ALE indicating that after the optimization of the parameters the synthesis time period was drastically reduced to 10.5 min. No further change in the SPR characteristics was observed with increase in the synthesis time duration.

Figure 4.25 (b) shows the SPR spectrum indicating the formation of AgNPs using TLE over the synthesis time duration of 24 h. Increase in the intensity of the SPR peak at 412 nm was observed as the synthesis time proceeded marking the beginning of the reduction process of Ag^+ ions to Ag^0 indicating increase in the rate of nucleation. The nucleation process continued till 9 min of the synthesis time duration as indicated by blueshifted intense peak. However at 10.5 min of synthesis, the SPR peak with high intensity, shifted to 420 nm (characteristic of AgNPs) marking the beginning of the growth of AgNPs. This increase in the intensity indicated the formation of a large number of small sized AgNPs. The SPR peak intensity reached the maximum at 30 min of the reaction time and no further change in the SPR spectra with progress of synthesis time duration was seen indicating that the synthesis of AgNPs was completed within time duration of 30 min.

Thus, the optimization of synthesis process parameters brought about tremendous reduction in the synthesis time period without any change in the morphological characteristics of the AgNPs. This reduction in the synthesis time duration implies the rapidness and simplicity of the overall AgNPs synthesis process using ALE and TLE.

The process of synthesis of AgNPs using plant bioactive compounds for the reduction of the $AgNO_3$ as a precursor salt into nanoparticles does not involve any

harsh process conditions such as elevated temperature and toxic chemical reagents, solvents or surfactants unlike the chemical and physical routes of synthesis and yields AgNPs that are monodispersed with small size range. The process harnesses the untapped potency of bioactive components that remain unutilized from the large amount of biowaste generated in the form of foliage from timber industry and as an agrowaste. This process focuses on utilizing resources that do not possess agro-industrial value and channelling it towards the synthesis of AgNPs through a benign and ecofriendly route of green synthesis.

4.5 Characterization of AgNPs synthesized using ALE and TLE

4.5.1 Characterization of AgNPs synthesized using the aqueous extract of *T.catappa* leaves

The AgNPs synthesized using 5% ALE and 20 mM AgNO$_3$ solution in 1:4 (v/v) ratio at an initial alkaline pH condition of 11 at the ambient temperature of 28±2 ºC were analyzed using different characterization techniques to determine its morphological characteristics and to provide qualitative assessment of various biomolecules encapsulating the synthesized AgNPs.

4.5.1.1 UV-Vis Spectral analysis

Nanoscale silver is intense brown in colour and the appearance of this characteristic colour is often considered as a visual confirmation of the formation of AgNPs (Maria et al. 2015; Basavaraja et al. 2011, Jain, 2009, Song and Kim, 2009,). AgNPs are extraordinarily efficient at absorbing and scattering light. Their interaction with light depends on the size and the shape of the nanoparticles (Kelly et al. 2003). Preliminary confirmation of AgNP formation during the synthesis was provided by the visual observation of brown colour in the synthesis mixture as shown in Figure 4.2(b) of section 4.2 (A). Second level confirmation of AgNPs was determined through UV-Vis Spectrophotometry analysis of the synthesis mixture containing AgNPs. Metallic AgNPs possess strong surface plasmon resonance due to the collective oscillation of surface electrons in visible wavelength region. The understanding of surface plasmon resonance provides the relationship between the plasmon and the morphological characteristics of the AgNPs. Figure 4.26 presents the

SPR spectra of the AgNPs synthesized using ALE. As discussed in section 4.2.2, the SPR band of AgNPs synthesized using ALE is sharp and intense with peak centred at 420 nm indicating the formation of a large number of smaller sized monodispersed AgNPs. However, a peak split with a narrow difference in excitation energy levels of the two peaks (section 4.2.2) indicates the formation of nearly isotropic AgNPs.
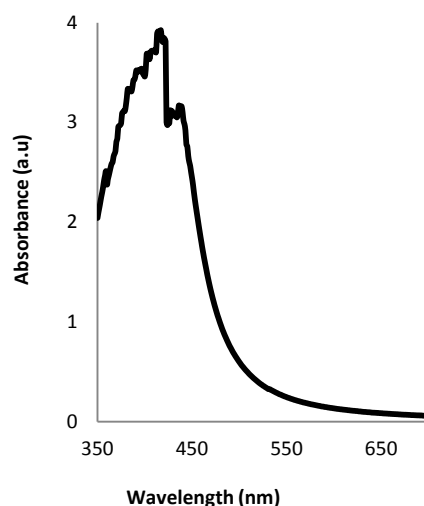
Figure 4.26 SPR spectra of the synthesis mixture containing AgNPs synthesized using ALE

4.5.1.2 SEM analysis

The morphological analysis of the AgNPs synthesized using ALE is as shown in the SEM image in Figure 4.19 of section 4.2.5 (A) and it reveals the presence of large number of monodispersed and nearly isotropic, quasi spherical shaped AgNPs with size range of 18 nm to 38 nm and approximate size of 20.8 nm as determined using Image J software.

4.5.1.3 XRD analysis of AgNPs synthesized using ALE

X-Ray Diffractogram of the AgNPs synthesized using ALE is shown in Figure 4.27 and revealed the presence of peaks at 2θ values of 38.35, 44.69, 64.76, 77.65 and 81.79 belonging to (111), (200), (220), (311) and (211) planes of face centred cubic structure (FCC) of metallic crystalline silver (JCPDS Data Card No- 04-0783). The average crystallite size of AgNPs was determined using DeBye-Shrerrer's formula and found to be 8.27 nm. The synthesis of FCC crystalline AgNPs by plant based

synthesis route has been widely reported (Song and Kim, 2009; Chandran et al. 2006; Vigneshwaran et al. 2006 b; Li et al. 2007; Ahmad et al. 2003 a; Sun and Xia, 2002).
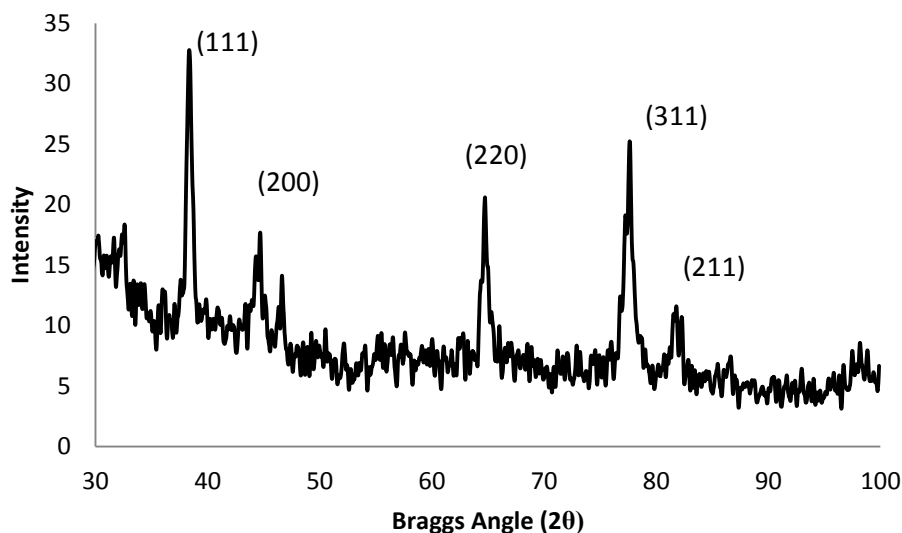
Figure 4.27 X-ray diffraction pattern obtained from AgNPs synthesized using ALE.

4.5.1.4 Particle size distribution analysis of AgNPs synthesized using ALE

The size distribution of the AgNPs synthesized using ALE as obtained from Particle size distribution analysis by DLS is shown in Figure 4.28 and it revealed that the hydrodynamic size of the AgNPs in aqueous colloidal solution lie in the range of 9-35 nm with an average size of 10.9 nm. The narrow size range indicates the presence of fairly monodispersed AgNPs and the average size obtained is found to be almost similar to the crystallite size obtained through XRD analysis.
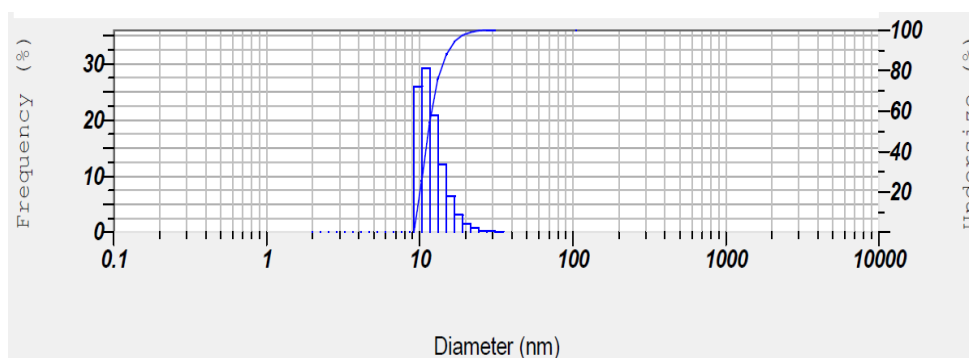
Figure 4.28 Size distribution histogram of AgNPs synthesized using ALE

Table 4.12 of section 4.5.2.4 compares the size of AgNPs synthesized using other plant resources and ALE. The average size of AgNPs synthesized using ALE is smaller than those synthesized using other plant resources, though the size range is broader than the few others.

4.5.1.5 Zeta potential analysis and stability of AgNPs synthesized using ALE

A common way to evaluate the stability of colloidal dispersions is by determining the magnitude of zeta potential. It is a very good index of the magnitude of the electrostatic repulsive interaction between particles. The zeta potential (ζ -ZP) is a function of the surface charge which develops when any material is placed in a liquid. In dispersions where value of the ζ potential is close to zero (isoelectric point), particles tend to agglomerate. At highly negative or positive values of ζ potential (more than 25 mV or less than -25mV (nanoComposix, 2003) particles in dispersions tend to repel each other.

In an electrostatically stabilized dispersion, charges generated on the surface of the AgNP prevent or control agglomeration. Steric stabilization takes place when large molecules adsorb on to the surface of AgNPs; introducing physical barriers between them. A combination of electrostatic and steric mechanisms produces electrosteric stabilization (Mandzy et al. 2005). All three stabilization mechanisms prevent nanoparticles from agglomerating thereby leading to the stability of the particle dispersion.The zeta (ζ) potential is the electrostatic potential at the boundary dividing the compact layer and the diffuse layer of the colloidal particles. Reduction or increase in the ζ potential is related to the presence of the dissociated functional groups that result in the zeta potential changes depending on the ionic nature of polyelectrolyte; negatively charged groups (e.g., carboxylic groups) cause decrease of ζ, whereas the positively charged groups (e.g., amino groups) contribute to the increase in the zeta potential value (Ostolska and Wiśniewska, 2014).

The zeta potential value of AgNPs synthesized using ALE was determined according to the methodology described in section 3.6.5 of Chapter 3. The zeta potential value of AgNPs synthesized using ALE was found to be -36.7 mV with water as a solvent and electrode voltage of 3.3 V at 25 ºC and the zeta potential measurement is provided in Appendix IX. The zeta potential values above ±25 mV

indicates good stability of AgNPs. The zeta potential values of AgNPs synthesized by other plant resources are shown in Table 4.13 of section 4.5.2.5 further in this Chapter.

The zeta potential value for AgNPs synthesized using ALE is better than those synthesized by other plant resources from literature. The value being smaller than those reported in the literature indicates it superior stability. The AgNPs synthesized using ALE exhibited anionic surface charge. The stability of AgNPs synthesized using ALE in aqueous colloidal solution was determined for a time duration of 6 months at specific time intervals using UV-Vis spectroscopy as described in section 3.6.7 and the SPR spectra of the AgNPs obtained was analysed. Figure 4.29 shows that the SPR spectra of the aqueous colloidal solution of AgNPs synthesized using ALE did not show any significant change in the spectra indicating the stability of the AgNPs.
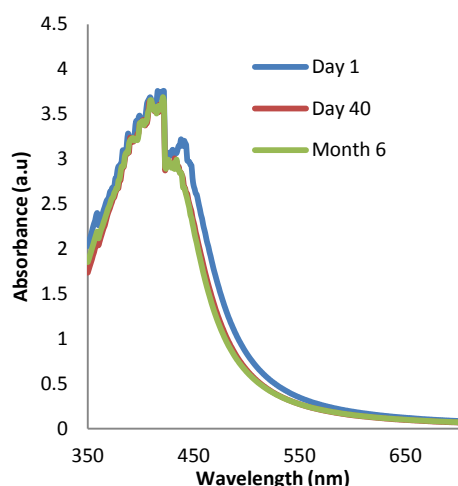
Figure 4.29 SPR spectra of aqueous colloids of AgNPs over time duration of 6 months synthesized using ALE

4.5.1.6 TEM analysis of AgNPs synthesized using ALE

To obtain a better insight into the morphological characteristics, TEM analysis was performed on the AgNPs synthesised using ALE. The TEM image is shown in Figure 4.30 and the particles were found to be quasi-spherical. The average size of the AgNPs synthesized using ALE was determined from the TEM analysis using Image J software (Number of nanoparticles=48) and was found to be 10.56 nm. The size range of the particles was found to be of 4.56 nm to 20 nm. It indicates that the AgNPs

synthesized are with a narrow size range and thus monodispersed. The presence of capping around the nanoparticles is evident in the TEM image, showing that the nanoparticles are encapsulated in the layer formed by the capping agents in ALE.
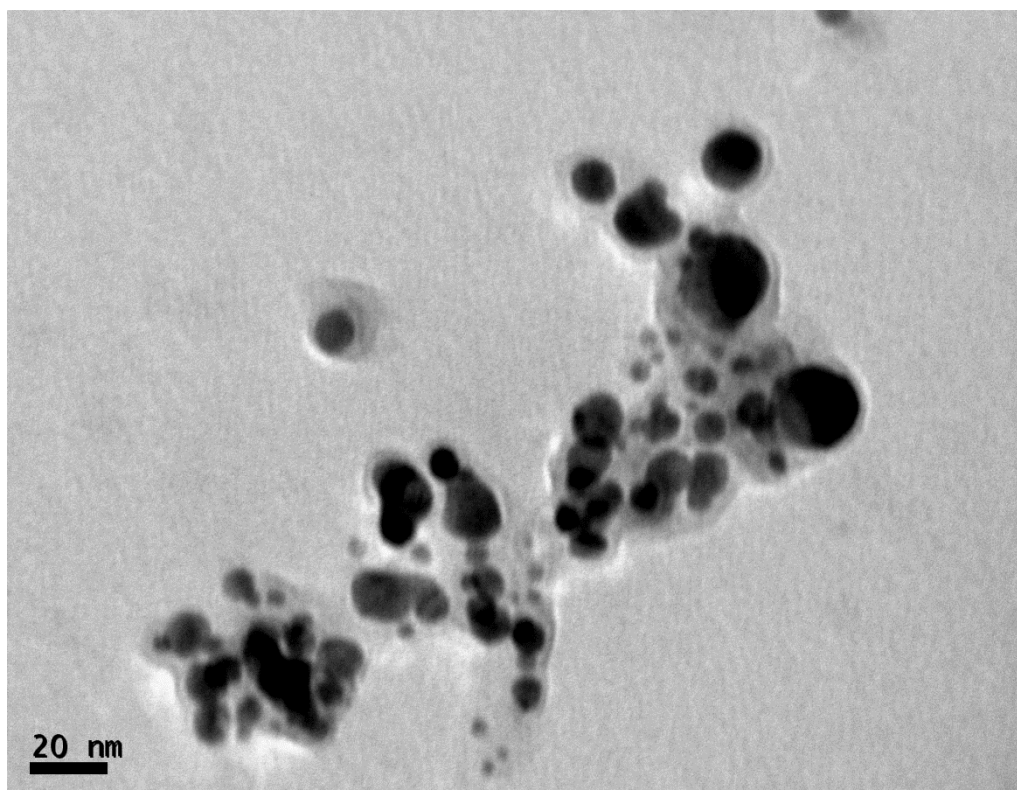
Figure 4.30 TEM image of AgNPs synthesized using ALE

4.5.1.7 EDS analysis of AgNPs synthesized using ALE

EDS analysis of the AgNPs was performed using SEM to determine its elemental composition (Rao et al. 2013 a; Gardea-Torresday et al. 2002). The spectra obtained as depicted below in Figure 4.31 reveals the presence of elemental peaks belonging to silver as well as that for carbon and oxygen. The signal peak for silver was found to be very strong in comparison to that of oxygen and carbon revealing the formation of AgNPs. The presence of peaks belonging to carbon and oxygen reveal that the AgNPs synthesized using the aqueous extract of *T.catappa* leaves are covered by organic capping agents of plant origin. It supports the presence of encapsulating layer around the nanoparticles as viewed through TEM. Similar findings were reported by Cruz et al. (2010) who observed a signal peak belonging to elemental carbon in the EDS spectra of AgNPs synthesized by *Lippia citriodora* (Lemon

Verbena) and they attributed it for the presence of plant bioactive compounds in the sample.
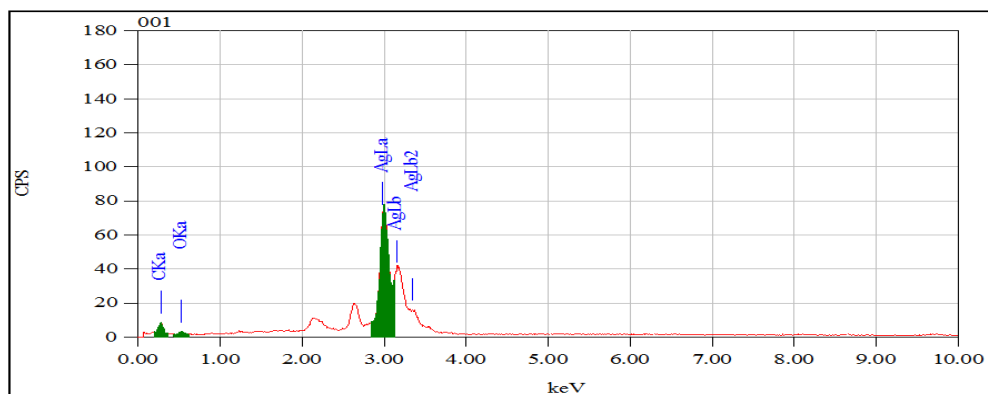
Figure 4.31 EDS analysis of AgNPs synthesized using 5%ALE and 20mM of precursor salt in the volume ratio 1:4, under alkaline pH 11.

The presence of these capping agents make AgNPs synthesized using biobased routes more efficient than chemically synthesized AgNPs, as biological capping moieties are readily identified and are acceptable by organisms in the field of therapeutical and medical applications (Kora and Sashidhar, 2015; MacCuspie, 2011; Govindaraju et al. 2009). Chemically synthesized AgNPs are known to be decorated by harsh surfactants acting as capping agents rendering them bio-incompatible for medical applications (Baker et al. 2013; Von White et al. 2012).

4.5.1.8 FTIR analysis of AgNPs synthesized using ALE

Plant based synthesis lead to the formation of AgNPs that are capped with bioactive compounds present in the plant extract used in the synthesis. FTIR analysis has been widely used by researchers as an important analytical tool for examining and determining the capping agents present on the surface of the AgNPs (Aromal and Philip, 2011; Duran et al.2011; Iravani, 2011; Das et al. 2011; Philip et al. 2011; Kaviya et al. 2011; Raut et al. 2010; Bar et al. 2009)
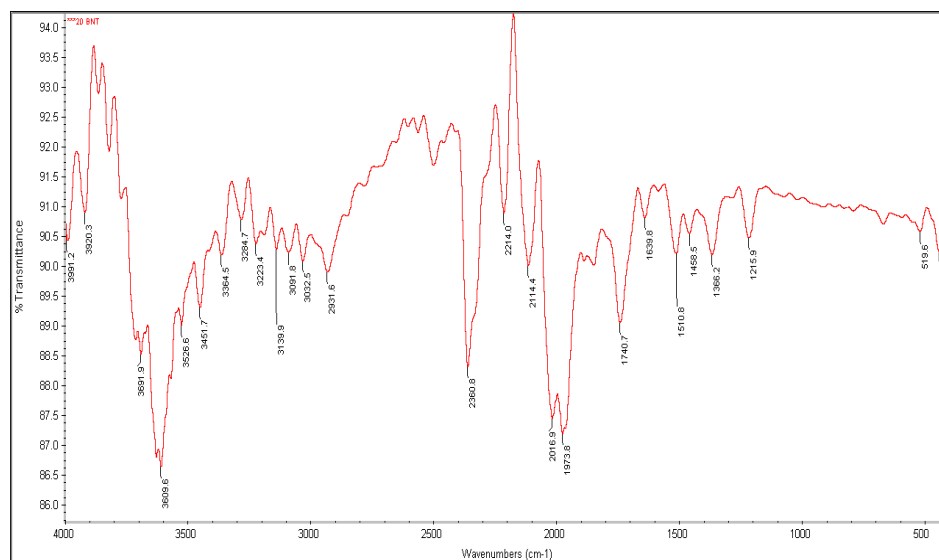
Figure 4.32 FTIR spectra of AgNPs synthesized using 5%ALE and 20mM of precursor salt in the volume ratio 1:4, under alkaline pH 11.

FTIR analysis of the synthesized AgNPs further validated the presence of capping agents on the surface of the AgNPs. In the IR spectra presented in Figure 4.32, a strong peak at 3609 cm^{-1} indicates the presence of N-H stretching vibrations (Ashokumar et al. 2014). The peaks belonging to 3991cm^{-1} to 3609cm^{-1} belong to the –C- of the carboxylic group. Peak 3451cm^{-1} indicates the vibration of O-H groups of the phenols. The peak at 3364cm^{-1} indicates the N-H group from the peptides. 2931.6cm^{-1} peak belongs to asymmetric stretching of C-H bonds. While the medium peaks centered around 2114cm^{-1} belong to the C=C variables, Carboxylic acid group (C=O) stretching is indicated by the small peaks at 1740.7cm^{-1} and 1366.2cm^{-1} (Philip, 2010; Narayan and Sakthivel, 2008), peak 1639.8cm^{-1} indicates the presence of aromatic rings and the amine groups are confirmed by the peak at 1510.8cm^{-1} (Bansal et al. 2005), The peak at 1215.9cm^{-1} represents the C-O stretching indicating polyol stretching. The presence of various organic groups on the surface of the synthesized AgNPs indicates the role of plant bioactive compounds in encapsulation of the AgNPs as capping agents.

4.5.2 Characterization of AgNPs synthesized using TLE

4.5.2.1 UV-Vis Spectral analysis

Figure 4.32 shows the SPR of AgNPs synthesized using 10 % TLE and 20 mM of $AgNO_3$ in the volume ratio of 1:4 (v/v) with an initial alkaline pH of 11 at ambient synthesis temperature of 28±2 ºC. The SPR is sharp, narrow and centred at 420 nm, indicating the formation of large number of smaller sized, nearly isotropic AgNPs as discussed in section 4.4 previously.
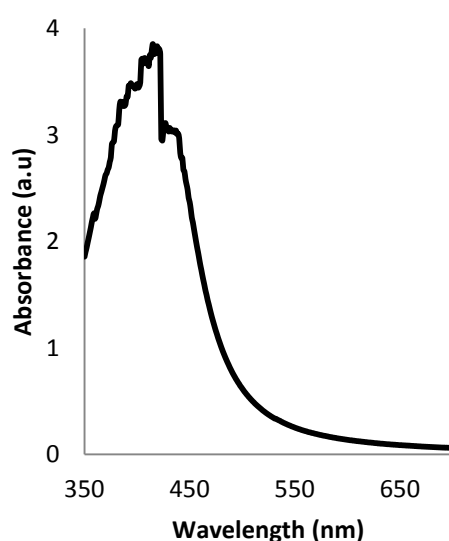
Figure 4.33 SPR spectra of synthesis mixture containing AgNPs synthesized using TLE

4.5.2.2 SEM analysis of AgNPs synthesized using TLE

Figure 4.21 in section 4.2.5 (B) presents the SEM image of AgNPs synthesized using TLE and it reveals the presence of AgNPs with a size range of 18.6 nm to 38 nm with an approximate size of 21.6 nm. The particles are nearly isotropic with quasi spherical shape.

4.5.2.3 XRD analysis of AgNPs synthesized using TLE

Figure 4.34 reveals peaks in the X ray diffractogram obtained from AgNPs synthesized using TLE with 2θ values of 38.03, 46.23, 64.35 and 77.17 belonging to (111), (200), (220), (311) planes of face centred cubic (FCC) structure of crystalline metallic silver. Several researchers reported the synthesis of FCC structured AgNPs using biological sources as reducing agents (Zargar et al. 2012; Philip, 2011; Philip

and Unni, 2011; Guzman et al. 2011; Ahmad et al. 2010 b). The average crystallite size of the AgNPs was determined using De-bye Sherrer`s equation and was found to be 14.12 nm.
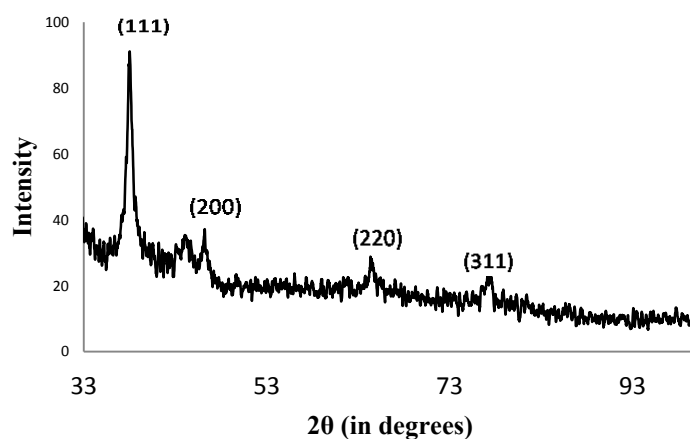
Figure 4.34 X-ray diffraction pattern obtained from AgNPs synthesized using TLE

4.5.2.4 Particle size distribution analysis

The size distribution of the AgNPs synthesized using the extract of TLE as obtained from particles size distribution analysis using dynamic light scattering technique is shown in Figure 4.35 and it revealed that the size of the AgNPs lie in the range of 19-50 nm. The average size of the particles was determined to be 20.4 nm which is in agreement with the SEM analysis and greater than the crystallite size determined using XRD. Table 4.12 shows the particle size of AgNPs synthesized using various plant resources.
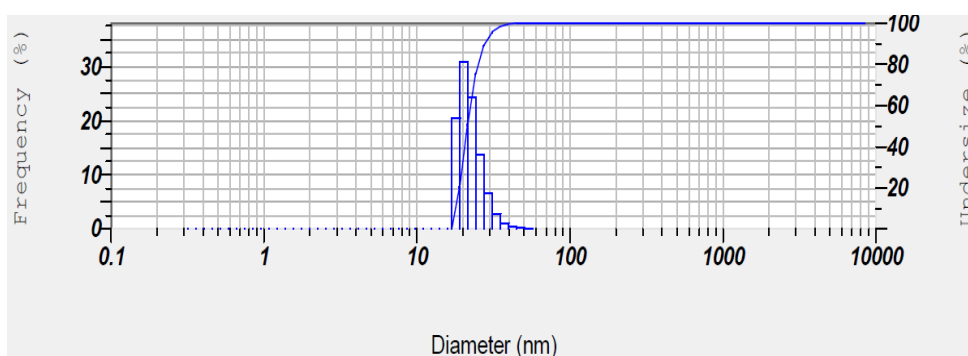
Figure 4.35 Size distribution histogram of AgNPs synthesized using TLE

Table 4.12 Particle size of AgNPs synthesized using various plant resources.

Plant Source	Size of AgNPs synthesized (nm)	References
Azadirachta indica	50-100	Shankar et al.2004
Aloe vera	15-20	Chandran et al. 2006
Emblica Officinalis	10-20	Ankamwar et al.2005 a
Cinnamomum camphora	55-80	Huang et al.2007a
Tamarind Leaf Extract	20-40	Ankamwar et al.2005 b
Carica papaya	25-50	Jain et al.2009
Parthenium hysterophorus L	40-50	Parashar et al.2009
Diopyros kaki)	15-19	Song and Kim, 2008
Camellia sinensis	30-40	Vilchis-Nestoret al. 2008
Eucalyptus hybrida	50-150	Dubey et al. 2009
ALE	9-35 (10.9) nm	Present study
TLE	19-50 (20.4) nm	Present study

As seen in Table 4.12 the AgNPs synthesized using TLE with average particle size of 20.4 nm and size range of 19-50 nm were found to be larger than those synthesized using ALE. However the size of AgNPs obtained in the present study are comparable to the size of particles synthesized by other researchers.

4.5.2.5 Zeta potential analysis and stability of AgNPs synthesized using TLE

The zeta potential value of AgNPs synthesized using TLE was determined according to the methodology described in section 3.6.5 of Chapter 3. The zeta potential value and was found to be -36.5 mV (Zeta potential measurement is provided in Appendix IX) with water as a solvent and electrode voltage of 3.3 V at 25 ºC. The zeta potential value above +25 mV and below -25 mV indicates very stable AgNPs (nanoComposix, 2003). Table 4.13 shows the zeta potential value of AgNPs synthesized using various plant resources.

The AgNPs synthesized using plant extracts were found to possess anionic surface charge as seen in Table 4.13. The zeta potential value of AgNPs synthesized using TLE in the present study were found to be better than the zeta potential value of AgNPs synthesized using various other plant resources shown in Table 4.13 and almost similar to those synthesized using ALE. The zeta potential value of AgNPs synthesized using ALE and TLE show good stability of the particles and indicates their stable dispersions in aqueous solution. However to evaluate the stability of TLE based AgNPs in aqueous solution; UV-Vis spectroscopy of the aqueous AgNPs

colloidal solution was performed at specific time intervals for a duration of 6 months as described in section 3.6.7 and the SPR spectra of the AgNPs obtained was analysed. Figure 4.36 shows that the SPR spectra remained unchanged over a duration of over a time duration of 6 months and did not show any signs of aggregation indicating good stability of the AgNPs synthesized using TLE.

Table 4.13 Zeta potential value of AgNPs synthesized using various plant resources

Plant Source	Zeta Potential value	Reference
Fruit extract of *Tanacetum vulgare*	-26 mV	Dubey et al. 2010
Callicarpa maingayi Stem Bark Extract	-35.5 ± 3.7 mV	Shameli et al. 2012
Citrus limon aqueous extract	−29 mV	Prarthna et al. 2011a
Terminalia chebula fruit extract	−35.6 mV	Edison and Sethuraman, 2012.
Pergularia daemia plant latex	−27.4 mV	Patil et al. 2012
Melia azedarach Linn leaf extract	−24.9 mV	Sukirtha et al. 2012
Extract of Oak Fruit Hull (Jaft)	−25.3 mV	Heydari and Rashidipour, 2015
ALE	-36.7 mV	Present Study
TLE	-36.5 mV	Present Study
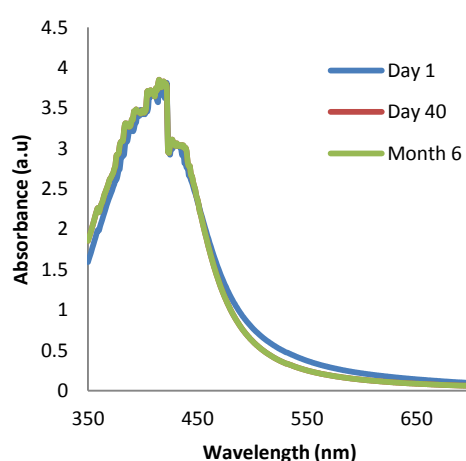
Figure 4.35 SPR spectra of aqueous colloids of AgNPs over time duration of 6 months synthesized using TLE

4.5.2.6 TEM analysis of AgNPs synthesized using TLE

TEM image of AgNPs synthesized using TLE is presented in Figure 4.37 revealed the presence of quasi spherical AgNPs. The average size of the AgNPs was calculated using Image J software and determined as 22 nm and was found to lie in a a narrow size range of 5 nm to 28.3 nm indicating the monodispersity of the particles. The presence of capping around the nanoparticles is evident in the TEM image, showing that the nanoparticles are encapsulated by a layer of capping agents in TLE. The average size obtained by TEM analysis matched with those obtained through SEM and DLS analysis with marginal differences.
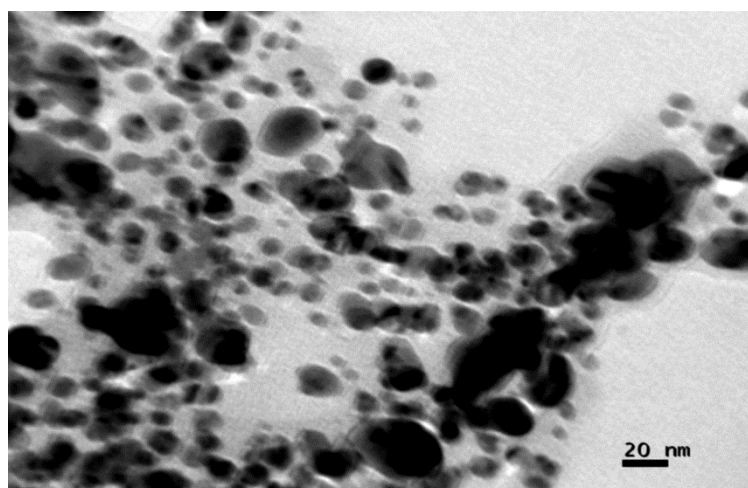
Figure 4.37 TEM image of AgNPs synthesized using TLE

4.5.2.7 EDS analysis of AgNPs synthesized using TLE

The presence of elemental peaks belonging to Carbon and Oxygen in Figure 4.38, in addition to the elemental silver peak indicates the presence of plant origin capping agents on the AgNPs signifying the role of the bioactive components present in TLE as capping agents.
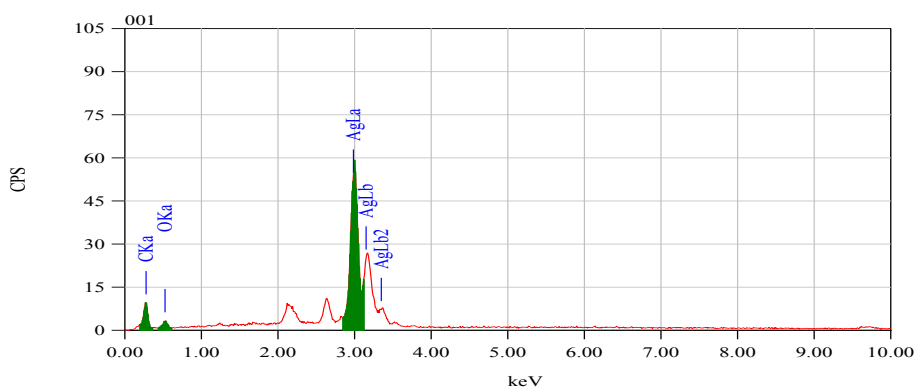
Figure 4.37 EDS analysis of AgNPs synthesized using TLE

4.5.2.8 FTIR analysis of AgNPs synthesized using TLE

Significant results pertaining to the involvement of the plant based bioactive components in the capping of AgNPs were further obtained by subjecting the AgNPs to FTIR analysis.

The IR spectra in Figure 4.39 revealed a sharp peak at 2358 cm^{-1} which can be attributed to the N- H stretching vibrations, 1218.8 cm^{-1} to C-O stretching of polyols like hydroxyflavones, 1010cm^{-1}to C-N stretching vibrations of aliphatic amines or to alcohols and phenols indicating that phenols also play an important role in the reduction of the precursor salt. The peak at 1362.7 cm^{-1} indicates the presence of residual NO$_3^-$ along with the synthesized nanoparticles, 1580.4 cm^{-1} can be attributed to C-O stretching vibrations, while 2916.1 cm^{-1} and 2848.5 cm^{-1} correspond to amide linkages (Prathna et al. 2011; Krishnaraj et al. 2010). The fingerprint thus obtained suggests that, bound and unbound amide linkages belonging to aromatic rings, ethers and polyphenols are the bioactive components that act as reducing and stabilizing agents in the synthesis of AgNPs.
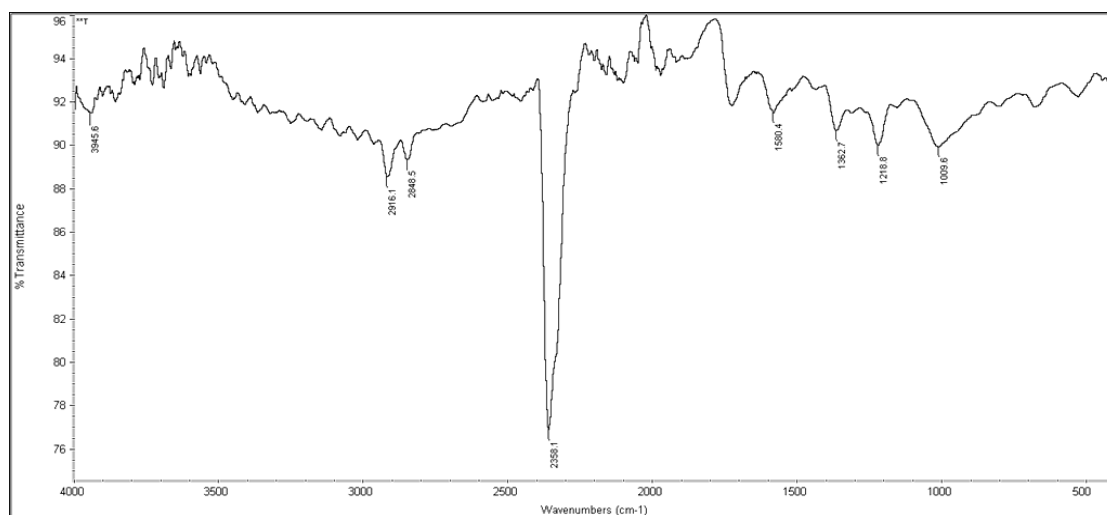
Figure 4.39 FTIR spectra of AgNPs synthesized using TLE

The presence of plant bioactive compounds encapsulating the AgNPs being synthesized has been widely studied and reported (Dipankar and Murugan, 2012; MubarakAli et al. 2011; Jain et al. 2009; Bar et al. 2009; Li et al. 2007).

In the present study, AgNPs were successfully synthesized using agrowaste resources such as *T.catappa* leaves extract and *T.grandis* Linn. f leaves extract. The bioactive compounds present in them were channelled towards the reduction of the

precursor salt i.e., $AgNO_3$ to AgNPs and were also determined to be acting as capping agents around the AgNPs synthesized using the plant leaf extracts. The careful selection and precise control of process parameters such as precursor salt ($AgNO_3$) solution concentration, concentration of leaf powder suspension used for the extraction, volume ratios of the extract and the $AgNO_3$ solution and pH of the synthesis mixture were found to be important and these parameters are known to have unambiguous control over the characteristics and the conversion of Ag^+ ions to yield AgNPs. The process can be fine tuned to synthesize AgNPs on a large scale. Understanding the influence of process parameters and knowledge on optimum set of conditions on the synthesis of AgNPs, provides researchers a better edge in controlling the process to obtain desired characteristics of AgNPs. Bioactive components such as phenols, antioxidants and flavonoids play a crucial role in the reduction of precursor salt and its subsequent capping were also determined through the reduction in the concentration of the bioactive compounds after the synthesis of AgNPs. These AgNPs were found to be stable and monodispersed with a narrow size range.

Bacterial based synthesis of AgNPs

Studies have reported that similar to plant based methods, the microbial based methods for the synthesis of AgNPs are cost effective, ecofriendly and are carried out under ambient conditions of synthesis while leaving a lesser chemical foot print on the environment and considered as greener and cleaner process. These processes have been reported to yield nanoparticles with distinct characteristics which serve for their unique applications. As presented in Section 2.3.3 of Chapter 2, microbial resources such as bacteria, yeast and fungi have been reported to mediate the biobased synthesis of AgNPs (Duran et al. 2011; Geriecke and Pinches, 2006; Duran et al. 2005; Nair and Pradeep, 2002).

In the current research work, bacterial strains with susceptibility to silver rich environment and with the efficacy to synthesize extracellular AgNPs by reduction of silver precursor salt were isolated and identified. The influence of precursor salt solution concentration and pH of the synthesis medium on the synthesis of AgNPs by the cell free supernatants of the bacterial isolates was studied and their characterization was performed.

4.6. Isolation and screening of microorganisms for the synthesis of AgNPs

The bacterial strains were isolated from the dust laden soil from the workbench of a silversmith. This source of sample collection was chosen as it would increase the possibilities of isolating microorganisms with the efficiency of thriving in silver rich conditions such that they possess the machinery required for the synthesis of AgNPs. The isolation of the microbes was carried out by performing serial dilution of the sample collected according to the methodology described in section 3.3.3 of Chapter 3. $AgNO_3$ was chosen as the precursor salt for isolation of bacterial strains and for nanoparticle synthesis (Prabhu and Paulose, 2012; Rai et al. 2009; Moronez et al. 2005; Sun and Xia, 2002; Bragg and Rainnie, 1947; De and Bergsteinsson, 1947). The bacteria were cultured on solid agar medium enriched with 0.1 g/L of $AgNO_3$. The nutrient agar plates enriched with $AgNO_3$ were initially pale milky white in colour on inoculation. The inoculated plates were observed for the growth of bacterial colonies for a period of 24 h along with the reduction of the $AgNO_3$ present in the medium. The $AgNO_3$ reduction efficacy of the bacterial isolates was identified based on the visual observation of the clear zones surrounded by a brown band around the

bacterial colonies as shown in Figure 4.40 (a). Clear zone indicates the extracellular reduction of $AgNO_3$ in the agar medium in the vicinity of the colonies by the cells and the brown band around indicates the deposition of the synthesized zerovalent silver around the clear zone.
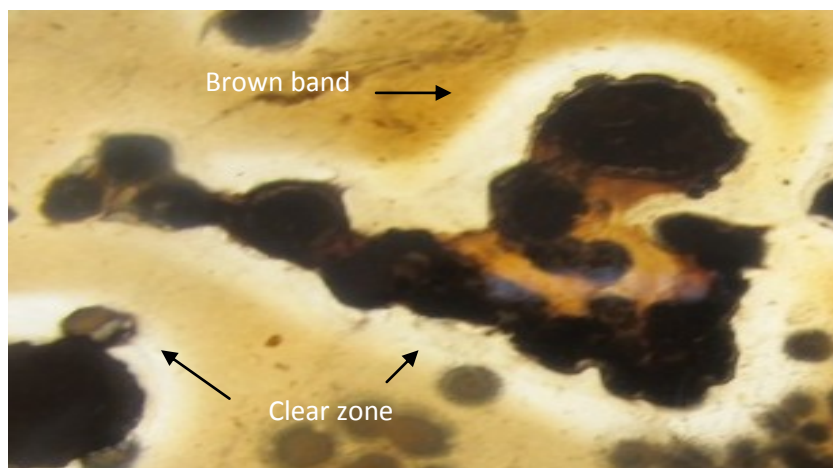
(a)

Figure 4.40 (a): Formation of clear zone indicating the reduction of $AgNO_3$ in the medium (b) Silver coating on the agar plate indicating formation of AgNPs

As observed in Figure 4.40 (a), the colonies with clear zones also exhibited intense brown colour, a characteristic colour of AgNPs indicating the intracellular reduction of $AgNO_3$ to Ag^0 by these bacterial colonies and accumulation. The reduced $AgNO_3$ as Ag^0 was seen as a metallic sheen at the inner basal surface of the Petridish as seen in Figure 4.40 (b). The characteristics displayed by the bacterial isolates confirmed that these strains possessed the ability to synthesize AgNPs. Table 4.14

presents the details of the colonies and their growth response to the silver content during isolation.

Table 4.14 Details of Colony characteristics used in the isolation of bacterial strains

Number of colonies	Characteristics in 24 h	Characteristics in 48 h	Inference
107	Brown colored with no clear zone around the colony	Brown colored with a few exhibiting less prominent clear zone around the colony	The bacteria were able to intracellularly reduce Ag^+ to Ag^0
11	No brown colored colony and with no clear zone	Disintegration and death of the colony or no clear zone with dim brown bands	The bacteria were not able to bring about either extracellular or intracellular reduction of Ag^+ to Ag^0 in 24 h
10	Brown colored colonies with clear zone and brown band around the clear zone	Brown colored colonies with clear zone and brown band around the clear zone	The bacteria were able to grow and tolerate silver and bring about both extracellular and intracellular reduction of Ag^+ to Ag^0

Out of the total 128 colonies formed, 107 were brown colored colonies with no clear zone and 10 colonies were brown colored with the clear zone and a brown band around. The brown colored colonies with no clear zones indicated that these cells possess the ability to intracellulary reduce Ag^+ to Ag^0, while the 10 brown colonies of varying colony characteristics exhibiting clear zone with a brown band around, indicated their ability to reduce Ag^+ ions to Ag^0 both extracellularly as well as intracellularly. A few of the brown colonies with no clear zone, showed the presence of clear zone with dim brown bands around after prolonged incubation period of upto 48 h. It showed that these colonies were also able to reduce Ag^+ to Ag^0 extracellularly, but with a slow rate. Thus, ten brown colonies which showed clear zones and brown bands in 24 h were chosen for further screening, owing to their ability to extracellularly reduce silver ions to zerovalent silver at a faster rate.

Intracellular synthesis of the AgNPs would involve challenges in recovering the AgNPs as it requires necessary steps to separate the bacterial biomass, lyses of the

bacterial cells, separation of unwanted cell material from the AgNPs and recovery of the AgNPs. The challenges involved in the intracellular synthesis of AgNPs can be overcome by synthesizing the AgNPs extracellularly.

The 10 bacterial isolates which showed capability to synthesize AgNPs extracellularly were further screened by inoculating them separately onto nutrient agar plates enriched with increasing $AgNO_3$ concentrations of 0.2 g/L, 0.4 g/L, 0.6 g/L, 0.8 g/L and 1 g/L to test for their reduction efficacy with high concentrations of $AgNO_3$. The isolates which were able to tolerate and produce a clear zone around the colonies with brown band around even in increased concentration of $AgNO_3$ were selected. These features indicate that the bacterial strains could tolerate high concentrations of Ag^+ ions and secreted extracellular metabolic enzymes that were capable of reducing the $AgNO_3$ present in the medium within the time duration of 24 h. Table 4.15 present the details of the tolerance and reduction capabilities of the isolated colonies with increasing concentration of $AgNO_3$.

Out of the ten bacterial isolates, five isolates namely 4S1, 4S2, 4S3, 6S1 and 8S1 exhibited tolerance towards $AgNO_3$ at higher concentrations and showed the presence of clear zones with brown band around indicating their ability to extracellulary reduce $AgNO_3$ to Ag^0. The isolate 6S1 could tolerate and reduce $AgNO_3$ upto 0.6g/L; 8S1 till 0.8 g/L and the isolates 4S1, 4S2 and 4S3 could tolerate and reduce $AgNO_3$ upto 0.4 g/L.

Thus, these five screened bacterial isolates with the ability to reduce higher concentrations of $AgNO_3$ to Ag^0 efficiently were found to be the candidates for the extracellular synthesis of AgNPs.

Table 4.15 Tolerance and reduction capacities demonstrated by the isolated bacterial strains

Isolates	Concentration of AgNO₃ in the growth medium				
	0.2 g/L	0.4 g/L	0.6 g/L	0.8 g/L	1 g/L
4S1	✓	✓	X	X	X
4S2	✓	✓	X	X	X
4S3	✓	✓	X	X	X
4	X	X	X	X	X
5	X	X	X	X	X
6S1	✓	✓	✓	X	X
7	X	X	X	X	X
8S1	✓	✓	✓	✓	X
9	X	X	X	X	X
10	X	X	X	X	X

As per the literature reports, the microbes for bacterial based synthesis of AgNPs with silver reducing ability were isolated from silver rich environment like electroplating industries (Babu and Gunasekaran, 2009), coastal mangrove sediment (Kathiresan et al. 2009), photographic waste and silver mining wastes (Priyadarshini et al. 2013). Isolation of a strain with the specific metabolic machinery to synthesize AgNPs provides better results in terms of the conversion and morphological aspects of the AgNPs being synthesized. Earlier reports have also proven that, the silver resistant strains could efficiently reduce AgNO₃ to Ag⁰ (Gericke and Pinches, 2006; De and Bergsteinsson, 1947). Though several reports of bacterial strains with the ability to biosynthesize AgNPs were reported in the literature, majority of the synthesis involving AgNPs were confined within the bacterial cell wall (Mouxing et al. 2006; Ahmad et al. 2003 b; Nair and Pradeep 2002). However, relatively a few reports on extracellular synthesis of AgNPs are available. As discussed earlier in this section, extracellular synthesis of AgNPs is desirable as it considerably reduces the number of downstream purification steps involved in the production of AgNPs (Ogi et al. 2010; Thakkar et al. 2010; Das et al. 2010; Gurunathan et al. 2009; Kalishwaralal et al. 2008). Thus, further studies on synthesis of AgNPs were conducted with the five bacterial strains 4S1, 4S2, 4S3, 6S1 and 8S1 which exhibited the ability to reduce Ag⁺ ions to Ag⁰.

4.7 Identification of the bacterial isolates by partial sequencing of 16s ribosomal RNA

The partial sequencing of 16S ribosomal RNA of the individual bacterial isolates 4S1, 4S2, 4S3, 6S1 and 8S1 was carried out by the protocol mentioned in Appendix VIII by Agharkar Research Institute, Pune, Maharashtra, India. The gene sequences of all the five bacterial strains are furnished in Appendix VIII and the BLASTn algorithm was used to compare the homology of the obtained gene sequences with that of the gene sequence database on National Centre for Biotechnology Information- GenBank.

The designated strains along with their accession numbers issued by GenBank and their Maximum identity values to its closest phylogenetic affiliation values are presented in Table 4.16.

Table 4.16 Bacterial genetic characterization details of the five bacterial isolates according to the partial sequencing of 16S ribosomal RNA gene and their GenBank accession number

Strain Designation	GenBank Accession ID	Strain Name	Accession ID of the Closest Phylogenetic Affiliation	Maximum identity
4S1	KP772325	*Brevundimonas vancanneytii* strain	AJ227779	99.81%
4S2	KP772326	*Leucobacter aridicollis* strain	AJ81047	99.01%
4S3	KP772328	*Leucobacter aridicollis* strain	AJ81047	97.13%
6S1	KP055785	*Enterobacter cloacae* strain	CP001918	99.8%
8S1	KP772327	*Alcaligenes aquatilis* strain	JX986974	99.33%

The significance of these strains with respect to the presence of the reduction machinery responsible for the reduction of the Ag^+ ions to Ag^0 is discussed in detail in section 4.9 of this chapter.

4.8 Synthesis of AgNPs with the isolated bacterial strains 4S1, 4S2, 4S3, 6S1 and 8S1

In order to evaluate the efficiency of the isolated bacterial strains to synthesize extracellular AgNPs in liquid medium, a detailed study was carried out. The cell free culture supernatants of the bacterial strains 4S1, 4S2, 4S3, 6S1 and 8S1 were obtained by the methodology described in section 3.5.5 of Chapter 3. A control containing 100 mL of sterile nutrient broth was also maintained. To 100 mL of the 24 h grown cell free supernatant of the bacterial strain and the control, equal volume of 1 mM AgNO$_3$ solution was added. The reaction was allowed to proceed for time duration of 24 h as described in section 3.3.5 of Chapter 3.

The synthesis mixtures were observed for visual change in colour, the appearance of brown colour being the indication for the formation of AgNPs. The synthesis mixtures containing the 24 h grown cell free supernatant of the bacterial strains exhibited brown colour while the control synthesis mixture did not exhibit any brown colour indicating that the formation of AgNPs occurred only in the presence of bacterial metabolic machinery. The brown colour of the AgNPs in the colloidal form is the characteristic that is visually observed for, in all the cases for the preliminary confirmation of its synthesis (Shahverdi et al. 2007; Ahmad et al. 2003, Bhainsa and Dsouza, 2003). Formation of brown colour in the synthesis medium is attributed to the formation of AgNPs (Rastogi and Arunachalam, 2011; Basavaraja et al. 2008; Bhainsa and D'Souza, 2006; and Duran et al. 2005; Mukherjee et al. 2001). This change in colour occurs through the surface plasmon vibration of the AgNPs (Wei et al. 2012, Balaji et al. 2009; Ingle et al. 2008). The visual confirmation of change in the colour of the synthesis medium to brown is indicative of the detail that the bacterial supernatant comprises of extracellular biocomponents that were responsible for the reduction of the AgNO$_3$ salt solution in the medium into AgNPs

Figure 4.41 (a) shows the changes in colour of the synthesis mixture during the synthesis of AgNPs. The figure showed that the synthesis mixtures turned from white to brown in 24 h indicating the formation of AgNPs.
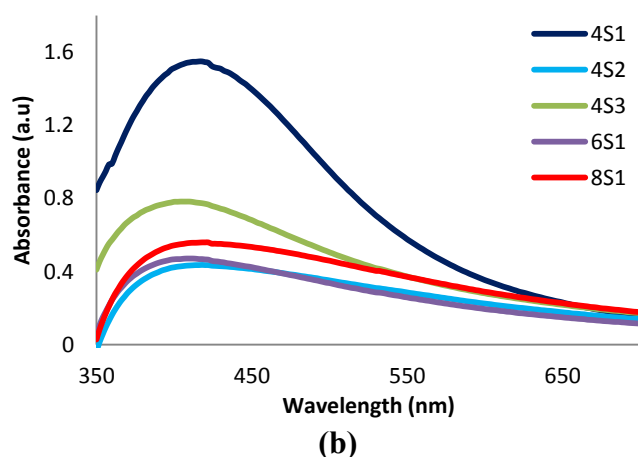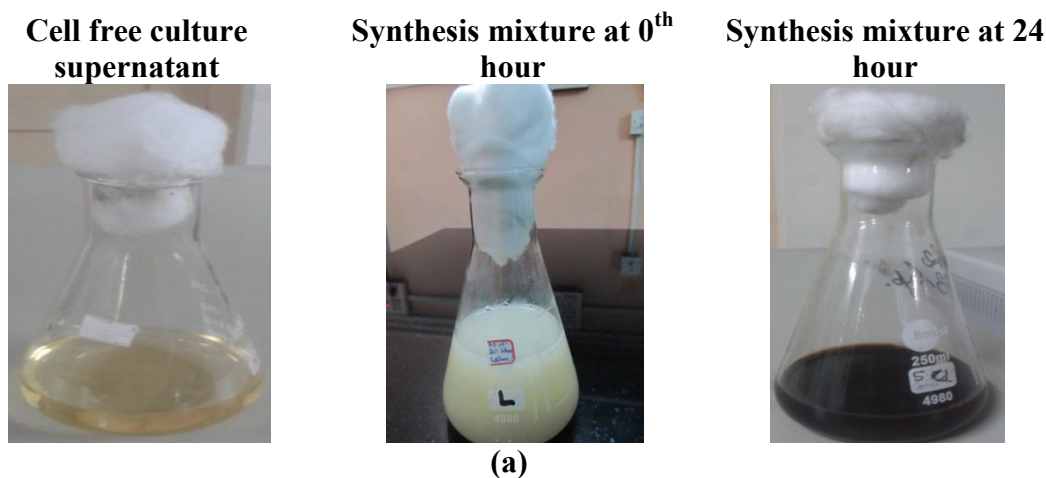
Figure 4.41 (a) Change in colour from the cell free culture supernatant, synthesis mixture at 0th hour and 24th hour of synthesis (b) SPR spectra of AgNPs in the synthesis mixture with 24 h cell free culture supernatant of bacterial isolates 4S1, 4S2, 4S3, 6S1 and 8S1.

The synthesis of AgNPs using the 24 h cell free culture supernatant of the bacterial strains 4S1, 4S2, 4S3, 6S1 and 8S1 was further confirmed by the UV-Vis spectral analysis of the synthesis mixtures for the characteristic SPR peaks. The spectral characterization of the AgNPs was performed according to the methodology described in section 3.3.5 of Chapter 3. Figure 4.41 (b) shows the characteristic SPR peaks for AgNPs synthesized in the cell free culture supernatants of bacterial isolates 4S1, 4S2, 4S3, 6S1 and 8S1 centred at 420 nm.

As discussed earlier, the SPR peak characteristic of metallic AgNPs occurs at 420 nm (Wei et al. 2012; Saifuddin et al. 2009; Ingle et al. 2009). This is due to the excitation of the surface electrons of the AgNPs in interaction with the incident electromagnetic radiation. Stepanov, (1997) and Stamplecoskie and Scaiano, (2010)

have reported that the SPR peak characteristics of AgNPs is highly influenced by their shape, size and the dielectric constant of the medium.

The SPR band of the AgNPs synthesized in the synthesis mixture containing the 24 h cell free supernatant of 4S1 bacterial strain and 1mM of the $AgNO_3$ solution in volume ratio of 1:1 after 24 h of synthesis time period exhibited a SPR peak which is slightly broader, with the highest intensity, and is redshifted in comparison to the SPR peaks obtained by the AgNPs synthesized using the cell free culture supernatants of strains 4S2, 4S3, 6S1 and 8S1. As discussed earlier, the higher intensity indicates that larger number of AgNPs are synthesized; the redshift and broadened SPR peak indicates the formation of large sized polydispersed AgNPs with a wide size range (Rodríguez-León et al. 2013; Darroudi et al. 2012; Guidelli et al. 2011; Basavaraja et al.2008). The peak intensities for AgNPs are in the order of 4S1> 4S3> 8S1> 6S1> 4S2. Table 4.17 shows the percentage conversion of Ag^+ ions to Ag^0 obtained by each of the bacterial strains, the average particle size, and approximate size range of the AgNPs and the shape of the particles being synthesized. The average particle size and size range were determined from SEM micrographs using Image J software. The SEM images of the AgNPs synthesized using the strains 4S1, 4S2, 4S3, 6S1 and 8S1 are presented in Figure 4.42 (a) to Figure 4.42 (e) respectively. The conversions obtained with the bacterial strains are less than 70% as shown in Table 4.14. The lower conversion may be due to lower rate of nuclei formation and the low rate of growth of the Ag nuclei owing to lower mass transfer rate of Ag^+ ions to the surface of Ag^0 nuclei caused by lower concentration gradient and subsequent reduction to Ag^0 on the surface resulting in slow growth of the nanoparticles. The morphological features as observed from SEM are presented in Table 4.17.

The conversion of Ag^+ ions is in the order of 4S1>4S3> 4S2>8S1>6S1. The higher peak intensities and larger conversions with 4S1 and 4S3 indicate the formation of large number of AgNPs. However, the size of the nanoparticles synthesized with 4S1 and 4S3 are larger with broad range (Table 4.17). The average size of the nanoparticles and the size range obtained with the strains followed the order of 4S1>4S3>4S2>6S1>8S1. Thus, though 4S1, 4S3 and 4S2 yielded higher conversion, the average sizes of AgNPs are larger with wide size range. The AgNPs synthesized using 4S1 and 4S3 are not with uniform morphological characteristics.

Table 4.17 Percentage conversion of Ag⁺ ions obtained in the synthesis mixtures containing the 24 h cell free supernatant of bacterial isolates 4S1, 4S2, 4S3, 6S1 and 8S1.

AgNPs synthesis medium of bacterial isolate	Percentage conversion of Ag$^+$ ions	Average Size of AgNPs(nm)	Average Size range of AgNPs (nm)	Shape of AgNPs synthesized
4S1	68.46	98.96	35-189.7	Cubical and Spherical
4S2	62.01	87.2	43-135.2	Quasi spherical
4S3	65.96	92.76	38-196.8	Polyhedral
6S1	51.72	79.4	47-130.3	Cubical
8S1	58.83	60.25	24-106.4	Quasi spherical

The percentage conversion of Ag$^+$ ions to Ag^0 obtained with 4S1was found to be 68.46% (Table 4.17) which is the highest amongst the percentage conversion obtained from all the bacterial strains. But in Figure 4.42 (a), the SEM image of AgNPs synthesized using the 24h cell free culture supernatant of strain 4S1 shows the formation of many particles of varying sizes with cubical and spherical shapes. The average particles size of AgNPs was found to be ~ 99 nm as shown in Table 4.17 and the size range was found to lie between 35-189.7 nm. The SPR peak (Figure 4.41) emanating from the AgNPs synthesized using the 24 h cell free culture supernatant of strains 4S2, 4S3, 6S1 and 8S1 also exhibited the characteristic peaks of AgNPs which were blue shifted from 420 nm and lower in intensity in comparison to the SPR peak of AgNPs synthesized using the 24 h cell free culture supernatant of 4S1 strain. The blue shift of the SPR peak from the characteristic wavelength of 420nm indicates the formation of smaller sized AgNPs (Rodríguez-León et al. 2013; Guidelli et al. 2011; Noguez et al. 2007; Abe et al.1982) as discussed earlier. For larger particle sizes these shifting in the SPR peaks of the AgNPs are caused by the phase shifts, due to the retardation of the electromagnetic waves along with the influence of the higher-order multipoles. While for the smaller AgNPs, the shift is due to the spill out of the conduction electrons, resulting in the electron density drop thus effecting the change in SPR position (Kreibig and Vollmer, 1995).

(a)

(b)

(c)

(d)

(e)
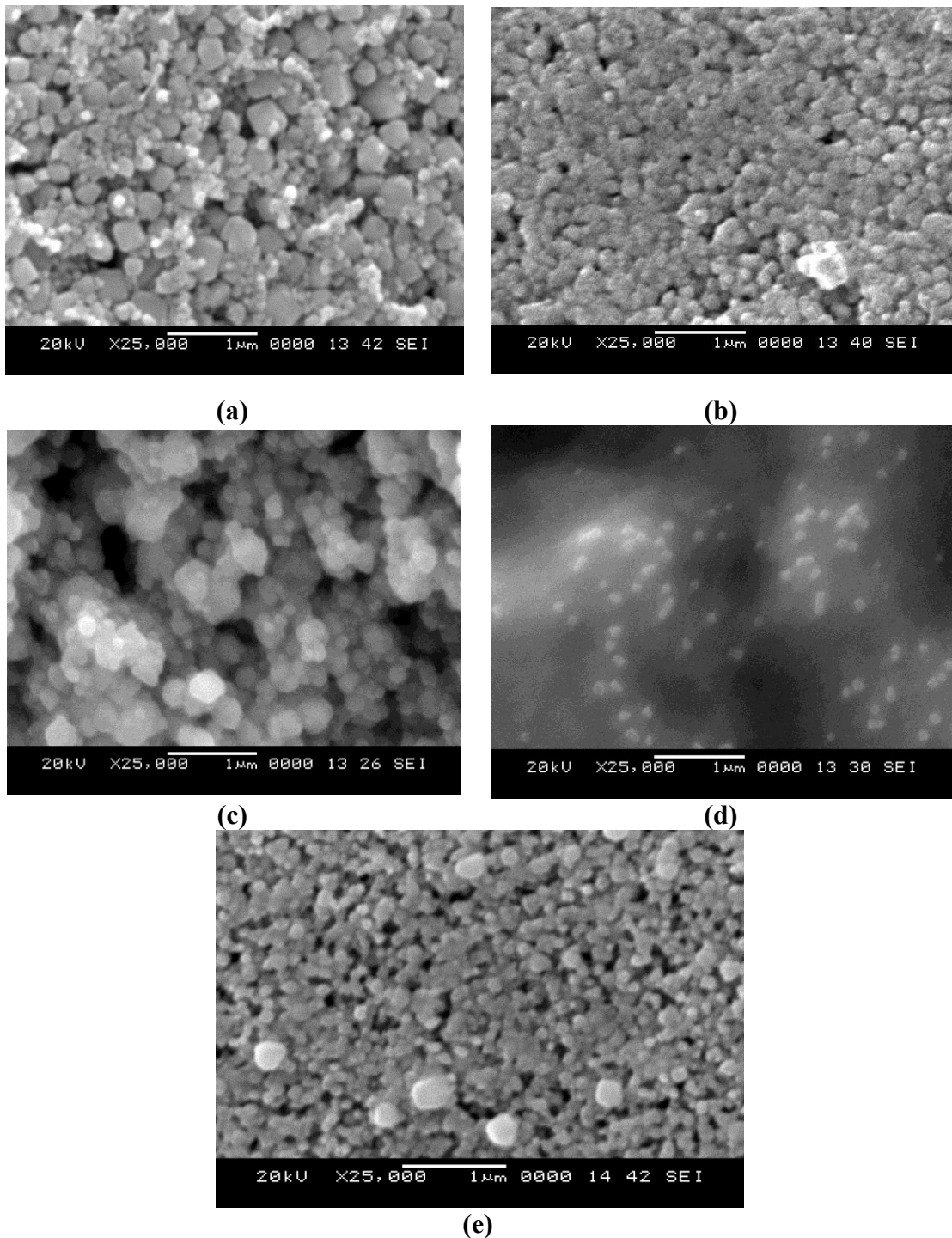
Figure 4.42 SEM Images of AgNPs synthesized using 1 mM of AgNO$_3$ and 24 h cell free supernatant of bacterial strain (a) 4S1 (b) 4S2 (c) 4S3 (d) 6S1 and (e) 8S1

Thus, it can be inferred that, even though the conversions obtained in the nanoparticle synthesis with 8S1 and 6S1 were lower, the size of the nanoparticles were smaller with the narrower size range. It indicates that the strains 6S1and 8S1

have the better potential to synthesize smaller AgNPs. The smallest average particle size was obtained by the AgNPs synthesized using the 24 h cell free culture supernatant of bacterial strain 8S1 of 60.25 nm with narrow distribution of size range which is highly desirable but with a lower conversion of 58.83%. SEM images (Figure 4.44(e)) and the morphological characteristics presented in Table 4.17, indicated that the strain 8S1 could synthesize quasispherical particles, whereas the AgNPs synthesized with the strain 6S1 are cubical. Bacterial strains such as *P. aeuginosa* (Husseiny et al. 2007), *B.casei*, (Kalishwarlal et al. 2010) *E.coli* (Minaeian et al. 2008) and *E. cloacae* (El-Shanshoury et al. 2011) have been used to synthesize AgNPs of varying sizes and shapes. This indicates that the shape and size of AgNPs synthesized depends on the bacterial strain employed for synthesis of the AgNPs as the metabolic machinery of each bacterium varies in terms of its genetic makeup, utilization of specific nutrients required for its growth as well as secretion of certain bacterial moieties. Hence influencing the rate of reduction of the precursor salt to Ag^0 nuclei and its subsequent growth into nanoparticles followed by its capping. Xia et al. (2013) have reported that capping agents control the shape and size of the nanoparticle being synthesized because it reduces the surface free energy of the particle surface through chemisorptions. The presence of different functional groups present on the surface of the AgNPs synthesized using the five bacterial isolates discussed further in section 4.11.2 indicates the presence of various capping agents secreted by the bacterial strains which may play a role in controlling the shape and size of the nanoparticle.

Further, the conversion may be enhanced and the nanoparticles with the better size and morphological characteristics may be synthesized by optimizing the synthesis parameters.

The synthesis of AgNPs by the cell free supernatants may occur due to the reduction of Ag^+ ions to Ag^0 by the action of extracellular enzymes secreted by the cells or their metabolite. However, the literature reports predominantly support that the microbial based synthesis process is governed by the action of extracellular enzymes secreted by the microbes (Kumar et al. 2007; Mandal et al. 2006; Ahmad et al. 2002). The present study indicates that the bacterial strains 4S1, 4S2, 4S3, 6S1 and

8S1 possess metabolic machinery for the extracellular synthesis of AgNPs by the reduction of Ag^+ to Ag^0.

The synthesis of AgNPs in a cell free condition increases the overall efficacy of the process by reducing the number of downstream processing steps in the production of AgNPs under ambient conditions of synthesis without the involvement of any harsh and elevated conditions of synthesis and use of toxic and expensive solvents/chemicals. Thus the bacterial strains isolated and selected based on the current study can be adopted for the synthesis of AgNPs.

This route is simple, benign and takes place at ambient conditions making it a reliable and promising process for the large scale production of AgNPs. However, manoeuvring of process parameters may be essential for the synthesis AgNPs with desired morphological characteristics and to enhance the conversion.

4.9 Determination of the bacterial metabolic machinery responsible for the reduction of Ag^+ ions

In the synthesis of nanoparticles using the cell free supernatant of the microbial strains, the extracellular enzymes secreted by the microbes during their growth or the metabolites may be responsible (Narayanan and Sakthivel, 2010; Sastry et al. 2003; Ahmad et al. 2002) for the reduction of precursor salt. Several researchers have reported that, the microbial based synthesis is caused by the extracellular enzymes (Duran et al. 2005; Mohanpuria et al. 2003). To test for, whether the cell metabolites are responsible for reduction of $AgNO_3$ to AgNPs, in the present study the cell free supernatant was initially subjected to heat treatment at 70º C for 3 h to deactivate the enzymes. The heat treated cell free supernatant was treated with the 1 mM $AgNO_3$ salt solution at 1:1 v/v ratio with unadjusted pH conditions and the evidence of AgNPs synthesis was tracked. No characteristic brown colour of AgNPs was observed, indicating the absence of AgNP formation by the heat treated cell free supernatant. It proved that the cell metabolites are not responsible for the reduction of silver nitrate to AgNPs. Thus, it is confirmed that the AgNPs were synthesized by the action of extracellular enzymes secreted during the growth of bacteria.

Literature reports (Gade et al. 2008; Ingle et al. 2008; Kumar et al. 2007a, b; He et al. 2007; Duran et al. 2005) support the presence of strong reducing machinery

in microbes capable of synthesizing extracellular AgNPs. Reports based on the partial purification and identification of the protein machinery associated with reduction of $AgNO_3$ into AgNPs considers that nitrate reductase is the protein moiety responsible for it.

In regard to the findings of experiments carried out by Kumar et al. (2007) involving the *in vitro* synthesis of AgNPs using nitrate reductase as the reducing enzyme, they suggested that *Fusarium oxysporum* strains must have a strong NADH dependent nitrate reductase. This was the first direct evidence for the involvement of nitrate reductase in the synthesis of AgNPs. NADH dependant nitrate reductases are one such class of enzymes that convert the nitrate in the medium to nitrite and the electron is transferred to the silver ion which gets reduced to zerovalent silver (Ag^+ to Ag^0). This mechanism is most widely accepted and has been proven in an independent study involving the fungus *F. oxysporum*, wherein the enzyme nitrate reductase was purified from the fungus and mixed with silver nitrate and NADPH in a test tube which apparently led to the synthesis of AgNPs with a formation of characteristic brown colour (Vaidyanathan et al. 2010).

In the present study, in order to identify the presence of NADH dependent nitrate reductase in the cell free supernatant, the crude 24 h cell free supernatant of the bacterial strains was partially purified using classical and traditional methods of protein purification such as ammonium sulphate precipitation to salt out the proteins, dialysis of the salted out proteins to remove the ionic contaminants and further concentration by reverse osmosis of the dialyzed samples followed by molecular weight determination through SDS PAGE. The detailed procedure is presented in Section 3.5 of Chapter 3.

Figure 4.43 shows the SDS PAGE image of the proteins present in the cell free supernatant of bacterial strains 4S1, 4S2, 4S3, 6S1 and 8S1 along with the standard protein marker.
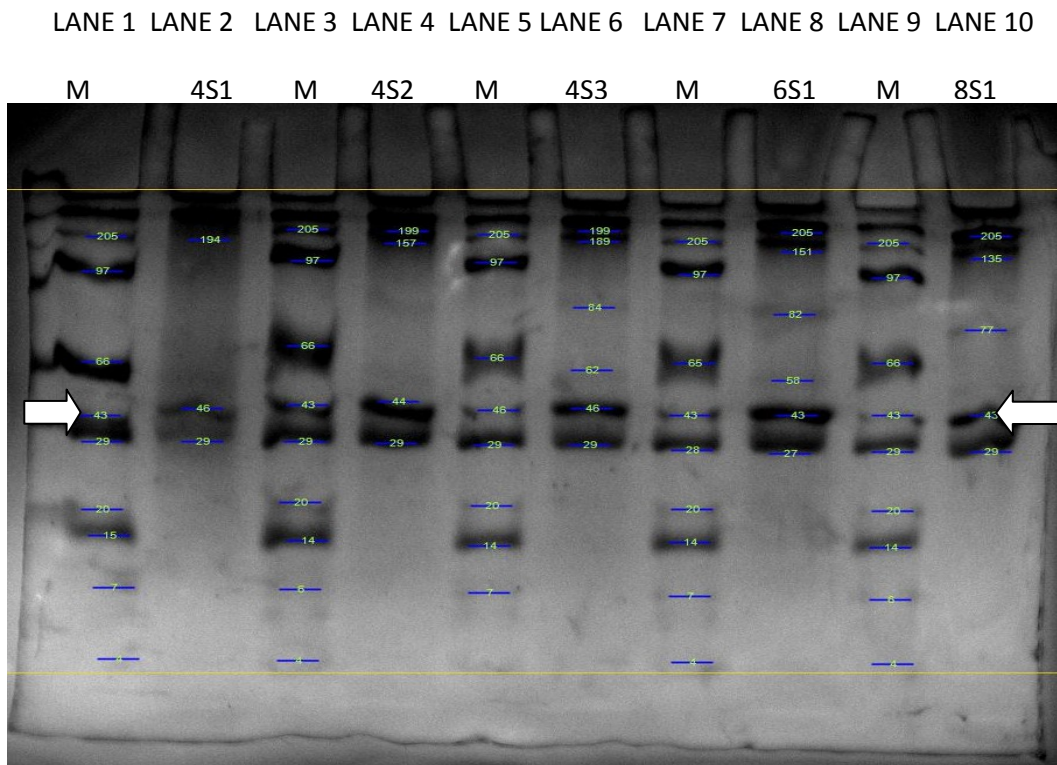
Figure 4.43 Coomassie Brilliant Blue stained SDS PAGE gel under UV light showing the molecular ladder and molecular weight of the bacterial proteins

Lanes 2, 4, 6, 8 and 10 in the SDS PAGE gel image shown in Figure 4.43 display the protein bands obtained after partial purification of the cell free supernatant of the bacterial strains 4S1, 4S2, 4S3, 6S1 and 8S1. The molecular weights of the bands observed in different lane belonging to strains 4S1, 4S2, 4S3, 6S1 and 8S1 are presented in Table 4.18.

Table 4.18 Molecular weights of the protein bands obtained from the SDS PAGE gel image

Bacterial Strain	Molecular weight of the protein found (kDa)
4S1	194, 46, 29
4S2	199, 167, 44, 29
4S3	199, 189, 84, 62,46, 29
6S1	205, 151, 82, 58, 43, 27
8S1	205, 135, 77, 43, 29

From Table 4.18, it is observed that two bands with molecular weights ranging around 46-43 kDa and 27-29 kDa are present in all the strains, indicating that all the five strains secrete these proteins during their growth. As per the literature reports, the protein with molecular weight of around 45 kDa belongs to NADH dependent nitrate reductase enzyme (Kumar et al. 2007 a) and the protein with molecular weight of around 27-29 kDa belongs to hydrolases (Rajakumar et al. 2012 b; Kirthi et al. 2011). As the precursor salt used for the synthesis of AgNPs is $AgNO_3$, these nitrate reductase enzymes would have been responsible for the reduction of $AgNO_3$ to Ag^0 and further growth of particles.

The mechanism of extracellular synthesis of nanoparticles with the nitrate salt of the metal as precursor using microbes is basically found to be nitrate reductase-based synthesis. The enzyme nitrate reductase secreted by microbes helps in the bioreduction of metal ions and synthesis of nanoparticles. A number of researchers supported the activity of nitrate reductase for extracellular synthesis of nanoparticles (Gade et al. 2008; Ingle et al. 2008; Kumar et al. 2007 a; He et al. 2007;Duran et al. 2005). Duran et al. (2005) reported that the enzyme reductase is responsible for the reduction of Ag^+ ions and the subsequent formation of AgNPs. The findings of Duran et al. (2005) were further confirmed by Ingle et al. (2008) in their study involving the determination of the role and signifying the presence of nitrate reductase wherein commercially available nitrate reductase disks were used in the determination of the role of nitrate reductase in the extracellular synthesis of AgNPs. Thus, it can be concluded that the enzyme NADH dependent reductase is associated with reduction of Ag^+ ions to Ag^0 in the case of microbial based synthesis of AgNPs. During the catalysis, nitrate is converted to nitrite, and an electron will be shuttled to the incoming Ag^+ ions. The secretion of NADH dependant nitrate reductase that is responsible for the reduction of Ag^+ ions to Ag^0 and subsequent formation of AgNPs has been excellently described in the organism *B. licheniformis* (Kalimuthu et al. 2008). Figure 4.44 presents the mechanism of the reduction of Ag^+ to Ag^0 as reported by He et al. (2007).
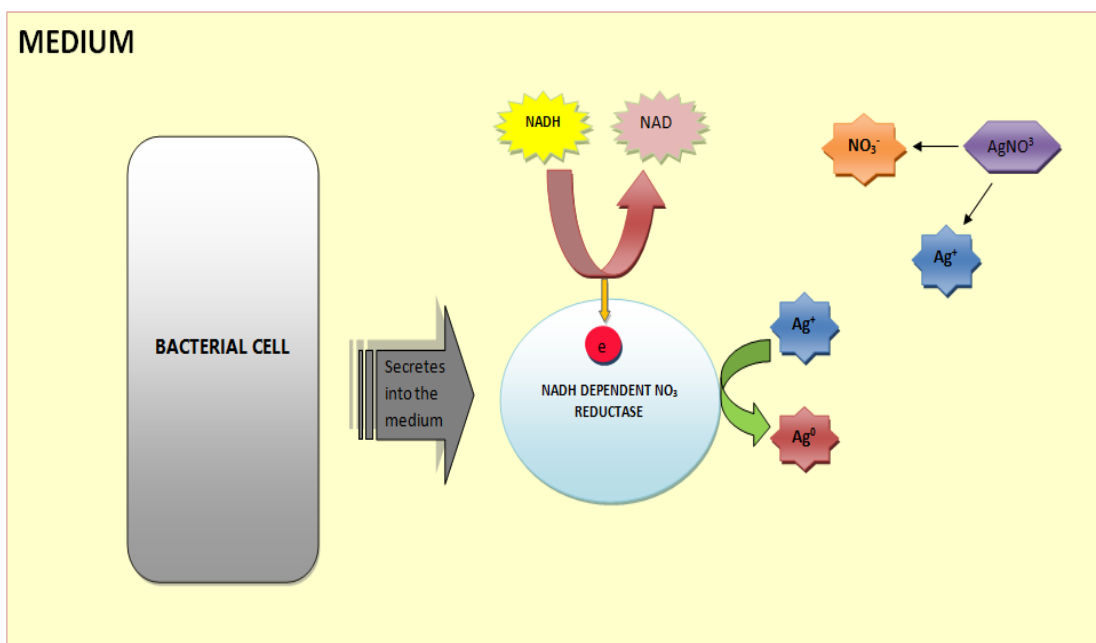
Figure 4.44 Proposed mechanisms for the reduction of AgNO$_3$ into AgNPs by bacteria

The bacterial isolate 4S1 was identified as *Brevundimaonas vancannyetii* strain with 99.81% identity; strains belonging to *Brevundimaonas* sp. were majorly isolated from marine areas with high saline conditions (Tsubouchi et al. 2013; Wang et al. 2012; Scotta et al. 2011; Estrala and Abraham, 2010). Also the strains were initially designated as *Pseudomonas* sp. but were later reclassified. Reports on the presence of nitrate reductase enzyme in some species belonging to *Brevundimaonas* genera are available (Srinandan et al. 2011; Montañez et al. 2009). The enzyme nitrate reductase is also present in the strain 4S1 thus substantiating the synthesis of AgNPs by this isolate. Reports pertaining to isolation of the genera *Brevundimaonas* and *Alcaligenes* from the Indian subcontinent are rare. The genera *Brevundimaonas* was recently isolated from Gujarat, India by Ghosh (2015).

Thus, the bacterial strains isolated were able to secrete nitrate reductases in their growth medium which later brought about the reduction of the AgNO$_3$ to AgNPs. It can be proposed that the strains were highly selective of nitrate as their substrate to carry out their metabolic processes hence were induced to produce the same during the isolation process. The selection of these strains has been proven to be justified in accordance to the ability of these strains to successfully synthesize AgNPs.

The bacterial strains belonging to similar genetic make-up as those isolated in the present study were reported to possess nitrate reductase. French et al. (1998), Bryant and Deluca, (1991) and Nivinskas and co-workers (1999) have shown that *Enterobacter cloacae* strain with which the isolated strain 6S1 shares the genetic identity; possess NADH- dependent nitrate reductase. *Leucobacter* sp., the genera to which strains 4S2 and 4S3 belong are known to harbor NADH dependant nitrate reductases and have been largely employed in hexavalent chromium reduction (Sarangi and Krishnan, 2008; Zhu et al 2008).

The bacterial isolate 8S1 was identified as *Alcaligenes aquatilis* strain with 99% homology. The homologous reference strain to 8S1 was isolated first by Van Trappen and co-workers (2005) in Germany and they reported the nitrite reduction efficiency by this strain under anaerobic conditions, but not the nitrate reduction efficiency. However, the strain 8S1 exhibited the presence of nitrate reductase enzyme which proves the novelty of the strain and its potential application in the synthesis of AgNPs.

All these strains were initially designated as *Pseudomonas* sp. but were later reclassified. *Pseudomonas* genera are known to contain a very strong nitrate reductase enzyme activity.

The reduction efficiency of strain 6S1 has already been explored and reported for the synthesis of nanoparticles. Shahverdi et al. (2007) have reported the extracellular synthesis of AgNPs using the culture supernatants of *Enterobacter cloacae* strains; however no studies on optimization have been reported by them. Losi and Frankenberger, (1997a and b) had also reported the extracellular synthesis of selenium nanoparticles by reduction of selenite by an isolated strain of *Enterobacter cloacae* from agricultural drainage water.

Except for the stain 6S1 which has been identified as *Enterobacter cloacae* sp. the other bacterial isolates belonging to the Genera of *Leucobacter,* (4S2 and 4S3), *Brevundimaonas* (4S1) and *Alcaligenes* (8S1) have never been reported for the synthesis of nanoparticles to the best of our knowledge. This makes the entire research on the synthesis of nanoparticles using these strains as novel in the field of bionanotechnology.

4.10 Effect of process parameters on the biobased synthesis of AgNPs by the cell free supernatants of the isolated bacterial strains

From the studies on the synthesis of AgNPs conducted using the culture supernatants of the bacterial strains 4S1, 4S2, 4S3, 6S1 and 8S1; it was evident that the culture supernatants were efficiently able to synthesize AgNPs by reducing the precursor salt in the synthesis mixture under ambient conditions of temperature (28 ± 2 ºC).

According to literature reports, the synthesis parameters greatly influence the characteristics of the nanoparticles synthesized and their yield. Precursor salt concentration and pH of the medium play an important role in the synthesis process (Hebbalalu et al. 2013; Vahabi et al. 2011; Li et al. 2011; Gurunathan et al. 2009; Kowshik et al. 2009). To obtain a better understanding of the influence of various parameters on the synthesis of AgNPs using the strains under study and to determine the best set of values for the synthesis of AgNPs with the desired morphological characteristics and to achieve maximum conversion, parameters such as the precursor salt concentration and initial pH of the synthesis mixture were varied and the effect was studied.

4.10.1 Effect of precursor salt (AgNO$_3$) solution concentration on the synthesis of AgNPs using the cell free supernatants of the bacterial strains

Substrate concentration plays an important role in determining the rate of any enzymatic process. In the present study AgNO$_3$ acts as a substrate which is reduced to zerovalent silver by the enzymatic action. Thus, the effect of AgNO$_3$ concentration in the synthesis mixture on synthesis of AgNPs using the cell free supernatants of the bacterial strains 4S1, 4S2, 4S3, 6S1 and 8S1 were studied. The studies were conducted by varying the concentration of AgNO$_3$ solution used to prepare the synthesis mixture, while keeping the total volume constant and the volume ratio of the cell free supernatant and the AgNO$_3$ solution constant at 1:1. The results are presented showing the effect of concentration of AgNO$_3$ solution used in preparing the synthesis mixture. However, the concentration of AgNO$_3$ in the synthesis mixture is one half the concentration of AgNO$_3$ solution added into it.

The 24 h grown cell free culture supernatant from each of the bacterial strains was obtained by adopting the methodology described in Section (3.3.5) of Chapter 3 and the nanoparticle synthesis was carried out with the varying concentration of $AgNO_3$ solution for a period of 24 h at the ambient temperature of 28±2 ℃ according to the methodology described in Section 3.3.6.1 of Chapter 3 with the unadjusted initial pH of the synthesis mixture as 7.0±0.2 units. The concentration of $AgNO_3$ solution added to the synthesis mixture was varied in the range of 1 mM to 500 mM in 1:1 volume ratio with that of the bacterial cell free supernatant, thus, the initial concentration of $AgNO_3$ in the synthesis mixture was varied in the range of 0.5 mM to 250 mM.

The SPR peaks of AgNPs synthesized using different concentrations of $AgNO_3$ solution with the cell free supernatants of the strains 4S1, 4S2, 4S3, 6S1 and 8S1 are shown in Figure 4.45, 4.47, 4.49, 4.51 and 4.53 respectively. Figure 4.46, 4.48, 4.50, 4.52 and 4.54 present the SEM images of AgNPs synthesized using the cell free culture supernatants of strains 4S1, 4S2, 4S3, 6S1 and 8S1 respectively. Table 4.16 shows the percentage conversion of Ag^+ ions by the cell free culture supernatants of bacterial strains 4S1, 4S2, 4S3, 6S1 and 8S1.

The SPR peak characteristics of AgNPs provides preliminary information on the morphological aspects of the AgNPs, where the wavelength at which the SPR peak occurs determines the dispersity of the AgNPs and the intensity of the SPR peak determines the relative number of AgNPs being synthesized (Zaki et al. 2011). The red and blue shift in the position of the SPR peak indicate the formation of large and small sized nanoparticles respectively (Basavaraja et al. 2008), while the broad and narrower peaks depicting the formation of polydispersed and monodispersed nature of the AgNPs (Evanoff and Chumanov, 2005) respectively.

Figure 4.45 shows the SPR peaks obtained from the AgNPs synthesized using the cell free supernatant of bacterial strain 4S1 with varying precursor salt solution concentration. The SPR peaks of AgNPs synthesized using 1 mM and 5mM solution are almost overlapping and wide indicating the formation of polydispersed AgNPs. The increase in the SPR intensity indicates the formation of a large number of AgNPs with increased concentration of $AgNO_3$ solution added. Table 4.16 also shows that with the increase in the concentration of $AgNO_3$ solution, the conversion of Ag^+ ions

by reduction to Ag^0 increases. The increase in both the number and conversion can be attributed to higher concentration of Ag^+ ions in the synthesis mixture, which increases the rate of reduction of Ag^+ ions to Ag^0, thus the nucleation and subsequent growth of nanoparticles occur at a higher rate. The increased rate of growth at the Ag^0 nuclei may be owing to higher rate of mass transfer of Ag^+ ions to the surface of Ag^0 nuclei due to higher concentration gradient and subsequent reduction to Ag^0 on the surface resulting in faster growth of the nanoparticles.
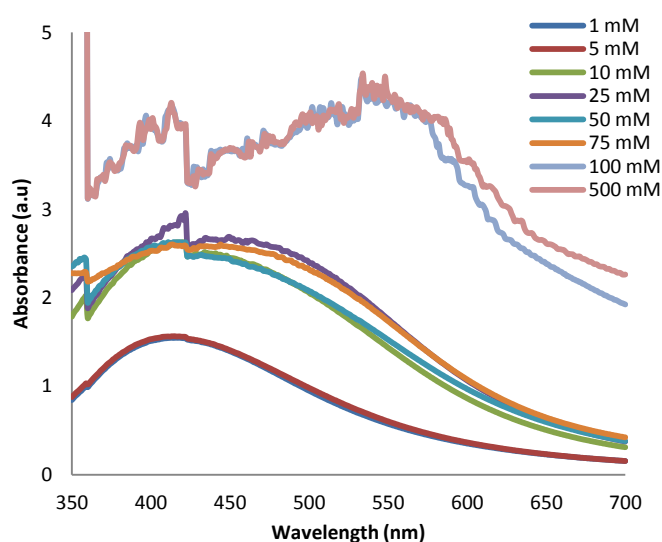
Figure 4.45 SPR spectra of AgNPs synthesized from synthesis mixtures containing 4S1 bacterial cell free culture supernatant and varying concentration of precursor salt solution in 1:1 volume ratios

The AgNPs synthesized using 75 mM of $AgNO_3$ as the precursor salt solution gave rise to a smooth, wide and high intensity SPR peak without any split indicating the formation of a large number of AgNPs with wide size range and without the presence of any anisotropy. Though, the SPR peaks obtained with 100 mM and 500 mM $AgNO_3$ solution are more intense as compared to the others, they yielded corrugated peaks with a split around 420 nm. Several peaks in the spectra are due to the increase in non uniform charge distribution over the particles resulting in the phase retardation. As the particle size increases it broadens the dipole resonance and excites higher multipole resonances like quadruple, octupole resonances leading to the formation of several peaks in the spectra. The difference in the energy level of the

resonances is manifested as the split in the SPR peak and the distance between the peaks (Evanoff and Chumanov, 2005).

The split in the SPR peak is obtained due to longitudinal and transverse polarization of the surface plasmon (Wang et al. 2010) in two different modes of dipole and quadrapole mode (Mie, 1908; Evanoff and Chumanov, 2005; Zhang et al. 2011). The two predominant plasmonic peaks are observed with AgNPs synthesized using 100 mM and 500 mM of $AgNO_3$ solution due to the polarization of longitudinal and transversal vibrations of the electrons on the surface of the AgNPs (Zhang et al. 2011; Evanoff and Chumanov 2005) which may be caused by non-spherical or anisotropic nanoparticles (Tian et al, 2005; Sun and Xia, 2002). A further insight into the anisotropic nature of the AgNPs synthesized by using 500 mM $AgNO_3$ solution and the cell free supernatant of strain 4S1 was obtained using SEM image provided in Figure 4.46, that shows the presence of a wide size range of AgNPs with varying morphological structures such as rods, tetrahedrons, bipyramids and spheres. The conversion was found to be lower (Table 4.19) for the AgNPs being synthesized with 100 mM and 500 mM of precursor salt solution. The conversion of Ag^+ ions increased upto 75 mM but with further increase in the concentration to 100 mM and 500 mM of $AgNO_3$ solution, the conversion decreased for AgNPs synthesis using strain 4S1.

Table 4.19 Percentage conversion of Ag^+ ions by the cell free culture supernatants of bacterial strains 4S1, 4S2, 4S3, 6S1 and 8S1

Precursor salt solution concentration used in the synthesis mixture	Percentage conversion of Ag^+ ions by the cell free culture supernatants of bacterial strains				
	4S1	4S2	4S3	6S1	8S1
1mM	68.46	62.01	65.96	51.72	58.83
5mM	73.46	63.83	66.48	59.43	62.65
10mM	75.78	66.14	71.91	62.7	64.96
25mM	78.1	74.0	79.31	68.6	69.5
50mM	83.75	77.46	85.43	76.6	72.74
75mM	87.88	88.89	89.54	89.3	89.99
100mM	81.02	80.17	84.22	91.17	93.94
500mM	74.73	79.69	74.66	70.1	Coagulation
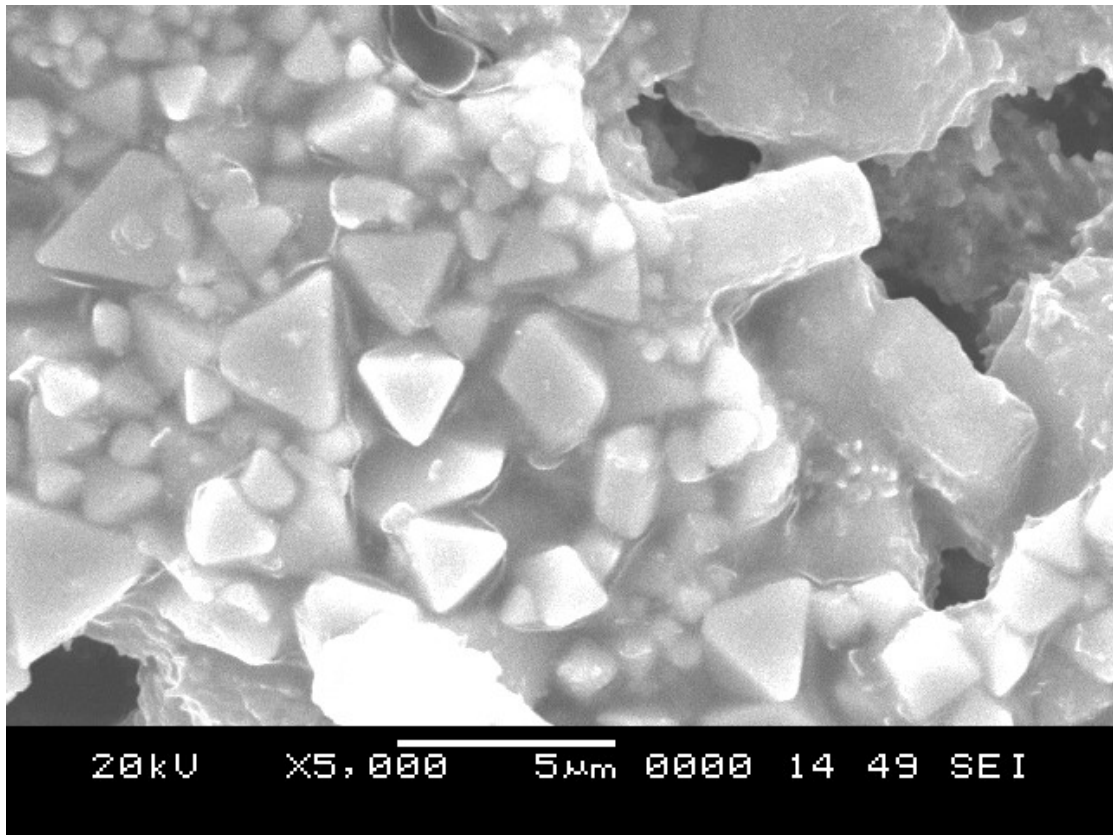
Figure 4.46 SEM image of AgNPs synthesized using 500 mM of AgNO$_3$ solution and cell free culture supernatant of strain 4S1 showing the formation of highly anisotropic AgNPs

According to Mie's theory small spherical or quasi-spherical nanocrystals exhibit a single SPR band; whereas anisotropic particles show two or three bands, depending on their shape. The symmetry of nanostructures determines the polarization ways which leads to the number of plasmonics being emitted (Ashkarran and Bayat, 2013; Xia et al. 2009). SPR spectra (Figure 4.45) indicates that anisotropic particles are formed at higher precursor salt solution of 100 mM and 500 mM and the conversion of Ag$^+$ to Ag^0 was found to decrease at concentrations above 75 mM (Table 4.19), though the intensity of SPR peak was found to be higher. The symmetry of the nanoparticles changes the intensity of the extinction spectra. Existence of sharp corners in the nanoparticles leads to accumulation of electrons in sharp corners than in the other parts .Therefore, the number of plasmons increases which further leads to increase in the intensity of the spectra (Ashkarran and Bayat, 2013; Xia et al. 2009). Thus, higher intensity peaks at 100 mM and 500mM does not

indicate large number of particles, but the anisotropic, non symmetric and sharp cornered nature of the AgNPs synthesized.

Thus, the AgNO$_3$ salt solution with the concentration of 75 mM was found to be optimum for the synthesis using the cell free culture supernatant of 4S1as it gave the highest conversion of Ag$^+$ ions of 87.88% with a smooth SPR peak indicating the formation of isotropic nanoparticles.
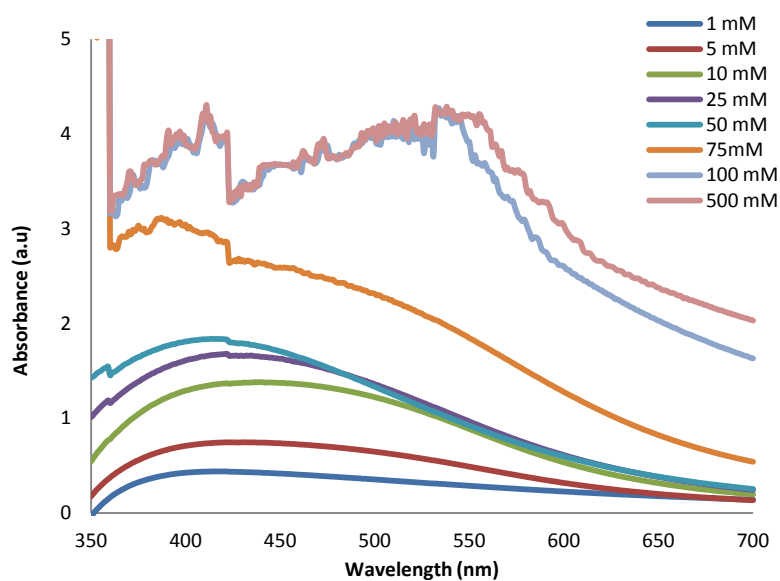
Figure. 4.47 SPR spectra of synthesis mixtures containing AgNPs synthesized using 4S2 bacterial culture supernatant and varying concentration of precursor salt solution in equal volume ratios

Similarly, Figure 4.47 shows the SPR peaks obtained from the AgNPs synthesized using the cell free supernatant of the bacterial strain 4S2 with varying concentrations of AgNO$_3$ solutions at an initial pH of 7.0 ± 0.2 units. The intensities of the SPR peaks of AgNPs was found to increase with an increase in the concentration of the precursor salt solution, but as the concentration was increased beyond 10 mM a split in the SPR peak emerged and became more prominent beyond 75 mM with a corrugation in the SPR peak at the concentration of 100 mM and 500 mM. Increase in the peak intensities with the increase in precursor salt concentration has been also reported by Shankar et al. (2003) and Tripathy et al. (2010) in their studies on microbial synthesis of AgNPs.

The presence of several small peaks and a prominent split in the SPR peak along with the wide difference in the dipole and quadrapole excitation shows that highly anisotropic AgNPs were synthesized at the concentration of 100 mM and 500

mM of AgNO$_3$. The number of small peaks in the SPR spectra of AgNPs synthesized using 100 mM and 500 mM AgNO$_3$ solution and cell free supernatant of strain 4S2 are many compared to the SPR of AgNPs synthesized using 75 mM of AgNO$_3$. Figure 4.48 shows the highly anisotropic nature of the AgNPs being synthesized using 500 mM of AgNO$_3$ as the precursor salt solution; varying shapes such as hexagons, tetrahedrons and bipyramidal structures with a wide size range can be observed. The SEM image shows the anisotropy of the AgNPs synthesized and is in agreement with the SPR analysis.

The highest conversion of Ag$^+$ ions of 89.94% (Table 4.19) was found to occur with 75 mM of AgNO$_3$ and resulted in a SPR peak with a small split and lesser width indicating the formation of a large number of AgNPs which are less anisotropic in structure. Thus 75 mM of the precursor salt solution was found to be the optimum precursor salt solution for the synthesis of AgNPs using cell free supernatant of the bacterial strain 4S2.
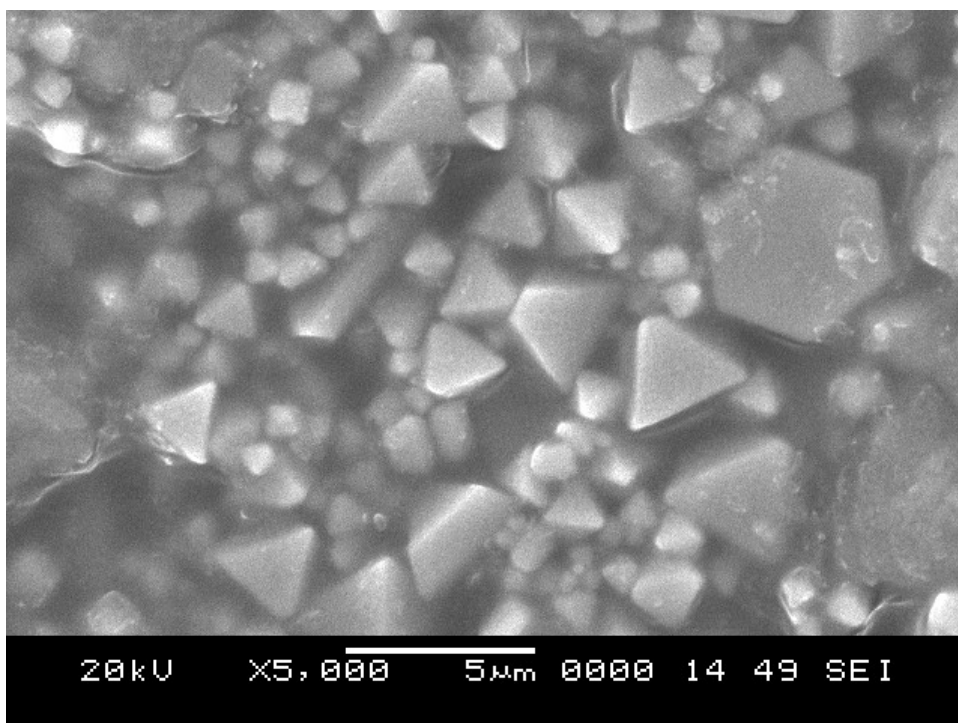
Figure 4.48 SEM image of AgNPs synthesized using 500 mM of AgNO$_3$ solution and cell free supernatant of strain 4S2 showing the formation of highly anisotropic AgNPs
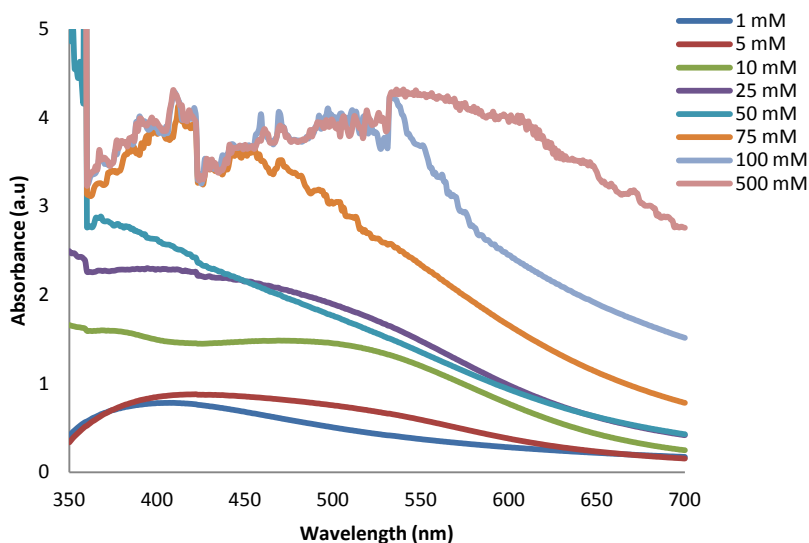
Figure. 4.49 SPR spectra of synthesis mixture containing AgNPs synthesized using 4S3 bacterial culture supernatant and varying concentration of precursor salt solution in equal volume ratios

Figure 4.49 shows the SPR peaks obtained from the synthesis mixtures containing AgNPs synthesized using the cell free supernatant of the bacterial strain 4S3. As discussed earlier the intensity of the SPR peak of AgNPs being synthesized in the synthesis mixture increased with an increase in the concentration of the $AgNO_3$ solution. The conversion of Ag^+ ions to Ag^0 increased with the increase in concentration of the precursor salt solution used for the synthesis of AgNPs (Table 4.19). Broad SPR bands with non prominent peaks are observed with AgNPs synthesized using $AgNO_3$ solutions of less than 50 mM, indicating particles of wide size range. The maximum conversion of 89.54% was obtained with 75 mM of the precursor salt solution used for the synthesis of AgNPs and was found to decrease with a further increase in the concentration of the precursor salt solution in the synthesis mixture. The multiple peaks and peak splits are observed with AgNPs synthesized using 75 mM, 100 mM and 500 mM $AgNO_3$ solutions which indicate the formation of anisotropic nanoparticles. However, the distance between dipole and the quadrapole maxima of the electron excitation modes in the SPR peak of AgNPs have become larger as the concentration of the $AgNO_3$ solution in the synthesis mixture was increased from 75 mM to 500 mM.

The SPR peak belonging to the AgNPs synthesized using 100 mM and 500 mM of AgNO$_3$ solution and the cell free supernatant of strain 4S3 showed large number of multiple peaks within a single SPR band indicating the highly anisotropic morphology of the AgNPs. The highest number of multiple peaks was observed with 500 mM of AgNO$_3$ solution. Figure 4.50 shows the SEM image of AgNPs synthesized using 500 mM of AgNO$_3$ and the cell free supernatant of strain 4S3; which clearly indicates the anisotropic nature of the AgNPs with a wide size range and diverse shapes.

The SPR bands obtained with AgNPs synthesized with 75 mM AgNO$_3$ solution and the cell free supernatant of strain 4S3 shows a dominant split in the peak at 422 nm, but the SPR spectra contains multiple peaks. Dominant peaks were not observed below 75 mM AgNO$_3$ solution concentration. Ag$^+$ concentrations above 75 mM, the multiple peaks are large in number as shown by highly corrugated spectra. Thus the AgNPs synthesized using 75 mM AgNO$_3$ solution may have lesser anisotropy and asymmetry compared to those synthesized using 100 mM and 500 mM AgNO$_3$ solution.
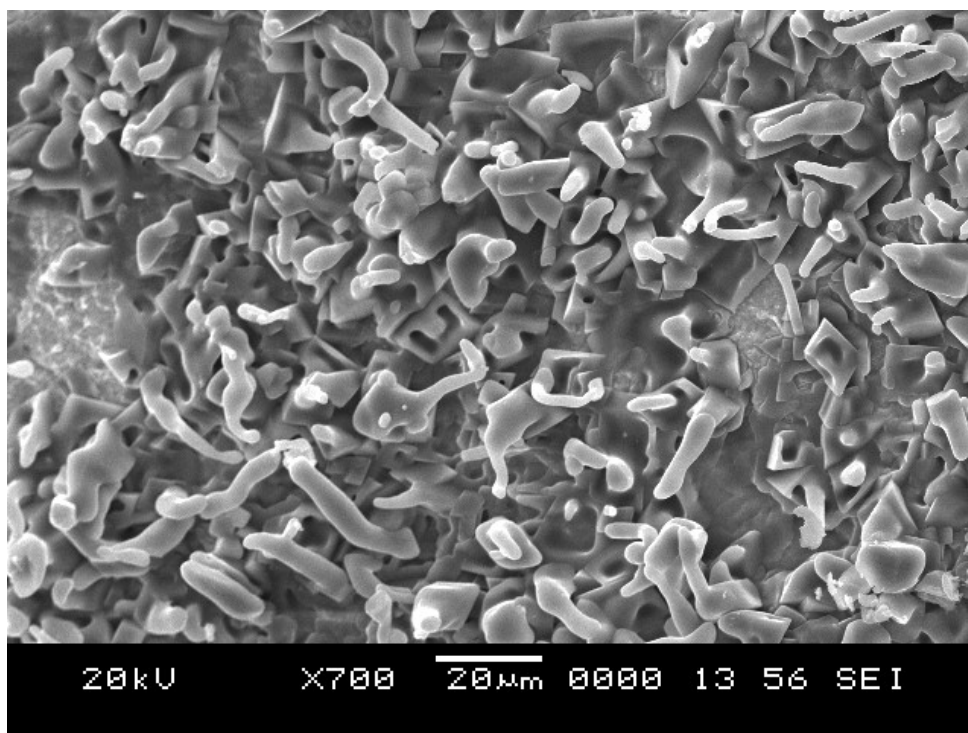
Figure 4.50 SEM image of AgNPs synthesized using 500 mM of AgNO$_3$ solution and cell free supernatant of strain 4S3 showing the formation of highly anisotropic AgNPs
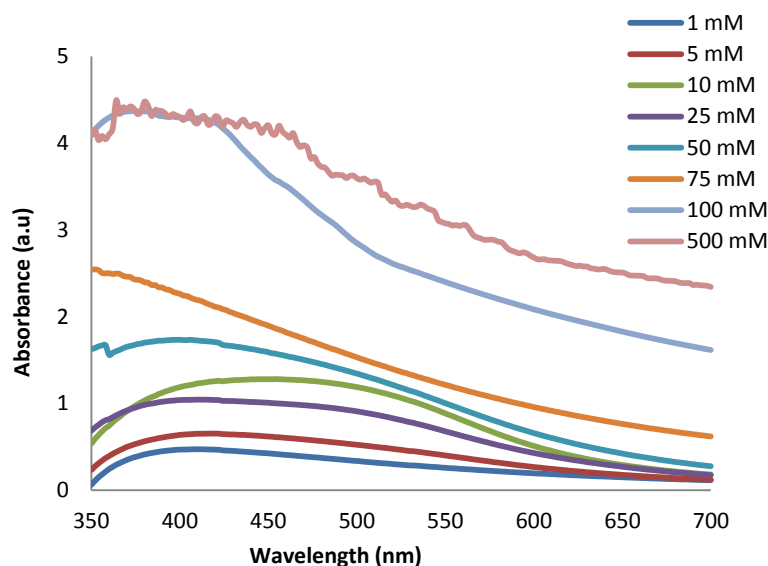
Figure. 4.51 SPR spectra of synthesis mixture containing AgNPs synthesized using 6S1 bacterial culture supernatant and varying concentration of precursor salt solution in 1:1 volume ratio

Thus, owing to maximum conversion (89.54%) obtained and less anisotropic characteristics observed through the spectral analysis, 75 mM of $AgNO_3$ solution was considered the optimum for the synthesis of AgNPs using the cell free supernatant of the bacterial strain 4S3.

Figure 4.51 shows the SPR spectra of AgNPs synthesized using the cell free supernatant of the bacterial strain 6S1 and varying concentrations of $AgNO_3$ solution in 1:1 volume ratio at an initial pH of 7.0±0.2 units at 24 h of the synthesis duration.

The SPR peaks were found to increase in intensity with increasing concentration of the $AgNO_3$ solution in the synthesis mixture. The AgNPs synthesized using 1 mM and 5 mM of the $AgNO_3$ solution gave rise to blue shifted peaks but the intensity of the SPR peak was lower indicating the formation of small number of AgNPs in the synthesis mixture and the conversion was also found to be low as shown in Table 4.19. This can be attributed to the lower concentrations of $AgNO_3$ in the synthesis mixture and the formation of large number of Ag nuclei, without the growth into AgNPs. The rate of growth of nuclei into AgNPs may be lesser owing to slower mass transfer rate caused by lower Ag^+ ions concentration gradient with the low concentration of the $AgNO_3$ salt solution in the synthesis mixture. Negligibly small number of AgNPs would have formed at 1 mM and 5 mM, as indicated by the

low intensity peaks. With increase in the concentration of AgNO$_3$ solution beyond 5 mM the appearance of a prominent peak of AgNPs occurred with increasing intensity as the concentration of the precursor salt solution was increased in the synthesis mixture. However, the peaks were broad indicating polydispersed nanoparticles with upto 75 mM AgNO$_3$ solution. However with 100 mM AgNO$_3$ solution the SPR peaks were of high intensities, blue shifted and smoother.

Similarly, the percentage conversion was also found to increase with an increase in the concentration of the AgNO$_3$ solution as seen in Table 4.19. The maximum conversion of Ag$^+$ ions to Ag^0 occurred at 100 mM and was found to decrease with further increase in the AgNO$_3$ solution in the synthesis mixture to 500 mM indicating that 100 mM of AgNO$_3$ solution is the optimum to bring about maximum conversion (91.17%) at 24 h of the synthesis duration and resulting in the formation of a high intensity, blue shifted, smoother SPR peak indicating the formation of a large number of small sized isotropic AgNPs.

The AgNPs synthesized with 500 mM AgNO$_3$ solution yielded a blue shifted peak with almost the same intensity as that obtained with 100 mM as seen in Figure 4.51. However, the conversion with 500 mM AgNO$_3$ solution was only 70.1% and was much lesser than that obtained with 100mM. The SPR band is found to contain several small peaks indicating the formation of highly anisotropic AgNPs which are undesirable. Figure 4.52 shows the SEM image of AgNPs synthesized using 500 mM of AgNO$_3$ solution with the cell free supernatant of strain 6S1 from which it is evident that a wide size range of AgNPs with varied anisotropic morphology are formed with 500 mM AgNO$_3$ solution . Through the SEM analysis it can be observed that 500 mM is unsuitable for the synthesis of AgNPs as it yields anisotropic morphology of the particles which is undesirable.

Thus, 100 mM of AgNO$_3$ solution which resulted in maximum conversion of 91.17% and indicated the formation of smaller and isotropic AgNPs from spectral analysis is considered as the optimum for the synthesis of AgNPs with 6S1.
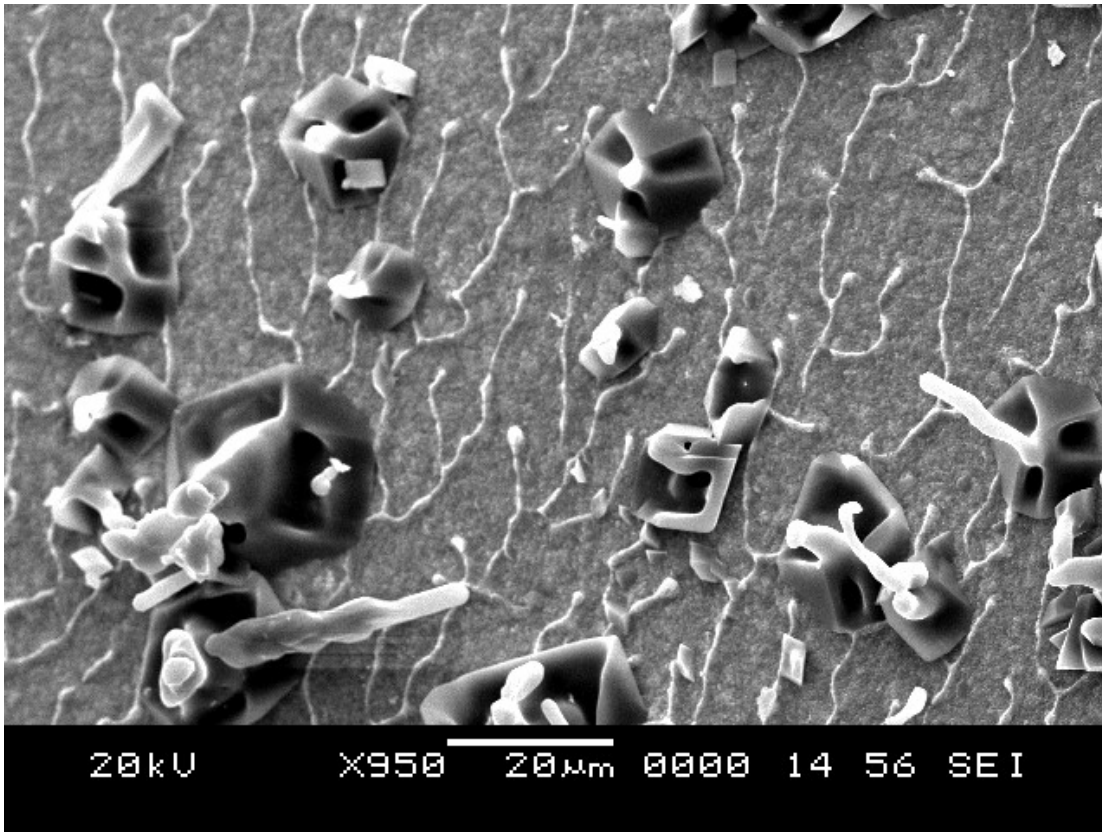
Figure 4.52 SEM image of AgNPs synthesized using 500 mM of AgNO₃ solution and cell free supernatant of strain 6S1 showing the formation of highly anisotropic AgNPs
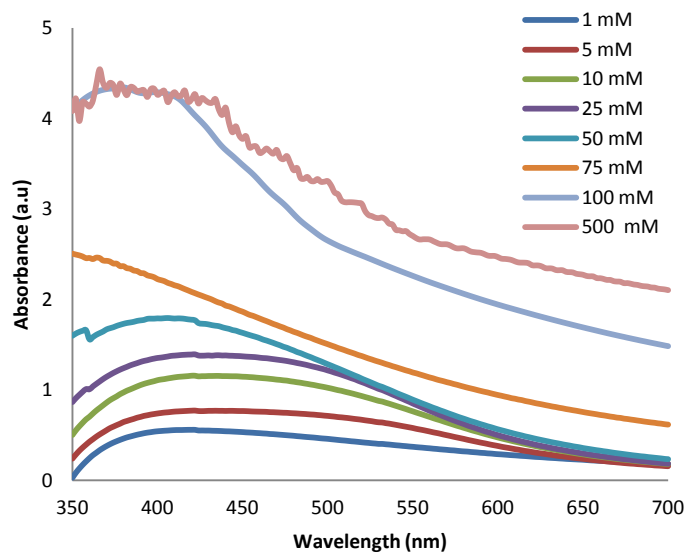
Figure. 4.53 SPR spectra of synthesis mixtures containing AgNPs synthesized using 8S1 bacterial culture supernatant and varying concentration of precursor salt solution in equal volume ratios

Similarly, the SPR spectra of AgNPs synthesized using the cell free supernatant of the bacterial strain 8S1 with varying concentrations of $AgNO_3$ solution in 1:1 volume ratios at an initial pH of 7.0±0.2 units at 24 h of the synthesis duration is shown in Figure 4.53.

The SPR peak intensities of the AgNPs synthesized using varying concentrations of the $AgNO_3$ solution in the synthesis mixture were found to be increasing in intensity in the order of increasing concentration of the $AgNO_3$ solution being used in the synthesis mixture. The percentage conversion of Ag^+ ions to Ag^0 was also found to increase in the same manner but decreased at the concentration above 100 mM as shown in Table 4.19. The AgNPs synthesized at lower concentration of precursor salt such as 1 mM, 5 mM, 10 mM, 25 mM and 50 mM gave rise to SPR peaks characteristic of AgNPs but very small splits in the SPR bands were observed at 25 mM and 50 mM $AgNO_3$ concentrations, indicating slightly anisotropic nature of the nanoparticles. With increase in $AgNO_3$ concentration, the SPR bands became narrower, indicating lower polydispersity.

The conversion of Ag^+ ions to Ag^0 was the maximum of 93.94% at 100 mM of the $AgNO_3$ solution used for the synthesis of AgNPs after 24 h of the synthesis period. SPR peak of AgNPs synthesized with 100 mM of the $AgNO_3$ solution was narrower, intense, smoother blue shifted as compared to the SPR peaks of AgNPs being synthesized with other concentrations of $AgNO_3$. The intense and blueshifted peak centred at 386 nm indicated the formation of many small sized AgNPs. Smoother and narrow bands indicate the formation of isotropic and narrow size range nanoparticles.

Coagulation was observed in case of the synthesis mixture prepared with the bacterial cell free culture supernatant of 8S1 and 500 mM of precursor salt solution indicating that the enzymes responsible for the reduction of Ag^+ ions to Ag^0 must have undergone poisoning of their catalytic sites thus leading to the change in the conformation of the active structure by the presence of high concentration of Ag^+ and NO_3^- ions. SEM analysis of the particles in Figure 4.54 obtained using 500 mM of $AgNO_3$ and the cell free supernatant of the strain 8S1 revealed large sized aggregates of the AgNPs with wide size range of the particles. This feature is also presented by the corrugated SPR band in Figure 4.53.
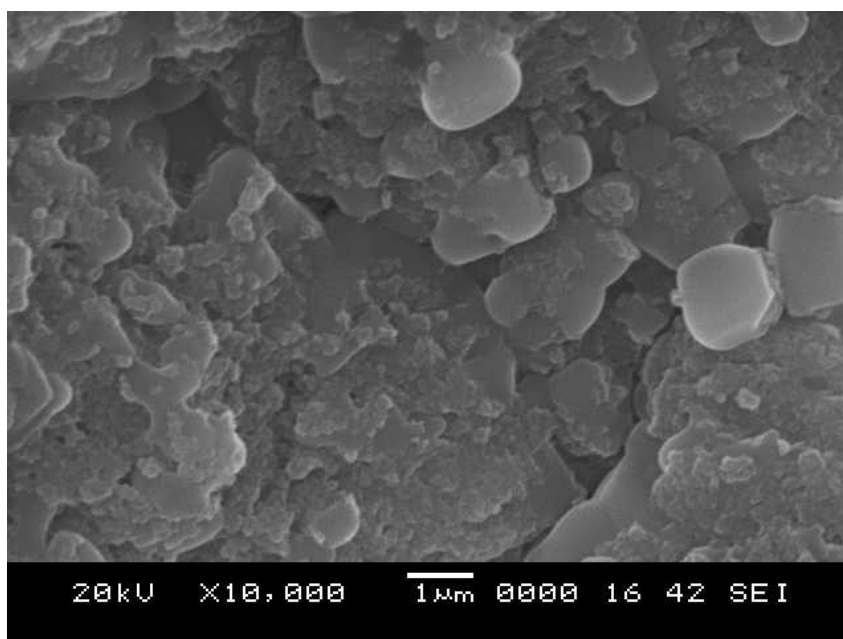
Figure 4.54 SEM image of AgNPs synthesized using 500 mM of AgNO₃ solution and cell free supernatant of strain 8S1 showing the formation of aggregates.

Thus, owing to maximum conversion and probable formation of small sized, isotropic AgNPs with the narrow size range as indicated by the nature of SPR band, 100 mM of $AgNO_3$ solution was considered to be the optimum for the synthesis of AgNPs using the cell free supernatant of bacterial strain 8S1.

Figure 4.55 consolidates the SPR peaks of AgNPs synthesized using $AgNO_3$ salt solution at the optimum concentration using the 24 h cell free supernatant of bacterial strains 4S1, 4S2, 4S3, 6S1 and 8S1. The percentage conversion of Ag^+ ions at the optimum precursor salt solution concentration is presented in Table 4.20.

Table 4.20 Percentage conversion Ag^+ ions obtained using the optimum precursor salt solution concentration with the bacterial cell free supernatant of strain 4S1, 4S2, 4S3, 6S1 and 8S1.

AgNPs synthesized using the bacterial supernatant	Optimum Concentration of AgNO₃ used for the synthesis of AgNPs	Percentage conversion Ag⁺ ions
4S1	75 mM	87.88
4S2	75 mM	88.89
4S3	75 mM	89.54,
6S1	100 mM	91.17
8S1	100 mM	93.94
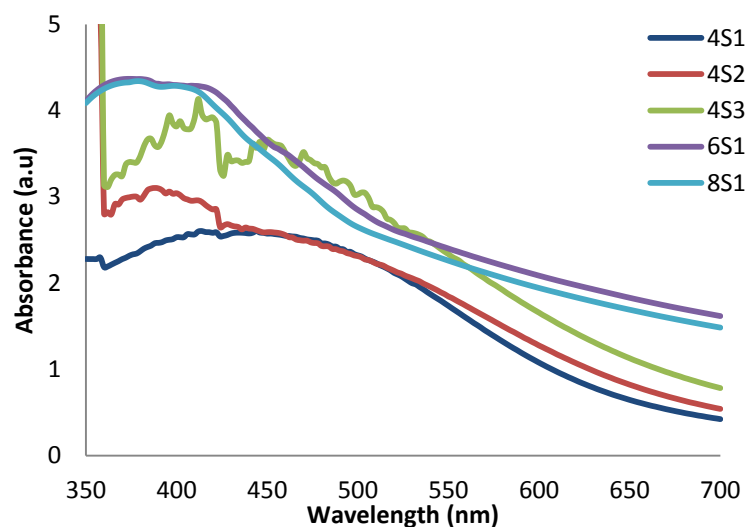
Figure 4.55 SPR spectra of synthesis mixtures containing AgNPs synthesized using the bacterial cell free culture supernatant and the precursor salt solution at optimum concentration

From Figure 4.55, it can be seen that the SPR peak obtained using 75 mM of AgNO$_3$ and 24 h cell free supernatant of bacterial strain 4S1 in 1:1 volume ratio with an initial synthesis mixture pH of 7.0±0.2 units is least in intensity than the SPR peaks obtained with the AgNPs synthesized using the bacterial strains 4S2, 4S3, 6S1 and 8S1 with their optimum concentrations of precursor salt solutions. The peak is broad and redshifted indicating that larger sized particles with a wide size range are formed and the conversion is found to be 87.88%. The conversion with 4S1 is also the lowest amongst all the bacterial strains. The SPR peak of AgNPs synthesized using the cell free supernatant of strain 4S2 with 75 mM AgNO$_3$ solution shows a split in the peak; the split results from the polarization of the AgNPs in two different modes of dipole and quadrapole mode (Zhang et al. 2011; Mie, 1908; Evanoff and Chumanov, 2005) and indicates the formation of non spherical, anisotropic AgNPs.

Similarly the SPR peak obtained from AgNPs synthesized using the cell free supernatant of strain 4S3 with 75 mM AgNO$_3$ solution is also found to contain a wide SPR peak with several small peaks indicating the formation of non spherical, highly anisotropic AgNPs with a conversion of 89.54%. The SPR peaks of AgNPs synthesized using the cell free supernatant of 6S1 and 8S1 with 100 mM (optimum) AgNO$_3$ solution are smoother, blue shifted and higher in intensity in comparison to the SPR peaks of AgNPs synthesized using other strains. The conversion as shown in

Table 4.20 is also the highest for AgNPs synthesized using strain 8S1 followed by 6S1. A small split in the SPR peaks of AgNPs being synthesized using 8S1 and 6S1 is observed at 395 nm and 390 nm respectively. The appearance of this small split indicates a minor deviation from spherical shape of the AgNPs being synthesized. However, the split is not pronounced or large as observed for the other strains. The SEM images of AgNPs synthesized using the cell free supernatant of 6S1 and 8S1 are shown in Figure 4.56 and Figure 4.57 respectively and their average size and particle size range are also given.

Figure 4.56 reveals the formation of quasi spherical shaped AgNPs with an average particle size of 58.78 nm and size range of 30-97 nm using the synthesis mixture prepared with the cell free supernatant of bacterial strain 6S1 and 100 mM of $AgNO_3$ solution. The SEM image and the particle size analysis results are in agreement with the analysis and interpretation of the spectral data presented in Figure 4.55. The intense, narrow and blue shifted SPR peak indicated the formation of large number of monodispersed AgNPs with a narrow size range of the particles
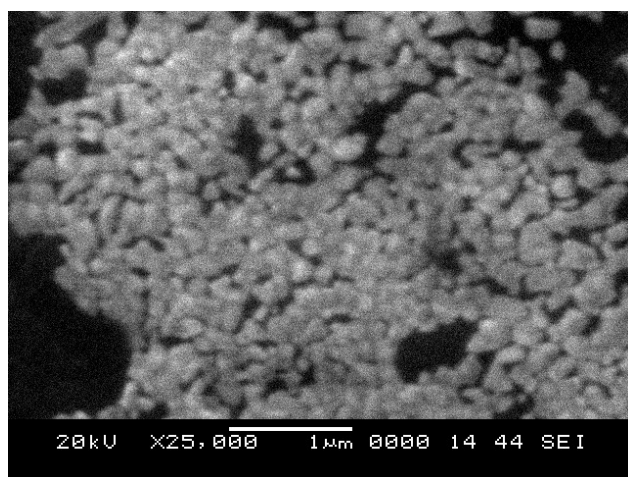
Size range of AgNPs synthesized
30-97 nm
Average Size of AgNPs synthesized
58.78 nm

Figure 4.56 SEM image of AgNPs synthesized using the 24 h cell free supernatant of strain 6S1 and 100 mM AgNO$_3$ solution

Figure 4.57 reveals the formation of spherical shaped AgNPs with an average particle size of 52.34 nm and average size range of 31-80.2 nm, synthesized using the 24 h cell free culture supernatant of bacterial strain 8S1 with 100 mM (optimum) $AgNO_3$ solution. The SEM image and the particle size analysis results are in agreement with the analysis and interpretation of the

spectral data presented in Figure 4.55. The SPR peak of AgNPs synthesized by 8S1 strain is narrower and blueshifted by 5 nm than the SPR peak of AgNPs synthesized using 6S1. The intense, narrow and blue shifted SPR peak indicates the formation of large number of monodispersed AgNPs with a narrow size range of the particles. The SEM image and particle size analysis also support the SPR characteristics. Thus AgNPs synthesized using the 24 h cell free supernatant of bacterial strain 8S1 is found to be spherical and smaller in size in comparison to the AgNPs synthesized using the 24 h cell free supernatant of bacterial strain 6S1.

Average Size range of AgNPs synthesized
31-80.2 nm
Average Size of AgNPs synthesized
52.34 nm
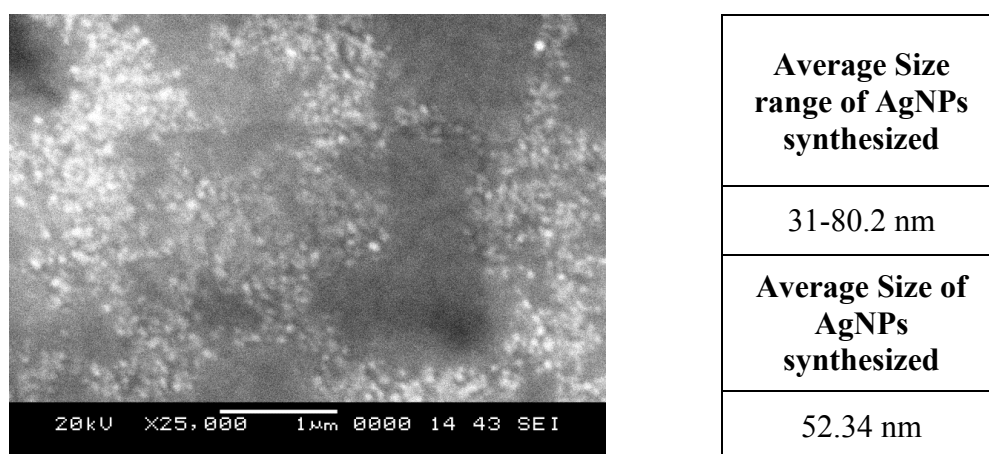
Figure 4.57 SEM image of AgNPs synthesized using the 24 h cell free supernatant of strain 8S1 and 100 mM AgNO$_3$ solution

Many researchers have established the precursor salt concentration to be a crucial factor in microbial based synthesis of AgNPs. Husseiny et al. (2015), Zaki et al. (2011), Otari et al. (2012), Kuber and Bhainsa, (2006) and Katherisan et al. (2009) have studied the effect of precursor salt solution concentration on the synthesis of AgNPs using microbes and have found that the concentration of the precursor salt used for the synthesis of AgNPs confers morphological characteristics to the nanoparticles being synthesized and also that increase in the concentration of the precursor salt solution beyond the optimum level increases the polydispersity of the particles being synthesized. The similar results have been obtained in the present study. The present study also proves that the concentration of precursor salt in the synthesis mixture determines the morphological characteristics of the AgNPs being

synthesized, enabling the synthesis of AgNPs with desirable morphological characteristics and dispersity for the specific applicability.

4.10.2 Effect of initial pH of the synthesis mixture on synthesis of AgNPs

The initial pH of the synthesis mixture has been proven to have a pronounced effect on the size and shape of AgNPs being synthesized (Gurunathan et al. 2009; Gericke and Pinches, 2006). To study the effect of initial pH of the mixture on synthesis of AgNPs, synthesis was carried out using 1:1 volume ratio of the optimum precursor salt solution and the 24 h grown bacterial cell free supernatant with varying initial pH as acidic pH 4, neutral (unadjusted) pH of 7.0± 0.2 and alkaline pH of 11 units.

The SPR peaks and the photographic image of AgNPs synthesized with acidic, neutral and alkaline initial pH conditions of the synthesis mixture containing $AgNO_3$ solution and the 24 h cell free supernatant of the strains 4S1, 4S2, 4S3, 6S1 and 8S1 after 24 h of synthesis time duration are shown in Figure 4.58 (a)-(e) and Figure 4.59 (a)-(e) respectively. Table 4.18 shows the percentage conversion of Ag^+ ions by the cell free supernatants of the bacterial strains 4S1, 4S2, 4S3, 6S1 and 8S1 under acidic, neutral and alkaline initial pH conditions of the synthesis mixture.

From the SPR spectra (Figure 4.58 (a)-(e)) of AgNPs synthesized using the cell free supernatants of the five bacterial strains, it can be seen that the intensity of the spectra increased with an increase in the initial pH of the synthesis mixture and highest intensities were observed with alkaline pH condition. Higher intensity is an indication of formation of large number of nanoparticles (Rodríguez-León et al. 2013; Guidelli et al. 2011; Basavaraja et al., 2008; Darroudi et al. 2012) under alkaline conditions. This is confirmed by the increase in conversion of Ag^+ with increase in pH and the highest conversion obtained with alkaline pH condition as presented in Table 4.21.

Table 4.21 Percentage conversion of Ag⁺ ions under initial pH conditions of synthesis medium using the 24 h cell free supernatant of bacterial strains 4S1, 4S2, 4S3, 6S1 and 8S1

Bacterial strain	Percentage conversion of Ag⁺ ions under different initial pH conditions		
	Acidic pH 4	Neutral (unadjusted) pH-7.0±0.2	Alkaline pH 11
4S1	34.57	87.88	91.59
4S2	36.42	88.89	92.86
4S3	31.84	89.54	92.04
6S1	18.64	91.17	96.6
8S1	20.1	93.94	98.98

The SPR peak of the AgNPs synthesized using initial acidic conditions of the synthesis mixture with the cell free supernatant of strain 4S1 as presented in Figure. 4.58(a) shows a split in the SPR band indicating anisotropic nature of the particles synthesized. The red shift of the dipole resonance towards 550 nm in the SPR peak indicates the formation of large sized particles and aggregation of the AgNPs (Rodríguez-León et al. 2013; Darroudi et al. 2012, Guidelli et al. 2011; Basavaraja et al. 2008) at acidic conditions which eventually settled as seen in the photographic image in Figure 4.59 (a). The intensity of the peak is low indicating that lesser number of AgNPs were synthesized at pH 4. SPR results are in agreement with the lower conversion of 34.57% as shown in Table 4.21.
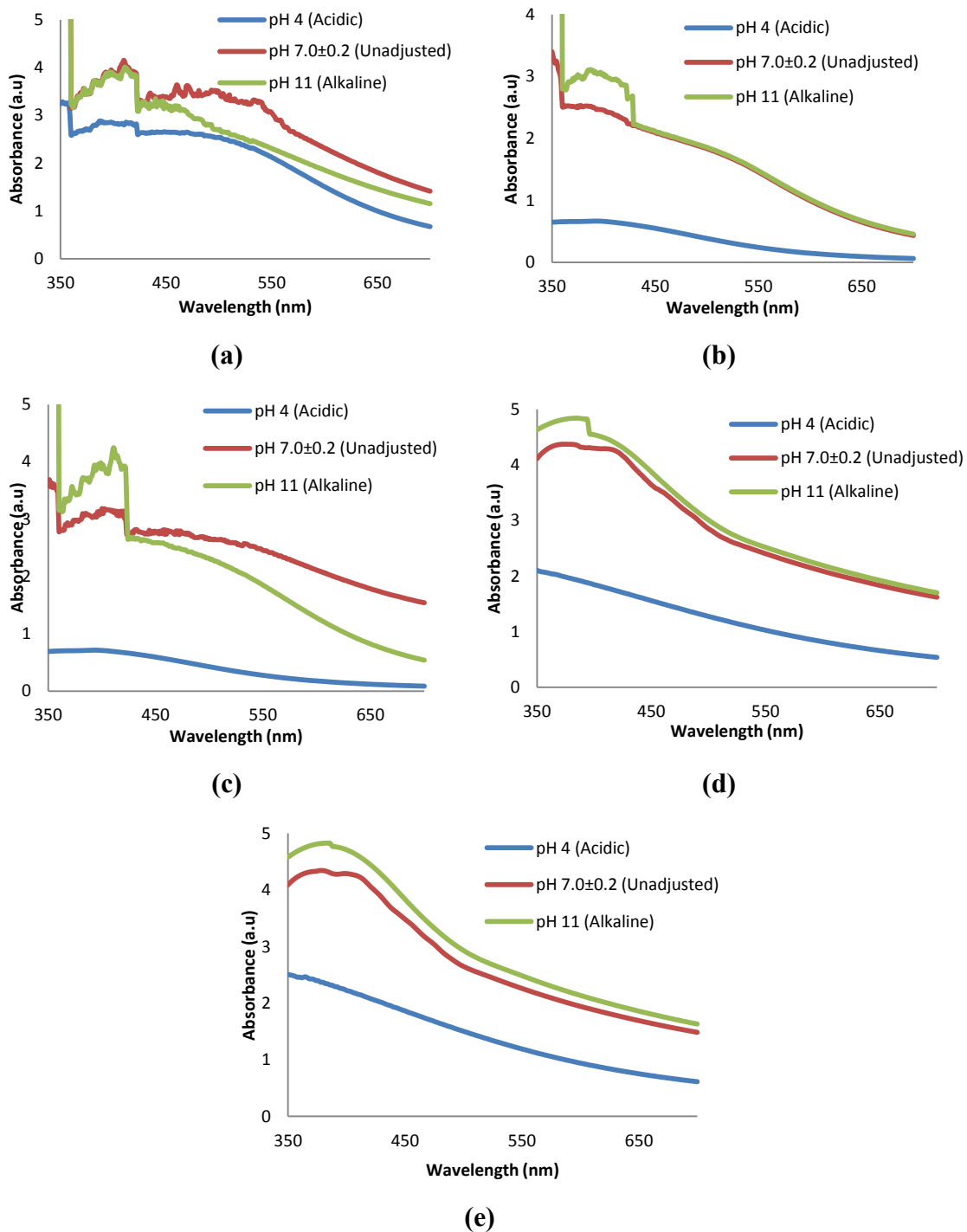
Figure 4.58 SPR spectra of synthesis mixtures for AgNPs synthesized using the optimum AgNO₃ solution under different initial conditions of pH using the cell free culture supernatant of strains (a) 4S1 (b) 4S2 (c) 4S3 (d) 6S1 and (e) 8S1
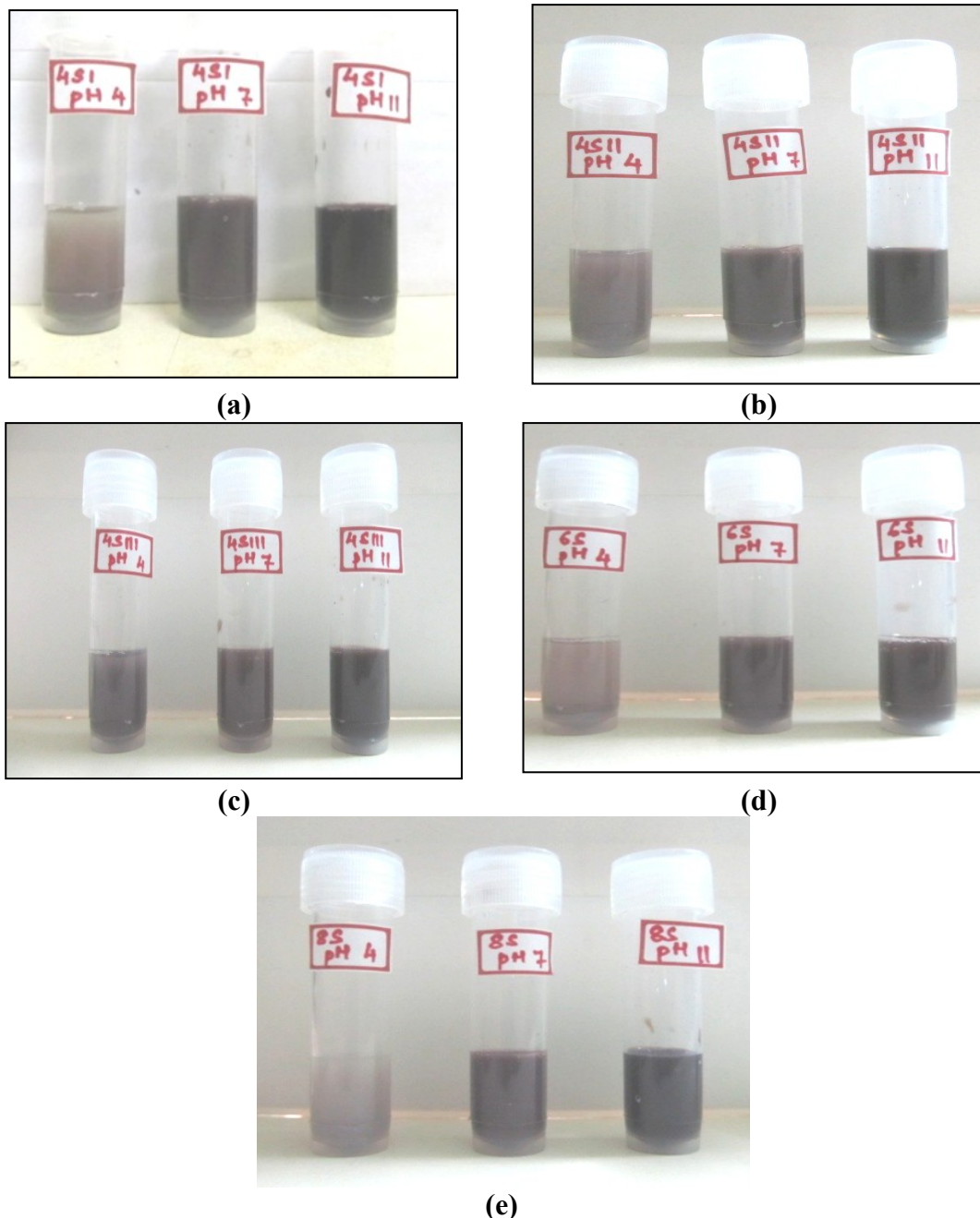
Figure 4.59 Photographic images showing the dispersion of AgNPs synthesized using the optimum precursor salt solution under different conditions of initial pH using the cell free culture supernatant of strains (a) 4S1 (b) 4S2 (c) 4S3 (d) 6S1 (e) 8S1

From Figure 4.58 (a) it can be seen that at initial neutral (unadjusted pH 7.0±0.2 units) conditions of synthesis, the SPR peak is intense, has a split, the dipole and quadrapole resonance modes are very distant from each other and is redshifted to 545 nm indicating the formation of a large number of anisotropic AgNPs with a broad

range of size distribution. The formation of well dispersed nanoparticles is visible in the photographic image shown as Figure 4.59 (a). The conversions is around 87.88% (Table 4.21) and is found to be higher than the conversion of Ag^+ ions obtained with acidic pH condition of 4. The SPR peak of AgNPs synthesized using alkaline condition of pH 11 in the synthesis mixture of cell free supernatant of strain 4S1 shows a narrow peak with high intensity and a split as presented in Figure 4.58 (a). The split indicates the dipole and the quadrapole resonance modes indicating the formation of anisotropic AgNPs and the distance between the two modes is less indicating that the particles synthesized have a smaller size distribution range as compared to those synthesized with initial acidic pH of 4 and under unadjusted pH condition of 7.0±0.2. Photograph of the synthesis mixture (Figure 4.59(a)) after synthesis showed well dispersed condition of the nanoparticles. The conversion of Ag^+ was found to be around 91.59%; which is the maximum amongst all the conditions of initial pH of the synthesis mixture.

Similarly the SPR peaks of AgNPs synthesized under initial acidic condition of pH 4 using the synthesis mixture prepared with optimum $AgNO_3$ solution of 75 mM and the cell free supernatant of either strain 4S2 (Figure 4.58 (b)) or 4S3 (Figure 4.58 (c)) did not reveal any characteristic peak belonging to AgNPs. Similarly, the absence of peaks characteristic of AgNPs in the SPR bands of AgNPs prepared with $AgNO_3$ solution of optimum concentration (100 mM) using the cell free supernatants of strain 6S1 (Figure 4.58 (d)) or 8S1 (Figure 4.58 (e)) at initial pH of 4, revealed that the AgNPs were not formed to a considerable extent at acidic conditions. The conversion (Table 4.21) obtained under acidic pH conditions are the lowest compared to that obtained with neutral and alkaline pH conditions with all the strains. Agglomeration and settling of the AgNPs was observed in the photographic images of AgNPs synthesized at initial pH 4 using the cell free supernatants of the bacterial strains 4S1 in Figure 4.59 (a), 4S2 in Figure 4. 59 (b), 4S3 in Figure 4.59 (c), 6S1 in Figure 4.59 (d) and 8S1 in Figure 4.59 (e) indicating that initial acidic pH of the synthesis mixture is unfavourable for the synthesis of AgNPs.

The SPR spectra obtained from AgNPs synthesized under initial neutral (unadjusted) conditions of pH 7.0±0.2 for the strains 4S1, 4S2 and 4S3 show the presence of several small peaks in their SPR as shown in Figure 4.58 (a), (b) and (c)

respectively indicating the synthesis of highly anisotropic AgNPs which is undesirable. However the conversion obtained under initial neutral pH conditions of synthesis for all the five strains was found to be higher than that obtained under initial acidic pH conditions as shown in Table 4.21. The SPR spectra of AgNPs synthesized using 100 mM of $AgNO_3$ and the cell free supernatant of strains 6S1 (Figure 4.58 (d)) and 8S1 (Figure 4.58 (e)) with initial pH of 7.0±0.2 (unadjusted) are smooth and blue shifted with high intensity compared to the SPR spectra of AgNPs synthesized using the strains 4S1, 4S2 and 4S3. The high intensity, blue shifted and smooth peaks indicate the formation of lesser number, smaller anisotropic shaped AgNPs. The photographic images of AgNPs synthesized under initial neutral pH of 7.0±0.2 with all the five bacterial strains show better dispersion of the AgNPs as compared to that of acidic pH (Figure 4.59 (a)-(e)).

Further, initial alkaline pH of 11 used for AgNPs synthesis using $AgNO_3$ solution of optimum concentration and the cell free culture supernatants resulted in a smoother and narrow SPR band with less number of peaks within it compared to that obtained from AgNPs synthesized using initial acidic and neutral conditions of synthesis mixture for all the five strains. The observation of intense, smoother and narrow SPR peaks (Figure 4.58 (a)-(e)) with high conversion (Table 4.21) indicates the formation of a large number smaller sized nearly isotropic AgNPs. Also the dispersion obtained with alkaline pH was better compared to acidic and neutral pH conditions as seen in the photographic images of AgNPs in Figure 4.59 (a)-(e) for all the five strains. The conversion obtained for AgNPs synthesized under initial alkaline pH of 11 was the highest for all the five strains as shown in Table 4.21. The conversion was found to increase (Table 4.21) with an increase in the initial pH of the synthesis mixture. Thus with regard to the spectral characteristics along with the high conversion and dispersion, initial alkaline pH conditions of the synthesis mixture is considered to be the optimum for the synthesis of small sized isotropic AgNPs. However, the SPR spectra for AgNPs synthesized with cell free supernatants of strains 4S1, 4S2, 4S3 and 6S1 show peak splits even at initial pH 11. With strains 4S1, 4S2 and 4S3 multiple small peaks were also observed indicating anisotropic nature of the AgNPs. But, with strain 6S1 at initial pH 11, the spectra is smoother with a single small split indicating nearly isotropic nature of AgNPs synthesized. The

spectrum of AgNPs synthesized with strain 8S1 is smooth with no visible peak split, thus indicating the formation of isotropic AgNPs at pH 11.

Through these studies it is evident that initial pH of the synthesis mixture highly influences the shape, size, conversion and dispersion of the AgNPs being synthesized and alkaline pH of 11 is found to be favourable for the synthesis of AgNPs using cell free supernatant of strain 4S1, 4S2, 4S3, 6S1 and 8S1.

The formation of anisotropic nanoparticles with low conversion and agglomeration under initial acidic pH of synthesis mixture for all the five strains can be attributed to the high proton concentration in acidic conditions of synthesis which may block the enzyme active sites for Ag^+ reduction or cause a change in the native protein structure of the enzyme responsible for the reduction of Ag^+ ions in the synthesis mixture thereby reducing the conversion. The capping agents on the surface of AgNPs may react with the prominent H^+ ions in the solution, thus destabilizing the surface charge on the AgNPs thereby leading to agglomeration. Thus, acidic pH influences the shape and size of the AgNPs leading to the formation of aggregated or anisotropic AgNPs. Similar observations were reported by Nayak et al. (2011) in their studies pertaining to the effect of initial pH of the synthesis mixture on the AgNPs being synthesized using the cell free supernatant of *Penicillium purpurogenum* NPMF wherein they reported the formation of anisotropic and large sized AgNPs at lower pH conditions of pH 4 and 5 and found that the AgNPs synthesized at higher pH conditions of pH 8 and 9 resulted in monodispersed and spherical shaped particles. They attributed this change in the shape and dispersion of the AgNPs to the proton concentration present in the synthesis mixture and its interaction with the nitrate reducing enzymes secreted by the microbe.

The conversion of AgNPs was found to be the highest with initial alkaline pH of the synthesis mixture. This high conversion of Ag^+ ions to Ag^0 can be attributed to the faster reduction of Ag^+ ions under alkaline conditions of synthesis, where $AgNO_3$ is readily reduced by the action of enzymes present in the bacterial culture supernatants. Oza et al. (2012) have also studied the effect of initial pH of synthesis mixture on AgNPs synthesis and have reported pH 10 to be favourable for the formation of monodispersed AgNPs than acidic pH. Also Qin et al. (2010) reported

that alkaline pH results in the formation of smaller AgNPs and the shape of the AgNPs changed from quasi spherical to spherical nanoparticles at pH 10.5.

The enzymes present in the cell free supernatant of the bacterial strains play an important role in bringing about the conversion of Ag^+ ions to Ag^0 in alkaline pH conditions as the amino, sulfhydryl and carboxylic groups present in the enzymes bear more negative charge and offer more affinity towards the Ag^+ ions at higher pH conditions thereby bringing about faster reduction and formation of a large number of Ag^0 nuclei contributing to the formation of thermodynamic-favoured spherical particles. The same groups bear a positive charge under low pH conditions lowering the reduction rate and the affinity hence not being favourable for the reduction and causing low conversion (Park et al. 2007). Under alkaline pH, the proteins involved in the synthesis may bind with silver at thiol regions (–SH) forming a –S–Ag bond, a clear indication of which aids the conversion of Ag^+ to Ag^0 . In addition, the alkaline ion (-OH) is very much required for the reduction of metal ions. Moreover, under alkaline conditions the ability of the enzyme responsible for the synthesis of silver nanoparticles increases (Sanghi and Verma, 2009). Thus initial alkaline pH of 11 of the synthesis mixture is favourable for the synthesis of AgNPs using the 24 h grown cell free supernatants of the bacterial strains and the optimum concentration of $AgNO_3$ solution in equal volume ratios under ambient conditions of synthesis.

The conversion under alkaline conditions of synthesis followed the order of 8S1>6S1>4S3>4S2>4S1. The strains 8S1 and 6S1 yielded the highest conversion under alkaline conditions of synthesis along with better spectral characteristics of intense, narrow, blue shifted and smoother SPR peaks (Figure 4.58 (d) and Figure 4.58 (e)) indicating the formation of large number of small sized, isotropic or nearly isotropic AgNPs with narrow size distribution range. Thus to gain a better insight into the morphological characteristics of the AgNPs synthesized with the strains 6S1 and 8S1, SEM analysis of the AgNPs synthesized under each of the initial pH condition was performed and is shown in Figure 4.60 (a)-(c) and Figure 4.61 (a)-(c) respectively. Table 4.22 and Table 4.23 present the average size and approximate size range of the AgNPs synthesized at different initial pH conditions of the synthesis mixture with the cell free culture supernatants of bacterial strains 6S1 and 8S1 respectively.

(a)   **(b)**

(c)
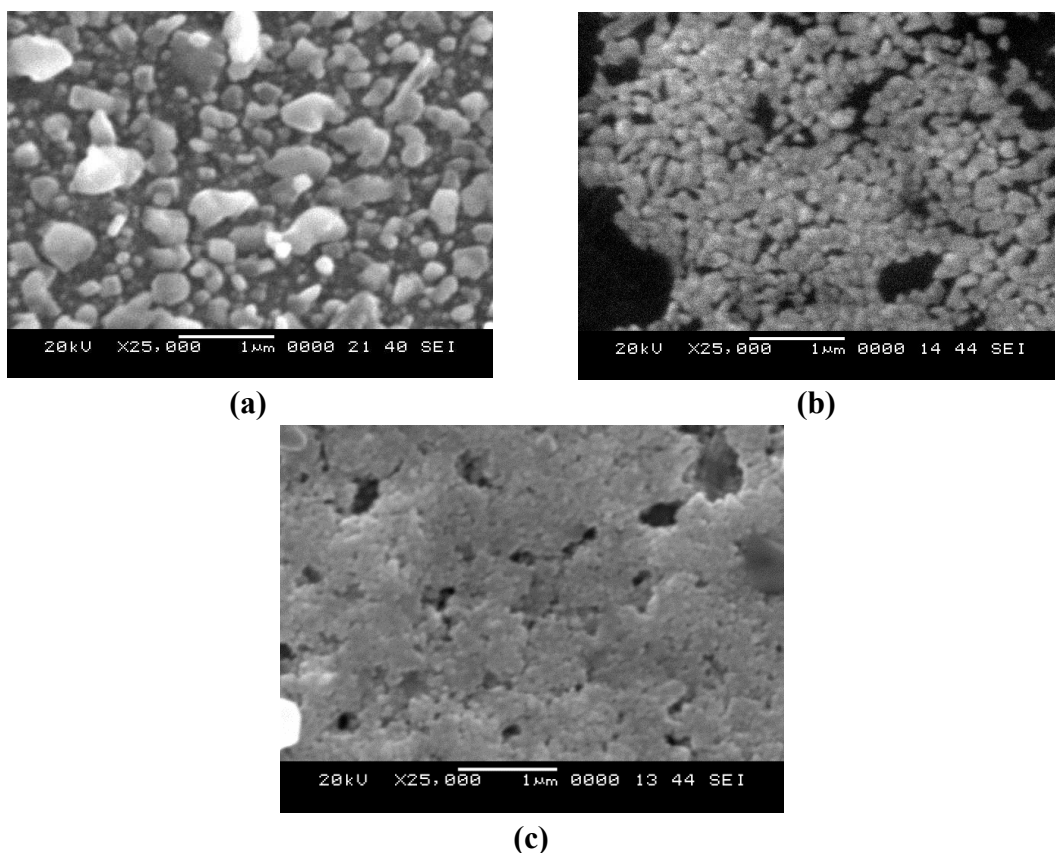
Figure 4.60 SEM images of AgNPs synthesized using culture supernatant of bacterial strain 6S1 at initial pH condition of (a) Acidic pH 4 (b) Neutral pH 7 and (c) Alkaline pH 11.

Figure 4.60 (a) shows the SEM image of the aggregated particles synthesized under initial acidic pH condition with strain 6S1. It can be seen that the aggregates are formed and are of highly polymorphic (anisotropic) and are large sized. The SPR results (Figure 4.58 (d)) along with the visual data obtained from the digital image (Figure 4.59(d)) of the AgNPs are in agreement with the result obtained through SEM analysis. The particles are of large size as shown in Table 4.22 with low conversion (Table 4.21). The SEM image in Figure 4.60 (b) of AgNPs synthesized under initial neutral pH of the synthesis mixture reveals the formation of fairly dispersed AgNPs which are nearly isotropic with quasi spherical shape and with an average size of 58.78 nm and narrower size range (Table 4.22) compared to that obtained with AgNPs synthesized at initial acidic pH condition of synthesis.

Table 4.22 Approximate size range and average particle size of AgNPs synthesized under different initial pH condition of the synthesis mixture using 24 h cell free culture supernatant of bacterial strain 6S1 and 100 mM AgNO$_3$ solution

Initial pH condition of the synthesis medium	Approximate size range of the particles	Average particle size
Acidic pH 4	96- 900 nm	734.28 nm
Neutral (unadjusted) pH 7.0±0.2	30-97 nm	58.78 nm
Alkaline pH 11	18.4-68 nm	38.05 nm

SEM image of the AgNPs synthesized using cell free supernatant of strain 6S1 at initial alkaline pH as shown in Figure 4.60 (c) reveals the formation of nearly isotropic, quasi spherical shaped, uniform sized AgNPs. As observed in Table 4.22 the average particle size is 38.05 nm with narrow size range, the size is smaller and the range is narrower than the AgNPs synthesized under initial acidic and neutral pH of the synthesis mixture. The narrow range of size distribution indicates the monodispersity of the AgNPs synthesized at initial pH 11.

To obtain further insight on the morphological characteristics of the AgNPs synthesized using 100 mM of AgNO$_3$ with the cell free supernatant of strain 6S1 with initial alkaline pH of 11, the particles were subjected to TEM analysis. Figure 4.61 presents the TEM image of AgNPs synthesized using strain 6S1.

From the TEM image in Figure 4.61 it can be seen that the AgNPs were found to be of an average size 38.32 nm as determined using Image J software and were found to be quasi spherical in shape. In addition, the presence of a transparent mass encapsulating the AgNPs can be observed which can be attributed to the capping material of bacterial origin.
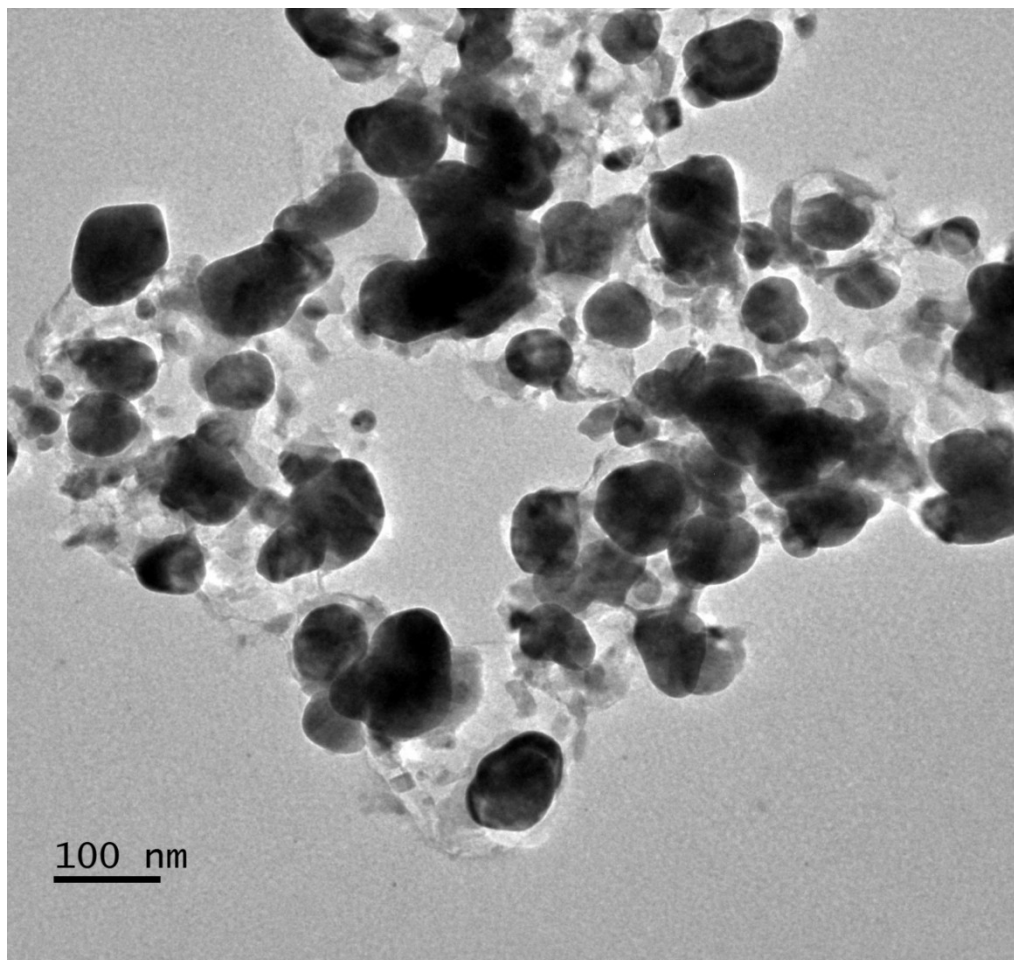
Figure 4.61 TEM image of AgNPs synthesized from the cell free culture supernatant of bacterial strain 6S1 with 100mM of AgNO$_3$ solution under alkaline condition of pH 11 at ambient temperature of synthesis

Similarly the AgNPs synthesized using the cell free supernatant of the strain 8S1 at different initial pH were also analyzed using SEM to obtain their morphological characteristics as shown in Figure 4.62 (a)-(c).

The SEM image obtained in Figure 4.62 (a) shows highly aggregated particles with no distinct shape and size suggestive of the aggregation of the particles obtained under acidic conditions of synthesis. The SEM image presented in Figure 4.62 (a) indicates the polydispersity of the particles being synthesized under acidic conditions. However, the SPR bands in Figure 4.58 (e) with neutral and alkaline pH were smoother, narrower with peak split of negligible magnitude indicating probable formation of isotropic, smaller sized AgNPs with uniform size distribution. The SEM images of AgNPs synthesized at neutral and alkaline pH presented in Figure 4.62 (b)

and Figure 4.62 (c) also show nearly spherical nanoparticles that confirm isotropic nature of the AgNPs synthesized, thus supporting the interpretations made by SPR analysis. Similarly, the size of AgNPs are small with narrow size range both at neutral and alkaline pH as observed in Table 4.23 supporting the SPR spectral interpretation. The SPR spectra for AgNPs synthesized at neutral pH (Figure 4.58 (e)) showed a broader and sharper peak as compared to that for AgNPs synthesized at alkaline pH and it was interpreted that owing to the sharper and narrower peak, the AgNPs synthesized at pH 11 are smaller sized with narrower size distribution than those synthesized at neutral pH. These interpretations are justified as observed in Table 4.23. The AgNPs synthesized at initial neutral conditions of synthesis are of size range 31-80.2 nm with average size of 52.34 nm, whereas those synthesized at alkaline pH are of narrower size range of 22-57 nm with smaller average size of around 29 nm. Thus, very small sized, almost isotropic and spherical AgNPs with narrow size distribution were synthesized at pH 11with the cell free supernatant of strain 8S1 using 100 mM (optimum) $AgNO_3$ solution.

Table 4.23 Average size range of the particles and Average particle size of AgNPs synthesized under different initial pH condition of the synthesis medium using the 24 h cell free supernatant of bacterial strain 8S1

Initial pH condition of the synthesis medium	Average size range of the particles	Average particle size
Acidic pH 4	Agglomeration, Not Determinable	Agglomeration, Not Determinable
Neutral (unadjusted) pH 7.0±0.2 units	31-80.2 nm	52.34 nm
Alkaline pH 11	22-57 nm	29.01 nm

(a)

(b)

(c)
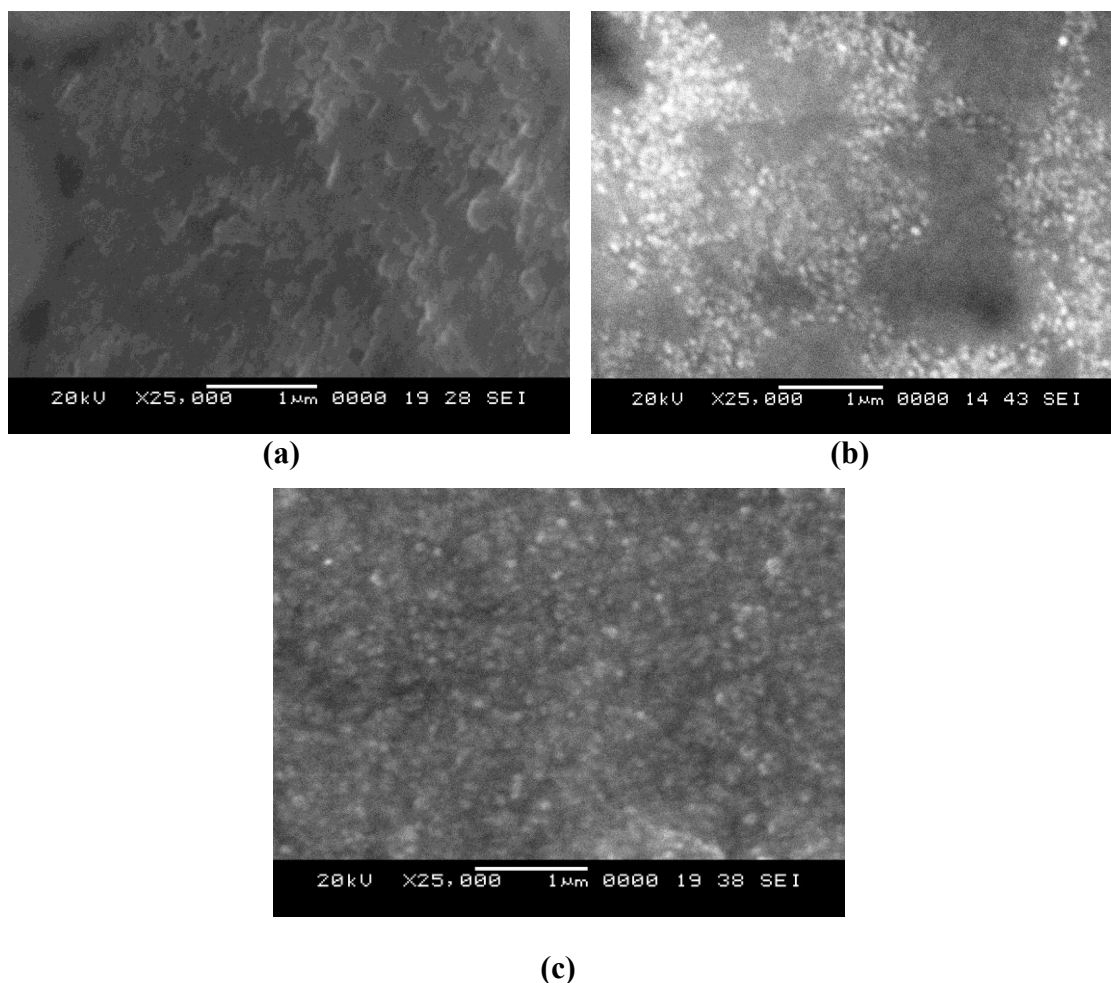
Figure 4.62 SEM images of AgNPs synthesized using culture supernatant of bacterial strain 8S1 at initial pH condition of (a) Acidic pH 4 (b) Neutral pH 7 and (c) Alkaline pH 11

To obtain a better insight into the morphological characteristics of AgNPs synthesized using the strain 8S1 under alkaline pH of 11, the AgNPs were subjected to TEM analysis and the image is presented in Figure 4.63.
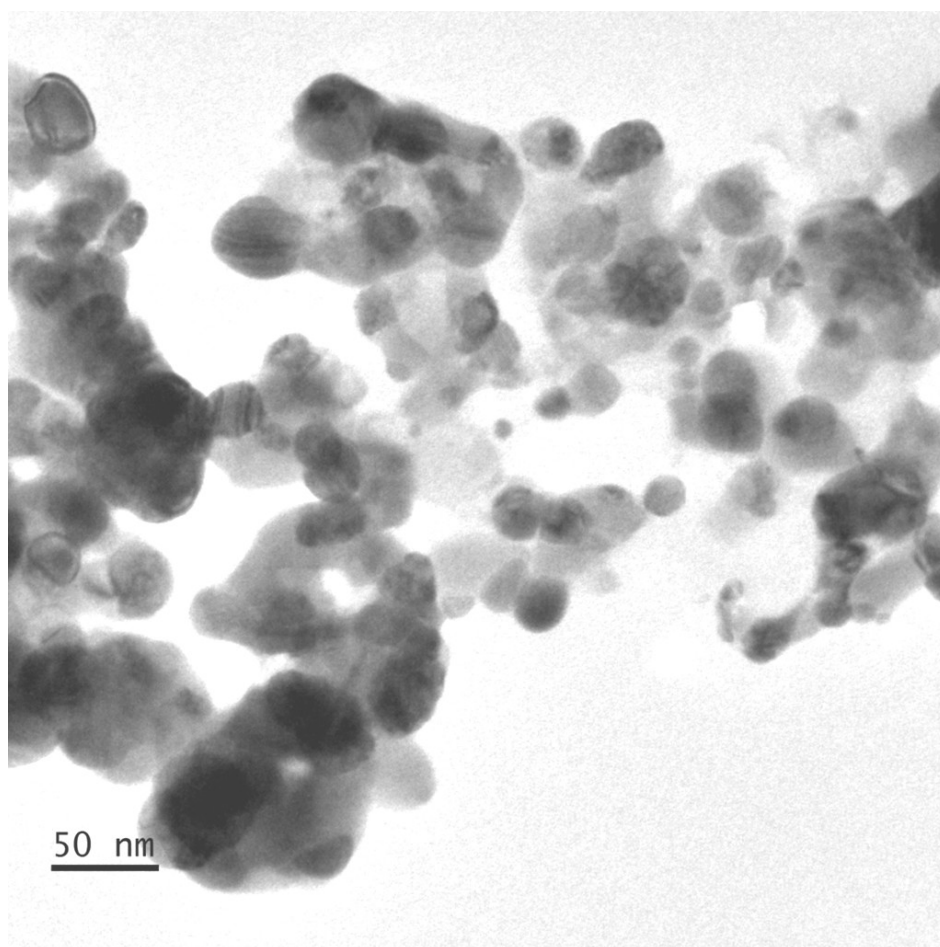
Figure 4.63 TEM image of AgNPs synthesized from the cell free culture supernatant of bacterial strain 8S1 with 100mM of AgNO₃ solution under alkaline condition of pH 11 at ambient temperature of synthesis

Figure 4.63 reveals the quasi spherical shaped morphology of the AgNPs with an average size of 22.01 nm; the particles are embedded in a translucent matrix indicating the presence of capping agents of bacterial origin. The TEM results are in agreement with the SEM results.

From these studies on the effect of initial pH of the synthesis mixture on the synthesis of AgNPs using the cell free culture supernatants of the five bacterial strains it can be concluded that pH of the synthesis mixture plays an important role in determining the dispersity and morphological characteristics of the AgNPs being synthesized. pH of the synthesis medium can be altered in order to synthesize AgNPs with desired morphological characteristics. This study also revealed that alkaline pH of the synthesis mixture is favourable for the synthesis of AgNPs, as it results in more isotropic, dispersed and small sized AgNPs. The synthesis with the cell free

supernatants of the strains 6S1 and 8S1 at alkaline initial pH yields isotropic, spherical AgNPs with the small size and narrow size distribution as compared to those synthesized with the strains 4S1,4S2 and 4S3. However the AgNPs synthesized with 8S1 were of smallest average size, narrowest size distribution with nearly spherical shape supporting perfect isotropy.

4.11 Characterization of AgNPs synthesized using the isolated strains of bacteria

As discussed in Section 2.9 of Chapter 2, characterization of the AgNPs provides us vital information regarding the morphological and physicochemical characteristics. The AgNPs synthesized in synthesis mixture prepared with $AgNO_3$ solution of optimum concentration as determined from the studies discussed in Section 3.3.6.1 and 24 h cell free supernatant of the isolated strains of bacteria in 1:1 volume ratio were characterized. The optimum concentrations of $AgNO_3$ solution used for the synthesis were 75 mM for strains 4S1, 4S2 and 4S3 and 100 mM for strains 6S1 and 8S1. The spectral characteristics, SEM images, the sizes and size ranges as analyzed with Image J analyzer software using the SEM image were presented in Section 4.10.2. The current section presents the EDS analysis for elemental composition, FTIR analysis for surface chemical groups, XRD analysis for crystallinity and crystallite size, particle size distribution and zeta potential determination using particle size analyzer.

4.11.1 EDS analysis of AgNPs synthesized using the cell free supernatant of the bacterial isolates

EDS analysis allows the determination of elemental composition of AgNPs synthesized. Figure 4.64 (a)-(e) show the EDS spectra of AgNPs synthesized using the 24 h cell free supernatant of bacterial strains 4S1, 4S2, 4S3, 6S1 and 8S1 respectively.
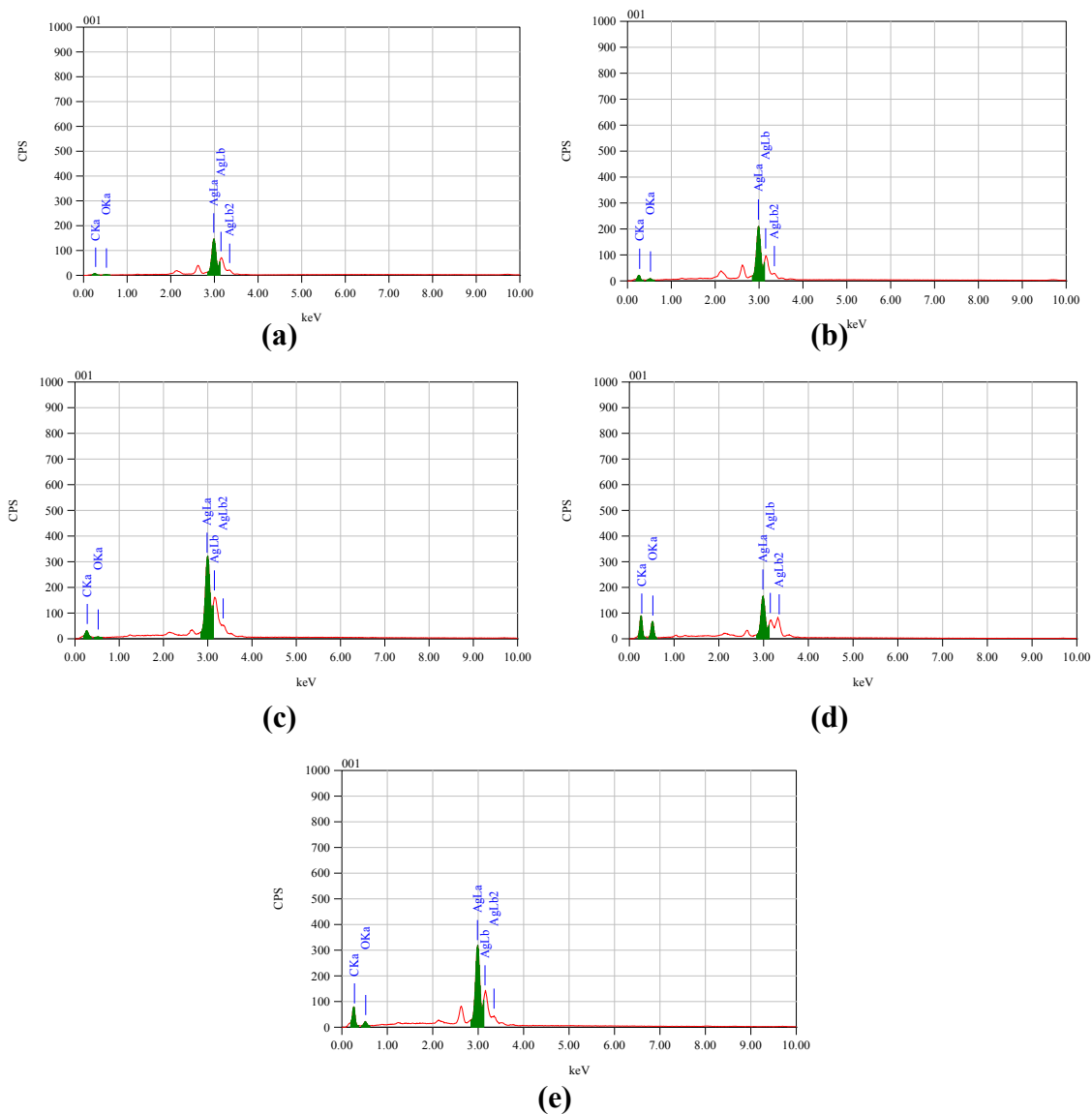
Figure 4.64 EDS spectrum of AgNPs synthesized using the cell free supernatant of bacterial strains (a) 4S1 (b) 4S2 (c) 4S3 (d) 6S1 and (e) 8S1

The EDS spectrum shows the presence of elemental silver, carbon and oxygen in AgNPs. The optical absorption peak is observed at approximately 3 keV, which is typical for the absorption of metallic silver nanocrystals (Fayaz et al. 2010). The presence of carbon and oxygen indicate existence of bacterial capping agents on the surface. The presence of capping agents imparts stability to the AgNPs being synthesized.

4.11.2 FTIR analysis of AgNPs synthesized using the cell free supernatant of the bacterial isolates

The AgNPs synthesized using the cell free bacterial supernatants of the isolates 4S1, 4S2, 4S3, 6S1 and 8S1 were processed according to the methodology described in section 3.3.5 of Chapter 3 and subjected to FTIR analysis to determine the presence of surface groups as an evidence of the capping agents which impart stability to the AgNPs.

Figure 4.65 to Figure 4.69 show the IR spectra of AgNPs synthesized using the cell free supernatants of bacterial strains 4S1, 4S2, 4S3, 6S1 and 8S1 respectively. Table 4.24 shows the wave numbers and the corresponding functional groups present on the surface of the AgNPs.
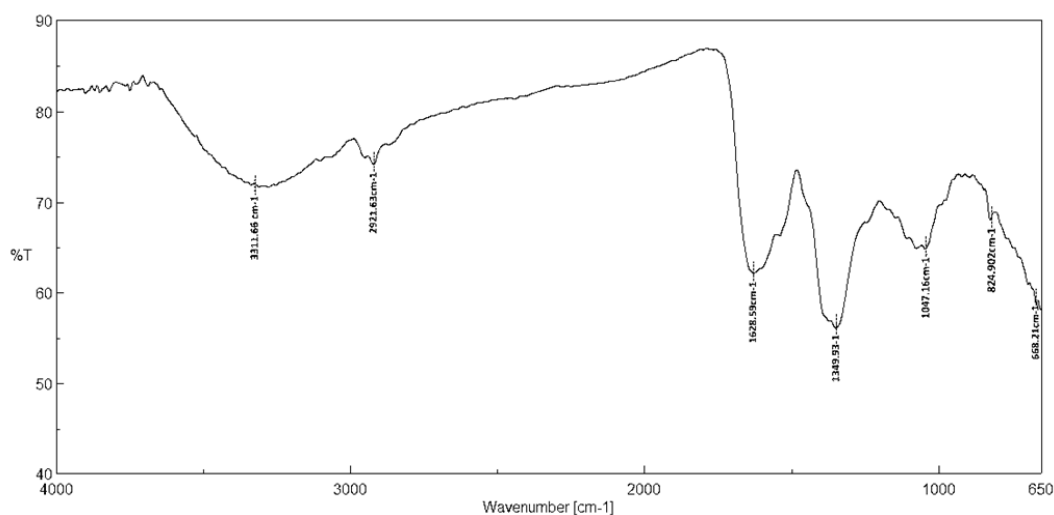
Figure 4.65 FTIR spectra of AgNPs synthesized using bacterial culture supernatant of 4S1
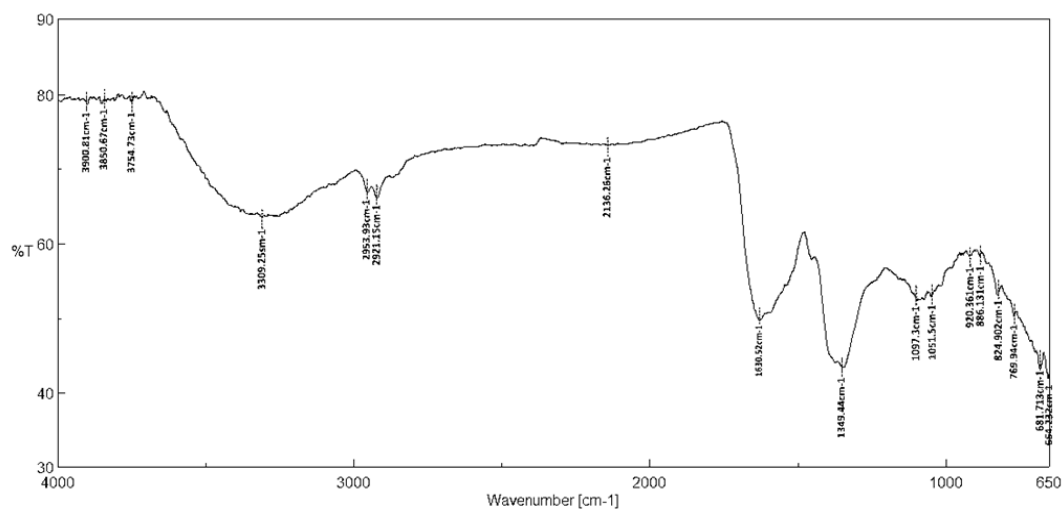
Figure 4.66 FTIR spectra of AgNPs synthesized using bacterial culture supernatant of 4S2
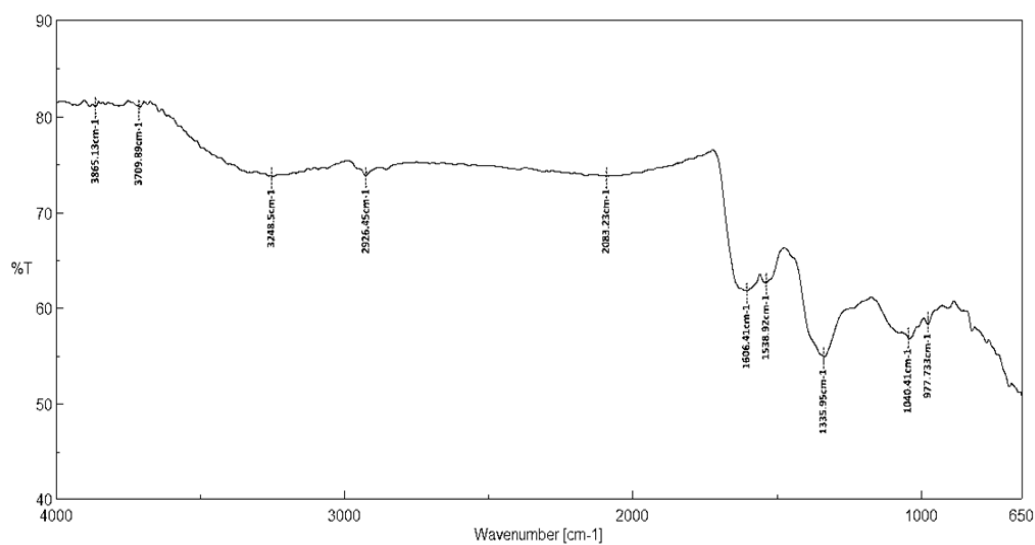
Figure 4.67 FTIR spectra of AgNPs synthesized using bacterial culture supernatant of 4S3
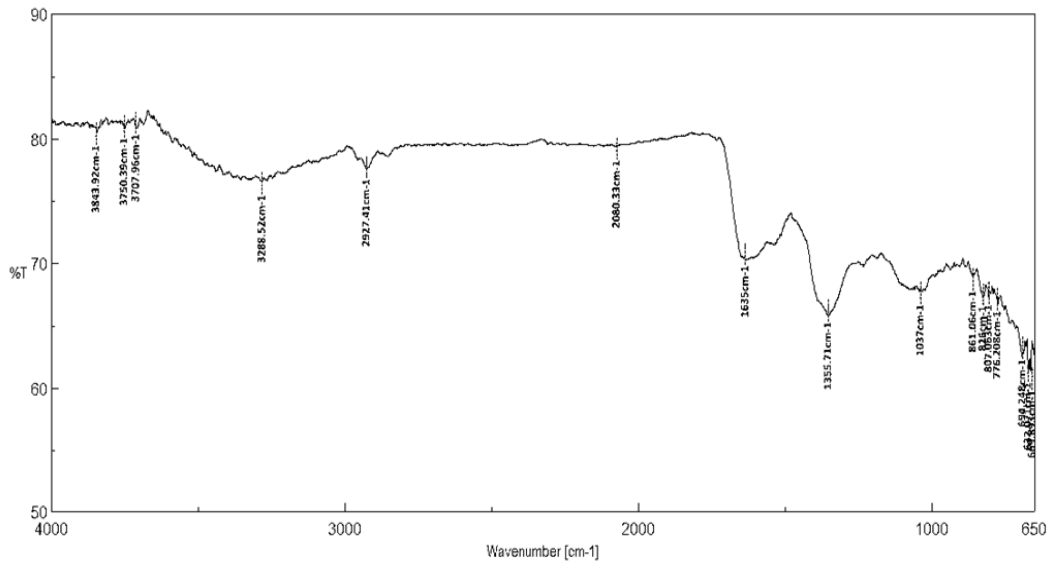
Figure 4.68 FTIR spectra of AgNPs synthesized using bacterial culture supernatant of 6S1
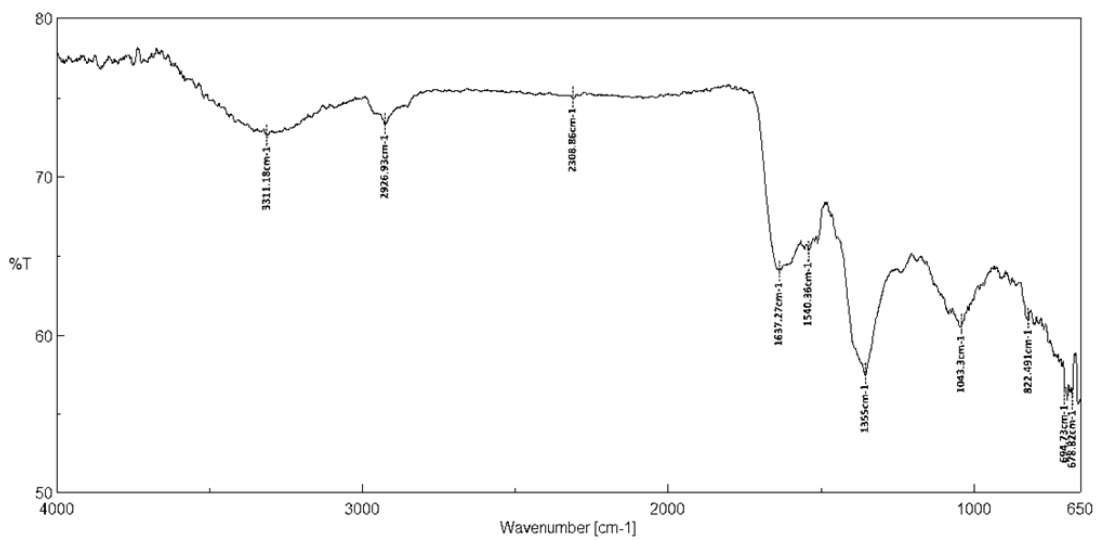
Figure 4.69 FTIR spectra of AgNPs synthesized using bacterial culture supernatant of 8S1

Table 4.24 Functional groups at various wave numbers on the surface of the AgNPs synthesized using the cell free supernatants of bacterial strains 4S1, 4S2, 4S3, 6S1 and 8S1

Bacterial source of AgNPs	Wave number (cm^{-1})	Functional Groups*
4S1	668.214	CH out of plane bending vibrations
	824.902	C=CH$_2$ vibrations
	1047.16	C–N stretching vibrations of the amine
	1349.93	COO- (carboxylate group) asymmetric and symmetric stretching
	1628.59	Carbonyl stretch vibrations in the amide linkages of proteins
	2921.63	weak C-H stretching vibration
	3311.66	O-H Stretching
4S2	664.232	CH out of plane bending vibrations
	681.713	
	769.94	C–H rock alkanes
	824.902	C=CH$_2$ vibrations
	886.131	
	920.361	stretching vibrations of C-O-CH3 and -OH bending of carboxylic acids
	1051.5	C–N stretching vibrations of the amine
	1097.3	
	1349.44	COO- (carboxylate group) asymmetric and symmetric stretching
	1630.52	Carbonyl stretch vibrations in the amide linkages of proteins
	2136.26	-OH stretching involved in P-OH
	2921.15	weak C-H stretching vibration
	2953.93	
	3309.25	O-H Stretching
	3754.73	
	3850.67	

Table 4.24 Continued...

AgNPs synthesized	Wave number (cm^{-1})	Functional Groups*
4S3	977.733	stretching vibrations of C-O-CH3 and -OH bending of carboxylic acids
	1040.41	C–N stretching vibrations of the amine
	1335.95	in-plane bending vibration of hydroxyl groups
	1538.92	-OH stretching involved in P-OH
	1606.41	Carbonyl stretch vibrations in the amide linkages of proteins
	2083.23	
	2926.45	weak C-H stretching vibration
	3248.5	O-H Stretching
	3709.89	
	3865.13	
6S1	694.248	CH out of plane bending vibrations
	776.208	C–H rock alkanes
	807.063	C=CH$_2$ vibrations
	826.83	
	861.06	
	1037.03	C–N stretching vibrations of the amine
	1355.71	in-plane bending vibration of hydroxyl groups
	1635.82	Carbonyl stretch vibrations in the amide linkages of proteins
	2080.33	–C≡C– stretch
	2927.41	weak C-H stretching vibration
	3288.52	O-H Stretching
	3707.96	
	3750.39	
	3843.92	
8S1	678.82	CH out of plane bending vibrations
	694.73	
	822.491	C=CH$_2$ vibrations
	1043.3	C–N stretching vibrations of the amine
	1355.23	COO- (carboxylate group) asymmetric and symmetric stretching
	1540.36	
	1637.27	Carbonyl stretch vibrations in the amide linkages of proteins
	2308.86	-OH stretching involved in P-OH
	2926.93	weak C-H stretching vibration
	3311.18	O-H Stretching

* Silverstein et al., 2014.

FTIR analysis of the AgNPs synthesized from the cell free culture supernatant of bacterial isolates 4S1, 4S2, 4S3, 6S1 and 8S1 revealed the presence of several functional groups (Table 4.24) belonging to protein moieties of bacterial origin.

Peaks belonging to the asymmetric stretching of C-H bonds, carbonyl stretch of amide I and N-H stretch vibrations of amide II, C-N stretching of aromatic and aliphatic amines were found to be common in all the synthesized AgNPs (Figure 4.65 to Figure 4.69) thereby validating the presence of proteinaceous capping agents encapsulating them. Similar results have been reported by Vigneshwaran et al. (2007) and Wei et al. (2012). The presence of all these peaks on the synthesized AgNPs strongly suggest that the AgNPs synthesized from the cell free supernatant of bacterial isolates are encapsulated by the proteinaceous moieties of bacterial origin. The hydroxyl group (-OH) of peptides such as Tyrosine, Glutamine and Asparagine have been reported as the most active group that bring about the capping.

4.11.3 XRD analysis of AgNPs synthesized using the cell free supernatant of the bacterial isolates

X-Ray Diffractogram of the AgNPs synthesized using the cell free supernatant of the bacterial isolates 4S1, 4S2, 4S3, 6S1 and 8S1 as shown in Figure 4.70 – Figure 4.74 respectively. The diffractograms revealed the presence of peaks at different Bragg's angle value (2θ values) with Miller indices (hkl) as shown in Figure 4.70–Figure 4.74 and enlisted in Table 4.25. The average crystallite sizes of AgNPs synthesized were determined using De-bye Shrerrer's formula presented as Eq. (3.1) in Section 3.6.2 of Chapter 3 and is also presented in Table 4.25.
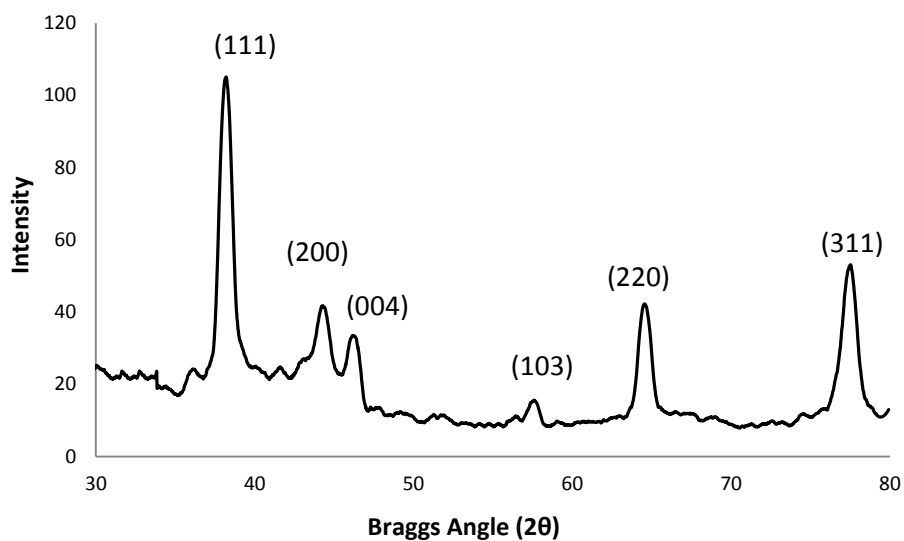
Figure 4.70 X-Ray Diffractogram of AgNPs synthesized using the 24 h cell free bacterial supernatant of isolate 4S1 in equal volume ratio with initial alkaline pH of 11 under ambient conditions of synthesis
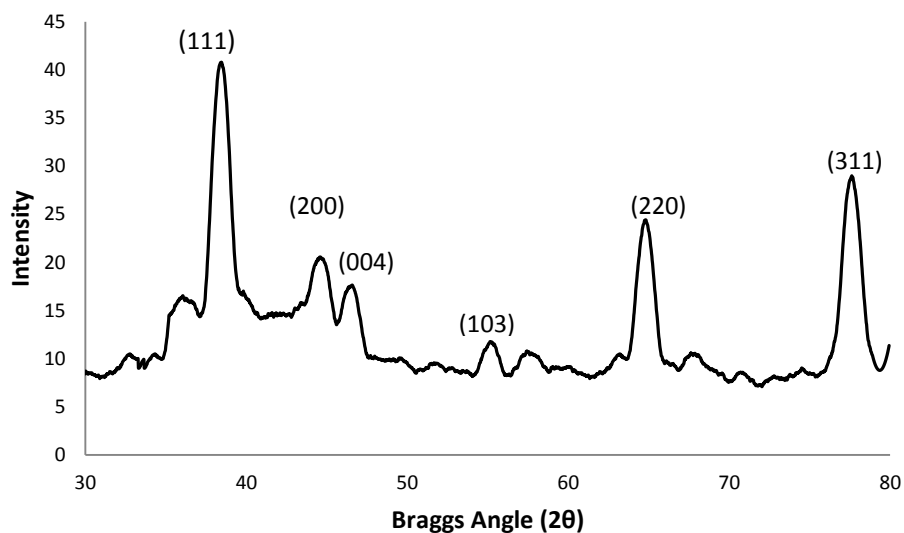
Figure 4.71 X-Ray Diffractogram of AgNPs synthesized using the 24 h cell free bacterial supernatant of isolate 4S2 in equal volume ratio with initial alkaline pH of 11 under ambient conditions of synthesis

222
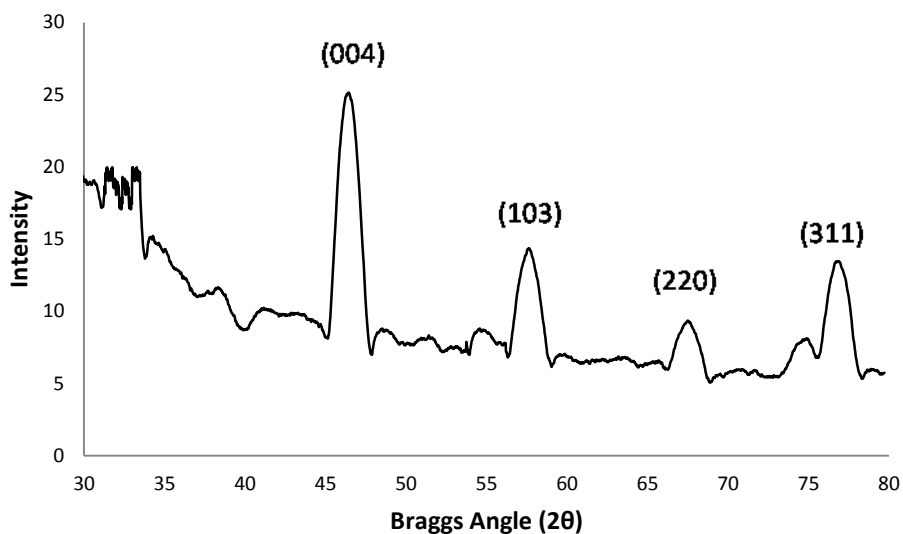
Figure 4.72 X-Ray Diffractogram of AgNPs synthesized using the 24 h cell free bacterial supernatant of isolate 4S3 in equal volume ratio with initial alkaline pH of 11 under ambient conditions of synthesis
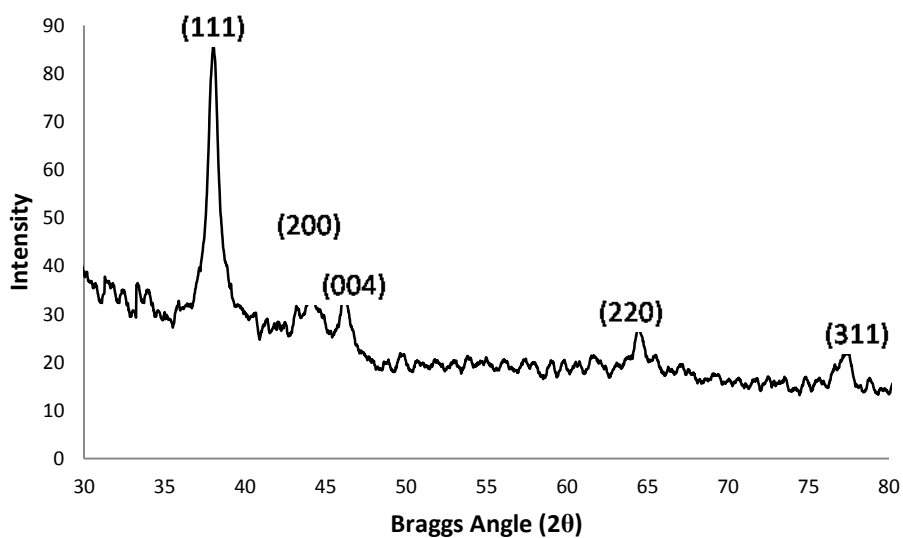
Figure 4.73 X-Ray Diffractogram of AgNPs synthesized using the 24 h cell free bacterial supernatant of isolate 6S1 in equal volume ratio with initial alkaline pH of 11 under ambient conditions of synthesis
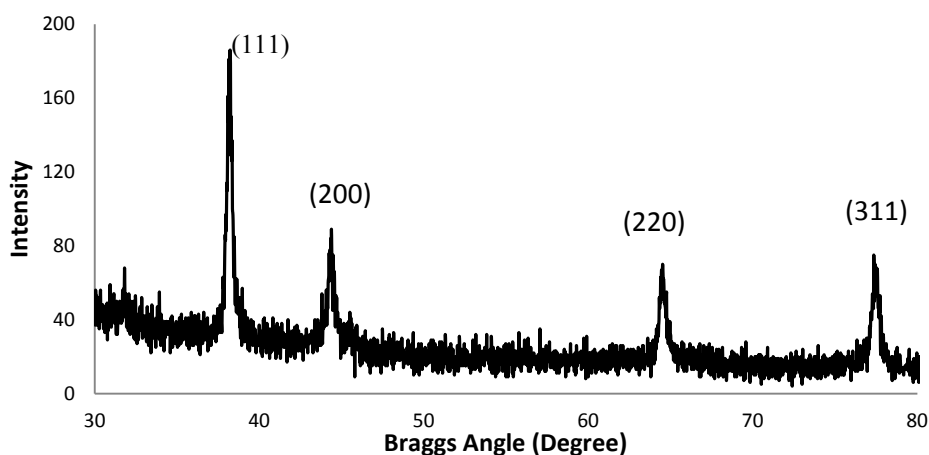
Figure 4.74 X-Ray Diffractogram of AgNPs synthesized using the 24 h cell free bacterial supernatant of isolate 8S1 in equal volume ratio with initial alkaline pH of 11 under ambient conditions of synthesis

Table 4.25 Bragg's angle (2θ) values with (hkl) values and the average crystallite size of AgNPs synthesized using the cell free supernatant of the bacterial strains

Source of AgNPs	Braggs angle (2θ) and Millers indices (hkl) value	Average crystallite size
4S1	38.4(111),44.36(200), 45.31(004),57.36(103), 64.46(220), 77.34(311)	80.9 nm
4S2	38.4(111),44.36(200), 45.31(004),57.36(103), 64.46(220), 77.34(311)	51.26nm
4S3	45.31(004),57.36(103), 64.46(220), 77.34(311)	70.7 nm
6S1	38.4(111),44.36(200), 45.31(004), 64.46(220), 77.34(311)	39.87 nm
8S1	38.4(111), 44.36(200), 64.46(220), 77.34(311)	23.47 nm

The AgNPs synthesized using the cell free supernatant of bacterial isolates 4S1, 4S2, 4S3, 6S1 and 8S1 under optimum conditions were found to be crystalline in structure as observed from the XRD. The XRD of AgNPs synthesized by the cell free supernatant of strain 8S1 exhibited the highest intensity of crystalline peaks and was found to contain only FCC structure, but the AgNPs synthesized using other strains were found to contain a mixture of FCC and hexagonal structure as seen in Table 4.25. The average crystallite size determined through XRD analysis was found to be

the lowest of 23.47 nm for AgNPs synthesized with the strain 8S1 The crystallite sizes of AgNPs synthesized are in the order 4S1 > 4S3> 4S2 > 6S1 > 8S1.

4.11.4 Particle size analysis of AgNPs synthesized using the cell free supernatant of the bacterial strains

The particle size analysis of AgNPs synthesized using the cell free supernatant of the bacterial strains 4S1, 4S2, 4S3, 6S1 and 8S1 was performed using Horiba Zetasizer SZ-100 Particle size analyzer by DLS technique according to the methodology described in section 3.6.5 of Chapter 3. The histograms showing the particle size distribution of the AgNPs synthesized using the cell free supernatant of bacterial strains 4S1, 4S2, 4S3, 6S1 and 8S1 with respective optimum precursor salt solution in 1:1 volume ratio with initial alkaline pH of the synthesis medium at 28±2 ºC are shown in Figure 4.75 to Figure 4.79 respectively. The particle size distribution range obtained from particle size analysis with the average particle sizes are shown in Table 4.26. The particle size is almost similar to that of obtained though XRD indicating the formation of single crystallite particles.
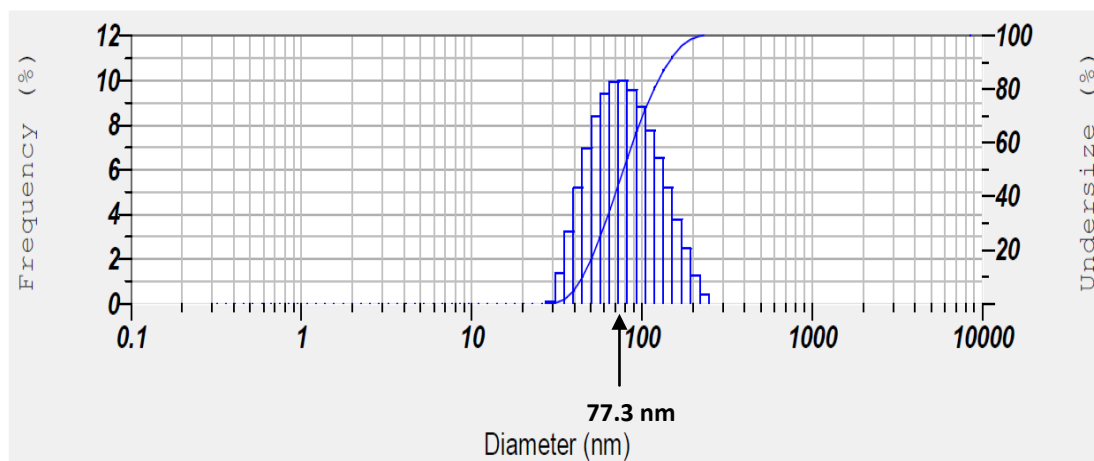
Figure 4.75 Particle size analysis of AgNPs synthesized using the 24 h cell free bacterial supernatant of isolate 4S1 in equal volume ratio with initial alkaline pH of 11 under ambient conditions of synthesis
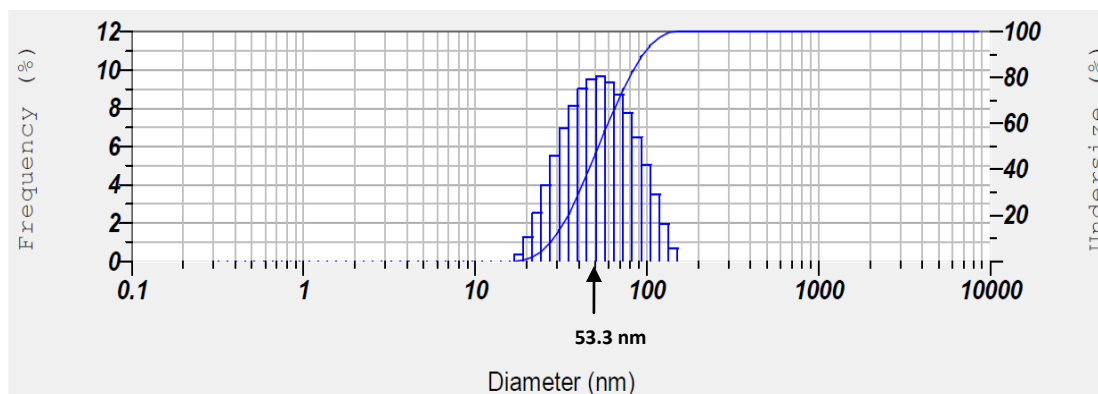
Figure 4.76 Particle size analysis of AgNPs synthesized using the 24 h cell free bacterial supernatant of isolate 4S2 in equal volume ratio with initial alkaline pH of 11 under ambient conditions of synthesis
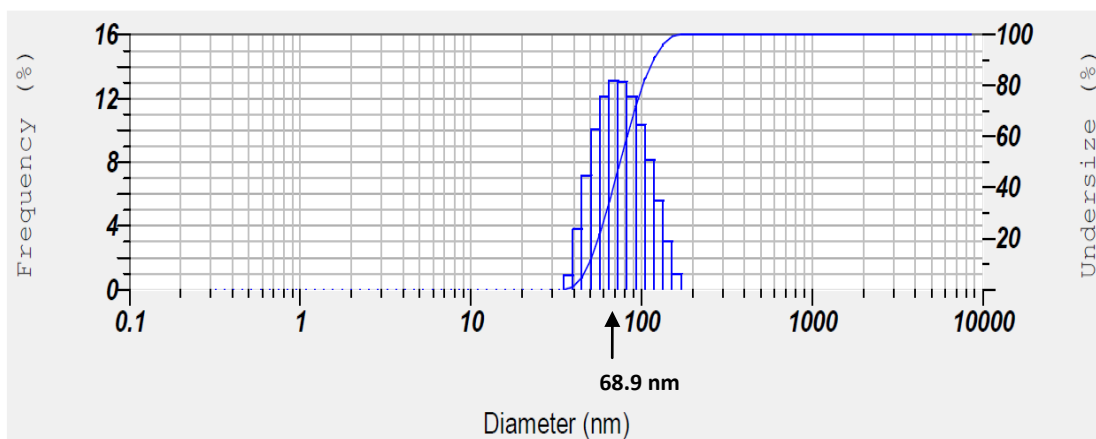
Figure 4.77 Particle size analysis of AgNPs synthesized using the 24 h cell free bacterial supernatant of isolate 4S3 in equal volume ratio with initial alkaline pH of 11 under ambient conditions of synthesis
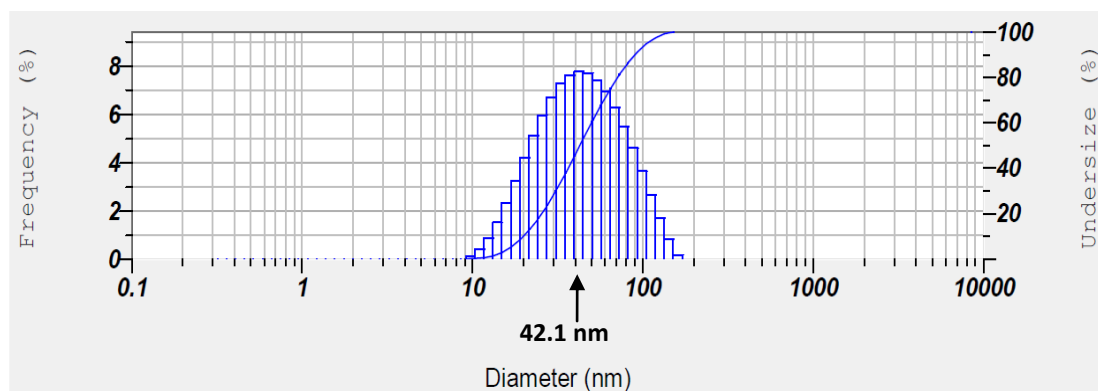
Figure 4.78 Particle size analysis of AgNPs synthesized using the 24 h cell free bacterial supernatant of isolate 6S1 in equal volume ratio with initial alkaline pH of 11 under ambient conditions of synthesis

226
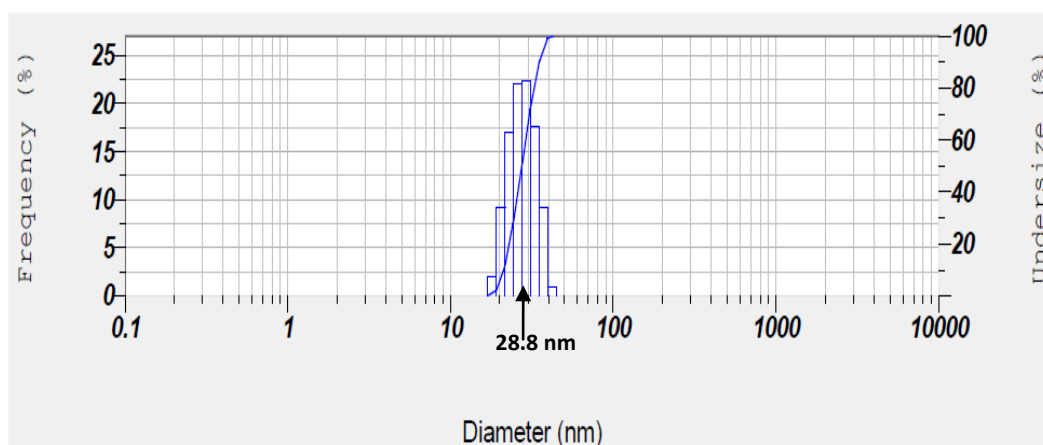
Figure 4.79 Particle size analysis of AgNPs synthesized using the 24 h cell free bacterial supernatant of isolate 8S1 in equal volume ratio with initial alkaline pH of 11 under ambient conditions of synthesis

Table 4.26 Particle size distribution of AgNPs synthesized using the 24 h cell free supernatant under alkaline pH conditions of 11

AgNPs synthesized using cell free culture supernatant of bacterial strain	Average Particle size	Average size range distribution
4S1	77.3 nm	30-250 nm
4S2	53.3 nm	19-150 nm
4S3	68.9 nm	35-190 nm
6S1	42.1 nm	9-190 nm
8S1	28.8 nm	18-46 nm

From the histograms shown in Figure 4.75 to Figure 4.79 and the details in Table 4.26 it is seen that the AgNPs synthesized using the cell free supernatant of strain 8S1 are the smallest in size of 28.8 nm and has a very narrow range of size distribution of 18-46 nm. Table 4.27 shows the comparison between the sizes of the AgNPs synthesized in the present study to the AgNPs synthesized using other microbial sources by other researchers.

From Table 4.27 it is understood that the sizes of AgNPs synthesized using the isolated strains 4S1, 4S2, 4S3, 6S1 and 8S1 in the present study are comparable with the sizes of AgNPs synthesized by other researchers. The size range distribution of AgNPs synthesized was in the order of 8S1 > 4S2 > 4S3 > 6S1 > 4S1. The average particle size of the AgNPs synthesized by the five strains followed the order of 8S1 > 6S1 > 4S2 > 4S3 > 4S1.

Table 4.27 Sizes of AgNPs synthesized using various bacterial strains

Microbe used	Location of the AgNP	Size of AgNPs synthesized (nm)	Reference
Morganella sp.	Extracellular	20-30	Parikh et al. 2008
Pseudomonas stutzeri	Intracellular	~200	Klaus et al. 2009
Klebsiella pneumoniae	Extracellular	5-32	Mokhtari et al. 2009
Aspergillus fumigatus	Extracellular	5-25	Bhainsa and D'Souza, 2006
Phaenerochaete chrysosporium	Extracellular	50–200	Vigneshwaran et al. 2006
Phoma sp. 3.2883	Extracellular	71.06–74.46	Chen et al. 2003
Fusarium accuminatum	Extracellular	5–40	Ingle et al. 2008
Aspergillus niger	Extracellular	20	Gade et al. 2008
Verticillium	Intracellular	25-30	Mukherjee et al. 2001
Staphylococcus aureus	Extracellular	160-180	Nanda and Saravanan, 2009
4S1	Extracellular	77.3 (30-250)	Present Study
4S2	Extracellular	53.3 (19-150)	Present Study
4S3	Extracellular	68.9 (35-190)	Present Study
6S1	Extracellular	42.1 (9-190)	Present Study
8S1	Extracellular	28.8 (18-46)	Present Study

However the narrowest size distribution along with the smallest size range was exhibited by the AgNPs synthesized using the cell free supernatant of strain 8S1 with 100 mM of AgNO$_3$ in equal volume ratio with initial alkaline pH of 11 at 28±2 ºC. The particle size as well as the size range of AgNPs synthesized by the strain 8S1 were found to be closer to the size range of particles synthesized by other researchers as presented in Table 4.27. Thus AgNPs synthesized by the strain 8S1 exhibits better morphological characteristics proving to be a suitable candidate to exhibit unique properties at nanoscale level.

4.11.5 Zeta potential analysis of AgNPs synthesized using the cell free supernatant of bacterial strains 4S1, 4S2, 4S3, 6S1 and 8S1

The FTIR data presented in section 4.11.2 reveals that the AgNPs synthesized using the cell free supernatant of strains 4S1, 4S2 and 4S3 except 6S1 and 8S1 reveal

the presence of carboxylic functional groups on the surface of the nanoparticles which may result in the decrease in the zeta potential value of the AgNPs synthesized using these strains, while presence of amide groups on the surface of AgNPs synthesized by the strains, may lead to increase in zeta potential value (Ostolska and Wiśniewska, 2014) as discussed in section 4.5.1.5. The colloidal suspensions exhibiting zeta potential value more than 25 mV and less than -25 mV are known to be stable (nanoComposix, 2003).

Table 4.28 shows the zeta potential of AgNPs dispersed in HPLC grade deionized water synthesized using the cell free supernatants of bacterial strain 4S1, 4S2, 4S3, 6S1 and 8S1. The AgNPs synthesized using the cell free supernatant of strain 8S1 exhibited a zeta potential value of -30.1 mV indicating good stability in aqueous solutions compared to other strains. However the AgNPs synthesized using the strains 4S1, 4S2, 4S3 and 6S1 exhibited limited stability as the zeta potential value range in between -14.5 and -21.2 mV. From Table 4.28 it can be deduced that the AgNPs synthesized using the cell free supernatant of the bacterial strains isolated in the present study exhibit zeta potential value which is in well agreement with those obtained by other researchers. The stability of AgNPs synthesized by all the five strains was further evaluated using SPR spectra analysis over a period of 6 months at specific time intervals. Figure 4.80 (a) to (e) present the SPR spectral data of AgNPs synthesized by strains 4S1, 4S2, 4S3, 6S1 and 8S1 respectively.

Table 4.28 Zeta potential values of AgNPs synthesized using the isolated bacterial strains 4S1, 4S2, 4S3, 6S1 and 8S1 compared with AgNPs synthesized using other microbial sources

Microbe used	Zeta potential value	Reference
Penicillium strain	-26.3 ± 0.2 mV	Sadowski et al. 2008
T.viridae strain	-27 mV	Fayaz et al. 2010
Pseudomonas aeruginosa	-9.59 mV	Kumar and Mamidyala, 2011
Escherichia hermannii, Citrobacter sedlakii, Pseudomonas putida	-12 mV to -30.4 mV	Saeb et al. 2014
Aspergillus niger	-13.7 mV	Kalaiselvan and Rajasekaran, 2009
4S1	-15.4 mV	Present Study
4S2	-14.5 mV	Present Study
4S3	-17.9 mV	Present Study
6S1	-21.2 mV	Present Study
8S1	-30.1 mV	Present Study

Figures 4.80 (a) to (e) show that there is no noticeable change in the SPR spectra or peak intensities of the AgNPs in the colloid for over the duration of 6 months indicating that the AgNPs remain dispersed over the specified period as a sol in aqueous media without agglomeration. Hence the AgNPs synthesized using the five bacterial strains are stable.

(a)

(b)

(c)

(d)

(e)
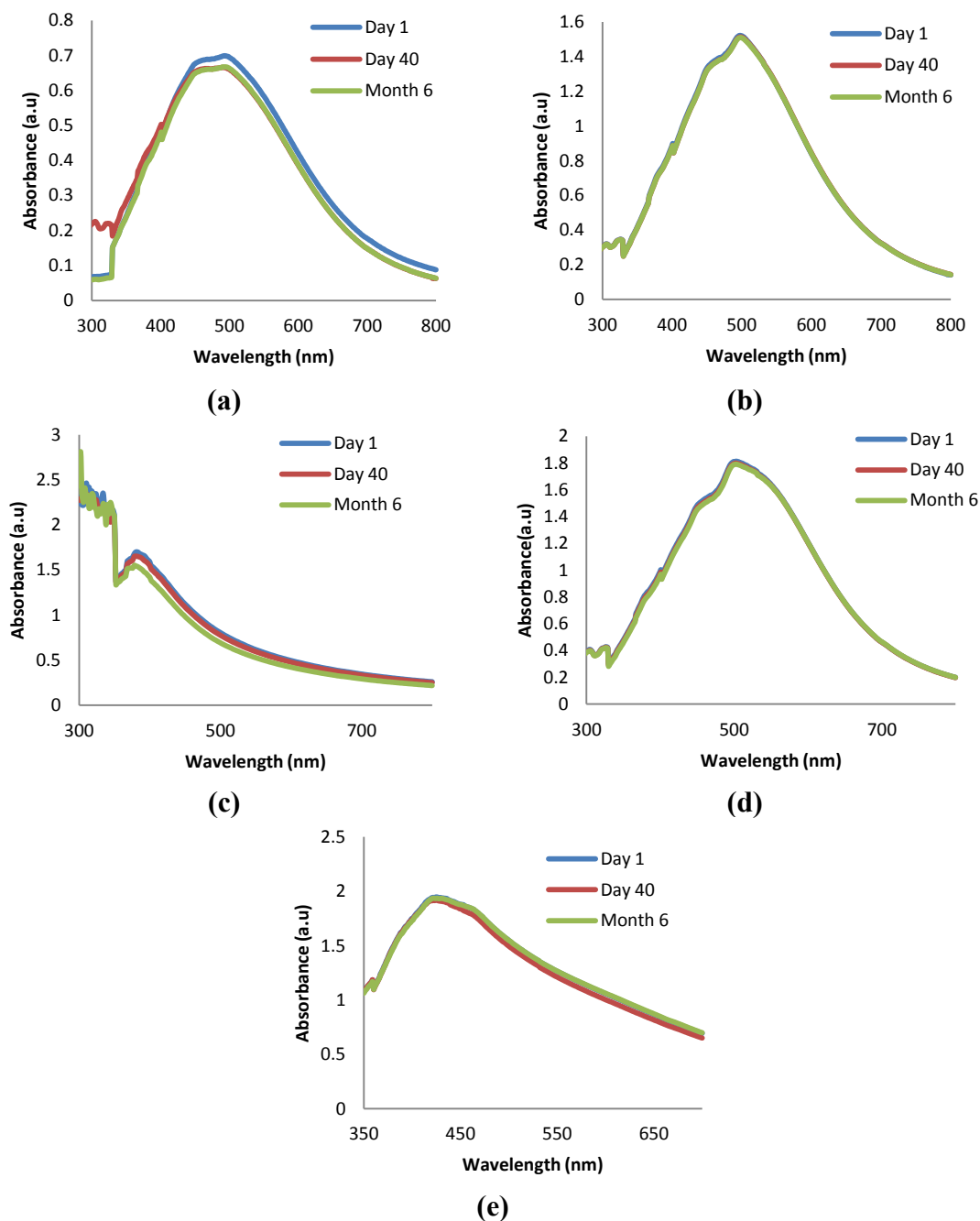
Figure 4.80 SPR spectra of AgNPs at different intervals of time as an indication of their stability using the cell free supernatant of strains (a) 4S1, (b) 4S2, (c) 4S3, (d) 6S1 and (e) 8S1.

4.12 Studies on application of AgNPs synthesized using plant and bacterial sources

4.12.1 Application of AgNPs synthesized using plant and bacterial sources as mercury sensors

AgNPs synthesized by the plant sources; ALE and TLE and with the bacterial culture supernatants of bacterial strains 4S1, 4S2, 4S3, 6S1, 8S1 and the AgNPs synthesized through chemical route were analyzed for their functionality as colorimetric sensors for the detection of mercury. AgNPs are known to exhibit characteristic brown colour when present in colloidal form. A change in the intensity of the brown colour indicates the change in the physicochemical aspect of AgNPs in response to the mercury added to the colloid. This aspect of the functionality of AgNPs shows their potential application in mercury sensors. The AgNPs synthesized using the extract of soap root plant as stabilizer and extract of Manna of hedysarum plant as a reducing agent demonstrated mercury sensing ability as reported by Farhadi et al. (2012).

Colloidal solutions of plant and bacterial based AgNPs were used to detect the presence of Hg^+ ions in aqueous $HgCl_2$ solution. 10 µL samples of $HgCl_2$ solution of concentration 1µg/µL was added to 3 mL of the colloidal suspension containing 0.3 mg of AgNPs. The spectra of the suspension were noted. The addition of 10 µL samples of $HgCl_2$ solution was continued till the colour of the colloidal suspension turned colourless. A representative photograph of the brown colour of the AgNPs colloidal solution before and after addition of Hg^{2+} ions are showed in Figure 4.81(a) and Figure 4.81(b). The spectra of the AgNPs suspension were taken after every addition of $HgCl_2$ solution. UV-Vis Spectra thus obtained with the AgNPs synthesized in the present study are presented in Figure 4.82 (a) to Figure 4.89 (a).

In each case of AgNPs tested with the addition of $HgCl_2$ solution there was a characteristic decrease in the absorption intensity and blue shift of the spectra was observed. Owing to the to the difference in the standard potential of 0.8 V (Ag^+/Ag) and 0.85 V (Hg^{2+}/Hg), the redox reaction between Ag^0 and Hg^{2+} can occur (Ravi et al. 2013). Table 4.29 presents the µg of $HgCl_2$ added and corresponding Hg^{2+} ion content in the colloidal suspension that reacted with $AgNO_3$ and the corresponding absorbance at the wavelength of maximum absorbance.

(a)   (b)

Figure 4.81 Representative photograph showing the change in colour of the AgNPs colloidal solution (a) Before the addition of HgCl$_2$ solution (b) After addition of HgCl$_2$ solution

The plots of absorbance vs. Hg^{2+} content in the colloidal suspension of different AgNPs were plotted and are shown in Figure 4.82 (b) to Figure 4.88 (b). The AgNPs exhibit a characteristic SPR peak indicating the number and morphological aspect of the particle. On addition of Hg^{2+} ions to the AgNPs colloidal solution a blue shift and decrease in the intensity of the SPR peak occurs (Figure 4.82(a) to Figure 4.88(a)). Hence the wavelength at which the blue shift occurred on the subsequent addition of Hg^{2+} ions was used to determine the absorbance. The plots in Figure 4.82(b) to Figure 4.88(b) are linear with the negative slope indicating a decrease in absorbance with increase in Hg^{2+} content. It is mandatory that a sensing element should provide linearity between its input variable and the output variable for any inference or measurement application. Figure 4.82 (b) to Figure 4.88 (b) shows linearity between the Hg^{2+} ion level (input variable) and the absorbance (output variable), thus implying the suitability of AgNP based sensing method for Hg^{2+} detection and concentration measurement. However, increasing the concentration of AgNPs in colloidal suspension may tend to increase the range of measurement of Hg^{2+} level. The maximum and minimum detectable Hg^{2+} ions by AgNPs synthesized using different plant and bacterial sources are presented in Table 4.30. The maximum detectable level was determined by the addition of Hg^{2+} ions to the colloidal solution till the solution turned colourless and no SPR peak was observed, while the minimum detectable level was determined by the maximum amount of Hg^{2+} ions added to the AgNPs colloidal solution that resulted in decrease in the intensity of SPR peak with a

prominent blue shift, the detailed methodology is described in section 3.7.1.4 of Chapter 3.

Table 4.29 Amount of HgCl$_2$ added and corresponding Hg^{2+} ion content in the colloidal suspension of AgNPs and their absorbance at wavelength of maximum absorbance.

AgNPs and Wavelength of Absorbance Maxima	Absorbance at wavelength of maximum absorbance (a.u)	Amount of HgCl$_2$ added to 3 mL of colloidal solution	Corresponding Hg^{2+} ion content in the colloidal suspension (µg)
ALE (382 nm)	1.846	10	4.25
	1.749	20	8.5
	1.701	30	12.75
	1.652	40	17
	1.592	50	21.25
	1.541	60	25.5
	1.439	70	29.75
	1.362	80	34
	1.254	90	38.25
	1.846	100	42.5
TLE (420 nm)	2.154	10	4.25
	2.1	20	8.5
	2.062	30	12.75
	1.981	40	17
	1.822	50	21.25
	1.691	60	25.5
4S1 (398 nm)	1.502	10	4.25
	1.439	20	8.5
	1.37	30	12.75
	1.3	40	17
	1.259	50	21.25
	1.183	60	25.5
4S2 (414 nm)	1.906	10	4.25
	1.883	20	8.5
	1.86	30	12.75
	1.844	40	17
	1.801	50	21.25
	1.73	60	25.5
	1.682	70	29.75
	1.647	80	34
	1.6	90	38.25
	1.547	100	42.5
	1.514	110	46.75
	1.469	120	51

Table 4.29 Continued...

AgNPs and Wavelength of Absorbance Maxima	Absorbance at wavelength of maximum absorbance (a.u)	Amount of HgCl₂ added to 3 mL of colloidal solution	Corresponding Hg²⁺ ion content in the colloidal suspension (µg)
4S3 (418 nm)	1.992	10	4.25
	1.884	20	8.5
	1.842	30	12.75
	1.802	40	17
	1.765	50	21.25
	1.746	60	25.5
	1.703	70	29.75
	1.635	80	34
	1.568	90	38.25
	1.504	100	42.5
	1.449	110	46.75
	1.381	120	51
	1.325	130	55.25
	1.232	140	59.5
	1.123	150	63.75
6S1(420 nm)	1.877	10	4.25
	1.842	20	8.5
	1.8	30	12.75
	1.725	40	17
	1.643	50	21.25
	1.588	60	25.5
	1.515	70	29.75
	1.427	80	34
	1.351	90	38.25
	1.24	100	42.5
	1.162	110	46.75
	1.063	120	51
	1.021	130	55.25
8S1 (414 nm)	1.529	10	4.25
	1.494	20	8.5
	1.405	30	12.75
	1.319	40	17
	1.204	50	21.25

(a)

y = -0.0163x + 1.9177
R² = 0.9839
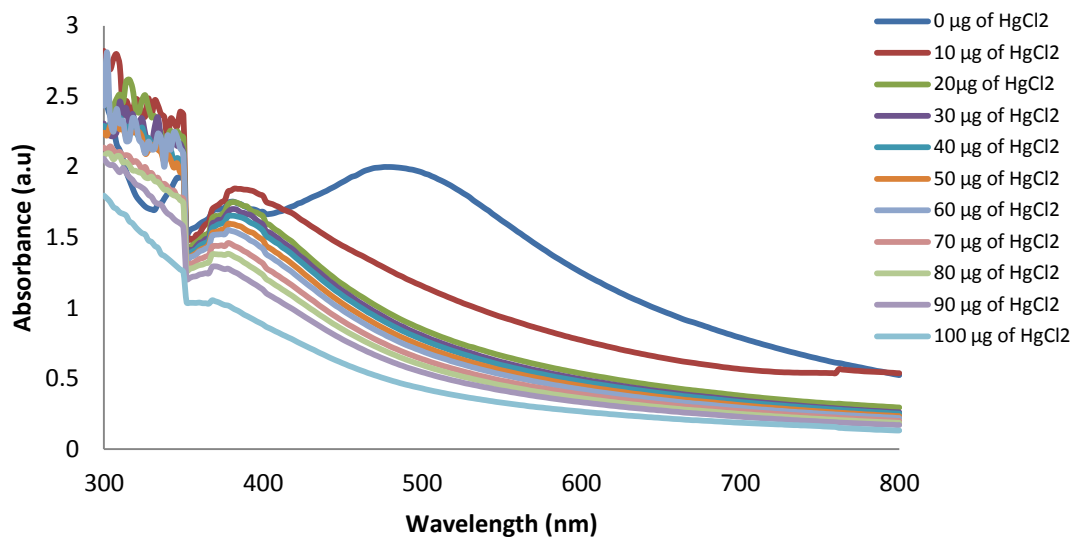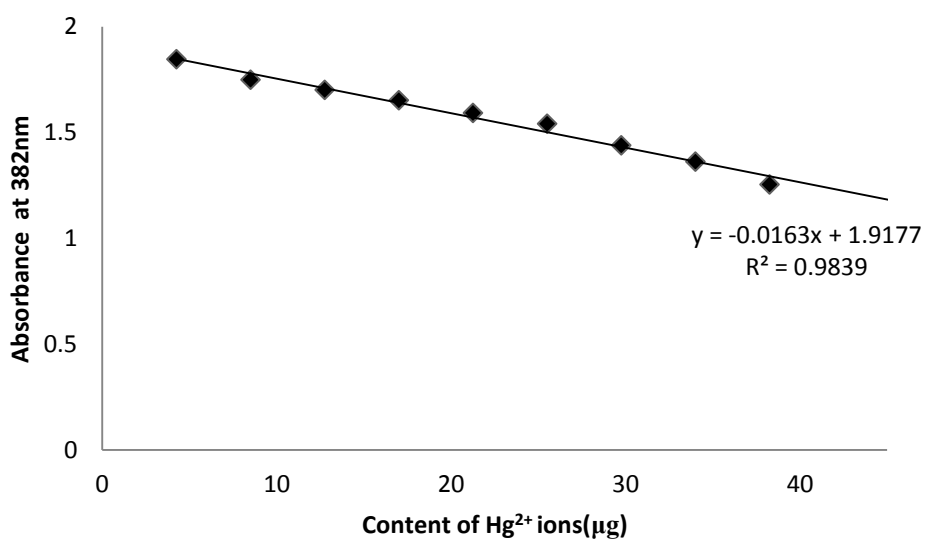
(b)

Figure 4.82 (a) SPR peaks obtained after addition of mercury to the colloidal suspension of AgNPs synthesized using ALE (b) Absorbance at 382 nm with different amount of mercury added to the colloidal suspension of AgNPs synthesized using ALE

(a)

$$y = -0.0217x + 2.2913$$
$$R^2 = 0.937$$
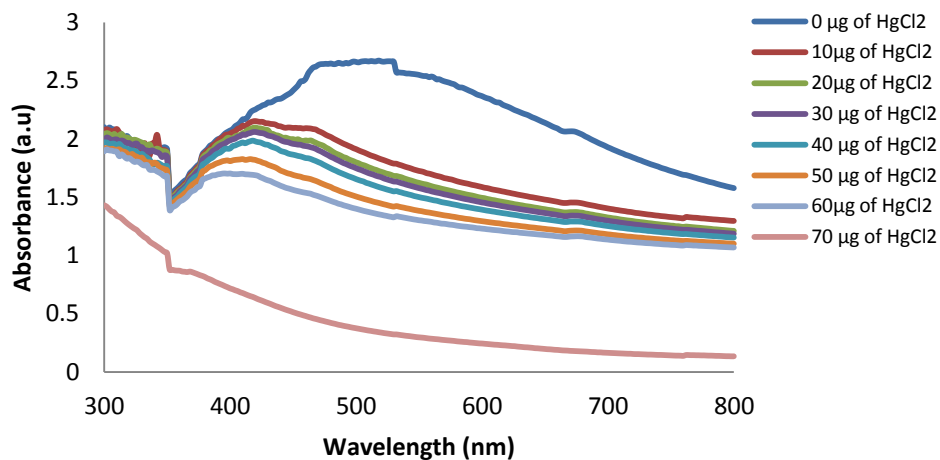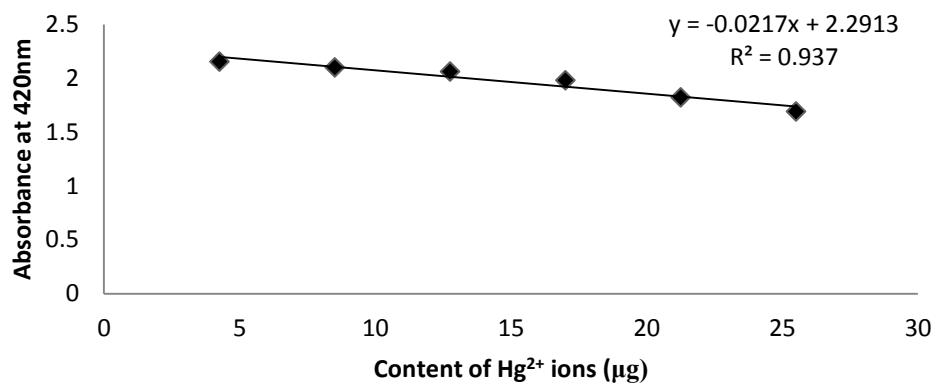
(b)

Figure 4.83 (a) SPR peaks obtained after addition of mercury to the colloidal suspension of AgNPs synthesized using TLE (b) Absorbance at 420 nm with different amount of mercury added to the colloidal suspension of AgNPs synthesized using TLE

236

(a)

y = -0.0148x + 1.5627
R² = 0.9961
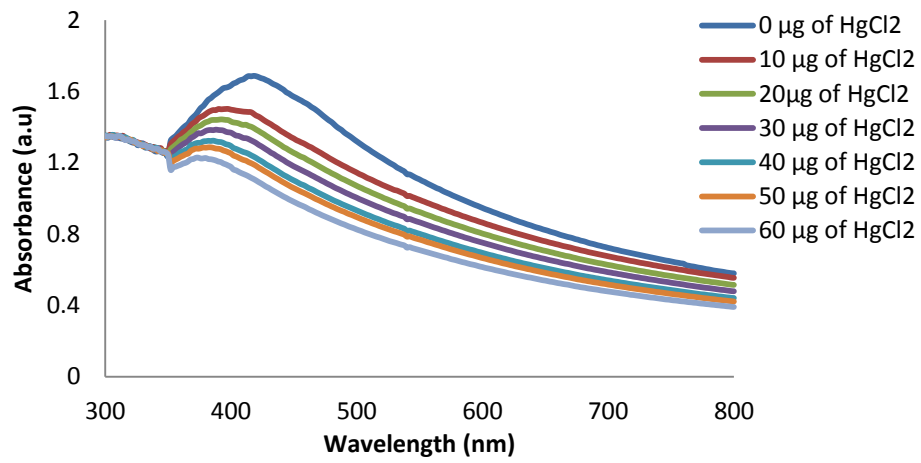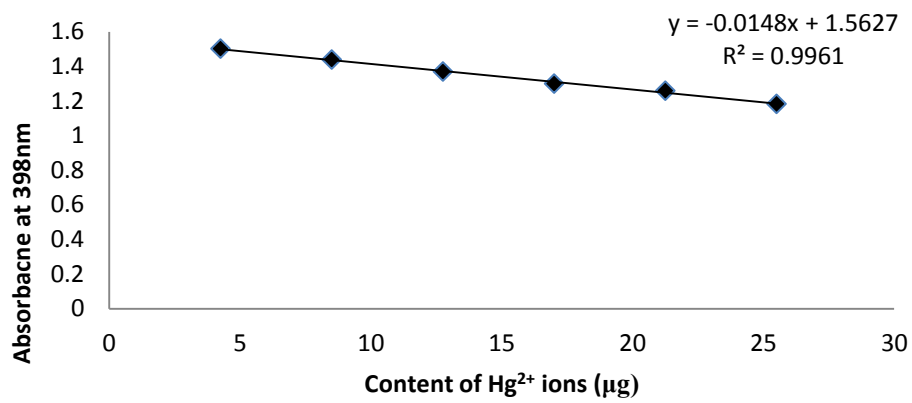
(b)

Figure 4.84 (a) SPR peaks obtained after addition of mercury to the colloidal suspension of AgNPs synthesized using 4S1 (b) Absorbance at 398 nm with different amount of mercury added to the colloidal suspension of AgNPs synthesized using 4S1

(a)

$$y = -0.0099x + 1.9808$$
$$R^2 = 0.9865$$
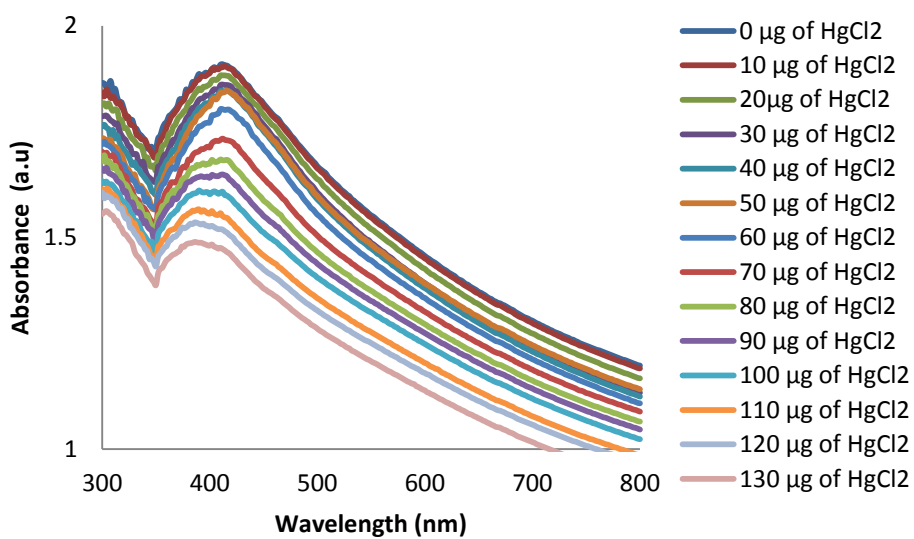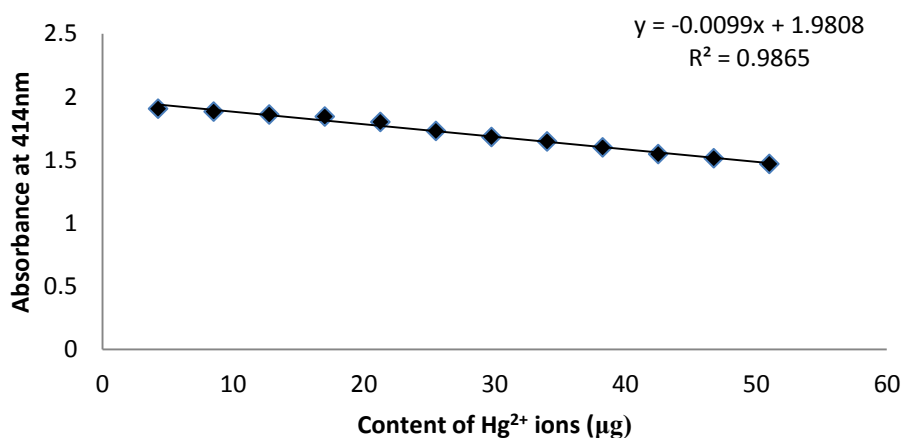
(b)

Figure 4.85 (a) SPR peaks obtained after addition of mercury to the colloidal suspension of AgNPs synthesized using 4S2 (b) Absorbance at 414 nm with different amount of mercury added to the colloidal suspension of AgNPs synthesized using 4S2

(a)

$$y = -0.0133x + 2.049$$
$$R^2 = 0.9798$$
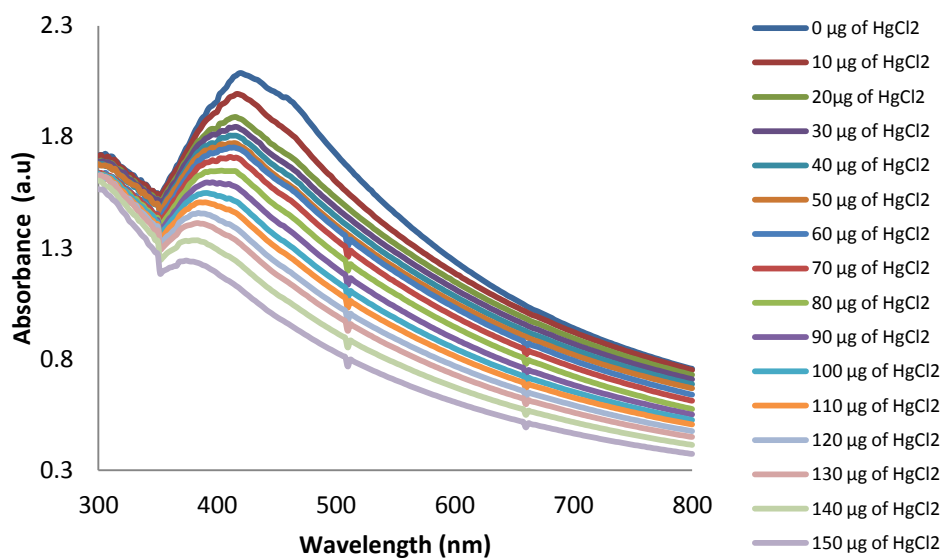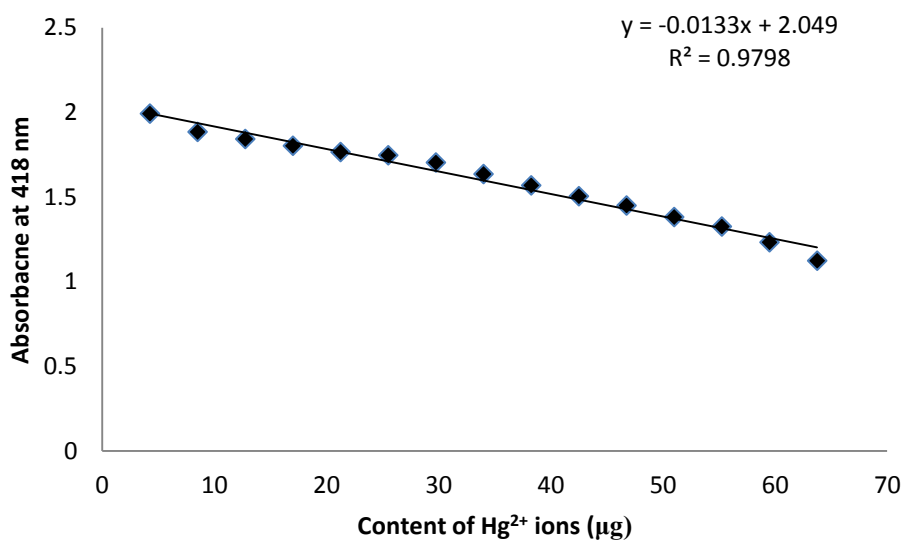
(b)

Figure 4.86 (a) SPR peaks obtained after addition of mercury to the colloidal suspension of AgNPs synthesized using 4S3 (b) Absorbance at 418 nm with different amount of mercury added to the colloidal suspension of AgNPs synthesized using 4S3

(a)

$y = -0.0178x + 2.0112$
$R^2 = 0.991$
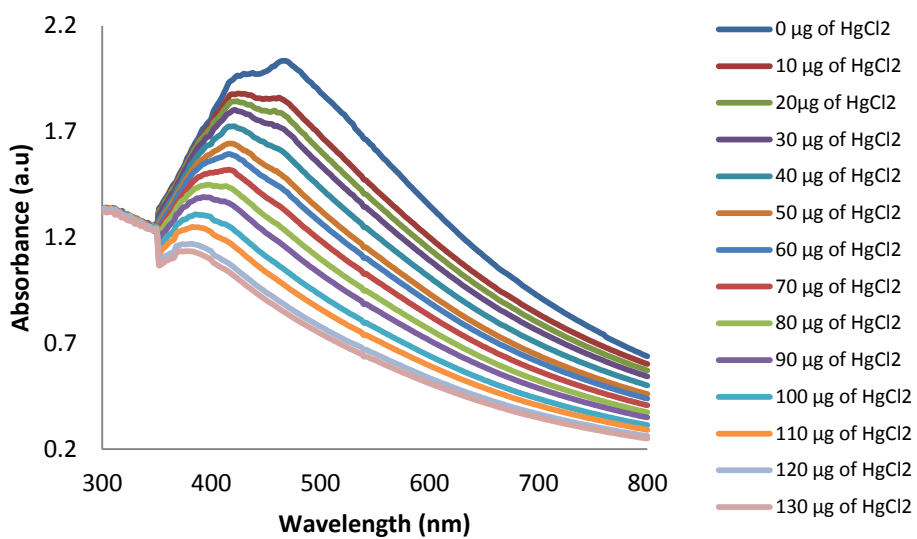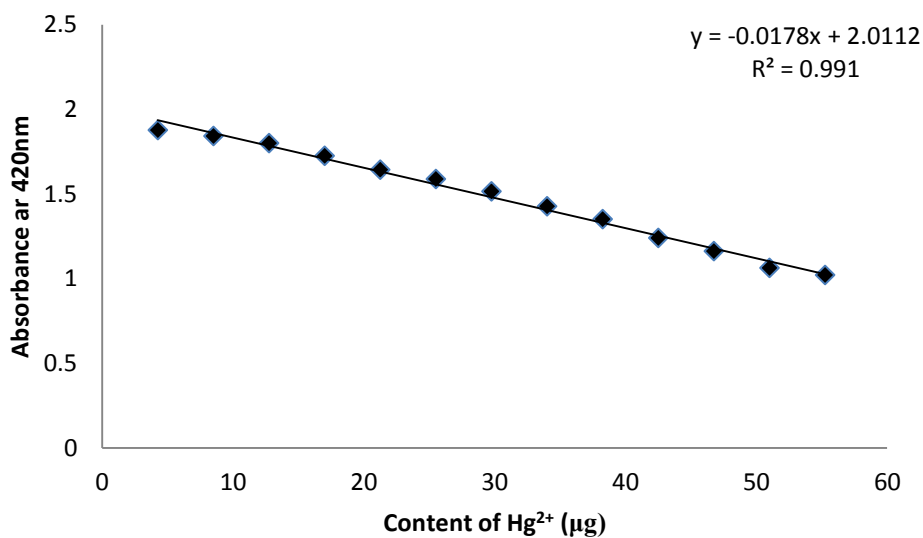
(b)

Figure 4.87 (a) SPR peaks obtained after addition of mercury to the colloidal suspension of AgNPs synthesized using 6S1 (b) Absorbance at 420 nm with different amount of mercury added to the colloidal suspension of AgNPs synthesized using 6S1

(a)

$$y = -0.0194x + 1.6377$$
$$R^2 = 0.9723$$
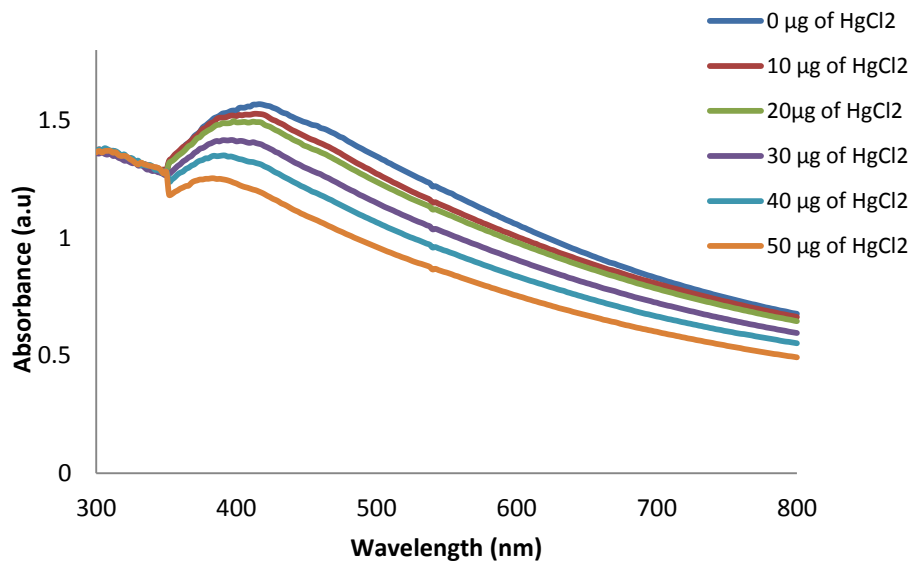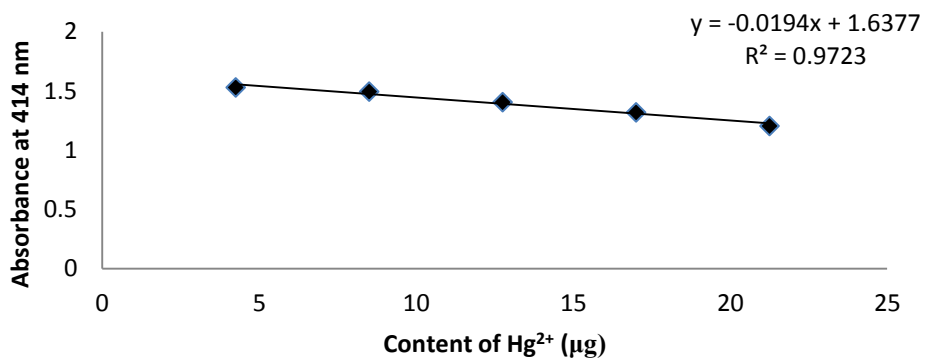
(b)

Figure 4.88 (a) SPR peaks obtained after addition of mercury to the colloidal suspension of AgNPs synthesized using 8S1 (b) Absorbance at 414 nm with different amount of mercury added to the colloidal suspension of AgNPs synthesized using 8S1
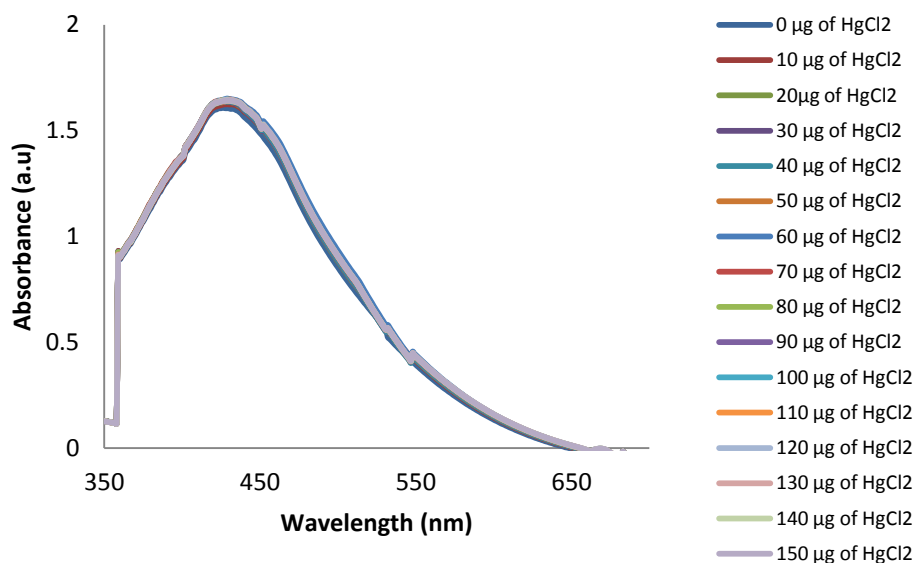
Figure 4.89 SPR Spectra of chemically synthesized AgNPs obtained after addition of mercury

Table 4.30: Maximum and Minimum content of Hg^{2+} ions detected by AgNPs synthesized through different sources

Routes		Source	Maximum content of Hg^{2+} ions detected (µg)	Minimum content of Hg^{2+} ions detected (µg)
Bio based	**Plant resources**	**ALE**	38.25	2.55
		TLE	25.5	2.125
	Bacterial Resources	**4S1**	25.5	2.975
		4S2	51.0	3.825
		4S3	63.75	4.25
		6S1	55.25	3.4
		8S1	21.25	1.275
Chemical	**Trisodium Citrate**	**Trisodium Citrate**	ND	ND

FTIR analysis presented in section 4.5.1.8, 4.5.2.8 and 4.11.2 showed that AgNPs synthesized using ALE and TLE are capped with bioactive phytocomponents, while AgNPs synthesized using bacterial sources are known to posses certain moieties of bacterial origin that act as capping and stabilizing agent. Thus, the surface of AgNPs is covered by these organic moieties. Such groups promote electrostatic–ionic attractions between the nanoparticle surface and mercury ion (Katok et al. 2012; Pradeep, 2009). The Hg^{2+} may interact with the AgNPs leading to redox reactions. A change in polarization of the surface of AgNPs by the Hg^{2+} ions may occur leading to

shift in plasmon resonance. Ag^0 is oxidized to Ag^+ by the Hg^{2+} on their surface and Hg^{2+} is reduced to Hg^0 leading to the formation of an amalgam, and thus leading to a blue shift on addition of Hg^{2+}. Both ALE and TLE based AgNPs showed minimum detection limit of 2.55 μg and 2.125 μg (Hg^{2+}) with the maximum detection level of 38.25 μg and 25.5 μg respectively.

The bacterial AgNPs synthesized using the bacterial strains exhibited maximum detection level of Hg^{2+} content in the order of 4S3>6S1>4S2>4S1>8S1 and minimum detection level of Hg^{2+} content in the order of 8S1>4S1>6S1>4S2>4S3. The lowest minimum detection level of Hg^{2+} content is exhibited by the AgNPs synthesized using 8S1 strain followed by AgNPs synthesized using TLE and ALE. However, the efficacy of these AgNPs in applicability as potential sensors for mercury is proved.

The AgNPs synthesized chemically by using trisodium citrate as the reducing and capping agent was also tested for its mercury sensor application according to the methodology described in Appendix VII. As shown in Figure 4.89, no shift in the SPR peak was observed on addition of Hg^{2+} and the spectra remained unaltered even after addition of upto 72.25 μg of Hg^{2+}, indicating that no interaction between Hg^{2+} ions and AgNPs occurred. The capping agents play an important role in promoting the interaction between Hg^{2+} and AgNPs. However, the charges present on citrate capped AgNPs may not attract Hg^{2+} ions onto the surface of AgNPs, thus preventing interaction between Hg^{2+} and AgNPs. The capping agent on the AgNPs synthesized using ALE and TLE are the natural organic moieties belonging to the class of phenolics and flavonoids that have been to exhibit preferential affinity towards the heavy metal ions depending on the organic moiety. Karthiga and Anthony (2013) have reported that gallic acid and catechin present in the extract of neem bark have affinity towards Hg^{2+} and thus AgNPs synthesized using neem bark extract showed their specific sensitivity to Hg^{2+} thus proving their potential applicability as selective Hg^{2+} sensor. Similarly, the AgNPs synthesized using the isolated bacterial strains also contain organic moieties as the surface capping and interact with Hg^{2+}.

For AgNPs synthesized through chemical route, even the addition of upto 72.25 μg of Hg^{2+}, did not result in any change in the SPR spectra of the AgNPs colloidal solution and this can be explained by the presence of surface charges on the

citrate capped AgNPs that may not enable the binding of the Hg^{2+} onto the surface of AgNPs and also might require a higher content of Hg^{2+} for detection. A further insight into the mechanism of AgNPs synthesized using biobased routes acting as mercury sensors can be gained by Figure 4.90.
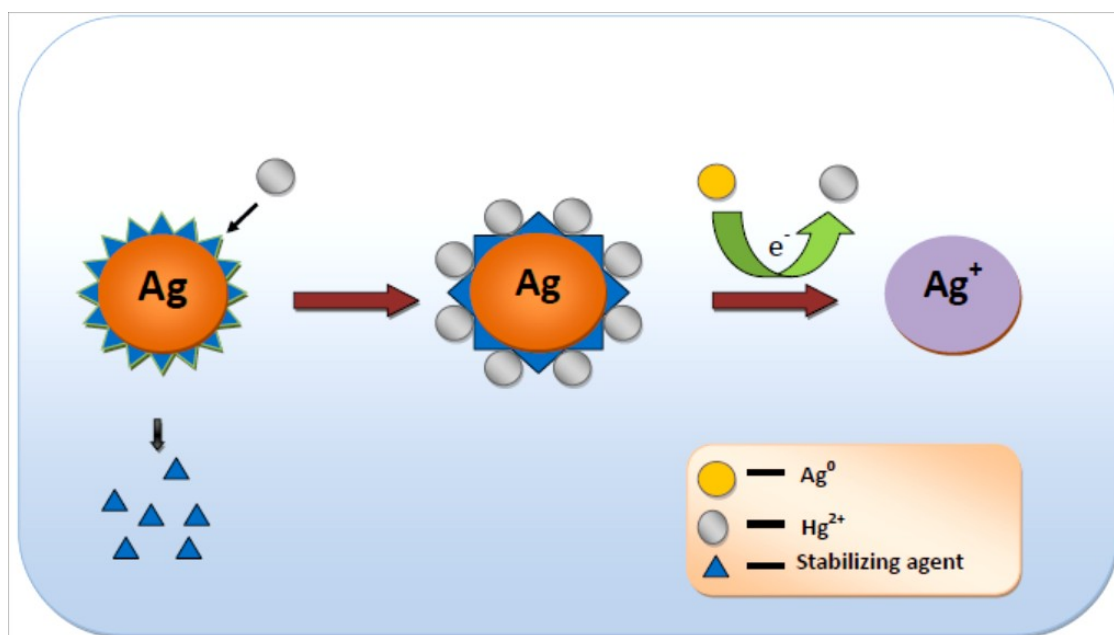
Figure 4.90 Mechanism of AgNPs synthesized using plant and bacterial sources acting as sensors for mercury

Mercury (II) ion with a closed-shell d^{10} configuration has no optical spectroscopic signature hence remain as colourless in solutions (Farhadi et al. 2012) while AgNPs exhibit characteristic brown colour. After addition of 10 µg of Hg^{2+} to AgNPs, the color of solution decreases accompanied by the blue shifting of the SPR band, and finally turns to colourless after the addition of the maximum content of Hg^{2+}. When mercury salt is added to the colloidal AgNP suspension, the presence of organic capping agents on the surface of AgNPs promotes electrostatic–ionic attractions between the nanoparticle surface and mercury ions (Katok et al. 2012; Pradeep, 2009). The mercury added is said to remove the stabilizing agents present on the surface of the AgNPs and reacting with the Ag core by a Redox reaction (Farhadi et al., 2012), thus converting Ag^0 to Ag^+ ions. Hg^{2+} gets reduced to Hg^0 on the surface of AgNPs, while oxidizing Ag^0 to Ag^+ ions. The size of AgNPs reduces as AgNPs react with Hg^+ to form Ag^+. Hg^0 forms tiny Hg-Ag colloidal amalgams with AgNPs,

thus changing the colour of the colloidal solution. When all the AgNPs are converted to Ag^+ ions by Hg^{2+}, the colloidal solution becomes colourless, indicating that the available Ag^0 in the colloidal suspension is just sufficient for the detection of the added quantity of mercury. It limits the maximum detectable mercury level for the given quantity of AgNPs.

In the present study, the AgNPs synthesized using ALE and TLE and the bacterial isolates 4S1, 4S2, 4S3, 6S1 and 8S1 were also tested for their applicability as sensors for different heavy metals such as Cr^{6+}, Ni, Cd^{2+}, Al^{3+} and Fe^{3+} using the similar methodology adopted for Hg sensor application. But no visual change in the color and other characteristics of AgNP colloidal suspension was observed on addition of the heavy metal salt solutions. Thus, the AgNPs synthesized using plant and bacterial sources reported in this study can be used as selective sensors for detection and measurement of Hg^{2+} in aqueous systems.

There are several reports on the use of AgNPs synthesized by different approaches for mercury sensor applications. However, in these studies the AgNPs were functionalized by the addition of chromophores or fluorophores (Zhu et al. 2006; Ros-Lis et al. 2005; Yang et al. 2005; Coronado et al. 2005; Guo et al. 2004) organic compounds (Chiang et al. 2008; Yoon et al. 2005), polymers (Liu et al. 2007) and oligonucleotides (Zhu et al. 2009), DNA (Liu and Lu. 2007) and proteins (Wegner et al. 2007) to facilitate the interaction between Hg^{2+} and AgNPs. AgNPs functionalized with rhodamine dye for Optical-electrochemical chemosensor for Hg^{2+} (Yang et al. 2007) have also been reported. But in the present study, the AgNPs were used as synthesized with no modification of the surface. The functionalization of the AgNP surface occurs during the synthesis process itself by the plant bioactive components, leading to an eco friendly approach for selective mercury sensing. The AgNPs synthesized using 8S1 showed minimum detectable level of 1.275 μg of Hg^{2+} followed by those synthesized by TLE and 4S1. The AgNPs synthesized in the present study showed very low Hg^{2+} minimum detection limit proving their potential for low level Hg^{2+} detection with high sensitivity.

These encouraging results could be used to develop a method for detection of unknown concentrations of mercury in contaminated water. A calibration plot can be plotted by using the absorbance value obtained at the wavelength of maximum

absorbance on addition of known concentrations of Hg^{2+} ions to the aqueous colloidal solution of AgNPs. This calibration plot can be further used to determine the concentration of the unknown sample of Hg^{2+} ions by using the absorbance value at the wavelength of maximum absorbance.

AgNPs as colorimetric sensors have a distinct advantage due to their simplicity, rapidity, sensitivity and ease of measurement in acting as transducer in converting the measured variable to optical signal form, thus exhibiting its potential as a sensor for real-time qualitative or quantitative analysis of mercury. The method demonstrated is very simple and easy to implement enabling the detection of mercury content in environmental systems such as in contaminated soil or water, in food samples or in aquatic organisms.

4.12.2 Antibacterial activity of plant and bacterial based AgNPs

Silver has been known for its antimicrobial properties. Though bulk silver is also antimicrobial in nature, nanosilver due to its size range provides high surface to volume ratio thereby providing an enhanced effect of antimicrobial activity. Silver at the nanoscale has established itself in the modern day, finding its way into medical applications such as topical gels, dental fillings and drug delivery systems. AgNPs have been adopted in coating of fabrics as they furnish antibacterial property and also aid in reducing odour (Klueh et al. 2000). As discussed in Section 2.3 of Chapter 2, AgNPs synthesized by various routes exhibit remarkable antimicrobial activity against various pathogenic strains of microbes such as *E.coli, K.pneumoniae, S.aureus* and have found profound applications due to these properties (Lohani et al. 2014; Osorio et al. 2012; Sharma et al. 2009; Moxham, 2008). Owing to their antibacterial property, AgNPs attract an increasing amount of scientific and industrial interest from fields such as textile science (Lee and Jeong, 2005) cosmetics (Kokura et al. 2010), medicine and water treatment (Jain and Pradeep, 2005). Thus, in the present study, the antibacterial activity of the AgNPs synthesized using ALE, TLE and different isolated bacterial strains were tested in terms ZOI and MIC against two water borne pathogens *E.coli* and *S.aureus,* to demonstrate their potential application as antibacterial agent in various fields.

Table 4.31 and Table 4.32 provide the details of antibacterial activity demonstrated by microbial based AgNPs against water borne pathogens *E.coli* and *S.aureus* respectively in terms of ZOI as determined through Agar Well diffusion technique. The antibacterial efficacy of AgNPs synthesized using biobased routes in terms of ZOI were compared with the chemically synthesized AgNPs which were prepared using citrate reduction method described in Appendix VII.

Table 4.31 Zone of inhibition formed by AgNPs for their antibacterial efficacy against *S.aureus*

Zone of inhibition observed (mm)		Photographic Image
Chemical AgNPs	**Biobased AgNPs**	
6±1	11±1 (4S1)	
6±1	9±1 (4S2)	
6±1	8±1 (4S3)	
6±1	9±1 (6S1)	
6±1	9±1 (8S1)	

Table 4.31 Continued...
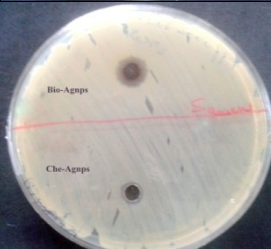
Zone of inhibition observed (mm)		Photographic Image
Chemical AgNPs	**Biobased AgNPs**	
6±2	**7±1 (ALE)**	
6±2	**9±1 (TLE)**	

Table 4.32 Zone of inhibition formed by AgNPs for their antibacterial efficacy against _E.coli_
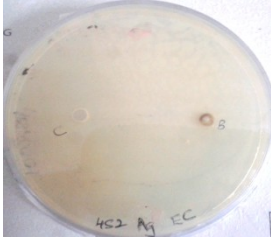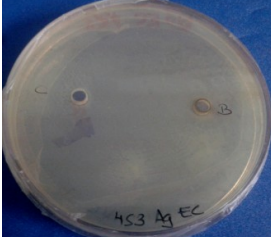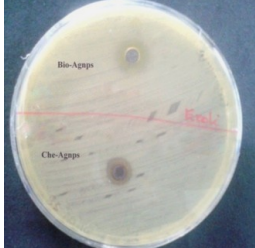
Zone of inhibition observed (mm)		Photographic Image
Chemical AgNPs	**Biobased AgNPs**	
6±1	**10±1 (4S1)**	
6±1	**8±1 (4S2)**	
6±1	**8±1 (4S3)**	

Table 4.32 Continued…

Zone of inhibition observed (mm)		Photographic Image
Chemical AgNPs	Chemical AgNPs	
6±1	8±1	
6±1	9±1	
7±1	10±1	
9±1	8±1	

Through the digital pictures showing ZOI presented in Table 4.31 and Table 4.32 it can be observed that AgNPs synthesized using the plant and bacterial based method exhibit higher ZOI against *E coli and S aureus* in the range of 7-11 mm and 8-10 mm respectively in comparison to those by chemically synthesized AgNPs of 5-6 mm. Thus AgNPs synthesized using the plant and bacterial based method were better antibacterial agents than the chemically synthesized AgNPs.

However, the antibacterial efficacy of the AgNPs was studied using the agar well diffusion technique which is not a precise method to analyze the antibacterial activity due to its semi quantitative nature, lower sensitivity and accuracy of the method of measurement of ZOI. Thus the antibacterial activity may better be represented in terms of MIC as it provides quantitative measurement of the level of

inhibition exhibited by any antibacterial agent against the test organism. MIC is defined as the lowest concentration of an antimicrobial that will inhibit the visible growth of a microorganism after overnight incubation (Andrews, 2001). MICs are used by diagnostic laboratories mainly to confirm resistance, but most often as a research tool to determine the *in vitro* activity of new antimicrobial.

The MIC of AgNPs synthesized using the leaf extracts: ALE, TLE and different bacterial strains 4S1, 4S2, 4S3, 6S1 and 8S1 against the water borne pathogens *E.coli and S.aureus* were determined using broth macrodilution method to quantitatively evaluate their antibacterial efficacy. In macrodilution method for MIC determination, a series of vials containing known concentrations of AgNPs in broth solutions with the test strain was prepared and the MIC was determined by observing the concentration of AgNP at which the growth of the test pathogen was inhibited after the period of incubation. The detailed methodology is presented in Section 3.7.1.2 of Chapter 3.

The MIC values of the AgNPs synthesized by using the leaf extracts and the bacterial strains against *E.coli* and *S.aureus* are presented in Table 4.33 along with their average particle size. The MIC of AgNPs synthesized using the isolated bacterial strain 8S1 (Table 4.33) exhibited the best antibacterial activity as compared to the AgNPs synthesized using other isolated strains (4S1, 4S2, 4S3, 6S1, 8S1) and the plant extracts (ALE or TLE), as indicated by the least value of MIC. However, the MIC of AgNPs synthesized using the isolated bacterial strains 4S2, 4S3 and 6S1 showed lower MIC values as compared to AgNPs synthesized using the isolated bacterial strain 4S1 and ALE, TLE. The antibacterial efficacy of all the synthesized AgNPs was found to be greater against *S aureus* as compared to that for *E Coli.*

In accordance with the zeta potential value of AgNPs synthesized using the bacterial and plant resources as presented in Table 4.28 of section 4.11.5, the AgNPs possessed anionic surface charge indicating their affinity towards cationic surfaces of the test pathogen. Thus the AgNPs exhibit better antibacterial activity towards *S.aureus* strain in comparison to *E.coli,* as *E.coli* possesses a net negative charge on its surface. The similarity in the charges on the surface of the AgNPs and *E.coli* must have caused the reduced efficacy of antibacterial activity of AgNPs against *E.coli.* Thus the higher affinity of AgNPs towards the *S.aureus* cell can be explained with

respect to the opposite surface charges present on the AgNPs as well as the test strain under study.

The size of the AgNPs synthesized using the plant extracts (ALE and TLE) and the cell free supernatant of the five isolated strains (4S1, 4S2, 4S3, 6S1and 8S1) was found to follow the order 4S1 > 4S3 > 4S2 > 6S1 > 8S1 > TLE > ALE. However the trend of lowest MIC exhibited by the AgNPs against *E.coli* followed the order of 8S1<4S2=4S3=6S1<TLE=ALE=4S1. However the sizes of the AgNPs synthesized using the ALE and TLE were found to be 10.9 nm and 20.4 nm respectively. These AgNPs exhibited the high MIC values against the test pathogens implying that size of the AgNPs alone is not the governing parameter in imparting the antibacterial property to it. The AgNPs synthesized using the strain 4S1 had the largest size and the same antibacterial efficacy as the AgNPs synthesized using ALE and TLE, further proving that other factors along with the size of the AgNPs act in a synergistic manner to confer the antibacterial property and also in determining the predominant mechanism involved in bringing about the cell death.

Table 4.33 Antibacterial efficacy of AgNPs synthesized using various resources against *E.coli* and *S.aureus*

Source	MIC against *E.coli* (µg/mL)	MIC against *S.aureus* (µg/mL)	Size
T.catappa leaves extract	25.6	25.6	10.9 nm
T.grandis Linn f.leaves extract	25.6	12.8	20.4 nm
4S1	25.6	25.6	77.3 nm
4S2	6.4	3.2	53.3 nm
4S3	6.4	3.2	68.9 nm
6S1	6.4	3.2	42.1 nm
8S1	3.2	1.6	28.8 nm

Studies pertaining to antimicrobial activity of AgNPs propose different routes of action causing the cell death. However certain amount of ambiguity exists in determining the exact mechanism which brings about the cell death. Several reports suggest that the morphological characteristics as well as the concentration of the AgNPs play a role in antimicrobial effect by causing damage to the cell membranes which promote permeable structural changes in the bacterial cell wall (Hashimoto et al. 2012; Rolim et al. 2012; Periasamy et al. 2012; Lazar, 2011). A study pertaining to antimicrobial activity of AgNPs against *E. coli* (Lazar et al. 2011) confirmed that a

gap in the integrity bilayer was created due to the accumulation of the AgNPs on the membrane predisposing it to cell death. Several studies have proven the size dependent antimicrobial activity of AgNPs (Wu et al. 2014; Tamayo et al. 2014). AgNPs are also known to possess higher surface to volume ratio compared to bulk material, facilitating the interaction between the bacterial cell and the AgNPs. Zeta potential and size of the AgNPs play a pivotal role in confirming the antimicrobial activity against pathogens as electrostatic forces are known to strongly develop between the surfaces with opposite charges. Once the AgNPs come in contact with the bacterial cell wall/ penetrate it, Ag^+ ions bind to membrane protein, creating reactive oxygen species or bind to the nucleic acids (Wu et al. 2014) and ribosomes thereby inhibiting the replication, transcription and translation and facilitating cell death (Mirzajani et al. 2011; Jung et al. 2008; Morones, 2005; Bury et al. 1999). Shape dependent antimicrobial activity of AgNPs has been reported by Pal et al. (2007).

Table 4.34 shows the MIC of AgNPs synthesized using various plant and microbial sources against *E.coli* and *S.aureus* as reported by other researchers. From Table 4.34 it can be observed that the MIC values exhibited by the AgNPs synthesized using the isolated strains (4S1, 4S2, 4S3, 6S1, 8S1) and the plant extracts (ALE or TLE) in the present study are found to be similar of more often better in antibacterial efficacy with lower MIC value when compared to the MIC values of AgNPs reported by other researchers indicating the potency of the AgNPs synthesized using biobased routes (Plant leaf extracts and cell free culture supernatant of isolated bacterial strains) of the current study in antimicrobial applications. Thus in the present study, along with the size and the type of surface charge possessed by the AgNPs, several other factors like the shape and presence of capping agents may impart an overall synergistic effect to the antimicrobial property of a particular nanoparticle.

It can be concluded that the AgNPs synthesized using the bacterial isolate 8S1 has the best antibacterial efficacy compared to other AgNPs. The AgNPs synthesized using strains 4S2, 4S3 and 6S1 also have good antibacterial efficacy. However the antibacterial efficacy of AgNPs synthesized using ALE, TLE and strain 4S1 are marginal but comparable with those reported in literature.

Table 4.34 Antibacterial efficacy of AgNPs synthesized using various resources against *E.coli* and *S.aureus*

Source	MIC against *E.coli* (μg/mL)	MIC against *S.aureus* (μg/mL)	References
Desmodium triflorum	27	53	Ahmad et al. 2010
Ocimum sanctum (Tulsi) leaf extract	0.314	1.25	Singhal et al. 2011
Tea leaf extract	>50.0	-	Sun et al. 2014
Abelia grandiflora	25	3.12	Sharma et al. 2014
Carica papaya leaf extract	100	100	Banala et al. 2015
Cashew Gum	6.75	13.5	Quelemes et al. 2013
edible mushroom *Pleurotus florida*	-	20.0	Bhat et al. 2011
Dalbergia spinosa leaves	300	300	Muniyappan and Nagarajan, 2014
Schizophyllum Commune	0.4–30	1.6–47	Chan and Mashitah, 2013
Grape Seed Extract	-	25.5	Xu et al. 2014
Cassia roxburghii DC. aqueous extract	9.8	12.4	Balashanmugam and Kalaichelvan, 2015
Exiguobacterium sp. KNU1	6.25	25	Tamboli and Lee, 2013
Acinetobacter calcoaceticus	150–600	>1000	Singh et al. 2013
Cryptosporiopsis ericae PS4	17	14	Devi and Joshi, 2014
***T.catappa* leaves extract**	25.6	25.6	Present Study
***T.grandis* Linn f.leaves extract**	25.6	12.8	Present Study
4S1	25.6	25.6	Present Study
4S2	6.4	3.2	Present Study
4S3	6.4	3.2	Present Study
6S1	6.4	3.2	Present Study
8S1	3.2	1.6	Present Study

4.12.3 The applicability of AgNPs as antibacterial coating on cotton fabric

The antibacterial efficacy of coated cotton fabric (Table 4.35 and Table 4.36) was tested against water borne pathogens such as, *E. coli* and *S. aureus.* Cotton is worn globally and the coating of AgNPs imparts antibacterial property to the cotton fabric. The AgNPs coated antibacterial fabrics can be multifunctional as they can

serve the purpose of eliminating disease causing pathogens, reduce odour and sweat. With these facets antibacterial fabrics find promising wide applicability in military, health care, and packaging sectors. The antibacterial property of AgNPs coated cotton fabric was tested by measuring the ZOI around the coated fabric as discussed in section 3.7.1.3 of Chapter 3.

Table 4.35 shows the images of agar plates showing the ZOI around the cotton swatches coated with the AgNPs synthesized using ALE, TLE and five bacterial isolates along with chemically synthesized AgNPs (Marked as C) and a control swatch containing water as the solvent (Marked as Cont). Both the test strains, *S.aureus* and *E.coli* are found in water and are pathogenic in nature.

Table 4.35 Antibacterial property of cotton fabric swatches coated with AgNPs synthesized using ALE, TLE and bacterial isolates against *E.coli* and *S.aureus*

Source	Photographic image of Agar plates showing ZOI (mm)	
	E.coli	*S.aureus*
ALE		
TLE		
4S1		
4S2		

Table 4.35 Continued…
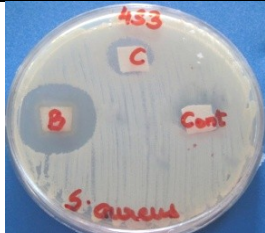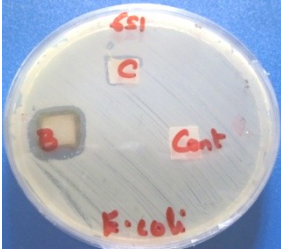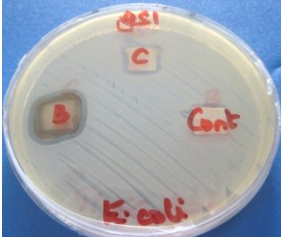
Source	Photographic image of Agar plates showing ZOI (mm)	
	E.coli	*S.aureus*
4S3		
6S1		
8S1		

Table 4.36 Zone of inhibition formed by AgNPs coated upon cotton swatches against water borne pathogens *E.coli* and *S.aureus*

Sources	Zone of inhibition observed (mm)	
	E.coli	*S.aureus*
ALE	20±1	30±1
TLE	20±1	28±1
4S1	20±1	25±1
4S2	20±1	30±1
4S3	20±1	31±1
6S1	21±1	32±1
8S1	21±1	34±1
Chemically synthesized AgNPs	8±1	10±1

Table 4.36 shows the ZOI value for AgNPs synthesized using ALE, TLE, bacterial isolates and chemically synthesized AgNPs. As seen in the Table 4.36, the ZOI value exhibited by the AgNPs synthesized using plant and bacterial resources is higher against *S.aureus* and *E.coli* compared to that of chemically synthesized AgNPs; validating the hypothesis that biologically synthesized AgNPs possess an edge over chemically synthesized AgNPs. The AgNPs synthesized using ALE, TLE and the five bacterial isolates exhibited larger value of ZOI against *S.aureus* compared to that of *E.coli.*

The ZOI values for cotton swatches coated with AgNPs synthesized using 6S1 and 8S1 strains are almost similar against *E.coli,* whereas the AgNPs synthesized using 8S1 showed better antibacterial efficacy compared to AgNPs synthesized *using* 6S1 against *S.aureus*. The efficacy of AgNPs synthesized using ALE, TLE and strains 4S1, 4S2, 4S3 are similar but inferior to those synthesized using 6S1 and 8S1 against *E.coli*. But the efficacy of AgNPs synthesized using ALE was better than that of TLE against *S.aureus*. The efficacy of AgNPs synthesized using TLE and 4S1 are further inferior compared to other AgNPs against *S.aureus*.

The coated AgNPs impart antibacterial property to the fabric, increasing the multifunctionality of fabric. The antibacterial fabric may be used in wound dressing, surgical wears, hospital uniforms, school uniform and socks. These AgNPs may be coated onto bag filter fabrics used for water disinfection in water treatment facilities.

Encouraging results validate the antibacterial efficacy and potency of AgNPs synthesized using plant extracts and bacteria, rendering it as a simple, rapid, low cost and green synthetic process that can be employed in the antibacterial coating for fabrics to meet the demand for comfortable, clean, and hygienic textile goods.

The biological resources such as ALE, TLE and the cell free supernatant of isolated strains 4S1, 4S2, 4S3, 6S1 and 8S1 could be effectively used for the synthesis of AgNPs and these AgNPs exhibited mercury sensing and antibacterial properties, thus showing their potential use as mercury sensors and as antibacterial agents to be used in textile, wound dressings, military clothing, uniforms and other areas where antibacterial coatings would be preferential.

ALE and TLE were reported to possess several phytocomponents and the cell free supernatants of isolated strains 4S1, 4S2, 4S3, 6S1 and 8S1 contain enzymes and

several other components of bacterial origin that play a crucial role in the synthesis of the AgNPs. Thus these resources were further tested for their efficacy in synthesizing, a semiconductor oxide; TiO_2-NPs that has several applications such as self cleaning materials, antifogging applications, disinfection and antimicrobial, air and water cleaning applications.

However the TiO_2-NPs could not be synthesized using plant extracts (ALE and TLE) but the cell free supernatant of the isolated bacterial strains 4S1, 4S2, 4S3, 6S1 and 8S1 showed promise in the synthesis of TiO_2-NPs. Thus, the next part of the thesis deals with the studies on the synthesis of TiO_2-NPs by the isolated bacteria and the application of the synthesized TiO_2-NPs.

PART B

Bacterial based synthesis of TiO$_2$-NPs

4.13 Bacterial based synthesis of TiO₂-NPs

TiO_2-NPs are the highly sought semiconductor nanoparticles for their photocatalytic property (Ni et al. 2007; Thompson and Yates, 2005; Linsebigler, et al. 1995). It is due to this fact that TiO_2-NPs are used in catalytic reactions (Dai et al. 2008), self cleaning materials (Parkin and Palgrave, 2005), paints (Maggos et al. 2007) and pigments (Ceresa et al. 1983), cosmetics (Auffan et al. 2010), dielectrics (Campbell et al. 1997), in applications associated with gas sensing (Wang et al. 2008; Karunagaran et al. 2005; Lin et al. 1997), photochromic devices (Ohko et al. 2003; Suzuki et al. 2001) and solar cells (Nazeeruddin et al. 2011; Mor et al. 2006; Liu and Bach et al. 1998), in drug delivery (Song et al. 2009; Aydil, 2009; Kayser et al. 2005; Parveen et al. 2012; Zhang et al. 2012), diagnostics (Wu et al. 2007), artificial implants (Geetha et al. 2009; Streicher et al. 2007) and tissue engineering (Ma et al. 2005).

Biobased synthesis of TiO_2-NPs is cost effective, ecofriendly and involves the usage of natural resources for the synthesis of TiO_2-NPs under ambient conditions of synthesis as discussed in Chapter 2. As presented in Section 2.3 of Chapter 2, microbial resources such as bacteria and fungi have been reported to mediate the synthesis of TiO_2-NPs (Órdenes-Aenishanslins et al. 2014; Rajakumar et al. 2012b; Dhandapani et al. 2012; Kirthi et al. 2011).

In the current research work, the bacterial strains with the efficacy to synthesize AgNPs were also tested for their efficacy to synthesize TiO_2-NPs followed by evaluation of the photocatalytic activity of TiO_2-NPs.

4.13.1 Synthesis of TiO₂-NPs using the bacterial strains 4S1, 4S2, 4S3, 6S1 and 8S1

In order to evaluate the efficacy of the bacterial strains 4S1, 4S2, 4S3, 6S1and 8S1 to synthesize TiO_2-NPs, a preliminary shake flask study was conducted. It was crucial to determine whether the bacterial strains isolated with the specificity to synthesize AgNPs were capable of synthesizing TiO_2-NPs.

Hence, 1 g of the precursor salt, K_2TiF_6 was added to 100 mL of the 24 h grown culture solutions of bacterial strains 4S1, 4S2, 4S3, 6S1and 8S1 and a control flask containing only the sterile growth medium. The flasks were further incubated for

24 h. The detailed methodology for these experiments is presented in Section 3.4.2 of Chapter 3. The flasks containing the culture medium along with the precursor salt was observed for visual changes. The change in the colour of the medium from turbid yellow to turbid white along with a little white deposit was observed. The representative photographic image of the 24 h grown cell free culture supernatant of strain 8S1 is shown in Figure 4.91 (a). The control flask did not show any colour change, turbidity or deposition indicating that TiO_2-NPs formation did not occur in the absence of bacterial enzymes. The occurrence of colour change on the synthesis of TiO_2-NPs is presented by a representative photographic image for the strain 8S1 as Figure 4.91(b).

Figure 4.91 (a) Representative photograph of the 24h grown cell free supernatant of strain 8S1 (b) photograph of TiO_2-NPs synthesized using 24h cell free supernatant of strain 8S1

Several researchers (Dhandapani et al. 2012; Kirthi et al. 2011; Prasad et al. 2007) have attributed the formation of white turbidity along with deposits in the synthesis medium for the synthesis of TiO_2-NPs by microbial based routes. Hence the preliminary evaluation of the bacterial strains 4S1, 4S2, 4S3, 6S1 and 8S1 to synthesize TiO_2-NPs proved that the bacterial isolates were capable of reducing the precursor salt into TiO_2-NPs. The formation of white deposits in the synthesis medium confirmed that the synthesized nanoparticles were extracellular. Intracellular synthesis of the TiO_2-NPs would involve the necessary steps for lyses of the bacterial cells, to separate the bacterial biomass, separation of unwanted materials of bacterial origin from the TiO_2-NPs followed by the separation of the TiO_2-NPs from the

cytoplasmic content. Thus, the bacterial species under study which can synthesize the TiO$_2$–NPs extracellularly are favourable.

However, the challenges faced in terms of recovery of nanoparticles from the synthesis mixture and the separation of microbial biomass associated with the nanoparticles need to be countered. These challenges can be overcome by adopting a cell free, enzymatic/metabolite based synthesis process. However, for a cell free synthesis process, it is highly desirable that the TiO$_2$-NPs synthesized by the bacterial strains are extracellular. In, the present study, the preliminary experiments confirmed that the TiO$_2$-NPs synthesized by 4S1, 4S2, 4S3, 6S1and 8S1 are extracellular and thus these bacteria are the potential candidates for a cell free nanoparticle synthesis process.

Cell free synthesis of TiO$_2$-NPs would lead to increase in the overall efficacy of the production process as this would reduce the number of the downstream processing steps in the production of TiO$_2$-NPs.

Thus, further studies on the synthesis of TiO$_2$–NPs were carried out in the cell free environment using the metabolic machinery of these strains of bacteria. For these studies, the bacterial strains 4S1, 4S2, 4S3, 6S1 and 8S1were grown in NB medium for 24 h as described in Section 3.3.5 of Chapter 3. One gram of precursor salt was added to 100 mL of cell free supernatant obtained after separation of the biomass from the nutrient media, thus forming 10 g/L precursor salt concentration in the cell free synthesis media. The synthesis process was continued for a period of 24 h as described in Section 3.4.2 of Chapter 3. Change in colour of the synthesis media from yellow to white with appearance of white deposits confirmed the formation of TiO$_2$-NPs, thus proving that the strains secreted extracellular enzymes that were capable of synthesizing TiO$_2$-NPs from K$_2$TiF$_6$. It confirmed the possibility of cell free synthesis of TiO$_2$-NPs using the bacterial strains 4S1, 4S2, 4S3, 6S1 and 8S1.

To confirm the role of extracellular bacterial metabolic machinery involved in the synthesis of TiO$_2$-NPs; the 24 h grown cell free culture supernatant of the bacterial strains 4S1, 4S2, 4S3, 6S1 and 8S1 was obtained by following the methodology described in section 3.3.5 of Chapter 3. The 24 h cell free supernatant of all the bacterial strains were heated to 70ºC in a water bath for 3 h to enable the denaturation of bacterial proteins. The precursor salt was added to these solutions and observed for

the synthesis of TiO$_2$-NPs for a time duration of 24 h. After the synthesis period there was no visual observation of change in either the colour of the medium or the formation of white deposits indicating the synthesis of TiO$_2$-NPs. Thus from this study it was proven that extracellular synthesis is not brought about by the metabolites but the extracellular proteinaceous molecules secreted by the bacteria are responsible for the synthesis of TiO$_2$-NPs.

4.14 Determination of the bacterial metabolic machinery responsible for the reduction of Ti^{4+} ions

Extracellular enzymes secreted by microbes are known to bring about the reduction of the precursor salt to nanoparticles. Bacteria are known to secrete hydrolytic enzymes to use macromolecules of organic polymers as nutrients, such enzymes break down polymers of big molecules into smaller units to penetrate plasmatic membrane. Bansal and co-workers (2005) identified various genera of fungi for the extracellular synthesis of nanoparticles that were able to synthesize TiO$_2$-NPs from K$_2$TiF$_6$ and found that extracellular hydrolytic enzymes of small molecular weight were responsible for the synthesis of TiO$_2$-NPs and were found to be in the molecular weight range of 20-28 kDa as determined through SDS-PAGE.

Thus in the present study the cell free culture supernatant of the strains were subjected to partial purification of the enzymes by ammonium sulphate precipitation, dialysis, concentration of the proteins and further subjected to SDS PAGE to test for the presence of hydrolytic enzymes. The molecular weight of the extracellular proteins secreted by the bacteria into the cell free supernatant was also determined through SDS PAGE according to the methodology described in section 3.5 of Chapter 3. The Coomassie Brilliant Blue stained Gel image obtained under UV light is shown in Figure 4.92.

Figure 4.92 shows the SDS PAGE gel image with odd lanes containing the ladder while the even lanes containing the bands in the supernatant of the five bacterial strains. It can be observed that low molecular weight proteins belonging to 29 kDa have been identified in the lanes belonging to the cell free supernatant of bacterial strains 4S1, 4S2, 4S3, 6S1 and 8S1. Similar protein with a molecular weight of 20-24 kDa was determined by Bansal et al. (2005) in their studies pertaining to the

extracellular synthesis of TiO_2-NPs using K_2TiF_6 as the precursor salt. These low molecular weight proteins were determined to belong to hydrolases class of enzymes and they are known to bring about the conversion of K_2TiF_6 to TiO_2-NPs by hydrolysis of TiF_6^-. Jha et al. (2009a) had used *Lactobacillus* and Yeast cells for the synthesis of TiO_2-NPs and found that membrane bound oxidoreductase enzymes of the microbes were responsible for the synthesis of TiO_2-NPs. Rajakumar et al. (2012 b) synthesized TiO_2-NPs using the biomass of *A.flavus* and have attributed oxygenases present in the cytosol to the synthesis. Kirthi et al. (2011) have also attributed the synthesis of intracellular TiO_2-NPs from its precursor salt to the membrane bound oxidoreductases. All the enzymes discussed so far belong to the class of hydrolytic enzymes-hydrolases. Hence, in the present study the conversion of K_2TiF_6 as the precursor salt to TiO_2-NPs is attributed to hydrolysis by the class of low molecular weight extracellular oxidoreductases enzymes with a molecular weight of ~29 kDa.
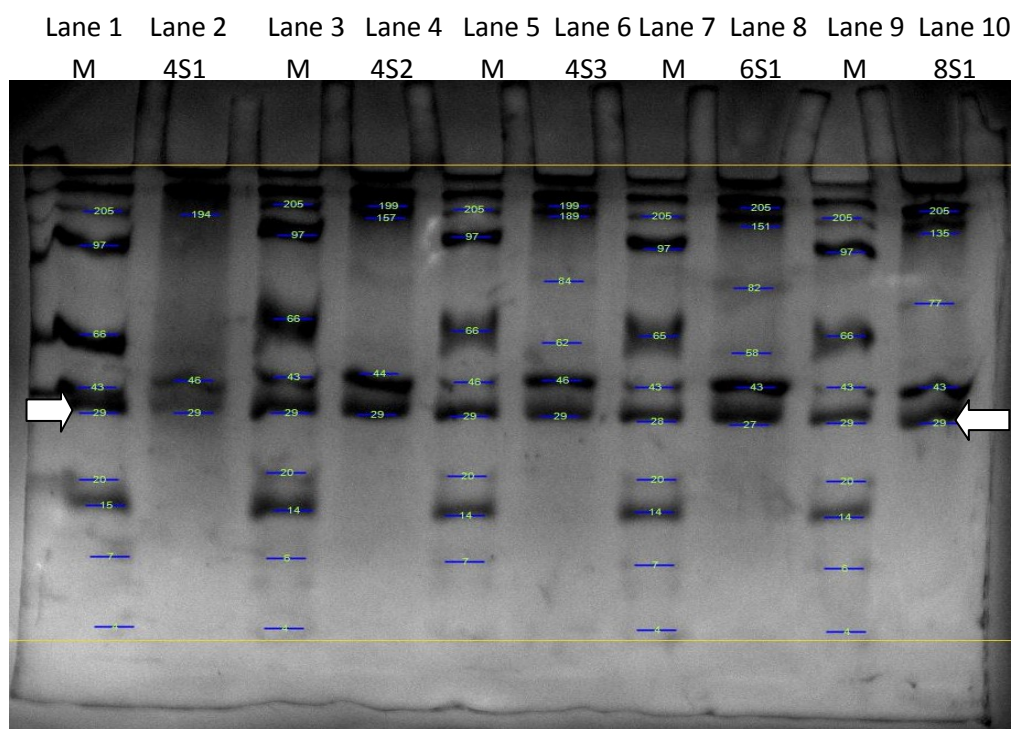
Figure 4.92 Coomassie Brilliant Blue stained SDS PAGE Gel image under UV light showing the protein ladder and the molecular weight of the bacterial proteins

4.15 Effect of synthesis process parameters on the synthesis of TiO$_2$-NPs by the cell free culture supernatants of the bacterial strains 4S1, 4S2, 4S3, 6S1and 8S1

The synthesis of nanoparticles by cell free supernatant is governed by the presence of enzymes and any enzymatic process is greatly influenced by the pH and temperature (Palmer, 1991) of the medium along with concentration of the precursor salt. Jha et al. (2007) have reported that pH of the synthesis mixture governs the rate of the particle synthesis. Thus, the effects of these parameters on the synthesis of TiO$_2$-NPs by the cell free supernatants of the bacterial strains were studied.

4.15.1 Effect of precursor salt concentration on the synthesis of TiO$_2$-NPs using the cell free supernatants of the bacterial strains

The synthesis of TiO$_2$-NPs was carried out using the cell free supernatants of the bacterial strains 4S1, 4S2, 4S3, 6S1and 8S1. The 24 h grown cell free culture supernatant of the bacterial strain was obtained by adopting the methodology described in Section (3.3.5) of Chapter 3 and the studies on the effect of precursor salt concentration was carried out with the varying concentration of K$_2$TiF$_6$ that served as the precursor salt as explained in Section 3.4.3.1 of Chapter 3. The concentration of K$_2$TiF$_6$ salt added to the synthesis mixture was varied in the range of 5 g/L to 15 g /L, thus the concentration of the precursor salt in the synthesis mixture remained the same. The synthesis process was allowed to continue for a period of 24 h at the ambient temperature of 28±2ºC. The initial pH of the synthesis mixture was not adjusted and found to be 7.0±0.2. The amount of residual Ti^{+4} ions present in the synthesis mixture after the separation of nanoparticles was analyzed using AAS and the percentage conversion of Ti^{+4} was determined using the methodology in Appendix I.

The percentage conversion obtained with each of the bacterial strain is presented in Table 4.37. The percentage conversion increased with the increase in precursor salt concentration from 5 g/L to 10 g/l. However, with further increase in precursor salt concentration to 15 g/L, the conversion decreased. This trend was observed in TiO$_2$-NP synthesis with all the bacterial strains. As the concentration of precursor salt increases the rate of synthesis increases owing to easier availability of Ti^{+4} ions to the enzyme active sites. Increased rate yielded higher conversion at any

time in the synthesis mixture with 10 g/L precursor salt, as compared to that at 5 g/L. However, further increase in precursor salt concentration to 15 g/L led to decrease in conversion.

High ionic strength at higher concentration leads to disruption or blockage of native active sites of the enzymes, thus reducing the rate of hydrolysis of K_2TiF_6 to TiO_2. The fluoride ions in the solution may also bind onto the enzyme, thus denaturing the enzymes (Marquis et al. 2003) leading to lower conversion to TiO_2.

Table 4.37 Conversion of Ti^{+4} ions obtained with different precursor salt concentrations by the culture mixture of the isolates

Bacterial Isolate	Percentage conversion of Ti^{+4} ions with precursor salt concentration		
	5g/L	10g/L	15g/L
4S1	37.85	**76.73**	42.11
4S2	48.72	**73.53**	62.37
4S3	18.38	**65.20**	56.92
6S1	38.4	**61.89**	40.36
8S1	53.46	**84.01**	45.97

The highest conversion was obtained by using a precursor salt concentration of 10 g/L with all the bacterial strains 4S1, 4S2, 4S3, 6S1 and 8S1. On comparison of the conversions of Ti^{+4} ions obtained by using the cell free culture supernatants of different strains at 10 g/L concentration of precursor salt, the maximum conversion of 84.01% was obtained with 8S1 strain as observed in Table 4.37. The SEM images of TiO_2-NPs synthesized using the cell free culture supernatant of bacterial strain 8S1 at different concentrations of K_2TiF_6 are shown in Figure 4.93 to Figure 4.95. The presence of distinct particles was not observed with precursor salt concentration of 5g/L as shown in Figure 4.93, indicating that the particle formation did not occur. The converted Ti^{+4} ions would have formed the nuclei, but the growth would not have occurred due to presence of very low concentration of the salt. Lower rate of mass transfer due to lower concentration gradient would have resulted in reduced growth rate and thus no distinct particles were formed. But, formation of distinct particles was observed with 10g/L concentration of K_2TiF_6 as observed in Figure 4.94. The particles are polymorphic and anisotropic with polygonal structures and are flaked. The particles were of the average size range 322nm indicating that the conditions used

for the synthesis such as pH and precursor salt concentration could not yield nanosized particles. At a precursor salt concentration of 15 g/L polymorphic, polygonal particles with still higher average size range of 787 nm were formed (Fig 4.95). Owing to larger sized particles and lower conversion obtained with 15 g/L as compared to that with 10 g/L, precursor salt concentration of 10 g/L was found to be the optimum in the range studied. EDS spectra of the TiO_2 particles synthesized with different concentrations of precursor salt using cell free supernatant of the strain 8S1 are presented in Figure 4.96 (a), (b) and (c). From the EDS spectra it can be seen that the content of Fluoride was the highest in the TiO_2 particles prepared using 15 g/L concentration of precursor salt. The elemental analysis of TiO_2 particles reveals the presence of titanium and oxygen supporting the formation of TiO_2 particles. Presence of potassium and fluorine ions on the particle surface indicates that these ions also may have doped onto the particle surface. Presence of Carbon and phosphorous may be attributed to the organic capping of bacterial origin on the surface of the particles.

However, it was deduced that further optimization of pH may be necessary to obtain the particles with better characteristics in terms of size, surface and morphology.
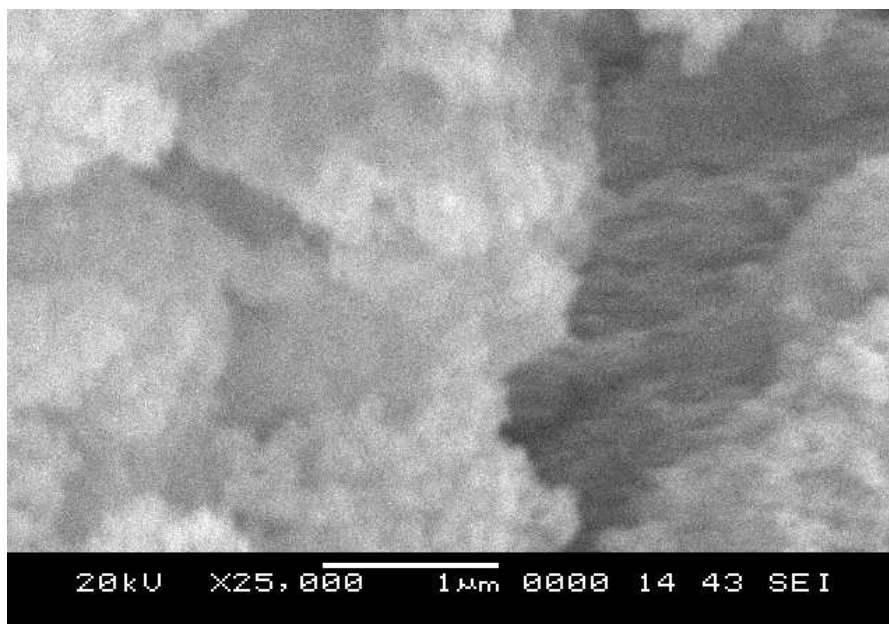
Figure 4.93 SEM analysis of TiO₂ synthesized using bacterial strain 8S1 using of precursor salt concentration of 5 g/L
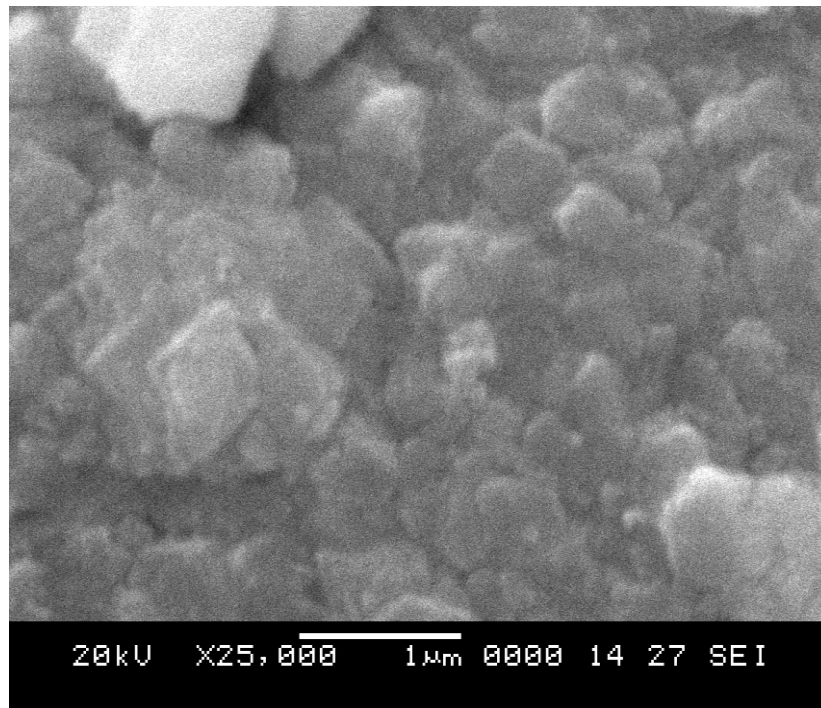
Figure 4.94 SEM analysis of TiO₂ synthesized using bacterial strain 8S1 using of precursor salt concentration of 10 g/L

| (a) | (b) |
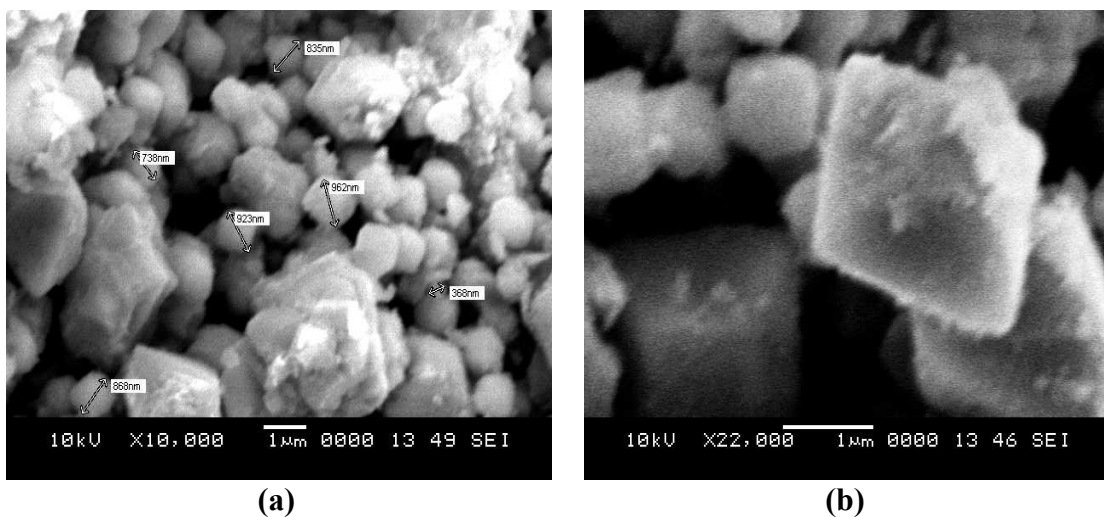
Figure 4.95 (a) SEM analysis of TiO₂ synthesized using bacterial strain 8S1 using precursor salt concentration of 15 g/L (b) Magnified image of TiO₂-NPs synthesized using 15 g/L using 8S1 strain.
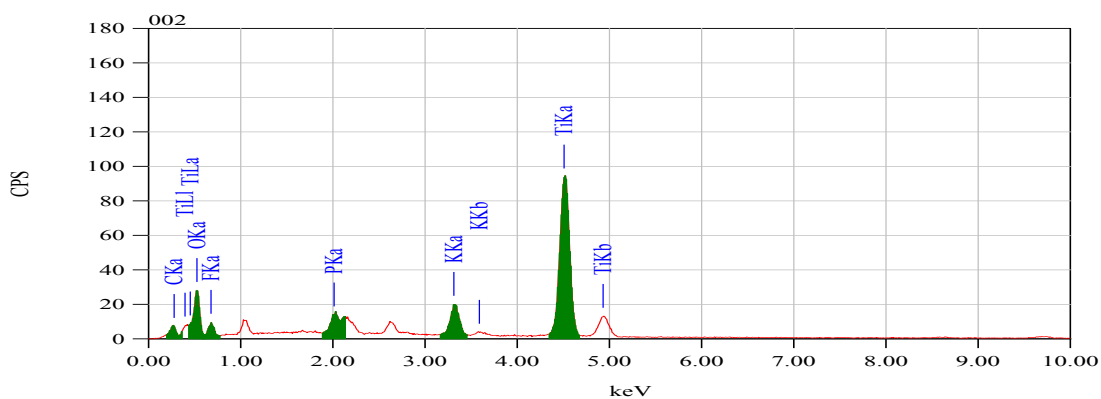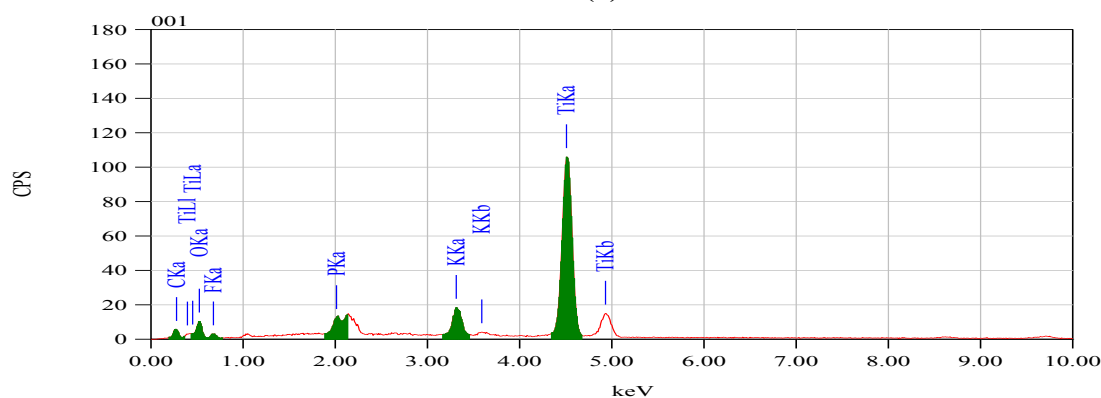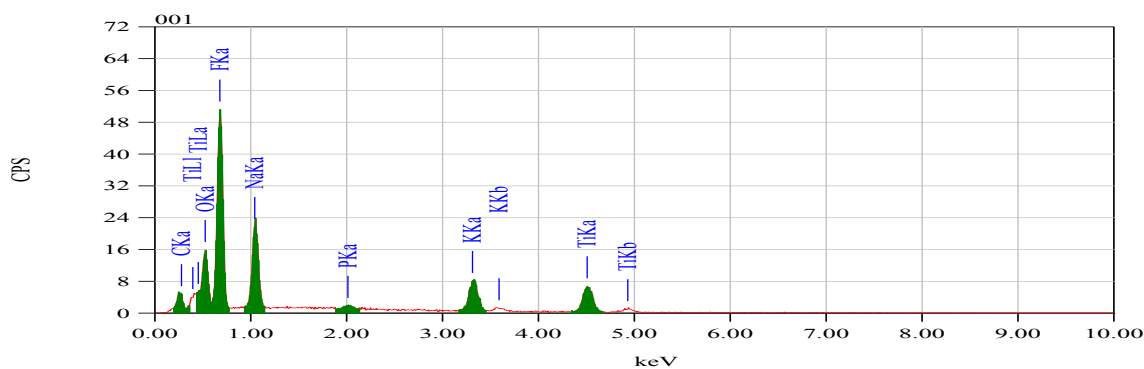
Figure 4.96 EDS analysis of particles obtained through the synthesis mixture containing cell free supernatant of 8S1 and different concentrations of precursor salt (a) 5g/L , (b) 10 g/L (c) 15 g/L

4.15.2 Effect of pH of the reaction mixture on synthesis of TiO_2-NPs

In the synthesis of nanoparticles using the microbial cell free culture supernatant, the pH of the synthesis mixture plays a pivotal role in controlling the morphological and dispersion characteristics of the nanoparticles (Hebbalalu et al.

2013; Li et al. 2011; Vahabi et al. 2011; Gurunathan et al. 2009a; Kowshik et al. 2009). Thus, the effect of pH of the synthesis mixture on the synthesis of TiO_2-NPs using the bacterial cell free culture supernatant was studied. The synthesis of TiO_2 particles was carried out in the reaction mixture comprising of 100 mL of the cell free culture supernatant with the precursor salt concentration of 10 g/L and at varying initial pH conditions of acidic pH 4, unadjusted pH of 7.0±0.2 units and at alkaline pH of 11. The cell free culture supernatant of each of the bacterial isolates 4S1, 4S2, 4S3, 6S1 and 8S1 was obtained according to the methodology described in section 3.3.5 of Chapter 3 and the studies were carried out according to the methodology explained in section 3.4.3.2 of Chapter 3 with initial pH conditions of acidic pH 4, normal unadjusted pH of 7.0±0.2 units and at alkaline pH of 11.

The percentage conversion of Ti^{+4} ions to TiO_2-NPs was calculated using the residual Ti^{+4} ions content are presented in Table 4.40.

Table 4.38 Percentage conversion of Ti^{+4} ions in the synthesis of TiO_2-NPs using bacterial strains 4S1, 4S2, 4S3, 6S1 and 8S1

Bacterial isolate	Percentage conversion of Ti^{+4} ions		
	pH 4	pH 7.0 ± 0.2	pH 11
4S1	33.73	76.73	86.78
4S2	37.85	73.53	81.96
4S3	48.48	65.20	71.41
6S1	34.92	61.89	92.15
8S1	41.74	84.01	93.79

The percentage conversion of Ti^{+4} ions obtained after the synthesis using the synthesis mixtures containing the cell free supernatant of the bacterial strains 4S1, 4S2, 4S3, 6S1 and 8S1 with initial acidic pH of the synthesis mixtures, resulted in low conversion of Ti^{+4} ions in comparison to those with the alkaline pH of 11 and the unadjusted pH of nearly neutral. With increase in initial pH of the synthesis mixture, the percentage conversion increased with the maximum conversion occurring at pH 11. These studies revealed that alkaline pH favoured the synthesis of TiO_2-NPs with an increase in the conversion with increasing pH of the synthesis mixture. The low molecular weight extracellular hydrolytic enzymes secreted by the bacteria responsible for the synthesis of TiO_2-NPs are found to work efficiently under neutral to alkaline conditions (pH 7- pH 11) with the higher efficiency at alkaline conditions.

As observed in Table 4.38, highest percentage conversion of Ti^{+4} ions to TiO_2-NPs was obtained using the bacterial strain 8S1 followed by the strain 6S1. The SEM images of the nanoparticles synthesized using the five strains 4S1, 4S2, 4S3, 6S1 and 8S1 with initial pH of 11 are presented in Figure 4.97 to Figure 4.101 respectively to provide better insight into the morphological characteristics of the TiO_2-NPs. The size range and the average size of the synthesized TiO_2-NPs at initial pH 11 were calculated by Image J software using the SEM images and the results are presented in Table 4.39.
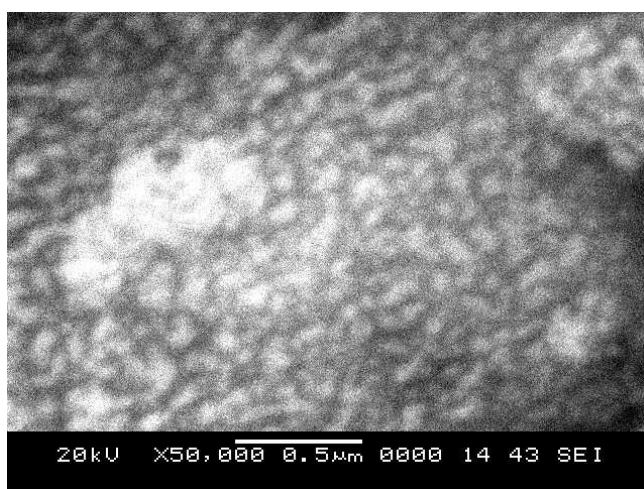
Figure 4.97 SEM image of TiO$_2$-NPs synthesized using 4S1 bacterial cell free culture supernatants with initial alkaline pH 11
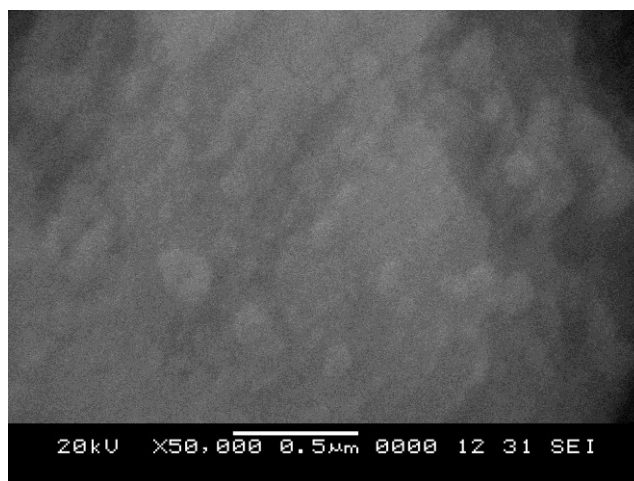
Figure 4.98 SEM image of TiO$_2$-NPs synthesized using 4S2 bacterial cell free culture supernatants with initial alkaline pH 11
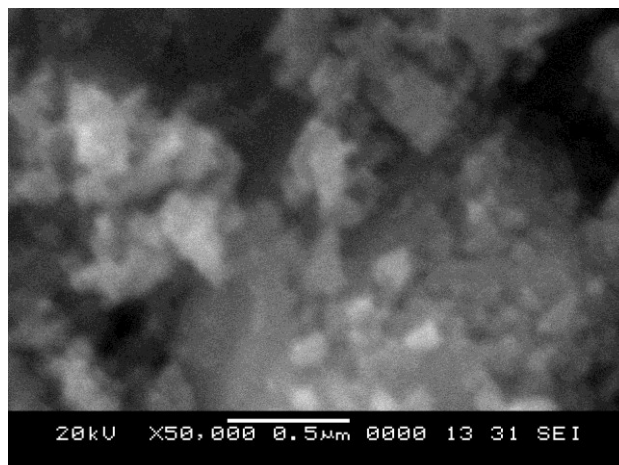
Figure 4.99 SEM image of TiO$_2$-NPs synthesized using 4S3 bacterial cell free culture supernatants with initial alkaline pH 11

Figure 4.100 SEM image of TiO$_2$-NPs synthesized using 6S1 bacterial cell free culture supernatants with initial alkaline pH 11
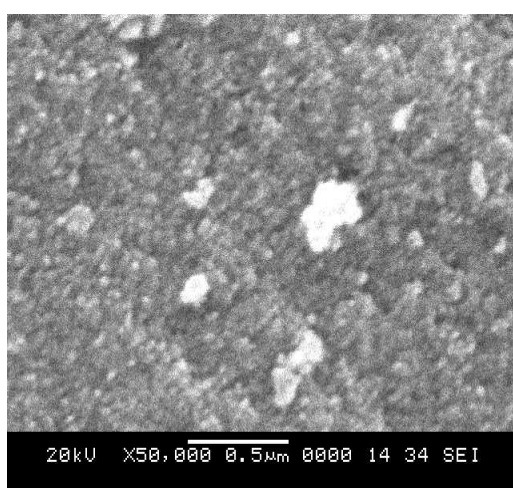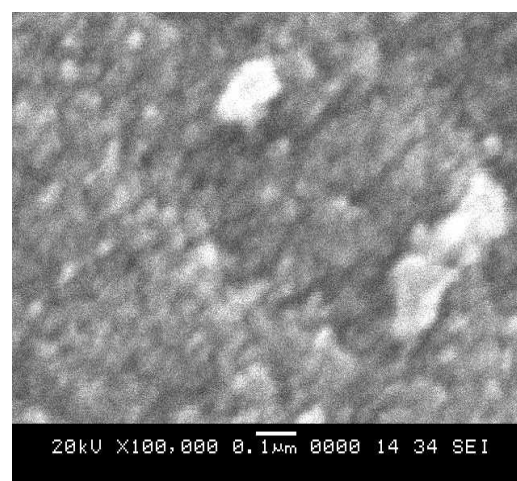
| (a) | (b) |

Figure 4.101 SEM images of TiO$_2$-NPs synthesized using 8S1 bacterial cell free culture supernatants with (a) initial alkaline pH condition of 11 and (b) Magnified SEM image

Table 4.39 Average particle size and size range of TiO$_2$-NPs by SEM images using Image J software

Bacterial isolate	Average particle size of TiO$_2$-NPs (nm)	Average particles size range (nm)
4S1	53.30	35-92.7
4S2	119.01	62.9-178.4
4S3	73.23	58-111.2
6S1	84.87	63-98.27
8S1	18.7	9.29-23.1

As seen in the SEM images Figure 4.97 and Figure 4.101, TiO$_2$-NPs synthesized using the cell free supernatant of bacterial strain 4S1 and 8S1 are distinct and quasi spherical shaped. However the particles synthesized from 4S1 as seen in Figure 4.97 and Table 4.39 exhibit larger average size and size range compared to TiO$_2$-NPs synthesized using 8S1 (Figure 4.101 and Table 4.39). The TiO$_2$-NPs synthesized using the cell free supernatant of bacterial strains 4S2, 4S3 and 6S1 lead to the formation of larger sized, aggregated particles with polymorphic shapes as seen in Figure 4.98, Figure 4.99 and Figure 4.100 respectively. The average particle size and the size range of particles synthesized using the strain 4S2, 4S3 and 6S1 as shown in Table 4.39 are higher than the sizes obtained through strains 4S1 and 8S1.

The TiO$_2$-NPs synthesized using the cell free supernatant of bacterial strain 8S1 (8S1-TiO$_2$-NPs) were found to have the smallest size distribution range of 9.29 nm-23.1 nm. The size distribution range was in the order of 8S1 < 4S1 < 4S3 < 6S1 < 4S2.

8S1-TiO$_2$-NPs synthesized at alkaline initial pH (pH 11) (Figure 4.101 (a) and (b)) revealed the formation of monodispersed TiO$_2$-NPs with the average size of around 18.7 nm which is even lower than the average particle size of TiO$_2$-NPs synthesized at neutral (unadjusted) initial pH of the synthesis mixture. The average size of 8S1-TiO$_2$-NPs at neutral (unadjusted) initial pH of the synthesis mixture was found to be 322nm and the size range was 90-645nm as seen in Figure 4.94 of section 4.15.1. However, with unadjusted and alkaline pH conditions, the particle size distribution ranges were very narrow indicating the formation of monodispersed TiO$_2$-

NPs, the size of nanoparticles synthesized with initial pH 11 was one order of magnitude lower than that obtained with the unadjusted (neutral) pH condition.

The cell free culture supernatant of 8S1 strain with 10 g/L of precursor salt concentration   in the synthesis mixture with initial pH 11 yielded the highest conversion of ~94%, with minimum average particle size of 18.7 nm, well dispersed, distinct and quasi spherical shaped particles with the narrowest size distribution as compared to those obtained with other strains. The particles thus prepared are distinct and of uniform size as observed in Figure 4.101 (a) and (b).

4.16 Characterization of the TiO$_2$-NPs synthesized using bacterial isolates

4.16.1 XRD analysis of TiO$_2$-NPs synthesized using bacterial isolates

The TiO$_2$-NPs synthesized using the cell free culture supernatants of bacterial strains 4S1, 4S2, 4S3, 6S1 and 8S1 were subjected to XRD analysis. The X-Ray diffractograms of the TiO$_2$-NPs synthesized from each of these bacterial strains are presented in Figure 4.102 to 4.106. Phases are demarcated with their initial alphabets such as Brookite (B) and Anatase (A) Monoclinic (U).
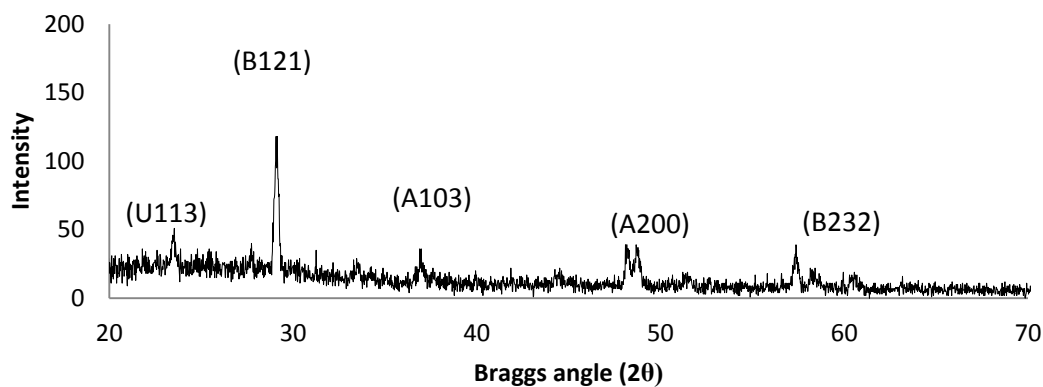
Figure 4.102 X Ray diffractogram of TiO$_2$-NPs obtained by cell free culture supernatant of bacterial isolate 4S1
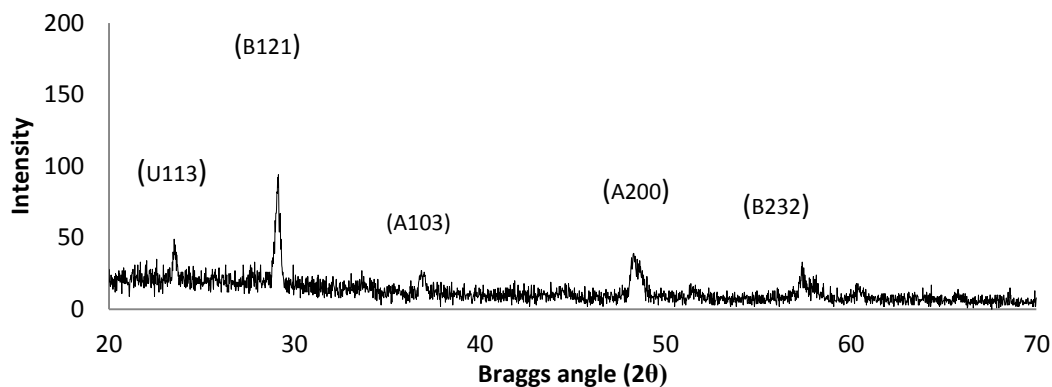
Figure 4.103 X Ray diffractogram of TiO$_2$-NPs obtained by cell free culture supernatant of bacterial isolate 4S2
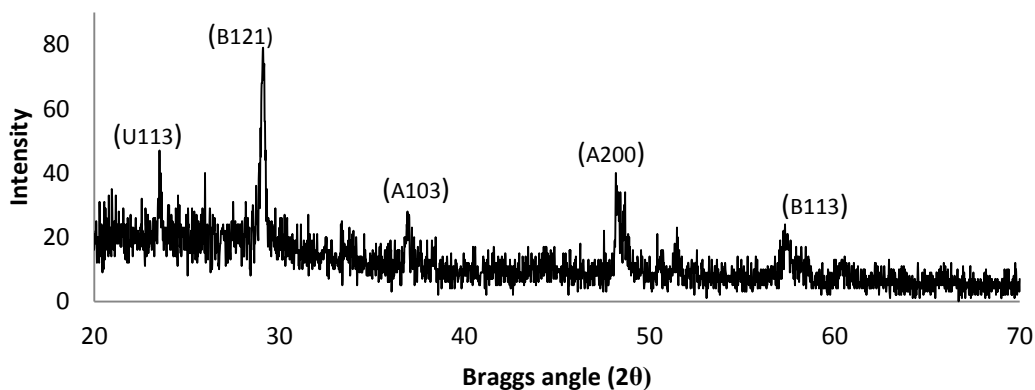
Figure 4.104 X Ray diffractogram of TiO$_2$-NPs obtained by cell free culture supernatant of bacterial isolate 4S3
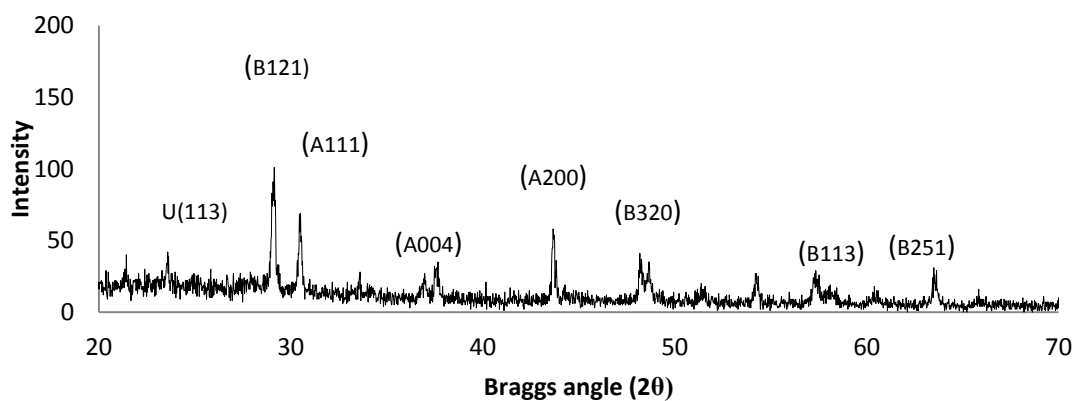
Figure 4.105 X Ray diffractogram of TiO$_2$-NPs obtained by cell free culture supernatant of bacterial isolate 6S1

276
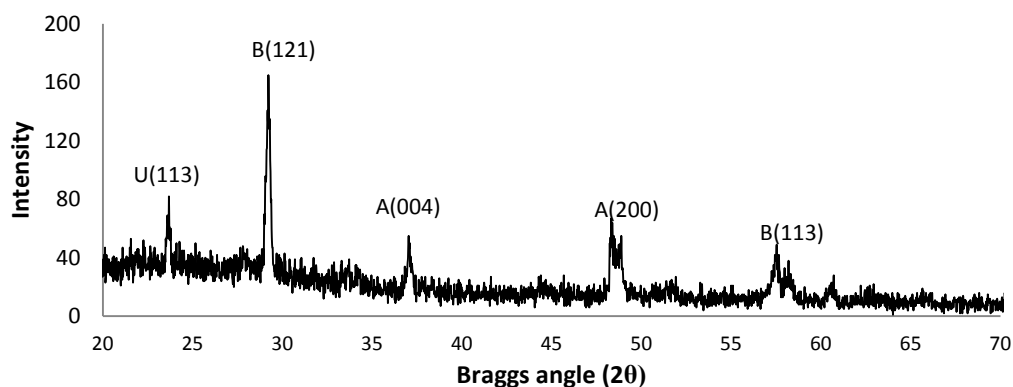
Figure 4.106 X Ray diffractogram of TiO$_2$-NPs obtained by cell free culture supernatant of bacterial isolate 8S1

As observed from the appearance of peaks in XRD, belonging to lattices of U (113), B(121), A (103), A (200) and B (232) at Braggs angle value of 25.42, 29.08, 36.98, 48.1 and 57.4 respectively (JCPDS data card: 21-1272, 29-1360 and 38-0088) shown in Figure 4.102, the TiO$_2$-NPs synthesized using 4S1 were found to be crystalline containing the brookite and anatase phase of TiO$_2$ along with an unidentified monoclinic phase of TiO$_2$. The average crystallite size of particles was calculated according to DeBye Scherrer`s formula in Eq. 3.1 and was found to be 55 nm which is in agreement with the particle size obtained using SEM analysis.

Similarly peaks belonging to brookite and anatase phase and monoclinic phase of titanium dioxide were found in all the X-ray diffractograms of TiO$_2$-NPs synthesized using the cell free supernatants of strains 4S1, 4S2, 4S3, 6S1 and 8S1. The Braggs angle (2θ) and their corresponding Miller indices (hkl values) along with the average crystallite size of the TiO$_2$-NPs was calculated according to DeBye Scherrer`s formula in Eq. 3.1 as shown in Table 4.40.

Table 4.40 Braggs Angle (2θ), Miller Indices (hkl value) and average crystallite size of TiO$_2$-NPs synthesized using the cell free supernatants of bacterial strains

Bacterial Strain	Braggs Angle (2 θ)and Miller Indices (hkl value)	Average crystallite size (nm)
4S1	23.46 U (113), 29.06 B(121), 36.88 A(103), 48.08 A (200), 57.36 B(232)	55
4S2	23.5 U (113), 29.08 B(121), 36.76 A(103), 48.24 A (200), 57.32 B(232)	108.0
4S3	23.5 U(113), 29.08 B(121), 36.9 A (103), 48.16 A(200), 57.3 B (113)	81.6
6S1	23.56 U (113), 29.1 B(121), 30.42 A(111), 43.64 A(200), 54.18 B (320), 54.22 B(113), 63.48 B(251)	79.83
8S1	26.67 U(113), 29.21 B(121), 36.99 A(004), 48.35 A(200), 57.49 B(113)	4.27

TiO$_2$ usually occurs in three predominant crystal forms; Rutile (Tetragonal), Anatase (Tetragonal) and Brookite (Rhombohedral). Rutile is the most stable form of TiO$_2$, while brookite has been found to be the most stable polymorph form of nanoparticles in the 11-35nm range (Markham and Upreti, 1965). The brookite phase of TiO$_2$ is rarely studied in comparison with the common anatase and rutile phases, as it is difficult to obtain it in pure form. However, recently researchers have reported the photocatalytic activity of Brookite (Fujishima et al. 2008). DiPaola et al. (2013) and demonstrated that Brookite exhibits better photocatalytic activity in comparison to anatase and rutile. In addition, there exists ambiguity over the recognition of the light-induced activity of Brookite phase, in spite of its higher band gap energy of 3.4 eV (Koelsch et al. 2002). It had been reported that alkaline conditions and the presence of alkaline or alkaline earth metals favour the formation of brookite phase (Truong et al. 2011). In the present study, the alkaline pH conditions and the use of K$_2$TiF$_6$ as precursor salt was used for the synthesis that provides potassium as the alkaline metal ion in the synthesis mixture and it may attribute to the formation of brookite phase.

The TiO$_2$-NPs synthesized using the cell free culture supernatant of bacterial strain 8S1 showed the smallest average crystallite size of 4.27 nm. The average crystallite size followed the order of 8S1< 4S1<6S1<4S3< 4S2. The presence of brookite phase in addition to anatase phase of TiO$_2$ has been reported to exhibit better photocatalytic activity by Kandiel et al. (2010). Thus, the TiO$_2$–NPs synthesized using the cell free supernatant of bacterial strains 4S1, 4S2, 4S3, 6S1 and 8S1

containing both anatase and brookite phase may feature as the potential photocatalysts.

4.16.2 Particle size analysis of TiO$_2$-NPs

The particle size analysis of TiO$_2$-NPs was determined using the dynamic scattering technique using Zetasizer SZ-100 according to the methodology described in section 3.6.5 of Chapter 3.

Figure 4.107 to Figure 4.111 show the particle size distribution histograms of TiO$_2$-NPs synthesized using the 24 h cell free culture supernatants of the bacterial strains 4S1, 4S2, 4S3, 6S1 and 8S1 under alkaline pH respectively.
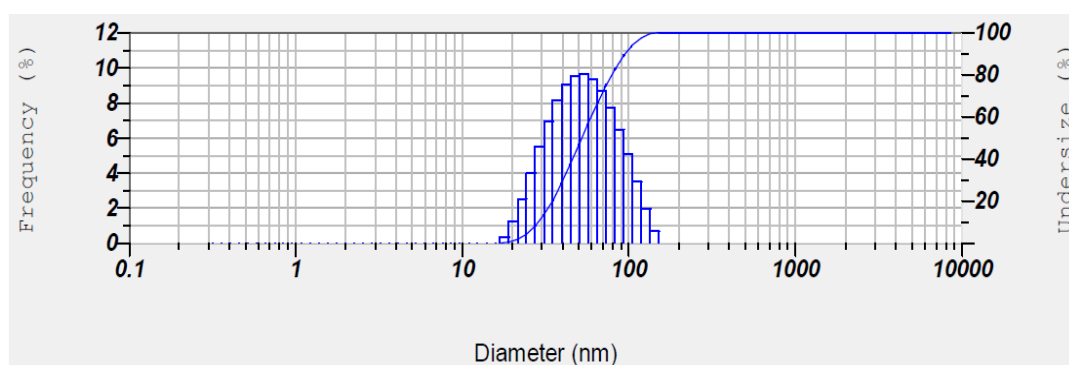
Figure 4.107 Particle size distribution of TiO$_2$-NPs synthesized using 4S1 strain
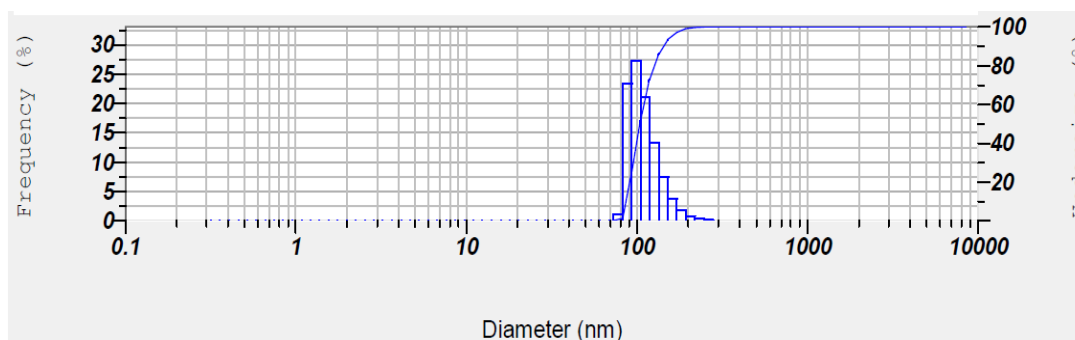
Figure 4.108 Particle size distribution of TiO$_2$-NPs synthesized using 4S2 strain
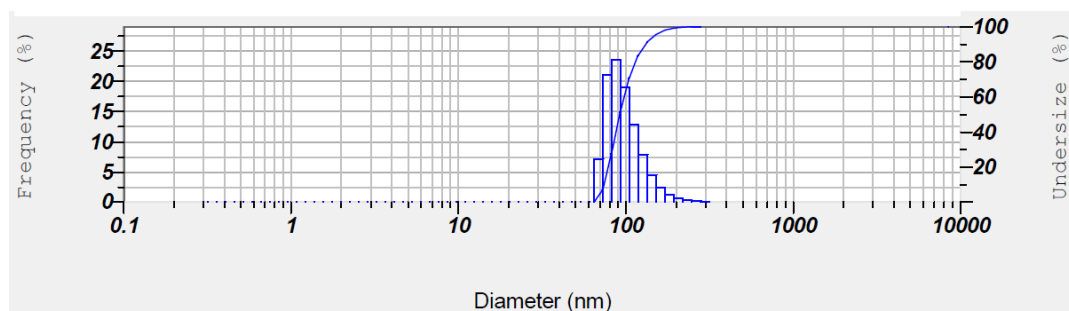
Figure 4.109 Particle size distribution of TiO$_2$-NPs synthesized using 4S3 strain
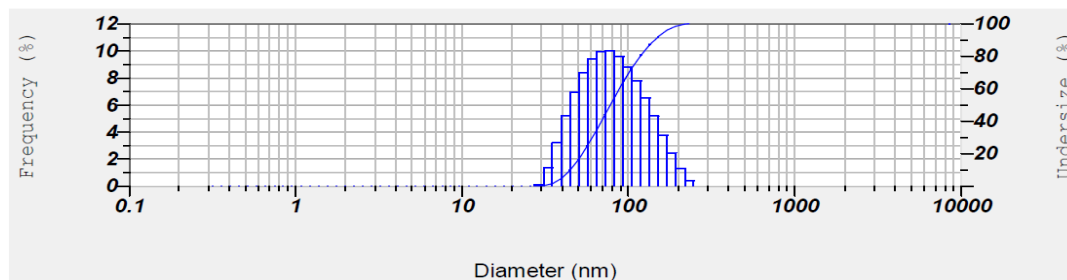
Figure 4.110 Particle size distribution of TiO₂-NPs synthesized using 6S1 strain
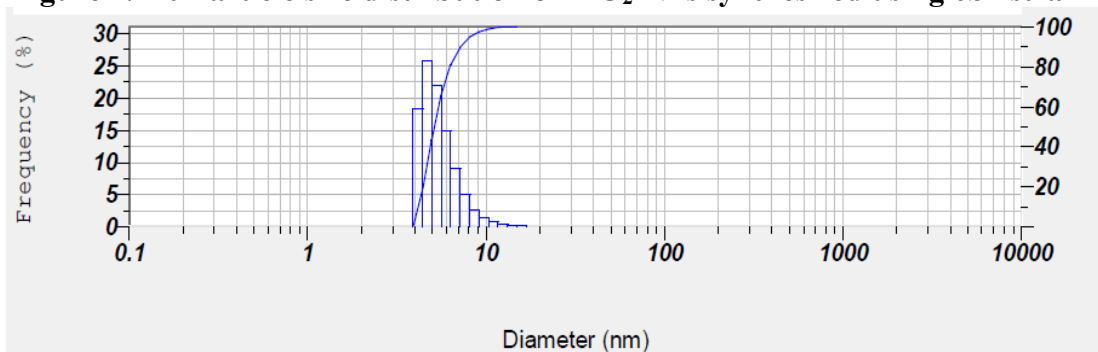
Figure 4.111. Particle size distribution of TiO₂-NPs synthesized using 8S1 strain

Table 4.41 shows the particle size distribution range and average particle size of TiO₂-NPs synthesized using the strains 4S1, 4S2, 4S3, 6S1 and 8S1 as analyzed using DLS.

Table 4.41 Average size and size range of TiO₂-NPs obtained by Particle size distribution analysis

TiO₂-NPs synthesized using the supernatant	Average size of the TiO₂-NPs	Size range of TiO₂-NPs
4S1	53.6 nm	19 nm-150 nm
4S2	98.4 nm	78 nm- 290 nm
4S3	87.0 nm	65.5 nm -320 nm
6S1	77.3 nm	30 nm -250 nm
8S1	4.97 nm	4 nm-18 nm

8S1-TiO₂-NPs synthesized were found to possess a narrow range of size distribution along with the smallest average size compared to TiO₂-NPs synthesized using other strains as shown in Table 4.41. The particle sizes of TiO₂-NPs determined using particle size distribution analysis by DLS technique are in reasonable good agreement with the average crystallite sizes determined using XRD in section 4.16.1. The morphological characteristics of 8S1-TiO₂-NPs make it an interesting and potential candidate for the exploration of its applicability features. The average size of

TiO$_2$–NPs synthesized by using various plant and bacterial sources is shown in Table 4.42.

Table 4.42 Sizes of TiO$_2$-NPs synthesized using various plant and bacterial sources

Source	Size of TiO$_2$–NPs synthesized	References
Saccharomyces cerevisiae	18 nm	Jha et al. 2009a
Lactobacillus sp.	30 nm	Prasad et al. 2007
Bacillus subtilis	66-77 nm	Kirthi et al. 2011
Leaf extract of *Nyctanthes arbor-tristis*	100 nm	Sundrarajan et al.2011
Aqueous extract of *Jatropha curcas* L. latex	25-110 nm	Hudlikar et al. 2012
Aspergillus flavus	62- 74 nm	Rajakumar et al. 2012a
Leaf aqueous extract of *Eclipta prostrate*	49.5 nm	Rajakumar et al. 2012b
Annona squamosa peel extract	26 nm	Roopan et al. 2012
Bacillus subtilis	10-30 nm	Dhandapani et al. 2012
Leaf extract of *Catharanthus roseus*	65 nm	Velayutham et al. 2012
Flower aqueous extract of *Calotropis gigantea*	160-220 nm	Marimuthu et al. 2013
Planomicrobium sp.	100–500 nm	Malarkodi et al. 2013
Propionibacterium jensenii	65 nm	Babitha et al. 2013
Aeromonas hydrophila	40.5 nm	Jayaseelan et al. 2013
Leaf extract of *Solanum trilobatum*	70 nm	Rajakumar et al. 2014
4S1	53.6 nm (19-150 nm)	Present Study
4S2	98.4 nm (78- 290 nm)	Present Study
4S3	87.0 nm (65.5-320 nm)	Present Study
6S1	77.3 nm (30-250 nm)	Present Study
8S1	4.97 nm (4-18 nm)	Present Study

The sizes of TiO$_2$-NPs synthesized in the present study are comparable with the size of the TiO$_2$-NPs synthesized using various other sources as reported in Table 4.42 with 8S1-TiO$_2$-NPs being the smallest in size.

4.16.3 Zeta potential analysis of TiO$_2$-NPs

As discussed earlier in section 4.11.5 colloidal suspensions exhibiting zeta potential value more than 25 mV and less than -25 mV are known to be stable (nanoComposix, 2003). The zeta potential value of the TiO$_2$-NPs colloids obtained by

all the five strains was determined according to the methodology described in section 3.6.5 of Chapter 3.

The zeta potential measurements of all the five TiO_2-NPs colloids are presented in Appendix XI and the zeta potential values are shown below in Table 4.43 and compared with the zeta potential values reported by other researchers.

Table 4.43 Zeta potential value of TiO_2-NPs synthesized in the present study and other routes

Route of TiO_2-NPs Synthesis	Zeta Potential Value	References
4S1	-32.3 mV	Present study
4S2	-32.3 mV	Present study
4S3	-34.0 mV	Present study
6S1	-38.4 mV	Present study
8S1	61.3 mV	Present study
Sol gel synthesis (Chemical)	47.7 mV	Mohammadi et al. 2006.
laser pyrolysis powders	-40 and -55 mV	Sentein et al. 2009
Commercial nanocrystalline titania (TiO_2) with particle size of less than 25 nm, Sigma Aldrich. Germany	-29 mV	Tso et al. 2010
Titanium (IV) oxide nanopowder 99.5% rutile ~10 nm × 40 nm (TiO_2 rutile),Sigma-Aldrich, Schnelldorf, Germany.	-40.9 ± 3 mV	Bihari et al. 2008.
Titanium (IV) oxide nanopowder 99.7% anatase Sigma-Aldrich, Schnelldorf, Germany.	-18.7 ± 0.4	Bihari et al. 2008.

The zeta potential values of all the TiO_2-NPs synthesized using the cell free supernatants of strains 4S1, 4S2, 4S3, 6S1 and 8S1 shown in Table 4.43 exhibited values outside the range of ±30 mV indicating the excellent stability of the nanoparticles in colloidal form with water at ambient conditions. The stability of the TiO_2-NPs synthesized using the bacterial isolates exhibited good stability and is comparable or better than the stability of TiO_2-NPs synthesized using various synthesis routes as shown in Table 4.43. The stability of the TiO_2-NPs colloids followed the order of 8S1>6S1> 4S3>4S2>4S1, with the zeta potential value of the 8S1-TiO_2-NPs being highly positive compared to the TiO_2-NPs synthesized using

other strains. The high positive zeta potential value of 8S1-TiO$_2$-NPs indicates the superior stability of these particles over other particles synthesized. The synthesized TiO$_2$-NPs have promising prospect in terms of applicability studies as they are found to be stable.

4.16.4 FTIR analysis of TiO$_2$-NPs

FTIR spectra of the TiO$_2$-NPs synthesized using the five isolated bacterial strains 4S1, 4S2, 4S3, 6S1 and 8S1 are shown in Figure 4.112 to Figure 4.116 respectively and it revealed the presence of certain functional groups along with the particles. The presence of these functional groups indicates that the TiO$_2$-NPs synthesized using the bacterial cell free culture supernatants must be encapsulated by moieties belonging to bacterial origin. Reports of bacterial TiO$_2$-NPs synthesis by various researchers suggest the presence of proteinaceous moieties capping the TiO$_2$-NPs. The FTIR analysis provides us details regarding the capping agents encapsulating the TiO$_2$-NPs being synthesized. The characteristic peak of TiO$_2$-NPs occurs at wave numbers ranging from 450 cm^{-1} to 750 cm^{-1}. The same is observed in the IR spectrum of the TiO$_2$-NPs synthesized from the bacterial isolates in the present study.
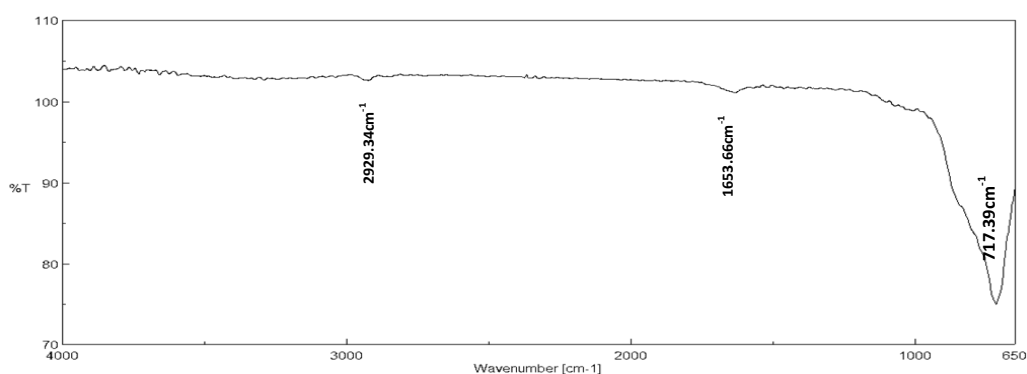
Figure 4.112 FTIR spectrum of TiO$_2$-NPs synthesized from bacterial isolate 4S1
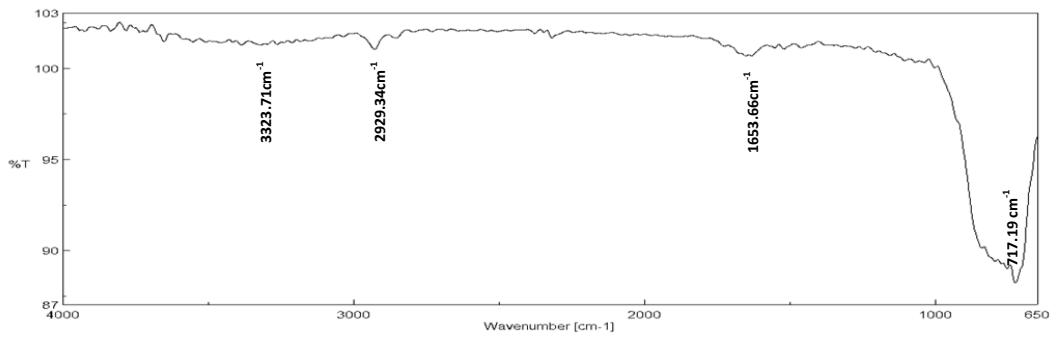
Figure 4.113 FTIR spectrum of TiO$_2$-NPs synthesized from bacterial isolate 4S2
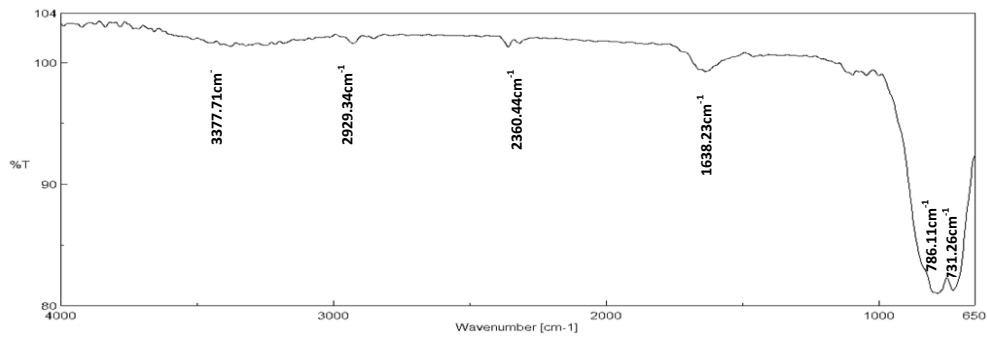
Figure 4.114 FTIR spectrum of TiO$_2$-NPs synthesized from bacterial isolate 4S3
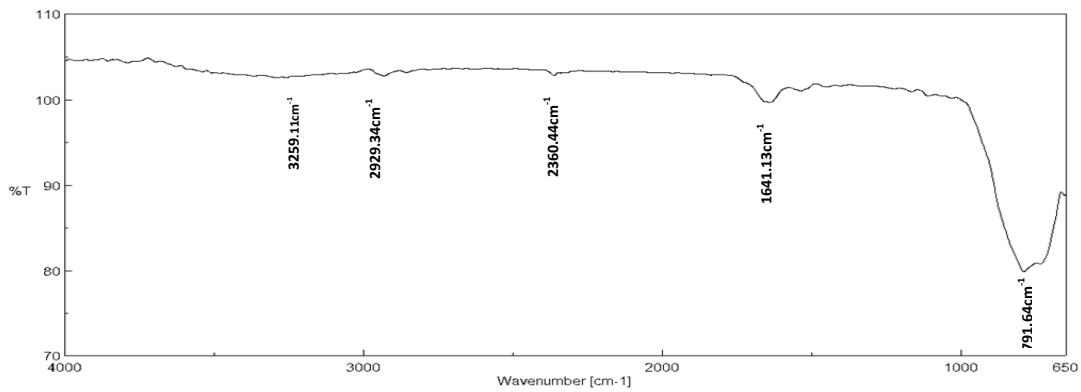
Figure 4.115 FTIR spectrum of TiO$_2$-NPs synthesized from bacterial isolate 6S1
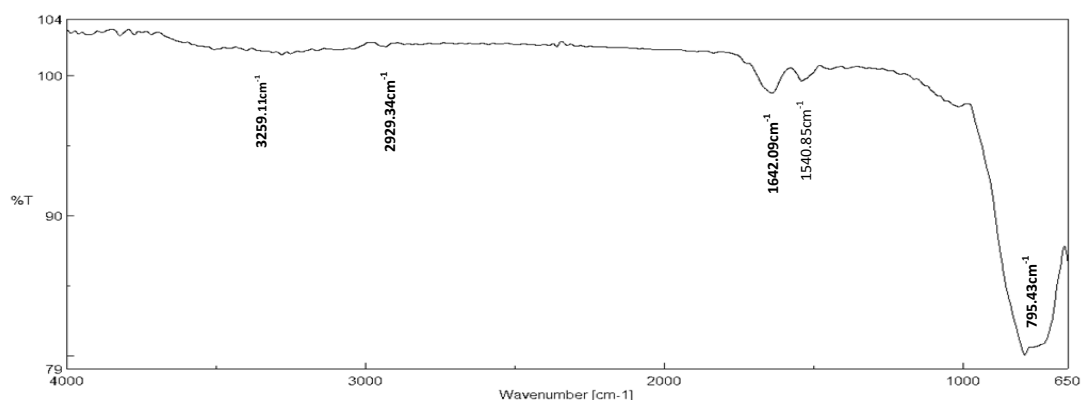
Figure 4.116 FTIR spectrum of TiO₂-NPs synthesized from bacterial isolate 8S1
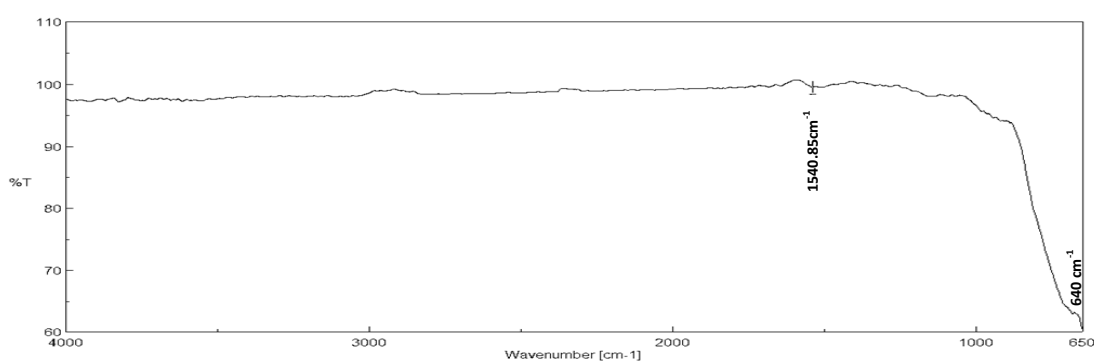
Figure 4.117 FTIR spectrum of Degussa P-25 TiO₂-NPs

Table 4.44 presents the wavenumbers of functional groups detected by FTIR analysis of TiO₂-NPs synthesized by the bacterial strains 4S1, 4S2, 4S3, 6S1 and 8S1.

Table 4.44 Wavenumbers of functional groups detected by FTIR analysis of TiO₂-NPs synthesized by the bacterial strains

TiO₂-NPs	Wavenumber of Peaks observed in FTIR
4S1	2929.34 cm^{-1}, 1653.66 cm^{-1}, 717.39 cm^{-1}
4S2	3323.71 cm^{-1}, 2929.34 cm^{-1}, 1653.66 cm^{-1}, 727.99 cm^{-1}
4S3	3377.71 cm^{-1}, 2929.34 cm^{-1}, 2360.44 cm^{-1}, 786.81 cm^{-1}, 731.26 cm^{-1}
6S1	3259.11 cm^{-1}, 2929.34 cm^{-1}, 2360.44 cm^{-1},1641.11 cm^{-1}, 791.63 cm^{-1}
8S1	3259.11 cm^{-1}2929.34 cm^{-1},1642.09 cm^{-1}, 1540.85 cm^{-1}, 795.49 cm^{-1}
Degussa P25	1540.85 cm^{-1}, 640 cm^{-1}

The TiO₂-NPs samples synthesized using the bacterial strains exhibited the main bands at 400-700 cm^{-1}, which are attributed to Ti-O stretching and Ti-O-Ti

bridging stretching modes (Yu et al. 2003; Peiró et al. 2001). The regions of 1400-1750 cm^{-1} are attributed to bending vibrations of O-H and N-H. The peaks occurring at other wavelengths such as 2929.34 cm^{-1}, 2380.44 cm^{-1} belong to the C=O and N-H vibrations due to the presence of amide and amine groups (Órdenes-Aenishanslins et al. 2014), the presence of these functional groups confirm that the TiO$_2$-NPs are encapsulated with proteinaceous moieties of bacterial origin. These bacterial moieties may serve as the capping agents and provide stability to the TiO$_2$-NPs synthesized. The presence of large number of protein moieties may not favour the photocatalytic activity of TiO$_2$-NPs synthesized as they may poison the photocatalytic sites on the surface of the TiO$_2$-NPs (Yu et al. 2003b).

The minor peaks occurring at around 3400 cm^{-1} and 1634 cm^{-1} in the IR spectra rises from the -OH scissoring bond of chemisorbed water, and the Ti-O-Ti stretching band that begins after 1000 cm^{-1} and below (Smith et al. 2015; Wang et al. 2009; Jia et al. 2008). The low intensity of the peaks belonging to the adsorbed H$_2$O molecules is also observed in Figure 4.117 of Degussa P25. Degussa P25 shows the peak belonging to adsorbed water molecules but the peak intensity is higher in the FTIR spectra belonging to 8S1-TiO$_2$-NPs indicating that these TiO$_2$-NPs can exhibit better photocatalytic activity than Degussa P25.

Considering the photocatalytic activity, it has been reported that when TiO$_2$-NPs are photoexcited, an electron-hole pair generates in TiO$_2$. The electrons tend to reduce the Ti^{+4} charged to Ti^{+3} state, but on the other hand, the generated hole reacts with the bridging site oxygen resulting in oxygen vacancy. Water molecules can heal these oxygen vacancies, producing absorbed OH groups which make the surface hydrophilic thereby increasing the photocatalytic activity of TiO$_2$-NPs (Watanabe et al. 1999).The intensity of peak around 1600cm^{-1} for the TiO$_2$-NPs synthesized using strains 4S1, 4S2, 4S3 and 6S1 is lower than that of 8S1 which may lead to decreased photocatalytic activity by these TiO$_2$-NPs.

The FTIR spectra of Degussa P25 (Figure 4.117) and 8S1-TiO$_2$-NPs are almost similar except the presence of peaks belonging to chemisorbed water molecules which are more in TiO$_2$-NPs synthesized using strain 8S1.

4.16.5 Determination of Band gap energy of TiO₂-NPs synthesized using the cell free bacterial supernatants

The term "band gap" refers to the specific minimum amount of energy for the transition of electrons from the valance band to the conduction band. In case of semiconductors and light active substances, it is very crucial to determine the band gap energy as it provides the information regarding the range of wavelength under which the photoactive substance performs best.

In case of semiconductor TiO₂-NPs the band gap has been associated with the photocatalytic activity in the UV or Visible region of light. Higher band gap energy of TiO₂-NPs indicates that they can absorb only at UV light region. In the case of anatase there is a consensus that the absorption edge is around 3.2 eV, associated with indirect transitions (Asahi et al. 2007, Hosaka et al. 1997; Hosaka et al. 1996) with rutile exhibiting band gap energy of 3.06 eV (Amtout and Leonelli 1995; Glassford and Chelikowsky, 1992; Pascual et al. 1978). Brookite is the least studied titania phase and experimental band gap energies ranging from 3.1 to 3.4 eV have been reported, both smaller and larger than the anatase band gap, and there appears to be no consensus on whether direct or indirect transitions dominate the optical response (Li et al. 2007; Koelsch et al. 2004).

The band gap energy of TiO₂-NPs was determined using the methodology presented in section 3.6.8 of Chapter 3. The UV-Vis absorbance spectra of the TiO₂-NPs showing the absorbance extinction wavelength are given in Figure 118 (a) to (e) for TiO₂-NPs synthesized using 4S1, 4S2, 4S3, 6S1 and 8S1 respectively and the band gap energy determined using Method A (Dharma and Pisal, Perklin Elmer, 2012) described in section 3.6.8 of Chapter 3 for TiO₂-NPs synthesized using the cell free supernatants are enlisted in Table 4.45. The Band gap energy along with the electron transitions of the TiO₂-NPs were also determined by the Method B described by Ghobadi et al. (2013) in section 3.6.8 of Chapter 3. The best linear fit for absorption spectra was obtained for m (index value) =2 indicating indirect allowed transitions, and the plots for TiO₂-NPs are shown in Figure 4.119 (a) to (e). The Band gap energy values determined using method A and method B are given in Table 4.45. The band gap energies obtained by both the methods were found to be closer and in agreement with each other.
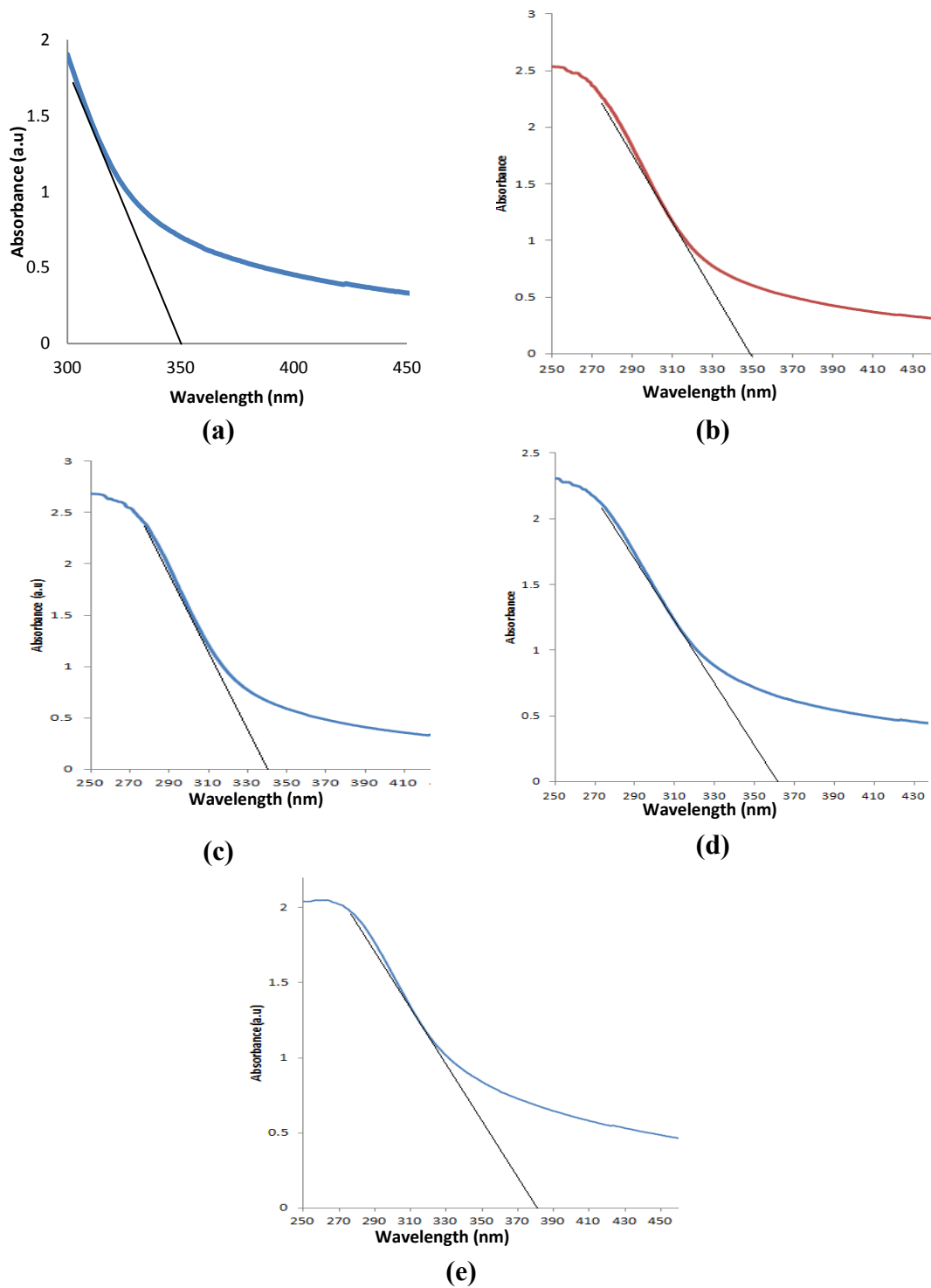
Figure 4.118 Determination of band gap energy using UV-Vis Spectra of TiO$_2$-NPs synthesized using bacterial strains (a) 4S1 (b) 4S2 (c) 4S3 (d) 6S1 (e) 8S1
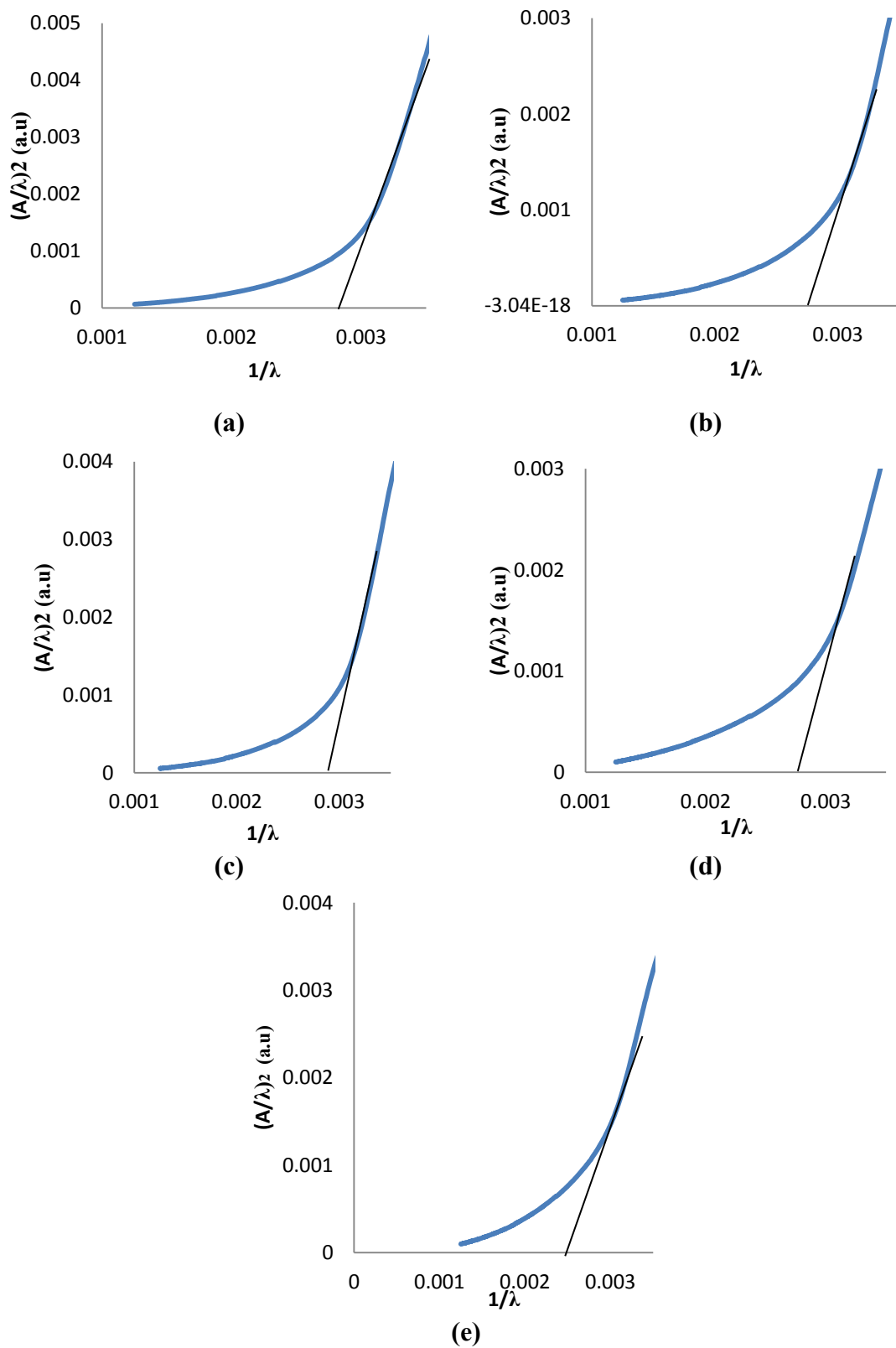
Figure 4.119 Absorption spectrum fitting plots of TiO₂-NPs synthesized using the cell free supernatant of bacterial strains (a) 4S1 (b) 4S2 (c) 4S3 (d) 6S1 (e) 8S1

Table 4.45 Band gap energy of TiO$_2$-NPs synthesized using the cell free supernatant of bacterial strains

Strain used for the synthesis of TiO$_2$-NPs	Method A	Method B
4S1	3.55 eV	3.534 eV
4S2	3.55 eV	3.58 eV
4S3	3.65 eV	3.657 eV
6S1	3.45 eV	3.43 eV
8S1	3.23 eV	3.19 eV

The band gap energy determined for TiO$_2$-NPs was found to range between 3.23 eV and 3.65 eV. Experimental band gap energies ranging from 3.1 to 3.4 eV have been reported for brookite, but there is disagreement on whether the optical response is attributable to direct or indirect transitions (DiPaola et al. 2013). However, in the present study, a mixture of brookite and anatase phase was found to be present in all the TiO$_2$-NPs and the optical response was determined to be indirect allowed transition.

The lowest band gap energy was observed for 8S1-TiO$_2$-NPs indicating that these TiO$_2$-NPs can absorb UV light radiation in an efficient manner.

8S1-TiO$_2$-NPs exhibit the characteristics of an ideal photocatalyst with lower band gap energy of 3.23 eV. The TiO$_2$-NPs contains a mixture of brookite phase and anatase phase as determined by XRD analysis (Section 4.16.1). They offer more hydrophilic surface area due the smaller size and the presence of surface adsorbed water molecules as observed through FTIR analysis (Section 4.16.4). Hence, the TiO$_2$-NPs synthesized in the present study were evaluated for their photocatalytic efficacy in the degradation of environmental pollutants.

4.16.7 EDS analysis of 8S1-TiO$_2$-NPs

EDS analysis of 8S1-TiO$_2$-NPs synthesized with 10 g/L of precursor salt with initial alkaline pH of 11 revealed the presence of elemental Titanium, phosphorous and carbon peaks as seen in Figure 4.120. The presence of carbon and phosphorous in the EDS spectrum suggest towards the presence of bacterial capping agents on the surface of the TiO$_2$-NPs which may impart stability to it.
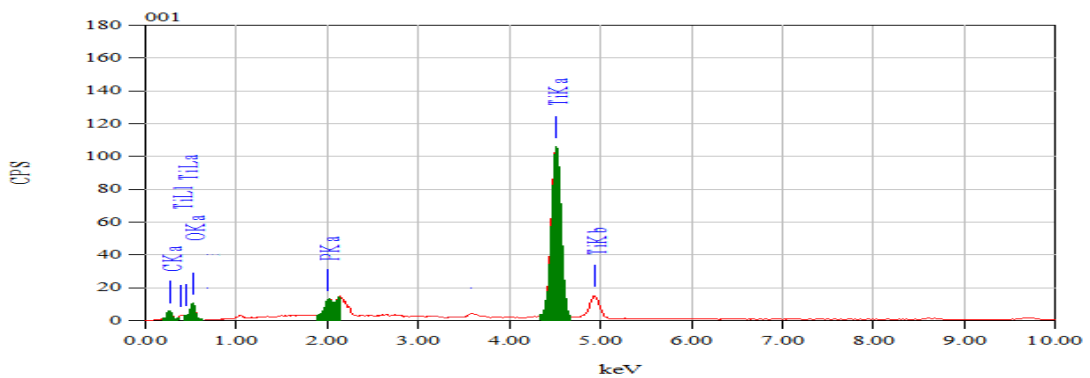
Figure 4.120: EDS spectra of 8S1-TiO₂-NPs synthesized using the synthesis mixture containing the cell free culture supernatant of bacterial strain 8S1 and 10 g/L precursor salt at pH 11.

4.16.8 TEM analysis of 8S1-TiO₂-NPs

The TEM analysis of the TiO₂-NPs in Figure 4.121 revealed the presence of small TiO₂-NPs, almost quasi spherical shaped with an average size of around 4.2 nm. The particles seem to be embedded in a translucent matrix which can be attributed to the presence of capping agents of bacterial origin.
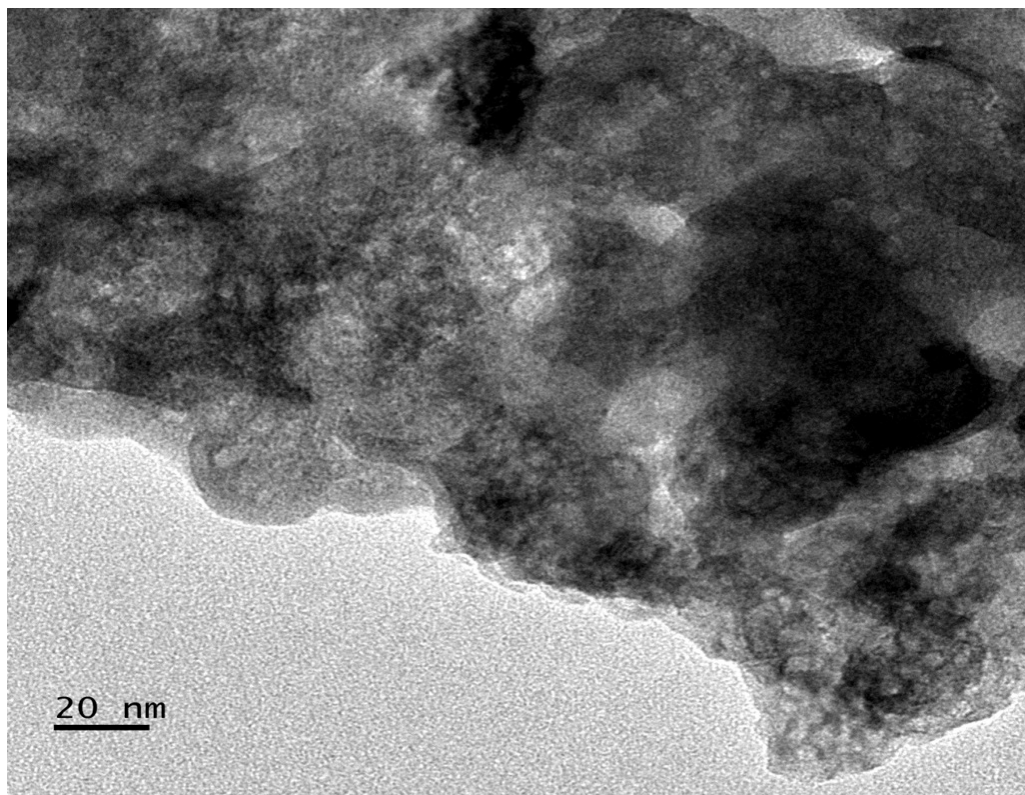
Figure 4.121 TEM analysis of TiO₂-NPs synthesized using strain 8S1

4.17 Photocatalytic activity of TiO$_2$-NPs

The construction of TiO$_2$ nano-structures with interesting morphologies and properties has recently attracted considerable attention and many TiO$_2$ nanostructural materials have been fabricated and used for photocatalysis applications (Choi et al. 2007; Joo et al. 2005; Li et al. 2004; Nagaveni et al. 2004; Xu et al. 2002). Section 4.14.1 showed that TiO$_2$-NPs could be synthesized using the cell free culture supernatants of the isolates 4S1, 4S2, 4S3, 6S1 and 8S1.The photocatalytic activity of these bacterial based TiO$_2$-NPs were tested in terms of photocatalytic degradation of two model compounds; AB 129 dye and RBB dye. The photocatalytic activity was also compared with that of commercially available Degussa P25 nanoparticles.

4.17.1 Photocatalytic activity of TiO$_2$-NPs synthesized using the cell free culture supernatant of isolated bacterial strains

The TiO$_2$-NPs synthesized using the cell free supernatant of each of the bacterial isolate 4S1, 4S2, 4S3, 6S1 and 8S1 were evaluated for their photocatalytic activity in the degradation of AB 129 dye and RBB dye as model compounds under visible and UV light irradiation according to the methodology described in section 3.8.2.1 of Chapter 3. Two lamps of 18W power each were used in these experiments with the total power of 36W for both UV and visible light irradiation studies.

The time course variation of degradation of AB 129 dye and RBB dye in presence of TiO$_2$-NPs synthesized using the cell free supernatants of five bacterial strains under UV light irradiation are presented in Figure 4.122 and Figure 4.123 for AB 129 and RBB dye respectively.
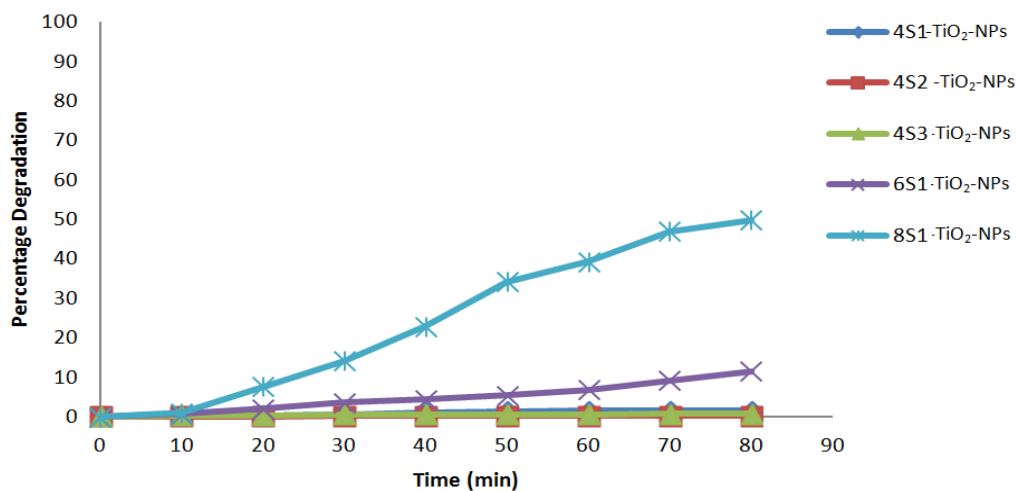
Figure 4.122 Percentage degradation of Acid Blue dye by TiO$_2$-NPs synthesized using the isolated strains under UV light irradiation. Conditions: UV lamp power =36 W, UV light intensity=5.85 mW/cm^2,Catalyst loading =0.1 g /L, initial pH=6.5, Initial dye concentration=10 mg/L

Figure 4.122 shows that 8S1-TiO$_2$-NPs were able to successfully degrade 50% of 10 mg/L of AB 129 dye in the time duration of 80 min. The TiO$_2$-NPs synthesized using 6S1 could bring about 11.5% degradation of AB 129 within 80 min of the reaction time. However, the dye could not be degraded in the presence of TiO$_2$-NPs synthesized using the cell free supernatants of the other strains. The initial rate of AB 129 dye degradation with 8S1-TiO$_2$-NPs was calculated to be 0.3855 mg/L/min with 10 mg/L initial dye concentration.
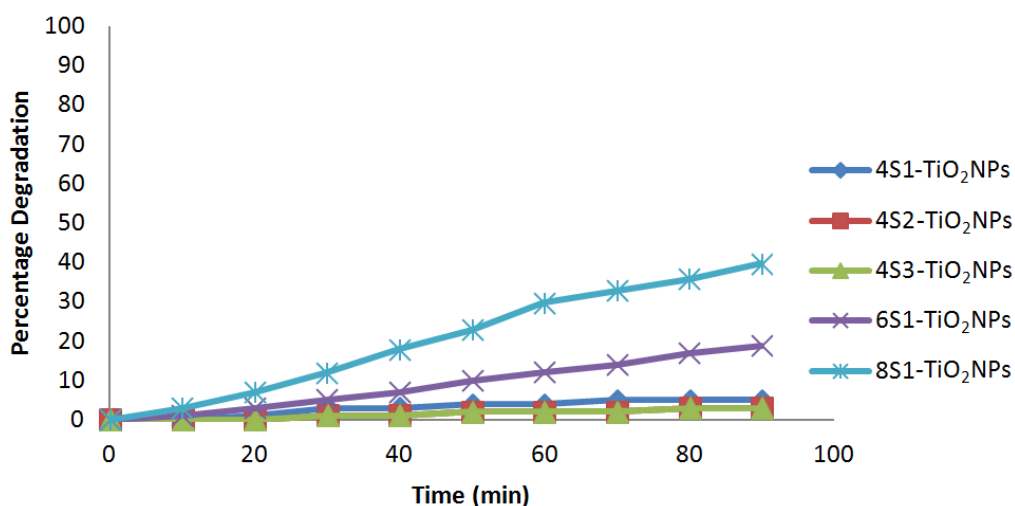
Figure 4.123 Percentage degradation of RBB dye by TiO$_2$-NPs synthesized using the cell free supernatant of the isolated strains under UV light irradiation Conditions: UV lamp power =36 W ,UV light intensity=5.85 mW/cm^2, Catalyst loading =0.1 g /L, initial pH=7.5, Initial dye concentration= 10 mg/L

The time course variation of degradation of RBB dye in the presence of TiO_2-NPs synthesized using the cell free supernatants of five bacterial strains under UV light irradiation is presented in Figure 4.12 Under UV light irradiation, around 39.6 % of RBB dye of 10 mg/L concentration was successfully degraded in the time duration of 90 min in the presence of 8S1-TiO_2-NPs whereas around 18.8 % degradation of RBB could be achieved in the presence of TiO_2-NPs synthesized using 6S1 within the same reaction time period. The photocatalysis using TiO_2-NPs synthesized using the cell free supernatants of other strains did not result in noticeable degradation of RBB dye. The rate of RBB dye degradation with 8S1-TiO_2-NPs was found to be the highest compared to that by other strains and the initial rate was calculated to be 0.297 mg/L/min. Low initial rate of degradation of 0.099 mg/L/min was achieved in the presence of TiO_2-NPs synthesized from strain 6S1. The TiO_2-NPs synthesized from strains 4S1, 4S2 and 4S3 did not show any photocatalytic degradation of RBB dye.

These studies reveal that the TiO_2-NPs synthesized using the cell free supernatants of the strains 8S1 and 6S1 possess photocatalytic activity under UV light irradiation and the activity of 8S1-TiO_2-NPs were superior to those synthesized using 6S1. However, the TiO_2-NPs synthesized using other strains did not show any noticeable UV photocatalytic activity.

The time course variations of degradation of the dyes in the presence of TiO_2-NPs synthesized using the cell free supernatants of five bacterial strains under visible light irradiation are presented in Figure 4.126 and Figure 4.127 for AB 129 and RBB dye respectively.
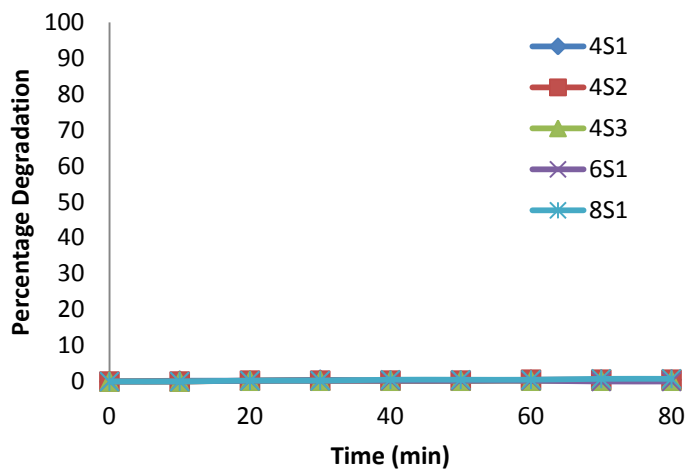
Figure 4.124. Percentage degradation of AB129 dye by TiO$_2$-NPs synthesized using the cell free supernatant of strains 4S1, 4S2, 4S3, 6S1 and 8S1 under visible light irradiation. Conditions: Visible lamp power= 36 W, Visible light intensity= 84.7X10^3 Lux, Catalyst loading= 0.1 g/L, Initial pH= 6.5, Initial dye concentration= 10 mg/L
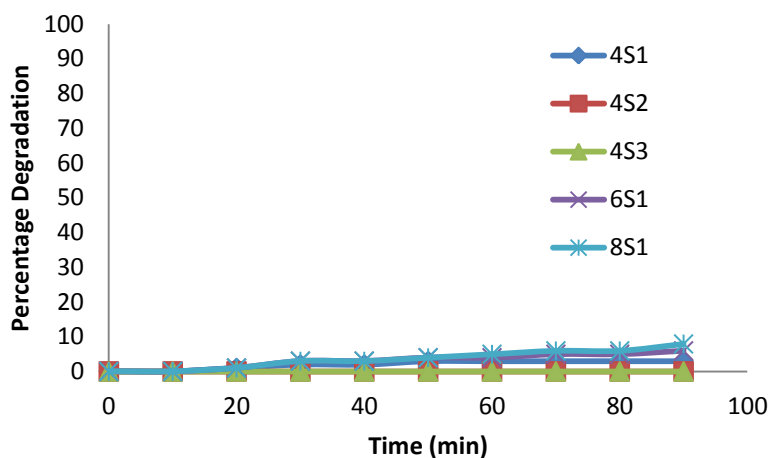
Figure 4.125. Percentage degradation of RBB dye by TiO$_2$-NPs synthesized using the cell free supernatant of strains 4S1, 4S2, 4S3, 6S1 and 8S1 under visible light irradiation. Conditions: Visible lamp power= 36 W, Visible light intensity=84. 7X10^3 Lux, Catalyst loading= 0.1 g/L, Initial pH= 6.5, Initial dye concentration= 10 mg/L

As observed in Figure 4.124, no noticeable degradation of AB 129 dye occurred under visible light irradiation in the presence of TiO$_2$-NPs that were synthesized using the cell free supernatants of bacterial strains 4S1, 4S2, 4S3, 6S1 and 8S1. Degradation of RBB dye under visible light irradiation in the presence of TiO$_2$-

NPs that were synthesized using the cell free supernatants of the isolated bacterial strains were only marginal (Figure 4.125). These results prove that these TiO_2-NPs do not possess appreciable visible light photocatalytic activity.

8S1-TiO_2-NPs exhibited better photocatalytic degradation of the dyes under low intensity UV light and visible light compared to the TiO_2-NPs synthesized using strain 6S1. However, the photocatalytic efficiency of 8S1-TiO_2-NPs was higher when illuminated by UV light, but only marginal under visible light.

As TiO_2 is illuminated with a photon of energy lesser than its band gap width, electron and hole formation does not take place to initiate the photocatalytic degradation. In the present study, the photon energy of visible light is not adequate for the electron-hole formation, as band gap energy of TiO_2-NPs as presented in Table 4.40 of section 4.15.6 is above 3.2 eV suggesting that these catalysts can be activated only by the shorter wavelength UV light. Thus, the TiO_2-NPs synthesized using the cell free supernatants of the five isolated bacterial strains failed to exhibit considerable visible light photocatalytic activity. Hence, these TiO_2-NPs as synthesized are not suitable for use as photocatalyst under visible light.

The higher photocatalytic activity of brookite phase can be attributed to the bond length of Ti- O and O-O of 1.87-2.04 A° and 2.49 A° which is the longest than that of anatase and rutile phase; thereby decreasing the degree of orbital interactions within a bond with increasing bond distance. The degree of photocatalytic activity of TiO_2 is proportional to the number of electrons emitted by ultraviolet energy.

The probability of electron emission is strongly related to the electron density near the Fermi energy. Density of states (DOS) value of the Fermi energy in brookite-type TiO_2 is bigger than that in rutile or even in anatase phase. The photocatalytic efficiency of the material depends on the crystallinity of the material, surface area, shape of the particle, band gap, and the amount of electrons around the Fermi energy. The DOS of brookite phase suggests that the photocatalytic efficiency of highly crystallized brookite phase TiO_2 might be better than that of anatase when the structural conditions are similar (Young and Park et al. 2009). As observed in Figure 4.102 to Figure 4.106 depicting the XRD patterns of the nanoparticles, the brookite and anatase phase intensities of 8S1-TiO_2-NPs are the highest that resulted in better

photocatalytic activity. Thus, it can be noted that 8S1-TiO$_2$-NPs exhibits promissory criterion for photocatalytic activity under UV light.

The percentage degradation achieved with TiO$_2$-NPs synthesized using 6S1 was not very appreciable even under UV light. The studies on photocatalytic degradation AB 129 dye and RBB dye revealed that 8S1-TiO$_2$-NPs were able to photocatalytically degrade the dyes under UV light irradiation. However, maximum percentage degradation of only around 50% of AB 129 and 40% of RBB at initial concentrations of 10 mg/L could be achieved with the catalyst loading of 0.1 g/L when 8S1-TiO$_2$-NPs were used as photocatalysts under UV light irradiation. Thus, further studies were conducted to improve the photocatalytic degradation of the dyes by employing a reactor model with better design and high power UV light source to increase the light absorption.

4.18 Photocatalytic degradation of AB 129 dye and RBB dye under irradiation with 80 W UV lamp in immersion well quartz reactor using 8S1-TiO$_2$-NPs

The rate of photocatalysis depends on the intensity of the light reaching the reaction mixture. The intensity of light reaching the reaction mixture may be enhanced by using high power UV lamps and by using a quartz surface between the light source and the reaction mixture. Thus to improve the efficiency of photocatalysis by increasing the intensity of UV light, the high power UV lamps mounted in a quartz immersion well were employed for photocatalysis of dyes using the 8S1-TiO$_2$-NPs.

As determined in the previous section, 8S1-TiO$_2$-NPs were able to degrade AB129 dye and RBB dye under low intensity UV light. Hence further studies on photocatalysis of the two model dyes was carried out with 8S1-TiO$_2$-NPs in an immersion well quartz reactor illuminated with 80 W medium pressure UV lamp as described in section 3.8.2.2 of Chapter 3. Figure 4.126 shows the time course degradation of AB 129 dye in the quartz reactor. It can be observed that high intensity UV lamp could bring about efficient degradation of the dye of about 99.74% with an initial degradation rate of 0.95 mg/L/min. Experiments were also performed (i) under UV light irradiation in the absence of TiO$_2$-NPs and (ii) in the absence of light with the TiO$_2$-NPs, according to the methodology described in section 3.8.2.2 of Chapter 3. Dye removal was not observed under these conditions as seen in Figure 4.126 which

indicated that no appreciable photodegradation or dye adsorption on TiO_2 surface occurred. Dye was efficiently removed under irradiation with 80W UV lamp and in the presence of TiO_2-NPs which confirmed that the process of degradation of dyes occurred by photocatalysis. Similar results were observed in the degradation of RBB dye by irradiation under high UV lamp in the presence of TiO_2-NPs.
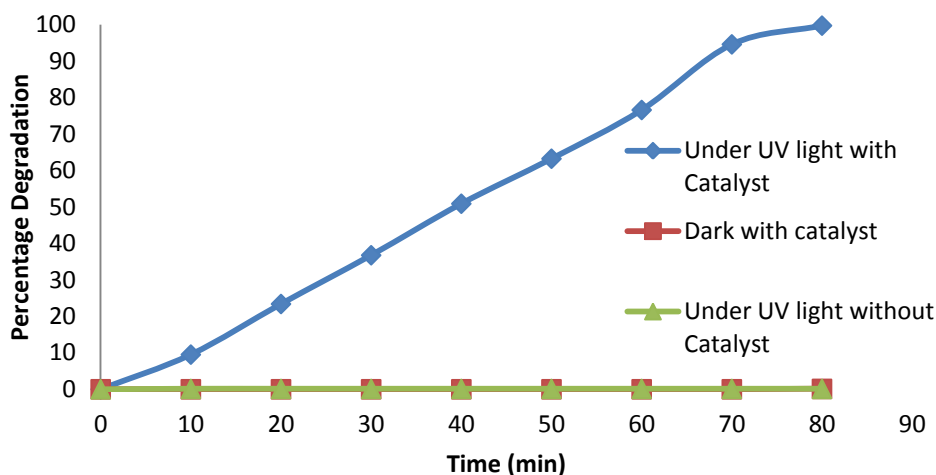
Figure 4.126.Photocatalytic degradation of AB 129 by 8S1-TiO₂-NPs in immersion well quartz reactor using 80 W UV lamp. Conditions: UV lamp power=80 W; UV light intensity=11.2 mW/cm², Catalyst loading= 0.1 g/L, Initial pH= 6.5, Initial dye concentration= 10 mg/L

Figure 4.127 shows the photocatalytic degradation of RBB dye in immersion well quartz reactor using 80 W UV lamp.
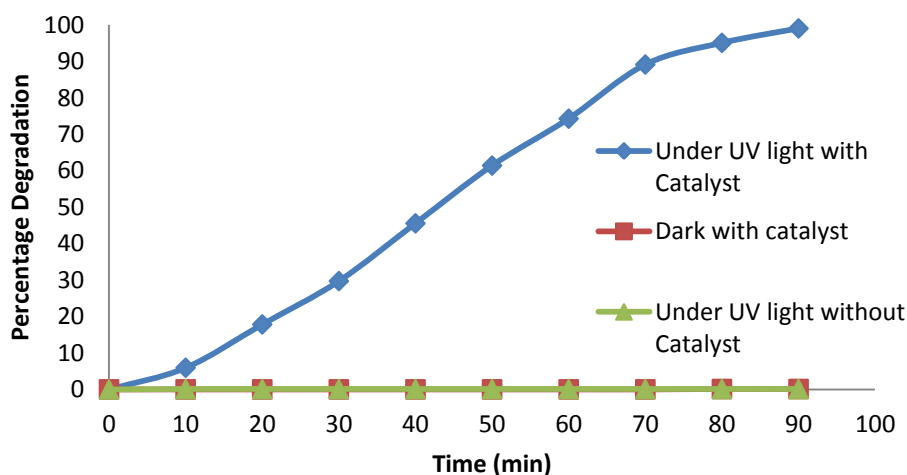
Figure 4.127 Photocatalytic degradation of RBB dye by 8S1-TiO₂-NPs in immersion well quartz reactor using 80 W UV lamp. Conditions; UV light intensity=11.2 mW/cm²,Catalyst loading= 0.1 g/L, Initial pH= 7.5, Initial dye concentration= 10m g/L

The TiO$_2$ catalysts synthesized using the cell free supernatant of bacterial strain 8S1 were able to degrade 99% of RBB dye in 90 min with an initial rate of 0.891 mg/L/min proving that high intensity UV light could facilitate the efficient degradation RBB dye. Experiments performed under dark and in the absence of catalyst revealed that no photolytic degradation or adsorption of the dye contributed onto the dye removal process by TiO$_2$-NPs.

Thus from the photocatalysis studies it can be determined that 8S1-TiO$_2$-NPs are able to efficiently degrade both the model dyes under high intensity UV light with greater than 99% degradation in 80-90 min. Hence, further studies were conducted under irradiation with 80 W UV lamps in quartz reactor. Further the suitability of these photocatalysts for degradation of dyes from effluents at higher concentrations was investigated.

4.18.1 Effect of initial dye concentration on photocatalytic degradation of the dyes in immersion well quartz reactor using 8S1-TiO$_2$-NPs

As industrial wastewaters may contain dyes at varying concentration it is important to study the effect of initial dye concentration on photocatalytic degradation of the dyes.

The effect of initial dye concentration on the photocatalytic degradation was studied by conducting experiments with AB-129 and RBB dyes in immersion well quartz reactor illuminated using 80 W UV lamp at initial dye concentrations of 10 mg/L and 25 mg/L with catalyst loading of 0.1 g/L. The initial pH of the reaction mixture was unadjusted and was found to be 6.5 and 7.5 for AB 129 and RBB dyes respectively. The effect of initial dye concentration on photocatalytic degradation of AB129 dye and RBB dyes are presented in Figure 4.128 and Figure 4.129 respectively.

As seen in Figure 4.128 increase in the initial concentration from 10 mg/L to 25 mg/L of AB129 dye caused the reduction in the rate of the photocatalytic degradation with decrease in initial rate from 0.951 mg/L/min to 0.186 mg/L/min respectively. 99.74 % degradation of 10 mg/L AB 129 dye was achieved within 80 min of the reaction duration with 0.1 g/L catalyst loading, whereas only 45% degradation of 25 mg/L of the dye was achieved with the same catalyst loading.
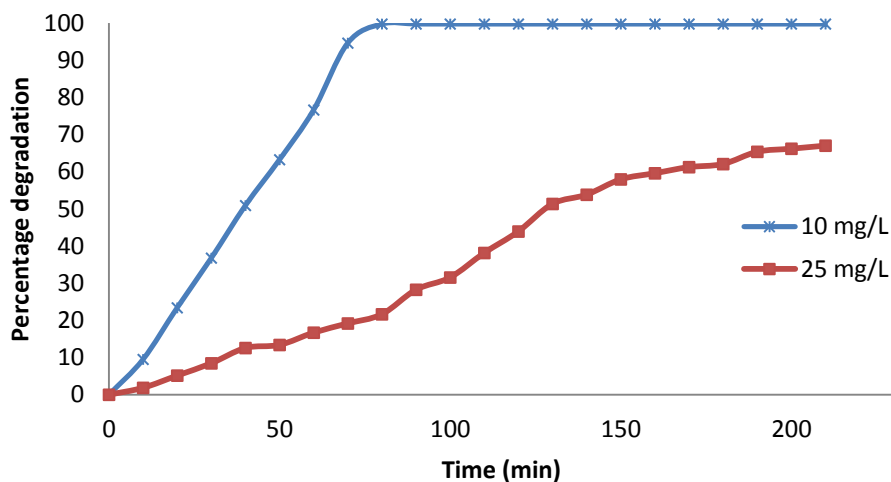
Figure 4.128 Photocatalytic degradation of AB129 dye by TiO₂-NPs synthesized using the cell free supernatant of strain 8S1 in immersion well quartz reactor using 80 W UV lamp. Conditions; UV light intensity=11.2 mW/cm², Catalyst loading= 0.1 g/L, Initial pH= 6.5

Figure 4.129 shows the effect of initial dye concentration on photocatalytic degradation of RBB dye.
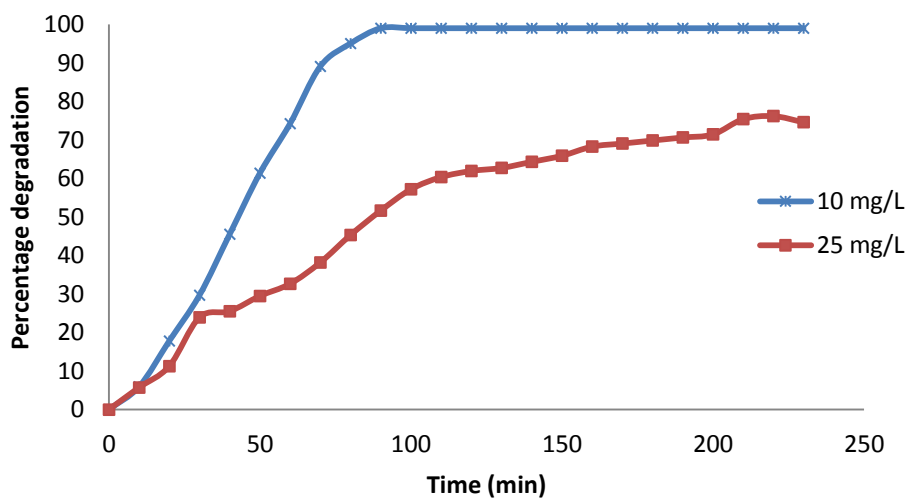
Figure 4.129 Photocatalytic degradation of RBB dye by TiO₂-NPs synthesized using the cell free supernatant of strain 8S1in immersion well quartz reactor using 80 W UV lamp. Conditions; UV light intensity=11.2 mW/cm²,Catalyst loading= 0.1 g/L, Initial pH= 7.54

As seen in Figure 4.129 increase in the initial concentration from 10 mg/L to 25 mg/L of RBB dye caused the reduction in the initial rate of the photocatalytic degradation from 0.891 mg/L/min to 0.5645 mg/L/min. 99.09% degradation of 10

mg/L RBB dye was achieved within 100 min of the reaction duration while only 57.22% was obtained with 25 mg/L within the same time duration.

The decrease in the rate of photocatalytic degradation with increase in initial concentration of the dye can be attributed to the reduction in the generation of OH^- radicals on the surface of catalyst as the active sites on the surface of the catalyst are covered with the dye molecules as the initial dye concentration is increased (Kashif and Ouyang, 2009). The catalyst loading being the same in either of the cases, the available active photocatalytic sites on the TiO_2 surface remain the same, while the number of dye molecules in the reaction mixture increases with increase in concentrations. Owing to lower active sites, the dye molecules need to compete for the sites, thus photocatalytic degradation rate decreases with the increase in dye concentration (Shet and Shetty, 2015).

Another possible cause for decrease in the rate of degradation could be the UV- shielding effect of the dye. With a high initial concentration of the dye, the UV light entering the reaction mixture is absorbed by the dye molecules, limiting its penetration to the surface of the catalyst thus reducing the efficiency of the photocatalytic reaction (So et al. 2002; Grzechulska and Morawski, 2002; Mills et al. 1993). The irradiation intensity is much higher near to the irradiated side (reaction zone) where majority of the photocatalytic degradation occurs (Sakthivel et al. 2003). Increase in the initial dye concentration brings about retardation in the penetration of light thereby decreasing the degradation at sufficiently long distances from the reaction zone.

Thus from this study it can be concluded that as the initial concentration of dyes increases, the requirement of catalyst surface needed for the degradation also increases. Thus, further the effect of catalyst loading on the degradation of the dyes was studied.

4.18.2 Effect of catalyst loading on photocatalytic degradation of the dyes in immersion well quartz reactor using 8S1-TiO$_2$-NPs

Catalyst loading is one of the prime parameter that governs the rate of degradation in a photocatalytic reaction. To avoid unnecessary usage of excess catalyst and to ensure total absorption of light photons for efficient

photomineralization of the dye, the optimum amount of catalyst must be used. The loading of the catalyst used for the photocatalytic degradation of the dye is dependent on the concentration of the initial concentration of the dye (Herrmann, 1999).

The effect of catalyst loading on photocatalytic degradation of the dyes was studied using 8S1-TiO$_2$-NPs under irradiation with 80W UV lamp in immersion well quartz reactor. Figure 4.130 shows the percentage degradation of 25 mg/L of AB 129 dye and Figure 4.131 shows the percentage degradation of 25 mg/L RBB dye with different catalyst loadings of 0.1 g/L, 0.25 g/L and 0.5 g/L of 8S1-TiO$_2$-NPs.The pH of the solution was unadjusted.
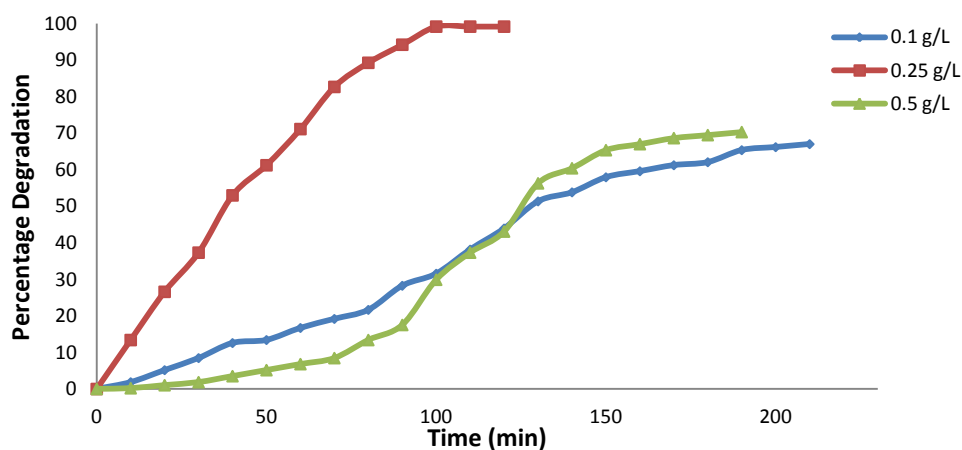
Figure 4.130. Effect of catalyst loading on the photocatalytic degradation of AB 129 by 8S1-TiO$_2$-NPs. Conditions; Initial pH= 6.5, Initial dye concentration= 25 mg/L

The initial rate of degradation of AB 129 dye with 0.1 g/L, 0.25 g/L and 0.5 g/L of catalyst loading were found to be 0.0464 mg/L/min, 0.335 mg/L/min and 0.021 mg/L/min respectively. The initial rate of the degradation increased with the increase in catalyst loading from 0.1 g/L to 0.25 g/L and then decreased when the catalyst loading was increased to 0.5 g/L. The initial rate was the maximum at the catalyst loading of 0.25 g/L with AB 129 dye. 99% degradation of 25 mg/L AB129 dye with 0.25 g/L of catalyst loading occurred within 120 min of the reaction duration while only ~43% of degradation occurred with 0.1 g/L and 0.5 g/L of catalyst loading. Thus, the maximum degradation of AB129 was achieved with 0.25 g/L catalyst loading.

The effect of catalyst loading was also studied in the photocatalytic degradation of RBB dye and is shown in Figure 4.131.
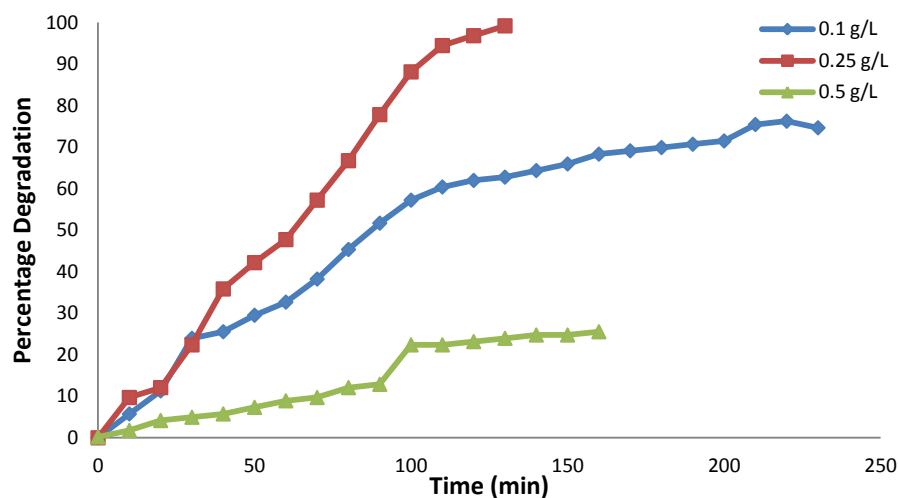
Figure 4.131. Effect of catalyst loading on the photocatalytic degradation of RBB dye by 8S1-TiO₂-NPs. Conditions; Initial pH= 7.5, Initial dye concentration= 25 mg/L

The initial rate of RRB dye degradation increased from 0.144 mg/L/min to 0.243 mg/L/min as the initial dye concentration increased from 0.1 g/L to 0.25 g/L. But with further increase in catalyst loading to 0.5 g/L, the initial rate of degradation decreased to 0.045 mg/L/min. Thus the highest initial rate of 25 mg/L RRB dye degradation occurred with catalyst loading of 0.25 g/L. 75% of RBB dye degradation was observed with a reaction time of 230 min with the catalyst loading of 0.1 g/L. However with the catalyst loading of 0.25 g/L, 99% of 25 mg/L RBB dye was degraded in the reaction period of 130 min. But further increase in catalyst loading to 0.5 g/L resulted in only 25.54% degradation in the time duration of 160 min.

Thus, from the studies on effect of catalyst loading it is observed that the efficiency of photocatalytic degradation of dyes in terms of rate of degradation increases with the increase in catalyst loading upto a certain value, but further increase in catalyst loading above this limit results in decreased degradation of the dyes. The highest initial rate of degradation and maximum percentage degradation at any time was observed with 0.25 g/L of catalyst loading in the degradation of both AB129 and RBB dyes. This can be explained in terms of the active sites present on the surface of the catalyst and the penetration of the light into the reaction mixture. With the increase in catalyst loading the number of active sites available for the degradation of dye molecules increase, leading to increase in rate of electron hole generation and hydroxyl radical formation. This enhances the rate of degradation of

303

the dyes. However, further increase in catalyst loading to 0.5 g/L resulted in decrease in the degradation of the dyes. The decrease in the degradation rate with increased catalyst loading is said to occur due to deactivation of activated catalyst by collision with ground state catalyst (Neppolian et al. 2002).The availability of active sites increases with the increase in the catalyst loading however the penetration of light decreases causing shrinkage in the photoactivated reaction volume (Konstantinou and Albanis, 2004; Neppolian et al. 2002). Thus, the decrease in the degradation rates can be rationalized in terms of availability of active sites on catalyst surface and the light penetration of photoactivating light into reaction mixture. At very high catalyst loading, agglomeration of the catalyst may also take place which makes the active sites unavailable for the catalysis (So et al. 2002; Lea and Adesina, 1998).The optimum catalyst loading depends on the geometry, working conditions of the photoreactor and the type of UV-lamp (power and wavelength). Thus owing to higher initial rates and the maximum percentage degradation obtained at the end of fixed time period of irradiation as compared to other catalyst loadings, the optimum catalyst loading were found to be 0.25 g/L for degradation of 25 mg/L of AB 129 and RBB dyes in the immersion well quartz reactor with 80W UV lamp.

From these studies, it was found that for degradation 25 mg/L dye, a catalyst loading of 0.25 g/L was the optimum based on maximum degradation. Thus, the dye to catalyst loading ratio of 1:10 is favourable for the degradation of AB 129 and RBB dyes. This ratio is determined by the synergetic effect of available active sites for the dye molecules present in the reaction mixture, and the light penetration effect. Further the effect of initial dye concentration on the degradation of the dye was studied, while keeping the dye to catalyst ratio constant at 1:10. Thus, the photocatalytic degradation of AB 129 dye and RBB dye using 8S1-TiO$_2$-NPs was carried out in the immersion well reactor according to the methodology described in Section 3.8.2.3 of Chapter 3. Experiments were performed with dye concentration of 50 mg/L and catalyst loading of 0.5g/L. Thus, the dye to catalyst ratio was maintained at 1:10 while the initial concentration of the dye was doubled. The initial pH of the reaction medium was unadjusted (6.5 for AB 129 dye and 7.5 units for RBB dye).

Figure 4.132 shows the comparison of the photocatalytic degradation of 25 mg/L and 50 mg/L AB 129 dye under optimum dye to catalyst loading ratio of 1:10.
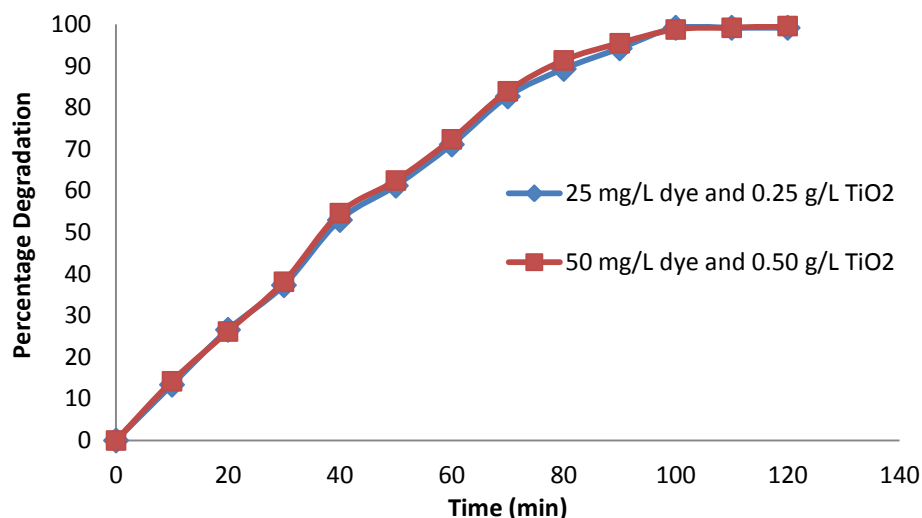
Figure 4.132 Effect of increase in initial dye concentration at fixed dye to catalyst ratio on the degradation of AB 129 dye using 8S1-TiO₂-NPs with 1:10 dye to catalyst ratio, Initial pH= 6.5

As seen in Figure 4.132, the percentage degradation at any time during the photocatalysis were the same with both 25 mg/L and 50 mg/L dye concentration. Almost complete degradation of the dye could be achieved in 120 minute in both the cases. Similar results were observed in Figure 4.133 showing the comparison of the photocatalytic degradation of 25 mg/L and 50 mg/L RBB dye under optimum dye to catalyst loading ratio of 1:10. Almost complete degradation of the dye could be achieved in 130 minute in both the cases. It indicates that, when optimal dye to catalyst ratio was provided, the active sites available for dye degradation on the catalyst are just appropriate for the degradation of the dye molecules with a fast rate. The dye molecules need not compete for the bare active sites and the probability of their collision with the active sites is the same even when the dye concentration was doubled owing to doubling of the catalyst loading. It also implies that the effects of hindrance to light penetration by increased catalyst loading or increase in dye concentration are not dominant. The possibility of aggregation of the catalyst particles owing to the presence of large number of particles in the given volume is also minimal. If the hindrance to light penetration effect or catalyst particle aggregation had occurred, it would have led to decreased rate of photocatalysis with 50 mg/L dye concentration, as in this case both the catalyst loading and dye concentrations doubled. The similar rate of photocatalysis with both 25 mg/L and 50 mg/L dye indicates that the provision of enough number of active sites for degradation of the

dyes is the governing factor. However, there may be a limiting dye concentration and catalyst loading condition above which light penetration effects or particle aggregation effects may become dominant.
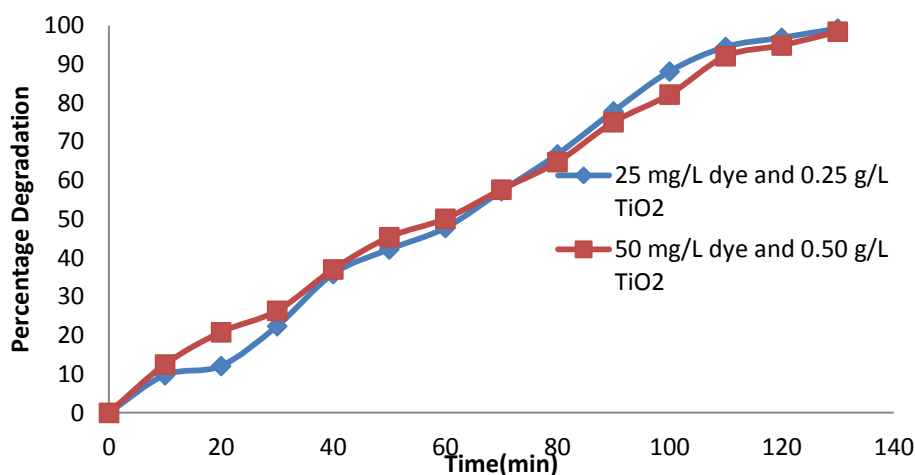
Figure 4.133. Effect of increase in initial dye concentration at fixed dye to catalyst ratio on the degradation of RBB dye using 8S1-TiO$_2$- NPs with 1:10 dye to catalyst ratio, Initial pH= 7.54

From these studies it may be concluded that maximum degradation of AB 129 and RBB using 8S1-TiO$_2$-NPs as photocatalysts can be achieved under unadjusted initial pH conditions with dye to catalyst ratio of 1:10 as the optimum.

4.18.3 Effect of initial pH of the reaction mixture on the photocatalytic degradation of the dyes with the 8S1-TiO$_2$-NPs

The pH of the reaction mixture plays multiple roles in the photocatalysis of dyes, as it influences the ionization state of the catalyst, reactants and reaction products (Fox and Dulay, 1993). pH changes of the reaction mixture can thus influence the adsorption of dye molecules onto catalyst, which is an important step for the photocatalytic oxidation to take place (Fox and Dulay, 1993). Acid-base properties of the metal oxide surfaces can have considerable implications upon their photocatalytic activity. The catalyst tends to agglomerate under acidic conditions and the surface area available for dye adsorption and photon absorption would be reduced resulting in lower degradation reaction rates (Konstantinou and Albanis, 2004; Bahnemann et al. 1994). At low pH conditions (Acidic), reduction by electrons in conduction band may play a very important role in the degradation of dyes. The positive holes act as the predominant oxidation species at acidic pH conditions

whereas at neutral or high pH levels hydroxyl radicals act as the major species (Sakthivel et al. 2003). Thus, the favourable pH condition required for maximum degradation of dyes is influenced by different opposing and contributing effects. However, the dominant phenomena for the given dye-catalyst system may govern the optimum pH condition. Thus, in the present work the effect of pH on the photocatalytic degradation of AB 129 and RBB dyes in the presence of 8S1-TiO$_2$-NPs was studied.

To study the influence of initial pH, photocatalysis experiments were conducted in quartz immersion well reactor with initial dye concentration of 25 mg/L and a catalyst loading of 0.25 g/L. The experiments were conducted at the initial pH conditions of acidic pH 3, alkaline pH 10 and the normal (unadjusted) pH (6.5 for AB 129 dye and 7.5 for RBB dye). Figure 4.134 shows the percentage degradation of 25 mg/L AB 129 dye with 0.25 g/L of catalyst loading at varying pH conditions.
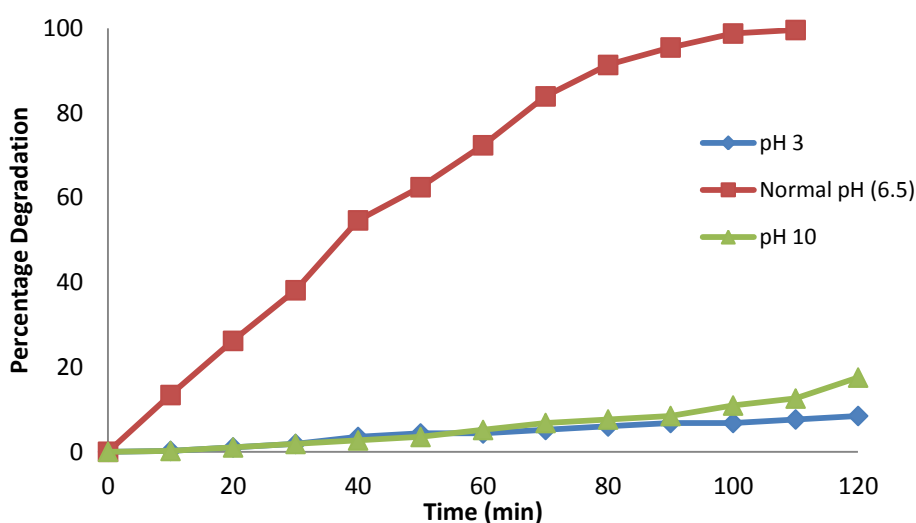
Figure 4.134. Effect of initial pH of the reaction medium on photocatalytic degradation of AB 129 dye using 8S1-TiO$_2$-NPs under irradiation with 80W UV lamp, Conditions: Catalyst loading= 0.25 g/L, Initial dye concentration= 25 mg/L
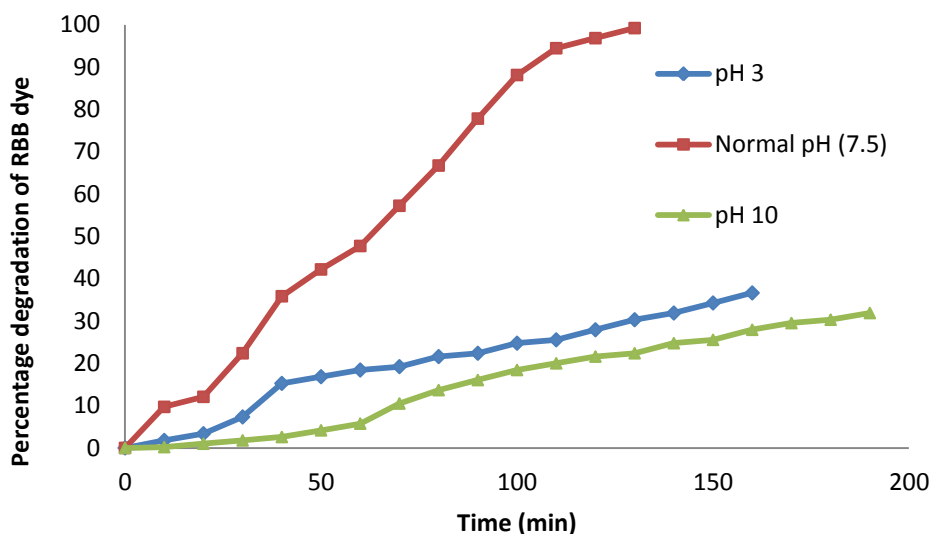
Figure 4.135. Effect of initial pH of the reaction medium on photocatalytic degradation of RBB dye using 0.25 g/L of 8S1-TiO₂-NPs catalyst loading using 80W UV lamp, Conditions: Catalyst loading= 0.25 g/L, Initial dye concentration= 25 mg/L

As seen in Figure 4.134, the unadjusted pH of 6.5 units for AB 129 dye gave the highest degradation of 99% within time duration of 110 min with an initial reaction rate of 0.335 mg/L/min. As seen in Figure 4.135, the initial rate of the degradation RBB dye with initial unadjusted condition of 7.5 and catalyst loading of 0.25 g/L was determined to be 0.243 mg/L/min. Maximum degradation of 99% RBB was achieved within a time period of 130 min.

This can be attributed to the optimal interaction of the dye molecules and the surface of the catalyst due to the reduction in the Coulombic charges under pH 6.5 or pH 7.5 resulting in higher degradation rate of AB 129 dye and RBB dyes respectively.

The acidic pH of 3 units with an initial reaction rate of 0.00515 mg/L/min resulted in lower percentage degradation of 17.5% in 120 min indicating that high acidic pH condition was not favourable for the degradation of AB 129 dye. Similarly, 36.63% of RBB dye was degraded in the time duration of 160 min with an initial reaction rate of 0.04455 mg/L/min. Thus, it can be seen that the photocatalysis rate decreased as the initial pH was reduced from the unadjusted condition (near neutral) to acidic pH of 3.As reported by Bahnemann et al. (1994) and Konstantinou and Albanis, (2004) the reduction in the photocatalysis under acidic initial pH of the

solution can be attributed to the decrease in the availability of the surface area of the catalyst due to agglomeration.

Alkaline initial pH condition of 10 units of the reaction mixture also resulted in lower percentage of dye degradation of 8.45% in 120 min (Figure 4.134) with an initial rate of reaction of 0.02577 mg/L/min for AB129 and an initial degradation rate of 0.01238 mg/L/min resulting in only 32% degradation of RBB dye degradation within a time duration of 190 min (Figure 4.1375). Thus lowest degradation of dyes were achieved under alkaline initial pH conditions indicating that alkaline pH conditions of the reaction medium is unsuitable for the photocatalytic degradation of RBB dye. In alkaline solution OH$^{\bullet}$ are easily generated by the oxidation of more hydroxide ions available on the surface of the catalyst (Shourong et al. 2007, Conçalves et al. 1999; Galindo et al. 2000). This can lead to an increase in the degradation. However in initial alkaline pH of the reaction mixture, Coulombic repulsion between the negative charged surface of photocatalyst and the hydroxide anions could hinder the formation of OH$^{\bullet}$ radicals and bring about a decrease in the photocatalysis (Konstantinou and Albanis, 2004).

Thus from this study of effect of initial pH of the reaction mixture on degradation of AB 129 dye and RBB dyes, it was found that maximum degradation of AB 129 dye was observed at the normal (unadjusted) pH of 6.5 and that of RBB was observed at the normal (unadjusted) pH of 7.5.

Similar reports pertaining to maximum dye degradation at normal pH of (6-7) have been reported by Poulios and Aetopoulou (1999) and Tang et al. (1997) in their studies on degradation of AB 129 and RBB dyes respectively using Degussa P25 as the catalyst. They have also observed a decrease in the degradation rate at acidic and alkaline pH. Also the pH of the reaction mixture can be related with changes in the specification of the dye causing protonation or deprotonation of the dye, which in turn changes its adsorption characteristics and redox activity (Neppolian et al. 2002).

This study pertaining to the effect of initial pH of the reaction mixture on the photocatalytic degradation of both the model dyes proves that normal (unadjusted) initial pH (AB 129 dye -6.5 and RBB -7.54) resulted in the highest dye degradation in comparison to that of acidic (pH 3) and alkaline pH (pH 11) conditions, thus proving

that near neutral pH of the mixture may be considered favourable for the degradation of AB129 and RBB dyes using 8S1-TiO$_2$ photocatalyst.

4.19 Comparison of photocatalytic activity of 8S1-TiO$_2$-NPs and Degussa P25 in terms of degradation of dyes

The efficacy of 8S1-TiO$_2$-NPs as photocatalysts was compared with that of commercially available TiO$_2$ catalyst (Degussa P25) in terms of photocatalytic degradation of AB129 and RBB dyes under UV light irradiation. The photocatalysis experiments were conducted in a quartz immersion well reactor with unadjusted pH condition and at the optimum dye to catalyst ratio of 1:10 as obtained from the studies reported in earlier sections.

Figure 4.136 shows the degradation of 50 mg/L of AB129 dye under optimum dye to catalyst loading of 1:10 using 8S1-TiO$_2$-NPs and Degussa P25.
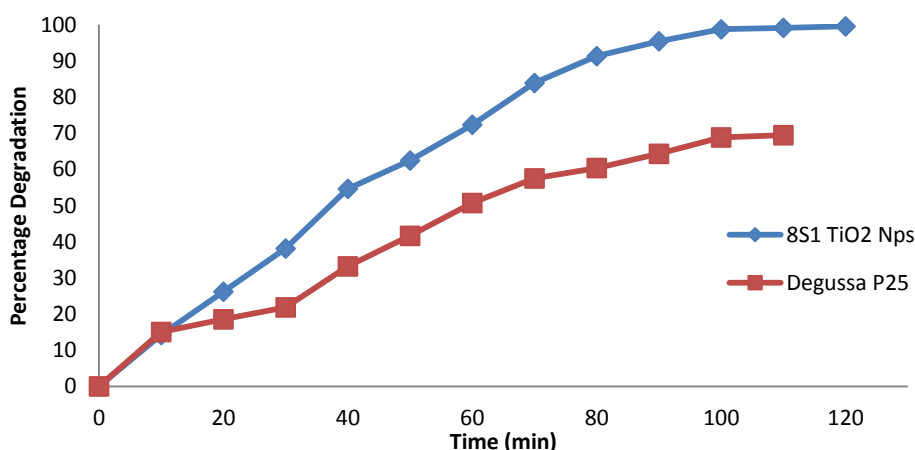
Figure 4.136. Percentage degradation of AB 129 dye using 8S1- TiO$_2$- NPs and Degussa P25. Conditions: Initial pH of the reaction medium = 6.5 pH, Initial dye concentration = 50 mg/L, Catalyst loading = 50 g/L

It can be deduced from Figure 4.136 that 8S1-TiO$_2$-NPs brought about 99.6% degradation of 50 mg/L AB 129 dye within 120 min of the reaction time and with initial reaction rate of 0.712 mg/L/min.
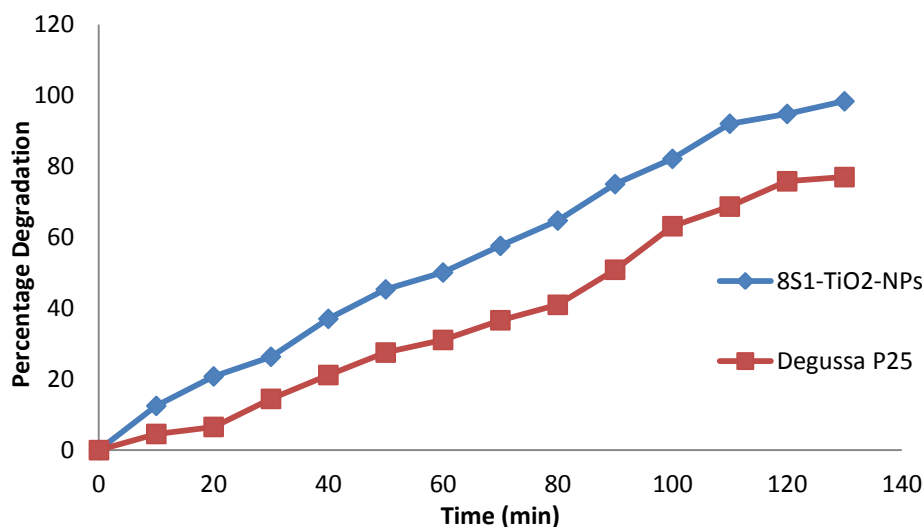
Figure 4.137 Percentage degradation of RBB dye using 8S1-TiO$_2$-NPs and Degussa P25. Conditions: Initial pH of the reaction medium = 7.54 pH, Initial dye concentration = 50 mg/L, Catalyst loading = 50 g/L.

Similarly as seen in Figure 4.137 around 99% degradation of 50 mg/L RBB dye could be achieved in 110 minutes. However, only 70% of the dye degradation could be achieved in 110 min at an initial reaction rate of 0.464 mg/L/min with Degussa P25 as a photocatalyst under similar set of experimental conditions.

The higher percentage degradation and rate of degradation could be achieved with the 8S1-TiO$_2$-NPs due to its crystallinity and content of Anatase and Brookite phases of TiO$_2$. Recently, studies have shown that mixtures of anatase-rutile or brookite-anatase were more active than anatase alone (Shah et al. 2008 and Miyagi et al. 2004). The 8S1-TiO$_2$-NPs were of smaller size of ~4.2 nm, while Degussa P25 contains Anatase and rutile phase with an average size of 21 nm. Owing to the smaller size and the presence of brookite and anatase phases, 8S1-TiO$_2$-NPs exhibited superior photocatalytic activity than Degussa P25 in the photocatalytic degradation of the dyes.

The photocatalytic activity exhibited by 8S1-TiO$_2$-NPs in the degradation of model compounds shows that the particles can be further used in applications wherein photocatalysis play a prime role.

4.20. Kinetics of AB 129 dye and RBB dye degradation using 8S1-TiO$_2$-NPs

Determination of rate equation governing photocatalytic process and evaluation of kinetic parameters are crucial from the view point of feasibility and

commercialization of the photocatalytic process at a large scale. Study on kinetics is important to facilitate the design of photocatalytic reactors.

The concentration-time data obtained by conducting the photocatalytic degradation of 50 mg/L AB129 dye and RBB dyes with dye to catalyst ratio of 1:10 and unadjusted pH of the reaction mixture in immersion well quartz reactor with 80W UV lamp power were used for the evaluation of kinetics of photocatalysis of the dyes. The rates of AB 129 dye and RBB dye degradation were obtained by drawing tangents on the plots of dye concentration vs. time data at different time intervals and by finding the slopes of these tangents. The dye concentrations at these times were also noted.

Langmuir-Hinshelwood (L-H) mechanism is predominantly applicable for the heterogeneous catalytic degradation (Ollis and Serpone 1989; Fox and Dulay 1993; Hoffmann et al. 1995). The L–H model was established to describe the dependence of the observed reaction rate on the solute concentrations.

The L–H model showing the effect of dye concentration on the rate of degradation is given in the form of Eq 4.1 (Matthews, 1991).

$$(-r) = \frac{K_{obs} K_r [C_{dye}]}{1 + K_r [C_{dye}]} \quad \text{............ Eq. 4.1}$$

Where $(-r)$ is the reaction rate of the dye being degraded, C_{dye} is the concentration of the dye, K_{obs} is the constant related to adsorption and K_r is the reaction rate constant.

Thus, the suitability of L-H model to predict the kinetics of photocatalytic degradation of AB 129 and RBB dyes using 8S1-TiO$_2$-NPs was tested. The rate-concentration data were fitted on to the linear form of L-H kinetic model presented as Eq. 4.2.

$$\frac{1}{-r} = \frac{1}{K_{obs} K_r [C_{dye}]} + \frac{1}{K_{obs}} \quad \text{...Eq. 4.2}$$

To estimate the parameters, it has been customary to write Eq. 4.1 in linear form using the reciprocals as shown in Eq.4.2 and then to plot the reciprocal of reaction rate, 1/(-r), versus the reciprocal of concentration, 1/C_{dye}. The plot of 1/-r vs. 1/C_{dye} was plotted and is shown in Figure 4.138 and Figure 4.139 for AB 129 and RBB dyes respectively. The plots in Figure 4.138 and Figure 4.139 are found to be

312

linear showing that the photocatalytic degradation of AB 129 and RBB dyes using 8S1-TiO$_2$-NPs obeys the L-H kinetics. According to L-H model, adsorption of the dye molecules on the surface of the catalyst is assumed to be the slowest and the rate determining step.

The values of kinetic parameters were estimated from the slope and intercept of the lines. The values of kinetics parameters (K_{obs} and K_r) are presented in Table 4.48 for degradation of AB 129 dye and RBB dye by UV photocatalysis.
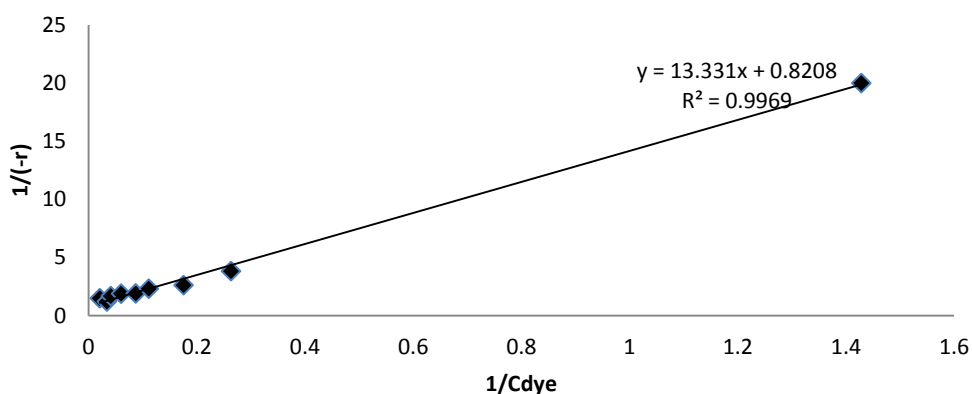
Figure 4.138 Plot of linear form of L-H kinetic model for AB 129 dye using 8S1-TiO$_2$-NPs
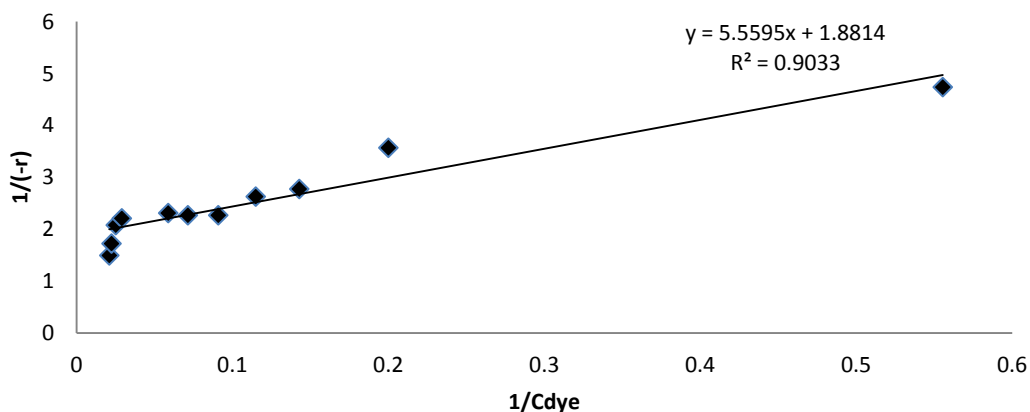
Figure 4.139 Plot of linear form of L-H kinetic model for RBB dye using 8S1-TiO$_2$-NPs

Table 4.46 Kinetic Parameters and goodness of fit obtained from the linearity plot of degradation of AB 129 dye and RBB dye

Kinetic Parameters	AB 129 dye	RBB dye
K_r (mg/L/min)	1.218	0.5315
K_{obs} (L/mg)	16.24	0.3384
Goodness of fit		
SSE	0.899	0.7943
R^2	0.9969	0.9033
RMSE	0.3584	0.2971

Table 4.46 shows Sum of squared error (SSE), Coefficient of determination (R^2) and Root mean square Error (RMSE) for the fit of data to L-H kinetic model. The values confirm the goodness of fit and thus the L-H model is found to be the valid model for the prediction of kinetics of degradation of AB129 and RBB by UV photocatalysis using 8S1-TiO_2-NPs. As L-H model fits the heterogeneous degradation of AB 129 and RBB dye it is confirmed that adsorption of the dye molecules on the surface of the catalyst is the rate determining step.

In the reported study, TiO_2-NPs were successfully synthesized using the bacterial isolates 4S1, 4S2, 4S3, 6S1 and 8S1. These strains were known to possess necessary metabolic machinery which could bring about the synthesis of TiO_2-NPs by the hydrolysis of K_2TiF_6 salt added to the synthesis medium containing the cell free supernatants of the bacterial strains. The parameters affecting the morphological characteristics of TiO_2-NPs such as concentration of the precursor salt and initial pH of the synthesis mixture were studied. Bacterial strain 8S1 yielded the smallest TiO_2-NPs with an average size of ~4.2 nm with highest crystallinity and content of Anatase and Brookite phases of TiO_2 and exhibited cationic surface charge and excellent stability with a zeta potential value of 61.3 mV. 8S1-TiO_2-NPs possessed a band gap energy value of 3.23 eV and were able to successfully degrade the azo dyes; AB 129 and RBB by photocatalysis and with better efficacy compared to Degussa P25 under UV light irradiation. The kinetics of degradation followed L-H model indicating that the photocatalysis is adsorption controlled process. The results obtained in the present study shows it as a promising photocatalyst, enabling its applications in areas related to disinfection of water and degradation of pollutants in air and water. The photocatalytic efficiency of 8S1-TiO_2-NPs can be further used in applications such as self cleaning materials, antifogging applications, disinfection and antimicrobial applications, air and water cleaning applications.

CHAPTER 5
SUMMARYAND
CONCLUSIONS

The research work presented in this report, emphasizes on the use of benign and eco friendly route of synthesis of AgNPs and TiO$_2$-NPs. The AgNPs were synthesized using plant extracts and the cell free supernatants of isolated bacterial strains. Tropical plant resources that possess low agro-economic value such as leaves and fruit peels which were readily available in large surplus as an agro or food processing industry waste were screened on the basis of their efficacy to reduce the AgNO$_3$ to AgNPs and the leaves of *T.catappa* (Indian Almond tree) and *T.grandis* Linn F (Teak tree) were chosen for the synthesis of AgNPs. The influence of synthesis parameters such as concentration of the leaf extract, precursor salt solution concentration, ratio of the extract to the precursor salt solution concentration in the synthesis mixture and initial pH of the mixture along with the processes adopted to prepare the extract of the leaves on the synthesis of AgNPs were studied. The optimum conditions of these parameters were selected based on the spectral and morphological characteristics of the AgNPs such as isotropic nature, monodispersity, size and shape along with good conversion.

Bacterial strains were isolated from a silver rich environment and screened based on their ability to reduce higher concentrations of Ag$^+$ ions to zerovalent silver at faster rates. Five bacterial strains named: 4S1, 4S2, 4S3, 6S1 and 8S1 were selected for the synthesis of extracellular AgNPs and were identified as *Brevundimonas vancanneytii* strain, *Leucobacter aridicollis* strain, *Enterobacter cloacae* strain and *Alcaligenes aquatilis* strain by 16S rRNA sequencing. The bacterial metabolic machinery responsible for the reduction of Ag$^+$ ions to AgNPs was also determined.

The influence of the synthesis process parameters such as precursor salt solution concentration and the initial pH of the synthesis mixture on the extracellular synthesis of AgNPs were studied and the optimum conditions were determined based on the conversion as well as the morphological and spectral characteristics of the AgNPs synthesized. The AgNPs thus synthesized using the bacterial isolates, aqueous leaf extracts of *T.catappa* (ALE) and *T.grandis* Linn F (TLE) were characterized using UV-Vis spectroscopy, XRD, SEM, TEM, EDS, FTIR and Particle size analyzer and their morphological characteristics were studied. The application potentials of the AgNPs as antibacterial agents and colorimetric sensors for the detection of mercury were evaluated.

Plant leaf extracts and bacterial strains with the efficacy to synthesize AgNPs were also tested for their ability to synthesize TiO_2-NPs. The TiO_2-NPs could be successfully synthesized extracellularly using the bacterial strains in the cell free environment. The influence of synthesis parameters such as concentration of the precursor salt (K_2TiF_6) and initial pH of the synthesis mixture were studied and the optimum conditions were determined based on the conversion as well as the morphological characteristics of the TiO_2-NPs being synthesized. The TiO_2-NPs were characterized and were tested for their photocatalytic activity in terms of the degradation of two model organic compounds- AB129 and RBB dyes.

The salient findings of the present research work are summarized as below:

Synthesis, Characterization and applications of AgNPs

- AgNPs were successfully synthesized using ALE, TLE and the cell free supernatant of the isolated bacterial strains: 4S1, 4S2, 4S3, 6S1 and 8S1.

- Major classes of bioactive components present in ALE and TLE such as phenols, antioxidants and flavonoids were found to play a role in the synthesis of AgNPS with dominant contribution of antioxidants as reducing agents; while phenols and flavonoids acted as capping agents.

- AgNPs synthesized with 5% ALE prepared by open solvent heating method and 20 mM of $AgNO_3$ solution in the volume ratio of 1:4 with an initial alkaline pH of 11 at an ambient temperature of 28± 2 ℃ with a conversion of ~99.8% were found to be isotropic, monodispersed and quasi spherical shaped in the narrow size range of 9-35 nm with an average size of 10.9 nm.

- AgNPs synthesized using 10% TLE prepared using open solvent heating method with 20 mM of $AgNO_3$ solution in the volume ratio of 1:4 with an initial alkaline pH of 11 at an ambient temperature of 28± 2 ℃ with a conversion of ~99 % were found to be isotropic, monodispersed and quasi spherical shaped with an average size of 20.4 nm and a narrow size range of 19-50 nm.

- The rate of synthesis of AgNPs was enhanced under optimum conditions with no compromise on the spectral characteristics of the AgNPs being synthesized.

- The AgNPs synthesized using ALE and TLE were found to be encapsulated within a capping as revealed by TEM, FTIR and EDX confirming the role of plant bioactive components in the extract as capping agents.

- Initial alkaline pH of 11 in the synthesis mixture was found to be the optimum for synthesis of AgNPs with all the bacterial isolates. The optimum concentration of $AgNO_3$ solution used in the synthesis mixture was found to be 75 mM for strains 4S1, 4S2 and 4S3 and 100 mM for strains 6S1 and 8S1.

- TEM analysis revealed that the AgNPs synthesized using the strain 6S1 with a conversion of 96.6% were monodispersed, nearly isotropic and covered with capping agents of bacterial origin. The AgNPs were in the average size range of ~38 nm. While the AgNPs synthesized using the strain 8S1 with a conversion of 98.9% were smaller than those obtained by strain 6S1 and nearly isotropic, monodispersed and quasi spherical shaped with an average size of ~22 nm. The average sizes obtained thorugh TEM and SEM were in agreement.

- Presence of NADH dependant nitrate reductase enzyme with a molecular wight of ~ 44 kDa in bacterial superantnat of the strains indicated that these enzymes were involved in the synthesis of AgNPs by reducing the Ag^+ ions.

- AgNPs synthesized using ALE, TLE, 4S1, 4S2, 4S3, 6S1 and 8S1 were found to be crystalline and FCC structured.

- The SPR spectra of AgNPs in colloidal solutions synthesized using the plant and the bacterial sources did not show any change in characteristics over a period of 6 months revealing that the particles were stable. The zeta potential value of AgNPs synthesized using bacterial strains 4S1, 4S2, 4S3 and 6S1 indicated moderate stability while those synthesized using ALE, TLE and 8S1 indicated good stability of AgNPs.

- EDS and FTIR analysis of AgNPs synthesized using the bacteria revealed the presence of several functional groups of bacterial origin with proteins, amines and sugar moieties being the major classes of molecules encapsulating the AgNPs.

- AgNPs synthesized using the leaf extracts and the bacterial isolates could be used as good antibacterial agents and as sensors for detecting and measuring trace level of mercury in water. These properties were found to be superior as compared to chemically synthesized AgNPs.

Synthesis, Characterization and application of TiO₂-NPs

- The cell free supernatants of the bacterial strains 4S1, 4S2, 4S3, 6S1 and 8S1 used for the synthesis of AgNPs could also facilitate the synthesis of TiO$_2$-NPs. Hydrolytic enzymes with a molecular weight of ~29 kDa present in the cell free supernatants were found responsible for the synthesis of TiO$_2$-NPs.

- The cell free culture supernatant of 8S1 strain with 10 g/L of precursor salt concentration in the synthesis mixture with initial pH 11 yielded TiO$_2$-NPs which are quasi spherical shaped, monodispersed and encapsulated by capping material of bacterial origin with an average size of ~4 nm as revealed through TEM and with the highest conversion of 94%. The crystallite size by XRD analysis approximately matched with the particle size.

- The X-ray diffractograms of the TiO$_2$-NPs synthesized using all the bacterial strains were crystalline in nature and exhibited peaks belonging to brookite, anatase and an unknown monoclinic phases of TiO$_2$ with highest intensity of Brookite phase in 8S1-TiO$_2$-NPs. 8S1-TiO$_2$-NPs were monodispersed with a very narrow size range, excellent stability and lowest band gap energy value of 3.23 eV as compared to TiO$_2$-NPs synthesized using other strains.

- FTIR spectra revealed the presence of least content of proteins and the highest content of chemisorbed hydroxyl molecules in TiO$_2$-NPs synthesized with 8S1 as compared to those synthesized by the other strains.

- 8S1-TiO$_2$-NPs and 6S1-TiO$_2$-NPs showed photocatalytic activity in terms of degradation of Acid blue and RBB dyes from aqueous solutions on irradiation with UV lamps, with 8S1-TiO$_2$-NPs exhibiting the highest activity. Enhanced rate of photocatalytic degradation of both the dyes was achieved in quartz immersion well reactor.

- Optimum conditions of reaction parameters for photocatalytic degradation in a quartz immersion well reactor by irradiation with 80W UV lamp were found to be initial dye to catalyst loading ratio of 1:10 and unadjusted, near neutral condition of pH which brought about almost complete degradation of 50 mg/L of the dyes within 120 min proving 8S1-TiO$_2$-NP as a promising photocatalyst and enabling its applications in areas related to disinfection of water and degradation of pollutants

in air and water. The kinetics of degradation followed Langmuir Hinshelwood model, thus the process of photocatalysis is adsorption controlled.

It is concluded that the synthesis processes developed in the current study could nature mine the biobased entities from the new plant and bacterial sources for the synthesis of AgNPs and TiO_2-NPs under ambient conditions with no requirement of elevated pressure and temperature, toxic, hazardous chemicals or solvents, thus making it less energy intensive process with low chemical footprint on the environment. The process proves itself to be an ecofriendly, cost effective and beneficial route for the synthesis of AgNPs and TiO_2-NPs. The optimum conditions of synthesis determined through this study can facilitate the design and operation of large scale synthesis of these nanoparticles. For plant based synthesis of AgNPs, the extraction of bioactive components can be done using solid liquid extraction equipments and further agitated vessels maybe used for the large scale synthesis of AgNPs. While for microbial synthesis of nanoparticles, the bacteria of interest can be grown in large scale reactors, followed by large scale centrifugation to separate the supernatant from the biomass. The supernatant may further be reacted with the precursor salt in agitated reactors for the synthesis of nanoparticles. However further research on optimization of reactor operating conditions and scale up of the reactors can be pursued.

Higher conversions achievable in the synthesis processes with the favourable morphological characteristics and stability makes it economically and technologically feasible and promising. The AgNPs synthesized exhibited good antibacterial activity and mercury sensing property while TiO_2-NPs proved to be efficient photocatalysts. The AgNPs synthesized by these processes can find their applications into antibacterial and fabrics find wide applicability in military, health care and packaging sectors and in other various support matrices concerning hygienic and sterility demands.

These AgNPs can also be used for detection of trace amount of mercury to determine the pollution levels in air or water and in foodstuff. The TiO_2-NPs synthesized can be used as photocatalysts predominantly in wastewater treatment, water disinfection and self cleaning materials such as ceramics, glass and coatings, cosmetics, degradation of organic contaminants, in paints and printing inks,

SCOPE FOR FUTURE STUIDES

- Large scale synthesis of AgNPs and TiO$_2$-NPs in reactors and optimization of reactor operating conditions

- Synthesis of other nanoparticles and nanocomposite structures using the plant and bacterial sources used in the present research work.

- To study the photocatalytic activity of the TiO$_2$-NPs synthesized on the degradation of other organic molecules and disinfection of water

- To study the kinetics of nanoparticle synthesis

REFERENCES

Abe, H., Charle, K.P., Tesche, B. and Schulze, W. (1982). "Surface plasmon absorption of various colloidal metal particles." *Chem. Phys.,* 68(1), 137-141.

Ahluwalia, V., Kumar, J., Sisodia, R., Shakil, N.A. and Walia, S. (2014). "Green synthesis of silver nanoparticles by *Trichoderma harzianum* and their bio-efficacy evaluation against Staphylococcus *aureus* and *Klebsiella pneumonia." Ind. Crops Prod.*, 55, 202-206.

Ahmad, A., Mukherjee, P., Mandal, D., Senapati, S., Khan, M.I., Kumar, R. and Sastry, M. (2002). "Enzyme mediated extracellular synthesis of CdS nanoparticles by the fungus, *Fusarium oxysporum." J. Am. Chem. Soc.*, 124(41), 12108-12109.

Ahmad, A., Mukherjee, P., Senapati, S., Mandal, D., Khan, M.I., Kumar, R. and Sastry, M. (2003a). "Extracellular biosynthesis of silver nanoparticles using the fungus *Fusarium oxysporum." Colloids Surf. B: Biointerfaces,* 28(4), 313-318.

Ahmad, A., Senapati, S., Khan, M.I., Kumar, R., Ramani, R., Srinivas, V. and Sastry, M. (2003b). "Intracellular synthesis of gold nanoparticles by a novel alkalotolerant actinomycete, *Rhodococcus* species." *Nanotechnol.,* 14(7), 824.

Ahmad, B., Ali, J. and Bashir, S. (2013). "Optimization and effects of different reaction conditions for the bioinspired synthesis of silver nanoparticles using *Hippophae rhamnoides* linn. leaves aqueous extract." *World Appl. Sci. J.*, *22*(6), 836-843.

Ahmad, N., Sharma, S., Alam, M.K., Singh, V.N., Shamsi, S.F., Mehta, B.R. and Fatma, A. (2010 b). "Rapid synthesis of silver nanoparticles using dried medicinal plant of basil." *Colloids Surf. B: Biointerfaces,* 81(1), 81-86.

Ahmad, N., Sharma, S., Singh, V.N., Shamsi, S.F., Fatma, A. and Mehta, B.R. (2010a). "Biosynthesis of silver nanoparticles from *Desmodium triflorum*: a novel approach towards weed utilization." *Biotechnology Research International*, *2011*.

Ahmed, S., Ahmad, M., Swami, B.L. and Ikram, S. (2016). "A review on plants extract mediated synthesis of silver nanoparticles for antimicrobial applications: A green expertise." *J. Adv. Res.*, 7(1), 17-28.

Aiyelaagbe, O.O. and Osamudiamen, P.M. (2009). "Phytochemical screening for active compounds in Mangifera indica leaves from Ibadan, Oyo State." *Plant Sci. Res.*, 2(1), 11-13.

Akaighe, N., MacCuspie, R.I., Navarro, D.A., Aga, D.S., Banerjee, S., Sohn, M. and Sharma, V.K. (2011). "Humic acid-induced silver nanoparticle formation under environmentally relevant conditions." *Environ. Sci. Technol.*, 45(9), 3895-3901.

Ali, R. and Hassan, S.H. (2008). "Degradation studies on paraquat and malathion using TiO_2/ZnO based photocatalyst." *Mal. J. Anal. Sci.*, 12(1), 77-87.

Ammala, A., Hill, A.J., Meakin, P., Pas, S.J. and Turney, T.W. (2002). "Degradation studies of polyolefins incorporating transparent nanoparticulate zinc oxide UV stabilizers." *J. Nanopart. Res.*, *4*(1-2), 167-174.

Amtout, A. and Leonelli, R. (1995). "Optical properties of rutile near its fundamental band gap." *Phys. Rev. B:*, *51*(11), 6842.

Ankamwar, B., Chaudhary, M. and Sastry, M. (2005). "Gold nanotriangles biologically synthesized using tamarind leaf extract and potential application in vapor sensing." *Synthesis and Reactivity in Inorganic, Metal-Organic and Nano-Metal Chemistry*, *35*(1), 19-26. (b)

Ankamwar, B., Damle, C., Ahmad, A. and Sastry, M. (2005a). "Biosynthesis of gold and silver nanoparticles using *Emblica officinalis* fruit extract, their phase transfer and transmetallation in an organic solution." *J. Nanosci.Nanotechnol.*, *5*(10), 1665-1671.

Anttonen, M.J. and Karjalainen, R.O. (2005). "Environmental and genetic variation of phenolic compounds in red raspberry." *J. Food Compos. Anal.*, *18*(8), 759-769.

Arana, J., Nieto, J.M., Melián, J.H., Rodrıguez, J.D., Dıaz, O.G., Peña, J.P., Bergasa, O., Alvarez, C. and Méndez, J. (2004). "Photocatalytic degradation of formaldehyde containing wastewater from veterinarian laboratories." *Chemosphere*, *55*(6), 893-904.

Arico, A.S., Bruce, P., Scrosati, B., Tarascon, J.M. and Van Schalkwijk, W. (2005). "Nanostructured materials for advanced energy conversion and storage devices." *Nat. Mater.*, *4*(5), 366-377.

Asahi, R., Taga, Y., Mannstadt, W. and Freeman, A.J. (2000). "Electronic and optical properties of anatase TiO_2." *Phys. Rev. B:*, *61*(11), 7459.

Ashkarran, A.A. and Bayat, A. (2013). "Surface plasmon resonance of metal nanostructures as a complementary technique for microscopic size measurement." *Int. Nano Lett.*, 3(1), 1-10.

Ashokkumar, S., Ravi, S., Kathiravan, V. and Velmurugan, S. (2014). "Synthesis, characterization and catalytic activity of silver nanoparticles using *Tribulus terrestris* leaf extract." *Spectrochim. Acta. A: Mol. Biomol. Spectrosc.*, 121, 88-93.

Atwater, H.A. and Polman, A. (2010). "Plasmonics for improved photovoltaic devices." *Nat. Mater.*, 9(3), 205-213.

Auffan, M., Pedeutour, M., Rose, J., Masion, A., Ziarelli, F., Borschneck, D., Chaneac, C., Botta, C., Chaurand, P., Labille, J. and Bottero, J.Y. (2010). "Structural degradation at the surface of a TiO_2-based nanomaterial used in cosmetics." *Environ. Sci. Technol.*, 44(7), 2689-2694.

Augugliaro, V., Baiocchi, C., Prevot, A.B., García-López, E., Loddo, V., Malato, S., S., Marcí, G., Palmisano, L., Pazzi, M. and Pramauro, E. (2002). "Azo-dyes

photocatalytic degradation in aqueous suspension of TiO_2 under solar irradiation." *Chemosphere*, *49*(10), 1223-1230.

Babitha, S. and Korrapati, P.S. (2013). "Biosynthesis of titanium dioxide nanoparticles using a probiotic from coal fly ash effluent." *Mater. Res. Bull.,* 48(11), 4738-4742.

Babu, M.G. and Gunasekaran, P. (2009). "Production and structural characterization of crystalline silver nanoparticles from *Bacillus cereus* isolate." *Colloids Surf. B: Biointerfaces, 74*(1), 191-195.

Bach, U., Lupo, D., Comte, P., Moser, J.E., Weissörtel, F., Salbeck, J., Spreitzer, H. and Grätzel, M. (1998). "Solid-state dye-sensitized mesoporous TiO_2 solar cells with high photon-to-electron conversion efficiencies." *Nat.*, 395(6702), 583-585.

Badawy, A.M.E., Luxton, T.P., Silva, R.G., Scheckel, K.G., Suidan, M.T. and Tolaymat, T.M. (2010). "Impact of environmental conditions (pH, ionic strength, and electrolyte type) on the surface charge and aggregation of silver nanoparticles suspensions." *Environ. Sci. Technol.*, 44(4), 1260-1266.

Bahnemann, D., Cunningham, J., Fox, M.A., Pelizzetti, E., Pichat, P., Serpone, N. and Crosby, D.G. (1994). "Aquatic and surface photochemistry". *Lewis, Boca Raton, FL*, 261.

Bajpai, M., Pande, A., Tewari, S.K. and Prakash, D. (2005). "Phenolic contents and antioxidant activity of some food and medicinal plants." *Int. J. **Food** Sci. Nutr.*, 56(4), 287-291.

Baker, S., Rakshith, D., Kavitha, K.S., Santosh, P., Kavitha, H.U., Rao, Y. and Satish, S. (2013). "Plants: emerging as nanofactories towards facile route in synthesis of nanoparticles." *BioImpacts: BI*, 3(3), 111.

Balaji, D.S., Basavaraja, S., Deshpande, R., Mahesh, D.B., Prabhakar, B.K. and Venkataraman, A. (2009). "Extracellular biosynthesis of functionalized silver nanoparticles by strains of *Cladosporium cladosporioides* fungus." *Colloids Surf. B: Biointerfaces,* 68(1), 88-92.

Balashanmugam, P. and Kalaichelvan, P.T. (2015). "Biosynthesis characterization of silver nanoparticles using *Cassia roxburghii* DC. aqueous extract, and coated on cotton cloth for effective antibacterial activity." *Int. J. Nanomed.*, *10* (Suppl 1),

Balzani, V., Credi, A. and Venturi, M. (2002). "The Bottom-Up Approach to Molecular-Level Devices and Machines." *Chem. Eur. J.*, 8(24), 5524-5532.

Banala, R.R., Nagati, V.B. and Karnati, P.R. (2015). "Green synthesis and characterization of Carica papaya leaf extract coated silver nanoparticles through X-ray diffraction, electron microscopy and evaluation of bactericidal properties." ***Saudi J. Biol. Sci.***, 22(5), 637-644.

Bankar, A., Joshi, B., Kumar, A.R. and Zinjarde, S. (2010). "Banana peel extract mediated novel route for the synthesis of silver nanoparticles." *Colloids Surf. A Physicochem. Eng. Asp.,* 368(1), 58-63.

Bansal, V., Rautaray, D., Ahmad, A. and Sastry, M. (2004). "Biosynthesis of zirconia nanoparticles using the fungus *Fusarium oxysporum.*" *J. Mater. Chem.*, *14*(22), 3303-3305.

Bansal, V., Rautaray, D., Bharde, A., Ahire, K., Sanyal, A., Ahmad, A. and Sastry, M. (2005). "Fungus-mediated biosynthesis of silica and titania particles." *J. Mater. Chem.*, 15(26), 2583-2589.

Bar, H., Bhui, D.K., Sahoo, G.P., Sarkar, P., De, S.P. and Misra, A. (2009). "Green synthesis of silver nanoparticles using latex of *Jatropha curcas.*" *Colloids Surf., A.*, 339(1), 134-139.

Barnard, A.S., Lin, X.M. and Curtiss, L.A. (2005). "Equilibrium morphology of face-centered cubic gold nanoparticles > 3 nm and the shape changes induced by temperature." *J. Phys. Chem. B.*, 109(51), 24465-24472.

Barnes, W.L., Dereux, A. and Ebbesen, T.W. (2003). "Surface plasmon subwavelength optics." *Nat.*, 424(6950), 824-830.

Basavaraja, S., Balaji, S.D., Lagashetty, A., Rajasab, A.H. and Venkataraman, A. (2008). "Extracellular biosynthesis of silver nanoparticles using the fungus *Fusarium semitectum.*" *Mater. Res. Bull.,* 43(5), 1164-1170.

Basu, S., Maji, P. and Ganguly, J. (2016). "Rapid green synthesis of silver nanoparticles by aqueous extract of seeds of Nyctanthes arbor-tristis." *Appl. Nanosci.*, 6(1), 1-5.

Benedix, R., Dehn, F., Quaas, J. and Orgass, M. (2000). "Application of titanium dioxide photocatalysis to create self-cleaning building materials." *Lacer*, 5, 157-168.

Benn, T. M. and Westerhoff, P. (2008). Nanoparticle silver released into water from commercially available sock fabrics. *Environ. Sci. Technol.,* 42(11), 4133-4139.

Benzie, I.F. and Strain, J.J. (1996). "The ferric reducing ability of plasma (FRAP) as a measure of "antioxidant power": the FRAP assay." *Anal. Biochem.,* 239(1), 70-76.

Berneth, H., Hoheisel, W., Neigl, R. and Womelsdorf, H. (2007). *U.S. Patent No. 7,190,506*. Washington, DC: U.S. Patent and Trademark Office.

Berry, J. and Bjorkman, O. (1980). "Photosynthetic response and adaptation to temperature in higher plants." *Annu. Rev. Plant Physiol.*, 31(1), 491-543.

Bhainsa, K.C. and D'souza, S.F. (2006). "Extracellular biosynthesis of silver nanoparticles using the fungus *Aspergillus fumigatus.*" *Colloids Surf. B: Biointerfaces,* 47(2), 160-164.

Bhat, R., Deshpande, R., Ganachari, S.V., Huh, D.S. and Venkataraman, A. (2011). "Photo-irradiated biosynthesis of silver nanoparticles using edible mushroom *Pleurotus florida* and their antibacterial activity studies." *Bioinorg. Chem. Appl*.

Bhushan, B. (2010). "*Springer handbook of nanotechnology.*" Springer Science and Business Media.

Bihari, P., Vippola, M., Schultes, S., Praetner, M., Khandoga, A.G., Reichel, C. A., Coester, C., Tuomi, T., Rehberg, M. and Krombach, F. (2008). "Optimized dispersion of nanoparticles for biological in vitro and in vivo studies." *Part. Fibre Toxicol.*, 5(1), 1.

Bindhu, M.R. and Umadevi, M. (2013). "Synthesis of monodispersed silver nanoparticles using *Hibiscus cannabinus* leaf extract and its antimicrobial activity." *Spectrochim. Acta. A: Mol. Biomol. Spectrosc.,* 101, 184-190.

Biswas, K., Chattopadhyay, I., Banerjee, R.K. and Bandyopadhyay, U. (2002). "Biological activities and medicinal properties of neem (*Azadirachta indica*)." *Current Science-Bangalore*, 82(11), 1336-1345.

Bocco, A., Cuvelier, M.E., Richard, H. and Berset, C. (1998). "Antioxidant activity and phenolic composition of citrus peel and seed extracts." *J. Agric. Food. Chem.*, 46(6), 2123-2129.

Boelens, M.H. and Jimenez, R. (1989). "The chemical composition of the peel oils from unripe and ripe fruits of bitter orange, Citrus aurantium L. ssp. amara engl." *Flavour. Fragr. J.*, 4(3), 139-142.

Bradley, E.L., Castle, L. and Chaudhry, Q. (2011). "Applications of nanomaterials in food packaging with a consideration of opportunities for developing countries." *Trends Food Sci. Technol.*, 22(11), 604-610.

Bragg, P.D. and Rainnie, D.J. (1974). "The effect of silver ions on the respiratory chain of *Escherichia coli.*" *Can. J. Microbiol.*, 20(6), 883-889.

Brause, R., Moeltgen, H. and Kleinermanns, K. (2002). "Characterization of laser-ablated and chemically reduced silver colloids in aqueous solution by UV/VIS spectroscopy and STM/SEM microscopy." *Appl. Phys. B.*, 75(6-7), 711-716.

Bruce, P.G., Scrosati, B. and Tarascon, J.M. (2008). "Nanomaterials for rechargeable lithium batteries." *Angew. Chem. Int. Ed.*, 47(16), 2930-2946.

Bryant, C. and Deluca, M. (1991). "Purification and characterization of an oxygen-insensitive NAD(P)H nitroreductase from *Enterobacter cloacae.*" *J. Biol. Chem.*, 266(7), 4119-4125.

Bunghez, I.R., Barbinta Patrascu, M.E., Badea, N.M., Doncea, S.M., Popescu, A. and Ion, R.M. (2012). "Antioxidant silver nanoparticles green synthesized using ornamental plants." *J. Optoelectron. Adv. Mater.*, 14(11), 1016.

Burda, C., Lou, Y., Chen, X., Samia, A.C., Stout, J., & Gole, J.L. (2003). "Enhanced nitrogen doping in TiO2 nanoparticles." *Nano Lett.*, 3(8), 1049-1051.

Burnside, S.D., Shklover, V., Barbé, C., Comte, P., Arendse, F., Brooks, K., & Grätzel, M. (1998). "Self-organization of TiO_2 nanoparticles in thin films." *Chem. Mater.*, 10(9), 2419-2425.

Burrell, R.E., Wright, J.B., Lam, K., Naylor, A.G., Moxham, P.H., Gillis, S.H. and Schechter, P. (2008). *U.S. Patent No. 7,470,437*. Washington, DC: U.S. Patent and Trademark Office.

Bury, N.R. and Wood, C.M. (1999). "Mechanism of branchial apical silver uptake by rainbow trout is via the proton-coupled Na^+ channel." *Am. J. Physiol. Regul. Integr. Comp. Physiol.*, 277(5), 1385-1391.

Campbell, S.A., Gilmer, D.C., Wang, X.C., Hsieh, M.T., Kim, H.S., Gladfelter, W.L. and Yan, J. (1997). "MOSFET transistors fabricated with high permitivity TiO_2 dielectrics." *IEEE Trans. Electron Devices.*, 44(1), 104-109.

Canter, P.H., Thomas, H. and Ernst, E. (2005). "Bringing medicinal plants into cultivation: opportunities and challenges for biotechnology." *Trends Biotechnol.*, *23*(4), 180-185.

Caro, C., Sayagues, M.J., Franco, V., Conde, A., Zaderenko, P. and Gámez, F. (2016). "A hybrid silver-magnetite detector based on surface enhanced Raman scattering for differentiating organic compounds." *Sens. Actuators, B.*, 228, 124-133.

Carp, O., Huisman, C.L. and Reller, A. (2004). "Photoinduced reactivity of titanium dioxide." *Prog. Solid State Chem.*, 32(1), 33-177.

Castellano, J.J., Shafii, S. M., Ko, F., Donate, G., Wright, T.E., Mannari, R.J. and Robson, M.C. (2007). "Comparative evaluation of silver-containing antimicrobial dressings and drugs." *Int. Wound J.*, 4(2), 114-122.

Ceresa, E.M., Burlamacchi, L. and Visca, M. (1983). "An ESR study on the photoreactivity of TiO_2 pigments." *J. Mater. Sci.*, 18(1), 289-294.

Chan, Y.S. and Mashitah, M.D. (2013). "Biosynthesis of silver nanoparticles from *Schizophyllum commune* and *in-vitro* antibacterial and antifungal activity studies." *J. Phy. Sci.*, 24(2), 83-96.

Chandran, S.P., Chaudhary, M., Pasricha, R., Ahmad, A. and Sastry, M. (2006). "Synthesis of gold nanotriangles and silver nanoparticles using *Aloevera* plant extract." *Biotechnol. Progr.*, 22(2), 577-583.

Chaudhry, Q., Scotter, M., Blackburn, J., Ross, B., Boxall, A., Castle, L., Aitken, R. and Watkins, R. (2008). "Applications and implications of nanotechnologies for the food sector." *Food Addit. Contam.*, 25(3), 241-258.

Chen, D., Qiao, X., Qiu, X. and Chen, J. (2009). "Synthesis and electrical properties of uniform silver nanoparticles for electronic applications." *J. Mater. Sci.*, 44(4), 1076-1081.

Chen, J.C., Lin, Z.H. and Ma, X.X. (2003). "Evidence of the production of silver nanoparticles via pretreatment of *Phoma* sp. 3.2883 with silver nitrate." *Lett. Appl. Microbiol.*, 37(2), 105-108.

Chen, P.S., Li, J.H., Liu, T.Y. and Lin, T.C. (2000). "Folk medicine *Terminalia catappa* and its major tannin component, punicalagin, are effective against bleomycin-induced genotoxicity in Chinese hamster ovary cells." *Cancer Lett.*, 152(2), 115-122.

Chen, X. and Mao, S.S. (2007). "Titanium dioxide nanomaterials: synthesis, properties, modifications, and applications." *Chem. Rev.*, 107(7), 2891-2959.

Cheng, C.L., Sun, D. ., Chu, W.C., Tseng, Y.H., Ho, H.C., Wang, J.B., Chung, P.H., Chen, J.H., Tsai, P.J., Lin, N.T. and Yu, M.S. (2009). "The effects of the bacterial interaction with visible-light responsive titania photocatalyst on the bactericidal performance." *J. Biomed. Sci.*, 16(1), 1.

Chiang, C.K., Huang, C.C., Liu, C.W. and Chang, H.T. (2008). "Oligonucleotide-based fluorescence probe for sensitive and selective detection of mercury (II) in aqueous solution." *Anal. Chem.*, *80*(10), 3716-3721.

Chimentao, R.J., Kirm, I., Medina, F., Rodriguez, X., Cesteros, Y., Salagre, P. and Sueiras, J.E. (2004). "Different morphologies of silver nanoparticles as catalysts for the selective oxidation of styrene in the gas phase." *Chem. Commun.*, (7), 846-847.

Choi, H., Stathatos, E. and Dionysiou, D.D. (2007). "Photocatalytic TiO_2 films and membranes for the development of efficient wastewater treatment and reuse systems." *Desalin.*, 202(1), 199-206.

Chol, S.U.S. (1995). "Enhancing thermal conductivity of fluids with nanoparticles." *ASME-Publications-Fed*, 231, 99-106.

Chopade, V., Tankar, A., Pande, V., Tekade, A., Gowekar, N., Bhandari, S. and Khandake, S. (2008). "*Pongamia pinnata*: Phytochemical constituents, traditional uses and pharmacological properties: A review." *International journal of green pharmacy*, 2(2), 72.

Chowdhury, I.H., Ghosh, S., Roy, M. and Naskar, M.K. (2015). "Green synthesis of water-dispersible silver nanoparticles at room temperature using green *carambola* (star fruit) extract." *J. Sol-Gel Sci. Technol.*, 73(1), 199-207.

Christensen, L., Vivekanandhan, S., Misra, M. and Mohanty, A.K. (2011). "Biosynthesis of silver nanoparticles using *murraya koenigii* (curry leaf): an investigation on the effect of broth concentration in reduction mechanism and particle size." *Adv. Mat. Lett.*, 2(6), 429-434..

Chyau, C.C., Tsai, S.Y., Ko, P.T. and Mau, J.L. (2002). "Antioxidant properties of solvent extracts from *Terminalia catappa* leaves." *Food Chem.*, 78(4), 483-488.

Colvin, V.L., Schlamp, M.C. and Alivisatos, A.P. (1994). "Light-emitting-diodes made from cadmium selenide nanocrystals and a semiconducting polymer." *Nat.*, 370(6488), 354-357.

Comiskey, B., Albert, J.D., Yoshizawa, H. and Jacobson, J. (1998). "An electrophoretic ink for all-printed reflective electronic displays." *Nat.*, 394(6690), 253-255.

Contado, C. and Pagnoni, A. (2008). "TiO_2 in commercial sunscreen lotion: flow field-flow fractionation and ICP-AES together for size analysis." *Anal. Chem.*, *80*(19), 7594-7608.

Coronado, E., Galan-Mascaros, J.R., Marti-Gastaldo, C., Palomares, E., Durrant, J.R., Vilar, R., Gratzel, M. and Nazeeruddin, M.K. (2005). "Reversible colorimetric probes for mercury sensing." *J. Am. Chem. Soc.*, 127(35), 12351-12356.

Creran, B., Yan, B., Moyano, D.F., Gilbert, M.M., Vachet, R.W. and Rotello, V. M. (2012). "Laser desorption ionization mass spectrometric imaging of mass barcoded gold nanoparticles for security applications." *Chem. Commun.*, 48(38), 4543-4545.

Cruz, D., Falé, P.L., Mourato, A., Vaz, P.D., Serralheiro, M.L. and Lino, A.R.L. (2010). "Preparation and physicochemical characterization of Ag nanoparticles biosynthesized by *Lippia citriodora* (Lemon Verbena)." *Colloids Surf. B: Biointerfaces,* 81(1), 67-73.

Cui, D., Tian, F., Coyer, S.R., Wang, J., Pan, B., Gao, F. and Zhang, Y. (2007). "Effects of Antisense-Myc-Conjugated Single-Walled Carbon Nanotubes on HL-60Cells." *J. Nanosci. Nanotechnol.*, 7(4-1), 1639-1646.

Dai, K., Peng, T., Chen, H., Zhang, R. and Zhang, Y. (2008). Photocatalytic degradation and mineralization of commercial methamidophos in aqueous titania suspension. *Environ. Sci. Technol.,* 42(5), 1505-1510.

Dai, L. (Ed.). (2006). Carbon nanotechnology: recent developments in chemistry, physics, materials science and device applications. *Elsevier.*

Daneshvar, N., Salari, D. and Khataee, A.R. (2003). "Photocatalytic degradation of azo dye acid red 14 in water: investigation of the effect of operational parameters." *J. Photochem. Photobiol. A.,* 157(1), 111-116.

Daniel, M.C. and Astruc, D. (2004). "Gold nanoparticles: assembly, supramolecular chemistry, quantum-size-related properties, and applications toward biology, catalysis, and nanotechnology." *Chem. Rev.*, 104(1), 293-346.

Darroudi, M., Zak, A.K., Muhamad, M.R., Huang, N.M. and Hakimi, M. (2012). "Green synthesis of colloidal silver nanoparticles by sonochemical method." *Mater. Lett.*, 66(1), 117-120.

Das, R., Nath, S.S., Chakdar, D., Gope, G. and Bhattacharjee, R. (2010). "Synthesis of silver nanoparticles and their optical properties." *Journal J. Exp. Nanosci.*, 5(4), 357-362.

Das, R.K., Gogoi, N. and Bora, U. (2011). "Green synthesis of gold nanoparticles using *Nyctanthes arbortristis* flower extract." *Bioprocess and biosystems engineering.*, 34(5), 615-619.

Dauthal, P. and Mukhopadhyay, M. (2013). "In-vitro free radical scavenging activity of biosynthesized gold and silver nanoparticles using *Prunus armeniaca* (apricot) fruit extract." *J. Nanopart. Res.*, 15(1), 1-11.

De V, F. H. and Bergsteinsson, I. (1947). U.S. Patent No. 2,424,083. Washington, DC: U.S. Patent and Trademark Office.

Deljou, A. and Rhamjou, Z. (2016). "Green extracellular synthesis of silver nanoparticles using thermophilic *Bacillus* sp. AZ1 and its antimicrobial activity against some human pathogens bacteria." *Iran. J. Biotechnol*.

Devi, L.S. and Joshi, S.R. (2014). "Evaluation of the antimicrobial potency of silver nanoparticles biosynthesized by using an endophytic fungus, *Cryptosporiopsis ericae* PS4." *J. Microbiol.*, 52(8), 667-674.

Dhandapani, P., Maruthamuthu, S. and Rajagopal, G. (2012). "Bio-mediated synthesis of TiO_2 nanoparticles and its photocatalytic effect on aquatic biofilm." *J. Photochem. Photobiol., B*, 110, 43-49.

Dharma, J. and Pisal, A. "Simple Method of Measuring the Band Gap Energy Value of TiO_2 in the Powder Form." (Copyright ©2009-2102), PerkinElmer, Inc.

Di Paola, A., Bellardita, M. and Palmisano, L. (2013). "Brookite, the least known TiO_2 photocatalyst." *Catal.*, 3(1), 36-73.

Diebold, U. (2003). "The surface science of titanium dioxide." *Surf. Sci. Rep.*, 48(5), 53-229.

Dinesh, D., Murugan, K., Madhiyazhagan, P., Panneerselvam, C., Kumar, P.M., Nicoletti, M., Jiang, W., Benelli, G., Chandramohan, B., Suresh, U. (2015). "Mosquitocidal and antibacterial activity of green-synthesized silver nanoparticles from *Aloe vera* extracts: towards an effective tool against the malaria vector *Anopheles stephensi*." *Parasitol. Res.,* 114(4), 1519-1529.

Dipankar, C. and Murugan, S. (2012). "The green synthesis, characterization and evaluation of the biological activities of silver nanoparticles synthesized from *Iresine herbstii* leaf aqueous extracts." *Colloids Surf. B: Biointerfaces,* 98, 112-119.

Dirix, Y., Bastiaansen, C., Caseri, W. and Smith, P. (1999). "Oriented pearl-necklace arrays of metallic nanoparticles in polymers: a new route toward polarization-dependent color filters." *Adv. Mater.*, 11(3), 223-227.

Ditlbacher, H., Krenn, J.R., Lamprecht, B., Leitner, A. and Aussenegg, F.R. (2000). "Spectrally coded optical data storage by metal nanoparticles." *Opt. Lett.*, 25(8), 563-565.

Dong, W. and Zhu, C. (2003). "Optical properties of surface-modified CdO nanoparticles." *Opt. Mater.*, 22(3), 227-233.

Dubas, S.T., Kumlangdudsana, P. and Potiyaraj, P. (2006). "Layer-by-layer deposition of antimicrobial silver nanoparticles on textile fibers." *Colloids Surf. A Physicochem. Eng. Asp.*, 289(1), 105-109.

Dubey, M., Bhadauria, S. and Kushwah, B.S. (2009). "Green synthesis of nanosilver particles from extract of Eucalyptus hybrida (safeda) leaf." *Dig. J. Nanomater. Biostruct.*, 4(3), 537-543.

Dubey, S.P., Lahtinen, M., Särkkä, H. and Sillanpää, M. (2010). "Bioprospective of *Sorbus aucuparia* leaf extract in development of silver and gold nanocolloids." *Colloids Surf. B: Biointerfaces,* 80(1), 26-33.

Duncan, T.V. (2011). "Applications of nanotechnology in food packaging and food safety: barrier materials, antimicrobials and sensors." *J. Colloid Interface Sci.*, 363(1), 1-24.

Durán, N., Marcato, P.D., Alves, O.L., De Souza, G.I. and Esposito, E. (2005). "Mechanistic aspects of biosynthesis of silver nanoparticles by several *Fusarium oxysporum* strains." *J.Nanobiotechnol.*, 3(1), 1.

Durán, N., Marcato, P.D., Durán, M., Yadav, A., Gade, A. and Rai, M. (2011). "Mechanistic aspects in the biogenic synthesis of extracellular metal nanoparticles by peptides, bacteria, fungi, and plants." *Appl. Microbiol. Biotechnol.*, 90(5), 1609-1624.

Dwivedi, A.D. and Gopal, K. (2010). "Biosynthesis of silver and gold nanoparticles using Chenopodium album leaf extract." *Colloids Surf. A Physicochem. Eng. Asp., 369*(1), 27-33.

Edison, T.J.I. and Sethuraman, M.G. (2012). "Instant green synthesis of silver nanoparticles using *Terminalia chebula* fruit extract and evaluation of their catalytic activity on reduction of methylene blue." *Process Biochem.*, 47(9), 1351-1357.

Edison, T.J.I. and Sethuraman, M.G. (2013). "Biogenic robust synthesis of silver nanoparticles using *Punica granatum* peel and its application as a green catalyst for the reduction of an anthropogenic pollutant 4-nitrophenol." *Spectrochim. Acta. A: Mol. Biomol. Spectrosc.,* 104, 262-264.

Edwards, P.P. and Thomas, J.M. (2007). "Gold in a Metallic Divided State—From Faraday to Present-Day Nanoscience." *Angew. Chem. Int. Ed. Engl.*, 46(29), 5480-5486.

Elghanian, R., Storhoff, J.J., Mucic, R.C., Letsinger, R.L. and Mirkin, C.A. (1997). "Selective colorimetric detection of polynucleotides based on the distance-dependent optical properties of gold nanoparticles." *Sci.*, 277(5329), 1078-1081.

El-Nour, K.M.A., Eftaiha, A.A., Al-Warthan, A. and Ammar, R.A. (2010). "Synthesis and applications of silver nanoparticles." *Arabian J. Chem.*, 3(3), 135-140.

El-Sayed, M.A. (2001). "Some interesting properties of metals confined in time and nanometer space of different shapes." *Acc. Chem. Res.*, 34(4), 257-264.

El-Shanshoury, A.E.R.R., ElSilk, S.E. and Ebeid, M.E. (2011). "Extracellular biosynthesis of silver nanoparticles using *Escherichia coli* ATCC 8739, *Bacillus subtilis* ATCC 6633, and *Streptococcus thermophilus* ESh1 and their antimicrobial activities." *ISRN Nanotechnol*, *2011*.

Elumalai, E.K., Prasad, T.N.V.K.V., Hemachandran, J., Therasa, S.V., Thirumalai, T. and David, E. (2010). "Extracellular synthesis of silver nanoparticles using leaves of Euphorbia hirta and their antibacterial activities." *J Pharm Sci Res.*, 2(9), 549-554.

Epling, G.A. and Lin, C. (2002). "Photoassisted bleaching of dyes utilizing TiO_2 and visible light." *Chemosphere*, 46(4), 561-570.

Estrela, A.B. and Abraham, W.R. (2010). "*Brevundimonas vancanneytii* sp. nov., isolated from blood of a patient with endocarditis." *Int. J. Syst. Evol. Microbiol.*, 60(9), 2129-2134.

Esumi, K., Tano, T., Torigoe, K. and Meguro, K. (1990). "Preparation and characterization of bimetallic palladium-copper colloids by thermal decomposition of their acetate compounds in organic solvents." *Chem. Mater.*, 2(5), 564-567.

Evanoff, D.D. and Chumanov, G. (2004). "Size-controlled synthesis of nanoparticles. 2. Measurement of extinction, scattering, and absorption cross sections." *J. Phys. Chem. B.*, 108(37), 13957-13962.

Evanoff, D.D. and Chumanov, G. (2005). "Synthesis and optical properties of silver nanoparticles and arrays." *Chem. Phys. Chem.*, 6(7), 1221-1231.

Fan, Y.M., Xu, L.Z., Gao, J., Wang, Y., Tang, X.H., Zhao, X.N. and Zhang, Z.X. (2004). "Phytochemical and antiinflammatory studies on Terminalia catappa." *Fitoterapia*, 75(3), 253-260.

Fang, F., Li,J.M., Pan, Q.H. and Huang, W.D. (2007). "Determination of red wine flavonoids by HPLC and effect of aging." *Food Chem.*, 101(1), 428-433.

Faraday, M. (1991). "*The Correspondence of Michael Faraday: 1811-December 1831, letters 1-524* (Vol. 1). F. A. James (Ed.). Iet.

Farhadi, K., Forough, M., Molaei, R., Hajizadeh, S. and Rafipour, A. (2012). "Highly selective Hg^{2+} colorimetric sensor using green synthesized and unmodified silver nanoparticles." *Sens. Actuators, B.*, 161(1), 880-885.

Fayaz, A.M., Balaji, K., Girilal, M., Yadav, R., Kalaichelvan, P.T. and Venketesan, R. (2010). "Biogenic synthesis of silver nanoparticles and their synergistic effect with antibiotics: a study against gram-positive and gram-negative bacteria." *Nanomed. Nanotechnol. Biol. Med.*,6(1), 103-109.

Fayaz, A.M., Balaji, K., Kalaichelvan, P.T. and Venkatesan, R. (2009). "Fungal based synthesis of silver nanoparticles—an effect of temperature on the size of particles." *Colloids Surf. B: Biointerfaces,* 74(1), 123-126.

Fortina, P., Kricka, L.J., Graves, D.J., Park, J., Hyslop, T., Tam, F., Halas, N., Surrey, S. and Waldman, S.A. (2007). "Applications of nanoparticles to diagnostics and therapeutics in colorectal cancer." *Trends Biotechnol.*, 25(4), 145-152.

Fox, C.L. and Modak, S.M. (1974). "Mechanism of silver sulfadiazine action on burn wound infections." *Antimicrob. Agents Chemother.*, 5(6), 582-588.

Fox, M.A. and Dulay, M.T. (1993). "Heterogeneous photocatalysis." *Chem. Rev.*, 93, 341–357.

Freeman, R.G., Grabar, K.C., Allison, K.J. and Bright, R.M. (1995). "Self-assembled metal colloid monolayers: an approach to SERS substrates." *Sci.*, 267(5204), 1629.

French, C.E., Nicklin, S. and Bruce, N.C. (1998). "Aerobic degradation of 2, 4, 6-trinitrotoluene by *Enterobacter cloacae* PB2 and by pentaerythritol tetranitrate reductase." *Appl. Environ. Microbiol.*, 64(8), 2864-2868.

Fu, J. K., Zhnag, W.D., Liu, Y.Y., Lin, Z.Y., Yao, B.X., Weng, S.Z. and Zeng, J.L. (1999). "Characterization of adsorption and reduction of noble metal ions by bacteria." *Chemical Journal Of Chinese Universities-Chinese Edition-*, 20, 1454-1456.

Fujishima, A. (1972). "Electrochemical photolysis of water at a semiconductor electrode." *Nat.*, 238, 37-38.

Fujishima, A. and Zhang, X. (2006). "Titanium dioxide photocatalysis: present situation and future approaches." *C.R. Chim.*, 9(5), 750-760.

Fujishima, A., Kohayakawa, K. and Honda, K. (1975). "Hydrogen production under sunlight with an electrochemical photocell." *J. Electrochem. Soc.*, 122, 1487-1489.

Fujishima, A., Rao, T.N. and Tryk, D.A. (2000). "Titanium dioxide photocatalysis." *J. Photochem. Photobiol., C*, 1(1), 1-21.

Fujishima, A., Zhang, X. and Tryk, D.A. (2008). "TiO$_2$ photocatalysis and related surface phenomena." *Surf. Sci. Rep.*, *63*(12), 515-582.

Gade, A., Gaikwad, S., Tiwari, V., Yadav, A., Ingle, A. and Rai, M. (2010). "Biofabrication of silver nanoparticles by *Opuntia ficus*-indica: in vitro antibacterial activity and study of the mechanism involved in the synthesis." *Curr. Nanosci.*, 6(4), 370-375.

Gade, A.K., Bonde, P., Ingle, A.P., Marcato, P.D., Duran, N. and Rai, M.K. (2008). "Exploitation of *Aspergillus niger* for synthesis of silver nanoparticles." *J. Biobased Mater. Bioenergy*, 2(3), 243-247.

Galindo, C., Jacques, P. and Kalt, A. (2000). "Photodegradation of the aminoazobenzene acid orange 52 by three advanced oxidation processes: UV/H$_2$O$_2$, UV/TiO$_2$ and VIS/TiO$_2$: comparative mechanistic and kinetic investigations." *J. Photochem. Photobiol. A.,* 130(1), 35-47.

Ganaie, S.U., Abbasi, T. and Abbasi, S.A. (2015). "Green synthesis of silver nanoparticles using an otherwise worthless weed Mimosa (*Mimosa pudica*): feasibility and process development toward shape/size control." *Part. Sci. Technol.*, 33(6), 638-644.

Gao, J., Tang, X., Dou, H., Fan, Y., Zhao, X. and Xu, Q. (2004). "Hepatoprotective activity of *Terminalia catappa* L. leaves and its two triterpenoids." *J. Pharm. Pharmacol.*, 56(11), 1449-1455.

Garcia, M. A., Merino, J. M., Fernández Pinel, E., Quesada, A., De la Venta, J., Ruíz González, M. L., Castro, G.R., Crespo, P., Llopis, J., González-Calbet, J.M. and Hernando, A. (2007). "Magnetic properties of ZnO nanoparticles." *Nano lett.*, 7(6), 1489-1494.

Gardea-Torresdey, J.L., Parsons, J.G., Gomez, E., Peralta-Videa, J., Troiani, H. E., Santiago, P. and Yacaman, M. J. (2002). "Formation and growth of Au nanoparticles inside live alfalfa plants." *Nano Lett.*, 2(4), 397-401.

Geetha, M., Singh, A. K., Asokamani, R. and Gogia, A.K. (2009). "Ti based biomaterials, the ultimate choice for orthopaedic implants–a review." *Prog. Mater Sci.*, 54(3), 397-425.

Gericke, M. and Pinches, A. (2006). "Biological synthesis of metal nanoparticles." *Hydrometallurgy*, 83(1), 132-140.

Ghaffari-Moghaddam, M. and Hadi-Dabanlou, R. (2014). "Plant mediated green synthesis and antibacterial activity of silver nanoparticles using *Crataegus douglasii* fruit extract." *J. Ind. Eng. Chem.*, 20(2), 739-744.

Ghobadi, N. (2013). "Band gap determination using absorption spectrum fitting procedure." *Int. Nano Lett.*, 3(1), 1-4.

Ghosh, A., Chandratre, K., Chaudhary, A., Chaudhary, S., Badani, N., Chaudhary, P. S., Dhawan, D., Vudathala, S. and Chikara, S.K. (2015). "Whole-genome sequencing of Brevundimonas diminuta XGC1, isolated from a tuberculosis patient in Gujarat, India." *Genome announcements*, 3(3), e00686-15.

Glassford, K.M. and Chelikowsky, J.R. (1992). "Optical properties of titanium dioxide in the rutile structure." *Phys. Rev. B:*, 45(7), 3874.

Goncalves, M.S., Oliveira-Campos, A.M., Pinto, E.M., Plasencia, P.M. and Queiroz, M.J.R. (1999). "Photochemical treatment of solutions of azo dyes containing TiO_2." *Chemosphere*, 39(5), 781-786.

Govindaraju, K., Kiruthiga, V., Kumar, V.G. and Singaravelu, G. (2009). "Extracellular synthesis of silver nanoparticles by a marine alga, *Sargassum wightii Grevilli* and their antibacterial effects." *J. Nanosci. Nanotechnol.*, 9(9), 5497-5501.

Gregory, P.E. and Vinson, K.D. (1990). *U.S. Patent No. 4,952,278*. Washington, DC: U.S. Patent and Trademark Office.

Grzechulska, J. and Morawski, A.W. (2002). "Photocatalytic decomposition of azo-dye acid black 1 in water over modified titanium dioxide." *Appl. Catal. B Environ.,* 36(1), 45-51.

Guidelli, E.J., Ramos, A.P., Zaniquelli, M.E.D. and Baffa, O. (2011). "Green synthesis of colloidal silver nanoparticles using natural rubber latex extracted from *Hevea brasiliensis*." *Spectrochim. Acta. A: Mol. Biomol. Spectrosc.,* 82(1), 140-145.

Guo, X., Qian, X. and Jia, L. (2004). "A highly selective and sensitive fluorescent chemosensor for Hg^{2+} in neutral buffer aqueous solution." *J. Am. Chem. Soc.*, 126(8), 2272-2273.

Gurunathan, S., Kalishwaralal, K., Vaidyanathan, R., Venkataraman, D., Pandian, S.R.K., Muniyandi, J., Hariharan, N. and Eom, S.H. (2009a). "Biosynthesis, purification and characterization of silver nanoparticles using *Escherichia coli.*" *Colloids and Surfaces B: Biointerfaces*, 74(1), 328-335.

Gurunathan, S., Lee, K.J., Kalishwaralal, K., Sheikpranbabu, S., Vaidyanathan, R. and Eom, S.H. (2009b). "Antiangiogenic properties of silver nanoparticles." *Biomater., 30*(31), 6341-6350.

Guzman, M., Dille, J. and Godet, S. (2012). "Synthesis and antibacterial activity of silver nanoparticles against gram-positive and gram-negative bacteria." *Nanomed. Nanotechnol. Biol. Med.*, 8(1), 37-45.

Haes, A.J., Haynes, C.L., McFarland, A.D., Schatz, G.C., Van Duyne, R.P. and Zou, S. (2005). "Plasmonic materials for surface-enhanced sensing and spectroscopy." *Mrs Bulletin*, 30(05), 368-375.

Hamilton, J.F. and Baetzold, R.C. (1979). "Catalysis by small metal clusters." *Sci.*, 205(4412), 1213-1220.

Han, C., Zhang, L. and Li, H. (2009). "Highly selective and sensitive colorimetric probes for Yb^{3+} ions based on supramolecular aggregates assembled from β-cyclodextrin–4, 4′-dipyridine inclusion complex modified silver nanoparticles." *Chem. Commun.*, 24, 3545-3547.

Haruta, M., Kageyama, H., Kamijo, N., Kobayashi, T. and Delannay, F. (1989). "Fine structure of novel gold catalysts prepared by coprecipitation." *Stud. Surf. Sci. Catal.*, *44*, 33-42.

Hashimoto, K., Irie, H. and Fujishima, A. (2005). "TiO_2 photocatalysis: a historical overview and future prospects." *Jpn. J. Appl. Phys.*, *44*(12R), 8269.

Hashimoto, M.C., Prates, R.A., Kato, I.T., Nunez, S.C., Courrol, L.C. and Ribeiro, M.S. (2012). "Antimicrobial Photodynamic Therapy on Drug-*resistant Pseudomonas aeruginosa*-induced Infection- An *In Vivo* Study *Photochem. Photobiol.,* 88(3), 590-595.

He, S., Guo, Z., Zhang, Y., Zhang, S., Wang, J. and Gu, N. (2007). "Biosynthesis of gold nanoparticles using the bacteria *Rhodopseudomonas capsulata*." *Mater. Lett.*, 61(18), 3984-3987.

Hebbalalu, D., Lalley, J., Nadagouda, M.N. and Varma, R.S. (2013). "Greener techniques for the synthesis of silver nanoparticles using plant extracts, enzymes, bacteria, biodegradable polymers, and microwaves." *ACS Sustain. Chem. Eng.*, 1(7), 703-712.

Herrmann, J.M. (1999). "Heterogeneous photocatalysis: fundamentals and applications to the removal of various types of aqueous pollutants." *Catal. Today*, 53(1), 115-129.

Heydari, R. and Rashidipour, M. (2015). "Green synthesis of silver nanoparticles using extract of oak fruit hull (Jaft): synthesis and in vitro cytotoxic effect on MCF-7 cells." *Int J Breast Cancer, 2015*.

Higashisaka, K., Yoshioka, Y. and Tsutsumi, Y. (2015). "Applications and Safety of Nanomaterials Used in the Food Industry." *Food Saf.*, 3(2), 39-47.

Hoffman, A.J., Mills, G., Yee, H. and Hoffmann, M.R. (1992). "Q-sized cadmium sulfide: synthesis, characterization, and efficiency of photoinitiation of polymerization of several vinylic monomers." *J. Phys. Chem.*, 96(13), 5546-5552.

Hoffmann, M.R., Martin, S.T. Choi, W. and D. W. Bahnemann, D. (1995). "Environmental Applications of Semiconductor Photocatalysis." *Chem. Rev.,* 95, 69-96.

Hofstadler, K., Bauer, R., Novalic, S. and Heisler, G. (1994). "New reactor design for photocatalytic wastewater treatment with TiO_2 immobilized on fused-silica glass fibers: photomineralization of 4-chlorophenol." *Environ. Sci. Technol.*, 28(4), 670-674.

Hosaka, N., Sekiya, T., Satoko, C. and Kurita, S. (1997). "Optical properties of single-crystal anatase TiO_2." *J. Phys. Soc. Jpn.*, 66(3), 877-880.

Hotze, E. M., Phenrat, T., and Lowry, G. V. (2010). "Nanoparticle aggregation: challenges to understanding transport and reactivity in the environment." *J. of Environ. Quality*, 39(6), 1909-1924.

Houas, A., Lachheb, H., Ksibi, M., Elaloui, E., Guillard, C. and Herrmann, J. M. (2001). "Photocatalytic degradation pathway of methylene blue in water." *Appl. Catal. B Environ.,* 31(2), 145-157.

http://blast.ncbi.nlm.nih.gov/Blast.cgi?PAGE=Nucleotides&PROGRAM=blastn&BLAST_PROGRAMS=blastn&PAGETYPE=BlastSearch&DATABASE=refseq_rna&DESCRIPTIONS=100&EQ_TEXT=arabidopsis%5Borgn%5D&QUERY=8033

http://doi.org/10.1016/S2221-1691(13)60148-3

http://dx.doi.org/10.1016/j.matlet.2014.03.026

Huang, J., Li, Q., Sun, D., Lu, Y., Su, Y., Yang, X., Wang, H., Wang, Y., Shao, W., He, N. and Hong, J. (2007). "Biosynthesis of silver and gold nanoparticles by novel sundried *Cinnamomum camphora* leaf." *Nanotechnol.*, 18(10), 105104.

Huang, J., Zhan, G., Zheng, B., Sun, D., Lu, F., Lin, Y., Chen, H., Zheng, Z., Zheng, Y. and Li, Q. (2011). "Biogenic silver nanoparticles by *Cacumen platycladi* extract: synthesis, formation mechanism, and antibacterial activity." *Ind. Eng. Chem. Res.*, 50(15), 9095-9106.

Hudlikar, M., Joglekar, S., Dhaygude, M. and Kodam, K. (2012). "Green synthesis of TiO_2 nanoparticles by using aqueous extract of *Jatropha curcas* L. latex." *Mater. Lett.*, 75, 196-199.

Hunter, R.J., 1986. "In: Foundations Colloid Science, vol. 1. Oxford University Press, New York. Hunter, R. J. (1987)." Foundations of colloid science, vol. I-II., 992-1052.

Husseiny, S.M., Salah, T.A. and Anter, H.A. (2015). "Biosynthesis of size controlled silver nanoparticles by *Fusarium oxysporum*, their antibacterial and antitumor activities." *Beni-Suef University Journal of Basic and Applied Sciences*, 4(3), 225-231.

Ibrahem, K.H., Salman, J.A.S. and Ali, F.A. (2014). "Effect of Titanium Nanoparticles Biosynthesis by *Lactobacillus Crispatus* on Urease, Hemolysinand Biofilm Forming by Some Bacteria Causing Recurrent UTI in Iraqi Women." *Eur. Sci. J.*, 10(9).

Imam, H., Elsayed, K.A., Ismail, L.Z. and Afify, M. (2013). "Fabrication of Silver Nanoparticles by Laser Ablation in Liquid Solution." *Life Sci.J.*, 10(4).

Ingle, A., Gade, A., Pierrat, S., Sonnichsen, C. and Rai, M. (2008). "Mycosynthesis of silver nanoparticles using the fungus *Fusarium acuminatum* and its activity against some human pathogenic bacteria." *Curr. Nanosci.*, 4(2), 141-144.

Ingle, A., Rai, M., Gade, A. and Bawaskar, M. (2009). "*Fusarium solani:* a novel biological agent for the extracellular synthesis of silver nanoparticles." *J. Nanopart. Res.*, 11(8), 2079-2085.

Iravani, S. (2011). "Green synthesis of metal nanoparticles using plants." *Green Chem.*, 13(10), 2638-2650.

Jacobs, J.J., Skipor, A.K., Black, J., m Urban, R. and Galante, J.O. (1991). "Release and excretion of metal in patients who have a total hip-replacement component made of titanium-base alloy." *J. Bone Joint Surg. Am.*, 73(10), 1475-1486.

Jagtap, U.B. and Bapat, V.A. (2013). "Green synthesis of silver nanoparticles using *Artocarpus heterophyllus* Lam. seed extract and its antibacterial activity." *Ind. Crops Prod.*, 46, 132-137.

Jain, D., Daima, H.K., Kachhwaha, S. and Kothari, S.L. (2009). "Synthesis of plant-mediated silver nanoparticles using papaya fruit extract and evaluation of their anti microbial activities." *Dig. J. Nanomater. Biostruct.*, 4(3), 557-563.

Jain, P. and Pradeep, T. (2005). "Potential of silver nanoparticle-coated polyurethane foam as an antibacterial water filter." *Biotechnol. Bioeng.*, 90(1), 59-63.

Jain, P.K., Huang, X., El-Sayed, I.H. and El-Sayed, M.A. (2007). "Review of some interesting surface plasmon resonance-enhanced properties of noble metal nanoparticles and their applications to biosystems." *Plasmonics*, 2(3), 107-118.

Jain, P.K., Huang, X., El-Sayed, I.H. and El-Sayed, M.A. (2008). "Noble metals on the nanoscale: optical and photothermal properties and some applications in imaging, sensing, biology, and medicine." *Acc. Chem. Res.*, 41(12), 1578-1586.

Janczyk, A., Krakowska, E., Stochel, G. and Macyk, W. (2006). "Singlet oxygen photogeneration at surface modified titanium dioxide." *J. Am. Chem. Soc.*, 128(49), 15574-15575.

Jang, H.D., Kim, S.K. and Kim, S.J. (2001). "Effect of particle size and phase composition of titanium dioxide nanoparticles on the photocatalytic properties." *J. Nanopart. Res.*, 3(2-3), 141-147.

Jayaseelan, C., Rahuman, A.A., Roopan, S.M., Kirthi, A.V., Venkatesan, J., Kim, S. K., Iyappan, M. and Siva, C. (2013). "Biological approach to synthesize TiO_2 nanoparticles using *Aeromonas hydrophila* and its antibacterial activity." *Spectrochim. Acta. A: Mol. Biomol. Spectrosc.,* 107, 82-89.

Jeng, H.A. and Swanson, J. (2006). "Toxicity of metal oxide nanoparticles in mammalian cells." *J. Environ. Sci. Health., Part A.*,41(12), 2699-2711.

Jeon, S. and Braun, P.V. (2003). "Hydrothermal synthesis of Er-doped luminescent TiO_2 nanoparticles." *Chem. Mater.*, 15(6), 1256-1263.

Jha, A.K., Prasad, K. and Kulkarni, A.R. (2009). "Synthesis of TiO_2 nanoparticles using microorganisms." *Colloids and Surfaces B: Biointerfaces*, 71(2), 226-229.(a)

Jha, A.K., Prasad, K., Kumar, V. and Prasad, K. (2009a). "Biosynthesis of silver nanoparticles using *Eclipta leaf.*" *Biotechnol. Progr.*, 25(5), 1476-1479.

Jia, H., Xiao, W.J., Zhang, L., Zheng, Z., Zhang, H. and Deng, F. (2008). "In situ L-hydroxyproline functionalization and enhanced photocatalytic activity of TiO 2 nanorods." *J. Phys. Chem. C.*, 112(30), 11379-11384.

Jiang, H., Moon, K.S., Zhang, Z., Pothukuchi, S. and Wong, C.P. (2006). "Variable frequency microwave synthesis of silver nanoparticles." *J. Nanopart. Res.*, 8(1), 117-124.

Jiang, Z.J., Liu, C.Y. and Sun, L.W. (2005). "Catalytic properties of silver nanoparticles supported on silica spheres." *J. Phys. Chem. B.*, 109(5), 1730-1735.

Jiménez, M., Ignacio Maldonado, M., Rodríguez, E. M., Hernández-Ramírez, A., Saggioro, E., Carra, I. and Sánchez Pérez, J.A. (2015). "Supported TiO_2 solar photocatalysis at semi-pilot scale: degradation of pesticides found in citrus processing industry wastewater, reactivity and influence of photogenerated species." *J. Chem. Technol. Biotechnol.*,90(1), 149-157.

Jones, A.C. and Chalker, P.R. (2003). "Some recent developments in the chemical vapour deposition of electroceramic oxides." *J. Phys. D: Appl. Phys.*, 36(6), R80.

Joo, J., Kwon, S.G., Yu, T., Cho, M., Lee, J., Yoon, J. and Hyeon, T. (2005). "Large-Scale Synthesis of TiO_2 Nanorods via Nonhydrolytic Sol-Gel Ester Elimination Reaction and Their Application to Photocatalytic Inactivation of E. c oli." *J. Phys. Chem. B.,* 109(32), 15297-15302.

Juibari, M.M., Abbasalizadeh, S., Jouzani, G.S. and Noruzi, M. (2011). "Intensified biosynthesis of silver nanoparticles using a native extremophilic Ureibacillus thermosphaericus strain." *Mater. Lett.*, 65(6), 1014-1017.

Jung, W.K., Koo, H.C., Kim, K.W., Shin, S., Kim, S.H. and Park, Y.H. (2008). "Antibacterial activity and mechanism of action of the silver ion in *Staphylococcus aureus* and *Escherichia coli*." *Appl. Environ. Microbiol.*, 74(7), 2171-2178.

Kabashin, A.V. and Meunier, M. (2003). "Synthesis of colloidal nanoparticles during femtosecond laser ablation of gold in water." *J. Appl. Phys.*, 94(12), 7941-7943.

Kačenka, M., Kaman, O., Jirák, Z., Maryško, M., Žvátora, P., Vratislav, S. and Lukeš, I. (2014). "Magnetic properties of La^{1-}xSrxMnO$_3$ nanoparticles prepared in a molten salt." *J. Appl. Phys.*, 115(17), 17B525.

Kahl, M., Voges, E., Kostrewa, S., Viets, C. and Hill, W. (1998). "Periodically structured metallic substrates for SERS." *Sens. Actuators, B*, 51(1), 285-291.

Kahrilas, G.A., Wally, L.M., Fredrick, S.J., Hiskey, M., Prieto, A.L. and Owens, J.E. (2013). "Microwave-assisted green synthesis of silver nanoparticles using orange peel extract." *ACS Sustain. Chem. Eng.*, 2(3), 367-376.

Kaida, T., Kobayashi, K., Adachi, M. and Suzuki, F. (2003). "Optical characteristics of titanium oxide interference film and the film laminated with oxides and their applications for cosmetics." *J. Cosmet. Sci.*, 55(2), 219-220.

Kainz, Q.M. and Reiser, O. (2014). "Polymer-and dendrimer-coated magnetic nanoparticles as versatile supports for catalysts, scavengers, and reagents." *Acc. Chem. Res.*, 47(2), 667-677.

Kaiser, J.P., Diener, L. and Wick, P. (2013). "Nanoparticles in paints: A new strategy to protect façades and surfaces?" *J. Phys. Conf. Ser.,* 429(1),12-36.

Kalaiselvan, V. and Rajasekaran, A. (2009). "Biosynthesis of silver nanoparticles from *Aspergillus niger* and evaluation of its wound healing activity in experimental rat model." *Int. J. Pharm. Tech. Res*, 4, 1523-1529.

Kalimuthu, K., Babu, R.S., Venkataraman, D., Bilal, M. and Gurunathan, S. (2008). "Biosynthesis of silver nanocrystals by *Bacillus licheniformis*." *Colloids Surf. B: Biointerfaces,* 65(1), 150-153.

Kalishwaralal, K., Deepak, V., Pandian, S.R.K., Kottaisamy, M., BarathManiKanth, S., Kartikeyan, B. and Gurunathan, S. (2010). "Biosynthesis of silver and gold nanoparticles using *Brevibacterium casei." Colloids Surf. B: Biointerfaces,* 77(2), 257-262.

Kalishwaralal, K., Deepak, V., Ramkumarpandian, S., Nellaiah, H. and Sangiliyandi, G. (2008). "Extracellular biosynthesis of silver nanoparticles by the culture supernatant of *Bacillus licheniformis*." *Mater. Lett.*, 62(29), 4411-4413.

Kalyanasundharam, S. and Prakash, M.J. (2015). "Biosynthesis and characterization of titanium dioxide nanoparticles using *pithecellobium dulce* and *lagenaria siceraria* aqueous leaf extract and screening their free radical

scavenging and antibacterial properties." *International Letters of Chemistry, Physics and Astronomy*, *50*, 80.

Kangwansupamonkon, W., Lauruengtana, V., Surassmo, S. and Ruktanonchai, U. (2009). "Antibacterial effect of apatite-coated titanium dioxide for textiles applications." *Nanomed. Nanotechnol. Biol. Med.*, 5(2), 240-249.

Kaosa-ard, A. (1981). "Teak (*Tectona grandis* Linn. f) its natural distribution and related factors." *Nat. His. Bulletin Siam. Soc.*, 29, 55-74.

Karthiga, D. and Anthony, S.P. (2013). "Selective colorimetric sensing of toxic metal cations by green synthesized silver nanoparticles over a wide pH range." *RSC Adv.*, 3(37), 16765-16774.

Karunagaran, B., Uthirakumar, P., Chung, S.J., Velumani, S. and Suh, E.K. (2007). "TiO_2 thin film gas sensor for monitoring ammonia." *Mater. Charact.*, 58(8), 680-684.

Karuppiah, P. and Mustaffa, M. (2013). "Antibacterial and antioxidant activities of Musa sp. leaf extracts against multidrug resistant clinical pathogens causing nosocomial infection." *Asian Pac. J. Trop. Biomed.*, 3(9), 737-742.

Kashif, N. and Ouyang, F. (2009). "Parameters effect on heterogeneous photocatalysed degradation of phenol in aqueous dispersion of TiO_2." *J. Environ. Sci.*, 21(4), 527-533.

Kasthuri, J., Kathiravan, K. and Rajendiran, N. (2009). "Phyllanthin-assisted biosynthesis of silver and gold nanoparticles: a novel biological approach." *J. Nanopart. Res.*, 11(5), 1075-1085.

Katangur, P., Patra, P.K. and Warner, S.B. (2006). "Nanostructured ultraviolet resistant polymer coatings." *Polym. Degrad. Stab.*, 91(10), 2437-2442.

Kathiresan, K., Manivannan, S., Nabeel, M.A. and Dhivya, B. (2009). "Studies on silver nanoparticles synthesized by a marine fungus, *Penicillium fellutanum* isolated from coastal mangrove sediment." *Colloids Surf. B: Biointerfaces,* 71(1), 133-137.

Katok, K.V., Whitby, R.L., Fukuda, T., Maekawa, T., Bezverkhyy, I., Mikhalovsky, S.V. and Cundy, A.B. (2012). "Hyperstoichiometric interaction between silver and mercury at the nanoscale." *Angew. Chem. Int. Ed.*, 51(11), 2632-2635.

Kaviya, S., Santhanalakshmi, J., Viswanathan, B., Muthumary, J. and Srinivasan, K. (2011). "Biosynthesis of silver nanoparticles using *Citrus sinensis* peel extract and its antibacterial activity." *Spectrochim. Acta. A: Mol. Biomol. Spectrosc.,* 79(3), 594-598.

Kayser, O., Lemke, A. and Hernandez-Trejo, N. (2005). "The impact of nanobiotechnology on the development of new drug delivery systems." *Current Pharm. Biotechnol.*, 6(1), 3-5.

Kelly, K.L., Coronado, E., Zhao, L.L. and Schatz, G.C. (2003). "The optical properties of metal nanoparticles: the influence of size, shape, and dielectric environment." *J. Phys. Chem. B.*, 107(3), 668-677.

Khalil, M.M., Ismail, E.H., El-Baghdady, K.Z. and Mohamed, D. (2014). "Green synthesis of silver nanoparticles using olive leaf extract and its antibacterial activity." *Arabian J. Chem.*, 7(6), 1131-1139.

Khlebtsov, N.G., Trachuk, L.A. and Mel'nikov, A.G. (2005). "The effect of the size, shape, and structure of metal nanoparticles on the dependence of their optical properties on the refractive index of a disperse medium." *Opt. Spectrosc.*, 98(1), 77-83.

Khot, L.R., Sankaran, S., Maja, J.M., Ehsani, R. and Schuster, E.W. (2012). "Applications of nanomaterials in agricultural production and crop protection: a review." *Crop Prot.*, 35, 64-70.

Kim, J.S., Kuk, E., Yu, K.N., Kim, J.H., Park, S.J., Lee, H.J. and Kim, Y.K. (2007). "Antimicrobial effects of silver nanoparticles." *Nanomed. Nanotechnol. Biol. Med.*, 3(1), 95-101.

Kirthi, A.V., Rahuman, A.A., Rajakumar, G., Marimuthu, S., Santhoshkumar, T., Jayaseelan, C., Elango, G., Zahir, A.A., Kamaraj, C. and Bagavan, A. (2011). "Biosynthesis of titanium dioxide nanoparticles using bacterium *Bacillus subtilis*." *Mater. Let.*, 65(17), 2745-2747.

Klasen, H.J. (2000). "Historical review of the use of silver in the treatment of burns. I. Early uses." *Burns*, 26(2), 117-130.

Klaus, T., Joerger, R., Olsson, E. and Granqvist, C.G. (1999). "Silver-based crystalline nanoparticles, microbially fabricated." *Proc. Natl. Acad. Sci.*, 96(24), 13611-13614.

Klaus-Joerger, T., Joerger, R., Olsson, E. and Granqvist, C.G. (2001). "Bacteria as workers in the living factory: metal-accumulating bacteria and their potential for materials science." *Trends Biotechnol.*, 19(1), 15-20.

Klueh, U., Wagner, V., Kelly, S., Johnson, A. and Bryers, J.D. (2000). "Efficacy of silver-coated fabric to prevent bacterial colonization and subsequent device-based biofilm formation." *J. Biomed. Mater. Res.*, 53(6), 621-631.

Ko, T.F., Weng, Y.M. and Chiou, R.Y.Y. (2002). "Squalene content and antioxidant activity of *Terminalia catappa* leaves and seeds." *J. Agric. Food. Chem.*, 50(19), 5343-5348.

Kobayashi, M., Petrykin, V., Tomita, K. and Kakihana, M. (2011). "Hydrothermal synthesis of brookite-type titanium dioxide with snowflake-like nanostructures using a water-soluble citratoperoxotitanate complex." *J. Cryst. Growth*, 337(1), 30-37.

Koelsch, M., Cassaignon, S., Guillemoles, J.F. and Jolivet, J.P. (2002). "Comparison of optical and electrochemical properties of anatase and brookite TiO 2 synthesized by the sol–gel method." *Thin Solid Films*, 403, 312-319.

Koelsch, M., Cassaignon, S., Minh, C.T.T., Guillemoles, J.F. and Jolivet, J.P. (2004). "Electrochemical comparative study of titania (anatase, brookite and rutile) nanoparticles synthesized in aqueous medium." *Thin Solid Films*, 451, 86-92.

Kögel, I. and Zech, W. (1985). "The phenolic acid content of cashew leaves (*Anacardium occidentale* L.) and of the associated humus layer, Senegal." *Geodermal.*, 35(2), 119-125.

Kogure, K. and Hama, S. (2015). "Nanomaterials for Cosmetics. In *Encyclopedia of Polymeric Nanomaterials* (pp. 1349-1352)." Springer Berlin Heidelberg.

Kokura, S., Handa, O., Takagi, T., Ishikawa, T., Naito, Y. and Yoshikawa, T. (2010). "Silver nanoparticles as a safe preservative for use in cosmetics." *Nanomed. Nanotechnol. Biol. Med.*, 6(4), 570-574.

Konan, N.A. and Bacchi, E.M. (2007). "Antiulcerogenic effect and acute toxicity of a hydroethanolic extract from the cashew (*Anacardium occidentale* L.) leaves." *J. Ethnopharmacol.*, 112(2), 237-242.

Konishi, Y., Ohno, K., Saitoh, N., Nomura, T., Nagamine, S., Hishida, H., Takahashi, Y. and Uruga, T. (2007). "Bioreductive deposition of platinum nanoparticles on the bacterium *Shewanella algae*." *J. Biotechnol.*, 128(3), 648-653.

Konstantinou, I. and Albanis, T.A. (2004). "TiO2-assisted photocatalytic degradation of azo dyes in aqueous solution: kinetic and mechanistic investigations." *Appl. Catal. B: Environ.*, 49, 1–14.

Konstantinou, I.K., Sakellarides, T.M., Sakkas, V.A. and Albanis, T.A. (2001). "Photocatalytic degradation of selected s-triazine herbicides and organophosphorus insecticides over aqueous TiO_2 suspensions." *Environ. Sci. Technol.,* 35(2), 398-405.

Konwarh, R., Gogoi, B., Philip, R., Laskar, M.A. and Karak, N. (2011). "Biomimetic preparation of polymer-supported free radical scavenging, cytocompatible and antimicrobial "green" silver nanoparticles using aqueous extract of *Citrus sinensis* peel." *Colloids and Surfaces B: Biointerfaces*, 84(2), 338-345.

Kora, A.J. and Sashidhar, R.B. (2015). "Antibacterial activity of biogenic silver nanoparticles synthesized with gum ghatti and gum olibanum: a comparative study." *J. Antibiot.*, 68(2), 88-97.

Kore KJ, Jadhav PJ, Shetty RV, Shetty SC. (2011). "Diuretic activity of *Tectona grandis* leaves aqueous extract in wistar rats." *Int. J. Pharmaceutical Res. and deve.,* 3(7), 141-146.

Kowshik, M., Ashtaputre, S., Kharrazi, S., Vogel, W., Urban, J., Kulkarni, S. K. and Paknikar, K.M. (2002). "Extracellular synthesis of silver nanoparticles by a silver-tolerant yeast strain MKY3." *Nanotechnol.,* 14(1), 95.

Krajarathinam, K., Dheeba, B., Nageshwari, K. and Kannan, K. (2014). "Biosynthesis and characterization of intracellular TiO_2 nanoparticles by *Lactobacillus* sp: and its potential application in decolourization of methyl orange dyes." *Int. J. Pharm. Pharm. Sci.*, 7(2), 225-229.

Kreibig, U. and Vollmer, M. (1995). "Theoretical Considerations. In *Optical Properties of Metal Clusters* (pp. 13-201)." Springer Berlin Heidelberg.

Kühn, K.P., Chaberny, I.F., Massholder, K., Stickler, M., Benz, V.W., Sonntag, H.G. and Erdinger, L. (2003). "Disinfection of surfaces by photocatalytic oxidation with titanium dioxide and UVA light." *Chemosphere*, 53(1), 71-77.

Kuiters, A.T. and Denneman, C.A.J. (1987). "Water-soluble phenolic substances in soils under several coniferous and deciduous tree species." *Soil Biol. Biochem.*, 19(6), 765-769.

Kulkarni, N. and Muddapur, U. (2014). "Biosynthesis of metal nanoparticles: a review." *J. Nanotechnol.*, *2014*.

Kumar, A., Vemula, P.K., Ajayan, P.M. and John, G. (2008). "Silver-nanoparticle-embedded antimicrobial paints based on vegetable oil." *J. Nanotechnol.*, 7(3), 236-241.

Kumar, C.G. and Mamidyala, S.K. (2011). "Extracellular synthesis of silver nanoparticles using culture supernatant of *Pseudomonas aeruginosa.*" *Colloids Surf. B: Biointerfaces,* 84(2), 462-466.

Kumar, D.A., Palanichamy, V. and Roopan, S.M. (2014). "Green synthesis of silver nanoparticles using *Alternanthera dentata* leaf extract at room temperature and their antimicrobial activity." *Spectrochim. Acta. A: Mol. Biomol. Spectrosc.,* 127, 168-171.

Kumar, S.A., Abyaneh, M.K., Gosavi, S.W., Kulkarni, S.K., Pasricha, R., Ahmad, A. and Khan, M.I. (2007). "Nitrate reductase-mediated synthesis of silver nanoparticles from $AgNO_3$." *Biotechnol. Lett*, 29(3), 439-445.(a)

Kumar, S.A., Ansary, A.A., Ahmad, A. and Khan, M.I. (2007). "Extracellular biosynthesis of CdSe quantum dots by the fungus, *Fusarium oxysporum.*" *J. Biomed. Nanotechnol.*, 3(2), 190-194.(b)

Kumar, S.H., Prasad, C., Venkateswarlu, S., Venkateswarlu, P. and Jyothi, N.V. V. (2015). "Green Synthesis of Silver Nanoparticles Using Aqueous Solution of

Syzygium cumini Flowering Extract and its Antimicrobial Activity." *Indian Journal of Advances in Chemical Science*, 3(4), 299-303.

Kumar, V.V. and Anthony, S.P. (2014). "Silver nanoparticles based selective colorimetric sensor for Cd^{2+}, Hg^{2+} and Pb^{2+} ions: tuning sensitivity and selectivity using co-stabilizing agents." *Sens. Actuators, B.*, 191, 31-36.

Kvítek, O., Siegel, J., Hnatowicz, V. and Švorčík, V. (2013). "Noble metal nanostructures influence of structure and environment on their optical properties." *J. Nanomater.*, 111.

LaBean, T.H. and Li, H. (2007). "Constructing novel materials with DNA." *Nano Today.*, 2(2), 26-35.

Laemmli, U. K. (1970). "Cleavage of structural proteins during the assembly of the head of bacteriophage T4." *Nat.*, *227, 680-685*.

Lakshmipathy, R., Reddy, B.P., Sarada, N.C., Chidambaram, K. and Pasha, S.K. (2015). "Watermelon rind-mediated green synthesis of noble palladium nanoparticles: catalytic application." *Appli. Nanosci.*, 5(2), 223-228.

Lazar, V. (2011). "Quorum sensing in biofilms–how to destroy the bacterial citadels or their cohesion/power?." *Anaerobe*, 17(6), 280-285.

Lea, J. and Adesina, A.A. (1998). "The photo-oxidative degradation of sodium dodecyl sulphate in aerated aqueous TiO_2 suspension." *J. Photochem. Photobiol. A., 118*(2), 111-122.

Lee, H.J. and Jeong, S.H. (2005). "Bacteriostasis and skin innoxiousness of nanosize silver colloids on textile fabrics." *Textile Research Journal*, 75(7), 551-556.

Lee, J.S., Han, M.S. and Mirkin, C.A. (2007). "Colorimetric Detection of Mercuric Ion (Hg^{2+}) in Aqueous Media using DNA-Functionalized Gold Nanoparticles." *Angew. Chem. Int. Ed.*, 119(22), 4171-4174.

Lee, P.C. and Meisel, D. (1982). "Adsorption and surface-enhanced Raman of dyes on silver and gold sols." *J. Phys. Chem.*, 86(17), 3391-3395.

Lengke, M.F., Fleet, M.E. and Southam, G. (2007). "Biosynthesis of silver nanoparticles by filamentous cyanobacteria from a silver (I) nitrate complex." *Langmuir*, 23(5), 2694-2699.

Lévy, M., Lagarde, F., Maraloiu, V.A., Blanchin, M.G., Gendron, F., Wilhelm, C. and Gazeau, F. (2010). "Degradability of superparamagnetic nanoparticles in a model of intracellular environment: follow-up of magnetic, structural and chemical properties." *Nanotechnol.*, 21(39), 395103.

Li, G., He, D., Qian, Y., Guan, B., Gao, S., Cui, Y., Yokoyama, K. and Wang, L. (2011). "Fungus-mediated green synthesis of silver nanoparticles using *Aspergillus terreus*." *Int. J. Mol. Sci.*, 13(1), 466-476.

Li, H. and Bian, Y. (2009). "Selective colorimetric sensing of histidine in aqueous solutions using cysteine modified silver nanoparticles in the presence of Hg^{2+}" *Nanotechnol.*, 20(14), 145502.

Li, J.G., Tang, C., Li, D., Haneda, H. and Ishigaki, T. (2004). "Monodispersed Spherical Particles of Brookite-Type TiO_2: Synthesis, Characterization, and Photocatalytic Property." *J. Am. Ceram. Soc.*, 87(7), 1358-1361.

Li, K., Stockman, M.I. and Bergman, D.J. (2005b). "Optical Frequency Mixing at Coupled Gold Nanoparticles." *Phys. Rev. Lett.*, 72, 153401.

Li, S., Shen, Y., Xie, A., Yu, X., Qiu, L., Zhang, L. and Zhang, Q. (2007a). "Green synthesis of silver nanoparticles using *Capsicum annuum* L. extract." *Green Chem.*, 9(8), 852-858.

Li, X. Z., Liu, H., Cheng, L.F. and Tong, H.J. (2003a). "Photocatalytic oxidation using a new catalyst TiO_2 microsphere for water and wastewater treatment." *Environ. Sci. Technol.*, *37*(17), 3989-3994.

Li, X., Xu, H., Chen, Z.S. and Chen, G. (2011). "Biosynthesis of nanoparticles by microorganisms and their applications." *J. Nanomater.*, 8.

Li, Y., Wu, Y. and Ong, B.S. (2005a). "Facile synthesis of silver nanoparticles useful for fabrication of high-conductivity elements for printed electronics." *J. Am. Chem. Soc.*, *127*(10), 3266-3267.

Liguras, D.K., Kondarides, D.I. and Verykios, X.E. (2003). "Production of hydrogen for fuel cells by steam reforming of ethanol over supported noble metal catalysts." *Appl. Catal. B Environ.*, 43(4), 345-354.

Lin, H.M., Keng, C.H. and Tung, C.Y. (1997). "Gas-sensing properties of nanocrystalline TiO_2." *Nanostruct. Mater.*, 9(1), 747-750.

Ling, J., Sang, Y. and Huang, C. Z. (2008). "Visual colorimetric detection of berberine hydrochloride with silver nanoparticles." *J. Pharm. Biomed. Anal.,* 47(4), 860-864.

Linic, S., Christopher, P. and Ingram, D.B. (2011). "Plasmonic-metal nanostructures for efficient conversion of solar to chemical energy." *Nat. Mater.*, 10(12), 911-921.

Linsebigler, A.L., Lu, G. and Yates Jr, J.T. (1995). "Photocatalysis on TiO_2 surfaces: principles, mechanisms, and selected results." *Chem. Rev.*,95(3), 735-758.

Liu, B. and Aydil, E.S. (2009). "Growth of oriented single-crystalline rutile TiO2 nanorods on transparent conducting substrates for dye-sensitized solar cells." *J. Am. Chem. Soc.*, *131*(11), 3985-3990.

Liu, H. and Toshima, N., (1992). *J. Chem. Soc. Chem. Commun.*, 1095.

Liu, J. and Lu, Y. (2007). "Rational Design of "Turn-On" Allosteric DNAzyme Catalytic Beacons for Aqueous Mercury Ions with Ultrahigh Sensitivity and Selectivity." *Angew. Chem.*, 119(40), 7731-7734.

Liu, X., Tang, Y., Wang, L., Zhang, J., Song, S., Fan, C. and Wang, S. (2007). "Optical detection of mercury (II) in aqueous solutions by using conjugated polymers and label-free oligonucleotides." *Adv. Mater.*, 19(11), 1471-1474.

Lohani, A., Verma, A., Joshi, H., Yadav, N. and Karki, N. (2014). "Nanotechnology-based cosmeceuticals." *ISRN dermatol.*

Loo, Y.Y., Chieng, B.W., Nishibuchi, M. and Radu, S. (2012). "Synthesis of silver nanoparticles by using tea leaf extract from Camellia sinensis." *Int. J. Nanomed.*, 7, 4263.

López, R. and Gómez, R. (2012). "Band-gap energy estimation from diffuse reflectance measurements on sol–gel and commercial TiO_2: a comparative study." *J. Sol-Gel Sci. Technol.*, 61(1), 1-7.

López-Ortega, A., Estrader, M., Salazar-Alvarez, G., Roca, A.G. and Nogués, J. (2015). "Applications of exchange coupled bi-magnetic hard/soft and soft/hard magnetic core/shell nanoparticles." *Phys. Rep.*, 553, 1-32.

Losi, M.E. and Frankenberger, W.T. (1997). "Reduction of selenium oxyanions by *Enterobacter cloacae* SLD1a-1: isolation and growth of the bacterium and its expulsion of selenium particles." *Appl. Environ. Microbiol.*,63(8), 3079-3084.(a)

Losi, M.E. and Frankenberger, W.T. (1997). "Reduction of selenium oxyanions by Enterobacter cloacae strain SLD1a-1: Reduction of selenate to selenite." *Environ. Toxicol. Chem.*, 16(9), 1851-1858.(b)

Lu, W. and Lieber, C.M. (2007). "Nanoelectronics from the bottom up." *Nat. Mater.*, 6(11), 841-850.

Lukman, A.I., Gong, B., Marjo, C.E., Roessner, U. and Harris, A.T. (2011). "Facile synthesis, stabilization, and anti-bacterial performance of discrete Ag nanoparticles using *Medicago sativa* seed exudates." *J. Colloid Interface Sci.*, *353*(2), 433-444.

Luo, W., Hu, W. and Xiao, S. (2008). "Size effect on the thermodynamic properties of silver nanoparticles." *J. Phys. Chem.C.*, 112(7), 2359-2369.

Lyon, J.L., Fleming, D.A., Stone, M.B., Schiffer, P. and Williams, M.E. (2004). "Synthesis of Fe oxide core/Au shell nanoparticles by iterative hydroxylamine seeding." *Nano Lett.*, 4(4), 719-723.

Ma, Z., Kotaki, M., Inai, R. and Ramakrishna, S. (2005). "Potential of nanofiber matrix as tissue-engineering scaffolds." *Tissue Eng.*, 11(1-2), 101-109.

Maaz, K., Mumtaz, A., Hasanain, S.K. and Ceylan, A. (2007). "Synthesis and magnetic properties of cobalt ferrite ($CoFe_2O_4$) nanoparticles prepared by wet chemical route." *J. Magn. Magn. Mater.*, 308(2), 289-295.

MacCuspie, R.I. (2011). "Colloidal stability of silver nanoparticles in biologically relevant conditions." *J. Nanopart. Res.*, 13(7), 2893-2908.

Machida, M., Norimoto, K. and Kimura, T. (2005). "Antibacterial activity of photocatalytic titanium dioxide thin films with photodeposited silver on the surface of sanitary ware." *J. Am. Ceram. Soc.*, 88(1), 95-100.

Maggos, T., Bartzis, J.G., Leva, P. and Kotzias, D. (2007). "Application of photocatalytic technology for NOx removal." *Appl. Phys. A.*, 89(1), 81-84.

Maier, S.A., Brongersma, M.L., Kik, P.G., Meltzer, S., Requicha, A.A. and Atwater, H.A. (2001). "Plasmonics-a route to nanoscale optical devices." *Adv. Mater.*, 13(19), 1501-1505.

Maier, S.A., Kik, P.G., Atwater, H.A., Meltzer, S., Harel, E., Koel, B.E. and Requicha, A.A. (2003). "Local detection of electromagnetic energy transport below the diffraction limit in metal nanoparticle plasmon waveguides." *Nat. Mater.*, 2(4), 229-232.

Malarkodi, C., Chitra, K., Rajeshkumar, S., Gnanajobitha, G., Paulkumar, K., Vanaja, M. and Annadurai, G. (2013). "Novel eco-friendly synthesis of titanium oxide nanoparticles by using *Planomicrobium* sp. and its antimicrobial evaluation." *Der Pharmacia Sinica*, 4(3), 59-66.

Malato, S., Blanco, J., Richter, C., Braun, B. and Maldonado, M.I. (1998). "Enhancement of the rate of solar photocatalytic mineralization of organic pollutants by inorganic oxidizing species." *Appl. Catal. B Environ.,* 17(4), 347-356.

Mallikarjuna, K., Dillip, G.R., Narasimha, G. and John Sushrna, N. (2012). "Phytofabrication and Characterization of Silver Nanoparticles from Piper betle Broth." *Research Journal of Nanoscience and nanotechnology*, 2(1), 17-23.

Mandal, D., Bolander, M.E., Mukhopadhyay, D., Sarkar, G. and Mukherjee, P. (2006). "The use of microorganisms for the formation of metal nanoparticles and their application." *Appl. Microbiol. Biotechnol.*, 69(5), 485-492.

Mandzy, N., Grulke, E. and Druffel, T. (2005). "Breakage of TiO_2 agglomerates in electrostatically stabilized aqueous dispersions." *Powder Technol.*, 160(2), 121-126.

Maness, P.C., Smolinski, S., Blake, D.M., Huang, Z., Wolfrum, E.J. and Jacoby, W.A. (1999). "Bactericidal activity of photocatalytic TiO_2 reaction: toward an understanding of its killing mechanism." *Appl. Environ. Microbiol.*, 65(9), 4094-4098.

Mansur, H.S., Grieser, F., Marychurch, M.S., Biggs, S., Urquhart, R.S. and Furlong, D.N. (1995). "Photoelectrochemical properties of 'Q-state'CdS particles in arachidic acid Langmuir–Blodgett films."*J. Chem. Soc., Faraday Trans.*, 91(4), 665-672.

Maria, B.S., Devadiga, A., Kodialbail, V.S. and Saidutta, M.B. (2015). "Synthesis of silver nanoparticles using medicinal *Zizyphus xylopyrus* bark extract." *Appl. Nanosci.*, *5*(6), 755-762.

Marimuthu, S., Rahuman, A.A., Jayaseelan, C., Kirthi, A.V., Santhoshkumar, T., Velayutham, K., K., Bagavan, A., Kamaraj, C., Elango, G., Iyappan, M. and Siva, C. (2013). "Acaricidal activity of synthesized titanium dioxide nanoparticles using Calotropis *gigantea* against *Rhipicephalus microplus* and *Haemaphysalis bispinosa*." *Asian Pac. J. Trop. Biomed.*, 6(9), 682-688.

Markham, M.C. and Upreti, M.C. (1965). "Photoelectric effects at semiconductor electrodes." *J. Catal*., 4(2), 229-238.

Marquis, R.E., Clock, S.A. and Mota-Meira, M. (2003). "Fluoride and organic weak acids as modulators of microbial physiology." *FEMS Microbiol. Rev.*, 26(5), 493-510.

Matthews, R.W. (1991). "Photooxidative degradation of coloured organics in water using supported catalysts TiO_2 on sand." *Water. Res.*, 25(10), 1169-1176.

Mau, J.L., Ko, P.T. and Chyau, C.C. (2003). "Aroma characterization and antioxidant activity of supercritical carbon dioxide extracts from Terminalia catappa leaves." *Food Res. Int.*, *36*(1), 97-104.

Medina-Ramirez, I., Bashir, S., Luo, Z. and Liu, J.L. (2009). "Green synthesis and characterization of polymer-stabilized silver nanoparticles." *Colloids Surf. B: Biointerfaces,* 73(2), 185-191.

Mengyue, Z., Shifu, C. and Yaowu, T. (1995). "Photocatalytic degradation of organophosphorus pesticides using thin films of TiO_2." *J. Chem. Technol. Biotechnol.*, 64(4), 339-344.

Merkus HG, "Dynamic light scattering" in *Particle Size Measurements: Fundamentals, Practice, Quality,* 2009, Springer, Netherlands, 301-302.

Mie, G. (1908). "Beiträge zur Optik trüber Medien, speziell kolloidaler Metallösungen." *Ann. Phys.*, *330*(3), 377-445.

Mills, A., Davies, R.H. and Worsley, D. (1993). "Water purification by semiconductor photocatalysis." *Chem. Soc. Rev.*, *22*(6), 417-425.

Mills, A., Hodgen, S. and Lee, S. K. (2005). "Self-cleaning titania films: an overview of direct, lateral and remote photo-oxidation processes." *Res. Chem. Intermed.*, 31(4), 295-308.

Millstone, J.E., Hurst, S.J., Métraux, G.S., Cutler, J.I. and Mirkin, C.A. (2009). "Colloidal gold and silver triangular nanoprisms." *Small*, 5(6), 646-664.

Minaeian, S., Shahverdi, A.R., Nohi, A.S. and Shahverdi, H.R. (2008). "Extracellular biosynthesis of silver nanoparticles by some bacteria." *J. Sci. IAU*, 17(66), 1-4.

Mirzajani, F., Ghassempour, A., Aliahmadi, A. and Esmaeili, M.A. (2011). "Antibacterial effect of silver nanoparticles on *Staphylococcus aureus*." *Res. Microbiol.*, 162(5), 542-549.

Mittal, A.K., Bhaumik, J., Kumar, S. and Banerjee, U.C. (2014). "Biosynthesis of silver nanoparticles: elucidation of prospective mechanism and therapeutic potential." *J. Colloid Interface Sci.*, 415, 39-47.

Miyagi, T., Kamei, M., Mitsuhashi, T., Ishigaki, T. and Yamazaki, A. (2004). "Charge separation at the rutile/anatase interface: a dominant factor of photocatalytic activity." *Chem. Phys. Lett.*, 390(4), 399-402.

Mo, S.D. and Ching, W.Y. (1995). "Electronic and optical properties of three phases of titanium dioxide: rutile, anatase, and brookite." *Physical Review B*, 51(19), 13023.

Mohammadi, M.R., Cordero-Cabrera, M.C., Ghorbani, M. and Fray, D.J. (2006). "Synthesis of high surface area nanocrystalline anatase-TiO_2 powders derived from particulate sol-gel route by tailoring processing parameters." *J. Sol-Gel Sci. Technol.*, 40(1), 15-23.

Mohanpuria, P., Rana, N.K. and Yadav, S.K. (2008). "Biosynthesis of nanoparticles: technological concepts and future applications." *J. Nanopart. Res.,* 10(3), 507-517.

Mokhtari, N., Daneshpajouh, S., Seyedbagheri, S., Atashdehghan, R., Abdi, K., Sarkar, S., Sarkar, S., Minaian, S., Shahverdi, H.R. and Shahverdi, A.R. (2009). "Biological synthesis of very small silver nanoparticles by culture supernatant of *Klebsiella pneumonia*: The effects of visible-light irradiation and the liquid mixing process." *Mater. Res. Bull.,* 44(6), 1415-1421.

Montañez, A., Abreu, C., Gill, P.R., Hardarson, G. and Sicardi, M. (2009). "Biological nitrogen fixation in maize (*Zea mays* L.) by 15N isotope-dilution and identification of associated culturable diazotrophs." *Biol. Fertil. Soils*, 45(3), 253-263.

Mor, G.K., Shankar, K., Paulose, M., Varghese, O.K. and Grimes, C.A. (2006). "Use of highly-ordered TiO_2 nanotube arrays in dye-sensitized solar cells." *Nano. lett*, 6(2), 215-218.

Morones, J.R., Elechiguerra, J.L., Camacho, A., Holt, K., Kouri, J. B., Ramírez, J.T. and Yacaman, M.J. (2005). "The bactericidal effect of silver nanoparticles." *Nanotechnol.*, 16(10), 2346.

Mouxing, F.U., Qingbiao, L.I., Daohua, S.U.N., Yinghua, L.U., Ning, H.E., Xu, D.E.N.G., Huixuan, W. and Huang, J. (2006). "Rapid preparation process of silver nanoparticles by bioreduction and their characterizations." *Chin. J. Chem. Eng.*, 14(1), 114-117.

Mu, L. and Sprando, R.L. (2010). "Application of nanotechnology in cosmetics." *Pharm. Res.*, 27(8), 1746-1749.

MubarakAli, D., Thajuddin, N., Jeganathan, K. and Gunasekaran, M. (2011). "Plant extract mediated synthesis of silver and gold nanoparticles and its antibacterial activity against clinically isolated pathogens." *Colloids and Surfaces B: Biointerfaces*, 85(2), 360-365.

Mubayi, A., Chatterji, S., Rai, P.M. and Watal, G. (2012). "Evidence based green synthesis of nanoparticles." *Adv Mat Lett*, 3(6), 519-525.

Mude, N., Ingle, A., Gade, A. and Rai, M. (2009). "Synthesis of silver nanoparticles using callus extract of *Carica papaya*—a first report." *J. Plant Biochem. Biotechnol.*, 18(1), 83-86.

Mukherjee, P., Ahmad, A., Mandal, D., Senapati, S., Sainkar, S. R., Khan, M.I., Parishcha, R., Ajaykumar, P.V., Alam, M., Kumar, R. and Sastry, M. (2001a). "Fungus-mediated synthesis of silver nanoparticles and their immobilization in the mycelial matrix: a novel biological approach to nanoparticle synthesis." *Nano Lett.*, *1*(10), 515-519.

Mukherjee, P., Ahmad, A., Mandal, D., Senapati, S., Sainkar, S.R., Khan, M.I., Ramani, R., Parischa, R., Ajayakumar, P.V., Alam, M. and Sastry, M. (2001b). "Bioreduction of AuCl4⁻ ions by the fungus, *Verticillium* sp. and surface trapping of the gold nanoparticles formed." *Angew. Chem. Int. Ed.*, *40*(19), 3585-3588.

Müller, A., Behsnilian, D., Walz, E., Gräf, V., Hogekamp, L. and Greiner, R. (2016). "Effect of culture medium on the extracellular synthesis of silver nanoparticles using *Klebsiella pneumoniae, Escherichia coli and Pseudomonas jessinii*." *Biocatal. Agric. Biotechnol.*, 6, 107-115.

Muniyappan, N. and Nagarajan, N.S. (2014). "Green synthesis of silver nanoparticles with Dalbergia spinosa leaves and their applications in biological and catalytic activities." *Process Biochem.*, 49(6), 1054-1061.

Murugan, K., Senthilkumar, B., Senbagam, D. and Al-Sohaibani, S. (2014). "Biosynthesis of silver nanoparticles using *Acacia leucophloea* extract and their antibacterial activity." *Int. J. Nanomed.*, 9, 2431-2438.

Muthukumaran, U., Govindarajan, M., Rajeswary, M. and Hoti, S.L. (2015). "Synthesis and characterization of silver nanoparticles using *Gmelina asiatica* leaf extract against filariasis, dengue, and malaria vector mosquitoes." *Parasitol. Res.*, 114(5), 1817-1827.

Nadagouda, M.N. and Varma, R.S. (2008). "Green synthesis of silver and palladium nanoparticles at room temperature using coffee and tea extract." *Green Chem.*, 10(8), 859-862.

Nadtochenko, V., Denisov, N., Sarkisov, O., Gumy, D., Pulgarin, C. and Kiwi, J. (2006). "Laser kinetic spectroscopy of the interfacial charge transfer between membrane cell walls of *E. coli* and TiO_2." *J. Photochem. Photobiol. A.*, 181(2), 401-407.

Nagaveni, K., Sivalingam, G., Hegde, M.S. and Madras, G. (2004). "Photocatalytic degradation of organic compounds over combustion-synthesized nano-TiO_2." *Environ. Sci. Technol.*, 38(5), 1600-1604.

Nain, P., Saini, V., and Sharma, S. (2012). "In-vitro antibacterial and antioxidant activity of *Emblica officinalis* leaves extract." *Int. J. Pharm. Sci.*, 4(1), 385-389.

Nair, B. and Pradeep, T. (2002). "Coalescence of nanoclusters and formation of submicron crystallites assisted by *Lactobacillus* strains." *Cryst. Growth Des.*, 2(4), 293-298.

Naka, K., Yaguchi, M. and Chujo, Y. (1999). "Synthesis of poly (oxyethylene)-grafted palladium clusters." *Chem. Mater.*, 11(4), 849-851.

Nakajima, A., Hashimoto, K., Watanabe, T., Takai, K., Yamauchi, G. and Fujishima, A. (2000). "Transparent superhydrophobic thin films with self-cleaning properties." *Langmuir*, 16(17), 7044-7047.

Nakata, K. and Fujishima, A. (2012). "TiO2 photocatalysis: design and applications." *J. Photochem. Photobiol., C*, 13(3), 169-189.

Nanda, A. and Saravanan, M. (2009). "Biosynthesis of silver nanoparticles from Staphylococcus aureus and its antimicrobial activity against MRSA and MRSE." *Nanomed. Nanotechnol. Biol. Med.*, 5(4), 452-456.

nanoComposix, (2003). http://nanocomposix.com/collections/silver

Narayanan, K.B. and Sakthivel, N. (2008). "Coriander leaf mediated biosynthesis of gold nanoparticles." *Mater. Lett.*, 62(30), 4588-4590.

Narayanan, K.B. and Sakthivel, N. (2010). "Biological synthesis of metal nanoparticles by microbes." *Adv. Colloid Interface Sci.*,156(1), 1-13.

Naskar, S., Pillay, S.A. and Chanda, M. (1998). "Photocatalytic degradation of organic dyes in aqueous solution with TiO_2 nanoparticles immobilized on foamed polyethylene sheet." *J. Photochem. Photobiol. A.*, 113(3), 257-264.

Nasrollahzadeh, M., Babaei, F., Sajadi, S.M. and Ehsani, A. (2014). "Green synthesis, optical properties and catalytic activity of silver nanoparticles in the synthesis of N-monosubstituted ureas in water." *Spectrochim. Acta. A: Mol. Biomol. Spectrosc.,* 132, 423-429.

Nayak, R.R., Pradhan, N., Behera, D., Pradhan, K.M., Mishra, S., Sukla, L.B. and Mishra, B.K. (2011). "Green synthesis of silver nanoparticle by *Penicillium purpurogenum* NPMF: the process and optimization." *J. Nanopart. Res.*, 13(8), 3129-3137.

Nazeeruddin, M.K., Pechy, P., Renouard, T., Zakeeruddin, S.M., Humphry-Baker, R., Comte, P., Liska, P., Cevey, L., Costa, E., Shklover, V. and Spiccia, L. (2001). "Engineering of efficient panchromatic sensitizers for nanocrystalline TiO_2-based solar cells." *J. Am. Chem. Soc.*, 123(8), 1613-1624.

Neppolian, B., Choi, H.C., Sakthivel, S., Arabindoo, B. and Murugesan, V. (2002). "Solar light induced and TiO_2 assisted degradation of textile dye reactive blue 4." *Chemosphere*, 46(8), 1173-1181.

Neppolian, B., Sakthivel, S., Arabindoo, B., Palanichamy, M. and Murugesan, V. (1998). "Photocatalytic degradation of textile dye commonly used in cotton fabrics." *Stud. Surf. Sci. Catal.*, 113, 329-335.

Ni, M., Leung, M.K., Leung, D.Y. and Sumathy, K. (2007). "A review and recent developments in photocatalytic water-splitting using TiO_2 for hydrogen production." *Renewable Sustainable Energy Rev.*, 11(3), 401-425.

Nidavani, R.B. and Mahalakshmi, A.M. (2014). "Teak (*Tectona grandis* linn.): A renowned timber plant with potential medicinal values." *Inter J Pharm Pharm Sci*, 6(1), 48-54.

Niraimathi, K.L., Sudha, V., Lavanya, R. and Brindha, P. (2013). "Biosynthesis of silver nanoparticles using *Alternanthera sessilis* (Linn.) extract and their antimicrobial, antioxidant activities." *Colloids Surf. B: Biointerfaces,*102, 288-291.

Nivinskas, H., Koder, R.L., Anusevicius, Z., Sarlauskas, J., Miller, A.F. and Cenas, N. (1999). "Two-electron reduction of nitroaromatic compounds by *Enterobacter cloacae* NAD(P)H nitroreductase: description of quantitative structure-activity relationships." *Acta Biochim. Pol.*, 47(4), 941-949.

Njagi, E.C., Huang, H., Stafford, L., Genuino, H., Galindo, H.M., Collins, J.B., Hoag, G.E. and Suib, S.L. (2010). "Biosynthesis of iron and silver nanoparticles at room temperature using aqueous sorghum bran extracts." *Langmuir*, 27(1), 264-271.

Noguchi, T., Fujishima, A., Sawunyama, P. and Hashimoto, K. (1998). "Photocatalytic degradation of gaseous formaldehyde using TiO_2 film." *Environ. Sci. Technol.*, 32(23), 3831-3833.

Noguez, C. (2007). "Surface plasmons on metal nanoparticles: the influence of shape and physical environment." *J. Phys. Chem. C*, 111(10), 3806-3819.

Nosaka, A.Y., Kojima, E., Fujiwara, T., Yagi, H., Akutsu, H. and Nosaka, Y. (2003a). "Photoinduced changes of adsorbed water on a TiO_2 photocatalytic film as studied by 1H NMR spectroscopy." *J. Phys. Chem. B.,* 107(44), 12042-12044.

Nosaka, Y., Daimon, T., Nosaka, A.Y. and Murakami, Y. (2004). "Singlet oxygen formation in photocatalytic TiO 2 aqueous suspension." *Phys. Chem. Chem. Phys.*, 6(11), 2917-2918.

Nosaka, Y., Komori, S., Yawata, K., Hirakawa, T. and Nosaka, A.Y. (2003b). "Photocatalytic OH radical formation in TiO_2 aqueous suspension studied by several detection methods." *Phys. Chem. Chem. Phys.*, 5(20), 4731-4735.

Nosaka, Y., Nakamura, M. and Hirakawa, T. (2002). "Behavior of superoxide radicals formed on TiO_2 powder photocatalysts studied by a chemiluminescent probe method." *Phys. Chem. Chem. Phys.*, 4(6), 1088-1092.

Nwanya, A.C., Ugwuoke, P.E., Ejikeme, P.M., Oparaku, O.U. and Ezema, F.I. (2012). "*Jathropha curcas* and *citrus aurantium* leaves dye extract for use in dye sensitized solar cell with TiO_2 films." *Int. J. Electrochem. Sci*, 7, 11219-11235.

O'regan, B. and Grfitzeli, M. (1991). "A low-cost, high-efficiency solar cell based on dye-sensitized." *Nat.*, 353(6346), 737-740.

Ohko, Y., Tatsuma, T., Fujii, T., Naoi, K., Niwa, C., Kubota, Y. and Fujishima, A. (2003). "Multicolour photochromism of TiO2 films loaded with silver nanoparticles." *Nat. Mater.*, *2*(1), 29-31.

Ollis, D.F. and Serpone, N. (1989). "Heterogeneous Photocatalysis in the Environment: Application to Water Purification. Photocatalysis: Fundamentals and Applications." *John Wiley and sons*, 650- 655.

Oluwafemi, O.S., Lucwaba, Y., Gura, A., Masabeya, M., Ncapayi, V., Olujimi, O. O. and Songca, S.P. (2013). "A facile completely 'green'size tunable synthesis of maltose-reduced silver nanoparticles without the use of any accelerator." *Colloids and Surfaces B: Biointerfaces*, 102, 718-723.

Opeke, L. K. (1992). *Tropical tree crops*. Spectrum Books Ltd.

Órdenes-Aenishanslins, N.A., Saona, L.A., Durán-Toro, V.M., Monrás, J.P., Bravo, D.M. and Pérez-Donoso, J.M. (2014). "Use of titanium dioxide nanoparticles biosynthesized by *Bacillus mycoides* in quantum dot sensitized solar cells." *Microb. Cell Fact.*, 13(1), 1.

Ordonez, A. A. L., Gomez, J. D. and Vattuone, M. A. (2006). "Antioxidant activities of Sechium edule (Jacq.) Swartz extracts." *Food chem.*, 97(3), 452-458.

Osório, I., Igreja, R., Franco, R. and Cortez, J. (2012). "Incorporation of silver nanoparticles on textile materials by an aqueous procedure." *Mater. Lett.*, 75, 200-203.

Ostolska, I. and Wiśniewska, M. (2014). "Application of the zeta potential measurements to explanation of colloidal Cr_2O_3 stability mechanism in the presence of the ionic polyamino acids." *Colloid. Polym. Sci.*, 292(10), 2453-2464.

Otari, S.V., Patil, R.M., Ghosh, S.J. and Pawar, S.H. (2014). "Green phytosynthesis of silver nanoparticles using aqueous extract of *Manilkara zapota* (L.) seeds and its inhibitory action against *Candida* species." *Mater. Lett.*, 116, 367-369.

Otari, S.V., Patil, R.M., Nadaf, N.H., Ghosh, S.J. and Pawar, S.H. (2012). "Green biosynthesis of silver nanoparticles from an actinobacteria *Rhodococcu*s sp." *Mater. Lett.*, 72, 92-94.

Owolabi, M.S., Lawal, O.A., Ogunwande, I.A., Hauser, R.M. and Setzer, W.N. (2013). "Chemical composition of the leaf essential oil of *Terminalia catappa* L. growing in southwestern Nigeria." *American Journal of Essential Oils and Natural Products*, 1(1), 51-54.

Oza, G., Pandey, S., Shah, R. and Sharon, M. (2012). "Extracellular fabrication of silver nanoparticles using *Pseudomonas aeruginosa* and its antimicrobial assay." *Adv. Appl. Sci. Res.*, 3, 1776-1783.

Pal, S., Tak, Y.K. and Song, J.M. (2007). "Does the antibacterial activity of silver nanoparticles depend on the shape of the nanoparticle? A study of the gram-negative bacterium *Escherichia coli*." *Appl. Environ. Microbiol.*, 73(6), 1712-1720.

Palmer, T. (1991). "Understanding enzymes." *E. Horwood.*

Panáček, A., Kvítek, L., Prucek, R., Kolar, M., Vecerova, R., Pizurova, N., Sharma, V.K., Nevečná, T.J. and Zboril, R. (2006). "Silver colloid nanoparticles: synthesis, characterization, and their antibacterial activity." *J. Phys. Chem. B.*, 110(33), 16248-16253.

Parashar, V., Parashar, R., Sharma, B. and Pandey, A. C. (2009). "Parthenium leaf extract mediated synthesis of silver nanoparticles: a novel approach towards weed utilization." *Dig. J. Nanomater. Biostruct*, 4(1), 45-50.

Parikh, R.Y., Singh, S., Prasad, B.L.V., Patole, M.S., Sastry, M. and Shouche, Y.S. (2008). "Extracellular synthesis of crystalline silver nanoparticles and molecular evidence of silver resistance from *Morganella* sp.: towards understanding biochemical synthesis mechanism." *Chem. Bio. Chem.*, 9(9), 1415-1422.

Park, J.K., Kim, J.K. and Kim, H.K. (2007) "TiO_2–SiO_2 composite filler for thin paper." *J. Mater. Process. Technol.*, 186(1), 367-369.

Park, J.Y., Lee, C., Jung, K.W. and Jung, D. (2009). "Structure related photocatalytic properties of TiO2." *Bull. Korean Chem. Soc.*, 30(2), 402-404.

Park, S.J., Taton, T.A. and Mirkin, C.A. (2002). "Array-based electrical detection of DNA with nanoparticle probes." *Sci.*, 295(5559), 1503-1506.

Park, T.J., Papaefthymiou, G.C., Viescas, A.J., Moodenbaugh, A.R. and Wong, S.S. (2007). "Size-dependent magnetic properties of single-crystalline multiferroic $BiFeO_3$ nanoparticles." *Nano lett.*, 7(3), 766-772.

Parkin, I.P. and Palgrave, R.G. (2005). "Self-cleaning coatings." *J. Mater.Chem.*, 15(17), 1689-1695.

Parveen, S., Misra, R. and Sahoo, S.K. (2012). "Nanoparticles: a boon to drug delivery, therapeutics, diagnostics and imaging." *Nanomed. Nanotechnol. Biol. Med.*, 8(2), 147-166.

Pascual, J., Camassel, J. and Mathieu, H. (1978). "Fine structure in the intrinsic absorption edge of TiO_2." *Phys. Rev. B*, 18(10), 5606.

Patil, C.D., Borase, H.P., Patil, S.V., Salunkhe, R.B. and Salunke, B.K. (2012). "Larvicidal activity of silver nanoparticles synthesized using *Pergularia daemia* plant latex against Aedes aegypti and *Anopheles stephensi* and nontarget fish *Poecillia reticulata*." *Parasitol. Res.*, 111(2), 555-562.

Peiró, A. M., Peral, J., Domingo, C., Domenech, X. and Ayllón, J.A. (2001). "Low-temperature deposition of TiO_2 thin films with photocatalytic activity from colloidal anatase aqueous solutions." *Chem. Mater.*, 13(8), 2567-2573.

Perelshtein, I., Applerot, G., Perkas, N., Guibert, G., Mikhailov, S. and Gedanken, A. (2008). "Sonochemical coating of silver nanoparticles on textile fabrics (nylon, polyester and cotton) and their antibacterial activity." *Nanotechnol.*, 19(24), 245705.

Periasamy, S., Joo, H.S., Duong, A.C., Bach, T.H.L., Tan, V.Y., Chatterjee, S.S., Cheung, G.Y. and Otto, M. (2012). "How *Staphylococcus aureus* biofilms develop their characteristic structure." *Proc. Natl. Acad. Sci.*, 109(4), 1281-1286.

Perkowski, J., Bzdon, S., Bulska, A. and Józwiak, W.K. (2006). "Decomposition of detergents present in car-wash sewage by titania photo-assisted oxidation." *Pol. J. Environ. Stud.*, *15*(3), 457-465.

Peteros, N.P. and Uy, M.M. (2010). "Antioxidant and cytotoxic activities and phytochemical screening of four Philippine medicinal plants." *Journal of Medicinal Plants Research*, 4(5), 407-414.

Phanjom, P., Zoremi, E., Mazumder, J., Saha, M. and Baruah, S. B. (2012). "Green synthesis of silver nanoparticles using leaf extract of *Myrica esculenta*." *Int. J. NanoSci. Nanotechnol.*, 3, 73-79.

Philip, D. (2010). "Green synthesis of gold and silver nanoparticles using Hibiscus rosa sinensis." *Physica E*, 42(5), 1417-1424.

Philip, D. (2011). "Mangifera Indica leaf-assisted biosynthesis of well-dispersed silver nanoparticles." *Spectrochim. Acta. A: Mol. Biomol. Spectrosc.,* 78(1), 327-331.

Philip, D. and Unni, C. (2011). "Extracellular biosynthesis of gold and silver nanoparticles using Krishna tulsi (*Ocimum sanctum*) leaf." *Physica E*, 43(7), 1318-1322.

Philip, D., Unni, C., Aromal, S. A. and Vidhu, V.K. (2011). "Murraya koenigii leaf-assisted rapid green synthesis of silver and gold nanoparticles." *Spectrochim. Acta. A: Mol. Biomol. Spectrosc., 78*(2), 899-904.

Philip, J., Shima, P.D. and Raj, B. (2008). "Nanofluid with tunable thermal properties." *TC*, *13*, 14.

Pileni, M.P. (2000). "Fabrication and physical properties of self-organized silver nanocrystals." *Pure Appl. Chem.*, 72(1-2), 53-65.

Popov, A.P., Priezzhev, A.V., Lademann, J. and Myllylä, R. (2005). "TiO2 nanoparticles as an effective UV-B radiation skin-protective compound in sunscreens." *J. Phys. D: Appl. Phys.*, 38(15), 2564.

Pottier, A., Chanéac, C., Tronc, E., Mazerolles, L., & Jolivet, J.P. (2001). "Synthesis of brookite TiO2 nanoparticles by thermolysis of TiCl4 in strongly acidic aqueous media." *J. Mater. Chem.*, 11(4), 1116-1121.

Poulios, I. and Aetopoulou, I. (1999). "Photocatalytic degradation of the textile dye reactive orange 16 in the presence of TiO_2 suspensions." *Environ. Technol.*, *20*(5), 479-487.

Prabhawathi, V., Sivakumar, P.M. and Doble, M. (2012). "Biological Synthesis of Silver Nanoparticles and their Functional Properties." *Nanoscience and Advancing Computational Methods in Chemistry: Research Progress: Research Progress*, 162.

Prabhu, D., Arulvasu, C., Babu, G., Manikandan, R. and Srinivasan, P. (2013). "Biologically synthesized green silver nanoparticles from leaf extract of Vitex negundo L. induce growth-inhibitory effect on human colon cancer cell line HCT15." *Process Biochem.*, 48(2), 317-324.

Prabhu, S. and Poulose, E.K. (2012). "Silver nanoparticles: mechanism of antimicrobial action, synthesis, medical applications, and toxicity effects." *Int. Nano. Lett.,* 2(1), 1-10.

Pradeep, T. (2009). "Noble metal nanoparticles for water purification: a critical review." *Thin solid films*, 517(24), 6441-6478.

Prakash, A., Sharma, S., Ahmad, N., Ghosh, A. and Sinha, P. (2011). "Synthesis of AgNps by *Bacillus cereus* bacteria and their antimicrobial potential." *J. Biomater. Nanobiotechnol.*, 2(2), 155.

Prasad, K., Jha, A.K. and Kulkarni, A.R. (2007). "*Lactobacillus* assisted synthesis of titanium nanoparticles." *Nanoscale Res. Lett.*, 2(5), 248.

Prathna, T.C., Chandrasekaran, N., Raichur, A.M. and Mukherjee, A. (2011). "Kinetic evolution studies of silver nanoparticles in a bio-based green synthesis process." *Colloids Surf. A Physicochem. Eng. Asp.,* 377(1), 212-216.

Prathna, T.C., Chandrasekaran, N., Raichur, A.M. and Mukherjee, A. (2011). "Biomimetic synthesis of silver nanoparticles by *Citrus limon* (lemon) aqueous extract and theoretical prediction of particle size." *Colloids and Surfaces B: Biointerfaces*, 82(1), 152-159.

Priya, M.M., Selvi, B.K. and Paul, J.A. (2011). "Green synthesis of silver nanoparticles from the leaf extracts of Euphorbia hirta and Nerium indicum." *Dig. J. Nanomater. Biostruct.*, 6(2).

Priyadarshini, K.A., Murugan, K., Panneerselvam, C., Ponarulselvam, S., Hwang, J.S. and Nicoletti, M. (2012). "Biolarvicidal and pupicidal potential of silver nanoparticles synthesized using *Euphorbia hirta* against *Anopheles stephensi Liston* (Diptera: Culicidae)." *Parasitol. Res.*, 111(3), 997-1006.

Priyadarshini, S., Gopinath, V., Priyadharsshini, N. M., MubarakAli, D. and Velusamy, P. (2013). "Synthesis of anisotropic silver nanoparticles using novel strain, *Bacillus flexus* and its biomedical application." *Colloids and Surfaces B: Biointerfaces*, *102*, 232-237.

Qamar, M., Muneer, M. and Bahnemann, D. (2006). "Heterogeneous photocatalysed degradation of two selected pesticide derivatives, triclopyr and daminozid in aqueous suspensions of titanium dioxide." *J. Environ. Manage.*, 80(2), 99-106.

Quelemes, P.V., Araruna, F.B., de Faria, B.E., Kuckelhaus, S.A., da Silva, D.A., Mendonça, R.Z., Carla, E., Maria, S.S., Leite, J.R.S. (2013). "Development and antibacterial activity of cashew gum-based silver nanoparticles." *Int. J. Mol. Sci.*, 14(3), 4969-4981.

Rai, M., Kon, K., Ingle, A., Duran, N., Galdiero, S. and Galdiero, M. (2014). "Broad-spectrum bioactivities of silver nanoparticles: the emerging trends and future prospects." *Appl. Microbiol. Biotechnol.*, 98(5), 1951-1961.

Rai, M., Yadav, A. and Gade, A. (2009). "Silver nanoparticles as a new generation of antimicrobials." *Biotechnol. Adv., 27*(1), 76-83.

Rajakumar, G. and Rahuman, A.A. (2011). "Larvicidal activity of synthesized silver nanoparticles using *Eclipta prostrata* leaf extract against filariasis and malaria vectors." *Acta Trop.*, 118(3), 196-203.

Rajakumar, G., Rahuman, A.A., Jayaseelan, C., Santhoshkumar, T., Marimuthu, S., Kamaraj, C., Bagavan, A., Zahir, A.A., Kirthi, A.V., Elango, G. and Arora, P. (2014). "*Solanum trilobatum* extract-mediated synthesis of titanium dioxide

nanoparticles to control *Pediculus humanus capitis*, *Hyalomma anatolicum anatolicum* and *Anopheles subpictus*." *Parasitol. Res.*, 113(2), 469-479.

Rajakumar, G., Rahuman, A.A., Priyamvada, B., Khanna, V.G., Kumar, D.K. and Sujin, P. J. (2012a). "*Eclipta prostrata* leaf aqueous extract mediated synthesis of titanium dioxide nanoparticles." *Mater. Lett*, 68, 115-117.

Rajakumar, G., Rahuman, A.A., Roopan, S.M., Khanna, V.G., Elango, G., Kamaraj, C., Zahir, A.A. and Velayutham, K. (2012b). "Fungus-mediated biosynthesis and characterization of TiO_2 nanoparticles and their activity against pathogenic bacteria." *Spectrochim. Acta. A: Mol. Biomol. Spectrosc.,* 91, 23-29.

Rajamathi, M. and Seshadri, R. (2002). "Oxide and chalcogenide nanoparticles from hydrothermal/solvothermal reactions." *Curr. Opin. Solid State Mater. Sci.*, 6(4), 337-345.

Ramesh, P.S., Kokila, T. and Geetha, D. (2015). "Plant mediated green synthesis and antibacterial activity of silver nanoparticles using *Emblica officinalis* fruit extract." *Spectrochim. Acta. A: Mol. Biomol. Spectrosc.,* 142, 339-343.

Rani, D.S. and Nand, K. (2004). "Ensilage of pineapple processing waste for methane generation." *Waste Manage.*, 24(5), 523-528.

Rao, K.J. and Paria, S. (2013). "Green synthesis of silver nanoparticles from aqueous *Aegle marmelos* leaf extract." *Mater. Res. Bull.,* 48(2), 628-634.(a)

Rastogi, L. and Arunachalam, J. (2011). "Sunlight based irradiation strategy for rapid green synthesis of highly stable silver nanoparticles using aqueous garlic (Allium sativum) extract and their antibacterial potential." *Mater. Chem. Phys.*, *129*(1), 558-563.

Raut, R.W., Kolekar, N.S., Lakkakula, J.R., Mendhulkar, V.D. and Kashid, S. B. (2010). Extracellular synthesis of silver nanoparticles using dried leaves of *Pongamia pinnata* (L) pierre." *Nano-Micro Letters*, 2(2), 106-113.

Rauwel, P., Rauwel, E., Ferdov, S. and Singh, M.P. (2015). "Silver Nanoparticles: Synthesis, Properties, and Applications." *Adv. Mater. Sci. Eng.*, *2015*.

Raveendran, P., Fu, J. and Wallen, S.L. (2003). "Completely "green" synthesis and stabilization of metal nanoparticles." *J. Am. Chem. Soc.*, 125(46), 13940-13941.

Ravi, S.S., Christena, L.R., SaiSubramanian, N. and Anthony, S.P. (2013). "Green synthesized silver nanoparticles for selective colorimetric sensing of Hg^{2+} in aqueous solution at wide pH range." *Anal.*, *138*(15), 4370-4377.

Regan, O. and Grätzel, M. (1991) "A low-cost, high-efficiency solar cell based on dye-sensitized colloidal TiO_2 film." *Nat.*, 353, 737–740

RNCOS, (2015) Nanotechnology Market Outlook 2020, http://www.rncos.com/Market-Analysis-Reports/Nanotechnology-Market-Outlook-2020-IM687.htm

Roco, M. C. (2002). "NanotechnologyÐA frontier for engineering education." *Int. J. Eng. Educ.*, 18(5), 488-497.

Rodríguez-León, E., Iñiguez-Palomares, R., Navarro, R.E., Herrera-Urbina, R., Tánori, J., Iñiguez-Palomares, C. and Maldonado, A. (2013). "Synthesis of silver nanoparticles using reducing agents obtained from natural sources (*Rumex hymenosepalus* extracts)." *Nanoscale Res. Lett.*, 8(1), 1.

Roe, D., Karandikar, B., Bonn-Savage, N., Gibbins, B. and Roullet, J.B. (2008). "Antimicrobial surface functionalization of plastic catheters by silver nanoparticles." *J. Antimicrob. Chemother.*, 61(4), 869-876.

Roguska, A., Pisarek, M. andrzejczuk, M. and Lewandowska, M. (2014). "Synthesis and characterization of ZnO and Ag nanoparticle-loaded TiO_2 nanotube composite layers intended for antibacterial coatings." *Thin Solid Films*, *553*, 173-178.

Rolim, J.P., De-Melo, M.A., Guedes, S.F., Albuquerque-Filho, F.B., De Souza, J. R., Nogueira, N.A., Zanin, I.C., Rodrigues, L.K. (2012). "The antimicrobial activity of photodynamic therapy against *Streptococcus mutans* using different photosensitizers." *J. Photochem. Photobiol., B*, 106, 40-46.

Roopan, S.M., Bharathi, A., Prabhakarn, A., Rahuman, A.A., Velayutham, K., Rajakumar, G., Padmaja, R.D., Lekshmi, M., Madhumitha, G. (2012). "Efficient phyto-synthesis and structural characterization of rutile TiO_2 nanoparticles using *Annona squamosa* peel extract." *Spectrochim. Acta. A: Mol. Biomol. Spectrosc.,* 98, 86-90.

Roopan, S.M., Madhumitha, G., Rahuman, A.A., Kamaraj, C., Bharathi, A. and Surendra, T.V. (2013). "Low-cost and eco-friendly phyto-synthesis of silver nanoparticles using *Cocos nucifera* coir extract and its larvicidal activity." *Ind. Crops Prod.*, 43, 631-635.

Ros-Lis, J.V., Marcos, M.D., Mártinez-Máñez, R., Rurack, K. and Soto, J. (2005). "A Regenerative Chemodosimeter Based on Metal-Induced Dye Formation for the Highly Selective and Sensitive Optical Determination of Hg^{2+} Ions." *Angew. Chem. Int. Ed.*, 44(28), 4405-4407.

Sadhasivam, S., Shanmugam, P. and Yun, K. (2010). "Biosynthesis of silver nanoparticles by Streptomyces hygroscopicus and antimicrobial activity against medically important pathogenic microorganisms." *Colloids Surf. B: Biointerfaces, 81*(1), 358-362.

Sadowski, Z., Maliszewska, I.H., Grochowalska, B., Polowczyk, I. and Kozlecki, T. (2008). "Synthesis of silver nanoparticles using microorganisms." *Mater. Sci. Pol.*, 26(2), 419-424.

Saeb, A., Alshammari, A.S., Al-Brahim, H. and Al-Rubeaan, K.A. (2014). "Production of silver nanoparticles with strong and stable antimicrobial activity against highly pathogenic and multidrug resistant bacteria." *The Scientific World Journal*.

Saifuddin, N., Wong, C.W. and Yasumira, A.A. (2009). "Rapid biosynthesis of silver nanoparticles using culture supernatant of bacteria with microwave irradiation." *J. Chem.*, 6(1), 61-70.

Sakai, N., Fujishima, A., Watanabe, T. and Hashimoto, K. (2003). "Quantitative evaluation of the photoinduced hydrophilic conversion properties of TiO_2 thin film surfaces by the reciprocal of contact angle." *J. Phys. Chem. B.*, 107(4), 1028-1035.

Sakthivel, S., Neppolian, B., Shankar, M.V., Arabindoo, B., Palanichamy, M. and Murugesan, V. (2003). "Solar photocatalytic degradation of azo dye: comparison of photocatalytic efficiency of ZnO and TiO_2." *Sol. Energy Mater. Sol. Cells*, 77(1), 65-82.

Salkar, R.A., Jeevanandam, P., Aruna, S.T., Koltypin, Y. and Gedanken, A. (1999). "The sonochemical preparation of amorphous silver nanoparticles." *J. Mater. Chem.*, 9(6), 1333-1335.

Samadi, N., Golkaran, D., Eslamifar, A., Jamalifar, H., Fazeli, M.R. and Mohseni, F.A. (2009). "Intra/Extracellular Biosynthesis of Silver Nanoparticles by an Autochthonous Strain of *Proteus mirabilis* Isolated from Photographic Waste." *J. Biomed. Nanotechnol.*, 5(3), 247-253.

Sanghi, R. and Verma, P. (2009a). "A facile green extracellular biosynthesis of CdS nanoparticles by immobilized fungus." *Chem. Eng. J.*, 155(3), 886-891.

Sanghi, R. and Verma, P. (2009b). "Biomimetic synthesis and characterisation of protein capped silver nanoparticles." *Bioresour. Technol.,* 100(1), 501-504.

Sanguansri, P. and Augustin, M.A. (2006). "Nanoscale materials development–a food industry perspective." *Trends Food Sci. Technol.*, 17(10), 547-556.

Sankar, R., Rizwana, K., Shivashangari, K.S. and Ravikumar, V. (2015). "Ultra-rapid photocatalytic activity of *Azadirachta indica* engineered colloidal titanium dioxide nanoparticles." *Appl. Nanosci.*, 5(6), 731-736.

Santhoshkumar, T., Rahuman, A.A., Rajakumar, G., Marimuthu, S., Bagavan, A., Jayaseelan, CC., Zahir, A.A., Elango, G. and Kamaraj, C. (2011). "Synthesis of silver nanoparticles using *Nelumbo nucifera* leaf extract and its larvicidal activity against malaria and filariasis vectors." *Parasitol. Res.*, 108(3), 693-702.

Santos, K.D.O., Elias, W.C., Signori, A.M., Giacomelli, F.C., Yang, H. and Domingos, J.B. (2012). "Synthesis and catalytic properties of silver nanoparticle–linear polyethylene imine colloidal systems." *J. Phys. Chem. C*, 116(7), 4594-4604.

Sarangi, A. and Krishnan, C. (2008). "Comparison of in vitro Cr (VI) reduction by CFEs of chromate resistant bacteria isolated from chromate contaminated soil." *Bioresour. Technol.,* 99(10), 4130-4137.

Sastry, M., Ahmad, A., Khan, M.I. and Kumar, R. (2003). "Biosynthesis of metal nanoparticles using fungi and actinomycete." *Current science*, 85(2), 162-170.

Sathishkumar, G., Gobinath, C., Wilson, A. and Sivaramakrishnan, S. (2014). "*Dendrophthoe falcata* (Lf) Ettingsh (Neem mistletoe): a potent bioresource to fabricate silver nanoparticles for anticancer effect against human breast cancer cells (MCF-7)." *Spectrochim. Acta. A: Mol. Biomol. Spectrosc.,* 128, 285-290.

Sathishkumar, M., Sneha, K., Won, S.W., Cho, C.W., Kim, S. and Yun, Y.S. (2009). "*Cinnamon zeylanicum* bark extract and powder mediated green synthesis of nano-crystalline silver particles and its bactericidal activity." *Colloids Surf. B: Biointerfaces,* 73(2), 332-338.

Sathyavathi, R., Krishna, M.B., Rao, S.V., Saritha, R. and Rao, D.N. (2010). "Biosynthesis of silver nanoparticles using *Coriandrum sativum* leaf extract and their application in nonlinear optics." *Adv. Sci. Lett.*, 3(2), 138-143.

Satyavani, K., Ramanathan, T. and Gurudeeban, S. (2011). "Plant mediated synthesis of biomedical silver nanoparticles by using leaf extract of *Citrullus colocynthis." Research journal of nanoscience and nanotechnology*, 1(2), 95-101.

Saware, K. and Venkataraman, A. (2014). "Biosynthesis and characterization of stable silver nanoparticles using *Ficus religiosa* leaf extract: a mechanism perspective." *J. Cluster Sci.*, 25(4), 1157-1171.

Schmid, G. (1992). "Large clusters and colloids. Metals in the embryonic state." *Chem. Rev.*, 92(8), 1709-1727.

Schneider, K. and Schlegel, H. G. (1976). "Purification and properties of soluble hydrogenase from *Alcaligenes eutrophus* H 16." *Biochimica et Biophysica Acta (BBA)-Enzymology.*, 452(1), 66-80.

Scotta, C., Bennasar, A., Moore, E.R.B., Lalucat, J. and Gomila, M. (2011). "Taxonomic characterisation of ceftazidime-resistant Brevundimonas isolates and description of *Brevundimonas faecalis* sp. nov." *Syst. Appl. Microbiol.*, 34(6), 408-413.

Seger, B. and Kamat, P.V. (2009). "Fuel cell geared in reverse: photocatalytic hydrogen production using a TiO_2/Nafion/Pt membrane assembly with no applied bias." *J. Phys. Chem. C.*, 113(43), 18946-18952.

Sekiguchi, Y., Yao, Y., Ohko, Y., Tanaka, K., Ishido, T., Fujishima, A. and Kubota, Y. (2007). "Self-sterilizing catheters with titanium dioxide photocatalyst thin films for clean intermittent catheterization: Basis and study of clinical use." *International journal of urology*, 14(5), 426-430.

Senesac, L. and Thundat, T. G. (2008). "Nanosensors for trace explosive detection." *Mater. Today.*, *11*(3), 28-36.

Sentein, C., Guizard, B., Giraud, S., Yé, C. and Ténégal, F. (2009). "Dispersion and stability of TiO$_2$ nanoparticles synthesized by laser pyrolysis in aqueous suspensions." *J.Phys.: Conference Series,* 170(1), 12-13.

Seo, D., Yoon, W., Park, S., Kim, J. and Kim, J. (2008). "The preparation of hydrophobic silver nanoparticles via solvent exchange method." *Colloids Surf. A Physicochem. Eng. Asp.,* 313, 158-161.

Sergeev, B.M., Kasaikin, V.A., Litmanovich, E.A., Sergeev, G.B. and Prusov, A. N. (1999). "Cryochemical synthesis and properties of silver nanoparticle dispersions stabilised by poly (2-dimethylaminoethyl methacrylate)." *Mendeleev Commun.*, 9(4), 130-132.

Shah, R.R., Kaewgun, S., Lee, B.I. and Tzeng, T.R.J. (2008). "The antibacterial effects of biphasic brookite-anatase titanium dioxide nanoparticles on multiple-drug-resistant *Staphylococcus aureus*." *J. Biomed. Nanotechnol.*, 4(3), 339-348.

Shahverdi, A.R., Minaeian, S., Shahverdi, H. R., Jamalifar, H. and Nohi, A. A. (2007). "Rapid synthesis of silver nanoparticles using culture supernatants of *Enterobacteria*: a novel biological approach." *Process Biochem.*, 42(5), 919-923.

Shameli, K., Ahmad, M.B., Zamanian, A., Sangpour, P., Shabanzadeh, P., Abdollahi, Y. and Zargar, M. (2012). "Green biosynthesis of silver nanoparticles using *Curcuma longa* tuber powder." *Int. J. Nanomed*., 7, 5603.(a)

Shameli, K., Bin Ahmad, M., Jaffar Al-Mulla, E.A., Ibrahim, N.A., Shabanzadeh, P., Rustaiyan, A., Abdollahi, Y., Bagheri, S., Abdolmohammadi, S., Usman, M.S. and Zidan, M. (2012). "Green biosynthesis of silver nanoparticles using *Callicarpa maingayi* stem bark extraction." *Mol.*, 17(7), 8506-8517.

Shankar, S.S., Ahmad, A. and Sastry, M. (2003). "Geranium leaf assisted biosynthesis of silver nanoparticles." *Biotechnol. Progr.*, 19(6), 1627-1631.

Shankar, S.S., Rai, A., Ahmad, A. and Sastry, M. (2004). "Rapid synthesis of Au, Ag, and bimetallic Au core–Ag shell nanoparticles using Neem (*Azadirachta indica*) leaf broth." *J. Colloid Interface Sci.*, *275*(2), 496-502.

Sharma, G., Jasuja, N.D., Singhal, P. and Joshi, S.C. (2014). "Synthesis, characterization and antimicrobial activity of Abelia grandiflora assisted AgNPs." *J. Microb. Biochem. Technol.*

Sharma, V.K., Yngard, R.A. and Lin, Y. (2009). "Silver nanoparticles: green synthesis and their antimicrobial activities." *Adv. Colloid Interface Sci.*, 145(1), 83-96.

Shengrong, L., Juntao, Z., Liqin, D. and Jinghe, Z. (2005). "Study on the Synthesis Mechanism of Lube Oil Detergents Containing Metal Nanoparticles." *Petroleum Processing and Petrochemicals*, 36(7), 50.

Shet, A. and Shetty, V. (2015). "Photocatalytic degradation of phenol using Ag core-TiO$_2$ shell (Ag@ TiO$_2$) nanoparticles under UV light irradiation." *Environ. Sci. Pollut. Res.*, 1-10.

Shi, Z., Neoh, K.G., Kang, E.T. and Wang, W. (2006). "Antibacterial and mechanical properties of bone cement impregnated with chitosan nanoparticles." *Biomater.*, 27(11), 2440-2449.

Shibata, T., Irie, H., Ohmori, M., Nakajima, A., Watanabe, T. and Hashimoto, K. (2004). "Comparison of photochemical properties of brookite and anatase TiO$_2$ films." *Phys. Chem. Chem. Phys.*, 6(6), 1359-1362

Shipway, A.N. and Willner, I. (2001). "Nanoparticles as structural and functional units in surface-confined architectures." *Chem. Commun.*, (20), 2035-2045.

Shipway, A.N., Katz, E. and Willner, I. (2000). "Nanoparticle arrays on surfaces for electronic, optical, and sensor applications." *Chem. Phys. Chem.*, 1(1), 18-52.

Shourong, Z., Qingguo, H., Jun, Z. and Bingkun, W. (1997). "A study on dye photoremoval in TiO$_2$ suspension solution." *J. Photochem. Photobiol., A.*, 108(2), 235-238.

Shrivastava, S., Bera, T., Singh, S.K., Singh, G., Ramachandrarao, P. and Dash, D. (2009). "Characterization of antiplatelet properties of silver nanoparticles." *ACS Nano.*, 3(6), 1357-1364.

Šileikaitė, A., Prosyčevas, I., Puišo, J., Juraitis, A. and Guobienė, A. (2006). "Analysis of silver nanoparticles produced by chemical reduction of silver salt solution." *Mater. Sci.-Medzg.*, 12, 287-291.

Silverstein, R.M., Webster, F.X., Kiemle, D.J. and Bryce, D.L. (2014). "Spectrometric identification of organic compounds." John Wiley and Sons.

Singh, A.K., Talat, M., Singh, D.P. and Srivastava, O.N. (2010). "Biosynthesis of gold and silver nanoparticles by natural precursor clove and their functionalization with amine group." *J. Nanopart. Res.*, 12(5), 1667-1675.

Singh, P., Singh, H., Kim, Y.J., Mathiyalagan, R., Wang, C. and Yang, D.C. (2016). "Extracellular synthesis of silver and gold nanoparticles by *Sporosarcina koreensis* DC4 and their biological applications." *Enzyme Microb. Technol.*, 86, 75-83.

Singh, R., Wagh, P., Wadhwani, S., Gaidhani, S., Kumbhar, A., Bellare, J. and Chopade, B. A. (2013). "Synthesis, optimization, and characterization of silver nanoparticles from *Acinetobacter calcoaceticus* and their enhanced antibacterial activity when combined with antibiotics." *Int. J. Nanomedicine.*, 8, 4277-4290.

Singha, D., Barman, N. and Sahu, K. (2014). "A facile synthesis of high optical quality silver nanoparticles by ascorbic acid reduction in reverse micelles at room temperature." *J. Colloid Interface Sci.*, 413, 37-42.

Singhal, G., Bhavesh, R., Kasariya, K., Sharma, A.R. and Singh, R.P. (2011). "Biosynthesis of silver nanoparticles using *Ocimum sanctum* (Tulsi) leaf extract and screening its antimicrobial activity." *J. Nanopart. Res.*, 13(7), 2981-2988.

Singleton, V. L., Orthofer, R. and Lamuela-Raventos, R. M. (1999). "Analysis of total phenols and other oxidation substrates and antioxidants by means of folin-ciocalteu reagent." *Methods in enzymology*, 299, 152-178.

Sintubin, L., De Windt, W., Dick, J., Mast, J., van der Ha, D., Verstraete, W. and Boon, N. (2009). "Lactic acid bacteria as reducing and capping agent for the fast and efficient production of silver nanoparticles." *Appl. Microbiol. Biotechnol.*, 84(4), 741-749.

Smith, J.R., Amaya, K.R., Bredemeier, R.T., Banta, S. and Cropek, D. M. (2015). "Selective biomolecular photocatalytic decomposition using peptide-modified TiO$_2$ nanoparticles." *Appl. Catal. B Environ.,* 176, 315-324.

Sneha, K., Sathishkumar, M., Mao, J., Kwak, I.S. and Yun, Y.S. (2010). "*Corynebacterium glutamicum*-mediated crystallization of silver ions through sorption and reduction processes." *Chem. Eng. J.*, 162(3), 989-996.

So, C.M., Cheng, M.Y., Yu, J.C. and Wong, P.K. (2002). "Degradation of azo dye Procion Red MX-5B by photocatalytic oxidation." *Chemosphere*, *46*(6), 905-912.

Sobolev, K., Flores, I., Torres-Martinez, L.M., Valdez, P.L., Zarazua, E. and Cuellar, E.L. (2009). "Engineering of SiO$_2$ nanoparticles for optimal performance in nano cement-based materials. In *Nanotechnology in construction 3* (pp. 139-148). Springer Berlin Heidelberg.

Sondi, I. and Salopek-Sondi, B. (2004). "Silver nanoparticles as antimicrobial agent: a case study on *E. coli* as a model for Gram-negative bacteria." *J. Colloid Interface Sci.*, 275(1), 177-182.

Song, J.Y. and Kim, B.S. (2009). "Rapid biological synthesis of silver nanoparticles using plant leaf extracts." *Bioprocess. Biosyst. Eng.*, 32(1), 79-84.

Song, S., Yang, T., Li, Y., Pang, Z., Lin, L., Lv, M. and Han, S. (2009b). "Structural, electrical and optical properties of ITO films with a thin TiO$_2$ seed layer prepared by RF magnetron sputtering." *Vac.*, *83*(8), 1091-1094.(b)

Song, Y.Y., Schmidt-Stein, F., Bauer, S. and Schmuki, P. (2009a). "Amphiphilic TiO$_2$ nanotube arrays: an actively controllable drug delivery system." *J. Am. Chem. Soc.*, *131*(12), 4230-4232.

Sosa, I.O., Noguez, C. and Barrera, R.G. (2003). "Optical properties of metal nanoparticles with arbitrary shapes." *J. Phys. Chem. B.*, 107(26), 6269-6275.

Sowani, H., Mohite, P., Munot, H., Shouche, Y., Bapat, T., Kumar, A.R., Kulkarni, M. and Zinjarde, S. (2016). "Green synthesis of gold and silver nanoparticles by an actinomycete *Gordonia amicalis* HS-11: Mechanistic aspects and biological application." *Process Biochem.*, 51(3), 374-383.

Spatz, J.P., Chan, V.H., Mößmer, S., Kamm, F. M., Plettl, A., Ziemann, P. and Möller, M. (2002). "A combined top–down/bottom–up approach to the microscopic localization of metallic nanodots." *Adv. Mater.*, 14(24), 1827-1832.

Srinandan, C.S., Shah, M., Patel, B. and Nerurkar, A.S. (2011). "Assessment of denitrifying bacterial composition in activated sludge." *Bioresour. Technol.,* 102(20), 9481-9489.

Sriranjani, R., Srinithya, B., Vellingiri, V., Brindha, P., Anthony, S.P., Sivasubramanian, A. and Muthuraman, M.S. (2016). "Silver nanoparticle synthesis using Clerodendrum phlomidis leaf extract and preliminary investigation of its antioxidant and anticancer activities." *J. Mol. Liq.*, 220, 926-930.

Srivastava, P., Bragança, J., Ramanan, S.R. and Kowshik, M. (2013). "Synthesis of silver nanoparticles using haloarchaeal isolate *Halococcus salifodinae* BK3. " *Extremophiles*, 17(5), 821-831.

Stamplecoskie, K.G. and Scaiano, J.C. (2010). "Light emitting diode irradiation can control the morphology and optical properties of silver nanoparticles." *J. Am. Chem. Soc.*, 132(6), 1825-1827.

Stepanov, A.L. (2004). "Optical properties of metal nanoparticles synthesized in a polymer by ion implantation: a review." *Tech. Phys.*, 49(2), 143-153.

Streicher, R.M., Schmidt, M. and Fiorito, S. (2007). "Nanosurfaces and nanostructures for artificial orthopedic implants." *Nanomed.*, 2(6), 861-874.

Su, C., Hong, B.Y. and Tseng, C.M. (2004). "Sol–gel preparation and photocatalysis of titanium dioxide." *Catal. Today*, 96(3), 119-126.

Su, W., Zhang, J., Feng, Z., Chen, T., Ying, P., & Li, C. (2008). "Surface phases of TiO$_2$ nanoparticles studied by UV Raman spectroscopy and FT-IR spectroscopy." *J. Phys. Chem. C*, 112(20), 7710-7716.

Suganya, A., Murugan, K., Kovendan, K., Kumar, P.M. and Hwang, J.S. (2013). "Green synthesis of silver nanoparticles using *Murraya koenigii* leaf extract against Anopheles stephensi and Aedes aegypti." *Parasitol. Res.*, 112(4), 1385-1397.

Sukirtha, R., Priyanka, K.M., Antony, J.J., Kamalakkannan, S., Thangam, R., Gunasekaran, P., Krishnan, M. and Achiraman, S. (2012). "Cytotoxic effect of Green synthesized silver nanoparticles using *Melia azedarach* against in vitro HeLa cell lines and lymphoma mice model." *Process Biochem.*, *47*(2), 273-279.

Sul, Y.T. (2010). "Electrochemical growth behavior, surface properties, and enhanced in vivo bone response of TiO_2 nanotubes on microstructured surfaces of blasted, screw-shaped titanium implants." *Int. J. Nanomed.,* 5,87-100.

Sun, Q., Cai, X., Li, J., Zheng, M., Chen, Z. and Yu, C.P. (2014). "Green synthesis of silver nanoparticles using tea leaf extract and evaluation of their stability and antibacterial activity." *Colloids Surf. A Physicochem. Eng. Asp.,* 444, 226-231.

Sun, Y. and Xia, Y. (2002). "Shape-controlled synthesis of gold and silver nanoparticles." *Sci.*, 298(5601), 2176-2179.

Sun, Y.P., Atorngitjawat, P. and Meziani, M.J. (2001). "Preparation of silver nanoparticles via rapid expansion of water in carbon dioxide microemulsion into reductant solution." *Langmuir*, 17(19), 5707-5710.

Sunada, K., Kikuchi, Y., Hashimoto, K. and Fujishima, A. (1998). "Bactericidal and detoxification effects of TiO_2 thin film photocatalysts." *Environ. Sci. Technol.*, 32(5), 726-728.

Sunada, K., Watanabe, T. and Hashimoto, K. (2003). "Studies on photokilling of bacteria on TiO_2 thin film." *J. Photochem. Photobiol. A.*, 156(1), 227-233.

Sundrarajan, M. and Gowri, S. (2011). "Green synthesis of titanium dioxide nanoparticles by *Nyctanthes arbor-tristis* leaves extract." *Chalcogenide Lett*, 8(8), 447-451.

Suresh, A.K., Pelletier, D.A., Wang, W., Broich, M.L., Moon, J.W., Gu, B. and Doktycz, M.J. (2011). "Biofabrication of discrete spherical gold nanoparticles using the metal-reducing bacterium *Shewanella oneidensis*." *Acta Biomater.*, 7(5), 2148-2152.

Suzuki, M., Ito, T. and Taga, Y. (2001). "Photocatalysis of sculptured thin films of TiO_2." *Appl. Phys. Lett.*, 78(25), 3968-3970.

Tamayo, L.A., Zapata, P.A., Vejar, N.D., Azócar, M.I., Gulppi, M.A., Zhou, X., Thompson, G.E., Rabagliati, F.M. and Páez, M.A. (2014). "Release of silver and copper nanoparticles from polyethylene nanocomposites and their penetration into Listeria monocytogenes." *Adv. Mater. Sci. Eng. C*, 40, 24-31.

Tamboli, D.P. and Lee, D.S. (2013). "Mechanistic antimicrobial approach of extracellularly synthesized silver nanoparticles against gram positive and gram negative bacteria." *J. Hazard. Mater. B.,* 260, 878-884.

Tan, B., & Wu, Y. (2006). "Dye-sensitized solar cells based on anatase TiO_2 nanoparticle/nanowire composites." *J. Phys. Chem. B*, 110(32), 15932-15938.

Tanaka, Y., Sakai, H., Tsuke, T., Uesugi, Y., Sakai, Y. and Nakamura, K. (2011). "Influence of coil current modulation on TiO_2 nanoparticle synthesis using pulse-modulated induction thermal plasmas." *Thin Solid Films*, 519(20), 7100-7105.

Tang, W.Z. and An, H. (1995). "UV/TiO_2 photocatalytic oxidation of commercial dyes in aqueous solutions." *Chemosphere*, 31(9), 4157-4170.

Tang, W.Z., Zhang, Z., An, H., Quintana, M.O. and Torres, D.F. (1997). "TiO_2/UV photodegradation of azo dyes in aqueous solutions." *Environ. Technol.*, 18(1), 1-12.

Tarazona-Díaz, M.P., Viegas, J., Moldao-Martins, M. and Aguayo, E. (2011). "Bioactive compounds from flesh and by-product of fresh-cut watermelon cultivars." *J. Sci. Food Agric.*, 91(5), 805-812.

Tarimala, S., Kothari, N., Abidi, N., Hequet, E., Fralick, J. and Dai, L.L. (2006). "New approach to antibacterial treatment of cotton fabric with silver nanoparticle–doped silica using sol–gel process." *J. Appl. Polym. Sci.*, 101(5), 2938-2943.

Tattini, M., Galardi, C., Pinelli, P., Massai, R., Remorini, D. and Agati, G. (2004). "Differential accumulation of flavonoids and hydroxycinnamates in leaves of *Ligustrum vulgare* under excess light and drought stress." *New Phytologist*, 163(3), 547-561.

Thakkar, K.N., Mhatre, S.S. and Parikh, R.Y. (2010). "Biological synthesis of metallic nanoparticles." *Nanomed. Nanotechnol. Biol. Med.*, 6(2), 257-262.

Thamima, M. and Karuppuchamy, S. (2015). "Biosynthesis of titanium dioxide and zinc oxide nanoparticles from natural sources: A review." *Advanced Science, Engineering and Medicine*, 7(1), 18-25.

Thompson, D. (2007). "Michael Faraday's recognition of ruby gold: the birth of modern nanotechnology." *Gold Bull.*, 40(4), 267-269.

Thompson, T.L. and Yates Jr, J.T. (2005). "TiO_2-based photocatalysis: surface defects, oxygen and charge transfer." *Top. Catal.*, 35(3-4), 197-210.

Tian, F., Tian, F., Prina-Mello, A., Estrada, G., Beyerle, A., Möller, W. and Stoeger, T. (2008). "A novel assay for the quantification of internalized nanoparticles in macrophages." *Nanotoxicology*, 2(4), 232-242.

Tian, X., Chen, K. and Cao, G. (2006). "Seedless, surfactantless photoreduction synthesis of silver nanoplates." *Mater. Lett.*, *60*(6), 828-830.

Tien, D.C., Tseng, K.H., Liao, C.Y. and Tsung, T.T. (2008). "Colloidal silver fabrication using the spark discharge system and its antimicrobial effect on *Staphylococcus aureus*." *Medical engineering and physics*, 30(8), 948-952.

Tjong, S.C. (2007). "Novel nanoparticle-reinforced metal matrix composites with enhanced mechanical properties." *Adv. Eng. Mater.*, 9(8), 639-652.

Tolaymat, T.M., El Badawy, A.M., Genaidy, A., Scheckel, K.G., Luxton, T.P. and Suidan, M. (2010). "An evidence-based environmental perspective of manufactured silver nanoparticle in syntheses and applications: a systematic review and critical appraisal of peer-reviewed scientific papers." *Sci. Total Environ.*, 408(5), 999-1006.

Toma, F.L., Bertrand, G., Klein, D., Meunier, C. and Begin, S. (2008). "Development of photocatalytic active TiO_2 surfaces by thermal spraying of nanopowders." *J. Nanomater.*, *2008*, 58.

Tran, Q.H. and Le, A.T. (2013). "Silver nanoparticles: synthesis, properties, toxicology, applications and perspectives." *Adv. Nat. Sci.: Nanosci. Nanotechnol.*, 4(3), 033001.

Tripathi, R.M., Kumar, N., Shrivastav, A., Singh, P. and Shrivastav, B.R. (2013). "Catalytic activity of biogenic silver nanoparticles synthesized by *Ficus panda* leaf extract." *J. Mol. Catal. B: Enzym.*, *96*, 75-80.

Tripathy, A., Raichur, A.M., Chandrasekaran, N., Prathna, T. C. and Mukherjee, A. (2010). "Process variables in biomimetic synthesis of silver nanoparticles by aqueous extract of *Azadirachta indica* (Neem) leaves." *J. Nanopart. Res.*, 12(1), 237-246.

Trouiller, B., Reliene, R., Westbrook, A., Solaimani, P. and Schiestl, R.H. (2009). "Titanium dioxide nanoparticles induce DNA damage and genetic instability in vivo in mice." *Cancer Res.*, 69(22), 8784-8789.

Truong, Q.D., Kobayashi, M., Kato, H. and Kakihana, M. (2011). "Hydrothermal synthesis of hierarchical TiO_2 microspheres using a novel titanium complex coordinated by picolinic acid." *J. Ceram. Soc. Jpn.*, 119(1390), 513-516.

Tso, C.P., Zhung, C.M., Shih, Y.H., Tseng, Y.M., Wu, S.C. and Doong, R.A. (2010). "Stability of metal oxide nanoparticles in aqueous solutions." *Water Sci. Technol.*, 61(1), 127-133.

Tsubouchi, T., Shimane, Y., Usui, K., Shimamura, S., Mori, K., Hiraki, T., Tame, A., Uematsu, K., Maruyama, T. and Hatada, Y. (2013). "*Brevundimonas abyssalis* sp. nov., a dimorphic prosthecate bacterium isolated from deep-subsea floor sediment." *Int. J. Syst. Evol. Microbiol.*, 63(6), 1987-1994.

Tsuzuki, T. and McCormick, P.G. (2004). "Mechanochemical synthesis of nanoparticles." *J. Mater. Sci.*, 39(16-17), 5143-5146.

Turchi, C.S. and Ollis, D.F. (1990). "Photocatalytic degradation of organic water contaminants: mechanisms involving hydroxyl radical attack." *J. Catal.*, 122(1), 178-192.

Ulug, B., Turkdemir, M.H., Cicek, A. and Mete, A. (2015). "Role of irradiation in the green synthesis of silver nanoparticles mediated by fig (Ficus carica) leaf extract." *Spectrochim. Acta. A: Mol. Biomol. Spectrosc.,* 135, 153-161.

Uzunova-Bujnova, M., Kralchevska, R., Milanova, M., Todorovska, R., Hristov, D. and Todorovsky, D. (2010). "Crystal structure, morphology and photocatalytic activity of modified TiO$_2$ and of spray-deposited TiO$_2$ films." *Catal. Today*, 151(1), 14-20.

Vahabi, K., Mansoori, G.A. and Karimi, S. (2011). "Biosynthesis of silver nanoparticles by fungus *Trichoderma reesei*." *Insciences J*, *1*(1), 65-79.

Vaidyanathan, R., Gopalram, S., Kalishwaralal, K., Deepak, V., Pandian, S.R.K. and Gurunathan, S. (2010). "Enhanced silver nanoparticle synthesis by optimization of nitrate reductase activity." *Colloids and surfaces B: Biointerfaces*, 75(1), 335-341.

Valencia, S., Marín, J.M. and Restrepo, G. (2010). "Study of the bandgap of synthesized titanium dioxide nanoparticules using the sol-gel method and a hydrothermal treatment." *Open Materials Science Journal*, 4(1), 9-14.

Van Trappen, S., Tan, T.L., Samyn, E. and Vandamme, P. (2005). "*Alcaligenes aquatilis* sp. nov., a novel bacterium from sediments of the Weser Estuary, Germany, and a salt marsh on Shem Creek in Charleston Harbor, USA." *Int. J. Syst. Evol. Microbiol.*, 55(6), 2571-2575.

Vanaja, M., Gnanajobitha, G., Paulkumar, K., Rajeshkumar, S., Malarkodi, C. and Annadurai, G. (2013). "Phytosynthesis of silver nanoparticles by *Cissus quadrangularis*: influence of physicochemical factors." *J. Nanostructure Chem.*, 3(1), 1-8.

Varshney, R., Bhadauria, S. and Gaur, M. S. (2010). "Biogenic synthesis of silver nanocubes and nanorods using sundried *Stevia rebaudiana* leaves." *Adv Mat Lett*, 1(3), 232-237.

Veerasamy, R., Xin, T.Z., Gunasagaran, S., Xiang, T.F.W., Yang, E.F.C., Jeyakumar, N. and Dhanaraj, S.A. (2011). "Biosynthesis of silver nanoparticles using mangosteen leaf extract and evaluation of their antimicrobial activities." *Journal of Saudi Chemical Society*, *15*(2), 113-120.

Velayutham, K., Rahuman, A.A., Rajakumar, G., Santhoshkumar, T., Marimuthu, S., Jayaseelan, C., Bagavan, A., Kirthi, A.V., Kamaraj, C., Zahir, A.A. and Elango, G. (2012). "Evaluation of *Catharanthus roseus* leaf extract-mediated biosynthesis of titanium dioxide nanoparticles against *Hippobosca maculata* and *Bovicola ovis*." *Parasitol. Res.*, 111(6), 2329-2337.

Verma, V.C., Kharwar, R.N. and Gange, A.C. (2010). "Biosynthesis of antimicrobial silver nanoparticles by the endophytic fungus *Aspergillus clavatus*." *Nanomed.*, 5(1), 33-40.

Vigneshwaran, N., Ashtaputre, N.M., Varadarajan, P.V., Nachane, R.P., Paralikar, K.M. and Balasubramanya, R.H. (2007). "Biological synthesis of silver nanoparticles using the fungus *Aspergillus flavus*." *Mater. Lett.*, 61(6), 1413-1418.

Vigneshwaran, N., Kathe, A.A., Varadarajan, P.V., Nachane, R.P. and Balasubramanya, R.H. (2006a). "Biomimetics of silver nanoparticles by white rot fungus, *Phaenerochaete chrysosporium.*" *Colloids Surf. B: Biointerfaces,* 53(1), 55-59.

Vigneshwaran, N., Nachane, R.P., Balasubramanya, R.H. and Varadarajan, P.V. (2006b). "A novel one-pot 'green'synthesis of stable silver nanoparticles using soluble starch." *Carbohydr. Res.,* 341(12), 2012-2018.

Vijayaraghavan, K., Nalini, S.K., Prakash, N.U. and Madhankumar, D. (2012). "Biomimetic synthesis of silver nanoparticles by aqueous extract of *Syzygium aromaticum.*" *Mater. Lett., 75,* 33-35.

Vilchis-Nestor, A.R., Sánchez-Mendieta, V., Camacho-López, M.A., Gómez-Espinosa, R.M., Camacho-López, M.A. and Arenas-Alatorre, J.A. (2008). "Solventless synthesis and optical properties of Au and Ag nanoparticles using Camellia sinensis extract." *Mater. Lett., 62*(17), 3103-3105.

Vollath, D. (2008). "Nanomaterials." *An Introduction to Synthesis, Properties and Applications.*

Von White, G., Kerscher, P., Brown, R.M., Morella, J.D., McAllister, W., Dean, D. and Kitchens, C.L. (2012). "Green synthesis of robust, biocompatible silver nanoparticles using garlic extract." *J. nanometer.,* 55.

Walley, K.A., Khan, M.S.I. and Bradshaw, A.D. (1974). "The potential for evolution of heavy metal tolerance in plants. I. *Copper and zinc tolerance in Agrostis tenuis." Heredity,* 32, 309-319.

Wang, G.L., Xu, J.J. and Chen, H.Y. (2009). "Dopamine sensitized nanoporous TiO_2 film on electrodes: photoelectrochemical sensing of NADH under visible irradiation." *Biosens. Bioelectron.,* 24(8), 2494-2498.

Wang, J., Wang, X.J., Jiao, Y., Chu, M.W., Malac, M. and Li, Q. (2010). "Surface plasmon resonance in interacting Si nanoparticle chains." *Nanoscale.,* 2(5), 681-684.

Wang, J., Zhang, J., Ding, K., Xin, Y. and Pang, H. (2012). "*Brevundimonas viscosa* sp. nov., isolated from saline soil." *Int. J. Syst. Evol. Microbiol.,* 62(10), 2475-2479.

Wang, Y. and Herron, N. (1991). "Nanometer-sized semiconductor clusters: materials synthesis, quantum size effects, and photophysical properties." *J. Phys. Chem.,* 95(2), 525-532.

Wang, Y., Du, G., Liu, H., Liu, D., Qin, S., Wang, N., Hu, C., Tao, X., Jiao, J., Wang, J. and Wang, Z.L. (2008). "Nanostructured Sheets of TiO_2 Nanobelts for Gas Sensing and Antibacterial Applications." *Adv. Funct. Mater.,* 18(7), 1131-1137.

Wanyika, H., Gatebe, E., Kioni, P., Tang, Z. and Gao, Y. (2012). "Mesoporous silica nanoparticles carrier for urea: potential applications in agrochemical delivery systems." *J. Nanosci. Nanotechnol.*, 12(3), 2221-2228.

Warner, M.G., Reed, S.M. and Hutchison, J.E. (2000). "Small, water-soluble, ligand-stabilized gold nanoparticles synthesized by interfacial ligand exchange reactions." *Chem. Mater.*, 12(11), 3316-3320.

Watanabe, T., Nakajima, A., Wang, R., Minabe, M., Koizumi, S., Fujishima, A. and Hashimoto, K. (1999). "Photocatalytic activity and photoinduced hydrophilicity of titanium dioxide coated glass." *Thin solid films.*, 351(1), 260-263.

Wegner, K., Walker, B., Tsantilis, S. and Pratsinis, S.E. (2002). "Design of metal nanoparticle synthesis by vapor flow condensation." *Chem. Eng. Sci.*, 57(10), 1753-1762.

Wegner, S.V., Okesli, A., Chen, P. and He, C. (2007). "Design of an emission ratiometric biosensor from MerR family proteins: a sensitive and selective sensor for Hg^{2+}." *J. Am. Chem. Soc.*, 129(12), 3474-3475.

Wei, X., Luo, M., Li, W., Yang, L., Liang, X., Xu, L., Kong, P., Liu, H. (2012). Synthesis of silver nanoparticles by solar irradiation of cell-free *Bacillus amyloliquefaciens* extracts and $AgNO_3$. *Bioresour. Technol.*, 103, 273–278.

Weir, A., Westerhoff, P., Fabricius, L., Hristovski, K. and Von Goetz, N. (2012). "Titanium dioxide nanoparticles in food and personal care products." *Environ. Sci. Technol.*, 46(4), 2242-2250.

Weiss, J., Takhistov, P. and McClements, D.J. (2006). "Functional materials in food nanotechnology." *J. Food Sci.*, 71(9), R107-R116.

Wen, L., Lin, Z., Gu, P., Zhou, J., Yao, B., Chen, G. and Fu, J. (2009). "Extracellular biosynthesis of monodispersed gold nanoparticles by a SAM capping route." *J. Nanopart. Res.*, 11(2), 279-288.

Wiesenthal, A., Hunter, L., Wang, S., Wickliffe, J. and Wilkerson, M. (2011). "Nanoparticles: small and mighty." *Int.J. dermatol.*, 50(3), 247-254.

Wilcoxon, J.P., Williamson, R.L. and Baughman, R. (1993). "Optical properties of gold colloids formed in inverse micelles." *J. Chem. Phys.*, 98(12), 9933-9950.

Wiley, B., Sun, Y., Mayers, B. and Xia, Y. (2005). "Shape-controlled synthesis of metal nanostructures: the case of silver." *Chem. Eur. J.*, 11(2), 454-463.

Wolf, R., Matz, H., Orion, E. and Lipozencic, J. (2003). "Sunscreens-the ultimate cosmetic." *Acta Dermatovenerol. Croat.*, 11(3), 158-162.

Wong, C.P., Moon, K.S. and Li, Y. (2010). "*Nano-bio-electronic, photonic and MEMS packaging* (p. 297)." New York, NY, USA:: Springer.

Wu, D., Fan, W., Kishen, A., Gutmann, J.L. and Fan, B. (2014). "Evaluation of the antibacterial efficacy of silver nanoparticles against *Enterococcus faecalis* biofilm." *J. Endod.*, 40(2), 285-290.

Wu, H.P., Cheng, T.L. and Tseng, W.L. (2007). "Phosphate-modified TiO_2 nanoparticles for selective detection of dopamine, levodopa, adrenaline, and catechol based on fluorescence quenching." *Langmuir*, 23(14), 7880-7885.

Xia, X., Zeng, J., Zhang, Q., Moran, C. H., & Xia, Y. (2012). Recent developments in shape-controlled synthesis of silver nanocrystals. *J. Phy. Chem.C, 116*(41), 21647-21656.

Xia, Y., Xiong, Y., Lim, B. and Skrabalak, S. E. (2009). "Shape-Controlled Synthesis of Metal Nanocrystals: Simple Chemistry Meets Complex Physics?" *Angew. Chem. Int. Ed.*, 48(1), 60-103.

Xu, A.W., Gao, Y. and Liu, H.Q. (2002). "The preparation, characterization, and their photocatalytic activities of rare-earth-doped TiO_2 nanoparticles." *J. Catal.*, 207(2), 151-157.

Xu, H., Wang, L., Su, H., Gu, L., Han, T., Meng, F. and Liu, C. (2015). "Making Good Use of Food Wastes: Green Synthesis of Highly Stabilized Silver Nanoparticles from Grape Seed Extract and Their Antimicrobial Activity." *Food Biophys.*, 10(1), 12-18.

Yang, H., Zhou, Z., Huang, K., Yu, M., Li, F., Yi, T. and Huang, C. (2007). "Multisignaling optical-electrochemical sensor for Hg^{2+} based on a rhodamine derivative with a ferrocene unit." *Org. Lett.*, 9(23), 4729-4732.

Yang, H., Zhu, S. and Pan, N. (2004). "Studying the mechanisms of titanium dioxide as ultraviolet blocking additive for films and fabrics by an improved scheme." *J. Appl. Polym. Sci.*, 92(5), 3201-3210.

Yang, N. and Li, W.H. (2013). "Mango peel extract mediated novel route for synthesis of silver nanoparticles and antibacterial application of silver nanoparticles loaded onto non-woven fabrics." *Ind. Crops Prod.*, 48, 81-88.

Yang, Y.K., Yook, K.J. and Tae, J. (2005). "A rhodamine-based fluorescent and colorimetric chemodosimeter for the rapid detection of Hg^{2+} ions in aqueous media." *J. Am. Chem. Soc.*, 127(48), 16760-16761.

Yao, H., Miki, K., Nishida, N., Sasaki, A. and Kimura, K. (2005). "Large optical activity of gold nanocluster enantiomers induced by a pair of optically active penicillamines." *J. Am. Chem. Soc.*, 127(44), 15536-15543.

Yoffe, A. D. (2001). "Semiconductor quantum dots and related systems: electronic, optical, luminescence and related properties of low dimensional systems." *Adv. Phys.*, 50(1), 1-208.

Yoon, S., Albers, A.E., Wong, A.P. and Chang, C.J. (2005). "Screening mercury levels in fish with a selective fluorescent chemosensor." *J. Am. Chem. Soc.*, 127(46), 16030-16031.

Yoshida, H., Hirao, K., Nishimoto, J.I., Shimura, K., Kato, S., Itoh, H. and Hattori, T. (2008). "Hydrogen production from methane and water on platinum loaded titanium oxide photocatalysts." *J. Phys. Chem. C*, 112(14), 5542-5551.

Yu, J.C., Ho, W., Lin, J., Yip, H. and Wong, P.K. (2003a). "Photocatalytic activity, antibacterial effect, and photoinduced hydrophilicity of TiO_2 films coated on a stainless steel substrate." *Environ. Sci. Technol.*, 37(10), 2296-2301.(a)

Yu, J.C., Zhang, L., Zheng, Z. and Zhao, J. (2003b). "Synthesis and characterization of phosphated mesoporous titanium dioxide with high photocatalytic activity." *Chem. Mater.*, 15(11), 2280-2286.

Yu, J.G., Yu, H.G., Cheng, B., Zhao, X.J., Yu, J.C. and Ho, W.K. (2003c). "The effect of calcination temperature on the surface microstructure and photocatalytic activity of TiO_2 thin films prepared by liquid phase deposition." *J. Phys. Chem. B.*, 107(50), 13871-13879.

Zaki, S., El Kady, M.F. and Abd-El-Haleem, D. (2011). "Biosynthesis and structural characterization of silver nanoparticles from bacterial isolates." *Mater. Res. Bull.*, 46(10), 1571-1576.

Zargar, M., Shameli, K., Najafi, G.R. and Farahani, F. (2014). "Plant mediated green biosynthesis of silver nanoparticles using *Vitex negundo* L. extract." *J. Ind. Eng. Chem.*, 20(6), 4169-4175.

Zhang, H. (2012). "Daunorubicin-TiO." *Int. J. Nanomed.*, 7, 235-242.

Zhang, J. Z. and Noguez, C. (2008). "Plasmonic optical properties and applications of metal nanostructures." *Plasmonics*, 3(4), 127-150.

Zhang, S., Bao, K., Halas, N.J., Xu, H. and Nordlander, P. (2011). "Substrate-induced Fano resonances of a plasmonic nanocube: a route to increased-sensitivity localized surface plasmon resonance sensors revealed." *Nano. Lett.*, 11(4), 1657-1663.

Zhang, X., Fujishima, A., Jin, M., Emeline, A.V. and Murakami, T. (2006). "Double-layered TiO_2-SiO_2 nanostructured films with self-cleaning and antireflective properties." *J. Phys. Chem. B.*, 110(50), 25142-25148.

Zhang, X., Sun, H., Zhang, Z., Niu, Q., Chen, Y., & Crittenden, J.C. (2007). "Enhanced bioaccumulation of cadmium in carp in the presence of titanium dioxide nanoparticles." *Chemosphere,* 67(1), 160-166.

Zhang, X.T., Sato, O., Taguchi, M., Einaga, Y., Murakami, T. and Fujishima, A. (2005). "Self-cleaning particle coating with antireflection properties." *Chem. Mater.*, 17(3), 696-700.

Zhang, Y., Tang, Z.R., Fu, X. and Xu, Y.J. (2010). "TiO$_2$−graphene nanocomposites for gas-phase photocatalytic degradation of volatile aromatic pollutant: is TiO$_2$− graphene truly different from other TiO$_2$−carbon composite materials?" *ACS Nano.*, 4(12), 7303-7314.

Zhang, Z., Wang, C.C., Zakaria, R. and Ying, J.Y. (1998). "Role of particle size in nanocrystalline TiO$_2$-based photocatalysts." *J. Phys. Chem. B.*, 102(52), 10871-10878.

Zhao, H.E. and Shen, F. (2012). "The applied research of nanophase materials in sports engineering." *Advanced Materials Research*, 496, 126-129.

Zhao, J., Pinchuk, A.O., McMahon, J.M., Li, S., Ausman, L.K., Atkinson, A.L. and Schatz, G.C. (2008). "Methods for describing the electromagnetic properties of silver and gold nanoparticles." *Acc. Chem. Res.*, 41(12), 1710-1720.

Zhao, Y., Jiang, Y. and Fang, Y. (2006). "Spectroscopy property of Ag nanoparticles." *Spectrochim. Acta, Part A*, 65(5), 1003-1006.

Zheng, X., Xu, W., Corredor, C., Xu, S., An, J., Zhao, B. and Lombardi, J.R. (2007). "Laser-induced growth of monodisperse silver nanoparticles with tunable surface plasmon resonance properties and a wavelength self-limiting effect." *J. Phys. Chem. C*, 111(41), 14962-14967.

Zhong, C.J. and Maye, M.M. (2001). "Core–shell assembled nanoparticles as catalysts." *Adv. Mater.*, 13(19), 1507-1511.

Zhou, Y., Lin, W., Huang, J., Wang, W., Gao, Y., Lin, L., Li, Q., Lin, L. and Du, M. (2010). "Biosynthesis of gold nanoparticles by foliar broths: roles of biocompounds and other attributes of the extracts." *Nanoscale Res. Lett.*, 5(8), 1351.

Zhu, J., Liao, X. and Chen, H.Y. (2001). "Electrochemical preparation of silver dendrites in the presence of DNA." *Mater. Res. Bull.,* 36(9), 1687-1692.

Zhu, J., Liu, S., Palchik, O., Koltypin, Y. and Gedanken, A. (2000). "Shape-controlled synthesis of silver nanoparticles by pulse sonoelectrochemical methods." *Langmuir*, 16(16), 6396-6399.

Zhu, W., Yang, Z., Ma, Z. and Chai, L. (2008). "Reduction of high concentrations of chromate by *Leucobacter* sp. CRB1 isolated from Changsha, China." *World J. Microbiol. Biotechnol.*, 24(7), 991-996.

Zhu, X.J., Fu, S.T., Wong, W.K., Guo, J.P. and Wong, W.Y. (2006). "A Near-Infrared-Fluorescent Chemodosimeter for Mercuric Ion Based on an Expanded Porphyrin." *Angew. Chem.*, 118(19), 3222-3226.

Zhu, Z., Su, Y., Li, J., Li, D., Zhang, J., Song, S., Zhao, Y., Li, G. And Fan, C. (2009). "Highly sensitive electrochemical sensor for mercury (II) ions by using a mercury-specific oligonucleotide probe and gold nanoparticle-based amplification." *Anal. Chem.*, 81(18), 7660-F7666.

Zollinger, H. (2003). "Color chemistry: syntheses, properties, and applications of organic dyes and pigments." *John Wiley and Sons*.

Zuas, O., Hamim, N. and Sampora, Y. (2014). "Bio-synthesis of silver nanoparticles using water extract of *Myrmecodia pendan* (Sarang Semut plant)." *Mater. Lett.*, 123, 156-159.

APPENDICES

APPENDIX I

Analysis of residual Ag^+/Ti^{+4} ions concentration in the synthesis mixture and determination of conversion of Ag^+ ions using Atomic Absorption spectroscopy

To determine the conversion of Ag^+/Ti^{+4} ions in the synthesis mixture, the residual Ag^+/Ti^{+4} ions concentration in the synthesis mixture after the synthesis of AgNPs was measured. The synthesis mixture after 24 h of reaction time was centrifuged at 15000 rpm for 20 minutes and the supernatant with suitable dilutions was analysed using AAS (GBC 932-PLUS, USA) for concentration of residual Ag^+/Ti^{+4} ions.

Estimation of residual Ag^+ ions using Atomic Absorption spectroscopy

The silver standard stock solution of 1 mg/mL (Merck, Germany) for the estimation of Ag^+ ions was used to determine the concentration using Atomic Absorption spectroscopy (GBC 932 plus, USA). The stock solution was diluted several folds to obtain the concentrations of 3 mg/L,5 mg/L,7 mg/L, 9 mg/L and 11 mg/L as standard working solutions according to the silver estimation protocol of the AAS instrument. The silver lamp along with Air acetylene gas was used to determine the absorbance of Ag^+ ions. A calibration plot was plotted for the standard solutions. The samples containing unknown concentration of residual Ag^+ ions were suitably before AAS analysis and multiplied by the appropriate dilution factors after the analysis.

Conc (mg/L)	Absorbance (a.u)	
0	0	
3	0.25	
5	0.436	
7	0.58	
9	0.741	
11	0.89	
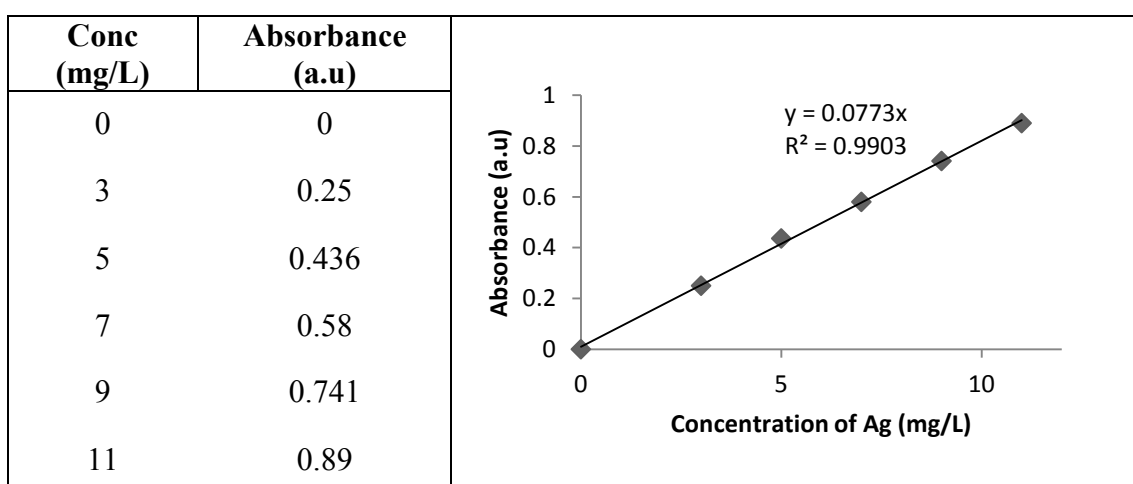
Fig A I (A) Sample calibration plot for the estimation of Ag^+ ions using AAS

Estimation of residual Ti^{+4} ions using Atomic Absorption spectroscopy

The titanium standard stock solution of 1mg/mL (Merck, Germany) for the estimation of Ti^{+4} ions was used to determine the concentration using Atomic Absorption spectroscopy (GBC 932 plus, USA). The stock solution was diluted several folds to obtain the concentrations of 5 mg/L, 10 mg/L, 15 mg/L, and 20 mg/L as standard working solutions according to the Ti^{+4} ions estimation protocol of the AAS instrument. The titanium lamp along with Nitrous gas was used to determine the absorbance of the Ti^{+4} ions. A calibration plot was plotted for the standard solutions. The samples containing unknown concentration of residual titanium ions were suitably diluted before AAS analysis and multiplied by the appropriate dilution factors after the analysis.

Conc (mg/L)	Absorbance (a.u)
0	0
5	0.015
10	0.027
15	0.037
20	0.052
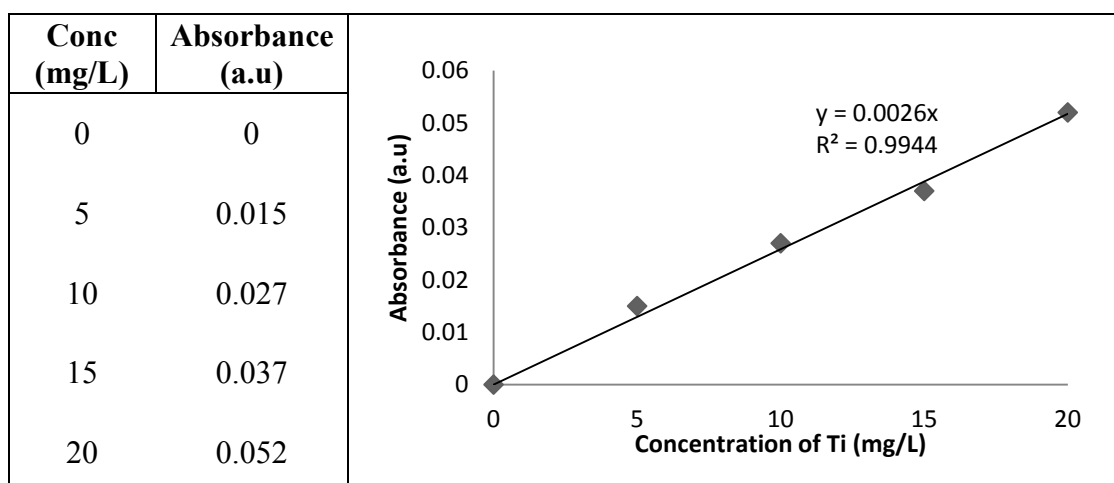
Fig A I (B) Sample calibration plot for the estimation of Ti^{+4} ions using AAS

Percentage conversion of Ag^+/Ti^{+4} ions to AgNPs/TiO$_2$-NPs was calculated using Eq. (A1)

$$Percentage\ conversion = \left(\frac{C_i - C_r}{C_i}\right) \times 100 \qquad \ldots\ldots\ldots.. (A1)$$

C_i=Initial concentration of Ag^+/Ti^{+4} ions in the reaction mixture before synthesis of nanoparticles, mg/L

C_r= Final (residual) concentration of Ag^+/Ti^{+4} ions in the reaction mixture after synthesis of nanoparticles, mg/L**.**

384

APPENDIX II

Estimation of total phenolic content

The total phenolic content (TPC) of extracts was measured using Folin-Ciocalteu method. A stock solution of 100 µg/mL of Gallic acid was prepared and working solution of concentration 10 µg/mL, 20 µg/mL, 30 µg/mL, 40 µg/mL and 50 µg/mL were prepared by suitable diluting the stock solution. 0.3 mL of the sample aliquot was drawn from each standard solution to be used for the assay. For the assay, 1.5 mL Folin-Ciocalteu's phenol reagent (Sigma) (10% v/v) and 1.2 mL 7.5% (w/v) Na_2CO_3 were added to 0.3 mL sample. The reaction mixture was thoroughly mixed and was incubated in the dark for 30 minutes before the absorbance was measured at 765 nm. Total phenolic content was determined in terms of µg of gallic acid equivalents (GAE)/mL using the calibrated data with gallic acid standards as depicted below.

Conc µg/mL	Absorbance (a.u)
0	0
10	0.115
20	0.279
30	0.402
40	0.579
50	0.664

y = 0.0137x
R^2 = 0.9947
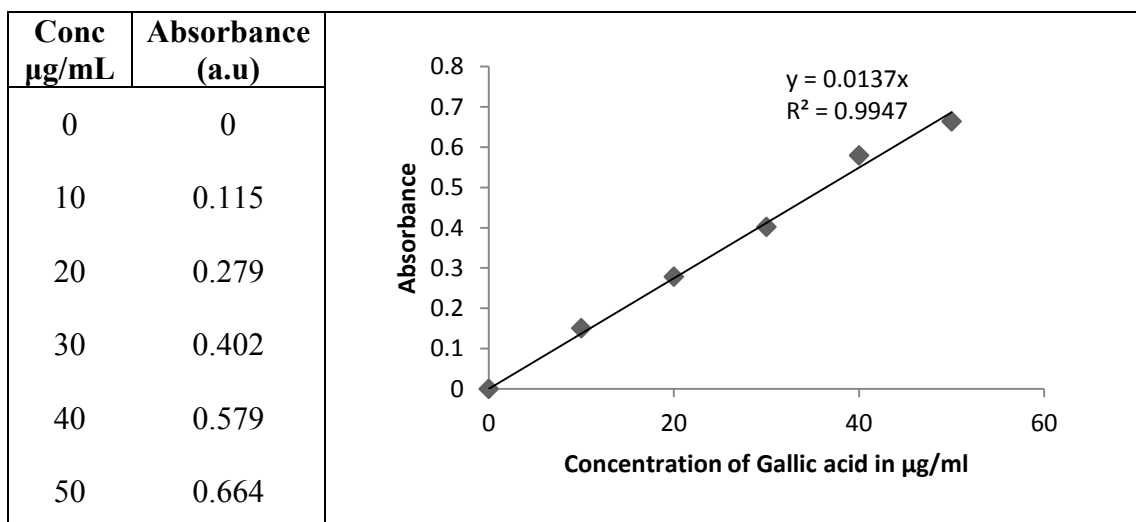
Fig A II Calibration plot for the determination of Total Phenolic content in plant extracts using gallic acid as standard

APPENDIX III

Estimation of Total Flavonoid Content

A stock solution of 200 µg/mL of Quercitin (Sigma Aldrich, India) was prepared and standard working solutions ranging from 20 µg/mL, 40 µg/mL, 60 µg/mL, 80 µg/mL and 100 µg/mL were prepared using the stock. 0.5 mL of the aliquot was drawn from each of the standard working solutions to be used in the assay for the determination of Total Flavonoid Content

The flavonoids contents in the standard working samples were determined spectrophotometrically using the method of Ordon-Ez et al. (2006) based on the formation of a complex flavonoid-aluminum. An amount of 0.5 ml of 2% $AlCl_3$ ethanol solution was added to 0.5 ml of sample in a clean test tube. After 1 h at room temperature, the absorbance from each of the test tube containing the solutions was measured at 420 nm. Formation of yellow color indicated the presence of flavonoids and was expressed as µg of Quercitin equivalent (QE)/mL.

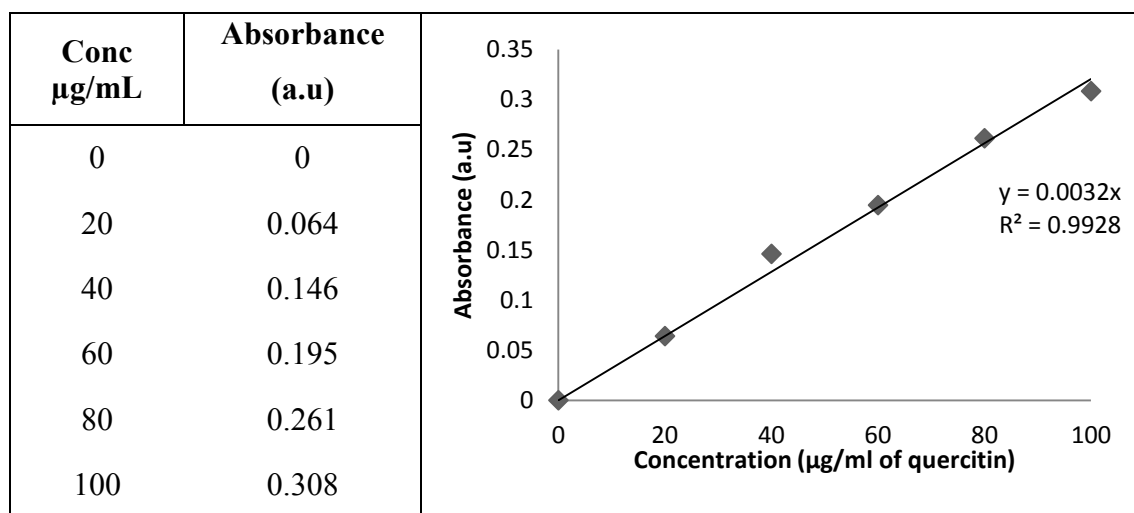| Conc µg/mL	Absorbance (a.u)
0	0
20	0.064
40	0.146
60	0.195
80	0.261
100	0.308

$y = 0.0032x$
$R^2 = 0.9928$

Fig A III Calibration plot for determination of Total Flavonoid Content using Quercitin

Estimation of Total Antioxidant Content

Total antioxidant activity (FRAP assay) of the plant extracts was determined wherein the stock solutions included 300mM acetate buffer (3.1 g $C_2H_3NaO_2-3H_2O$ and 16 mL $C_2H_4O_2$), pH 3.6, 10 mM TPTZ (2,4,6-tripyridyl- s-triazine) solution in 40mM HCl, and 20mM $FeCl_3-6H_2O$ solution. The fresh working solution was prepared by mixing 25 mL acetate buffer, 2.5mL TPTZ, and 2.5mL $FeCl_3-6H_2O$. The temperature of the solution was raised to 37^oC before using. A stock solution of 1 mM/mL of $FeSO_4$ was prepared and working solutions of 0.2 mM/mL, 0.4 mM/mL, 0.6 mM/mL, 0.8 mM/mL and 1 mM/mL were made by diluting the stock solution with deionized water. 0.2 mL of the sample aliquot from each of the standard working solutions were allowed to react with 3 mL of the FRAP solution prepared according to the specification mentioned in the previous paragraph for 30 min time duration in the dark condition. Readings of the colored product (ferrous tripyridyltriazine complex) were taken at 593 nm using UV Vis Spectrophotometer. The standard curve was linear between 200 μM and 1000μM of FeSO4. Results are expressed in terms of μM/mL of ferrous equivalents (FE).

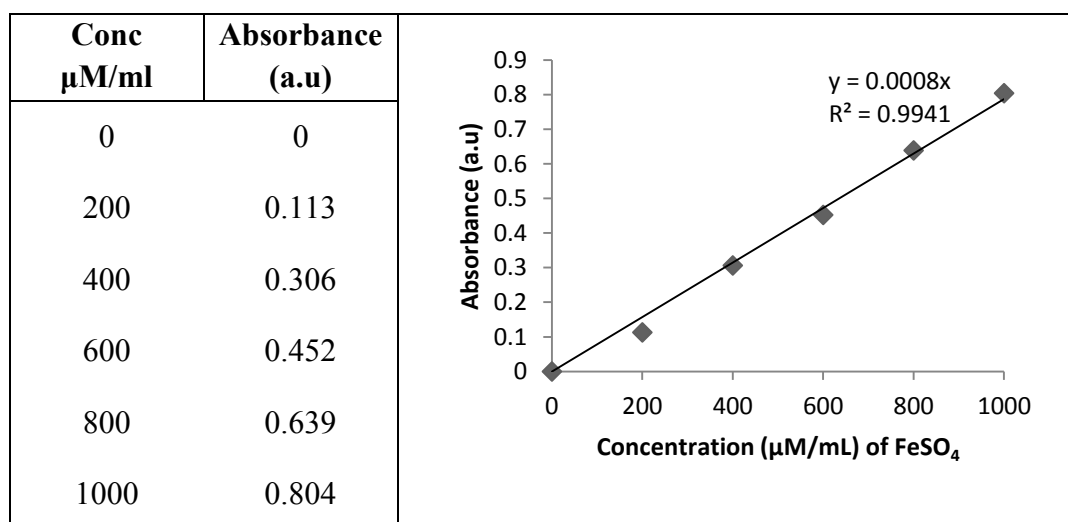| Conc μM/ml	Absorbance (a.u)
0	0
200	0.113
400	0.306
600	0.452
800	0.639
1000	0.804

$y = 0.0008x$
$R^2 = 0.9941$

Fig A IV Calibration plot for determination of total antioxidant content using Ferrous sulphate as standard

IDENTIFICATION OF THE BACTERIAL CULTURES BY 16S ribosomal RNA APPROACH

The bacterial cultures were sent for identification as isolated pure colonies in nutrient agar plates to Agharkar Research Institute, Pune.

The methodology followed by them is as follows:

The cultural sample was processed for identification in the following manner –

1. Genomic DNA was isolated from the culture by using Sigma's "GenElute Bacterial Genomic" DNA Kit.

2. PCR was carried out using the following combination of primers –

    FDD2 – RPP2 (universal primers for 1.5 kb fragment amplification for eubacteria).

The PCR was set using the following Mix:

ddH$_2$O	12.0µL
10 X PCR buffer	2.0 µL
dNTPs	2.0 µL
Forward primer	0.4 µL
Reverse primer	0.4 µL
Taq DNA Pol.	0.2 µL
Template DNA	3.0 µL
Total volume	**20.0** µL

Template DNA – Genomic DNA
Sequences of the primer pair used for amplification -
RPP2 – CCAAGCTTCTAGACGGITACCTTGTTACGACTT
FDD2 – CCGGATCCGTCGACAGAGTTTGATCITGGCTCAG

3. The PCR products obtained from above reactions were then processed for Cycle sequencing reaction (PCR performed using only one primer – RPP2)

4. Following the above reaction, the samples were cleaned up and loaded on the sequencer.(Avant 3100 Gene Analyser)

Protocol:

Total genomic DNA was isolated using GeneElute Genomic DNA isolation kit (Sigma,USA) as per the manufacturer's instructions and used as template for PCR. Each reaction mixture contained approximately 10 ng of DNA; 2.5 mM MgCl$_2$; 1X PCR buffer (Bangalore Genei, Bangalore, India); 200 µM each dCTP,

dGTP, dATP, and dTTP; 2 pmol of each, forward and reverse primer; and 1 U of Taq DNA polymerase (Bangalore Genei, Bangalore, India) in a final volume of 20 µl. FDD2 and RPP2 primers were used to amplify almost entire 16S rRNA gene, as described previously (Rawlings 1995). The PCR was performed using the Eppendorf Gradient Mastercycler system with a cycle of 94°C for 5 min; 30 cycles of 94º, 60º, and 72°C for 1 min each; and final extension at 72°C for 10 min, and the mixture was held at 4°C. The PCR product was precipitated using polyethylene glycol (PEG 6000, 8.5%) washed thrice-using 70% ethanol and dissolved in Tris-HCL (10mM, pH 8.0).

The ABI Prism BigDye Terminator Cycle Sequencing Ready Reaction kit (Applied Biosystems, Foster City, Calif.) was used for the sequencing of the PCR product. A combination of universal primers was chosen to sequence the nearly complete gene (Rawlings 1995; Muyzer et al. 1993). The sequencing reaction and template preparation were performed and purified in accordance with the directions of the manufacturer (Applied Biosystems). Samples were run on an ABI PRISM 3100 Genetic Analyzer (Applied Biosystems). The sequencing output was analyzed using the accompanying DNA Sequence Analyzer computer software (Applied Biosystems). The sequence was compared with National Center for Biotechnology Information GenBank entries by using the BLAST algorithm.

16S ribosomal RNA gene partial sequence of strain 4S1

GCCTGACGCAGCCATGCCGCGTGAATGATGAAGGTCTTAGGATTGTAAAATTCTTTCACCGGGGACG
ATAATGACGGTACCCGGAGAAGAAGCCCCGGCTAACTTCGTGCCAGCAGCCGCGGTAATACGAAGG
GGGCTAGCGTTGCTCGGAATTACTGGGCGTAAAGGGCGCGTAGGCGGATCGTTAAGTCAGAGGTG
AAATCCCAGGGCTCAACCCTGGAACTGCCTTTGATACTGGCGATCTTGAGTATGAGAGAGGTATGTG
GAACTCCGAGTGTAGAGGTGAAATTCGTAGATATTCGGAAGAACACCAGTGGCGAAGGCGACATAC
TGGCTCATTACTGACGCTGAGGCGCGAAAGCGTGGGGAGCAAACAGGATTAGATACCCTGGTAGTC
CACGCCGTAAACGATGATTGCTANTTGTCNGGCTGCATGCAGTTCGGTGACGCAANCTAACGCATTA
AGCCAATCCGCCTGGGGAANTACGGTCGCCNNGATTAAAACTCAAAAGGAATTGACGGGGGCCCC
GC

16S ribosomal RNA gene partial sequence of strain 4S2

CGCNAGCCTGATGCAGCAACGCCGCGTGAGGGATGACGGCCTTCGGGTTGTAAACCTCTTTTAGTA
GGGAAGAAGCGAAAGTGACGGTACCTGCAGAAAAAGCACCGGCTAACTACGTGCCAGCAGCCGCG
GTAATACGTAGGGTGCAAGCGTTGTCCGGAATTATTGGGCGTAAAGAGCTCGTAGGCGGCTTGTCG
CGTCTGCTGTGAAATCCCGGGGCTCAACCCCGGGCCTGCAGTGGGTACGGGCAAGCTAGAGTGCGG
TAGGGGAGATTGGAATTCCTGGTGTAGCGGTGGAATGCGCAGATATCAGGAGGAACACCGATGGC

GAAGGCAGATCTCTGGGCCGCTACTGACGCTGAGGAGCGAAAGCATGGGGAGCGAACAGGATTAG
ATACCCTGGTAGTCCATGCCGTAAACGTTGGGAACTAGATGTAGGGCCTGTTCCACGGGTTCTGTGT
CGTACCTAACGCATTAAGTTCCCCGCCTGGGGAGTACGGCCGCAAGGCTAAAAACTCAAAGGAATTG
ACGGGGGCCCGCACAAAGCGGCGGNACATGCGGAATTAATTCGATGCAACGCGAAAAAACCTTNA
CCAAGGCNTTGACATAACCCGAAAAC

16S ribosomal RNA gene partial sequence of strain 4S3

CGCAAGCCTGATGCAGCAACGCCGCGTGAGGGATGACGGCCTTCGGGTTGTAAACCTCTTTTAGTAG
GGAAGAAGCGAAAGTGACGGTACCTGCAGAAAAAGCACCGGCTAACTACGTGCCAGCAGCCGCGG
TAATACGTAGGGTGCAAGCGTTGTCCGGAATTATTGGGCGTAAAGAGCTCGTAGGCGGCTTGTCGC
GTCTGCTGTGAAATCCCGGGGCTCAACCCCGGGCCTGCAGTGGGTACGGGCAAGCTAGAGTGCGGT
AGGGGAGATTGGAATTCCTGGTGTAGCGGTGGAAATGCCCCAAATATCNAGGAGGGAACACCGAA
TTGGCCCAAAGGCAGAANTNTTTTTGGGNCCCCCTT

16S ribosomal RNA gene partial sequence of strain 6S1

```
AAGCCTGATGCAGCCATGCCGCGTGTATGAAGAAGGCCTTCGGGTTGTAAAGTACTTTCA
GCGGGGAGGAAGGTGTTGTGGTTAATAACCACAGCAATTGACGTTACCCGCAGAAGAAGC
ACCGGCTAACTCCGTGCCAGCAGCCGCGGTAATACGGAGGGTGCAAGCGTTAATCGGAAT
TACTGGGCGTAAAGCGCACGCAGGCGGTCTGTCAAGTCGGATGTGAAATCCCCGGGCTCA
ACCTGGGAACTGCATTCGAAACTGGCAGGCTGGAGTCTTGTAGAGGGGGGTAGAATTCCA
GGTGTAGCGGTGAAATGCGTAGAGATCTGGAGGAATACCGGTGGCGAAGGCGGCCCCCTG
GACAAAGACTGACGCTCAGGTGCGAAAGCGTGGGGAGCAAACAGGATTAGATACCCTGGT
AGTCCACGCCGTAAACGATGTCGATTTGGAGGTTGTGCCCTTGAGGCGTGGCTTCCGGAG
CTAACGCGTTAAATCGACCGCCTGGGGAGTACGGCCGCAAGGTTAAAACTCAAATGAATN
GACGGGGGCCCGC
```

16S ribosomal RNA gene partial sequence of strain 8S1

ANTGGGGAATTTTGGANAATGGGGGAAACCCTGATCCAGCCATCCCGCGTGTATGATGAAGGCCTT
CGGGTTGTAAAGTACTTTTGGCAGAGAAGAAAAGGTATCTCCTAATACGAGATACTGCTGACGGTAT
CTGCAGAATAAGCACCGGCTAACTACGTGCCAGCAGCCGCGGTAATACGTAGGGTGCAAGCGTTAA
TCGGAATTACTGGGCGTAAAGCGTGTAGGCGGTTCGGAAGAAAGATGTGAAATCCCAGGGCTCAA
CCTTGGAACTGCATTTTTAACTGCCGAGCTAGAGTATGTCAGAGGGGGGTAGAATTCCACGTGTAGC
AGTGAAATGCGTAAATATGTGGAGGAATACCGATGGCGAAGGCAGCCCCCTGGGATANTACTGACN
CTCANACACGAAAGCGTGGGGAGCNANCAGGATNAAATACCCTGGTANTCCCCCCCTAA

The phylogenetic trees of the bacterial strains 4S1, 4S2, 4S3, 6S1 and 8S1 obtained are presented below in Fig A V (A)-(E)

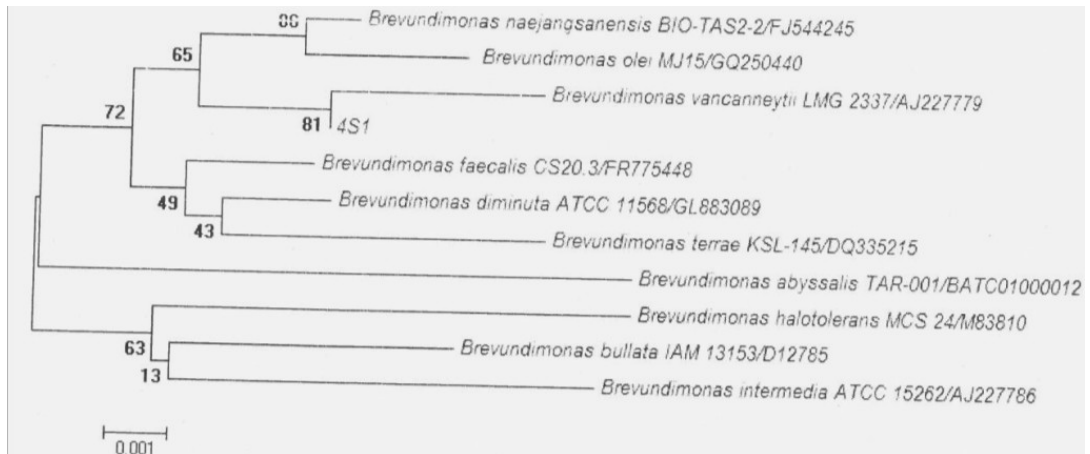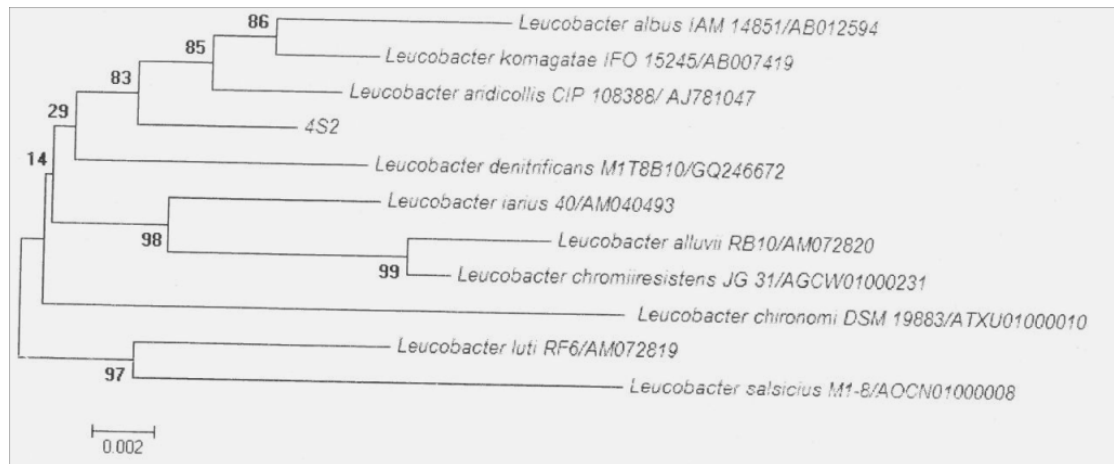**Fig A V (A) Phylogenetic tree of strain 4S1**
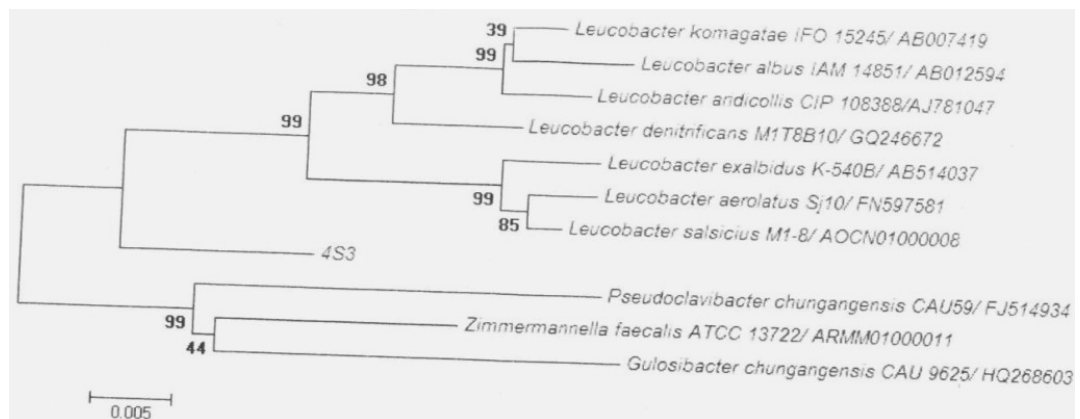

Fig A V (B) Phylogenetic tree of strain 4S2

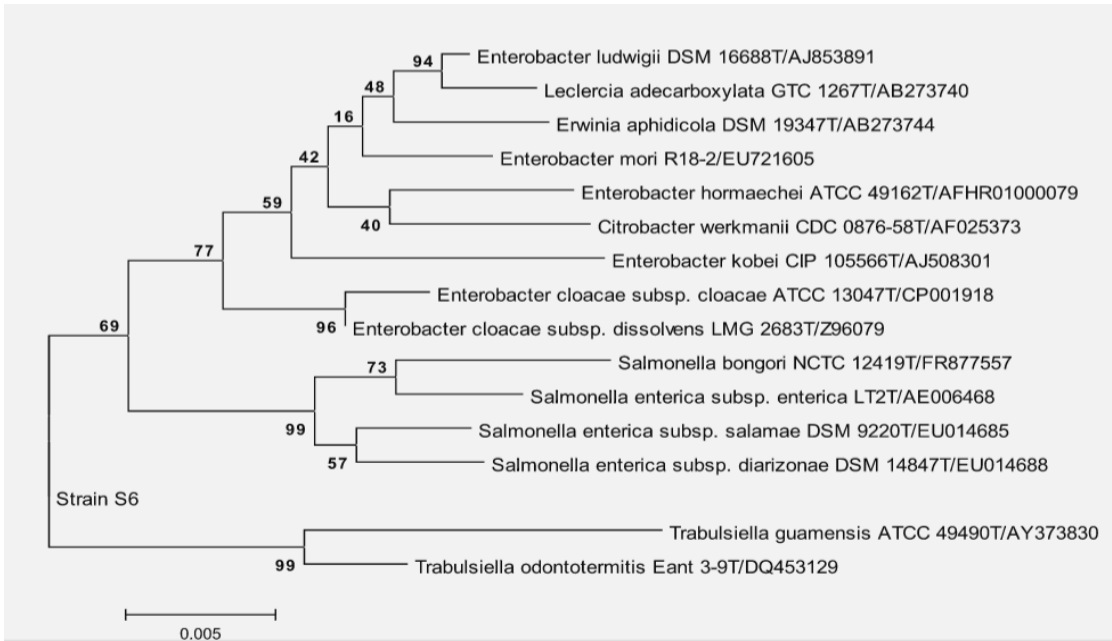**Fig A V (C) Phylogenetic tree of strain 4S3**

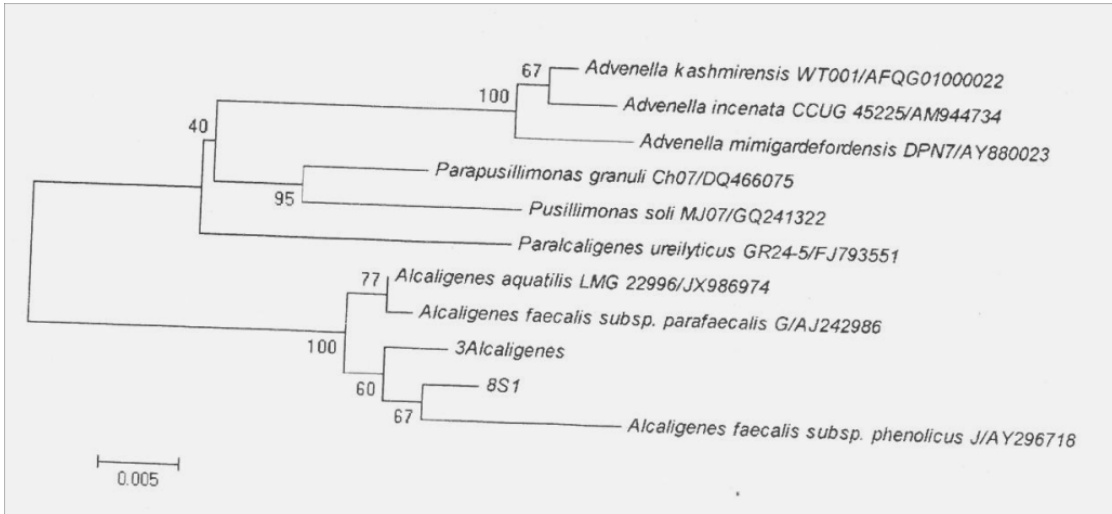**Fig A V (D) Phylogenetic tree of strain 6S1**

Fig A V (E) Phylogenetic tree of strain 8S1

APPENDIX VI

SDS PAGE of proteins for the determination of the molecular weight

SDS PAGE is routine method used for the qualitative characterisation of proteins in biological preparations and for the estimation of protein molecular masses.

A strongly anionic detergent sodium dodecyl sulfate (SDS) is used in combination with heat to dissociate the proteins before they are loaded on the gel. The denatured polypeptides bind to SDS and become negatively charged while exhibiting a consistent charge-to-mass ratio. The SDS-polypeptide complexes migrate through polyacrylamide gels with mobilities dependent on the size of the polypeptide.

Assembling the gel moulding cassette for the SDS PAGE

The glass plates along with the comb and spacers were cleaned thoroughly and rinsed with deionized water followed by ethanol and was dried under dust free conditions. The glass plates were aligned in the holders while achieving a leak proof condition.

Preparation of the gel

The resolving gel was prepared according to the recipe mentioned in section 2 below and the contents were mixed thoroughly before dispensing it into the gap assembled glass cassette with care as to not form any air bubbles. Enough space was left for casting the stacking gel and isobutanol was poured over the edge of the gel to prevent dehydration of the gel. The gel was left undisturbed in a vertical position for polymerization to occur.

The stacking gel was prepared according to the recipe mentioned in section 3 below and mixed thoroughly and carefully poured till the edge of the casting gel without the formation of any air bubble. The comb was inserted carefully into the stacking gel. The gel was left undisturbed in a vertical position for polymerization to occur.

Mounting the gel in the electrophoresis apparatus and electrophoretic separation

After the polymerization was complete the comb was carefully removed from the polymerized gel and the wells were washed with the SDS-PAGE running buffer (Section 4) to remove any unpolymerised acrylamide. The gel assembly was removed

from the clamp and placed onto the electrophoresis unit. The electrophoresis buffer was added to the unit till the edge of the gel cassette was completely immersed in it. The samples were loaded into the wells ensuring that the samples did not overflow from the respective wells. The electrical connections were made according to the manufacturer's specification.

The electrophoresis was performed at a constant voltage of 50V till the dye front reached the end of the gel. The process was stopped once the dye front reached the edge of the gel and the assembly was removed from the unit. The glass cassette containing the gel was separated and the gels were stained.

Preparation of the samples

The samples were mixed with the loading dye in a ratio of (2:1 v/v) and heated in boiling water for 1 min.

Coomassie staining

The gels were immersed in excess of Coomassie staining solution (Section 6) and were allowed to stand for at least 1 h before removing the stain. The gels were destained using the destaining solution (Section 5) until the stained protein bands were clearly distinguishable on a clear background.

Composition of gels and buffers used for Sodium Dodecyl Sulphate Poly Acrylamide Gel Electophoresis

1. **Acrylamide-bis-acrylamide solution**
   - 22.2% of acrylamide
   - 0.6% of bisacrylamide (stored in dark at 4^0C)
2. **Resolving Gel (12%), 10ml**
   - 5.41ml Acrylamide-bis-acrylamide
   - 3.75ml 1M Tris-Hcl, pH 8.8
   - 0.68ml Deionized H_2O
   - 0.1ml 10% SDS
   - 50µl 10% APS
   - 5 µl TEMED
3. **Stacking Gel (5%), 5ml**
   - 1.13ml Acrylamide-bis-acrylamide
   - 0.625ml 1M Tris-Hcl, pH 6.8
   - 3.17ml Deionized H_2O
   - 0.5ml 10% SDS
   - 25µl 10% APS

- 2.5µl TEMED
4. **Running Buffer**
     - 1.51g Tris base
     - 9.4g Glycine
     - 0.5g SDS
     - Deionized water upto 100ml
5. **De-staining Solution**
     - Deionized H_2O:Methanol:Acetic acid (50:40:10)
6. **Staining Solution**
     - 0.2% Coomassie Brilliant Blue in above solution
7. **Sample Loading Dye**
     - 1ml 0.5M Tris-Hcl, pH 8
     - 0.8ml Glycerol
     - 1.6ml 10% SDS
     - 0.4ml β-mercaptoethanol
     - 0.2ml 0.05% Bromophenol Blue
     - 4ml Deionized H_2O

Table A VI Protein markers and their molecular weights

Protein marker	Molecular weight (kDa)
Myosin, Rabbit Muscle	205
Phosphorylase b	97.4
Bovine Serum Albumin	66
Ovalbumin	43
Carbonic Anhydrase	29
Soyabean Trypsin Inhibitor	20.1
Lysozyme	14.3
Aprotinin	6.5
Insulin (α and β chains)	3

APPENDIX VII

Chemical synthesis of AgNPs

AgNPs were chemically synthesized using a citrate reduction method of boiling silver nitrate solution with sodium citrate as described by Fang et al. (2012). 100 mL of 1 mM $AgNO_3$ solution was boiled and 10 mL of 1% trisodium citrate was added to it dropwise, while the solution was continuously mixed on a heating mantle. As the reaction proceeded the solution turned brown red in colour and the reaction was continued till the colour of the reaction mixture turned yellowish green confirming the synthesis of AgNPs.

The colloidal solution was centrifuged at 15000rpm for 20 minutes. The supernatant was discarded and the settled AgNPs were dried at 90 ºC for 24 h. These nanoparticles were used for comparison with AgNPs synthesized using plant and bacterial sources.

APPENDIX VIII

Preparation of aqueous dye solutions

       100 mg/L of stock dye solution of AB 129 was prepared by dissolving 0.04 g of AB 129 dye (Purity- 25%) in distilled water to make upto 100 mL . 100 mg/L of stock solution of RBB dye was prepared by dissolving 0.022 g of RBB dye (Purity- ~50%) in distilled water to make upto 100 mL. Required concentrations of the dye solutions were prepared by suitably diluting the stock solutions with distilled water.

Estimation of Acid Blue degradation

A stock solution of 100 mg/L of the Acid Blue Dye (Sigma Aldrich) was made and a working solution of range 0- 25 mg/L was prepared in standard flasks with distilled water. The absorption maximum for Acid blue is found to be at 629nm. Aliquots of sample were drawn from the standard working solution and analyzed using UV-Vis Spectrophotometer. The standard graph was plotted by the concentration of the dye at X axis and Absorbance as Y axis giving rise to the standard equation y= 0.0097x with an R^2 value of 0.9978. The unknown samples of Acid Blue dye were diluted and analyzed for the dye content using the absorption maximum value and the final value was multiplied using the dilution factor.

Conc (mg/L)	Absorbance (a.u)
0	0
2.5	0.095
5.0	0.185
7.5	0.282
10	0.375
12.5	0.471
15	0.567
17.5	0.672
20	0.777
22.5	0.904
25	0.963

Fig A VIII (A) Calibration plot for the estimation of Acid Blue dye

Estimation of Remazol Brilliant Blue R Dye

A stock solution of 100 mg/L of the Remazol Brilliant Blue R Dye (Sigma Aldrich) was made and a working solution of range 0-25 mg/L was prepared in standard flasks with distilled water. The absorption maximum for Acid blue is found to be at 592nm. Aliquots of sample were drawn from the standard working solution and analysed using UV-Vis Spectrophotometer. The standard graph was plotted by the concentration of the dye at X axis and Absorbance as Y axis giving rise to the standard equation y= 0.0101x with an R^2 value of 0.9992. The unknown samples of Remazol Brilliant Blue R dye were diluted and analyzed for the dye content using the absorption maximum value and the final value was multiplied using the dilution factor.
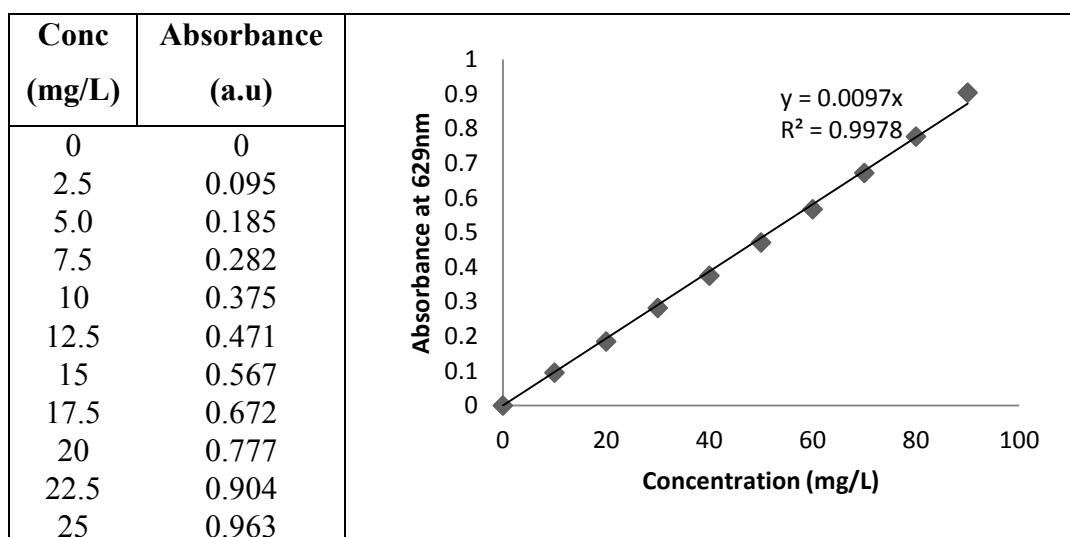
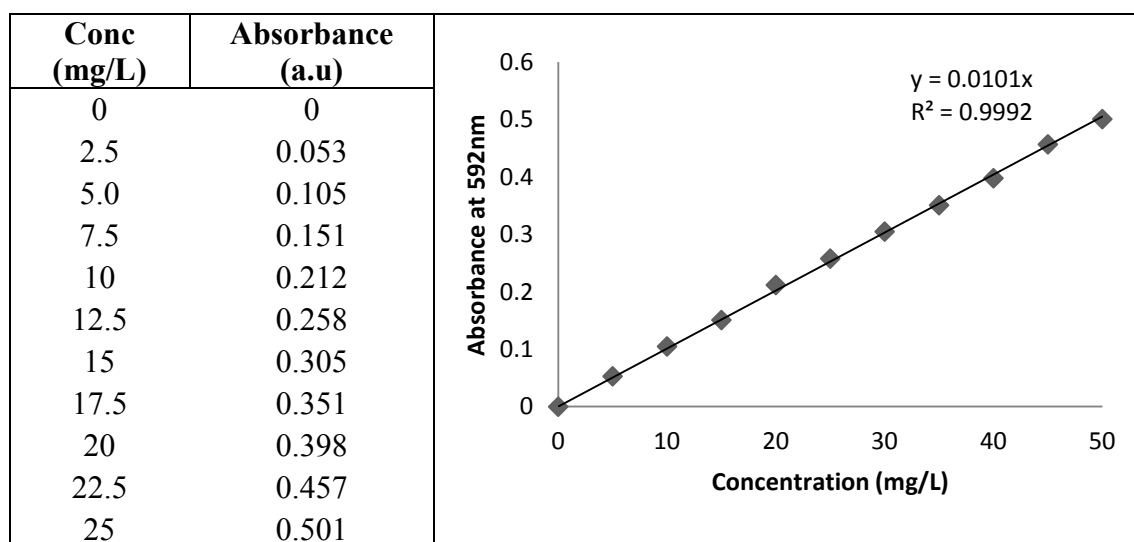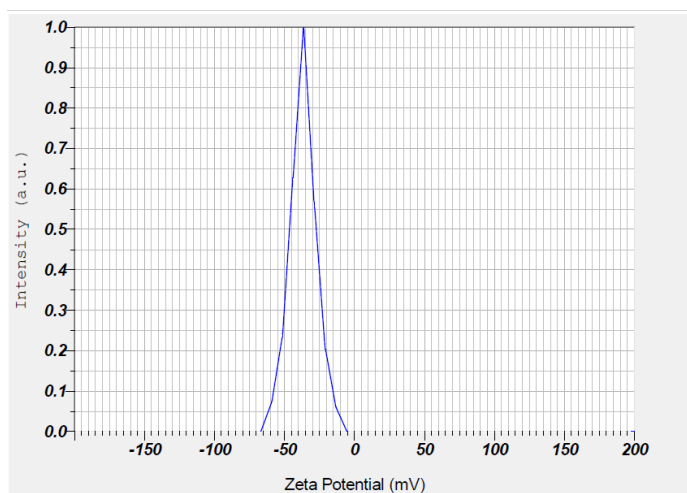| Conc (mg/L)	Absorbance (a.u)
0	0
2.5	0.053
5.0	0.105
7.5	0.151
10	0.212
12.5	0.258
15	0.305
17.5	0.351
20	0.398
22.5	0.457
25	0.501

Fig A VIII (B) Calibration plot for the estimation of Remazol Brilliant Blue R dye

APPENDIX IX

(i)
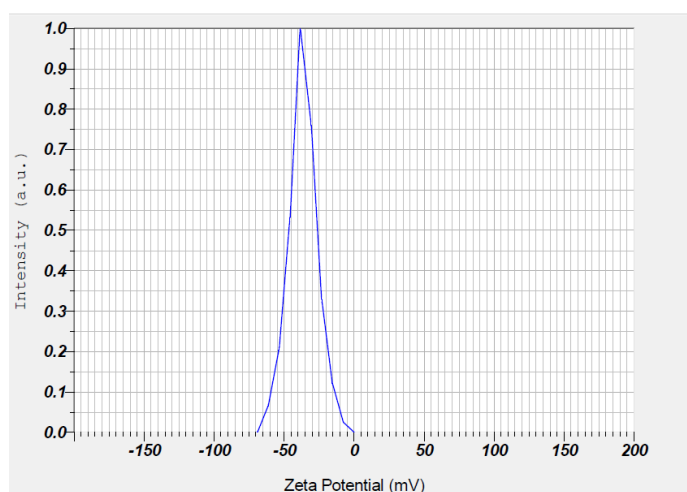
(ii)

Fig A IX(A) Zeta potential value of AgNPs synthesized using (i) ALE (ii) TLE

Fig A IX (B) Zeta potential measurements of AgNPs synthesized using the 24 h cell free supernatant of bacterial supernatants (i) 4S1 (ii) 4S2 (iii) 4S3 (iv) 6S1 and (v) 8S1

Fig A IX (C) Zeta potential graphs of TiO₂-NPs synthesized using the cell free supernatant of bacterial strain (i) 4S1 (ii) 4S2 (iii) 4S3 (iv) 6S1 and (v) 8S1

APPENDIX X

ಡಾ. ಶಿವರಾಮ ಕಾರಂತ ಪಿಲಿಕುಳ ನಿಸರ್ಗಧಾಮ

Dr. Shivaram Karantha Pilikula Nisarga Dhama

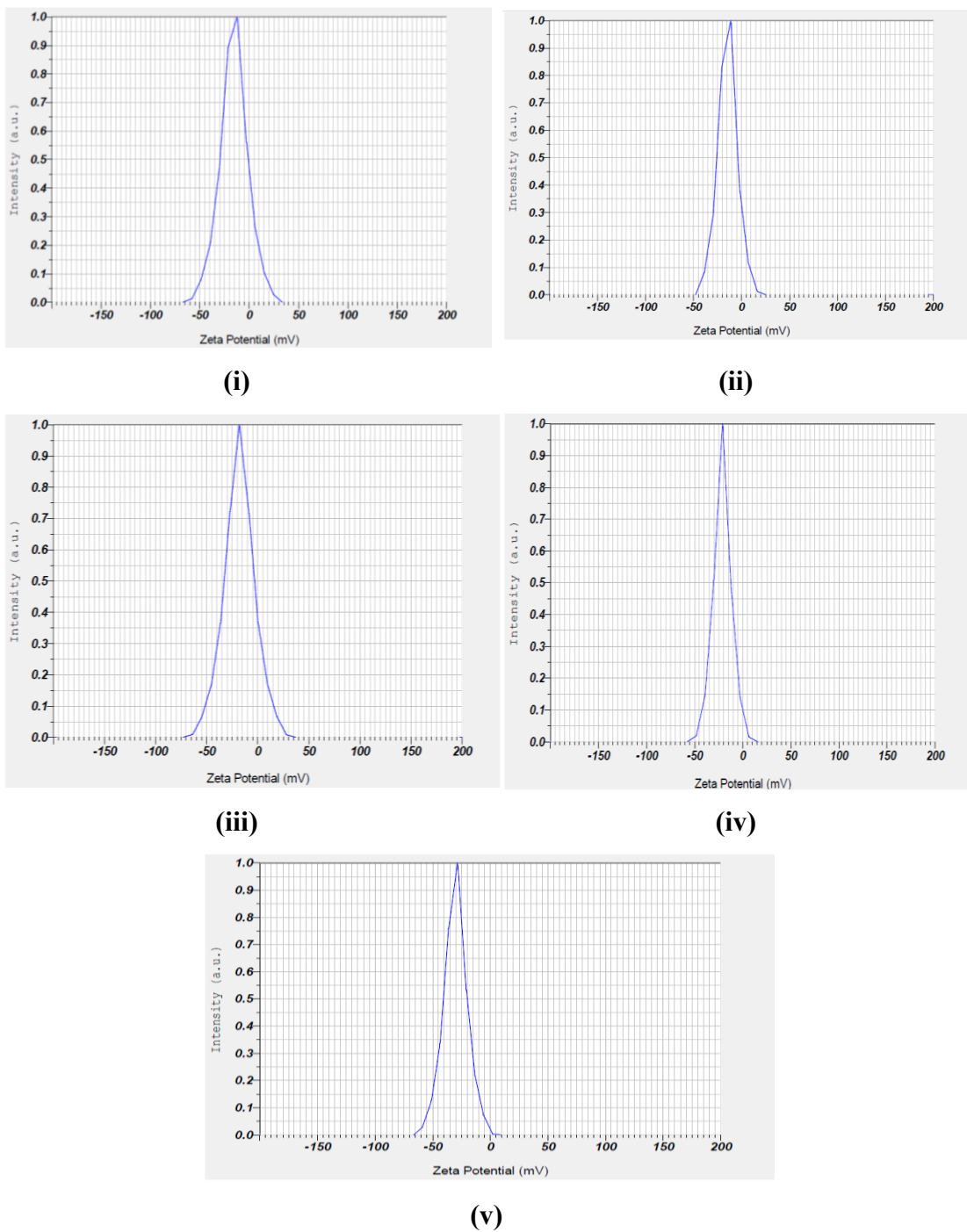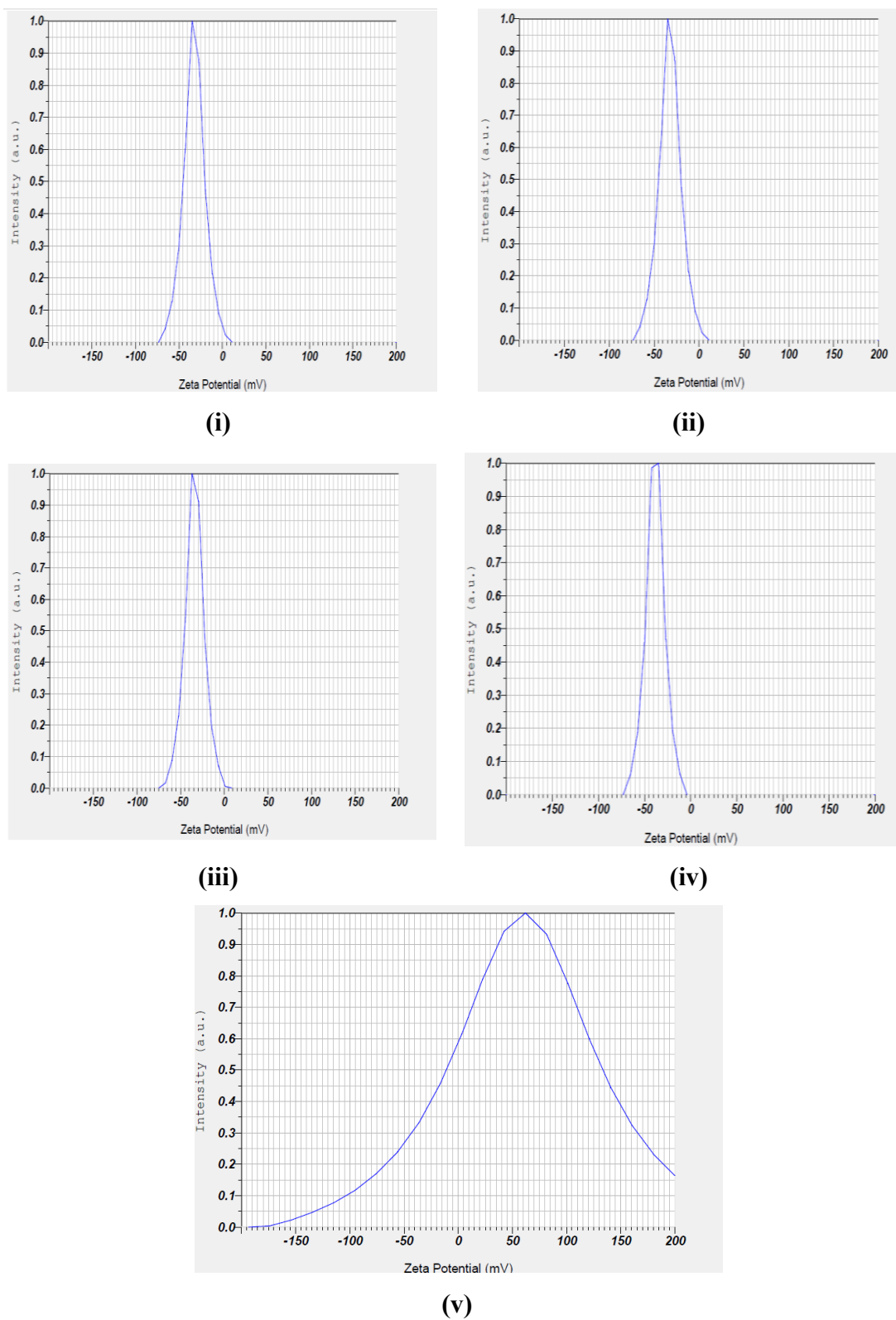ವಿಜ್ಞಾನ ಕೇಂದ್ರ, ಮೂಡುಶೆಡ್ಡೆ ಅಂಚೆ, ಮಂಗಳೂರು – 575 028, ದೂ : 0824 – 2263565 ಫ್ಯಾಕ್ಸ್ : 2263562
Science Centre, Moodushedde Post, Mangalore – 575 028 Ph : 0284 - 2263565 Fax : 2263562
Website : www.pilikula.com   E-mail: pilikula96@gmail.com
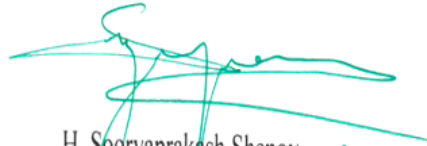
Date: 29. 01. 2015

Dr. H. Sooryaprakash Shenoy
Principal Scientist

This is to certify that two plant specimen samples were collected and submitted to us for identification by Ms. Aishwarya Devadiga, Dr. Vidya Shetty K and Dr. M. B Saidutta from Department of Chemical Engineering, National Institute of Technology, Karnataka, Surathkal- India. The plant samples were collected from the campus of National Institute of Technology, Karnataka, Surathkal and have been identified as *Tectona grandis* L. f (Lamiaceae) (Herbarium No- 2145) and *Terminalia catappa* L. (Combretaceae) (Herbarium No-0154). The specimens were processed and herbarium sheets were deposited at Pilikula Herbarium, Mangalore.

H. Sooryaprakash Shenoy
Principal Scientist
Dr. Shivarama Karantha
Pilikula Nisarga Dhama, Mangalore

RESEARCH PUBLICATIONS

- Devadiga, A., Shetty, K. V., and Saidutta, M. B. (2015). Timber industry waste-teak (*Tectona grandis* Linn.) leaf extract mediated synthesis of antibacterial silver nanoparticles. *International Nano Letters*, **Springer** *5*(4), 205-214.

- Devadiga, A., Shetty, K. V., and Saidutta, M. B. (2016). Effect of Precursor salt solution concentration on the size of silver nanoparticles synthesized using aqueous leaf extracts of *T.catappa* and *T.grandis* Linn f. - A green synthesis route. **Accepted for publication as a Book Chapter** in Materials, Energy and Environment Engineering, **Springer**.

- Maria, B. S., Devadiga, A., Kodialbail, V. S., & Saidutta, M. B. (2016) Solar photocatalytically active engineered silver nanoparticle synthesis using aqueous extract of mesocarp of *Cocos nucifera* (Red Spicata Dwarf). Accepted for publication. Journal of Experimental Nanoscience, **Taylor and Francis**. DOI: 10.1080/17458080.2016.1251622.

- Maria, B. S., Devadiga, A., Kodialbail, V. S., and Saidutta, M. B. (2015). Synthesis of silver nanoparticles using medicinal *Zizyphus xylopyrus* bark extract. Applied Nanoscience, **Springer** 5(6), 755-762.

Research Articles in Conference Proceedings

- Devadiga, A., Shetty, K. V., and Saidutta, M. B. (2012). "Isolation and Screening of Microorganisms from metal rich soil for biosynthesis of silver nanoparticles." Proceedings of National seminar on Biomolecules and biocatalysts in bioprocesses. St.Aloysius College, Mangalore , 8-9th March 2012. BBB-OP-02. pp.33- **Awarded Second Prize**

- Devadiga, A., Shetty, K. V., and Saidutta, M. B. (2012). "Biosynthesis of silver nanoparticles from *Pseudomonas* sp. Isolated and screened from metal rich soil." Proceedings of World Congress on Biotechnology-2012." Leonia International Conventional Centre, Hyderabad, 4-6th May 2012.

- Devadiga, A., Shetty, K. V., and Saidutta, M. B. (2013). "Biosynthesis of Nanosilver using aqueous leaf extract of *Terminalia catappa.*" International Conference on Recent Advances in Material Science and Technology, NITK, Surathkal, 17-19th January, 2013. OP-25, pp-18.

- Devadiga, A., Shetty, K. V., and Saidutta, M. B. (2015). "Presented a Paper entitled "Effect of Precursor salt solution concentration on the size of silver nanoparticles synthesized using the aqueous leaf extracts of *T.catappa* and *T.grandis* Linn F." International Conference on Advances in Chemical Engineering, NITK, Surathkal, 20-22th December. OP- 299, pp-61.

Ms. Aishwarya Devadiga

Email ID: aishwarya.d.88@gmail.com
Contact no: +91-9538947883

Personal details:

Date of Birth	30 August 1988
Nationality	Indian
Marital Status	Married
Spouse`s Name	Mr. Ambadas Nambivalap
Permanent Address	2-44/9, Ashraya Compound
	Beside HP Petrol Pump, NH 66
	Post Kulai- Hosabettu,
	Surathkal, Mangalore,
	Dakshina Kannada,
	Karnataka- 575019
	India

Educational qualification

Ph.D., Department of Chemical Engineering, NITK, Surathkal, Mangalore, Karnataka (2010 Onward).

Academic Background

- Doctor of Philosophy in Chemical Engineering from National Institute of Technology, Surathkal, Karnataka with CGPA of 7.27.
- Post Graduated in Biotechnology from St. Aloysius College, Mangalore with 76%
- Graduated in Biotechnology from St. Aloysius College, Mangalore with 78%
- Completed Pre-University from Govinda Dasa College, Surathkal with 79%
- Matriculated from S.M.E.M. School, Surathkal with 83%

Research Articles Published

- Devadiga, A., Shetty, K. V., and Saidutta, M. B. (2015). "Timber industry waste-teak (*Tectona grandis* Linn.) leaf extract mediated synthesis of antibacterial silver nanoparticles." *International Nano Letters*, Springer 5(4), 205-214.

- "Maria, B. S., Devadiga, A., Kodialbail, V. S., and Saidutta, M. B. (2015). "Synthesis of silver nanoparticles using medicinal *Zizyphus xylopyrus* bark extract." *Applied Nanoscience,* Springer 5(6), 755-762.

- Devadiga, A., Shetty, K. V., and Saidutta, M. B. (2015). "Effect of Precursor salt solution concentration on the size of silver nanoparticles synthesized using the aqueous leaf extracts of *T.catappa* and *T.grandis* Linn F." as a book chapter in Materials, Energy and Environment Engineering, **Springer**.

- Maria, B. S., Devadiga, A., Kodialbail, V. S., and Saidutta, M. B. (2015), "Solar Photocatalytically active engineered silver nanoparticle synthesis using aqueous extract of mesocarp of Cocos nucifera (Red Spicata Dwarf)." *Journal of Experimental Nanoscience.* doi: 10.1080/17458080.2016.1251622.

Research Articles in conference proceedings

- Devadiga, A., Shetty, K. V., and Saidutta, M. B. (2012). "Isolation and Screening of Microorganisms from metal rich soil for biosynthesis of silver nanoparticles." Proceedings of National seminar on Biomolecules and biocatalysts in bioprocesses. St.Aloysius College, Mangalore , 8-9th March 2012. BBB-OP-02. pp.33- **Awarded Second Prize**

- Devadiga, A., Shetty, K. V., and Saidutta, M. B. (2012). "Biosynthesis of silver nanoparticles from *Pseudomonas* sp. Isolated and screened from metal rich soil." Proceedings of World Congress on Biotechnology-2012." Leonia International Conventional Centre, Hyderabad, 4-6th May 2012.

- Devadiga, A., Shetty, K. V., and Saidutta, M. B. (2013). "Biosynthesis of Nanosilver using aqueous leaf extract of *Terminalia catappa.*" International Conference on Recent Advances in Material Science and Technology, NITK, Surathkal, 17-19th January, 2013. OP-25, pp-18.

- Devadiga, A., Shetty, K. V., and Saidutta, M. B. (2015). "Presented a Paper entitled "Effect of Precursor salt solution concentration on the size of silver nanoparticles synthesized using the aqueous leaf extracts of *T.catappa* and *T.grandis* Linn F." International Conference on Advances in Chemical Engineering, NITK, Surathkal, 20-22th December. OP- 299, pp-61.

Academic projects

- **Post Graduation Dissertation** entitled "Studies on Isolation, Screening, Mass Production and Application of Lipase" conducted at the Sangenomics Research Laboratory, Bangalore, India from October 2009- December 2009.

- **Graduation Dissertation** entitled "Isolation and Characterization of microorganisms from the Rhizosphere of rice plantations" conducted at the Department of Biotechnology, St. Aloysius College, Mangalore Karnataka, India from November 2007- April 2008.

- Underwent training in clinical laboratory techniques at A.J Hospital and Research Centre, Mangalore, Karnataka, India from September 2008- October 2008.

- **Graduate research project** entitled "Algae and Algal Products" for a period of two months September 2006-October 2006 conducted at St. Aloysius College, Mangalore Karnataka, India under the Bioscience Association.

Conferences/ workshop attended

- Presented a paper entitled "**Biosynthesis of silver nanoparticles by aqueous leaf extract of *Terminalia catappa***" in the International Conference on Recent Advances in Material Science and Technology held at NITK, Surathkal, Karnataka, India on January 17- 19, 2013.

- Presented a poster entitled "Biosynthesis of silver nanoparticles from *Pseudomonas sp.* Isolated and screened from metal rich soil" in the **World Congress on Biotechnology-2012** held at Leonia International Conventional Centre, Hyderabad, Andhra Pradesh, India on 04-06 May 2012.

- Presented a poster entitled "Isolation and Screening of Microorganism from metal rich soil for biosynthesis of nanoparticles" in the **International Conference on Advances in Biological Sciences,** held at Kannur University, Kannur, Kerala, India on 15-17 March 2012.

- Presented an paper entitled "Isolation and Screening of Microorganisms from metal rich soil for biosynthesis of silver nanoparticles. " in the **National seminar on Biomolecules and Biocatalysts in Bioprocesses** held at St.Aloysius College (Autonomous) Mangalore Karnataka, India on 8 and 9 March 2012 and was awarded "**Second Prize**".

- Presented a paper entitled " Biosynthesis of Silver nanoparticles by microbes" in the **National conference on perspectives of biotechnology in health care and industry** held at Alva`s College, Moodabidri, Mangalore Karnataka, India on 24-25 February 2012 and was awarded " **Best Presentation**"

- Participated in **Workshop on Nanobiotechnology** conducted by School of Interdisciplinary Science and Technology, I^{2}IT, Pune, Maharashtra, India held on 14- 16 March 2011.

- Presented a poster entitled "**Production of Lipase from bacteria and its application**" at "**infoVISION 2010**" **an IT and LIFE sciences Exhibition** at

AIMIT, St. Aloysius College, Mangalore, Karnataka, India on March 24- 26, 2010.

- Presented a poster entitled "Production of Bacterial Lipase and its application" in the National Level Seminar on **Biodiversity: An endless exploration** held at St. Aloysius College, Mangalore, Karnataka, India on February 22 2010.

- Presented a model entitled "Brain Tricks" **at IBRO sponsored "Brain Awareness Programme"** at St. Aloysius College, Mangalore, Karnataka, India on March 20-21, 2009.

- Presented a waste efficient model at the **BRNS-BARC National Seminar on "Sustainable Waste Management: Problems and Solutions"** held at St. Aloysius College, Mangalore, Karnataka, India on 29- 31 January 2009.

Technical skills

- Hands on experience in the synthesis of silver and titanium dioxide nanoparticles using different methods
- Characterization of nanomaterials,
- Proficient in basic and traditional microbiology techniques like cultivation, enumeration, isolation and preservation of microbes
- Proficient in handling equipments and instruments like High speed Centrifuges, Atomic absorption spectroscopy, UV-Vis spectrophotometer, Lyophilizer, Compound Microscope, Sonicator and conventional instruments used in microbiological studies like autoclave, laminar air flow, pH meter, incubated shakers and incubators, weighing balance.
- Proficient in handling instruments such as Scanning electron microscope, Particle size and Zeta potential analyzer.
- Familiar with basic and conventional techniques in molecular biology, bionanotechnology, Downstream process, Bioorganic chemistry, enzyme technology and concepts of chemical engineering.

Extracurricular Activities

* Consistent academic track record and have demonstrated general proficiency in subjects
* Have been a district level hockey player.
* Participated in many oratorical, quiz and dance competitions and won prizes
* Have been an active volunteer and have co-ordinator in various programmes and seminars held during the academic tenure.

Declaration

I hereby declare that the above-mentioned information are true to the best of my knowledge and I bear the responsibility for the correctness of the above-mentioned particulars.

Place: Surathkal, India

Date: / /   **(Aishwarya Devadiga)**